ADVANCES IN MICROALGAE BIOLOGY AND SUSTAINABLE APPLICATIONS

EDITED BY : Flavia Vischi Winck, Diego Mauricio Riaño-Pachón and Telma Teixeira Franco

frontiers Research Topics

About Frontiers

Frontiers is more than just an open-access publisher of scholarly articles: it is a pioneering approach to the world of academia, radically improving the way scholarly research is managed. The grand vision of Frontiers is a world where all people have an equal opportunity to seek, share and generate knowledge. Frontiers provides immediate and permanent online open access to all its publications, but this alone is not enough to realize our grand goals.

Frontiers Journal Series

The Frontiers Journal Series is a multi-tier and interdisciplinary set of open-access, online journals, promising a paradigm shift from the current review, selection and dissemination processes in academic publishing. All Frontiers journals are driven by researchers for researchers; therefore, they constitute a service to the scholarly community. At the same time, the Frontiers Journal Series operates on a revolutionary invention, the tiered publishing system, initially addressing specific communities of scholars, and gradually climbing up to broader public understanding, thus serving the interests of the lay society, too.

Dedication to Quality

Each Frontiers article is a landmark of the highest quality, thanks to genuinely collaborative interactions between authors and review editors, who include some of the world's best academicians. Research must be certified by peers before entering a stream of knowledge that may eventually reach the public - and shape society; therefore, Frontiers only applies the most rigorous and unbiased reviews.

Frontiers revolutionizes research publishing by freely delivering the most outstanding research, evaluated with no bias from both the academic and social point of view.

By applying the most advanced information technologies, Frontiers is catapulting scholarly publishing into a new generation.

What are Frontiers Research Topics?

Frontiers Research Topics are very popular trademarks of the Frontiers Journals Series: they are collections of at least ten articles, all centered on a particular subject. With their unique mix of varied contributions from Original Research to Review Articles, Frontiers Research Topics unify the most influential researchers, the latest key findings and historical advances in a hot research area! Find out more on how to host your own Frontiers Research Topic or contribute to one as an author by contacting the Frontiers Editorial Office: **researchtopics@frontiersin.org**
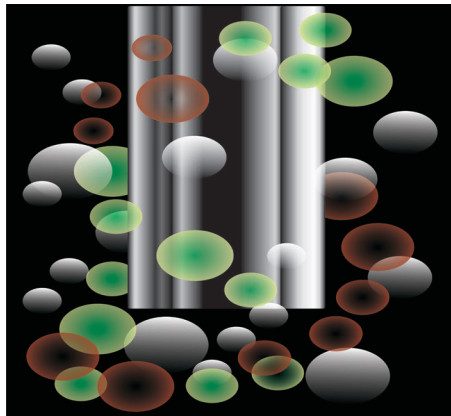
ADVANCES IN MICROALGAE BIOLOGY AND SUSTAINABLE APPLICATIONS

Topic Editors:
Flavia Vischi Winck, University of São Paulo, Brazil
Diego Mauricio Riaño-Pachón, Brazilian Center for Research in Energy and Materials, Brazil
Telma Teixeira Franco, State University of Campinas, Brazil

Semi-abstract illustration of the inside of a biorreactor containing microalgae cells (green dots), products (red dots) and gas bubbles (white dots).
Image by Flavia Vischi Winck

It has become more evident that many microalgae respond very differently than land plants to diverse stimuli. Therefore, we cannot reduce microalgae biology to what we have learned from land plants biology. However, we are still at the beginning of a comprehensive understanding of microalgae biology. Microalgae have been posited several times as prime candidates for the development of sustainable energy platforms, making thus the in-depth understanding of their biological features an important objective. Thus, the knowledge related to the basics of microalgae biology must be acquired and shared rapidly, fostering the development of potential applications.

Microalgae biology has been studied for more than forty years now and more intensely since the 1970's, when genetics and molecular biology approaches were integrated into the research programs. Recently, studies on the molecular physiology of microalgae have provided evidences on the particularities of these organisms, mainly in model species, such as Chlamydomonas reinhardtii. Of note, cellular responses in microalgae produce very interesting phenotypes, such as high lipid content in nitrogen deprived cells, increased protein content in cells under high CO_2 concentrations, the modification of flagella structure and motility in basal body mutant strains, the different ancient proteins that microalgae uses to dissipate the harmful excess of light energy, the hydrogen production in cells under sulfur deprivation, to mention just a few. Moreover, several research groups are using high-throughput and data-driven technologies, including "omics" approaches to investigate microalgae cellular responses at a system-wide level, revealing new features of microalgae biology, highlighting differences between microalgae and land plants.

It has been amazing to observe the efforts towards the development and optimization of new technologies required for the proper study of microalgae, including methods that opened new paths to the investigation of important processes such as regulatory mechanisms, signa-

ling crosstalk, chemotactic mechanisms, light responses, chloroplast controlled mechanisms, among others.

This is an exciting moment in microalgae research when novel data are been produced and applied by research groups from different areas, such as bioprocesses and biotechnology. Moreover, there has been an increased amount of research groups focused in the study of microalgae as a sustainable source for bioremediation, synthesis of bioproducts and development of bioenergy. Innovative strategies are combining the knowledge of basic sciences on microalgae into their applied processes, resulting in the progression of many applications that hopefully, will achieve the necessary degree of optimization for economically feasible large-scale applications.

Advances on the areas of basic microalgae biology and novelties on the essential cellular processes were revealed. Progress in the applied science showed the use of the basic science knowledge into fostering translational research, proposing novel strategies for a sustainable world scenario.

In this present e-book, articles presented by research groups from different scientific areas showed, successfully, the increased development of the microalgae research. Herewith, you will find articles ranging from bioprospecting regional microalgae species, through advances in microalgae molecular physiology to the development of techniques for characterization of biomass and the use of biomass into agriculture and bioenergy production.

This e-book is an excellent source of knowledge for those working with microalgae basic and applied sciences, and a great opportunity for researchers from both areas to have an overview of the amazing possibilities we have for building an environmentally sustainable future once the knowledge is translated into novel applications.

Table of Contents

frontiers
in Plant Science

Editorial: Advances in Microalgae Biology and Sustainable Applications

Flavia V. Winck[1]*, Diego M. Riaño-Pachón[2] and Telma T. Franco[3]

[1] *Department of Biochemistry, Institute of Chemistry, University of São Paulo, São Paulo, Brazil,* [2] *Brazilian Bioethanol Science and Technology Laboratory, Brazilian Center for Research in Energy and Materials, Campinas, Brazil,* [3] *School of Chemical Engineering, State University of Campinas, Campinas, Brazil*

The Editorial on the Research Topic

Advances in Microalgae Biology and Sustainable Applications

The further development of our societies will undoubtedly face many challenges, but currently we have the capacity, and the duty, to look for environmentally sustainable solutions to these challenges. In order to do so we must dedicate efforts toward the development of processes for the sustainable production of chemicals and energy. Microalgae are receiving increasing attention as candidates to develop sustainable processes; they have been proposed as feedstock for several purposes, such as energy production, biosynthesis of nutraceuticals, animal feed and bioremediation, to mention just a few (Skjanes et al., 2013; Wijffels et al., 2013). Recent understanding of diverse aspects of microalgae biology have revealed important differences at the cellular level between them and land plants (Perez-Garcia et al., 2011; Liu and Benning, 2013). The microalgae characteristics of unicellularity and mixotrophy, are of special interest for potential industrial applications (Lowrey et al., 2016). All of the above, is positioning microalgae as a viable solution for the sustainable production of fuels and chemicals (Skjanes et al., 2013; Moody et al., 2014).

Within this Frontiers research topic, we aimed to show important advances in the understanding of microalgae biology and the opportunities to translate basic knowledge into sustainable applications.

The articles making this collection highlight how different scientific areas should come together for the successful use of microalgae biomass in sustainable applications. Here you will find articles ranging from bioprospecting regional microalgae species, through advances in microalgae molecular physiology to the development of techniques for characterization of biomass and the use of biomass into agriculture and bioenergy production.

In this special research topic, Duong et al. tapped into the biodiversity of microalgae in aquatic Australian environments, resulting in the identification of the growth and lipid content in 16 novel isolates, from five different species (Duong et al.).

The further understanding of how microalgae cells can survive on aquatic environments implies understanding the mechanisms of nutrient assimilation. This was what Sanz-Luque et al. exemplified to us in a review of nitrate assimilation and its regulation in microalgae (Sanz-Luque et al.).

Notably, the study presented in Eitzinger et al. highlighted the identification of over 40 novel proteins that make part of the eyespot, i.e., a specialized optical device, and a complex pool of methylated proteins, in *Chlamydomonas reinhardtii*, contributing to a better understanding of the primordial visual system of microalgae and its possible connection to light responses (Eitzinger et al.).

Further research revealed candidate metabolic pathways sensitive to changes on the availability of carbon dioxide, as demonstrated by Winck et al. in a genomic scale modeling approach (Winck et al.), that suggested an important role of mitochondria and enzymes of the photorespiratory pathway during cell response to high availability of carbon dioxide.

Additionally, Steinbeck et al. described a detailed study of the sustainable light-driven production of Hydrogen in the model microalgae *Chlamydomonas*. The team of researchers demonstrated the importance of double mutation of proton-gradient regulation genes for hydrogen production, with increased oxygen consumption by the mutant strains and faster achievement of anaerobiosis and activation of hydrogenases in Sulfur deprivation conditions.

Therefore, the discovery of candidate genes and biological pathways and networks can foster the bioengineering of biological routes for enhanced biosynthesis of biomass and compounds of biotechnological interest. This is shown in the article by Ouyang et al. where they performed the functional analysis of the enzyme glycerol-3-phosphate acyltransferase from the oleaginous green microalgae *Lobosphaera incisa,* revealing that alterations on the gene sequence was important for increase the enzyme activity and phospholipid content when heterologous expressed in Yeast (Ouyang et al.).

However, novel methodological approaches to facilitate the characterization of microalgae biomass have to be developed and optimized and this is what we can see in the work of Shen et al. The authors performed the global profiling of lipids in microalgae for depicting fatty acids that can be applied as characteristics ones for measurement purposes, enabling lipid assessment in several strains (Shen et al.). A detailed analysis of several processes of microalgae dewatering (which could be understood as harvesting) methods, performed by Soomro et al, discussed an important problematic in the use of microalgal biomass as feedstock; the energy and financial costs associated to the production of microalgae biomass. The authors performed a life-cycle assessment analysis and proposed a combination of selected dewatering technologies for reducing costs and increasing biomass recovery (Soomro et al.).

One example of novel applications for the sustainable use of microalgae biomass residues generated by a global future microalgae industrial application was shown by Maurya et al. The authors performed the analysis of the sustainable use of microalgae biomass residues as substitute nitrogen fertilizer on *Zea mays* (maize) cultures, showing the possibility to substitute up to 75% of the total chemical nitrogen fertilizers provided to the plants.

Well succeed applications of microalgae biomass are now on the market, such as the production of Astaxanthin by the microalgae *Haematococcus pluvialis*. Astaxanthin is a potent antioxidant molecule, and a comprehensive review of *Haematococcus pluviallis* and the many aspects of the Astaxanthin properties, production and applications was provided by Shah et al.

The production of microalgae biomass for industrial scale applications is still been developed; however, as shown by Xiao et al. large amounts of biodiesel from microalgae biomass may be produced in a controlled process.

Besides the many challenges ahead on the development of massive production of microalgae biomass it has been demonstrated that human resources are available to achieve this goal, and to improve the capacity and diversity of applications of microalgae for sustainable applications worldwide.

Scientists from different fields of research, from basic science to applied science, are indeed contributing to the understanding of microalgae diversity, their complex cellular responses and phenotypes, which will certainly contribute to generate novel solutions for the development of microalgae-based sustainable applications, which are very much needed in present times.

AUTHOR CONTRIBUTIONS

FW draft the editorial text. FW, DR, and TF revised and approved the final version of the editorial text.

ACKNOWLEDGMENTS

REFERENCES

Liu, B., and Benning, C. (2013). Lipid metabolism in microalgae distinguishes itself. *Curr. Opin. Biotechnol.* 24, 300–309. doi: 10.1016/j.copbio.2012.08.008

Lowrey, J., Armenta, R. E., and Brooks, M. S. (2016). Nutrient and media recycling in heterotrophic microalgae cultures. *Appl. Microbiol. Biotechnol.* 100, 1061–1075. doi: 10.1007/s00253-015-7138-4

Moody, J. W., McGinty, C. M., and Quinn, J. C. (2014). Global evaluation of biofuel potential from microalgae. *Proc. Natl. Acad. Sci. U.S.A.* 111, 8691–8696. doi: 10.1073/pnas.1321652111

Perez-Garcia, O., Escalante, F. M., de-Bashan, L. E., and Bashan, Y. (2011). Heterotrophic cultures of microalgae: metabolism and potential products. *Water Res.* 45, 11–36. doi: 10.1016/j.watres.2010.08.037

Skjanes, K., Rebours, C., and Lindblad, P. (2013). Potential for green microalgae to produce hydrogen, pharmaceuticals and other high value products in a combined process. *Crit. Rev. Biotechnol.* 33, 172–215. doi: 10.3109/07388551.2012.681625

Wijffels, R. H., Kruse, O., and Hellingwerf, K. J. (2013). Potential of industrial biotechnology with cyanobacteria and eukaryotic microalgae. *Curr. Opin. Biotechnol.* 24, 405–413. doi: 10.1016/j.copbio.2013.04.004

Growth and lipid accumulation of microalgae from fluctuating brackish and sea water locations in South East Queensland—Australia

Van Thang Duong, Skye R. Thomas-Hall and Peer M. Schenk*

Algae Biotechnology Laboratory, School of Agriculture and Food Sciences, The University of Queensland, Brisbane, QLD, Australia

One challenge constraining the use of microalgae in the food and biofuels industry is growth and lipid accumulation. Microalgae with high growth characteristics are more likely to originate from the local environment. However, to be commercially effective, in addition to high growth microalgae must also have high lipid productivities and contain the desired fatty acids for their intended use. We isolated microalgae from intertidal locations in South East Queensland, Australia with adverse or fluctuating conditions, as these may harbor more opportunistic strains with high lipid accumulation potential. Screening was based on a standard protocol using growth rate and lipid accumulation as well as prioritizing fatty acid profiles suitable for biodiesel or nutraceuticals. Using these criteria, an initial selection of over 50 local microalgae strains from brackish and sea water was reduced to 16 strains considered suitable for further investigation. Among these 16 strains, the ones most likely to be effective for biodiesel feedstock were *Nitzschia* sp. CP3a, *Tetraselmis* sp. M8, *Cymbella* sp. CP2b, and *Cylindrotheca closterium* SI1c, reaching growth rates of up to 0.53 day^{-1} and lipid productivities of 5.62 μg mL^{-1}day^{-1}. Omega-3 fatty acids were found in some strains such as *Nitzschia* sp. CP2a, *Nitzschia* sp. CP3a and *Cylindrotheca closterium* SI1c. These strains have potential for further research as commercial food supplements.

Keywords: biodiesel, diatom, fatty acids, microalgae, omega-3 fatty acids

Introduction

Microalgae grow in most natural environments, typically aquatic and marine systems, but they are also found in soil, ice, rock pools or in volcanic water that can have extreme environmental fluctuations (Duong et al., 2012). Microalgae suffering from adverse or fluctuating conditions often have the ability to accumulate higher contents of biochemical products for survival, such as lipid, starch, protein or carotenoid contents (Lim et al., 2012). Microalgae can produce a variety of lipids that can be used by the food and biofuel industry (Huerlimann et al., 2010). For the production of biodiesel, fatty acids with a chain length of 14–18 carbons are preferable. Saturated fatty acids C14, C16, and C18 and unsaturated fatty acids such as C16:1, C16:2, C18:1, and C18:2 are the most important for producing good biodiesel quality (Schenk et al., 2008). This is because the other unsaturated fatty acids with 3 or 4 double bonds have reduced stability in storage (Knothe, 2006; Chisti, 2007).

The components of fatty acids, including saturated and unsaturated fatty acids produced by microalgae, differ for different species and strains (Renaud et al., 1994; Salama et al., 2013). The accumulation of fatty acid components can be controlled by environmental conditions such as temperature, nutrient availability and salinity (Renaud et al., 2002; Huerlimann et al., 2010). Alternatively, the necessary fatty acids can be developed using a chemical process. For example, unsaturated fatty acids from microalgae, especially fatty acids with 3 or 4 double-bonds, can be easily hydrogenated under partial catalysts (Jang et al., 2005), but it is preferable to identify and propagate microalgae that do not require secondary treatment to modify their fatty acid profile. Growth temperature is a major factor that dramatically influences lipid accumulation in general or lipid composition in particular. For instance, a higher growth temperature can stimulate lipid accumulation in microalgae or a lower growth temperature can lead to increased saturated fatty acid composition (Renaud et al., 2002).

The screening of microalgae is not limited to those suitable for biodiesel production, because microalgae also offer multiple bio-products that can be used in a variety of industry (Schenk et al., 2008; Huerlimann et al., 2010). For instance, unsaturated fatty acids containing more than three double bonds, including omega-3 fatty acids, are not preferable for biodiesel but they can be useful as nutritious food or feed supplement. These compounds currently have a high value and could compete with fish oil in terms of productivity and environmental sustainability (Adarme-Vega et al., 2014).

Although microalgae are known to produce considerable amounts of lipids this it is not true for all microalgal strains. The purpose of our research was to screen microalgal isolates collected from brackish and sea water and identify those with the highest growth and lipid production with desirable fatty acid composition. As lipid accumulation capacity of algae changes when subjected to adverse external factors, such as nutrient supply and environmental conditions (Huerlimann et al., 2010; Chen et al., 2011), the research focused on microalgae from sites that have known adverse or fluctuating environmental conditions (e.g., intertidal rock pools; Underwood, 1984). After isolating pure algal cultures, growth and lipid production were compared to establish which strains are most stable and productive and most likely to be effective as a feedstock source for biofuel production. In addition, strains which produce fatty acids suitable for the health food industry were identified.

Materials and Methods

Microalgae samples were collected from a variety of sites in the lower reaches of the Brisbane River, Stradbroke Island, and Sunshine Coast in South East Queensland—Australia. The samples represent different environmental conditions of tidal brackish river water (50 cm depth), rock pools and beaches. Two species from the Australian National Algae Culture Collection from the Commonwealth Scientific and Industrial Research Organisation (CSIRO) were used to compare growth and lipid production with the strains that were isolated from the field (**Table 1**). The microalgae were intentionally gathered from different environments to provide a diverse taxonomy, stored in a cold box and transferred to the laboratory for analysis.

Isolation and Preliminary Screening

Microalgae were cultured in f/2 medium at $25 \pm 1°C$ with a 12/12 h light/dark photoperiod at a light intensity of $120\,\mu mol$ photons $m^{-2}s^{-1}$ from fluorescent lights (Osram L36W/840) and constant bubbling conditions (LP-100 air pump, Shen-Zhen Xingrisheng Industrial Co. Ltd) in a temperature-controlled environment room. Single cells were isolated by a micropipette on an inverted microscope and grown in 96 wells plates before transferring to 100 mL flasks for pure cultivation as described previously (Duong et al., 2012). The isolation procedure was conducted with sterilized equipment and in the laminar flow. Single cells were isolated by the micromanipulation method and the pure culture was checked regularly for the presence of contaminating algae or high abundance of bacteria during inoculation and growth experiments. It should be mentioned that the cultures in this study are not axenic. While it can be excluded that they contain other microalgae or protists, they still contain associated bacteria. This was considered desirable as microalgae-associated bacteria often provide improved growth (Amin et al., 2012). Algal strains were then provisionally screened based on their ability for rapid growth and lipid fluorescence using Nile red staining as described by Lim et al. (2012).

Classification by DNA Sequencing

Microalgal biomass was collected at the late exponential phase of cultivation for DNA extraction. DNA extraction was performed using a phenol:chloroform method. After extraction, genomic DNA within the 18S rRNA region was amplified on a PCR machine by using the following primers: Forward 5′-GCGGTA ATTCCAGCTCCAATAGC-3′ and Reverse 5′-GACCATACT CCCCCCGGAACC-3′. The process followed was developed by Lim et al. (2012). PCR templates were then purified by using a Wizard SV Gel PCR Clean-Up System (Promega). For sequencing preparation, $5\,\mu L$ of a $25\,ng\,\mu L^{-1}$ PCR product were combined with $1\,\mu L$ of a $10\,\mu M$ solution of each of the above primers. The reaction was topped up to $12\,\mu L$ with Millipore water in a 1.5 mL tube and sent to the Australian Genome Research Facility (AGRF) at The University of Queensland for sequencing and analysis. The DNA sequence data was compared with Genbank entries for classification.

Standard Protocol for Growth Experiments

After obtaining pure cultures, all isolated strains were grown in f/2 medium following a cultivation protocol that used bubbling for aeration and mixing. The standard protocol can be briefly described as follows: All strains were inoculated with 5 mL from a recently grown master culture and cultured in 150 mL f/2 medium until the end of the exponential growth phase was reached (less than 10% cell density increase/day) before starting the standard growth experiment. This culture was then used as the inoculum at a ratio of 1/10 for 300 mL f/2 medium in 400 mL bottles that were connected to a bubbling system and exposed to 12/12 h light/dark photoperiod at a light intensity of $120\,\mu mol$ photons $m^{-2}s^{-1}$. Cells were counted daily by

TABLE 1 | Sources and accessions of microalgae used in this study.

Species	GPScoordinates	Species origin and collection time	Site status	Genbank accession number
Achnanthes sp. BR22.5_3	27°29′29.00S153°00′48.00E	Brisbane River (11.40 am 22/05/2012)	Brackish water	KF 360813
Bacillariophyta sp. B3	26°48′12.11S153°08′50.86E	Bullcock Beach (3 pm 12/06/2011)	Tidal rock pool	KF 360815
Bacillariophyta sp. SI1a	27°26′14.23S153°30′51.08E	Stradbroke Island (3 pm 07/07/2011)	Brackish rook pool	KF 360816
Chlorella sp. BR2	–	Brisbane River Lim et al., 2012	Brackish water	–
Cylindrotheca closterium SI1c	27°26′14.23S153°30′51.08E	Stradbroke Island (3 pm 07/07/2011)	Brackish rock pool	KF 360818
Cymbella cistuliformis CP2c	24°59′19.96S153°21′04.74E	Frazer Island, Champagne Pools (10 am 1/4/2012)	Tidal rock pool	KF 360819
Cymbella sp. CP2b	24°59′19.96S153°21′04.74E	Frazer Island, Champagne Pools (10 am 1/4/2012)	Tidal rock pool	KF 360820
Dunaliella tertiolecta	–	CSIRO Tasmania (CS-175/8)	–	–
Navicula sp. BR22.52	27°29′29.00S153°00′48.00E	Brisbane River (11.40 am 22/05/2012)	Brackish water	KF 360822
Navicula sp. CP6a	24°59′19.96S153°21′04.74E	Frazer Island, Champagne Pools (10 am 1/4/2012)	Tidal rock pool	KF 360823
Navicula sp. SI2d	27°25′33.82S153°31′45.70E	Stradbroke Island (3 pm 07/07/2011)	Tidal rock pool	KF 360824
Nitzschia sp. CP2a	24°59′19.96S153°21′04.74E	Frazer Island, Champagne Pools (10 am 1/4/2012)	Tidal rock pool	KF 360825
Nitzschia sp. CP3a	24°59′19.96S153°21′04.74E	Frazer Island, Champagne Pools (10 am 1/4/2012)	Tidal rock pool	KF 360826
Phaeodactylum tricornutum	–	CSIRO Tasmania (CS-29/8)	–	–
Tetraselmis sp. M8	–	Rock Pool Maroochydore, Lim et al., 2012	Tidal rock pool	JQ 423158
Thalassiosira rotula SI2a	27°25′33.82S153°31′45.70E	Stradbroke Island (3 pm 07/07/2011)	Tidal rock pool	KF 360828

using a hemocytometer. Nitrate concentrations were monitored daily until the nutrient levels reached zero (below detection). Nitrate was determined by using a colorimetric assay (API test kit) and measured on a spectrophotometer at a wavelength 545 nm. Growth rates were calculated by the following equation (Levasseur et al., 1993)

$$K' = \frac{ln\frac{N_2}{N_1}}{t_2 - t_1}$$

where N_1 and N_2 equal cell counts at time 1 (t_1) and time 2 (t_2), respectively. Doubling time was also calculated once the specific growth rate was known.

$$Doubling\ time = \frac{ln2}{K'}$$

Microalgae were cultured for another 3 days after the nitrate concentration in the medium became undetectable to induce lipid biosynthesis.

Fatty Acid Methyl Esters (FAME) Analysis

Samples for FAME analysis were collected when lipid accumulation reached its peak, after 3 days of starvation. A total of 4 mL of microalgal culture was collected and centrifuged at 8000 × g for 5 min. Biomass was collected and dried by a vacuum pump for 30 min. Lipids in the microalgal pellet were hydrolyzed and methyl-esterified in 300 μL of a 2% H_2SO_4 and methanol solution for 2 h at 80°C. Prior to the reaction, 50 μg of heneicosanoic acid (Sigma, USA) was added as internal standard. After the esterification step, 300 μL of 0.9% (w/v) NaCl solution and 300 μL of hexane were added and mixed for 20 s. To separate the phase, samples were centrifuged at 16,000 × g for 3 min. A total of 1 μL of hexane layer was injected into an Agilent 6890 gas chromatograph (GC) coupled to a 5975 MSD mass spectrometer

(MS). The running conditions were described by Agilent's RTL DBWax method (Brown, 1991).

Results

Growth of Selected Microalgal Strains

Out of 50 microalgal strains that were isolated, 16 were shortlisted based on their rapid growth and high lipid fluorescence following Nile red staining (**Figure 1** shows an example). Strains were then compared in standard growth and lipid accumulation assays to determine the most suitable strains as feedstock for biodiesel and/or nutraceuticals. The growth of microalgal strains in the collection is presented in two groups for easier comparison: diatoms and green microalgae. The fastest growing strain *Thalassiosira rotula* SI2a grew 5.3 times faster than the slowest growing strain *Bacillariophyta* sp. B3 (**Table 2**). Among the diatomaceous species, *Thalassiosira rotula* SI2a's cell density was 2.47×10^6 cells mL^{-1} and this strain exhibited the highest growth rate and lowest doubling time, achieving 0.64 day^{-1} and 1.09 days, respectively. The cell density of *Phaeodactylum tricornutum* reached 6.97×10^6 cells mL^{-1} and grew more after the standard assay's completion. The growth rate and doubling time of this strain was 0.49 day^{-1} and 1.42 days, respectively. *Cylindrotheca closterium* SI1c's growth reached a peak of 1.89×10^6 cells mL^{-1}. *Bacillariophyta* sp. SI1a, *Bacillariophyta* sp. B3, and *Navicula* sp. SI2d grew slowly and reached peaks of 3.18×10^5 cells mL^{-1}, 4.5×10^4 cells mL^{-1} and 1.18×10^5 cells mL^{-1}, respectively.

Dunaliella tertiolecta, *Chlorella* sp. BR2 and *Tetraselmis* sp. M8 were the fastest growing green algal strains. Cell density of three strains increased gradually and peaked after 7 to 9 days. The cell density peaks for *Chlorella* sp. BR2, *Tetraselmis* sp. M8, and *Dunaliella tertiolecta* were 2.46×10^6 cells mL^{-1}, 2.62×10^6 cells mL^{-1}, and 2.67×10^6 cells mL^{-1}, respectively. These strains had similar growth rates and doubling times (**Table 2**).
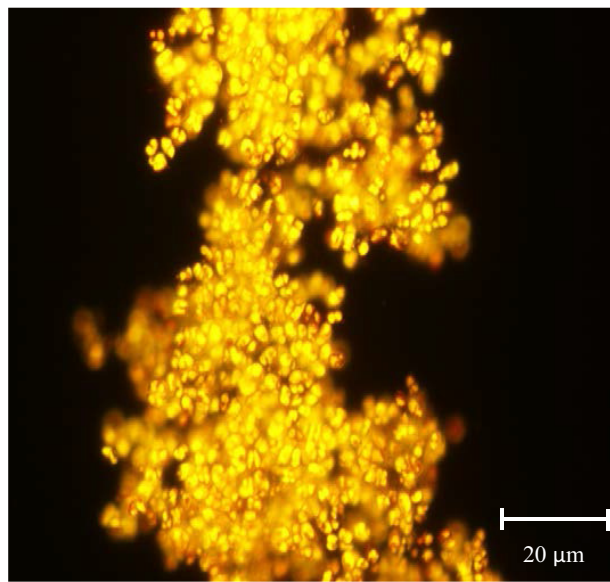
FIGURE 1 | *Cymbella* sp. CP2b after Nile red staining under fluorescence microscopy. Yellow droplets show lipid containing triacylglycerides and orange droplets show autofluorescence from chlorophyll. *Cymbella* sp. CP2b displayed fast growth rates and one of the highest lipid productivities (4.51 µg mL^{-1} day^{-1}).

TABLE 2 | Growth characteristics of the isolated strains in f/2 medium during the duration of the standard assay.

Species	Mean growth rate (µ day^{-1})	Doubling time (days)	Maximum cell density (x10^4 cells mL^{-1})
Achnanthes sp. BR22.5_3	0.13	5.48	28.50
Bacillariophyta sp. B3	0.12	5.96	6.17
Bacillariophyta sp. SI1a	0.32	2.16	31.83
Chlorella sp. BR2	0.45	1.54	245.83
Cylindrotheca closterium SI1c	0.53	1.31	189.00
Cymbella cistuliformis CP2c	0.26	2.65	28.67
Cymbella sp. CP2b	0.53	1.31	103.17
Dunaliella tertiolecta	0.46	1.51	266.83
Navicula sp. BR22.52	0.34	2.05	24.50
Navicula sp. CP6a	0.39	1.80	42.33
Navicula sp. SI2d	0.29	2.40	11.83
Nitzschia sp. CP2a	0.22	3.08	298.33
Nitzschia sp. CP3a	0.17	3.99	123.83
Phaeodactylum tricornutum	0.49	1.42	696.67
Tetraselmis sp. M8	0.43	1.60	262.17
Thalassiosira rotula SI2a	0.64	1.09	247.00

Shown are mean values from three separately-grown cultures each.

Nitrogen and phosphorous concentrations changed during the cultivation of the strains. Nitrate concentration in the medium decreased dramatically from day 3 to day 5 and nitrogen depletion occurred from day 5 to day 7 of the experiment. The concentration of phosphate decreased gradually over the experimental period. A depletion of phosphate occurred from day 7 to day 10. *Nitzschia* sp. CP2a and *Nitzschia* sp. CP3a consumed most nutrients among the strains tested (**Figure 2**).

Lipid Contents in Microalgae Collection

The result from GC/MS showed that all selected microalgal strains can produce fatty acids. Eighteen different fatty acids were detected, however not all strains produced all 18 fatty acids. There was no detection of some unsaturated fatty acid with 3 or 4 double bonds such as hexadecatrienoic acid, hexadecatetraenoic acid, and stearidonic acid in *Nitzschia* sp. CP2a, *Cymbella* sp. CP2b, *Cymbella cistuliformis* CP2c, *Nitzschia* sp. CP3a, and *Navicula* sp. CP6a. Total FAMEs ranged from 9.27 to 50.53 µg mL^{-1}. The highest FAME content was achieved for *Nitzchia* sp. CP3a and the lowest was measured for *Chlorella* sp. BR2 (**Figure 3**). Palmitic acid and stearic acid were dominant among the total fatty acids. The percentage of palmitic acid ranged from 19.83 to 37.65% in most of the strains, except for *Bacillariophyta* sp. SI1a, *Cylindrotheca closterium* SI1c, *Thalassiosira rotula* SI2a, and *Navicula* sp. SI2d. Stearic acid that accumulated in the strains ranged from 14.81 to 57.73%, except for *Nitzschia* sp. CP2a, *Cymbella* sp. CP2b, and *Nitzschia* sp. CP3a.

Interestingly, omega-3 eicosapentaenoic acid (EPA) and docosahexaenoic acid (DHA) were found in most of the strains. The highest EPA percentage of total FAMEs reached 30.85% for *Phaeodactylum tricornotum*, 14.49% for *Nitzschia* sp. CP3a, and

12.46% for *Nitzschia* sp. CP2a. DHA reached 1.11 and 1.36% for *Nitzschia* sp. CP3a and *Nitzschia* sp. CP2a, respectively. On average, saturated fatty acids were the major FAMEs in most strains; the highest values were found in *Thalassiosira rotula* SI2a (62.18%), *Bacillariophyta* sp. B3 (71.9%) and *Navicula* sp. CP6a (71.61%). However, total unsaturated fatty acids were higher than total saturated fatty acids in strains such as *Dunaliella tertiolecta* (62.08%), *Cylindrotheca closterium* SI1c (61.65%), and *Nitzschia* sp. CP3a (60.47%).

Discussion

All strains in the study were collected from estuary, coastal waters and rock pools where environmental conditions change frequently, especially changes of temperature, salinity, light exposure, and nutrients. The changes require microalgae to adapt and/or produce more biochemical products to ensure their survival (Lim et al., 2012). Lipid is one of the biochemical products that microalgae can produce along with starch under nutrient deprived conditions in the light (Schenk et al., 2008). Lipid productivities were highest for *Nitzschia* sp. CP3a (5.62 µg mL^{-1} day^{-1}), *Tetraselmis* sp. M8 (5.29 µg mL^{-1} day^{-1}), *Cymbella* sp. CP2b (4.51 µg mL^{-1} day^{-1}), and *Cylindrotheca closterium* SI1c (3.93 µg mL^{-1} day^{-1}). The value for *Tetraselmis* sp. M8 was higher than the lipid productivity previously reported for this strain when grown under laboratory conditions (2.1 µg mL^{-1} day^{-1}; Lim et al., 2012). It is interesting to note that all of these strains have been isolated from coastal rock pools subjected to tides. Their high lipid productivities suggest that these microalgae may be more opportunistic than others from more stable environments (e.g., stationary lakes or open ocean). A future study comparing the growth rates and lipid productivities
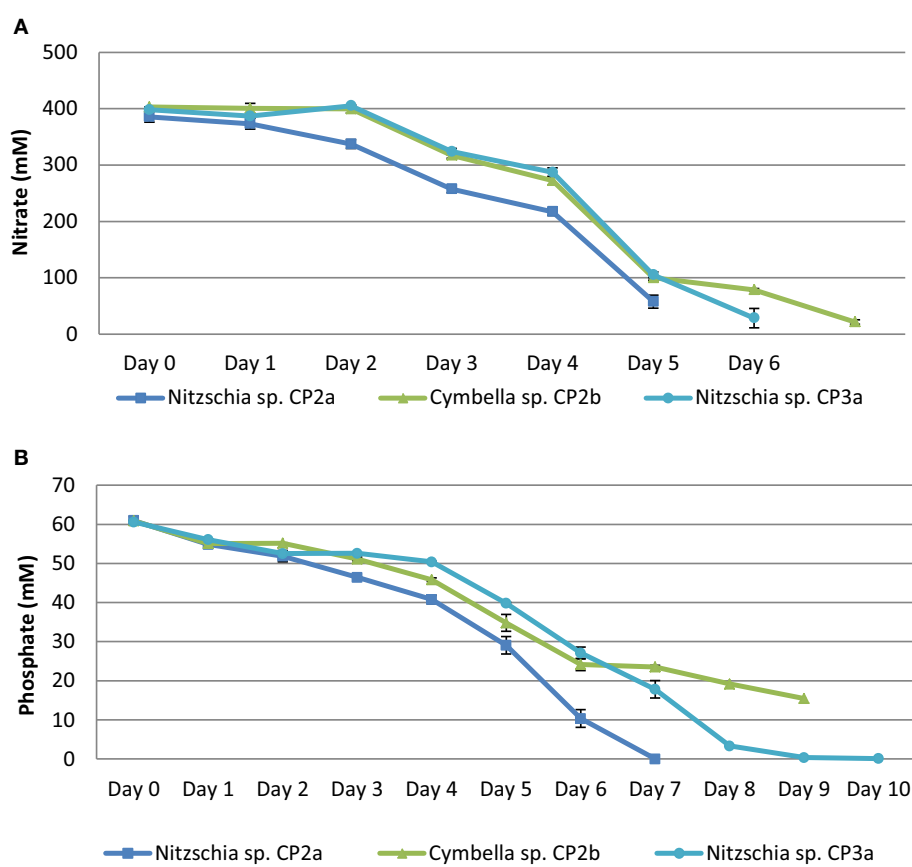
FIGURE 2 | Nitrate (A) and phosphate (B) depletion in growth medium (daily uptake) of *Cymbella* **sp. CP2b,** *Nitzschia* **sp. CP2a, and** *Nitzschia* **sp. CP3a.** Shown are mean values ± SEs from three separately-grown cultures each.
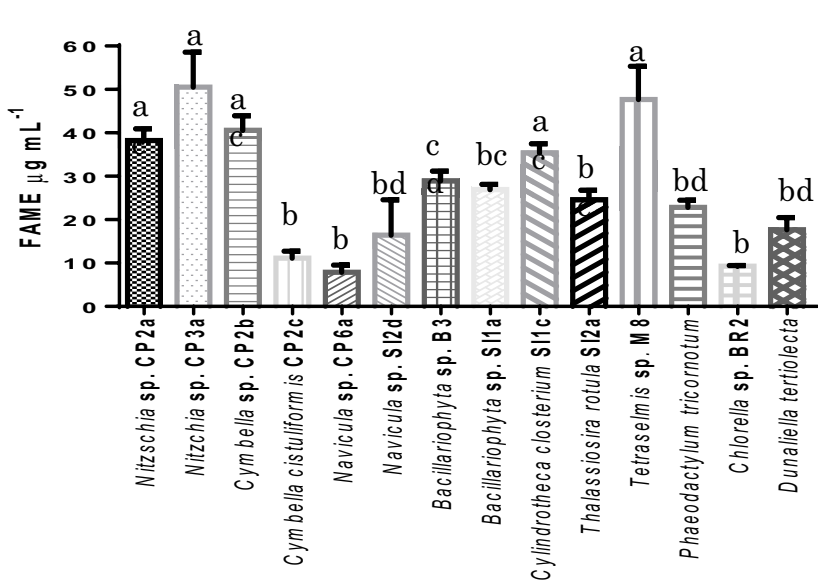
FIGURE 3 | Total fatty acid methyl esters (FAMEs) contents of the isolated microalgal strains, expressed in μg mL^{-1}. Shown are mean values ± SEs from three separately-grown cultures.

Different letters above bars indicate statistically significant differences ($p < 0.05$; Two-Way ANOVA, Tukey's HSD test using GraphPad Prism 6.0).

TABLE 3 | Fatty acid composition in percentage of total fatty acid methyl esters (FAMEs) of different microalgal strains collected in South East Queensland, Australia after cultivation to nitrate depletion and an additional 3 days of starvation.

Fatty acids	Bacillariophyta sp. B3	Bacillariophyta sp. S1a	Cylindrotheca closterium S1c	Thalassiosira rotula S1za	Navicula sp. S1zd	Tetraselmis sp. M8	Phaeodactylum tricornutum	Chlorella sp. BR2	Dunaliella tertiolecta	Nitzschia sp. CP2a	Cymbella sp. CP2b	Cymbella cistuliformis CP2c	Nitzschia sp. CP3a	Navicula sp. CP6a
Lauric (C12:0)	1.12	1.64	1.59	2.17	2.18	0.95	0.13	2.05	0.27	0.00	0.00	0.00	0.00	0.00
Myristic (C14:0)	21.32	0.74	0.63	0.66	0.81	0.93	8.74	1.65	0.47	5.96	9.56	6.73	5.33	4.88
Palmitic (C16:0)	23.64	0.88	0.23	1.27	1.12	28.33	29.31	31.68	19.87	30.10	37.65	30.22	28.82	37.04
Palmitoleic (C16:1)	0.45	1.43	4.66	1.19	1.37	1.79	0.21	4.71	0.35	31.57	38.26	21.31	27.28	15.75
Hexadecadienoic (C16:2)	5.08	13.72	8.97	3.18	6.56	14.59	0.43	1.42	1.44	2.80	1.60	2.49	3.33	1.63
Hexadecatrienoic (C16:3)	4.80	23.29	23.28	2.32	6.92	18.27	5.59	8.84	4.22	0.00	0.00	0.00	0.00	0.00
Hexadecatetraenoic (C16:4)	0.72	1.85	1.77	0.93	2.06	0.25	0.01	0.04	23.30	0.00	0.00	0.00	0.00	0.00
Stearic (C18:0)	25.15	39.13	35.21	57.73	52.32	19.79	14.81	29.28	16.65	5.71	6.56	20.39	5.25	28.74
Oleic (C18:1)	3.57	5.57	10.11	19.24	18.07	8.08	7.13	11.86	0.82	1.97	1.18	2.37	2.92	2.07
Linoleic (C18:2)	1.48	0.21	0.17	0.09	0.05	0.24	1.76	6.12	1.85	0.80	0.28	1.21	1.33	0.38
Linolenic (C18:3)	5.64	6.90	10.83	9.95	4.23	3.41	0.34	0.39	29.98	1.79	0.09	0.61	1.16	0.26
Stearidonic (C18:4)	0.10	0.15	0.20	0.10	0.15	0.14	0.00	0.13	0.00	0.00	0.00	0.00	0.00	0.00
Arachidic (C20:0)	0.52	0.18	0.42	0.17	0.11	0.26	0.60	1.28	0.57	0.19	0.20	0.77	0.13	0.95
Arachidonic (C20:4)	0.12	3.20	0.67	0.04	0.13	1.54	0.00	0.04	0.00	5.28	0.68	4.80	8.85	1.87
Eicosapentaenoic (EPA) (C20:5)	5.71	0.28	0.38	0.21	3.44	0.28	30.85	0.08	0.12	12.46	3.94	8.75	14.49	6.16
Behenic (C22:0)	0.15	0.40	0.27	0.18	0.19	0.34	0.00	0.00	0.00	0.00	0.00	0.00	0.00	0.00
Docosatetraenoic (C22:4)	0.26	0.25	0.29	0.32	0.18	0.44	0.00	0.00	0.00	0.00	0.00	0.00	0.00	0.00
Docosahexaenoic (DHA)(C22:6)	0.17	0.17	0.34	0.26	0.09	0.36	0.00	0.00	0.01	1.36	0.00	0.34	1.10	0.28
Saturated fatty acids (%)	71.90	42.96	38.35	62.18	56.73	50.60	53.59	65.93	37.82	41.96	53.97	58.11	39.53	71.61
Unsaturated fatty acids (%)	28.10	57.04	61.65	37.82	43.27	49.40	46.31	33.64	62.08	58.04	46.03	41.89	60.47	28.39
Total fatty acids (µg mL^{-1})	28.91	26.91	35.36	24.56	16.41	47.65	22.85	9.27	17.69	38.21	40.58	11.13	50.53	7.90
Lipid productivity (µg mL^{-1} day^{-1})	3.21	2.99	3.93	2.73	1.82	5.29	2.54	1.03	1.97	4.25	4.51	1.24	5.62	0.88

Shown are mean values from three separately-grown cultures each.

of microalgae isolated from stable and unstable environments may further substantiate this notion. High growth rates of these microalgae lead to rapid production of biomass while their high lipid accumulation capability is likely to assist in higher survival rates during adverse conditions. Interestingly, divergent from this trend is *Nitzschia* sp. CP3a which despite its high lipid productivity had a very slow growth rate. Further studies should be conducted to test the survival rates of these strains and if these correlate with their cellular lipid and/or starch contents.

Diatoms can survive in harsh environments (Seckbach, 2007) and usually produce more lipids in harsher environments (Lim et al., 2012). For this research, the difference of environmental conditions between natural habitats and the laboratory may have created a harsh environment that impacted on growth and chemical accumulation of microalgae tested. Many of the strains in this study adapted to their new environment and grew well under laboratory conditions. For instance, *Cymbella* sp. is a diatom that usually requires multi nutrients and minerals from natural sources (Tarapchak et al., 1983; Takeda, 1998). However, this strain grew well in f/2 medium and displayed one of the best growth rates (**Table 2**). The indoor growth experiments were set up for conditions similar to the natural habitats (temperature, nutrients, light). However, the indoor conditions are not identical to the natural conditions and the adaptability of the selected microalgae to the laboratory condition is a useful indicator of microalgae's ability to adapt to different external conditions which also will be encountered when grown at large scale for commercial purposes.

In addition, nutrient availability also affects diatom growth. For example, silica is the main components of the diatom cell wall. Changing nutrient availability may directly influence the structure of silica composition in the cell wall and affect diatom growth (Tarapchak et al., 1983). Thus optimizing nutrient availability can also substantially affect growth rates and biomass production. For example, increasing of nutrients or nitrogen leads to an increase of growth rate (Converti et al., 2009; Chen et al., 2011; Borowitzka and Moheimani, 2013). However, to enable a direct side-by-side comparison, a standard assay with unoptimized parameters was used in the current study. Clearly, higher growth rates and lipid productivities are achievable after careful cultivation optimization. For example, this has been achieved for *Tetraselmis* sp. M8 (Sharma et al., 2014). A comparison of growth rates among the fastest growth strains between the study and other publications has been undertaken. It showed that the growth of the strains in the present study was similar or faster to those in other studies for *Chlorella* sp. BR2, *Tetraselmis* sp. M8 (24.5 and 18.6% increase, respectively, compared to the study by Lim et al., 2012) or slightly lower for *Thalassiosira rotula* (23.4% reduction compared to the study by Doan et al., 2011). The difference may be due to a difference of strains used and growth conditions, such as air and nutrient supply, temperature, culture systems and photosynthesis periods (Renaud et al., 2002; Converti et al., 2009).

Total FAMEs results from GC/MS analysis showed that all 14 microalgal strains tested were lipid producers under the standard conditions used (**Table 3**). *Nitzschia* sp. CP3a was the highest lipid producer, followed by *Tetraselmis* sp. M8, *Cymbella* sp. CP2b, *Nitzschia* sp. CP2a and *Cylindrotheca closterium* SI1c. The lipid content produced by *Tetraselmis* sp. M8 was similar to the results of Lim et al. (2012). The proportion of saturated fatty acids reached more than 50% for most of the diatom strains and was dominated by myristic acid, palmitic acid, and stearic acid. These fatty acids are the main desirable components for biodiesel production (Schenk et al., 2008). Based on the above properties, we conclude that the two diatoms, *Cymbella* sp. CP2b and *Cylindrotheca closterium* SI1c, are potential strains that can be used to develop microalgal biofuel production.

Author Contributions

All authors designed the work, wrote the manuscript and approve the final version of the manuscript. VD acquired the material. VD, ST carried out the experiments, analyzed and interpreted the data. ST, PS critically revised the work and the manuscript.

Acknowledgments

References

Adarme-Vega, T. C., Thomas-Hall, S. R., and Schenk, P. M. (2014). Towards sustainable sources for omega-3 fatty acids production. *Curr. Opin. Biotechnol.* 28, 14–18. doi: 10.1016/j.copbio.2013.08.003

Amin, S. A., Parker, M. S., and Armbrust, E. V. (2012). Interactions between diatoms and bacteria. *Microbiol. Mol. Biol. Rev.* 76, 667–684. doi: 10.1128/MMBR.00007-12

Borowitzka, M., and Moheimani, N. (2013). Sustainable biofuels from algae. *Mitigat. Adaptat. Strateg. Glob. Change* 18, 13–25. doi: 10.1007/s11027-010-9271-9

Brown, M. R. (1991). The amino acid and sugar composition of sixteen species of microalgae used in mariculture. *J. Exp. Mar. Biol. Ecol.* 145, 79–99. doi: 10.1016/0022-0981(91)90007-J

Chen, M., Tang, H., Ma, H., Holland, T. C., Ng, K. Y. S., and Salley, S.O. (2011). Effect of nutrients on growth and lipid accumulation in the green algae *Dunaliella tertiolecta*. *Bioresour. Technol.* 102, 1649–1655. doi: 10.1016/j.biortech.2010.09.062

Chisti, Y. (2007). Biodiesel from microalgae. *Biotechnol. Adv.* 25, 294–306. doi: 10.1016/j.biotechadv.2007.02.001

Converti, A., Casazza, A. A., Ortiz, E. Y., Perego, P., and Del Borghi, M. (2009). Effect of temperature and nitrogen concentration on the growth and lipid content of *Nannochloropsis oculata* and *Chlorella vulgaris* for biodiesel production. *Chem. Eng. Process.* 48, 1146–1151. doi: 10.1016/j.cep.2009.03.006

Doan, T. T. Y., Sivaloganathan, B., and Obbard, J. P. (2011). Screening of marine microalgae for biodiesel feedstock. *Biomass Bioenerg.* 35, 2534–2544. doi: 10.1016/j.biombioe.2011.02.021

Duong, V. T., Li, Y., Nowak, E., and Schenk, P. M. (2012). Microalgae isolation and selection for prospective biodiesel production. *Energies* 5, 1835–1849. doi: 10.3390/en5061835

Huerlimann, R., de Nys, R., and Heimann, K. (2010). Growth, lipid content, productivity, and fatty acid composition of tropical microalgae for scale-up production. *Biotechnol. Bioeng.* 107, 245–257. doi: 10.1002/bit. 22809

Jang, E. S., Jung, M. Y., and Min, D. B. (2005). Hydrogenation for low trans and high conjugated fatty acids. *Compr. Rev. Food Sci. Food Saf.* 4, 22–30. doi: 10.1111/j.1541-4337.2005.tb00069.x

Knothe, G. (2006). Analyzing biodiesel: standards and other methods. *J. Am. Oil Chem. Soc.* 83, 823–833. doi: 10.1007/s11746-006-5033-y

Levasseur, M., Thompson, P. A., and Harrison, P. J. (1993). Physiological acclimation of marine phytoplankton to different nitrogen sources. *J. Phycol.* 29, 587–595. doi: 10.1111/j.0022-3646.1993.00587.x

Lim, D. K. Y., Garg, S., Timmins, M., Zhang, E. S. B., Thomas-Hall, S. R., Schuhmann, H., et al. (2012). Isolation and evaluation of oil producing microalgae from subtropical coastal and brackish waters. *PLoS ONE* 7:e40751. doi: 10.1371/journal.pone.0040751

Renaud, S. M., Parry, D. L., and Thinh, L.-V. (1994). Microalgae for use in tropical aquaculture I: gross chemical and fatty acid composition of twelve species of microalgae from the Northern Territory, Australia. *J. Appl. Phycol.* 6, 337–345. doi: 10.1007/BF02181948

Renaud, S. M., Thinh, L.-V., Lambrinidis, G., and Parry, D. L. (2002). Effect of temperature on growth, chemical composition and fatty acid composition of tropical Australian microalgae grown in batch cultures. *Aquaculture* 211, 195–214. doi: 10.1016/S0044-8486(01)00875-4

Salama, E.-S., Kim, H.-C., Abou-Shanab, R. I., Ji, M.-K., Oh, Y.-K., Kim, S.-H., et al. (2013). Biomass, lipid content, and fatty acid composition of freshwater *Chlamydomonas mexicana* and *Scenedesmus obliquus* grown under salt stress. *Bioprocess Biosyst. Eng.* 36, 827–833. doi: 10.1007/s00449-013-0919-1

Schenk, P. M., Thomas-Hall, S. R., Stephens, E., Marx, U., Mussgnug, J., Posten, C., et al. (2008). Second generation biofuels: high-efficiency microalgae for biodiesel production. *Bioenerg. Res.* 1, 20–43. doi: 10.1007/s12155-008-9008-8

Seckbach, J. (2007). *Algae and Cyanobacteria in Extreme Environments*, Vol. 11. Springer, Dordrecht: Springer Science and Business Media.

Sharma, K., Li, Y., and Schenk, P. M. (2014). UV-C-mediated lipid induction and settling, a step change towards economical microalgal biodiesel production. *Green Chem.* 16, 3539–3548. doi: 10.1039/C4GC00552J

Takeda, S. (1998). Influence of iron availability on nutrient consumption ratio of diatoms in oceanic waters. *Nature* 393, 774–777. doi: 10.1038/31674

Tarapchak, S. J., Slavens, D. R., Quigley, M. A., and Tarapchak, J. S. (1983). Silicon contamination in diatom nutrient enrichment experiments. *Can. J. Fish. Aquat. Sci.* 40, 657–664. doi: 10.1139/f83-088

Underwood, A. J. (1984). The vertical distribution and seasonal abundance of intertidal microalgae on a rocky shore in New South Wales. *J. Exp. Mar. Biol. Ecol.* 78, 199–220. doi: 10.1016/0022-0981(84)90159-X

Understanding nitrate assimilation and its regulation in microalgae

Emanuel Sanz-Luque, Alejandro Chamizo-Ampudia, Angel Llamas, Aurora Galvan and Emilio Fernandez *

Department of Biochemistry and Molecular Biology, University of Cordoba, Cordoba, Spain

Nitrate assimilation is a key process for nitrogen (N) acquisition in green microalgae. Among Chlorophyte algae, *Chlamydomonas reinhardtii* has resulted to be a good model system to unravel important facts of this process, and has provided important insights for agriculturally relevant plants. In this work, the recent findings on nitrate transport, nitrate reduction and the regulation of nitrate assimilation are presented in this and several other algae. Latest data have shown nitric oxide (NO) as an important signal molecule in the transcriptional and posttranslational regulation of nitrate reductase and inorganic N transport. Participation of regulatory genes and proteins in positive and negative signaling of the pathway and the mechanisms involved in the regulation of nitrate assimilation, as well as those involved in Molybdenum cofactor synthesis required to nitrate assimilation, are critically reviewed.

INTRODUCTION

The macroelement Nitrogen (N) is an essential component in key molecules of living mater. However, dinitrogen, the most abundant form either in the atmosphere or dissolved in waters, can only be used by fixing bacteria but is inaccessible to eukaryotic algae in general. Nevertheless, an uncommon symbiotic process between a unicellular cyanobacteria and a single-celled eukaryotic alga was described (Thompson et al., 2012). N can be incorporated in eukaryotic organisms from either organic or inorganic forms. The availability and concentrations of inorganic N sources, which in general are small, change depending on environments (Giordano and Raven, 2014) and usually limit growth and productivity. NH_4^+, NO_2^-, and NO_3^- the most frequent inorganic N sources assimilated by photosynthetic organisms show a different spatial distribution in oceans. In the euphotic zone of ocean waters (the area closer to the surface, which receives enough light for photosynthesis to be carried out), the estimated mean concentration of nitrate is about $7\,\mu M$ being those of ammonium and nitrite much smaller, 0.3 and 0.1, respectively. Whereas in the aphotic zone (just below the euphotic zone and unable to support photosynthetic or autotrophic growth) these values are 31, 0.01, 0.006 for nitrate, ammonium, and nitrite, respectively (Gruber, 2008). However, in the soil nitrate concentrations can be very variable from $10\,\mu M$ to 100 mM (Crawford, 1995). In natural surface waters, nitrate concentration is usually $<1\,\mu M$, but it can increase several orders of magnitude specifically in underground waters mainly due to contamination from plant fertilizers

or animal farms. Depending on colonized environments, microalgae own different adaptations for a proper N assimilation.

Interest of using *Chlamydomonas* in Nitrate Assimilation Studies

In this review, we will focus on nitrate assimilation in microalgae, which has generated basic knowledge and contributed significantly to the understanding of the pathway in crop plants (Ho and Tsay, 2010; Chardin et al., 2014; Krapp et al., 2014). Algae are a group of polyphyletic organisms, which evolved along different endosymbiotic events, thus the several species developed different and distinctive cell structures, grouping organizations, and metabolisms. Here, we will only refer to algae whose ancestors derive from a primary endosymbiotic event (de Clerck et al., 2012). They correspond to individuals from the group of Glaucocystophytes, Rhodophytes, and Chlorophytes. This latter group of chlorophytes is phylogenetically closely related to plants. Other algae groups add new layers of complexity, since they come from secondary and tertiary endosymbiotic events, with plastid loss, replacement, and gene transfers (Douglas, 1998; Keeling, 2010). Among those algae *Chlamydomonas reinhardtii* (referred herein as *Chlamydomonas*) has emerged as a very relevant experimental system, mostly due to the development of molecular and genetic tools useful in many different studies, such as the flagella structure and function, photosynthetic apparatus, chloroplast evolution, metabolism, or regulation under different stress conditions (Harris, 2009). Advances achieved in understanding of nitrate assimilation in this system (Fernandez and Galvan, 2007, 2008) were extrapolated to other algae and mostly to plants leading to remarkable progress (Xu et al., 2012; Bittner, 2014; Krapp et al., 2014). Many of the methodological tools in *Chlamydomonas* rely on its efficient transformation system, development of vectors (Kindle, 1990; León-Bañares et al., 2004; Neupert et al., 2012) and the sequencing of its genome (Merchant et al., 2007). In other algae, transformation methodology has been set up (Sun et al., 2006; Lerche and Hallmann, 2009, 2013, 2014; Hirata et al., 2011; Qin et al., 2012; Rathod et al., 2013; Talebi et al., 2013; Yamano et al., 2013), which will allow efficient techniques to appear as in *Chlamydomonas*. We will refer here to 10 Chlorophytes (using *Chlamydomonas* as a reference), two Rhodophytes, and a Glaucophyte, for which their genomes are sequenced and available in the public databases.

NITRATE ASSIMILATION

Overview of Nitrate Assimilation

The nitrate assimilation pathway from nitrate to amino acid is relatively simple at structural level. By contrast, its regulation to ensure the efficient assimilation of nitrate coupled to that of other environmental factors, is complex.

Overview in Chlamydomonas/Algae

In photosynthetic eukaryotes, nitrate assimilation is performed by two transport and two reduction steps: First, nitrate is transported into the cell, then a cytosolic Nitrate Reductase

(NR) catalyzes nitrate reduction to nitrite, which subsequently is transported into the chloroplast, where the enzyme Nitrite Reductase (NiR) catalyzes its reduction to ammonium (Guerrero et al., 1981; Fernandez and Galvan, 2007, 2008). Finally, ammonium is incorporated to carbon skeletons by rendering glutamate, through the glutamine synthetase/glutamine oxoglutarate amino transferase or glutamate synthase (GS/GOGAT) cycle (Miflin and Lea, 1975). First, ammonium is incorporated as the amide group of glutamine in a reaction involving glutamate and ATP (catalyzed by GS); then, the amide group is transferred reductively to α-oxoglutarate to form two molecules of glutamate.

Figure 1 summarizes the organization of enzymes/proteins for nitrate assimilation in *Chlamydomonas*. The assimilation of nitrate begins with its entry into the cell. The transport of nitrate and nitrite into the cell is a regulated and complex process in *Chlamydomonas* as suggested from the high number and types of proteins that participate (Fernandez and Galvan, 2007). The transporters are classified, based on their substrate specificity, affinity and expression characteristics, in: specific or bispecific, high and low affinity, constitutive and inducible transporters. From the structural point of view three families of proteins are involved in nitrate and/or nitrite transport in *Chlamydomonas*. They are NRT1 (NPF), NRT2, and NAR1 (Crawford and Glass, 1998; Forde, 2000; Galvan and Fernández, 2001; Forde and Cole, 2003; Fernandez and Galvan, 2007, 2008).

NRT1 Transporters Function

The NRT1 transporters belong to the PTR transporters (Peptide TRansporters), now renamed NPF for NRT1/PTR Family (Léran et al., 2014). There is a wide representation of these transporters in plant genomes (Krapp et al., 2014), however its presence in algal genomes is in low number if any. Most of the plant NRT1 genes encode low-affinity nitrate transporters (Tsay et al., 2007). The best-studied one is CHL1 from *Arabidopsis* (AtNRT1.1 or AtNPF2.6) and represents a paradigmatic protein. In fact, AtNRT1.1 is considered a transceptor with sensor and carrier functions (Tsay et al., 2007; Ho et al., 2009; Gojon et al., 2011). AtNRT1.1 is a dual affinity nitrate transporter that switches from high to low-affinity for nitrate, depending on the nitrate conditions and the phosphorylation/dephosphorylation of the threonine T101. At low nitrate conditions, AtNRT1.1 is phosphorylated by a CIPK23 protein kinase and functions as a high-affinity transporter. At high nitrate conditions AtNRT1.1 is dephosphorylated and is a low-affinity transporter (Liu et al., 1999; Ho et al., 2009). In addition AtNRT1.1 is involved in plant auxin transport and nitrate efflux (Tsay et al., 2007; Ho et al., 2009; Gojon et al., 2011).

NRT2 Transporters Function

The NRT2 proteins correspond to the NNP (Nitrate Nitrite Porter) family and belongs to the superfamily MFS (Major Facilitator Superfamily; Pao et al., 1998). *NRT2* genes are present into genomes of organisms able to assimilate nitrate like plants, algae, fungi, yeast and bacteria (Forde, 2000). The NRT2 proteins can transport nitrate or nitrite and some of them are two-component systems, which require a second protein,
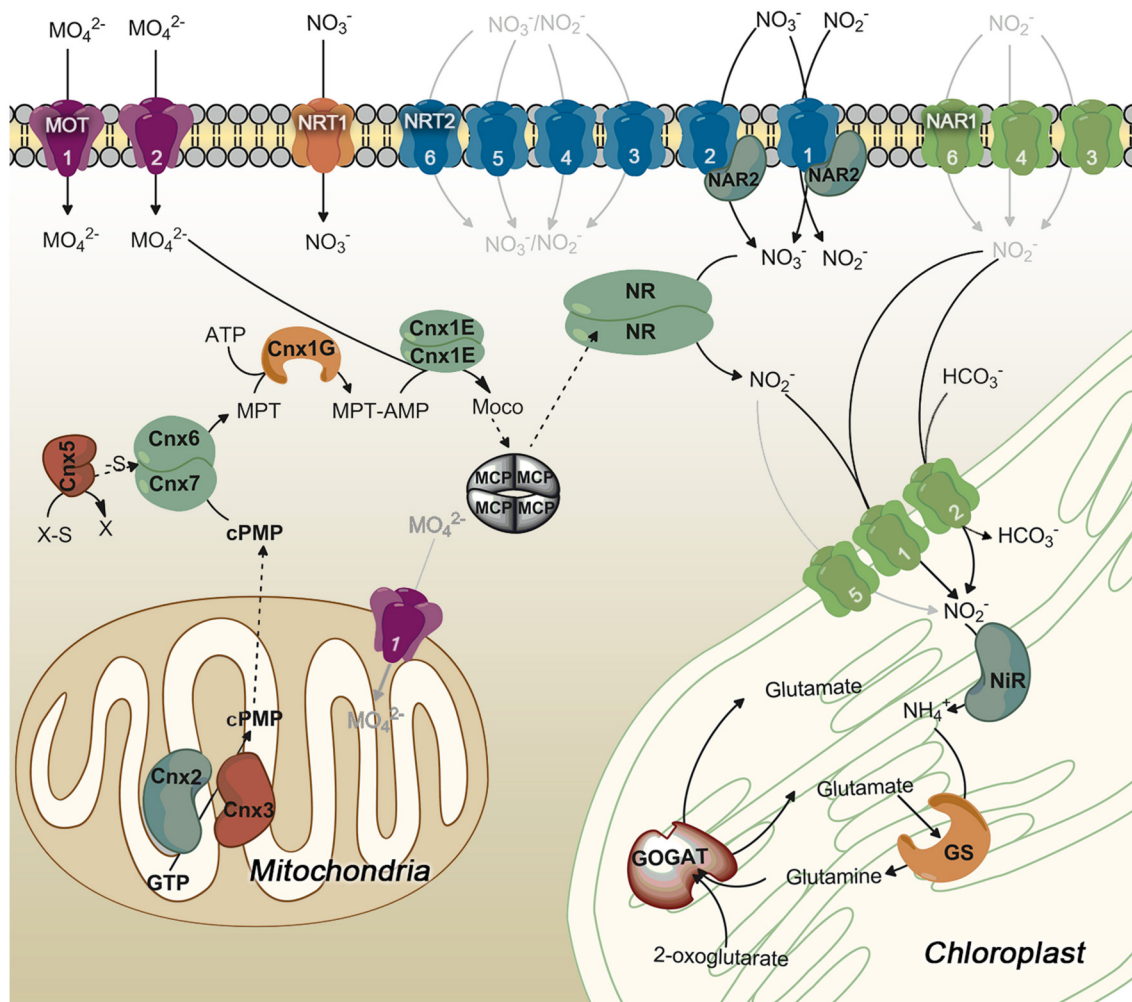
FIGURE 1 | General scheme of proteins involved in nitrate assimilation and molybdenum cofactor biosynthesis in *Chlamydomonas*. Those steps symbolized in gray lines are not empirically demonstrated. Proteins that mediate these hypothetic steps are represented in the most probable localization. Different colors are used for each family of transporters. Numbers on the transporters identify each family member.

NAR2, to be fully functional. NAR2 appears to be anchored to the membrane by a transmembrane domain (Quesada and Fernández, 1994; Tong et al., 2004; Okamoto et al., 2006; Orsel et al., 2006). In *Chlamydomonas* there are six NRT2 members but NAR2 is only required for functionality of NRT2.1 and NRT2.2 but not for other NRT2 transporters (Quesada and Fernández, 1994; Galván et al., 1996). Thus, in *Chlamydomonas* NRT2.1/NAR2 constitutes a bispecific high-affinity nitrate/nitrite transporter and NRT2.2/NAR2 is a high-affinity nitrate transporter (Fernandez and Galvan, 2007).

NAR1 Transporters Function

The family NAR1 (Nitrate Assimilation-Related component 1) is formed by transporters related to proteins called FNT (Formate Nitrite Transporters; Peakman et al., 1990; Suppmann and Sawers, 1994; Rexach et al., 2000). *Chlamydomonas* has six *NAR1* genes (*NAR1.1–6*; Mariscal et al., 2006). NAR1.1 is

a nitrite transporter to the chloroplast (Rexach et al., 2000), and NAR1.2 (LCIA) shows NO_2^- and HCO_3^- transport activity when expressed in *Xenopus* oocytes (Mariscal et al., 2006). More recently, it has been demonstrated that NAR1.2 (LCIA) is a chloroplast envelope HCO_3^- transporter and part of a CO_2-concentration mechanism (CCM) operating at very low CO_2 (Wang and Spalding, 2014; Yamano et al., 2015). The CCM is essential to accumulate CO_2 close to RUBISCO and make efficient photosynthesis in aquatic microalgae.

Nitrate Reductase Function

The enzyme NR catalyzes the reduction of nitrate to nitrite with electrons from NAD(P)H. In eukaryotes, NR is a homodimeric protein with subunits of about 100–120 kDa containing each one three prosthetic groups: FAD, b_{557} heme and Molybdenum cofactor (Moco) (Zhou and Kleinhofs, 1996). Algae typically contain a single gene encoding NR (Fernández et al., 1989;

Fernandez and Galvan, 2007) that, in addition to its physiological activity of nitrate reduction, has also two other activities. These partial activities can be assayed separately *in vitro*. The first one is the NAD(P)H-dehydrogenase or diaphorase, which catalyzes the transfer of electrons from pyridine nucleotides to artificial electron acceptors such as ferricyanide, dichlorophenol indophenol, or cytochrome c. This activity does not require the Moco domain. The second is the terminal activity, which catalyzes the transfer of electrons from artificial electron donors as flavins, bromophenol blue, or viologens (chemically reduced with dithionite) to nitrate (Solomonson et al., 1986; Caboche and Rouzé, 1990). This activity mostly requires the Moco domain.

Nitrite Reductase Function

Nitrite reduction to ammonium occurs in the stroma of chloroplasts and is catalyzed by the enzyme nitrite reductase (NiR). Reduced ferredoxin (Fd_{red}) generated as a consequence of the photosynthetic electron transport is the electron donor for nitrite reduction. In the dark, nitrite reduction can also occur from NADPH, generated in the oxidative pentose phosphate cycle, by mediation of Fd-$NADP^+$ oxidoreductase (Jin et al., 1998). Algal NiR, like in cyanobacteria and plants, is a monomer of approximately 63 kDa containing a [4Fe–4S] grouping and a siroheme as prosthetic groups. NiR is encoded by a single gene in *Chlamydomonas*, which is clustered with other genes essential for nitrate/nitrite assimilation (Guerrero et al., 1981; López-Ruiz et al., 1991; Quesada et al., 1993).

Incorporation of N into Amino Acids

Inorganic N is incorporated finally in form of organic N as glutamate by the action of GS/GOGAT (see above). *Chlamydomonas* contains four GS (GLN) (two cytosolic and two plastid-targeted), and two plastidic GOGAT, one dependent on NADH and the other on Fd_{red} (Cullimore, 1981; Cullimore and Sims, 1981a,b; Fischer and Klein, 1988; Chen and Silflow, 1996). GLN1 and GLN2 from *Chlamydomonas* have high sequence conservation and a similar octameric structure (Florencio and Vega, 1983a; Chen and Silflow, 1996). Chen and Silflow (1996) found three forms of GS in *Chlamydomonas*, but the sequencing of its genome detected four (Merchant et al., 2007). However, function and localization of these two additional GS (GLN3 and GLN4) have not been studied in detail.

In addition to GS/GOGAT, under certain stress conditions glutamate dehydrogenase (GDH) seems to be the predominant enzyme for ammonium incorporation in *Chlamydomonas*, catalyzing a reductive reaction of ammonium and α-oxoglutarate to yield glutamate (Muñoz-Blanco and Cárdenas, 1989). GDH is encoded by two genes (*GDH1* and *GDH2*) and has three isoenzymes located in the mitochondria, resulting very probably from combination of the two different subunits (Moyano et al., 1992; Vallon and Spalding, 2009). Under stress conditions such as N-starvation or high ammonium, the aminating activity of GDH varies inversely to that of GS. The GDH function seems to be related to the maintenance on glutamate levels in the cell when GS/GOGAT is inefficient, appearing to be more connected to carbon than to nitrogen metabolism (Muñoz-Blanco and Cárdenas, 1989; Moyano et al., 1995). Since GDH is related to

ammonium assimilation, which is not the topic of this review, it will not be mentioned any further.

Genes for Nitrate Assimilation in Algae

Table 1 (more details in Table S1) shows the genes and number of genes involved in nitrate assimilation in several Chlorophytes, Rhodophytes, and Glaucophytes algae with sequenced genomes.

The *NRT1 (NPF)* genes are represented in high number in plant genomes. In contrast, the algal genomes contain a very low number, two, one, or even none. For example, *Arabidopsis* has 53 NRT1 (NPF) but the number in plants varies between 51 (in *Capsella rubella*) and 139 (in *Malus domestica*; Crawford and Glass, 1998; Williams and Miller, 2001; Léran et al., 2014). *Chlamydomonas* has a unique *NRT1*, like most of the algal genomes analyzed. *Coccomyxa subellipsoidea* and *Chlorella NC64A* contain two, but the *NRT1* gene was not found in the microalgae *Micromonas pusilla* or *Chlorella paradoxa* (**Table 1**). This is relevant since, provided that the analyzed genomes are complete, it suggests that along evolution some important function mediated by NRT1 has been maintained in the different algae species, and that in plants, the complexity of the new tissues that were appearing required new functions, which were assumed by this family of proteins.

The NRT2 proteins, responsible for high affinity nitrate/nitrite transport (HATS), are present in all algal species. However, NAR2, which with NRT2 forms the two-components HATS appears in Chlorophytes algae, like in plants, but not in Rhodophytes or Glaucophytes (**Table 1**), suggesting that in these latter algae one-component nitrate HATS might be efficient enough to guarantee cell growth and performance. NAR2 is highly conserved between *Chlamydomonas* and *Volvox* but show a lower conservation with the other Chlorophytes. So far, *Chlamydomonas* is the alga with the highest number of *NRT2* genes, likewise for *NAR1* genes (six of each). Like *NAR2, NAR1* was not found in the genomes of Rhodophytes or Glaucophytes, and the number of *NAR1* genes is just one in species of *Micromonas*, *Ostreococcus,* and *Bathycoccus prasinos*. This is interesting because in *Chlamydomonas* two members of this NAR1 family have specialized functions. NAR1.1 is a nitrite transporter to the chloroplast clustered with the nitrate assimilation genes. The gene encoding this transporter is expressed in the presence of nitrate under the control of *NIT2*, which is the major regulatory gene for nitrate assimilation. All this suggests a role of NAR1.1 in nitrate assimilation (Fernandez and Galvan, 2007, 2008). On the other hand, *NAR1.2 (LCIA)* is not nitrate-regulated nor *NIT2*-dependent (Mariscal et al., 2006). NAR1.2 is expressed under low CO_2 conditions and is a HCO_3^- transporter to the chloroplast (Wang and Spalding, 2014; Yamano et al., 2015). The function of CrNAR1.3–6, as that of the single NAR1 in other microalgae species, has to be solved. The high number of these genes, NRT2 and NAR1, in *Chlamydomonas* might reflect an optimization in the utilization of those nutrients under many diverse environmental conditions.

Single genes encode NR and NiR in algae, excepting some particular cases as *Coccomyxa subellipsoidea* C-169, which has two NRs in its genome (**Table 1**). It is interesting to point out that in *Cyanidioschyzon merolae*, which lacks NiR gene (*NII1)*,

TABLE 1 | Nitrate and molybdenum assimilatory proteins in microalgae.
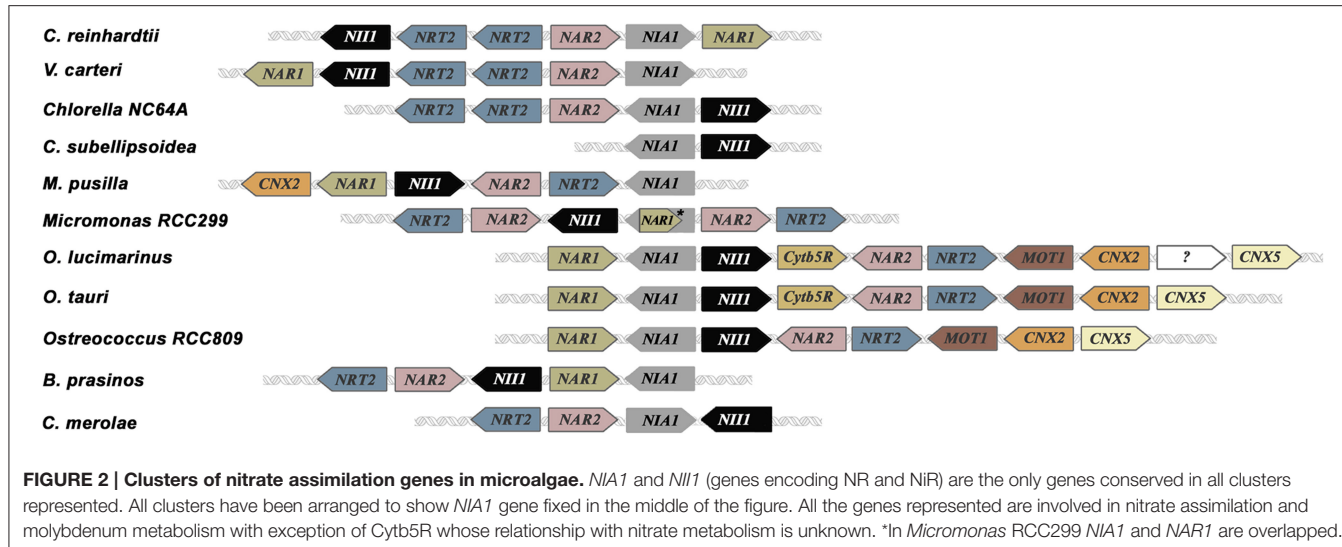
	Chlorophytes										Rhodophytes		Glaucophytes
	C. reinhardtii	V. carteri	C. subellipsoidea	M. pusilla	Micromonas RCC299	Chlorella NC64A	O. lucimarinus	Ostreococcus RCC809	O. tauri	B. prasinos	C. merolae	G. sulphuraria	C. paradoxa
NRT1	1	1	2	NF	1	2	1	1	1	1	1	1	NF
NRT2	6	3	1	1	3	2	1	1	1	1	1	1	2
NAR1	6	5	2	1	1	3	1	1	1	1	NF	NF	NF
NAR2	1	1	1	1	2	1	1	1	1	1	NF	NF	NF
NR	1	1	2	1	1	1	1	1	1	1	1	1	1
NiR	1	1	1	1	1	1	1	1	1	1	2	1	1
GLN	4	4	3	1	1	2	1	1	1	1	1	1	2
GSN/GSF	2	2	2	2	2	2	1	1	1	1	1	1	1
MCP	1	1	NF	NF	NF	NF	NF	NF	NF	NF	NF	NF	NF
MOT1	1	NF	1	NF	1	1	1	1	1	1	NF	NF	2
MOT2	2	2	2	2	2	2	2	2	2	2	1	1	1
CNX2	1	1	1	1	1	1	1	1	1	1	1	1	1
CNX3	1	1	1	1	1	1	1	2	1	1	1	1	1
CNX5	1	1	1	1	1	1	1	1	1	1	1	1	1
CNX6	1	1	1	1	1	1	1	1	1	1	1	1	1
CNX7	1	1	1	1	1	1	1	1	1	1	NF	NF	NF
CNX1G	1	1	1	1	1	1	1	1*	1*	1	1	1	NF
CNX1E	1	1	1	1	1	1	1	1*	1*	1	1	1	1
ABA3	1	1	1	NF	1	1	NF	NF	NF	1	NF	NF	NF

We have used the specific genome databases for each organism. Some proteins were already identified and annotated and others were found using BlastP and TBlastN. Chlamydomonas reinhardtii: Phytozome 10.2 (http://phytozome.jgi.doe.gov/pz/portal.html), for NAR1(192094) we used JGI v4 (http://genome.jgi-psf.org/). Volvox carteri, Coccomyxa subellipsoidea, Micromonas pusilla, Micromonas RCC299 and Ostreococcus lucimarinus: Phytozome 10.2. Chlorella NC64A, Ostreococcus RCC809 and Ostreococcus tauri: JGI. Bathycoccus prasinos: Genome.jp (www.genome.jp/kegg-bin/show_organism?org=bpg). Cyanidioschyzon merolae: Cyanidioschyzon merolae Genome Project (http://merolae.biol.s.u-tokyo.ac.jp/blast/blast.html). Galdieria Sulphuraria: (http://genomics.msu.edu/cgi-bin/galdieria/blast.cgi). Cyanophora paradoxa: (http://cyanophora.rutgers.edu/cyanophora/blast.php). Identified proteins are NRT1, NRT2, and NAR1, nitrate/nitrite transporters; NAR2, required component for high affinity nitrate transport; NR, Nitrate Reductase; NiR, Nitrite Reductase; GLN, Glutamine synthetase; GSN/GSF, Glutamate synthase; MCP, a Moco Carrier Protein; MOT1 and MOT2, Molybdate Transporters; Cnx2, Cnx3, Cnx5, Cnx6, Cnx7, Cnx1G, Cnx1E, and ABA3, Proteins of Molybdenum cofactor biosynthesis; Accession numbers of all these proteins are provided in Table S1. In Table S1 those proteins encoded by clustered genes are also indicated. (NF) indicates that proteins were not found in that organism. The asterisk (*) indicates that CNX1G and CNX1E are fused into a single chimeric gene in those algal species.

one sulfite reductase gene *CmSiRB* of the two annotated in its genome, *CmSiRA* and *CmSiRB*, encodes really a nitrite reductase (Sekine et al., 2009). Sulfite reductase and nitrite reductase have common structural and functional features (Crane and Getzoff, 1996). The nitrite reduction function of CmSiRB was deduced from its high NiR vs. its very low sulfite reductase activity, high expression in nitrate medium, and low in ammonium medium in contrast to *CmSiRA*, which is not affected by the presence of ammonium or nitrate. In addition, in the genome *CmSiRB* maps between a nitrate transporter and the NR genes (Sekine et al., 2009).

Clustering of nitrate assimilation genes appears commonly in fungi, cyanobacteria and algae (Johnstone et al., 1990; Frías et al., 1997; Fernandez and Galvan, 2008; McDonald et al., 2010; Maruyama and Archibald, 2012). In fungi the metabolic gene clusters are often associated with fungal virulence, and evolutionarily with pathways conferring some advantage over

competitors. They might have appeared by horizontal gene transfer (Slot and Hibbett, 2007; Wisecaver and Rokas, 2015). In plants, metabolic gene clusters are more common than suspected since the seminal work of Osbourn et al. (2012). However, the reasons for this clustering are not yet understood, but it is probable that this physical proximity of genes facilitates the coordination of their regulation and inheritance (Osbourn et al., 2012; Mugford et al., 2013; Nützmann and Osbourn, 2015). The clustering of nitrate assimilation genes in algae is analyzed in Table S1 and **Figure 2**. Though the particular genes clustered change in its role, order or orientation from species to species, it is interesting to point out that most of Chlorophytes have a complete set of genes for nitrate assimilation (*NRT2/NAR2/NIA1/NII1/NAR1*) with the exception of *Chlorella sp. NC64A,* which has three *NAR1* but none within the nitrate-cluster and *Cocomyxa subellipsoidea* in which genes are scattered in the genome. A curiosity is that *Chlorella* sp. NC64A, even

FIGURE 2 | Clusters of nitrate assimilation genes in microalgae. *NIA1* and *NII1* (genes encoding NR and NiR) are the only genes conserved in all clusters represented. All clusters have been arranged to show *NIA1* gene fixed in the middle of the figure. All the genes represented are involved in nitrate assimilation and molybdenum metabolism with exception of Cytb5R whose relationship with nitrate metabolism is unknown. *In *Micromonas* RCC299 *NIA1* and *NAR1* are overlapped.

having a complete set of all the genes needed for nitrate assimilation (transporters, reductases and Moco genes), has developed an alternative adaptation strategy to acquire N. This *Chlorella* strain is endosymbiotic with *Paramecium bursaria* and can use ammonium or amino acids but not nitrate or nitrite (Kamako et al., 2005). In this alga NiR and not NR activity is considerably stimulated by nitrate but the mechanisms responsible for this silencing of nitrate utilization are unknown.

Another curiosity is that *Ostreococcus* species contain in addition to genes for nitrate/nitrite transporters and reductases others for molybdate transport (*MOT1)* and metabolism (*CNX2* and *CNX5)*. Thus, the complete cluster in *Ostreococcus tauri* is: *NAR1-NIA1-NII1-Cytb5R-NAR2-NRT2-MOT1-CNX2-CNX5* (Derelle et al., 2006). In *Chlamydomonas* two gene clusters are present: one consists on *NII1-NRT2.2-NRT2.1-NAR2-NIA1-NAR1* and in the other *NRT2.3-AOX1* (*AOX1* encodes a mitochondrial alternative oxidase) (Quesada et al., 1998a,b). In *Micromonas* species two different clusters were described: *CNX2-NAR1-NII1-NAR2-NRT2-NIA1* (in *M. pusilla* CCMP1545), and *NRT2.1-NAR2.1-NII1-NAR1-NIA1-NAR2.2-NRT2.2* (in RCC299) (McDonald et al., 2010). A comparison between the different gene clusters for nitrate assimilation in microalgae is shown in **Figure 2**. It is remarkable how essential genes for nitrate assimilation have been maintained clustered during the different genetic events needed to configure the present organization.

Molybdate transporter genes (MOT), are present in the algal genomes highlighting the importance of this anion for a proper assimilation of nitrate (**Table 1**). Accordingly, the complete set of genes for Moco biosynthesis is represented in all the species analyzed. Interestingly, the *CNX1* gene, encoding the two domains (E and G) protein in plants, is split into two genes each one encoding a domain, *CNX1G* and *CNX1E*. However, some exceptions are found in *Ostreococcus tauri*, *Ostreococcus RCC809*, and *Bathycoccus prasinos* where these domains are merged in a single gene. By fusing those two genes from *Chlamydomonas reinhardtii* in chimeric constructions *CNX1E-G* or *CNX1G-E*,

it is shown that the orientation of the domains CNX1E and CNX1G does not affect the functionality of the chimeric CNX1 proteins (Llamas et al., 2007). This finding suggests that the fact of having two genes *CNX1E* and *CNX1G*, or just one *CNX1* with the orientation E-G as in plants, or G-E as in mammals is irrelevant. In contrast to other Moco genes, *ABA3* (Abscisic acid deficient 3, in plants; Bittner et al., 2001) is not generally present in the analyzed algae (**Table 1**). ABA3 is required for functionality of the Mo-hydroxylases, Xanthine Dehydrogenase, and Aldehyde Oxidase, by the transfer of a sulfur atom to the Mo-center (sulfuration step). Thus, it will be interesting to understand what is the effect of this lack in the metabolism of those algae. Similarly, *MCP* encoding a Moco Carrier Protein (Ataya et al., 2003; Fischer et al., 2006) seems to be involved in an efficient mechanism of Moco storage and protection. MCP has a significant conservation with MBP (Moco Binding Protein) from plants (Kruse et al., 2010), but it is only present in Volvocales and not in the other algal genomes analyzed (**Table 1**).

Additionally, it is interesting to point out that the *CNX5* gene for Moco biosynthesis was differentially conserved in the studied algae. *CNX5* from *Chlamydomonas* and *Volvox* are closely related but markedly different from *CNX5* genes from the other algae, which show a significant conservation among them. The reasons for this diversification are not clear.

Concerning the ammonium incorporation to amino acids, the corresponding genes were analyzed in algae (Ghoshroy and Robertson, 2015). GS (*GLN*) genes are well-represented in Volvocales in a number of 3 or 4. However, their particular role and localization has only been studied in *Chlamydomonas* (Florencio and Vega, 1983a; Chen and Silflow, 1996; Vallon and Spalding, 2009). The four GS genes encode cytosolic glutamine synthetases of type 1 (GLN1, GLN4) and plastidic GS of type 2 (GLN2, GLN3). The two isoforms of GS2 are highly conserved, and their genes located head to head in the genome suggesting a recent event of gene duplication in both *Chlamydomonas* and *Volvox* (Chen and Silflow, 1996; Vallon and Spalding, 2009). In the species of *Ostreococcus* and *C. merolae*, the single *GLN* gene

is more related to bacterial *GLN* than to plant-type *GLNs* present in other algae (**Table 1**). Genes for the plastidic NADH-GOGAT and Ferredoxin-GOGAT appear in Chlorophytes, however in Mamiellales, Rhodophytes, and Glaucophytes there appears only one (Ferredoxin-GOGAT).

REGULATION OF NITRATE ASSIMILATION

The regulation of nitrate acquisition is a complex process involving a network of proteins, many of them scarcely known. Majority of data available has been attained in *Chlamydomonas*. Below, we review some relevant regulatory aspects reported in microalgae.

In general, nitrate and ammonium have opposite effects over nitrate assimilation genes, which are referred to as positive (nitrate) and negative (ammonium) signals. Ammonium is the preferred N source due to its reduced state and energetically favorable assimilation. It is well-established that ammonium has a negative effect on nitrate assimilation at both transcriptional and posttranscriptional levels in *Chlamydomonas* (Fernandez and Galvan, 2008), especially in high CO_2 conditions. NR gene (*NIA1*) expression, widely studied in many algal species, is induced in nitrate medium and strongly repressed in ammonium medium (Loppes et al., 1999; Cannons and Shiflett, 2001; Llamas et al., 2002; Imamura et al., 2010). Also nitrate transporters are expressed after ammonium depletion in *Micromonas* (McDonald et al., 2010). In *Chlamydomonas*, when both positive and negative signals are present together, repression appears as a quantitative process that is not strictly sensitive to the ammonium concentration but to the nitrate/ammonium (N/A) balance (Llamas et al., 2002; de Montaigu et al., 2011). A determined ammonium concentration is less repressive in conditions of high nitrate (mM) than in low nitrate (μM). Nevertheless, in medium without ammonium, *NIA1* is similarly induced by low and high nitrate concentrations. This pattern points out to a finely tuned regulation mediated by the N/A balance. How this balance regulates *NIA1* is scarcely known and a complex network of proteins and signal molecules are starting to be unraveled in *Chlamydomonas*. To understand these positive and negative signaling pathways, an insertional mutant collection of about 22,000 mutants was obtained and screened for aberrant sensing of nitrate or ammonium. The selection of these phenotypes was possible because the mutagenized strain bears a reporter gene that responds positively to nitrate and negatively to ammonium (*pNIA1ARS*, a chimeric gene: promoter of *NIA1* fused to the arylsulfatase gene; González-Ballester et al., 2005). For the ammonium insensitive phenotype (AI), a broad range of insensitiveness is shown depending on the mutant but none of them is completely insensitive to ammonium (de Montaigu et al., 2011). The numerous mutants isolated together with the absence of a mutant totally insensitive to ammonium highlight a regulation mechanism that probably involves several independent pathways. In contrast, the nitrate insensitive mutants (NI) reveal a master gene, *NIT2*, needed for nitrate assimilation genes expression (Camargo et al., 2007). In addition, a number of NI mutants with partial phenotypes are identified that also illustrates the complexity of nitrate regulation (Higuera et al., 2014).

Positive Regulation of the Nitrate Assimilation Pathway

In photosynthetic organisms nitrate is not only an N source but also a signaling molecule (Crawford, 1995; Krapp et al., 2014). Nitrate induces expression of genes responsible for its assimilation. Proteins involved on nitrate sensing are scarcely known in microalgae. Several major transcription factors were identified in plants, fungi, yeast, and in some green and red algae. In *Chlamydomonas* the transcription factor NIT2 is essential for a proper upregulation of the main genes for nitrate assimilation (*NII1, NRT2.1, NRT2.2, NRT2.3, NAR2, NIA1, NAR1.1,* and *NAR1.6*; Quesada et al., 1993, 1994; Mariscal et al., 2006). Indeed, nit2 mutants are unable to grow in nitrate medium. The *NIT2* gene is also repressed by ammonium and induced in nitrate and N-free medium, highlighting that other yet unidentified transcription factors work upstream to *NIT2* (Camargo et al., 2007).

Structural characteristics of NIT2 show an RWP-RK domain (so called by the consensus sequence) within a leucine zipper domain; this motif may serve in dimerization and DNA binding (Camargo et al., 2007). This domain is also found in algal minus dominance (MID) proteins (Lin and Goodenough, 2007) and transcription factors from plants as the NIN-like proteins (NLP), some of them having a key role in regulating responses to nitrate availability (Konishi and Yanagisawa, 2013; Chardin et al., 2014). Actually, NLP7 seems to be a major player in the primary response to nitrate (Castaings et al., 2009; Marchive et al., 2013). Transcription factors containing RWP-RK domains are numerous in green algae but many of them have an unknown function. Proteins with significant homology to NIT2 have not been identified. However, it is noteworthy an RWP-RK transcription factor along the cluster of N metabolism related genes in *Micromonas pusilla*. Though clustering is not a strong evidence for its function, this gene is a good candidate to study in future experiments in this alga. Furthermore, other RWP-RK transcription factors that are upregulated in N starvation in *Chlamydomonas* (RWP1 and RWP10) have an expression that correlates with those of *LAO1* (encoding L-Amine Oxidase) and *CNX1E,* respectively (Gargouri et al., 2015). In addition to the RWP-RK domain, NIT2 shows a GAF domain at the N-terminal region of the protein. This motif could bind small molecules such as cGMP, NO or α-oxoglutarate (Little and Dixon, 2003; Rybalkin et al., 2003; Büsch et al., 2005). However, the function of this domain remains poorly studied, although it is known that it does not bind nitrate and is not involved in DNA binding (Camargo et al., 2007). Additionally, NIT2 possesses a glutamine-rich domain involved in protein-protein interactions, essential for NIT2 functionality, and a nuclear export sequence (NES) (Camargo et al., 2007). How NIT2 senses the nitrate signal for binding to different gene promoters is unknown. Nevertheless, a NES domain appears in the transcription factor NIRA involved in nitrate induction in *Aspergillus* (Narendja et al., 2002) and in NLP7 in *Arabidopsis* (Marchive et al., 2013). This NES sequence is involved in NIRA and NLP7

exportation to the cytosol in the absence of nitrate (Bernreiter et al., 2007; Marchive et al., 2013). In Chlamydomonas the NES domain of NIT2 is close to the GAF motif, thus binding of small molecules to GAF domain might expose or hide the NES domain facilitating its nuclear exportation. However, in *Chlamydomonas* NIT2 is important to activate nitrate-inducible genes and to upregulate genes in nitrate plus ammonium medium, a condition under which the nitrate assimilation genes are repressed, as the truncated hemoglobin *THB1* (Sanz-Luque et al., 2015). Therefore, a nuclear export would not be favorable in those conditions. Furthermore, NIT2 is also involved in the repression of genes downregulated by nitrate like the ammonium transporter *AMT1.1* (González-Ballester et al., 2004). It would be expected to find new proteins interacting with NIT2 to integrate the nitrate/ammonium balance and proportionate the specificity for a proper gene expression/regulation on each N condition.

In other green microalgae apart from *Chlamydomonas*, transcription factors involved in upregulating the nitrate assimilation genes are unknown. Nevertheless, in *Chlorella vulgaris* a unique GATA site is present in the promoter region of the NR gene (Dawson et al., 1996). This sequence works as a nitrate response element (NRE) and can bind specifically a *Neurospora crassa* NIT2 zinc-finger domain/glutathione S-transferase fusion protein. Thus, similar GATA-binding transcription factors could be responsible for the transcriptional regulation in this alga (Cannons and Shiflett, 2001). In the red alga *Cyanidioschyzon merolae* an R2R3-type MYB transcription factor, *MYB1*, has a key role in the nitrate upregulation of the main N assimilation genes (*NIA1, NII1, NRT2, AMT, GLN*). *MYB1*, as *CrNIT2*, is upregulated in nitrate and N-free medium and the transcription factor encoded binds directly to the promoter of all of these genes activating their expression (Imamura et al., 2009, 2010). This class of transcription factors is numerous in green algae but it has not been related to N metabolism. Nonetheless, two R2R3-type MYB type transcription factors directly bind to the promoter region of the glutamine synthetase gene in *Pinus sylvestris* (Gómez-Maldonado et al., 2004) and some MYB proteins are differentially regulated by the N source in *Arabidopsis* (Scheible, 2004). Thus, we could expect that MYB proteins would be also involved in N regulation in some algae.

In addition to NIT2, other regulatory protein NZF1 (nitrate zinc finger 1) involved in nitrate positive signaling was recently identified in *Chlamydomonas*. This is a tandem zinc finger protein CCCH-type that regulates *NIT2* expression and, indirectly, the nitrate assimilation genes (Higuera et al., 2014). NZF1 is proposed to have a role in *NIT2* polyadenylation. The nzf1 knockout mutant shows aberrant forms of polyadenylated *NIT2* mRNAs, which are not present in the wild type strain in nitrate medium. Thus, this nzf1 mutant has decreased levels of wild type *NIT2* transcript. Analogous transcription factors were not found in other algae, but a posttranscriptional regulation related to the mRNA stability is reported for the NR gene in *Chlorella vulgaris* (Cannons and Cannon, 2002). In this case, two different mRNAs are synthesized in response to short and long times of induction in nitrate. The long mRNA is less stable than the short version, which is induced in minutes when the

repressor (ammonium or derivatives) is removed or when the inductor (nitrate) appears. Differences between these mRNAs are located in the 5′UTR. This supposes a strategy to perform a rapid adaptation to the changing environmental conditions.

Transcriptomics analysis showed other transcription factors that are upregulated in N starvation. One of them is NRR1, which encodes a SQUAMOSA promoter-binding protein, SBP, responds early to N starvation, and has a relevant role in TAG accumulation. NRR1 is hypothesized as a "master" transcriptional regulator for reprogramming gene expression of N metabolism during N deprivation (Schmollinger et al., 2014; Gargouri et al., 2015). However, more transcriptomic and proteomic studies in nitrate medium would be required to shed light about new regulatory factors.

Negative Regulation of the Nitrate Assimilation Pathway

Nitrate assimilation is quickly blocked by ammonium addition. This is a common effect in the green algae studied. In fact, in higher plants, nitrate is essential to induce transcription of NR independently of ammonium. However, in algae removal of the repressor, or at least a shift in the balance N/A toward nitrate, is needed for induction (Cannons and Pendleton, 1994; de Montaigu et al., 2011). This repression is carried out at transcriptional (Quesada et al., 1993, 1998b; Berges, 1997; Loppes et al., 1999; Cannons and Shiflett, 2001; Imamura et al., 2010; de Montaigu et al., 2010) and posttranslational level (Florencio and Vega, 1983b; Franco et al., 1988; Galván et al., 1991, 1996). Some of the main players involved in transcriptional and posttranslational negative regulation of the nitrate assimilation pathway are briefly represented in **Figure 3**.

Transcriptional Regulation

Genes encoding the NR and high affinity nitrate/nitrite/transporters are repressed by ammonium but the mechanisms and the players involved are starting to be uncovered in *Chlamydomonas*. In this alga 40 ammonium insensitive mutants were isolated (González-Ballester et al., 2005) and some of them studied. One of them, the cyg56 mutant, is affected in a soluble guanylate cyclase (sGC) important for the ammonium-dependent repression (de Montaigu et al., 2010). These enzymes produce cGMP from GTP and are activated when NO binds to their heme group, which is found in the HNOB domain (Heme NO Binding; Iyer et al., 2003; Poulos, 2006). CYG56 is a key enzyme in ammonium sensing and the cyg56 mutant is less sensitive to NO donors than wild type strain (704) and responds similarly to cGMP addition. Pharmacological approaches, using different NO and cGMP donors and GC and phosphodiesterase inhibitors, highlight cGMP and NO as important signal molecules, and sGC as a relevant player for the repression of genes that respond negatively to ammonium. Some genes repressed by the NH_4^+-NO-CYG56-cGMP mechanism are *NIA1, NRT2.1, AMT1.1,* and *AMT1.2*. Guanylate cyclase activity is poorly studied in photosynthetic organisms because in higher plants the canonical sGC does not exist. Nevertheless, cGMP is gaining a significant role in many processes in plants (Maathuis, 2006) and some proteins without homology to GCs
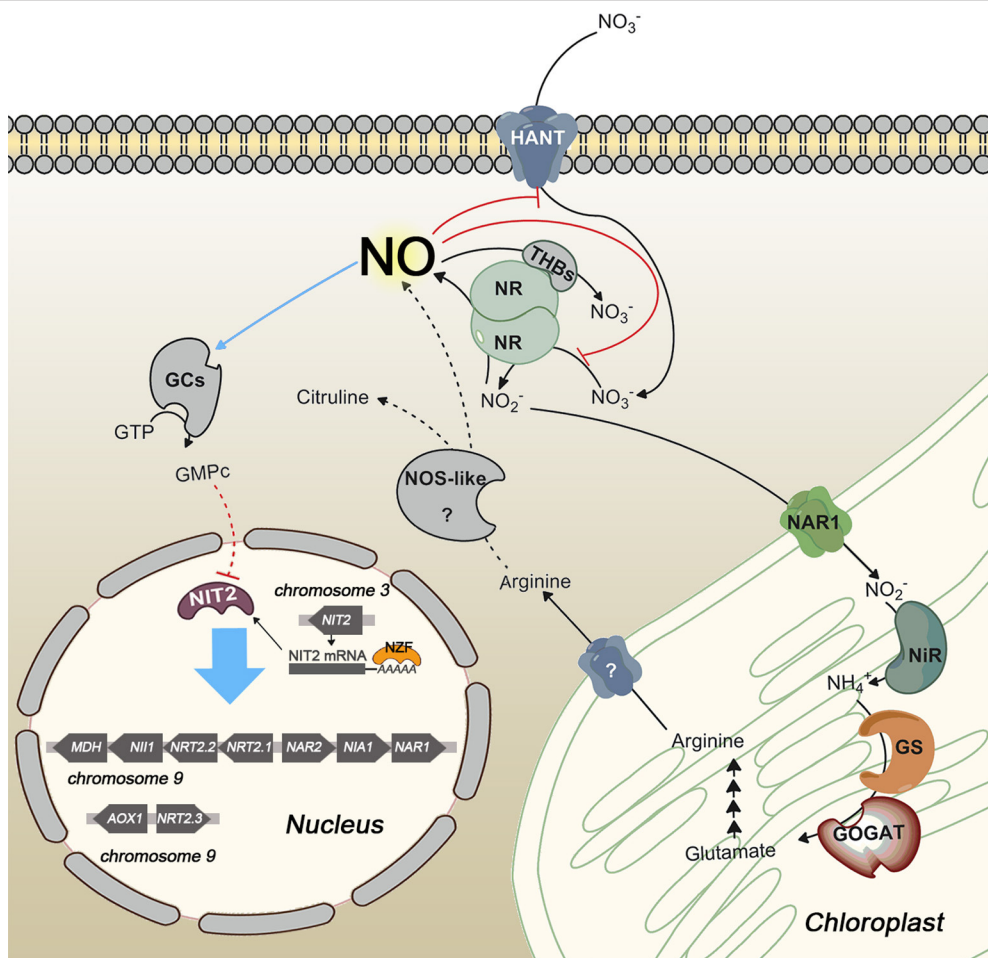
FIGURE 3 | Scheme of transcriptional and posttranslational negative regulation of nitrate assimilation in *Chlamydomonas*. Red and blue lines indicate inhibition and activation, respectively. Dashed lines represent hypothetic steps. NOS-like protein is an unidentified player that symbolizes the NOS activity reported in photosynthetic organisms. NO represses gene expression by activating a soluble guanylate cyclase (sGC) and inhibits NR activity and high affinity nitrate uptake. Two different sources of NO are represented, NR and a putative NOS enzyme. NO is scavenged by the complex NR/THB.

like kinases and hormone receptors have shown GC activity (Ludidi and Gehring, 2003; Kwezi et al., 2007; Meier et al., 2010). Unlike plants, in the Chlorophyta phylum canonical sGC can be found. The *Chlamydomonas reinhardtii* and *Volvox carteri* genomes encode two vast families of 57 and 63 adenylyl/guanylyl cyclase domains, respectively, with several soluble GC among their members. This huge amount of cyclase domains highlights the importance of cyclic nucleotides in these algae, with a close phylogenetic relationship. Other chlorophytes used in this work have none or few canonical cyclase domains encoded in their genomes as *C. subellipsoidea* (1), *M pusilla* (1), *Micromonas* sp. RCC299 (1), *O. tauri* (2), and *O. lucimarinus* (1).

How cGMP regulates gene expression is unknown. A possibility is that cGMP binds to GAF domain of NIT2 (Camargo et al., 2007) and regulates its structure and binding to specific promoters, but deeper studies have to be performed to address and clarify this mechanism. Due to the similarity observed in the components of the nitrate assimilation pathway and similar patterns of regulation, we could expect that cGMP would have

an important role in ammonium-mediated repression of nitrate assimilation genes in most of these algae. However, we propose that non-canonical GC, similar to those in plants, could have a relevant role in algae with few guanylate cyclase domains.

CYG56 expression is down-regulated in other AI mutants (de Montaigu et al., 2011). One of these strains (20.40) has a genome deletion affecting to nine putative genes; however, one of them was down-regulated in other AI mutants and is considered as a candidate for the AI phenotype. This gene codes a protein that shares homology with phosphofructokinases. In plants, these enzymes are regulated by 14-3-3 proteins (Kulma et al., 2004), like NR and GS (Finnemann and Schjoerring, 2000; MacKintosh and Meek, 2001), and may play a role in the cross-talk between nitrogen and carbon metabolisms. This mutant shows a high expression of *NIA1*, *NRT2.1,* and *AMT1.2* in nitrate medium, suggesting that this protein could be a general regulator rather than a specific player in ammonium sensing. Other relevant AI mutant (54.10) is affected in a gene, unidentified yet, that controls the expression of *CYG56* and *CDP1*, two genes that are

independently involved in ammonium sensing. *CDP1* also shows higher expression in ammonium media and codes a cysteine-rich protein. CDP1 has a very low conservation in photosynthetic eukaryotes and do not show homology with known proteins. Nevertheless, a well-conserved CDP1 is found in *Volvox*. These mutants as well as new players and their relationships, albeit poorly characterized at molecular level, are bringing out new knowledge about the complex network working in this alga for a proper ammonium sensing.

Concerning regulatory mechanisms in other green algae, few data have been reported. In *Chlorella sorokiniana*, *NRT2.1* gene encoding nitrate transporter is induced by nitrate involving phosphorylation/dephosphorylation events (Koltermann et al., 2003), however, the players that mediate this regulation are unknown.

Posttranslational Regulation

The ammonium-mediated negative effect over NR and nitrate transport was reported more than three decades ago. Ammonium addition, in cells induced with nitrate, inhibits in seconds the nitrate uptake (Florencio and Vega, 1982) and in minutes the NR activity (Franco et al., 1987). However, the mechanisms involved remain scarcely known. In plants, NR is regulated by phosphorylation of a serine residue, within a hinge region between the Moco and heme binding domains, followed by the binding of a 14-3-3 protein (MacKintosh and Meek, 2001; Lillo et al., 2004; Lambeck et al., 2012). Nevertheless, this serine residue is only conserved in higher plants and not in mosses nor algae (Medina-Andrés and Lira-Ruan, 2012). This points out that posttranslational regulation in microalgae should be different to that in plants and probably common with the most basal land plants, the mosses. Now, we are starting to understand how NR is post-translationally regulated in *Chlamydomonas*. NO not only triggers a cascade to repress transcription of the *NIA1* gene (see above, de Montaigu et al., 2010) but also partially inhibits the enzyme activity in a reversible way (Sanz-Luque et al., 2013). NO does not seem to interact directly with NR because the inhibitory effect appears when intact cells are treated but not when cell extracts or the *in vitro* recombinant NR are used. Recently, we have shown that the cytosolic truncated hemoglobin, THB1, has an important role in regulating NR activity (Sanz-Luque et al., 2015). This hemoglobin has NO dioxygenase activity (NOD) and takes up electrons from the FAD group of NR (diaphorase activity) to reduce its heme group. In the presence of NO, the reduced and oxygenated globin (THB1–Fe_2^+–O_2) catalyzes NO conversion to nitrate and decreases nitrate reduction by removing the reducing power available for NR. THB1 could also work with other reductase enzymes and probably mediate the control of other processes in the cell. However, due to its N-dependent transcriptional regulation we suggest that NR might be one of its most relevant partners. Curiously, two microalgae belonging to the class Raphidophyceae have the NR gene fused to a truncated hemoglobin (Stewart and Coyne, 2011). Authors hypothesize that this fusion confers a significant advantage to use the NO produced during bloom conditions as N source. These algae would be able to efficiently convert NO into nitrate by the NOD activity and subsequently to carry out the nitrate reduction.

In addition, other phosphorylatable serine residue, located in the hinge region 2 of NR between the FAD and heme domains, is highly conserved in both higher plants and algae. In *Arabidopsis*, MAPK6 phosphorylates this serine in NIA2 increasing the NR activity and NO production (Wang et al., 2010, 2014b).

Additionally, NO inhibits in a fast and reversible way the high affinity nitrate/nitrite transport (Sanz-Luque et al., 2013). Nitrate and nitrite uptakes of nitrate-induced cells are quickly halted after NO addition at low concentration, and normal rates of uptake recover after a few minutes, when NO disappears. In plants, two ways of regulation are described for nitrate transporters. NRT1.1, which is regulated by phosphorylation (Tsay et al., 2007; Ho et al., 2009) and some NRT2, which require association with the NAR2 protein to be active (Quesada et al., 1994; Zhou et al., 2000; Okamoto et al., 2006). Even so, the mechanisms and the players that connect the signal sensing with the posttranslational modification are unclear. NO could trigger cascades to phosphorylate or to modify directly the transporter or the accessory protein by S-nitrosylation.

Unlike NR and high affinity nitrate/nitrite transporters, NiR does not seem to be regulated by NO (Sanz-Luque et al., 2013). Regulatory mechanisms are unknown for NiR, although its activity depends on the reduced ferredoxin pool, which can be affected if photosynthesis decreases. That makes sense from a physiological point of view because this coordination avoids N loss, due to nitrite excretion, and possible toxic effects derived from nitrite accumulation. Under low photosynthetic activity rates NiR activity is low (Jin et al., 1998), resulting in the uncoupling of NR and NiR activities. Then nitrite production by NR can be higher than nitrite reduction to ammonium by NiR. Under this condition cells do not store the overproduced nitrite, which is excreted as an emergency strategy (Navarro et al., 2000). This excretion would entail loss of N and reducing power used for nitrate reduction. However, *Chlamydomonas* has a mechanism, which avoids such a disadvantage. In this alga one of the main NO sources is nitrite (Sakihama et al., 2002), and so, when nitrite accumulates, NR is able to synthetize NO with the subsequently inhibition of nitrate uptake and reduction until NR and NiR activities are coupled again (**Figure 3**).

The ammonium-dependent transcriptional and posttranslational regulation could be directly mediated by ammonium itself or by an ammonium derivative metabolite such as glutamine. Indeed, *CrAMT1.1* transcription (González-Ballester et al., 2004) or nitrite uptake (Galván et al., 1991), which are repressed and inhibited, respectively, by ammonium, are partially released of ammonium negative signaling by methione sulfoximine (MSX), an specific glutamine synthetase inhibitor. Glutamine has been described as an important N status reporter in many bacteria but in photosynthetic eukaryotes glutamine sensing is poorly understood. In many organisms glutamine is sensed by the PII protein, which is one of the most widespread signaling proteins in nature. These proteins are present in different kingdoms of life from bacteria to plants (Chellamuthu et al., 2013) and recently are reported in green algae as *Chlamydomonas* (Ermilova et al., 2013), *Chlorella* (Minaeva and Ermilova, 2015), and *Micromonas* (McDonald et al., 2010). Nevertheless, PII proteins are not conserved in

all photosynthetic algae, genome analysis failed to reveal any obvious PII homologs in the red alga *Cyanidioschyzon merolae* and diatoms (Uhrig et al., 2009).

PII proteins are responsible for the integration of N and carbon metabolisms as well as of the cellular energy status by regulating transcription factors, membrane transporters and metabolic enzymes (Uhrig et al., 2009). In bacteria there exist at least four recognized PII proteins and several targets identified. However, in most cyanobacteria, microalgae and higher plants the number of PII proteins seems to be reduced to one and its functionality is barely known (Ninfa and Jiang, 2005; Ermilova et al., 2013). In *Chlamydomonas*, like in the other photosynthetic organisms, PII protein (GLB1) is localized in the chloroplast (Ermilova et al., 2013) and activates N-acetyl-L-glutamate kinase (NAGK), a key enzyme of arginine biosynthesis (Chellamuthu et al., 2014). CrGLB1 binds glutamine at millimolar concentration and then interacts and activates NAGK. If α-oxoglutarate concentrations are high the complex is inhibited and NAGK activity decreases. Therefore, when N/C balance is shifted to N the arginine biosynthesis is enhanced. Thus, in these conditions arginine could be used as N-storage molecule or as NO precursor by a putative NO Synthase activity (NOS). Curiously, *Arabidopsis* PII mutants show higher nitrite uptake to the chloroplast than wt (Ferrario-Méry et al., 2008). Nevertheless, the PII role in algae and plants is starting to be unraveled. Recently, RNA-seq data have shown that *CrGLB1* is overexpressed in N starvation (Schmollinger et al., 2014) but its role in this condition is unknown. Additional studies will be necessary to elucidate the PII participation in the regulatory processes of the N assimilation pathway.

NO Metabolism

In the last years NO has emerged as an important signal molecule, which regulates many processes in plants and algae. A huge amount of publications have related it with essential roles in plant growth, development, defense (Delledonne et al., 1998; Corpas et al., 2004; He et al., 2004; Fernández-Marcos et al., 2011) and nitrate metabolism in plants and algae (Du et al., 2008; Jin et al., 2009; de Montaigu et al., 2010; Rosales et al., 2011; Sanz-Luque et al., 2013). Nevertheless, and despite the fact of being an important signal molecule involved in a vast number of processes, our knowledge about its synthesis and turnover in photosynthetic organisms is poor. Related to the synthesis, two different pathways are possible, the oxidative one from arginine, polyamines, or hydroxylamines, and the reductive one from nitrite (Wilson et al., 2008; Moreau et al., 2010; Gupta et al., 2011a). In photosynthetic organisms the main NO source described is NR that reduces nitrite to NO *in vivo* and *in vitro* using NAD(P)H as electron donor. This activity has been described in both plants (Yamasaki and Sakihama, 2000; Rockel et al., 2002) and algae (Mallick et al., 2000; Sakihama et al., 2002). Although the molecular basis of this enzymatic activity is not well-characterized, there exists a growing number of physiological processes regulated by a NR-dependent NO synthesis in plants and algae (Zhao et al., 2009; Hao et al., 2010; Lozano-Juste and León, 2010; Horchani et al., 2011; Wei et al., 2014; Sun et al., 2015). The NO synthesis by NR has

been estimated as 1% of the nitrate reducing capacity (Rockel et al., 2002). Thus, due to the higher affinity for nitrate than for nitrite, the NO production would require a low nitrate/nitrite balance. Indeed, experiments without nitrate are used to measure this activity (Sakihama et al., 2002), and when nitrate is added a significant delay is observed (Yamasaki and Sakihama, 2000) supporting the importance of a shifted nitrate/nitrite balance in NO synthesis by NR. As described above, NR-dependent NO synthesis would inhibit nitrate uptake and reduction with the aim of avoiding the accumulation of toxic nitrite and/or its excretion when NR and NiR are uncoupled.

In addition to NR, other reductive pathways for NO synthesis in photosynthetic organisms were described. Recently, a NR-independent NO source has been reported in *Chlamydomonas*, where nit2 mutants, with no expression of NR, showed NO increase in N-free medium after 20 h (Wei et al., 2014). Several of the alternative NO sources in plants are a plasma membrane-bound nitrite:NO reductase (Stöhr et al., 2001), which has been mainly studied in tobacco, and mitochondrial (Tischner et al., 2004; Gupta and Igamberdiev, 2011) and plastidic (Jasid et al., 2006) nitrite reduction. This reduction could be mediated by molybdoenzymes, as Amidoxime reducing component, of unknown function (Yang et al., 2015), Xanthine oxidoreductase in plants and animals (del Río et al., 2004; Gupta et al., 2011a) or Aldehyde oxidase (Li et al., 2009) and Sulfite oxidase (Wang et al., 2014a) reported only in animals albeit they could own a similar activity in plants. Finally, chemical apoplastic nitrite reduction to NO at acidic pHs has also been described (Bethke et al., 2004).

The oxidative production of NO in plant-like organisms is poorly known at molecular level. Arginine-dependent NO synthesis is mediated by NOS, but no protein with homology to animal and bacterial NOS has been found in plants. Even so, an arginine-dependent NO production has been physiologically described (Corpas et al., 2006, 2009; Moreau et al., 2010). Surprisingly, only two photosynthetic organisms bearing genes that encode animal-type NOS enzymes in their genomes have been reported up to date, the small algae *Ostreococcus tauri* and *Ostreococcus lucimanirus* (Foresi et al., 2010, 2015). The recently released genome of *Bathycoccus prasinos* (Moreau et al., 2012), other small alga from the Mamiellales clade of prasinophyceae as *Ostreococcus*, also has a gene encoding a NOS enzyme with 62% of similarity to *O. tauri* NOS (Kumar et al., 2015). Curiously, these primitive algae are species with small genomes and high horizontal gene transfer. In fact, a phylogenetic study suggests that around 5% of the *Bathycoccus prasinos* genome was originated by horizontal gene transfer (Moreau et al., 2012). This may explain why *Bathycoccus* and *Ostreococcus* are exceptional algae having genes that encode animal-type NOS enzymes.

Inhibition of nitrate reduction and uptake when nitrite concentration increases can be mediated by NO produced in a NR-dependent way; however, the NO source that performs the ammonium repression seems to depend on an arginine-dependent process in *Chlamydomonas*. Experiments with L-NAME (N_ω-Nitro-L-arginine methyl ester), an analog of arginine used as inhibitor of NOS, show a partial release of the ammonium repression of *NIA1* and other genes induced by nitrate and

repressed by ammonium (de Montaigu et al., 2010). Nevertheless, a role of NR in ammonium repression cannot be discarded.

Other important aspect of NO metabolism is its fast removal to avoid unspecific reactions producing toxic effects. Hemoglobins (Hb) have arisen as relevant proteins involved in NO scavenging. In plants, non-symbiotic Hbs have shown to have this role (Perazzolli et al., 2004; Gupta et al., 2011b). In algae, as described above, truncated Hbs are relevant players in this task. In *Chlamydomonas* a vast family of 12 truncated hemoglobins are found (Hemschemeier et al., 2013) and some of them were related to different physiological processes. Two of them THB1 and THB2 are differentially expressed by the N source, showing high transcription levels in nitrate and nitrate plus ammonium, and under the control of NIT2 (Johnson et al., 2014; Sanz-Luque et al., 2015). However, opposite responses to NO are observed for *THB1*, which is upregulated, and *THB2*, which is downregulated. In addition, as stated above, THB1 has NOD activity working with NR and using reducing power from NAD(P)H. Other recently studied truncated hemoglobins in *Chlamydomonas* are THB8, which is required for hypoxic survival in a process involving NO (Hemschemeier et al., 2013), or THB7, THB10, and THB11 that are overexpressed in the dark (Huwald et al., 2015). Some of these proteins (THB1-2-4-7-10-11) are biochemically characterized but our knowledge about their functions is poor (Ciaccio et al., 2015; Huwald et al., 2015; Rice et al., 2015). Therefore, in the last years this microalga has become an interesting organism to study the NO metabolism and functionality of these proteins. Truncated hemoglobins have also been identified in other *Chlamydomonas* species as well as in *Volvox carteri*, *Chlorella* sp. NC64A and *Micromonas pusilla* (Vázquez-Limón et al., 2012; Hemschemeier et al., 2013).

Additionally, other reactions that mediate NO scavenging are: spontaneous oxidation to nitrite; reaction with glutathione to store it as nitrosoglutathione (GSNO), which is the main NO reservoir *in vivo* in photosynthetic organisms (Wang, 2006); reaction with other ROS as superoxide anion to produce peroxynitrite, which works as a signal molecule in protein modification and, finally, reaction with metals as iron of heme groups (Moreau et al., 2010; Gupta et al., 2011a; Mur et al., 2013). Nevertheless, these mechanisms are less studied in algae.

Future Perspectives/Conclusions

The nitrate assimilation pathway is a relative simple process conserved in the majority of microalgae. This conservation highlights the importance of this pathway in the central metabolism of these organisms. This pathway owns an uptake step to incorporate nitrate into the cell, a first NR-mediated reduction followed by nitrite incorporation to chloroplasts and a second reduction step mediated by NiR. Finally N is incorporated into carbon skeletons by GS/GOGAT cycle.

Additionally, the key enzyme for nitrate assimilation (NR) harbors molybdenum cofactor, and subsequently the genes responsible for Moco biosynthesis are also highly conserved in most studied algae. In spite of the low structural complexity of this pathway its regulation is intricate. A complex protein network controlling nitrate assimilation is starting to be unraveled in *Chlamydomonas*. However, although structural genes for nitrate assimilation are well-conserved, being clustered in most algae, those involved in regulation show a lower conservation degree. Even so, a central role of NO and cGMP occurs in *Chlamydomonas,* and so the implication of these signal molecules in the regulation of other algae must be addressed. The higher diversification in the regulatory processes would allow a specific adaptation of each alga to its particular environment. At structural level, main differences are found in the number of transporters. *Chlamydomonas* is an alga with a high number of them, but other, algae with small genome sizes have transporter families with only one member. Probably, this would be a good reason to expect also a more complex regulation in *Chlamydomonas*. These features among others contribute to the high adaptability observed for this organism and have converted *Chlamydomonas* in a good model alga for basic science and biotechnological use. Nevertheless, future studies should improve our knowledge about the whole system of nutrient acquisition in algae, addressing not only assimilation of different N forms and its regulation but also their relationships with carbon, sulfur and phosphorus metabolisms. This understanding will allow us to develop many applications with algae and discover the real potential of these organisms on applied sciences.

SUPPLEMENTARY MATERIAL

The Supplementary Material for this article can be found online at: http://journal.frontiersin.org/article/10.3389/fpls.2015.00899

REFERENCES

Ataya, F. S., Witte, C. P., Galván, A., Igeño, M. I., and Fernández, E. (2003). Mcp1 encodes the molybdenum cofactor carrier protein in *Chlamydomonas*

reinhardtii and participates in protection, binding, and storage functions of the cofactor. *J. Biol. Chem.* 278, 10885–10890. doi: 10.1074/jbc.M211320200

Berges, J. (1997). Miniview: algal nitrate reductases. *Eur. J. Phycol.* 32, 3–8. doi: 10.1080/09541449710001719315

Bernreiter, A., Ramon, A., Fernández-Martínez, J., Berger, H., Araújo-Bazan, L., Espeso, E. A., et al. (2007). Nuclear export of the transcription factor NirA is a regulatory checkpoint for nitrate induction in *Aspergillus nidulans*. *Mol. Cell. Biol.* 27, 791–802. doi: 10.1128/MCB.00761-06

Bethke, P. C., Badger, M. R., and Jones, R. L. (2004). Apoplastic synthesis of nitric oxide by plant tissues. *Plant. Cell.* 16, 332–341. doi: 10.1105/tpc.017822

Bittner, F. (2014). Molybdenum metabolism in plants and crosstalk to iron. *Front. Plant. Sci* 5:28. doi: 10.3389/fpls.2014.00028

Bittner, F., Oreb, M., and Mendel, R. R. (2001). ABA3 is a molybdenum cofactor sulfurase required for activation of aldehyde oxidase and xanthine dehydrogenase in *Arabidopsis thaliana*. *J. Biol. Chem.* 276, 40381–40384. doi: 10.1074/jbc.C100472200

Büsch, A., Strube, K., and Friedrich, B. (2005). Transcriptional regulation of nitric oxide reduction in *Ralstonia eutropha* H 16. *Biochem. Soc. Trans.* 33, 193–194. doi: 10.1042/BST0330193

Caboche, M., and Rouzé, P. (1990). Nitrate reductase: a target for molecular and cellular studies in higher plants. *Trends Genet.* 6, 187–192. doi: 10.1016/0168-9525(90)90175-6

Camargo, A., Llamas, A., Schnell, R. A., Higuera, J. J., González-Ballester, D., Lefebvre, P. A., et al. (2007). Nitrate signaling by the regulatory gene *NIT2* in *Chlamydomonas*. *Plant. Cell* 19, 3491–3503. doi: 10.1105/tpc.106.045922

Cannons, A. C., and Cannon, J. (2002). The stability of the *Chlorella* nitrate reductase mRNA is determined by the secondary structure of the 5'-UTR: implications for posttranscriptional regulation of nitrate reductase. *Planta* 214, 488–491. doi: 10.1007/s00425-001-0679-z

Cannons, A. C., and Pendleton, L. C. (1994). Possible role for mRNA stability in the ammonium-controlled regulation of nitrate reductase expression. *Biochem. J.* 297, 561–565. doi: 10.1042/bj2970561

Cannons, A. C., and Shiflett, S. (2001). Transcriptional regulation of the nitrate reductase gene in *Chlorella vulgaris* : identification of regulatory elements controlling expression. *Curr. Genet.* 40, 128–135. doi: 10.1007/s002940100232

Castaings, L., Camargo, A., Pocholle, D., Gaudon, V., Texier, Y., Boutet-Mercey, S., et al. (2009). The nodule inception-like protein 7 modulates nitrate sensing and metabolism in *Arabidopsis*. *Plant J.* 57, 426–435. doi: 10.1111/j.1365-313X.2008.03695.x

Chardin, C., Girin, T., Roudier, F., Meyer, C., and Krapp, A. (2014). The plant RWP-RK transcription factors: key regulators of nitrogen responses and of gametophyte development. *J. Exp. Bot.* 65, 5577–5587. doi: 10.1093/jxb/eru261

Chellamuthu, V.-R., Alva, V., and Forchhammer, K. (2013). From cyanobacteria to plants: conservation of PII functions during plastid evolution. *Planta* 237, 451–462. doi: 10.1007/s00425-012-1801-0

Chellamuthu, V.-R., Ermilova, E. V., Lapina, T., Lüddecke, J., Minaeva, E., Herrmann, C., et al. (2014). A widespread glutamine-sensing mechanism in the plant kingdom. *Cell* 159, 1188–1199. doi: 10.1016/j.cell.2014.10.015

Chen, Q., and Silflow, C. D. (1996). Isolation and characterization of glutamine synthetase genes in *Chlamydomonas reinhardtii*. *Plant Physiol.* 112, 987–996. doi: 10.1104/pp.112.3.987

Ciaccio, C., Ocaña-Calahorro, F., Droghetti, E., Tundo, G. R., Sanz-Luque, E., Polticelli, F., et al. (2015). Functional and spectroscopic characterization of *Chlamydomonas reinhardtii* truncated hemoglobins. *PLoS ONE* 10:e0125005. doi: 10.1371/journal.pone.0125005

Corpas, F. J., Barroso, J. B., Carreras, A., Quirós, M., León, A. M., Romero-Puertas, M. C., et al. (2004). Cellular and subcellular localization of endogenous nitric oxide in young and senescent pea plants. *Plant Physiol.* 136, 2722–2733. doi: 10.1104/pp.104.042812

Corpas, F. J., Barroso, J. B., Carreras, A., Valderrama, R., Palma, J. M., León, A. M., et al. (2006). Constitutive arginine-dependent nitric oxide synthase activity in different organs of pea seedlings during plant development. *Planta* 224, 246–254. doi: 10.1007/s00425-005-0205-9

Corpas, F. J., Palma, J. M., del Río, L. A., and Barroso, J. B. (2009). Evidence supporting the existence of L-arginine-dependent nitric oxide synthase activity in plants. *New Phytol.* 184, 9–14. doi: 10.1111/j.1469-8137.2009.02989.x

Crane, B. R., and Getzoff, E. D. (1996). The relationship between structure and function for the sulfite reductases. *Curr. Opin. Struct. Biol.* 6, 744–756. doi: 10.1016/S0959-440X(96)80003-0

Crawford, N. M. (1995). Nitrate: nutrient and signal for plant growth. *Plant Cell* 7, 859–868. doi: 10.1105/tpc.7.7.859

Crawford, N. M., and Glass, A. (1998). Molecular and physiological aspects of nitrate uptake in plants. *Trends Plant Sci.* 3, 389–395 doi: 10.1016/S1360-1385(98)01311-9

Cullimore, J. V. (1981). Glutamine synthetase of *Chlamydomonas*: rapid reversible deactivation. *Planta* 152, 587–591. doi: 10.1007/BF00380832

Cullimore, J. V., and Sims, A. P. (1981a). Glutamine synthetase of *Chlamydomonas*: its role in the control of nitrate assimilation. *Planta* 153, 18–24. doi: 10.1007/BF00385313

Cullimore, J. V., and Sims, A. P. (1981b). Pathway of ammonia assimilation in illuminated and darkened *Chlamydomonas reinhardtii*. *Phytochemistry* 20, 933–940. doi: 10.1016/0031-9422(81)83002-6

Dawson, H. N., Pendleton, L. C., Solomonson, L. P., and Cannons, A. C. (1996). Cloning and characterization of the nitrate reductase-encoding gene from *Chlorella vulgaris*: structure and identification of transcription start points and initiator sequences. *Gene* 171, 139–145. doi: 10.1016/0378-1119(96)00063-7

de Clerck, O., Bogaert, K., and Leliaert, F. (2012). Diversity and evolution of algae: primary endosymbiosis. *Adv. Bot. Res.* 64, 55–86. doi: 10.1016/B978-0-12-391499-6.00002-5

Delledonne, M., Xia, Y., Dixon, R. A., and Lamb, C. (1998). Nitric oxide functions as a signal in plant disease resistance. *Nature* 394, 585–588. doi: 10.1038/29087

del Río, L. A., Corpas, F. J., and Barroso, J. B. (2004). Nitric oxide and nitric oxide synthase activity in plants. *Phytochemistry* 65, 783–792. doi: 10.1016/j.phytochem.2004.02.001

de Montaigu, A., Sanz-Luque, E., Galván, A., and Fernández, E. (2010). A soluble guanylate cyclase mediates negative signaling by ammonium on expression of nitrate reductase in *Chlamydomonas*. *Plant Cell* 22, 1532–1548. doi: 10.1105/tpc.108.062380

de Montaigu, A., Sanz-Luque, E., Macias, M. I., Galvan, A., and Fernandez, E. (2011). Transcriptional regulation of CDP1 and CYG56 is required for proper NH4+ sensing in *Chlamydomonas*. *J. Exp. Bot.* 62, 1425–1437. doi: 10.1093/jxb/erq384

Derelle, E., Ferraz, C., Rombauts, S., Rouzé, P., Worden, A. Z., Robbens, S., et al. (2006). Genome analysis of the smallest free-living eukaryote *Ostreococcus tauri* unveils many unique features. *Proc. Natl. Acad. Sci. U.S.A.* 103, 11647–11652. doi: 10.1073/pnas.0604795103

Douglas, S. E. (1998). Plastid evolution: origins, diversity, trends. *Curr. Opin. Genet. Dev.* 8, 655–661. doi: 10.1016/S0959-437X(98)80033-6

Du, S., Zhang, Y., Lin, X., Wang, Y., and Tang, C. (2008). Regulation of nitrate reductase by nitric oxide in Chinese cabbage pakchoi (*Brassica chinensis* L.). *Plant Cell Environ.* 31, 195–204. doi: 10.1111/j.1365-3040.2007.01750.x

Ermilova, E. V., Lapina, T., Zalutskaya, Z., Minaeva, E., Fokina, O., and Forchhammer, K. (2013). PII signal transduction protein in *Chlamydomonas reinhardtii*: localization and expression pattern. *Protist* 164, 49–59. doi: 10.1016/j.protis.2012.04.002

Fernandez, E., and Galvan, A. (2007). Inorganic nitrogen assimilation in *Chlamydomonas*. *J. Exp. Bot.* 58, 2279–2287. doi: 10.1093/jxb/erm106

Fernandez, E., and Galvan, A. (2008). Nitrate assimilation in *Chlamydomonas*. *Eukaryotic Cell* 7, 555–559. doi: 10.1128/EC.00431-07

Fernández, E., Schnell, R., Ranum, L. P., Hussey, S. C., Silflow, C. D., and Lefebvre, P. A. (1989). Isolation and characterization of the nitrate reductase structural gene of *Chlamydomonas reinhardtii*. *Proc. Natl. Acad. Sci. U.S.A.* 86, 6449–6453. doi: 10.1073/pnas.86.17.6449

Fernández-Marcos, M., Sanz, L., Lewis, D. R., Muday, G. K., and Lorenzo, O. (2011). Nitric oxide causes root apical meristem defects and growth inhibition while reducing PIN-FORMED 1 (PIN1)-dependent acropetal auxin transport. *Proc. Natl. Acad. Sci. U.S.A.* 108, 18506–18511. doi: 10.1073/pnas.1108644108

Ferrario-Méry, S., Meyer, C., and Hodges, M. (2008). Chloroplast nitrite uptake is enhanced in *Arabidopsis* PII mutants. *FEBS Lett.* 582, 1061–1066. doi: 10.1016/j.febslet.2008.02.056

Finnemann, J., and Schjoerring, J. K. (2000). Post-translational regulation of cytosolic glutamine synthetase by reversible phosphorylation and 14-3-3 protein interaction. *Plant J.* 24, 171–181. doi: 10.1046/j.1365-313x.2000.00863.x

Fischer, K., Llamas, A., Tejada-Jimenez, M., Schrader, N., Kuper, J., Ataya, F. S., et al. (2006). Function and structure of the molybdenum cofactor carrier protein from *Chlamydomonas reinhardtii*. *J. Biol. Chem.* 281, 30186–30194. doi: 10.1074/jbc.M603919200

Fischer, P., and Klein, U. (1988). Localization of nitrogen-assimilating enzymes in the chloroplast of *Chlamydomonas reinhardtii*. *Plant Physiol.* 88, 947–952. doi: 10.1104/pp.88.3.947

Florencio, F. J., and Vega, J. M. (1982). Regulation of the assimilation of nitrate in *Chlamydomonas reinhardii*. *Phytochemistry* 21, 1195–1200. doi: 10.1016/0031-9422(82)80110-6

Florencio, F. J., and Vega, J. M. (1983a). Separation, purification, and characterization of two isoforms of glutamine synthetase from *Chlamydomonas reinhardii*. *Z. Naturforsch. C* 38, 531–538.

Florencio, F., and Vega, J. (1983b). Utilization of nitrate, nitrite and ammonium by *Chlamydomonas reinhardtii*. *Planta* 158, 288–293. doi: 10.1007/BF00397329

Forde, B. G. (2000). Nitrate transporters in plants: structure, function and regulation. *Biochem. Biophys. Acta* 1465, 219–235. doi: 10.1016/S0005-2736(00)00140-1

Forde, B. G., and Cole, J. A. (2003). Nitrate finds a place in the sun. *Plant Physiol.* 131, 395–400. doi: 10.1104/pp.016139

Foresi, N., Correa-Aragunde, N., Parisi, G., Caló, G., Salerno, G., and Lamattina, L. (2010). Characterization of a nitric oxide synthase from the plant kingdom: NO generation from the green alga *Ostreococcus tauri* is light irradiance and growth phase dependent. *Plant Cell* 22, 3816–3830. doi: 10.1105/tpc.109.073510

Foresi, N., Mayta, M. L., Lodeyro, A. F., Scuffi, D., Correa-Aragunde, N., García-Mata, C., et al. (2015). Expression of the tetrahydrofolate-dependent nitric oxide synthase from the green alga *Ostreococcus tauri* increases tolerance to abiotic stresses and influences stomatal development in *Arabidopsis*. *Plant J.* 82, 806–821. doi: 10.1111/tpj.12852

Franco, A. R., Cárdenas, J., and Fernández, E. (1987). Involvement of reversible inactivation in the regulation of nitrate reductase enzyme levels in *Chlamydomonas reinhardtii*. *Plant Physiol.* 84, 665–669. doi: 10.1104/pp.84.3.665

Franco, A. R., Cárdenas, J., and Fernández, E. (1988). Regulation by ammonium of nitrate and nitrite assimilation in *Chlamydomonas reinhardtii*. *Biochem. Biophys. Acta* 951, 98–103. doi: 10.1016/0167-4781(88)90029-2

Frías, J. E., Flores, E., and Herrero, A. (1997). Nitrate assimilation gene cluster from the heterocyst-forming cyanobacterium *Anabaena* sp. strain PCC 7120. *J. Bacteriol.* 185, 5037–5044.

Galván, A., Córdoba, F., Cárdenas, J., and Fernández, E. (1991). Regulation of nitrite uptake and nitrite reductase expression in *Chlamydomonas reinhardtii*. *Biochem. Biophys. Acta.* 1074, 6–11. doi: 10.1016/0304-4165(91)90030-K

Galvan, A., and Fernández, E. (2001). Eukaryotic nitrate and nitrite transporters. *Cell. Mol. Life Sci.* 58, 225–233. doi: 10.1007/PL00000850

Galván, A., Quesada, A., and Fernández, E. (1996). Nitrate and nitrate are transported by different specific transport systems and by a bispecific transporter in *Chlamydomonas reinhardtii*. *J. Biol. Chem.* 271, 2088–2092. doi: 10.1074/jbc.271.4.2088

Gargouri, M., Park, J.-J., Holguin, F. O., Kim, M.-J., Wang, H., Deshpande, R. R., et al. (2015). Identification of regulatory network hubs that control lipid metabolism in *Chlamydomonas reinhardtii*. *J. Exp. Bot.* 66, 4551–4566. doi: 10.1093/jxb/erv217

Ghoshroy, S., and Robertson, D. L. (2015). Molecular evolution of nitrogen assimilatory enzymes in marine prasinophytes. *J. Mol. Evol.* 80, 65–80. doi: 10.1007/s00239-014-9659-3

Giordano, M., and Raven, J. A. (2014). Nitrogen and sulfur assimilation in plants and algae. *Aquat. Bot.* 118, 45–61. doi: 10.1016/j.aquabot.2014.06.012

Gojon, A., Krouk, G., Perrine-Walker, F., and Laugier, E. (2011). Nitrate transceptor(s) in plants. *J. Exp. Bot.* 62, 2299–2308. doi: 10.1093/jxb/erq419

Gómez-Maldonado, J., Avila, C., Torre, F., Cañas, R., Cánovas, F. M., and Campbell, M. M. (2004). Functional interactions between a glutamine synthetase promoter and MYB proteins. *Plant J.* 39, 513–526. doi: 10.1111/j.1365-313X.2004.02153.x

González-Ballester, D., Camargo, A., and Fernández, E. (2004). Ammonium transporter genes in *Chlamydomonas*: the nitrate-specific regulatory gene *Nit2* is involved in *Amt1;1* expression. *Plant Mol. Biol.* 56, 863–878. doi: 10.1007/s11103-004-5292-7

González-Ballester, D., de Montaigu, A., Higuera, J. J., Galván, A., and Fernández, E. (2005). Functional genomics of the regulation of the nitrate assimilation pathway in *Chlamydomonas*. *Plant Physiol.* 137, 522–533. doi: 10.1104/pp.104.050914

Gruber, N. (2008). "The marine nitrogen cycle: overview and challenges" in *Nitrogen in the Marine Environment*, eds D. G. Capone, D. A. Bronk, M. R. Mulholland, and E. J. Carpenter (San Diego: Academic Press), 1–50.

Guerrero, M. G., Vega, J. M., and Losada, M. (1981). The assimilatory nitrate-reducing system and its regulation. *Annu. Rev. Plant Physiol. Plant Mol. Biol.* 32, 169–204. doi: 10.1146/annurev.pp.32.060181.001125

Gupta, K. J., Fernie, A. R., Kaiser, W. M., and van Dongen, J. T. (2011a). On the origins of nitric oxide. *Trends Plant Sci.* 16, 160–168. doi: 10.1016/j.tplants.2010.11.007

Gupta, K. J., Hebelstrup, K. H., Mur, L. A. J., and Igamberdiev, A. U. (2011b). Plant hemoglobins: important players at the crossroads between oxygen and nitric oxide. *FEBS Lett.* 585, 3843–3849. doi: 10.1016/j.febslet.2011.10.036

Gupta, K. J., and Igamberdiev, A. U. (2011). The anoxic plant mitochondrion as a nitrite: NO reductase. *Mitochondrion* 11, 537–543. doi: 10.1016/j.mito.2011.03.005

Hao, F., Zhao, S., Dong, H., Zhang, H., Sun, L., and Miao, C. (2010). Nia1 and Nia2 are involved in exogenous salicylic acid-induced nitric oxide generation and stomatal closure in *Arabidopsis*. *J. Integr. Plant Biol.* 52, 298–307. doi: 10.1111/j.1744-7909.2010.00920.x

Harris, E. (2009). *The Chlamydomonas Sourcebook*. New York, NY: Academic Press.

He, Y., Tang, R.-H., Hao, Y., Stevens, R. D., Cook, C. W., Ahn, S. M., et al. (2004). Nitric oxide represses the *Arabidopsis* floral transition. *Science* 305, 1968–1971. doi: 10.1126/science.1098837

Hemschemeier, A., Düner, M., Casero, D., Merchant, S. S., Winkler, M., and Happe, T. (2013). Hypoxic survival requires a 2-on-2 hemoglobin in a process involving nitric oxide. *Proc. Natl. Acad. Sci. U.S.A.* 110, 10854–10859. doi: 10.1073/pnas.1302592110

Higuera, J. J., Fernandez, E., and Galvan, A. (2014). *Chlamydomonas*NZF1, a tandem-repeated zinc finger factor involved in nitrate signalling by controlling the regulatory gene *NIT2*. *Plant Cell Environ.* 37, 2139–2160. doi: 10.1111/pce.12305

Hirata, R., Takahashi, M., Saga, N., and Mikami, K. (2011). Transient gene expression system established in *Porphyra yezoensis* is widely applicable in Bangiophycean algae. *Mar. Biotechnol.* 13, 1038–1047. doi: 10.1007/s10126-011-9367-6

Ho, C.-H., Lin, S.-H., Hu, H.-C., and Tsay, Y.-F. (2009). CHL1 functions as a nitrate sensor in plants. *Cell* 138, 1184–1194. doi: 10.1016/j.cell.2009.07.004

Ho, C.-H., and Tsay, Y.-F. (2010). Nitrate, ammonium, and potassium sensing and signaling. *Curr. Opin. Plant Biol.* 13, 604–610. doi: 10.1016/j.pbi.2010.08.005

Horchani, F., Prévot, M., Boscari, A., Evangelisti, E., Meilhoc, E., Bruand, C., et al. (2011). Both plant and bacterial nitrate reductases contribute to nitric oxide production in *Medicago truncatula* nitrogen-fixing nodules. *Plant Physiol.* 155, 1023–1036. doi: 10.1104/pp.110.166140

Huwald, D., Schrapers, P., Kositzki, R., Haumann, M., and Hemschemeier, A. (2015). Characterization of unusual truncated hemoglobins of *Chlamydomonas reinhardtii* suggests specialized functions. *Planta* 242, 167–185. doi: 10.1007/s00425-015-2294-4

Imamura, S., Kanesaki, Y., Ohnuma, M., Inouye, T., Sekine, Y., Fujiwara, T., et al. (2009). R2R3-type MYB transcription factor, CmMYB1, is a central nitrogen assimilation regulator in *Cyanidioschyzon merolae*. *Proc. Natl. Acad. Sci. U.S.A.* 106, 12548–12553. doi: 10.1073/pnas.0902790106

Imamura, S., Terashita, M., Ohnuma, M., Maruyama, S., Minoda, A., Weber, A. P. M., et al. (2010). Nitrate assimilatory genes and their transcriptional regulation in a unicellular red alga *Cyanidioschyzon merolae*: genetic evidence for nitrite reduction by a sulfite reductase-like enzyme. *Plant Cell Physiol.* 51, 707–717. doi: 10.1093/pcp/pcq043

Iyer, L. M., Anantharaman, V., and Aravind, L. (2003). Ancient conserved domains shared by animal soluble guanylyl cyclases and bacterial signaling proteins. *BMC Genomics* 4:5. doi: 10.1186/1471-2164-4-5

Jasid, S., Simontacchi, M., and Bartoli, C. (2006). Chloroplasts as a nitric oxide cellular source. Effect of reactive nitrogen species on chloroplastic lipids and proteins. *Plant Physiol.* 142, 1246–1255. doi: 10.1104/pp.106.086918

Jin, C. W., Du, S. T., Zhang, Y. S., Lin, X. Y., and Tang, C. X. (2009). Differential regulatory role of nitric oxide in mediating nitrate reductase activity in roots of tomato (*Solanum lycocarpum*). *Ann. Bot.* 104, 9–17. doi: 10.1093/aob/mcp087

Jin, T., Huppe, H. C., and Turpin, D. H. (1998). *In vitro* reconstitution of electron transport from glucose-6-phosphate and NADPH to nitrite. *Plant Physiol.* 117, 303–309 doi: 10.1104/pp.117.1.303

Johnson, E. A., Rice, S. L., Preimesberger, M. R., Nye, D. B., Gilevicius, L., Wenke, B. B., et al. (2014). Characterization of THB1, a *Chlamydomonas reinhardtii* truncated hemoglobin: linkage to nitrogen metabolism and identification of lysine as the distal heme ligand. *Biochemistry* 53, 4573–4589. doi: 10.1021/bi5005206

Johnstone, I. L., McCabe, P. C., Greaves, P., and Gurr, S. J. (1990). Isolation and characterisation of the *crnA-niiA-niaD* gene cluster for nitrate assimilation in *Aspergillus nidulans*. *Gene* 90, 181–192. doi: 10.1016/0378-1119(90)90178-T

Kamako, S., Hoshina, R., Ueno, S., and Imamura, N. (2005). Establishment of axenic endosymbiotic strains of Japanese *Paramecium bursaria* and the utilization of carbohydrate and nitrogen compounds by the isolated algae. *Eur. J. Protist.* 41, 193–202. doi: 10.1016/j.ejop.2005.04.001

Keeling, P. J. (2010). The endosymbiotic origin, diversification and fate of plastids. *Philos. Trans. R. Soc. Lond. B Biol. Sci.* 365, 729–748. doi: 10.1098/rstb.2009.0103

Kindle, K. L. (1990). High-frecuency nuclear transformation of *Chlamydomonas reinhardtii*. *Proc. Natl. Acad. Sci. U.S.A.* 87, 1228–1232. doi: 10.1073/pnas.87.3.1228

Koltermann, M., Moroni, A., Gazzarini, S., Nowara, D., and Tischner, R. (2003). Cloning, functional expression and expression studies of the nitrate transporter gene from *Chlorella sorokiniana* (strain 211-8k). *Plant Mol. Biol.* 52, 855–864. doi: 10.1023/A:1025024821832

Konishi, M., and Yanagisawa, S. (2013). Arabidopsis NIN-like transcription factors have a central role in nitrate signalling. *Nat Commun.* 4, 1617. doi: 10.1038/ncomms2621

Krapp, A., David, L. C., Chardin, C., Girin, T., Marmagne, A., Leprince, A. S., et al. (2014). Nitrate transport and signalling in *Arabidopsis*. *J. Exp. Bot.* 65, 789–798. doi: 10.1093/jxb/eru001

Kruse, T., Gehl, C., Geisler, M., Lehrke, M., Ringel, P., Hallier, S., et al. (2010). Identification and biochemical characterization of molybdenum cofactor-binding proteins from *Arabidopsis thaliana*. *J. Biol. Chem.* 285, 6623–6635. doi: 10.1074/jbc.M109.060640

Kulma, A., Villadsen, D., Campbell, D. G., Meek, S. E., Harthill, J. E., Nielsen, T. H., et al. (2004). Phosphorylation and 14-3-3 binding of *Arabidopsis* 6-phosphofructo-2-kinase/fructose-2,6-bisphosphatase. *Plant J.* 37, 654–667. doi: 10.1111/j.1365-313X.2003.01992.x

Kumar, A., Castellano, I., Patti, F. P., Palumbo, A., and Buia, M. C. (2015). Nitric oxide in marine photosynthetic organisms. *Nitric Oxide* 47, 34–39. doi: 10.1016/j.niox.2015.03.001

Kwezi, L., Meier, S., Mungur, L., Ruzvidzo, O., Irving, H., and Gehring, C. (2007). The Arabidopsis thaliana brassinosteroid receptor (AtBRI1) contains a domain that functions as a guanylyl cyclase *in vitro*. *PLoS ONE* 2:e449. doi: 10.1371/journal.pone.0000449

Lambeck, I. C., Fischer-Schrader, K., Niks, D., Roeper, J., Chi, J.-C., Hille, R., et al. (2012). Molecular mechanism of 14-3-3 protein-mediated inhibition of plant nitrate reductase. *J. Biol. Chem.* 287, 4562–4571. doi: 10.1074/jbc.M111.323113

León-Bañares, R., Gonzalez-Ballester, D., Galván, A., and Fernández, E. (2004). Transgenic microalgae as green cell-factories. *Trends Biotechnol.* 22, 45–52. doi: 10.1016/j.tibtech.2003.11.003

Léran, S., Varala, K., Boyer, J.-C., Chiurazzi, M., Crawford, N. M., Daniel-Vedele, F., et al. (2014). A unified nomenclature of NITRATE TRANSPORTER 1/PEPTIDE TRANSPORTER family members in plants. *Trends Plant Sci.* 19, 5–9. doi: 10.1016/j.tplants.2013.08.008

Lerche, K., and Hallmann, A. (2009). Stable nuclear transformation of *Gonium pectorale*. *BMC Biotechnol.* 9:64. doi: 10.1186/1472-6750-9-64

Lerche, K., and Hallmann, A. (2013). Stable nuclear transformation of *Eudorina elegans*. *BMC Biotechnol.* 13:11. doi: 10.1186/1472-6750-13-11

Lerche, K., and Hallmann, A. (2014). Stable nuclear transformation of *Pandorina morum*. *BMC Biotechnol.* 14:65. doi: 10.1186/1472-6750-14-65

Li, H., Kundu, T. K., and Zweier, J. L. (2009). Characterization of the magnitude and mechanism of aldehyde oxidase-mediated nitric oxide production from nitrite. *J. Biol. Chem.* 284, 33850–33858. doi: 10.1074/jbc.M109.019125

Lillo, C., Meyer, C., Lea, U. S., Provan, F., and Oltedal, S. (2004). Mechanism and importance of post-translational regulation of nitrate reductase. *J. Exp. Bot.* 55, 1275–1282. doi: 10.1093/jxb/erh132

Lin, H., and Goodenough, U. W. (2007). Gametogenesis in the *Chlamydomonas reinhardtii* minus mating type is controlled by two genes, *MID* and *MTD1*. *Genetics* 176, 913–925. doi: 10.1534/genetics.106.066167

Little, R., and Dixon, R. (2003). The amino-terminal GAF domain of *Azotobacter vinelandii* NifA binds 2-oxoglutarate to resist inhibition by NifL under nitrogen-limiting conditions. *J. Biol. Chem.* 278, 28711–28718. doi: 10.1074/jbc.M301992200

Liu, K. H., Huang, C. Y., and Tsay, Y. F. (1999). CHL1 is a dual-affinity nitrate transporter of *Arabidopsis* involved in multiple phases of nitrate uptake. *Plant Cell* 11, 865–874. doi: 10.1105/tpc.11.5.865

Llamas, A., Igeño, M. I., Galván, A., and Fernández, E. (2002). Nitrate signalling on the nitrate reductase gene promoter depends directly on the activity of the nitrate transport systems in *Chlamydomonas*. *Plant J.* 30, 261–271. doi: 10.1046/j.1365-313X.2002.01281.x

Llamas, A., Tejada-Jiménez, M., González-Ballester, D., Higuera, J. J., Schwarz, G., Galvan, A., et al. (2007). *Chlamydomonas reinhardtii* CNX1E reconstitutes molybdenum cofactor biosynthesis in *Escherichia coli* mutants. *Eukaryotic Cell* 6, 1063–1067. doi: 10.1128/EC.00072-07

López-Ruiz, A., Verbelen, J. P., Bocanegra, J. A., and Diez, J. (1991). Immunocytochemical localization of nitrite reductase in green algae. *Plant Physiol.* 96, 699–704. doi: 10.1104/pp.96.3.699

Loppes, R., Radoux, M., Ohresser, M. C., and Matagne, R. F. (1999). Transcriptional regulation of the *Nia1* gene encoding nitrate reductase in *Chlamydomonas reinhardtii*: effects of various environmental factors on the expression of a reporter gene under the control of the *Nia1* promoter. *Plant Mol. Biol.* 41, 701–711. doi: 10.1023/A:1006381527119

Lozano-Juste, J., and León, J. (2010). Enhanced abscisic acid-mediated responses in nia1nia2noa1-2 triple mutant impaired in NIA/NR- and AtNOA1-dependent nitric oxide biosynthesis in *Arabidopsis*. *Plant Physiol.* 152, 891–903. doi: 10.1104/pp.109.148023

Ludidi, N., and Gehring, C. (2003). Identification of a novel protein with guanylyl cyclase activity in *Arabidopsis thaliana*. *J. Biol. Chem.* 278, 6490–6494. doi: 10.1074/jbc.M210983200

Maathuis, F. J. M. (2006). cGMP modulates gene transcription and cation transport in *Arabidopsis* roots. *Plant J.* 45, 700–711. doi: 10.1111/j.1365-313X.2005.02616.x

MacKintosh, C., and Meek, S. E. (2001). Regulation of plant NR activity by reversible phosphorylation, 14-3-3 proteins and proteolysis. *Cell. Mol. Life Sci.* 58, 205–214. doi: 10.1007/PL00000848

Mallick, N., Mohn, F. H., and Soeder, C. J. (2000). Evidence supporting nitrite-dependent NO release by the green microalga *Scenedesmus obliquus*. *J. Plant Physiol.* 157, 40–46. doi: 10.1016/S0176-1617(00)80133-9

Marchive, C., Roudier, F., Castaings, L., Bréhaut, V., Blondet, E., Colot, V., et al. (2013). Nuclear retention of the transcription factor NLP7 orchestrates the early response to nitrate in plants. *Nat. Commun.* 4, 1713. doi: 10.1038/ncomms2650

Mariscal, V., Moulin, P., Orsel, M., Miller, A. J., Fernández, E., and Galván, A. (2006). Differential regulation of the *Chlamydomonas Nar1* gene family by carbon and nitrogen. *Protist* 157, 421–433. doi: 10.1016/j.protis.2006.06.003

Maruyama, S., and Archibald, J. M. (2012). "Endosymbiosis, gene transfer, and algal cell evolution," in *Advances in Algal Cell Biology*, eds K. Heimann and C. Katsaros (Berlin: Walter de Gruyter GmbH), 21–41.

McDonald, S. M., Plant, J. N., and Worden, A. Z. (2010). The mixed lineage nature of nitrogen transport and assimilation in marine eukaryotic phytoplankton: a case study of *Micromonas*. *Mol. Biol. Evol.* 27, 2268–2283. doi: 10.1093/molbev/msq113

Medina-Andrés, R., and Lira-Ruan, V. (2012). *In silico* characterization of a nitrate reductase gene family and analysis of the predicted proteins from the moss *Physcomitrella patens*. *Commun. Integr. Biol.* 5, 19–25. doi: 10.4161/cib.18534

Meier, S., Ruzvidzo, O., Morse, M., Donaldson, L., Kwezi, L., and Gehring, C. (2010). The Arabidopsis wall associated kinase-like 10 gene encodes a functional guanylyl cyclase and is co-expressed with pathogen defense related genes. *PLoS ONE* 5:e8904. doi: 10.1371/journal.pone.0008904

Merchant, S. S., Prochnik, S. E., Vallon, O., Harris, E. H., Karpowicz, S. J., Witman, G. B., et al. (2007). The *Chlamydomonas* genome reveals the evolution of key animal and plant functions. *Science* 318, 245–250. doi: 10.1126/science.1143609

Miflin, B. J., and Lea, P. J. (1975). Glutamine and asparagine as nitrogen donors for reductant-dependent glutamate synthesis in pea roots. *Biochem. J.* 149, 403–409. doi: 10.1042/bj1490403

Minaeva, E., and Ermilova, E. (2015). Sequencing and expression analysis of the gene encoding PII signal protein in *chlorella variabilis* NC64A. *J. Plant Biochem. Physiol.* 2:142. doi: 10.4172/2329-9029.1000142

Moreau, H., Verhelst, B., Couloux, A., Derelle, E., Rombauts, S., Grimsley, N., et al. (2012). Gene functionalities and genome structure in *Bathycoccus prasinos* reflect cellular specializations at the base of the green lineage. *Genome Biol.* 13:r74. doi: 10.1186/gb-2012-13-8-r74

Moreau, M., Lindermayr, C., Durner, J., and Klessig, D. F. (2010). NO synthesis and signaling in plants - where do we stand? *Physiol. Plant.* 138, 372–383. doi: 10.1111/j.1399-3054.2009.01308.x

Moyano, E., Cárdenas, J., and Muño-Blanco, J. (1992). Purification and properties of three NAD(P)+ isozymes of l-glutamate dehydrogenase of *Chlamydomonas reinhardtii*. *Biochem. Biophys. Acta* 1119, 63–68.

Moyano, E., Cárdenas, J., and Munoz-Blanco, J. (1995). Involvement of NAD(P)+-glutamate dehydrogenase isoenzymes in carbon and nitrogen metabolism in *Chlamydomonas reinhardtii*. *Physiol. Plant* 94, 553–559. doi: 10.1111/j.1399-3054.1995.tb00967.x

Muñoz-Blanco, J., and Cárdenas, J. (1989). Changes in glutamate dehydrogenase activity of *Chlamydomonas reinhardili* under different trophic and stress conditions. *Plant Cell Environ.* 12, 173–182. doi: 10.1111/j.1365-3040.1989.tb01930.x

Mugford, S. T., Louveau, T., Melton, R., Qi, X., Bakht, S., Hill, L., et al. (2013). Modularity of plant metabolic gene clusters: a trio of linked genes that are collectively required for acylation of triterpenes in oat. *Plant Cell* 25, 1078–1092. doi: 10.1105/tpc.113.110551

Mur, L. A. J., Mandon, J., Persijn, S., Cristescu, S. M., Moshkov, I. E., Novikova, G. V., et al. (2013). Nitric oxide in plants: an assessment of the current state of knowledge. *AoB Plants* 5:pls052. doi: 10.1093/aobpla/pls052

Narendja, F., Goller, S. P., Wolschek, M., and Strauss, J. (2002). Nitrate and the GATA factor AreA are necessary for *in vivo* binding of *NirA*, the pathway-specific transcriptional activator of *Aspergillus nidulans*. *Mol. Microbiol.* 44, 573–583. doi: 10.1046/j.1365-2958.2002.02911.x

Navarro, M. T., Guerra, E., Fernández, E., and Galván, A. (2000). Nitrite reductase mutants as an approach to understanding nitrate assimilation in *Chlamydomonas reinhardtii*. *Plant Physiol.* 122, 283–290. doi: 10.1104/pp.122.1.283

Neupert, J., Shao, N., Lu, Y., and Bock, R. (2012). Genetic transformation of the model green alga *Chlamydomonas reinhardtii*. *Methods Mol. Biol.* 847, 35–47. doi: 10.1007/978-1-61779-558-9_4

Ninfa, A. J., and Jiang, P. (2005). PII signal transduction proteins: sensors of α-ketoglutarate that regulate nitrogen metabolism. *Curr. Opin. Microbiol.* 8, 168–173. doi: 10.1016/j.mib.2005.02.011

Nützmann, H. W., and Osbourn, A. (2015). Regulation of metabolic gene clusters in Arabidopsis thaliana. *New Phytol.* 205, 503–510. doi: 10.1111/nph.13189

Okamoto, M., Kumar, A., Li, W., Wang, Y., Siddiqi, M. Y., Crawford, N. M., et al. (2006). High-affinity nitrate transport in roots of *Arabidopsis* depends on expression of the *NAR2*-like gene *AtNRT3.1*. *Plant Physiol.* 140, 1036–1046. doi: 10.1104/pp.105.074385

Orsel, M., Chopin, F., Leleu, O., Smith, S. J., Krapp, A., Daniel-Vedele, F., et al. (2006). Characterization of a two-component high-affinity nitrate uptake system in *Arabidopsis*. Physiology and protein-protein interaction. *Plant Physiol.* 142, 1304–1317. doi: 10.1104/pp.106.085209

Osbourn, A., Papadopoulou, K. K., Qi, X., Field, B., and Wegel, E. (2012). Finding and analyzing plant metabolic gene clusters. *Methods Enzymol.* 517, 113–138. doi: 10.1016/B978-0-12-404634-4.00006-1

Pao, S. S., Paulsen, I. T., and Saier, M. H. (1998). Major facilitator superfamily. *Microbiol. Mol. Biol. Rev.* 62, 1–34.

Peakman, T., Crouzet, J., Mayaux, J. F., Busby, S., Mohan, S., Harborne, N., et al. (1990). Nucleotide sequence, organisation and structural analysis of the products of genes in the *nirB-cysG* region of the *Escherichia coli* K-12 chromosome. *Eur. J. Biochem.* 191, 315–323. doi: 10.1111/j.1432-1033.1990.tb19125.x

Perazzolli, M., Dominici, P., Romero-Puertas, M. C., Zago, E., Zeier, J., Sonoda, M., et al. (2004). *Arabidopsis* nonsymbiotic hemoglobin AHb1 modulates nitric oxide bioactivity. *Plant Cell* 16, 2785–2794. doi: 10.1105/tpc.104.025379

Poulos, T. L. (2006). Soluble guanylate cyclase. *Curr. Opin. Struct. Biol.* 16, 736–743. doi: 10.1016/j.sbi.2006.09.006

Qin, S., Lin, H., and Jiang, P. (2012). Advances in genetic engineering of marine algae. *Biotechnol. Adv.* 30, 1602–1613. doi: 10.1016/j.biotechadv.2012.05.004

Quesada, A., and Fernández, E. (1994). Expression of nitrate assimilation related genes in *Chlamydomonas reinhardtii*. *Plant Mol. Biol.* 24, 185–194. doi: 10.1007/BF00040584

Quesada, A., Galván, A., and Fernández, E. (1994). Identification of nitrate transporter genes in *Chlamydomonas reinhardtii*. *Plant J.* 5, 407–419. doi: 10.1111/j.1365-313X.1994.00407.x

Quesada, A., Galván, A., Schnell, R. A., Lefebvre, P. A., and Fernández, E. (1993). Five nitrate assimilation-related *loci* are clustered in *Chlamydomonas reinhardtii*. *Mol. Gen. Genet.* 240, 387–394.

Quesada, A., Gómez, I., and Fernández, E. (1998a). Clustering of the nitrite reductase gene and a light-regulated gene with nitrate assimilation loci in *Chlamydomonas reinhardtii*. *Planta* 206, 259–265. doi: 10.1007/s004250050398

Quesada, A., Hidalgo, J., and Fernández, E. (1998b). Three Nrt2 genes are differentially regulated in *Chlamydomonas reinhardtii*. *Mol. Gen. Genet.* 258, 373–377. doi: 10.1007/s004380050743

Rathod, J. P., Prakash, G., Pandit, R., and Lali, A. M. (2013). Agrobacterium-mediated transformation of promising oil-bearing marine algae *Parachlorella kessleri*. *Photosyn. Res.* 118, 141–146. doi: 10.1007/s11120-013-9930-2

Rexach, J., Fernández, E., and Galván, A. (2000). The *Chlamydomonas reinhardtii Nar1* gene encodes a chloroplast membrane protein involved in nitrite transport. *Plant Cell* 12, 1441–1453. doi: 10.1105/tpc.12.8.1441

Rice, S. L., Boucher, L. E., Schlessman, J. L., Preimesberger, M. R., Bosch, J., and Lecomte, J. T. J. (2015). Structure of *Chlamydomonas reinhardtii* THB1, a group 1 truncated hemoglobin with a rare histidine-lysine heme ligation. *Acta Crystallogr. F Struct. Biol. Commun.* 71, 718–725. doi: 10.1107/S2053230X15006949

Rockel, P., Strube, F., Rockel, A., Wildt, J., and Kaiser, W. M. (2002). Regulation of nitric oxide (NO) production by plant nitrate reductase *in vivo* and *in vitro*. *J. Exp. Bot.* 53, 103–110. doi: 10.1093/jexbot/53.366.103

Rosales, E. P., Iannone, M. F., Groppa, M. D., and Benavides, M. P. (2011). Nitric oxide inhibits nitrate reductase activity in wheat leaves. *Plant Physiol. Biochem.* 49, 124–130. doi: 10.1016/j.plaphy.2010.10.009

Rybalkin, S. D., Rybalkina, I. G., Shimizu-Albergine, M., Tang, X.-B., and Beavo, J. A. (2003). PDE5 is converted to an activated state upon cGMP binding to the GAF A domain. *EMBO J.* 22, 469–478. doi: 10.1093/emboj/cdg051

Sakihama, Y., Nakamura, S., and Yamasaki, H. (2002). Nitric oxide production mediated by nitrate reductase in the green alga *Chlamydomonas reinhardtii*: an alternative NO production pathway in photosynthetic organisms. *Plant Cell Physiol.* 43, 290–297. doi: 10.1093/pcp/pcf034

Sanz-Luque, E., Ocaña-Calahorro, F., de Montaigu, A., Chamizo-Ampudia, A., Llamas, A., Galván, A., et al. (2015). THB1, a truncated hemoglobin, modulates nitric oxide levels and nitrate reductase activity. *Plant J.* 81, 467–479. doi: 10.1111/tpj.12744

Sanz-Luque, E., Ocaña-Calahorro, F., Llamas, A., Galvan, A., and Fernandez, E. (2013). Nitric oxide controls nitrate and ammonium assimilation in *Chlamydomonas reinhardtii*. *J. Exp. Bot.* 64, 3373–3383. doi: 10.1093/jxb/ert175

Scheible, W. R. (2004). Genome-wide reprogramming of primary and secondary metabolism, protein synthesis, cellular growth processes, and the regulatory infrastructure of *Arabidopsis* in response to nitrogen. *Plant Physiol.* 136, 2483–2499. doi: 10.1104/pp.104.047019

Schmollinger, S., Mühlhaus, T., Boyle, N. R., Blaby, I. K., Casero, D., Mettler, T., et al. (2014). Nitrogen-sparing mechanisms in *Chlamydomonas* affect the transcriptome, the proteome, and photosynthetic metabolism. *Plant Cell* 26, 1410–1435. doi: 10.1105/tpc.113.122523

Sekine, K., Sakakibara, Y., Hase, T., and Sato, N. (2009). A novel variant of ferredoxin-dependent sulfite reductase having preferred substrate specificity for nitrite in the unicellular red alga *Cyanidioschyzon merolae*. *Biochem. J.* 423, 91–98. doi: 10.1042/BJ20090581

Slot, J. C., and Hibbett, D. S. (2007). Horizontal transfer of a nitrate assimilation gene cluster and ecological transitions in fungi: a phylogenetic study. *PLoS ONE* 2:e1097. doi: 10.1371/journal.pone.0001097

Solomonson, L. P., Barber, M. J., Robbins, A. P., and Oaks, A. (1986). Functional domains of assimilatory NADH:nitrate reductase from *Chlorella*. *J. Biol. Chem.* 261, 11290–11294.

Stewart, J. J., and Coyne, K. J. (2011). Analysis of raphidophyte assimilatory nitrate reductase reveals unique domain architecture incorporating a 2/2 hemoglobin. *Plant Mol. Biol.* 77, 565–575. doi: 10.1007/s11103-011-9831-8

Stöhr, C., Strube, F., Marx, G., Ullrich, W. R., and Rockel, P. (2001). A plasma membrane-bound enzyme of tobacco roots catalyses the formation of nitric oxide from nitrite. *Planta* 212, 835–841. doi: 10.1007/s004250000447

Sun, H., Li, J., Song, W., Tao, J., Huang, S., Chen, S., et al. (2015). Nitric oxide generated by nitrate reductase increases nitrogen uptake capacity by inducing lateral root formation and inorganic nitrogen uptake under partial nitrate nutrition in rice. *J. Exp. Bot.* 66, 2449–2459. doi: 10.1093/jxb/erv030

Sun, Y., Gao, X., Li, Q., Zhang, Q., and Xu, Z. (2006). Functional complementation of a nitrate reductase defective mutant of a green alga *Dunaliella viridis* by introducing the nitrate reductase gene. *Gene* 377, 140–149. doi: 10.1016/j.gene.2006.03.018

Suppmann, B., and Sawers, G. (1994). Isolation and characterization of hypophosphite–resistant mutants of *Escherichia coli*: identification of the FocA protein, encoded by the *pfl* operon, as a putative formate transporter. *Mol. Microbiol.* 11, 965–982. doi: 10.1111/j.1365-2958.1994.tb00375.x

Talebi, A. F., Tohidfar, M., Tabatabaei, M., Bagheri, A., Mohsenpor, M., and Mohtashami, S. K. (2013). Genetic manipulation, a feasible tool to enhance unique characteristic of *Chlorella vulgaris* as a feedstock for biodiesel production. *Mol. Biol. Rep.* 40, 4421–4428. doi: 10.1007/s11033-013-2532-4

Thompson, A. W., Foster, R. A., Krupke, A., Carter, B. J., Musat, N., Vaulot, D., et al. (2012). Unicellular cyanobacterium symbiotic with a single-celled eukaryotic alga. *Science* 337, 1546–1550. doi: 10.1126/science.1222700

Tischner, R., Planchet, E., and Kaiser, W. M. (2004). Mitochondrial electron transport as a source for nitric oxide in the unicellular green alga *Chlorella sorokiniana*. *FEBS Lett.* 576, 151–155. doi: 10.1016/j.febslet.2004.09.004

Tong, Y., Zhou, J.-J., Li, Z., and Miller, A. J. (2004). A two-component high-affinity nitrate uptake system in barley. *Plant J.* 41, 442–450. doi: 10.1111/j.1365-313X.2004.02310.x

Tsay, Y.-F., Chiu, C.-C., Tsai, C.-B., Ho, C.-H., and Hsu, P.-K. (2007). Nitrate transporters and peptide transporters. *FEBS Lett.* 581, 2290–2300. doi: 10.1016/j.febslet.2007.04.047

Uhrig, R. G., Ng, K. K. S., and Moorhead, G. B. G. (2009). PII in higher plants: a modern role for an ancient protein. *Trends Plant Sci.* 14, 505–511. doi: 10.1016/j.tplants.2009.07.003

Vallon, O., and Spalding, M. H. (2009). "Amino acid metabolism," in *The Chlamydomonas Sourcebook*, eds D. Stern and E. Harris (San Diego, CA: Academic Press), 115–158. doi: 10.1016/B978-0-12-370873-1.00012-5

Vázquez-Limón, C., Hoogewijs, D., and Vinogradov, S. N., Arredondo-Peter, R. (2012). The evolution of land plant hemoglobins. *Plant Sci.* 192, 71–81. doi: 10.1016/j.plantsci.2012.04.013

Wang, J., Krizowski, S., Fischer-Schrader, K., Niks, D., Tejero, J., Sparacino-Watkins, C., et al. (2014a). Sulfite oxidase catalyzes single-electron transfer at molybdenum domain to reduce nitrite to nitric oxide. *Antioxid. Redox Signal.* 23, 283–294. doi: 10.1089/ars.2013.5397

Wang, P., Du, Y., Li, Y., Ren, D., and Song, C.-P. (2010). Hydrogen peroxide-mediated activation of MAP kinase 6 modulates nitric oxide biosynthesis and signal transduction in *Arabidopsis*. *Plant Cell* 22, 2981–2998. doi: 10.1105/tpc.109.072959

Wang, P., Du, Y., and Song, C.-P. (2014b). Phosphorylation by MPK6. *Plant Signal. Behav.* 6, 889–891. doi: 10.4161/psb.6.6.15308

Wang, Y. (2006). S-Nitrosylation: an emerging redox-based post-translational modification in plants. *J. Exp. Bot.* 57, 1777–1784. doi: 10.1093/jxb/erj211

Wang, Y., and Spalding, M. H. (2014). Acclimation to very low CO2: contribution of limiting CO2 inducible proteins, LCIB and LCIA, to inorganic carbon uptake in *Chlamydomonas reinhardtii*. *Plant Physiol.* 166, 2040–2050. doi: 10.1104/pp.114.248294

Wei, L., Derrien, B., Gautier, A., Houille-Vernes, L., Boulouis, A., Saint-Marcoux, D., et al. (2014). Nitric oxide-triggered remodeling of chloroplast bioenergetics and thylakoid proteins upon nitrogen starvation in *Chlamydomonas reinhardtii*. *Plant Cell* 26, 353–372. doi: 10.1105/tpc.113.120121

Williams, L. E., and Miller, A. J. (2001). Transporters responsible for the uptake and partitioning of nitrogenous solutes. *Annu. Rev. Plant Physiol. Plant Mol. Biol.* 52, 659–688. doi: 10.1146/annurev.arplant.52.1.659

Wilson, I. D., Neill, S. J., and Hancock, J. T. (2008). Nitric oxide synthesis and signalling in plants. *Plant Cell Environ.* 31, 622–631. doi: 10.1111/j.1365-3040.2007.01761.x

Wisecaver, J. H., and Rokas, A. (2015). Fungal metabolic gene clusters-caravans traveling across genomes and environments. *Front. Microbiol.* 6:161. doi: 10.3389/fmicb.2015.00161

Xu, G., Fan, X., and Miller, A. J. (2012). Plant nitrogen assimilation and use efficiency. *Annu. Rev. Plant Biol.* 63, 153–182. doi: 10.1146/annurev-arplant-042811-105532

Yamano, T., Iguchi, H., and Fukuzawa, H. (2013). Rapid transformation of *Chlamydomonas reinhardtii* without cell-wall removal. *J. Biosci. Bioeng.* 115, 691–694. doi: 10.1016/j.jbiosc.2012.12.020

Yamano, T., Sato, E., Iguchi, H., Fukuda, Y., and Fukuzawa, H. (2015). Characterization of cooperative bicarbonate uptake into chloroplast stroma in the green alga *Chlamydomonas reinhardtii*. *Proc. Natl. Acad. Sci. U.S.A.* 112, 7315–7320. doi: 10.1073/pnas.1501659112

Yamasaki, H., and Sakihama, Y. (2000). Simultaneous production of nitric oxide and peroxynitrite by plant nitrate reductase: *in vitro* evidence for the NR-dependent formation of active nitrogen species. *FEBS Lett.* 468, 89–92. doi: 10.1016/S0014-5793(00)01203-5

Yang, J., Giles, L. J., Ruppelt, C., Mendel, R. R., Bittner, F., and Kirk, M. L. (2015). Oxyl and hydroxyl radical transfer in mitochondrial amidoxime reducing component-catalyzed nitrite reduction. *J. Am. Chem. Soc.* 137, 5276–5279. doi: 10.1021/jacs.5b01112

Zhao, M. G., Chen, L., Zhang, L. L., and Zhang, W. H. (2009). Nitric reductase-dependent nitric oxide production is involved in cold acclimation and freezing tolerance in *Arabidopsis*. *Plant Physiol.* 151, 755–767. doi: 10.1104/pp.109.140996

Zhou, J. J., Fernández, E., Galvan, A., and Miller, A. J. (2000). A high affinity nitrate transport system from *Chlamydomonas* requires two gene products. *FEBS Lett.* 466, 225–227. doi: 10.1016/S0014-5793(00)01085-1

Zhou, J., and Kleinhofs, A. (1996). Molecular evolution of nitrate reductase genes. *J. Mol. Evol.* 42, 432–442. doi: 10.1007/BF02498637

Proteomic Analysis of a Fraction with Intact Eyespots of *Chlamydomonas reinhardtii* and Assignment of Protein Methylation

Nicole Eitzinger[1†], Volker Wagner[2†], Wolfram Weisheit[2], Stefan Geimer[3], David Boness[1], Georg Kreimer[1†] and Maria Mittag[2†]*

[1] *Cell Biology, Department of Biology, Friedrich-Alexander-University Erlangen-Nuremberg, Erlangen, Germany,* [2] *Institute of General Botany and Plant Physiology, Faculty of Biology and Pharmacy, Friedrich Schiller University Jena, Jena, Germany,* [3] *Cell Biology and Electron Microscopy, University of Bayreuth, Bayreuth, Germany*

Flagellate green algae possess a visual system, the eyespot. In *Chlamydomonas reinhardtii* it is situated at the edge of the chloroplast and consists of two carotenoid rich lipid globule layers subtended by thylakoid membranes (TM) that are attached to both chloroplast envelope membranes and a specialized area of the plasma membrane (PM). A former analysis of an eyespot fraction identified 203 proteins. To increase the understanding of eyespot related processes, knowledge of the protein composition of the membranes in its close vicinity is desirable. Here, we present a purification procedure that allows isolation of intact eyespots. This gain in intactness goes, however, hand in hand with an increase of contaminants from other organelles. Proteomic analysis identified 742 proteins. Novel candidates include proteins for eyespot development, retina-related proteins, ion pumps, and membrane-associated proteins, calcium sensing proteins as well as kinases, phosphatases and 14-3-3 proteins. Methylation of proteins at Arg or Lys is known as an important posttranslational modification involved in, e.g., signal transduction. Here, we identify several proteins from eyespot fractions that are methylated at Arg and/or Lys. Among them is the eyespot specific SOUL3 protein that influences the size and position of the eyespot and EYE2, a protein important for its development.

Keywords: ATP synthase, *Chlamydomonas reinhardtii*, EYE2, eyespot proteome, phototaxis, protein methylation, SOUL heme-binding protein 3

INTRODUCTION

Many motile algae exhibit a peculiar photo-behavior: movement toward or away from the light source depending on the light intensity and quality. This behavior is known as positive or negative phototaxis. To allow such precise movement responses, many flagellate algae of all major phylogenetic lineages have developed specialized optical devices (eyespots), which are antennae that determine the direction of incident light (Foster and Smyth, 1980; Kreimer, 1994, 2009). In some warnowiid dinoflagellates, this structure is extremely complex and called ocelloid. Its ultrastructure bears apparent resemblance to camera-type eyes of some animals and has recently

been shown to be composed of different specialized cell organelles such as plastids, mitochondria, and vesicles. The occelloid is probably homologous to simpler dinoflagellate eyespot types, most of which involve parts of the chloroplasts (Dodge, 1984; Kawai and Kreimer, 2000; Gavelis et al., 2015; Hayakawa et al., 2015). In green algae, the functional eyespot is also a composed "organelle", involving local specializations from different subcellular compartments and highly ordered

carotenoid-rich globules inside the chloroplast. It is peripherally located in the cell and readily observable by bright-field microscopy as an orange- to red-colored spot (Melkonian and Robenek, 1984; Kreimer, 2009). In *Chlamydomonas reinhardtii*, the eyespot typically consists of two highly ordered layers of such globules, each subtended by a thylakoid (see **Figure 1A** for a schematic drawing). The outermost globule layer is attached to specialized areas of both the chloroplast envelope
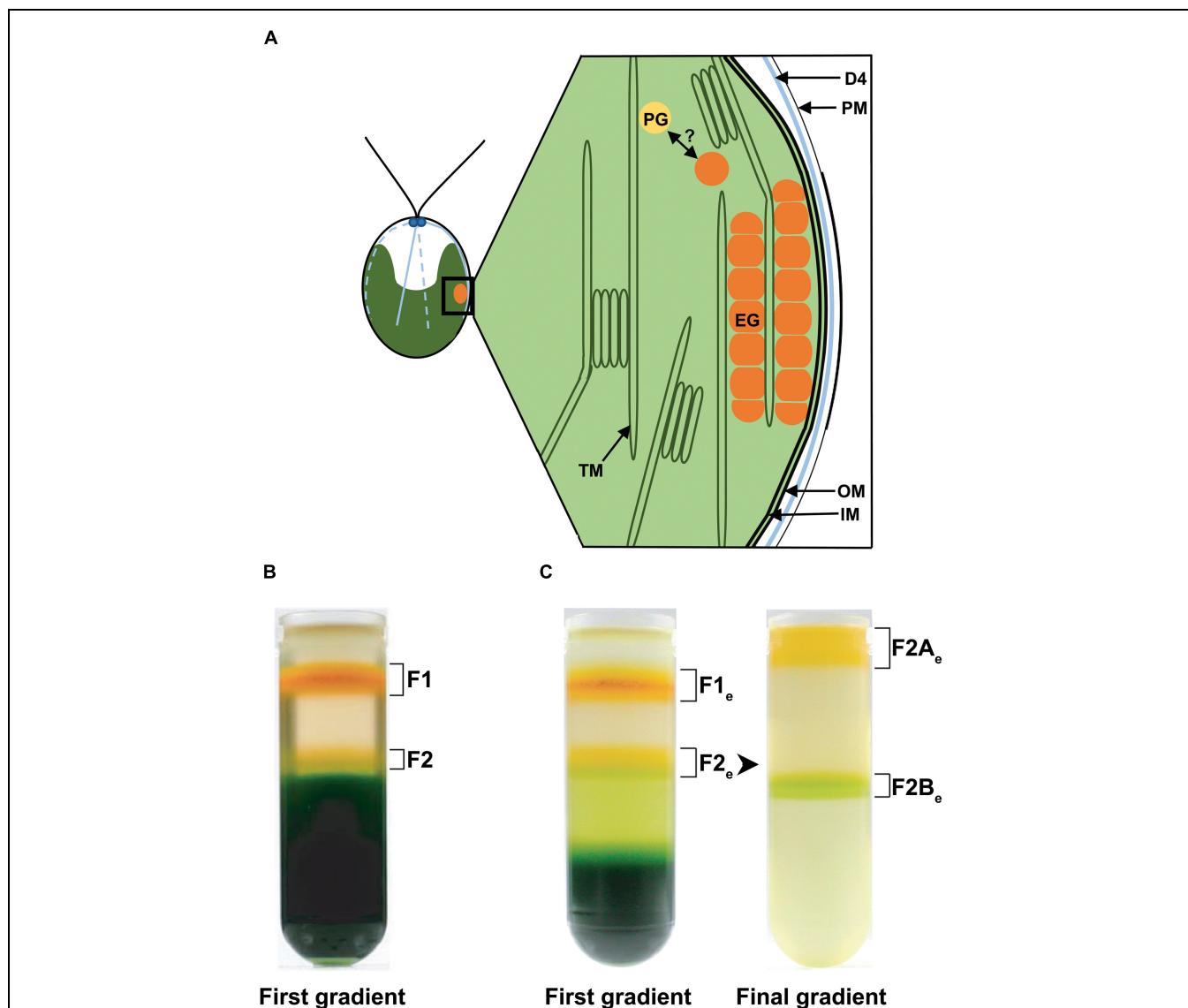
FIGURE 1 | Schematic drawing of the eyespot in *Chlamydomonas reinhardtii* and distribution of different fractions enriched in eyespots after flotation on discontinuous sucrose gradients. (A) Schematic longitudinal section through the eyespot in the region of the four stranded microtubular root (D4), which is important for eyespot positioning. The functional eyespot consists of local specializations of different compartments. The part of the plasma membrane (PM) overlying the eyespot globules (EG) is thickened and in close association with the inner and outer chloroplast envelope (IM/OM). The EG are in contact with the thylakoid membrane (TM) and arranged in layers, the outermost being also in contact with the chloroplast envelope. The possible link between plastoglobules (PG) and EG is indicated. **(B)** Separation of the cell homogenate in the first gradient using the established eyespot isolation method by Schmidt et al. (2006). **(C)** Separation of the cell homogenate in the first gradient using the here described (see Materials and Methods) modified cell rupture method for an extended ("e") eyespot fraction; separation of fraction 2 (F2$_e$) from these gradients in fraction 2A (F2A$_e$) and 2B (F2B$_e$) in the final gradient. Note the increased amount of F2$_e$ and the decreased amount of F1$_e$ and thylakoid debris in comparison to the original cell rupture method.

and the adjacent PM. The globule layers modulate the light intensity reaching the photoreceptors in the PM patch as the cell rotates around its longitudinal axis during forward swimming. They function as a combined absorption screen and quarter-wave interference reflector. Thereby, the contrast at the photoreceptors is increased up to eightfold, making the whole optical system highly directional (Foster and Smyth, 1980; Kreimer and Melkonian, 1990; Harz et al., 1992; Kreimer et al., 1992). Beside its function as a sensor for light direction and quality, the eyespot might have potential additional roles mainly for chloroplast function. There is, e.g., increasing evidence from both, ultrastructural and proteomic data, for a link between eyespot globules (EG) and plastoglobules (PG) and thereby for a more general role in chloroplast metabolism such as the biosynthesis of prenylquinones and carotenoids (Kreimer, 2009; Nacir and Bréhélin, 2013; Davidi et al., 2015). Whereas PG are directly connected with the thylakoids via the outer lipid leaflet of the TM (Austin et al., 2006), it is currently not known whether this is also true for the globules of the eyespot. Methods for the isolation of PG from green algae as well as EG and fragments are established (Kreimer et al., 1991; Renninger et al., 2001; Schmidt et al., 2006; Davidi et al., 2015).

Until 2005, only six proteins relevant to the structure and function of the eyespot of *C. reinhardtii* were identified, mainly based on genetic approaches. These included EYE2 and MIN1, two proteins important for eyespot assembly (Roberts et al., 2001; Dieckmann, 2003), two splicing variants of the abundant retinal binding protein COP, and the two unique seven-transmembrane domain photoreceptors, Channelrhodopsin1 (ChR1), and ChR2 serving as basis for the development of optogenetics (Deininger et al., 1995; Fuhrmann et al., 2001; Nagel et al., 2002; Sineshchekov et al., 2002; Suzuki et al., 2003; Hegemann and Nagel, 2013). As an in depth knowledge of the protein composition of this complex organelle is one prerequisite to understand its function at a molecular level, also proteomic approaches to a fraction strongly enriched in eyespot fragments were applied. Thereby, 203 different proteins covered with at least two different peptides were identified and some of them were shown to be phosphorylated (Schmidt et al., 2006; Wagner et al., 2008). Based on these proteomic approaches, recent functions in eyespot development have been demonstrated for SOUL3, one of the five SOUL heme-binding proteins in *C. reinhardtii* (Merchant et al., 2007; Schulze et al., 2013), Casein kinase 1 and the blue-light receptor Phototropin (Schmidt et al., 2006; Trippens et al., 2012). Additionally, evidence for a specialized localization of the alpha- and beta-subunit of the chloroplast ATP synthase and thereby probably function within the eyespot was found (Schmidt et al., 2007). The eyespots used in the proteomic approach by Schmidt et al. (2006) retained, however, only small parts of the eyespot membranes. Thus, it is well feasible that core membrane-associated eyespot proteins were not identified in this study. To further increase the understanding of eyespot related signaling processes in depth, knowledge of the protein composition of the membranes in its close vicinity is desirable. We thus developed a method that allows isolation of intact eyespots containing the two layers of lipid rich globules still associated with large parts of the

eyespot membranes and the adjacent PM as well as chloroplast envelope areas and analyzed this fraction by a proteomic approach.

Beside phosphorylation, protein methylation is an important posttranslational modification involved in the regulation of protein stability, localization, activity, and protein–protein interactions (Reinders and Sickmann, 2007; Biggar and Li, 2015). The importance of protein methylation at Arg and Lys residues in regulating protein activity is also becoming apparent in vascular plants and algae (e.g., Deng et al., 2010; Blifernez et al., 2011; Werner-Peterson and Sloboda, 2013). Recently, Arg and Lys methylation was reported for several chloroplast proteins (Alban et al., 2014). We therefore assigned protein methylation sites in the previous and currently analyzed eyespot fractions. In this study, we identify 742 proteins of the extended eyespot fraction, including numerous membrane-associated proteins as intended beside other candidates for eyespot development and signaling. We also assign protein methylation sites on two proteins with already demonstrated important functions for the eyespot (SOUL3 and EYE2; Roberts et al., 2001; Boyd et al., 2011; Schulze et al., 2013) and on 23 other proteins from the eyespot fractions, among them the alpha-, beta- and I-subunits of the chloroplast ATP synthase and a 14-3-3 protein.

MATERIALS AND METHODS

Isolation of the Different Eyespot Fractions

Growth of 20 L *C. reinhardtii* strain cw15 to late log-phase and isolation of fraction 1 (**Figure 1B**) enriched in eyespot fragments was done as previously described (Schmidt et al., 2006). The isolation of a fraction enriched in largely intact eyespots (F2A$_e$ in **Figure 1C**) was achieved by reducing the power and duration of the ultrasonic treatment (Bandelin Sonopuls HD2070, Microtip HS 73) to 16% output and seven cycles (15 s each interrupted by 15 s of cooling) during cell rupture. In addition, the submersion depth of the sonotrode tip was reduced to 1.5 cm. Eyespot fragments were separated by discontinuous sucrose gradients buffered with gradient stock solution (GSS) consisting of 12.5 mL sample brought to 42% (w/v) sucrose, 10 mL 31.8% (w/w), and 10 mL 20.5% (w/w) sucrose, overlaid with 5.5 mL GSS. After centrifugation (100,000 g, 105 min, 4°C), the orange-green bands (F2$_e$ in **Figure 1C**) at the interface of 20.5 and 31.8% sucrose were collected and brought to 35% (w/v) sucrose. Fraction F2$_e$ was further purified by flotation centrifugation (100,000 g, 60 min, 4°C) on discontinuous sucrose gradients (15 mL sample, 3 mL 31.8% [w/w] sucrose, 18 mL 25% [w/w] sucrose, and 2 mL 20.5% [w/w] sucrose). The yellow–orange 20.5% sucrose fractions (F2A$_e$) were collected and brought to 32% (w/v) sucrose. For concentration, 10 ml of this fraction were layered on 26 mL 42% (w/w) sucrose overlaid by 2 mL GSS and centrifuged again (100,000 g, 45 min, 4°C). The concentrated fraction F2A$_e$ was collected from the top of the gradient, directly extracted with chloroform:methanol:water (4:8:3) and the precipitated proteins were washed several times with methanol:chloroform (2:1, v/v)

to remove lipids and pigments before they were dissolved in 2x SDS sample buffer. Cell harvesting, buffers and all other treatments were otherwise done as described by Schmidt et al. (2006).

Crude Extract Preparation and Electrophoretic Methods

Log phase cultures were supplemented directly prior to cell harvesting with 1 mM phenylmethylsulfonyl fluoride (PMSF). Cells were harvested by centrifugation (2000 g, 10 min, 4°C), and pellets were suspended in TNED buffer (20 mM Tris, 80 mM NaCl, 1 mM EDTA, and 1 mM DTT, pH 7.5) supplemented with 1 mM PMSF and complete protease inhibitor cocktail (Roche), according to the instructions of the supplier. In the case of the cell-wall less strain cw15, aliquots (300 μl) of the suspended cells were directly mixed with methanol:chloroform (2:1, v:v; 1200 μL) for parallel protein precipitation and lipid/pigment removal. Cell wall-possessing strains were homogenized by sonication. Protein solubilization, SDS-PAGE and protein staining with silver or colloidal Coomassie were conducted as described by Schmidt et al. (2006). Gel loading based on equal protein content and immunoblot analyses followed standard techniques. Incubations with the monoclonal anti-modified (monomethyl, asymmetric dimethyl, and symmetric dimethyl) methyl-arginine antibody 7E6 (anti-Rm; company Covalab SAS, France, 1:2,500) were done overnight at 4°C.

Electron Microscopy

For fixation, aliquots of F2A$_e$ were diluted 1:1 with ice-cold 40% (w/v) BSA in GSS and mixed with cold glutaraldehyde (final concentration 3.1 or 6.3 %). The BSA/F2A$_e$ gel pieces were sliced in small pieces and fixed overnight in 25 mM Hepes/NaOH (pH 7.8) and 3.5% glutaraldehyde at 4°C. Samples were washed three times for 10 min with 25 mM Hepes/NaOH (pH 7.8) prior to a 2 h incubation at 4°C with osmium tetroxide (1% in 25 mM Hepes/NaOH, pH 7.8), followed by four washing steps with Millipore water. Dehydration, embedding in Epon and staining of ultrathin sections with uranyl acetate/lead citrate was done as described (Reynolds, 1963; Renninger et al., 2001). EM negatives were scanned and processed with Photoshop (Adope Systems).

Mass Spectrometry (MS) Analysis

In-Gel Digestion and Nano HPLC Electrospray Ionization Tandem MS (LC-ESI-MS/MS)

The gel was dissected into 50 bands and each gel slice was subjected to a washing procedure followed by an in gel digestion with trypsin as previously described (Schmidt et al., 2006). The pellets containing the tryptic peptides were resuspended in 5 μL 5% (v/v) acetonitrile/0.1% (v/v) formic acid and subjected to nano LC-ESI-MS using an UltiMate^{TM} 3000 nano HPLC (Dionex Corporation) with a flow rate of 300 nL/min coupled on-line with a linear ion trap electrospray-ionization (ESI) mass spectrometer (Finnigian^{TM} LTQ^{TM}, Thermo Electron Corp.) as described previously (Schmidt et al., 2006). The mass spectrometer was cycling between one full MS and MS/MS scans of the four most abundant ions. After each cycle, these peptide masses were excluded from analysis for 3 min.

Data Analysis

Data analysis was done using the Proteome Discoverer software (Version 1.4) from Thermo Electron Corp. including the SEQUEST algorithm (Link et al., 1999). Searches were done for tryptic peptides allowing two missed cleavages. The software parameters were set to detect lysine modifications (+14.016 for monomethyl, +28.031 for dimethyl, and +42.047 for trimethyl) and arginine modifications (+14.016 for monomethyl and +28.031 for dimethyl) with a maximum of four modifications of one type per peptide. Further, detection of variable methionine oxidation (+15.995) was enabled. Peptide mass tolerance was set to 1.5 Da in MS mode. In MS^2 mode, fragment ion tolerance was set up to 1 Da. The parameters for all database searches were set to achieve a false discovery rate (FDR) of not more than 1% for each individual analysis (Veith et al., 2009). All spectra used for the assignment of protein methylation were in addition manually validated and checked for the presence of the b- and/or y-type ions representing the methylation sites. In case that a methylation site is present on the first amino acid at the N-terminus of the peptide and therefore not present in the b- and y-type ions, these methylation sites were considered only when all other possible methylation sites in the peptide were validated as methylated or non-methylated, respectively. In case of trimethylated Lys residues, spectra were additionally screened for the presence of neutral loss events of trimethylamine (59 Da), which is a signature for trimethylation (Zhang et al., 2004; Erce et al., 2012). Data were searched against the *C. reinhardtii* database (Vs. 5.3.1), hosted by Phytozome (Vs. 9.1)[1], the mitochondrial database available from NCBI (NC001638, [gi:11467088]) and the chloroplast database[2]. Data from all runs were combined and further evaluated using an in house developed program. The peptide sequences of the gene models were compared to the NCBI protein database using BLAST (Altschul et al., 1997). For positive identification of both, protein and functional domain prediction, an internal cut-off E-value of 1e-05 was used. Transmembrane domain information was based on predictions by the programs TMHMM (Krogh et al., 2001), TMpred (Hofmann and Stoffel, 1993), and TopPred (von Heijnje, 1992). The GRAVY index was determined with ProtParam (Gasteiger et al., 2005). The mass spectrometry (MS) proteomics data have been deposited to the ProteomeXchange Consortium[3] via the PRIDE partner repository (Vizcaino et al., 2013) under the project description "Extended eyespot proteome and methylated proteins in the eyespot of *C. reinhardtii* strain cw15 (ID: PXD003254)".

Miscellaneous

Protein content was determined according to Neuhoff et al. (1979) with BSA as standard. Chlorophyll and carotenoids were determined as described by Lichtenthaler (1987). Spectra were recorded in 90% methanol with an Ultrospec 2100 pro (GE

---

[1]http://www.phytozome.net/chlamy.php

[2]http://www.chlamy.org/chloro/default.html

[3]http://proteomecentral.proteomexchange.org

Healtcare Life Science). Images of gradients, gels and blots were captured with a Coolpix 990 (Nikon) and processed with Photoshop (Adobe Systems).

RESULTS

Isolation and Characterization of a Fraction Enriched in Intact Eyespots

Based on a previously established method for the isolation of eyespot fragments from *C. reinhardtii* (Schmidt et al., 2006), we developed a procedure that allows the isolation of largely intact eyespot apparatuses. They contain the two layers of lipid rich globules with large parts of the eyespot associated membranes and adjacent PM areas. As a visual marker for enrichment of eyespots within the sucrose gradients, we first used the conspicuous yellow/orange to red color of the EG (**Figures 1B,C**). We noticed a deep orange-red fraction enriched in highly purified eyespot fragments (named F1; Schmidt et al., 2006), as well as an additional weak yellow–orange fraction (F2) apart from the bulk of the cell and chloroplast debris. F2 accumulates at the interface between 20.5 and 31.8% sucrose. At these sucrose concentrations, enrichment of largely intact eyespots with a high proportion of eyespot-associated membranes was described for the green alga *Spermatozopsis similis* (Kreimer et al., 1991). Thus, it seemed possible that the *Chlamydomonas* F2 fraction that was always present only in minute amounts may also bear intact eyespots. We therefore tried to optimize the yield of fraction F2 by variation of the ultrasonic treatment used for cell rupture. Best results were obtained upon a 50% reduction of the output power and cycle number (32 to 16% and 14 to 7 cycles) in combination with a reduction of the submersion depth of the sonotrode tip to 1.5 cm. For a clear differentiation between the different eyespot preparations, all fractions obtained by this modified cell rupture/purification strategy are characterized by the subscripted "e", which stands for extended eyespot. Although these reductions result in a clear loss in general cell rupture and thereby total yield of $F1_e$, the relative amount of $F2_e$, as judged by its color, was increased compared to the standard procedure (**Figures 1B,C**). $F2_e$ was further purified by an additional gradient centrifugation step to reduce contamination by thylakoids and other cell organelles. In this subsequent gradient, $F2_e$ splits up into two fractions: an orange–yellow ($F2A_e$) and a greenish-yellow ($F2B_e$) fraction (**Figure 1C**, final gradient). $F2A_e$ was finally concentrated by a floating centrifugation step. The total protein yields of $F2A_e$ varied between 28 and 46 μg when starting with 20 L of culture.

To verify enrichment of eyespots and to judge their intactness and purity, $F2A_e$ was analyzed by transmission electron microscopy (**Figure 2**). Indeed, a significant number of well-defined eyespots with intact globule layers are enriched in this fraction (**Figures 2A–D**). The close packing of the globules is largely preserved and the layers are still subtended by a thylakoid. The average size of the globules in these layers is well in the *in situ* range of 80–130 nm (Melkonian and Robenek, 1984). Analyses of 100 globules from different eyespots and sections yielded values of 114 ± 28 nm for the width and 121 ± 30 nm for the height,

respectively. Only a few EG were enlarged, probably by fusion. In addition, large parts of the chloroplast envelope, the PM and a fuzzy appearing material observed between the chloroplast envelope and the PM in the eyespot region *in situ* were frequently present (**Figures 2B,C**; Melkonian and Robenek, 1984; Kreimer, 2009). Additionally, less well-preserved eyespots predominantly with enlarged, possibly fused, globules were also observed (**Figure 2A**). Along with the intact eyespots, still possessing all eyespot membranes, varying amounts of the adjacent PM and chloroplast envelope were co-isolated (**Figures 2B,C**). Depending on their length, these membranes partially enwrapped the isolated eyespots as well as cell components not belonging to the functional eyespot, but located *in situ* in its close proximity like, e.g., grana thylakoids and ribosomes (**Figure 2C**). Major free contaminants were individualized fused globules associated with membranes, membrane vesicles of unknown origin as well as stroma and grana thylakoids (**Figures 2A,F**). Occasionally, also mitochondrial fragments were detected (**Figure 2E**). In summary, transmission electron microscopy confirmed enrichment of intact eyespots associated with all eyespot membranes. The gain in intactness of eyespots seems, however, accompanied by an inevitable increase of non-eyespot contaminants.

Spectral analysis of the pigments in fraction $F2A_e$ was performed for further characterization. The visual appearance of $F2A_e$ already indicates that carotenoids are strongly enriched. In vegetative cells of *C. reinhardtii*, carotenoids are found in the thylakoids, the chloroplast envelope and EG, whereas chlorophyll is solely present within thylakoids. A comparison of the amount of chlorophyll present in the crude extract (CE) with the amount of chlorophyll in fraction $F2A_e$ revealed that 0.015% of the total chlorophyll applied to the gradients remained there. The average carotenoid:chlorophyll ratio measured as the absorbance ratio 478 to 680 nm was 40 ± 12.6. These values indicate effective removal of the majority of free thylakoids not associated with the EG layers. Compared to fraction 1, however, these values are significantly higher (<0.0005% and 60–70; Schmidt et al., 2006). Spectra of methanol extracts of fraction $F2A_e$ were identical to those of fraction F1 in the range between 350 and 525 nm and revealed a typical carotenoid spectrum (**Figure 3A**). Major absorption peaks where at 446 and 470 nm and a shoulder at 423 nm.

The above analyses clearly shows that eyespot purity of the extended eyespot fraction $F2A_e$ was reduced compared to that of fraction F1 (Schmidt et al., 2006). Nonetheless, the significantly increased amount of eyespot associated membranes as well as of membrane areas adjacent to them in fraction $F2A_e$ offers the possibility to identify novel putative eyespot proteins and those present in close vicinity to this visual system via a proteomic approach. To get a first impression of possible differences in the protein patterns of the eyespot fractions, a comparative SDS-PAGE analysis was conducted (**Figure 3B**). As expected, the general protein pattern of the fractions enriched in eyespot fragments (F1) and intact eyespots ($F2A_e$) were similar to some extent indicating an overlap of a majority of proteins. In the complex protein patterns, however, also subtle but clear differences were resolved (see, e.g., the molecular mass ranges between 35 and 45 kDa and below 25 kDa). Their protein patterns
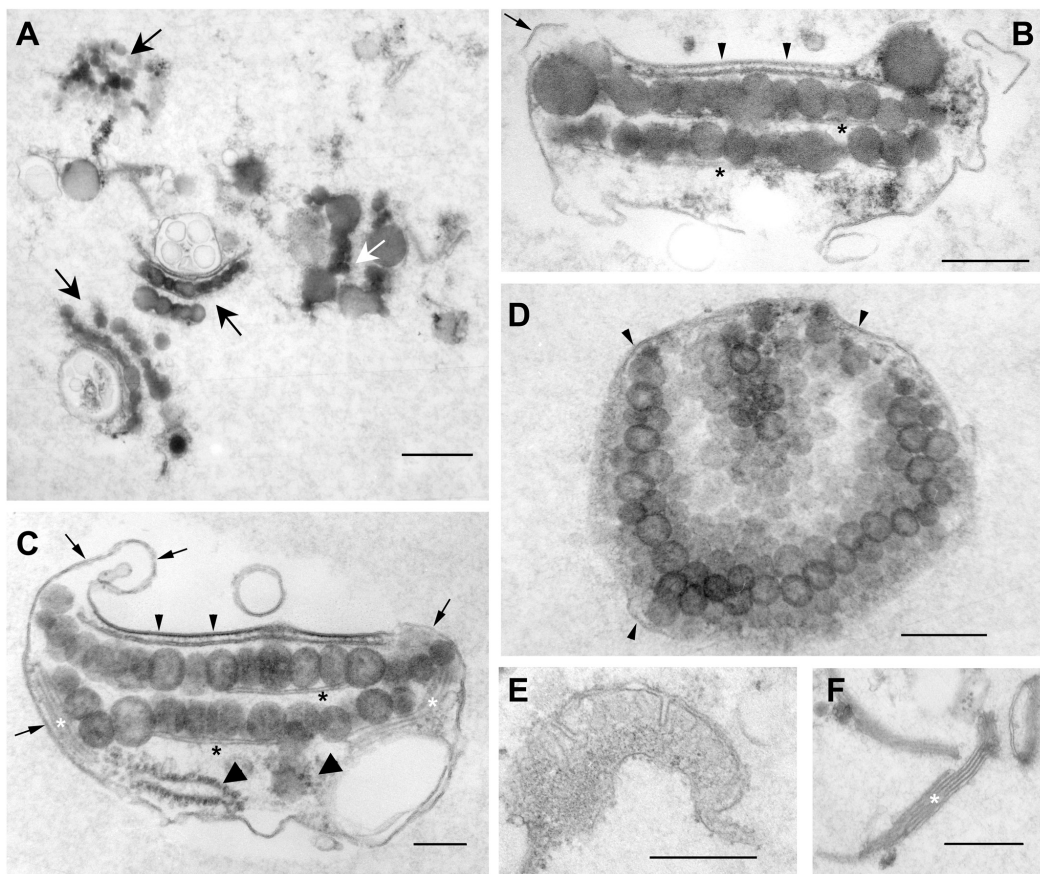
FIGURE 2 | Characterization of the extended eyespot fraction 2A (F2A$_e$) by transmission electron microscopy revealed enrichment of intact eyespots. Overview **(A)** and details **(B–F)**. **(A)** Black arrows indicate well-preserved eyespots, whereas the white arrow indicates structurally less well-preserved eyespots with fused EG; scale bar: 600 nm. **(B,C)** Cross-sections through isolated, double-layered eyespots associated with eyespot and other membranes. The globule layers are subtended by a thylakoid (black asterisk). Small arrowheads: plasma membrane area overlying the EG. Note the close association with the chloroplast envelope membranes and the thickened, electron-dense appearance of the plasma membrane in this region. In addition, the fuzzy fibrillar material typically observed *in situ* between the plasma membrane and chloroplast envelope in the region of the eyespot apparatus (Kreimer, 2009) is preserved. Small arrows point to normal plasma membrane regions tending to enwrap the globule layers and not eyespot-associated structures like a thylakoid stack (white asterisk) or ribosomes (large arrowheads); scale bars: 150 nm. **(D)** Tangential section through a globule layer. Arrowheads indicate membranes enclosing the eyespot; scale bar: 250 nm. **(E,F)** Co-isolated free mitochondrial fragment **(E)** and free thylakoid stack **(F)**; scale bars: 400 nm.
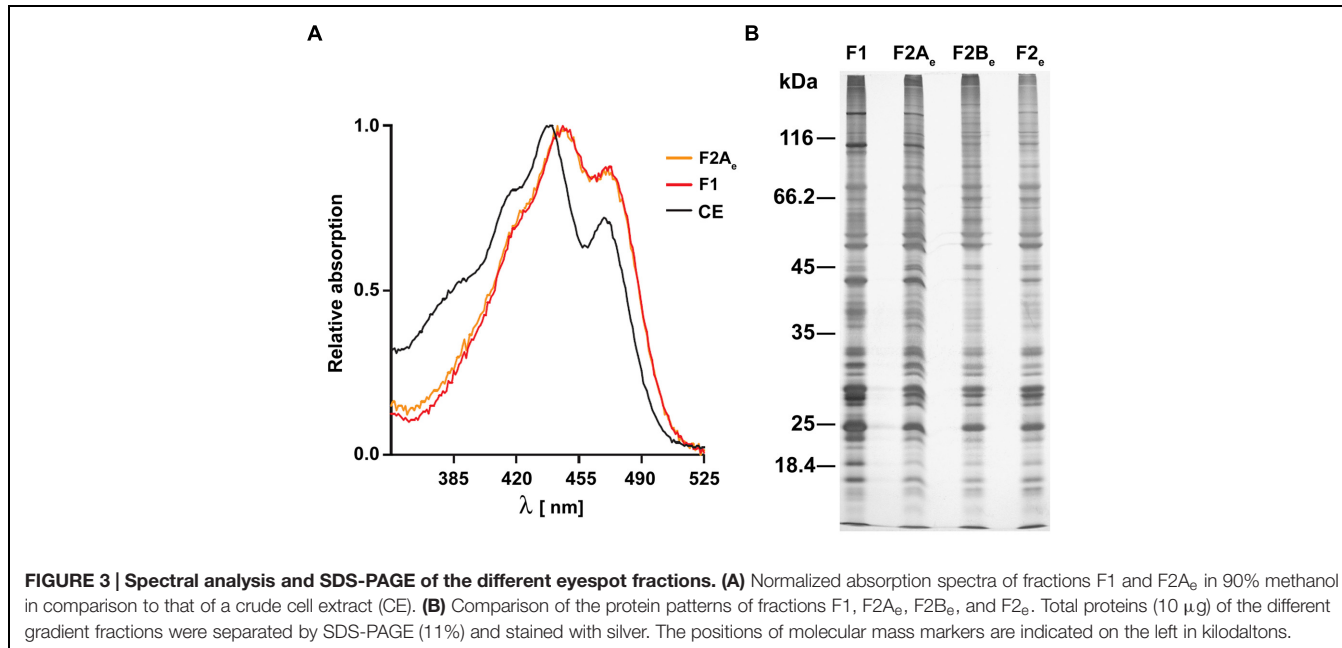
clearly differed also from those fractions with higher chlorophyll content (F2$_e$ and F2B$_e$). The protein pattern of fraction F2A$_e$ was highly reproducible in independent purifications [Supplemental Figure S1A (Data Sheet 1)].

The Proteome of the Extended Eyespot

To identify proteins of the enriched F2A$_e$ eyespot fraction by MS/MS, proteins from two independent eyespot isolations were combined, separated by SDS-PAGE and the gel was sliced into 50 pieces [Supplemental Figure S1B (Data Sheet 1)]. Following in-gel digestion with trypsin, the generated peptide fragments were subjected to LC-ESI-MS/MS analyses using a linear ion trap mass spectrometer (see Materials and Methods). In total, 742 proteins were identified with at least two different peptides and a FDR of ≤1. The majority of the 203 proteins identified in the former fraction F1 with at least two different peptides (Table 1 in Schmidt et al., 2006) were positively confirmed to be

present in the extended eyespot of F2A$_e$ [Supplemental Table S1 (Data Sheet 3) along with the currently identified peptides and values]. Supplemental Table S2 (Data Sheet 4) lists the 27 missing candidates, 10 of them (category ribosomes, translation, and DNA related) being obvious contaminants. Reasons for the differences are discussed later.

A selection of promising novel candidates with regard to eyespot development, signal transduction as well as membrane association and transporters is presented in **Table 1**. This selection is based on current knowledge about the eyespot apparatus, including its different complex associated subcellular structures as well as signaling pathways important for photoorientation, its development including mutant analysis as well as information on PG. Detailed information for all identified peptides of these selected candidates is given in Supplemental Table S3 (Data Sheet 5). We think that these categories enclose the primarily most interesting candidates to be

FIGURE 3 | Spectral analysis and SDS-PAGE of the different eyespot fractions. (A) Normalized absorption spectra of fractions F1 and F2A$_e$ in 90% methanol in comparison to that of a crude cell extract (CE). **(B)** Comparison of the protein patterns of fractions F1, F2A$_e$, F2B$_e$, and F2$_e$. Total proteins (10 µg) of the different gradient fractions were separated by SDS-PAGE (11%) and stained with silver. The positions of molecular mass markers are indicated on the left in kilodaltons.

studied functionally in the future. Supplemental Table S4 (Data Sheet 6) lists all further identified novel proteins along with their peptides from F2A$_e$ including also the putative contaminants. Among the novel candidates (**Table 1**), a protein involved in eyespot assembly, the Ser/Thr kinase EYE3 (Boyd et al., 2011), a retinal pigment epithelial membrane receptor as well as a protein with homologies to the eye pigment precursor transporter protein family (Vopalensky et al., 2012) were found. Moreover, two SOUL heme-binding proteins (SOUL2 and SOUL5) were identified. The so far known SOUL3 eyespot protein influences size and position of the eyespot (Schulze et al., 2013). Excitation of the ChR photoreceptors initiates a Ca^{2+}-based signaling cascade toward the flagella in the eyespot (reviewed by Hegemann and Berthold, 2009). Further, rapid reversible protein phosphorylation in isolated eyespots is strongly affected by free Ca^{2+} concentrations between 10^{-8} and 10^{-7} M (Linden and Kreimer, 1995) and both ChRs as well as SOUL3 are targets of kinases (Wagner et al., 2008). Therefore, the identification of six novel calcium-sensing and binding proteins as well as 11 different kinases and four phosphatases could be of high interest for understanding the signaling cascade network in the eyespot. Notably, a Ca^{2+}-dependent protein kinase 1 was identified with 11 different peptides. Moreover, two 14-3-3 proteins that interact with phosphorylated proteins and are key regulators in many vital cellular processes including signal transduction (Denison et al., 2011) were identified with eight and ten different peptides, respectively. Of note is also the fact that some of the kinases belong to the ABC1 kinase family such as EYE3 (**Table 1**). Homologs of two members of this family identified in the proteome of eyespot fraction F1 are present in PG of *Arabidopsis thaliana* and the beta-carotene PG of *Dunaliella bardawil* (Ytterberg et al., 2006; Lundquist et al., 2012; Davidi et al., 2015). Two of the newly identified ABC1 kinases with an AarF domain from the F2A$_e$ fraction [Cre09.g407800.t1.3 (AKC1),

Cre13.g570350.t1.3 (AKC4)] are also present in *Arabidopsis* PG (Lundquist et al., 2012). Additionally, AKC1 has a homolog in the plastoglobule proteome of *D. bardawil* (Davidi et al., 2015).

Among the novel candidates in the group of membrane associated/structural proteins are three PAP-fibrillin domain-containing proteins. Eight proteins of this group important for stabilization of PG and EG (Renninger et al., 2001; Ytterberg et al., 2006) were already identified in our previous analysis (Schmidt et al., 2006). In addition, Vesicle inducing protein in plastids (VIPP1) that is involved in the biogenesis of thylakoids (Rütgers and Schroda, 2013) has been also found with 11 different peptides (**Table 1**). VIPP1 was detected recently in an algal plastoglobule proteome and it was postulated that PG evolved from eyespot lipid droplets (Davidi et al., 2015). In addition, two fasciclin-like proteins with three and four FAS1 domains, respectively, might be of interest. FAS1 domains are present in many secreted, membrane-anchored proteins. Five transporters were found as well, underlining the enrichment of eyespot associated membranes (**Table 1**). In this group, identification of three P-type PM ATPases and a PM type Calmodulin-binding Ca^{2+}-transporting ATPase is of special interest. These types of proteins may be important for the resting membrane potential at the PM and thereby eventually also affect the excitation of the cell through the ChRs. As the currents of these photoreceptors are carried by Ca^{2+}, its extrusion in the eyespot region following ChR excitation will be important for signaling and adaptation. Due to the extreme close vicinity of the PM and the chloroplast envelope in the eyespot, also the chloroplast K$^+$/H$^+$-efflux antiporter 2 (KEA2) might affect the resting membrane potential in the eyespot region. KEA2, as one of the PM-type H$^+$-ATPases, was found with 11 different peptides. These different types of transporters thus might probably have important indirect functions in the context of eyespot related signaling.

TABLE 1 | Functional categorization of newly identified proteins from the extended eyespot fraction F2A$_e$.

Transcript name (Phytozome)	No. of different peptides	Function and/or homologies	TMDs[a]
Proteins important for eyespot development/retina related proteins			
Cre02.g105600.t1.3	4	Eyespot assembly protein EYE3, ABC1 kinase family	(+)
Cre12.g547300.t1.3	3	Eye Pigment Precursor Transporter (EPP) family protein	+
Cre12.g488350.t1.3	2	Retinal pigment epithelial membrane receptor	(+)
SOUL heme-binding proteins			
Cre13.g566850.t1.2	2	Similar to SOUL2	(+)
Cre06.g292400.t1.3	2	Similar to SOUL5	(+)
14-3-3 proteins			
Cre12.g559250.t1.2	10	14-3-3 protein	-
Cre06.g257500.t1.2	8	14-3-3 protein	-
Kinases[b]			
Cre17.g705000.t1.2	11	Calcium-dependent protein kinase 1	(+)
Cre09.g407800.t1.3	10	ABC1/COQ8 ser/thr kinase with an AarF (predicted unusual kinase) domain	(+)
Cre16.g663200.t1.3	10	Cyclic nucleotide dependent protein kinase	(+)
g8097.t1	9	Predicted protein with AarF (predicted unusual protein kinase) domain	(+)
g8097.t2 [c]	5	Predicted protein with AarF (predicted unusual protein kinase) domain	(+)
Cre13.g570350.t1.3; Cre13.g570350.t2.1	6	ABC-1-like kinase with an AarF (predicted unusual protein kinase) domain	+
g13907.t1	4	Predicted protein with AarF (predicted unusual protein kinase) domain	(+)
Cre06.g307100.t1.3	3	ABC1/COQ8 ser/thr kinase with an AarF domain	(+)
Cre16.g657350.t1.2	3	Protein with catalytic domain of serine/threonine protein kinases	(+)
Cre03.g168150.t1.2	2	Protein with catalytic domain of tyrosine kinase	(+)
Cre13.g571700.t1.3	2	Protein with catalytic domain of serine/threonine protein kinases	(+)
g17359.t1	2	Protein with catalytic domain of serine/threonine protein kinases	(+)
Phosphatases[b]			
Cre06.g292550.t1.2	3	Protein phosphatase 1	-
Cre09.g388750.t1.2	3	Phosphoinositide phosphatase	+
Cre06.g257850.t1.2	2	Serine/threonine protein phosphatase	-
Cre01.g030200.t1.2	2	Protein phosphatase 2C-like protein	-
Calcium-sensing and binding proteins			
Cre11.g468450.t1.2	6	Similar to centrin	-
Cre14.g615750.t1.1	4	Protein with EF-hand, calcium binding motif	(+)
Cre12.g559450.t1.3	4	Protein with a C2 domain (found in kinases and membrane trafficking proteins)	+
Cre03.g150300.t1.2	3	Protein with EF-hand, calcium binding motif	-
Cre03.g178150.t1.1	2	Similar to calmodulin	-
Cre15.g641250.t1.2	2	Protein with EF-hand, calcium binding motif	-
Membrane-associated/structural proteins, proteins with PAP-fibrillin domain			
Cre13.g583550.t1.2	11	VIPP1, Vesicle inducing protein in plastids 1	-
Cre03.g197650.t1.2	8	Protein with PAP-fibrillin domain	(+)
Cre12.g502250.t1.2	4	Protein with PAP-fibrillin domain	+
Cre12.g492600.t1.2	3	Fasciclin-like protein	+
Cre12.g492650.t1.2	2	Fasciclin-like protein	+
Cre11.g478850.t1.2	2	Protein with PAP-fibrillin domain	(+)
Transporter			
Cre10.g459200.t1.2	11	Plasma membrane-type proton ATPase	+
Cre04.g220200.t2.1; Cre04.g220200.t1.2; Cre04.g220200.t3.1	11	K$^+$/H$^+$-efflux antiporter 2 (KEA2, chloroplast inner envelope)	+
Cre09.g388850.t1.1	4	Calmodulin binding calcium-transporting ATPase (P-type/plasma membrane)	+
Cre03.g164600.t1.2;	4	Plasma membrane hydrogen ATPase	+
Cre03.g165050.t1.2	2	Plasma-membrane proton-efflux P-type ATPase	+

[a]*transmembrane domains, predictions done with TMHMM, TMpred, and TopPred (+, TMDs predicted by all three programs; (+), TMDs predicted by two programs; −, TMDs predicted by only one or no program);* [b]*Kinases and phosphatases that are putative signaling related;* [c]*Splice variant of g8097.t1. Function and/or homologies of depicted proteins were determined by NCBI BLASTp.*

Assignment of Protein Methylation

In recent years, increasing evidence points to the importance of diverse posttranslational protein modifications beside reversible phosphorylation in the regulation of protein stability, localization, activity and protein–protein interactions in cell organelles (e.g., Lehtimäki et al., 2015). One of them is methylation. In a recent study, 23 chloroplast proteins have been shown to be methylated at Lys and/or Arg residues (Alban et al., 2014). Methylation of these amino acids increases their basicity and hydrophobicity without altering their charge (Rice and Allis, 2001). As a part of the functional eyespot involves local specializations of the chloroplast (**Figure 1A**), it was of interest to find out whether methylated proteins are present in the eyespot fractions. Prior to an analysis via MS, we checked with a commercially available anti-methyl-Arg specific antibody recognizing monomethyl, asymmetric dimethyl, and symmetric dimethyl-Arg whether methylated proteins are still detectable after the isolation of eyespots (**Figure 4**). Immunoblot analysis of the proteins from fraction F1 with this antibody revealed four clearly and several weakly labeled protein bands. This result demonstrates that methylated proteins are still present in the eyespot fraction after the isolation procedure. Position, number, and intensity of labeled bands in a CE clearly differed, indicating that a specific subset of methylated proteins may occur in the eyespot fractions.

Mass spectrometry analysis of the peptides from both eyespot fractions resulted in the identification of 25 methylated proteins (**Tables 2** and **3**) where the methylation sites could be specified after additional manual evaluation of the spectra [Supplemental Figure S2 (Data Sheet 2), Supplemental Table S5 (Data Sheet 7)]. These proteins were characterized by 36 different methylated peptides and nine additional overlapping peptides having variations in the methylation status and/or sites and/or in oxidized versus non-oxidized Met. Six proteins are methylated at Lys and Arg residues, 17 proteins only at Lys residues, and two only at Arg residues. In total, we detected 10 Arg sites (nine mono and one dimethyl) and 42 Lys methylation sites (23 mono-, 14 di-, and 8 trimethylations; two of the residues were found mono- as well as dimethylated and one further residue di- as well as trimethylated; **Tables 2** and **3**). It should be mentioned that the identification of trimethylated Lys sides by LC-ESI-MS/MS is hampered by the fact that modification by acetylation is very close in mass (42.04695 vs. 42.01056 Da; Alban et al., 2014). Identification of neutral loss of trimethylamine (59 Da) being specific for trimethylation allows to discriminate (Zhang et al., 2004; Erce et al., 2012; Alban et al., 2014). All seven peptides (**Tables 2** and **3**) with potential trimethylated sites were therefore screened for neutral loss events by analyzing the spectra manually. In all corresponding spectra, b- and y-type ions of neutral loss fragments were found [Supplemental Figure S2 (Data Sheet 2)], indicating that there is trimethylation and not acetylation. Moreover, 14 methylated proteins were identified that are nucleic acid-related or considered as obvious contaminants. They are listed in Supplemental Table S6 (Data Sheet 8).

Interestingly, two proteins connected to eyespot development and positioning, EYE2 and SOUL3, as well as one of the
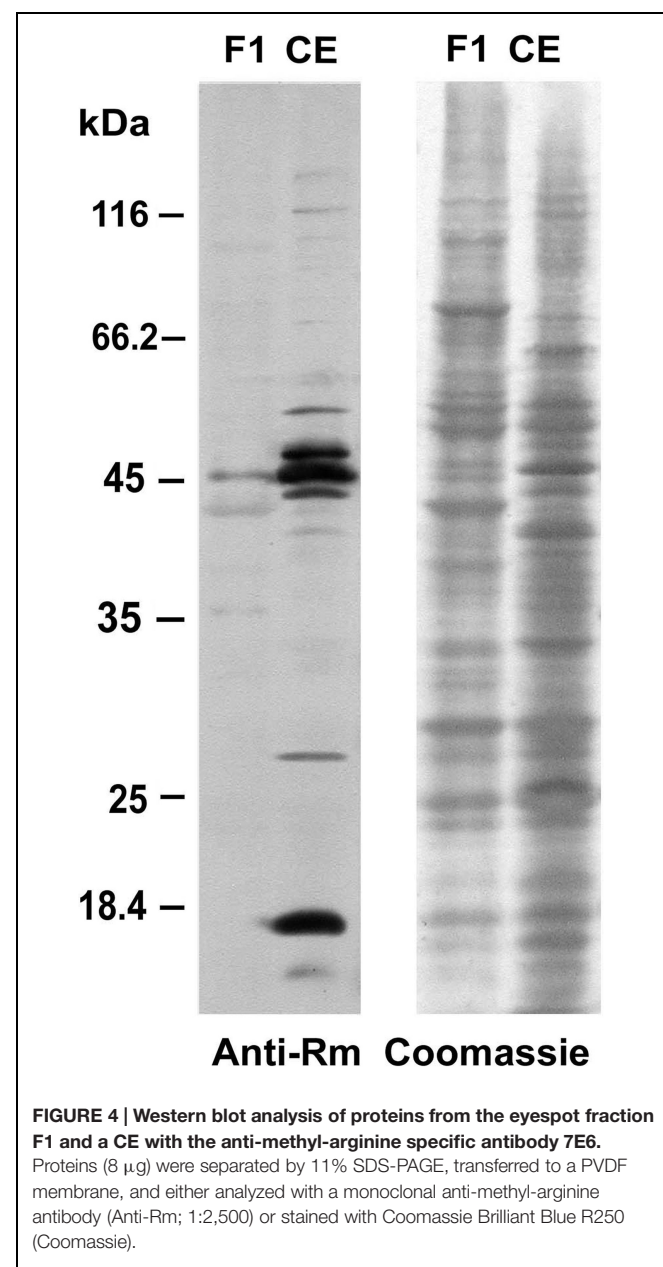
FIGURE 4 | Western blot analysis of proteins from the eyespot fraction F1 and a CE with the anti-methyl-arginine specific antibody 7E6. Proteins (8 μg) were separated by 11% SDS-PAGE, transferred to a PVDF membrane, and either analyzed with a monoclonal anti-methyl-arginine antibody (Anti-Rm; 1:2,500) or stained with Coomassie Brilliant Blue R250 (Coomassie).

14-3-3 proteins were detected among the methylated proteins. In the 14-3-3 protein, a methylated Arg and a dimethylated Lys residue were detected. As in the chloroplast of *Arabidopsis* (Alban et al., 2014), the *Chlamydomonas* chloroplast ATP synthase subunits alpha and beta both contain methylation sites. In addition, subunit I of the CF_0 membrane part of ATP synthase bears a trimethylation site. Also, other TM associated components bear methylation sites such as photosystem I and II components or the light harvesting complex protein Lhca7. N-terminal methylation of core light-harvesting complex proteins was shown before in purple photosynthetic bacteria (Wang et al., 2002). Furthermore, the photosystem I assembly protein Ycf4 was methylated at one Lys residue. In addition, methylated peptides of Ycf10, a transporter of the inner

TABLE 2 | Functional categorization of identified methylated proteins from the eyespot fractions F2A$_e$ and F1 (Schmidt et al., 2006).

Transcript name (Phytozome)	Function and/or homologies	Methylated peptide	z	Xcorr	x-times found
Proteins important for eyespot development					
Cre16.g666550.t1.2	SOUL3	QRQAFIMNDTCRmFLATDLKm[2a]	3	3.80	2
		–>QRQAFIMoNDTCRmFLATDLKm[2b]	3	3.51	1
Cre12.g509250.t1.1	EYE2, no eyespot	LTDDELIALVNSDPDLDKm[b]	2	4.40	1
14-3-3 proteins					
Cre12.g559250.t1.2	14-3-3 protein	DNLTLWTSDMoQDPAAGDDRmEGADMoKm[2]VEDAEP[a]	3	4.37	2
Photosynthesis/electron transport/light harvesting					
Cp genome	AtpB, ATP synthase subunit beta	FLSQPFFVAEVFTGSPGKm[2]YVSLAETIEG FGK[a,b]	3	5.97	6
		–>FLSQPFFVAEVFTGSPGKmYVSLAETIE GFGKm[a]	3	3.81	1
		ELQDIIAILGLDELSEEDRm[b]	2	3.51	2
		GMEVVDTGKm[2]PLSVPVGK[a]	2	2.91	1
		–>GMoEVVDTGKPLSVPVGKm[b]	2	3.09	1
		–>GMoEVVDTGKmPLSVPVGK[b]	2	2.81	1
		TVLIMoELINNIAKm[b]	2	2.73	1
Cp genome	AtpA, ATP synthase subunit alpha	SYLANSYPKm[2]YGEILR[a]	2	2.93	1
		SVYEPLATGLVAVDAMoIPVGRm[b]	2	3.38	1
Cp genome	AtpI, CF$_0$ ATP synthase subunit I	YVEPAAFLLPINVLEDFTKm[3]PLSLSFR[a]	3	3.11	1
Cre06.g261000.t1.2	10 kDa PS II polypeptide	GKm[2]GYGVYR[b]	1	2.26	2
		YEDKmYGANVDGYSPIYTPDLWTESGDSYTLGTK[a]	3	7.16	1
Cp genome	PetA, Cytochrome f	KmYSEMVVPILSPDPAKm[b]	2	2.60	1
		–>YSEMoVVPILSPDPAKm[b]	2	2.60	1
Cre16.g687900.t1.2	Lhca7, light-harvesting protein of PS I	NPGSQADGSFLGFTEEFKm[a]	2	3.48	5
Cp genome	PsbD, PS II D2 protein	AAEDPEFETFYTKm[a]	2	3.40	1
Cp genome	PsaB, PS I P700 chlorophyll a apoprotein A2	GYWQELIETLVWAHEKmTPLANLVYWKm[a]	3	3.40	1
Cp genome	Ycf4, PS I assembly protein	EIEKmQASELANFLQVSLEA[b]	2	2.77	1
Transporter					
Cp genome	CemA (Ycf10), inner envelope protein	FLKm[3]QLFSDVDNLVIQEYR[a]	3	3.10	1
		GSLDSIKmNKm[3]DISK[a]	3	3.00	1
g11711.t1	Similar to ATPase components of ABC transporters	LQTTKIGMLSEGQKm[2]SR[a]	2	3.28	1
Ferredoxin and thioredoxin-related proteins					
Cre11.g476750.t1.2	Ferredoxin-NADP reductase	KmGLCSNFLCDATPGTEISMoTGPTGK[a]	2	3.61	1
		–>KmGLCSNFLCDATPGTEISMTGPTGK[a]	2	3.42	1
		IPFWEGQSYGVIPPGTKmINSKm[2a]	3	3.82	1
		–>IPFWEGQSYGVIPPGTKINSKm[3a]	3	3.84	1
(Lipid) Metabolism					
g11946.t1, g11946.t2	Similar to Cytochrome b5 reductase	APDYSQGEVSGLLKm[2a]	2	3.32	3
Cre07.g349700.t1.2	Similar to 3-beta hydroxysteroid dehydrogenase/isomerase	ALVRDVSKmATSGSGLLAGVGSTTEVVR[b]	3	3.93	2
		–>ALVRmDVSKATSGSGLLAGVGSTTEVVR[b]	3	3.70	1
Cre01.g017100.t1.3	Similar to proteins with a acylglycerol/acyl-transferase domain	WFESFGAVKASPMAAFRm[2]LLR[a]	3	3.87	1

Km, methylated Lys; Km[2], dimethylated Lys; Km[3], trimethylated Lys (b and y ions of trimethylamin neutral loss events were found in the corresponding spectra indicating that trimethylation rather than acetylation is present); Rm, methylated Arg; Rm[2], dimethylated Arg; Mo, oxidized Met. If a peptide is marked with an arrow, the peptide above shows overlapping or identical sequences, but the number and/or status of methylation sites may be different or an oxidized Met may be present. [a]Peptide was identified in an analysis for methylated proteins from the extended eyespot fraction F2A$_e$. [b]Peptide was identified in an analysis for methylated proteins from the published eyespot proteome (Schmidt et al., 2006). Function and/or homologies of depicted proteins were determined by NCBI BLASTp.

chloroplast envelope possibly involved in H$^+$ extrusion into the cytosol in algae (Spalding, 2008), and the Ferredoxin-NADP reductase were found. This enzyme of *C. reinhardtii* was already characterized earlier as a methylated protein (Decottignies et al., 1995). It possesses three methylated Lys residues (Lys109, 115, and 161; as the first 26 amino acids were missing in the study from 1995, position of the Lys residues were changed according to the actual sequence of the protein). These positions are remarkably similar to those we obtained (Lys113, Lys162) and coincide in one case (Lys109). Additionally, several proteins of yet unknown functions bear methylation sites (**Table 3**). One protein, Cre01.g000900.t1.2

TABLE 3 | Methylated proteins of unknown function from the eyespot fractions F2A$_e$ and F1 (Schmidt et al., 2006).

Transcript name (Phytozome)	Function and/or homologies	Methylated peptide	z	Xcorr	x-times found
Cre06.g263250.t1.3	No significant hit in NCBI BLASTp	AAVADATGAASSAAADAKm[2a]	2	5.71	7
		AAVADATGAASSAATDAKm[2a]	2	4.20	3
Cp genome	ORF1995 unknown protein	MALEDLSKm[3]WKm[3a,b]	2	2.71	5
		SFDITSMTTTLPFYAGWDESLKm[2a]	2	4.61	3
		–>SFDITSMoTTTLPFYAGWDESLKm[2a]	2	3.59	1
Cre01.g000900.t1.2	Similar to conserved plant/cyanobacterial proteins of unknown functions, contains two DUF1350 domains	LATVAGQLGVSAATAPLEELSRm[a,b]	2	4.03	4
		FKDDSLDDTNNLVQLLQGSSSVGEVLDLTVRm[b]	3	4.35	1
Cp genome	ORF2971 unknown protein	VAMoLAELSLSNLSAKm[3]LDMITDLLVIIDSVRm[a]	3	3.31	1
		MoGQRmKmSQITLLEKm[a]	2	2.52	1
g2947.t1	No significant hit in NCBI BLASTp	ADGAAATATTAATGVLGAGFAKmADEAA ASATTAATGVLGAGFAKm[2a]	3	3.67	1
g14174.t1	No significant hit in NCBI BLASTp	GLGDVVGMKm[3]GPAAEINNGR[a]	2	3.33	1
Cre10.g438450.t1.3	No significant hit in NCBI BLASTp	GWGKm[2]LPDSGAALPAFLYKmHVLKm[a]	2	3.13	1

Km, methylated Lys; Km[2], dimethylated Lys; Km[3], trimethylated Lys (b and y ions of trimethylamin neutral loss events were found in the corresponding spectra indicating that trimethylation rather than acetylation is present); Rm, methylated Arg; Mo, oxidized Met. The peptide that is marked with an arrow shows an identical sequence, but an oxidized Met is present. [a]Peptide was identified in an analysis for methylated proteins from the extended eyespot fraction F2A$_e$. [b]Peptide was identified in an analysis for methylated proteins from the published eyespot proteome (Schmidt et al., 2006). Function and/or homologies of depicted proteins were determined by NCBI BLASTp.

with two DUF1350 domains, was methylated only at Arg residues.

DISCUSSION

The functional eyespot apparatus involves parts of numerous subcellular compartments including different membranes, proteins for its development and positioning, as well as proteins known from PG that seem to be involved in its structural organization and preservation. In addition, proteins involved in signaling, adaptational responses, and biochemical pathways, like, e.g., retinal biosynthesis, are part of this light sensitive organelle. Due to its high ultrastructural complexity and its diverse associated processes, selection criteria for proteins associated specifically with the eyespot cannot be derived on the basis of a simple routine workflow procedure. Moreover, conserved targeting sequences for the eyespot are not evident so far and some proteins in the eyespot also occur in additional compartments such as Casein kinase 1 or Phototropin (Schmidt et al., 2006; Trippens et al., 2012). Comparable green algal eyespot proteomes (beside the one in Schmidt et al., 2006) are still missing, but algal lipid droplets and higher plant plastoglobule proteomes are known and can be used for comparison (e.g., Lundquist et al., 2012; Davidi et al., 2015). Moreover, mutant screens for the eyespot are available (e.g., Boyd et al., 2011). All these literature based information has been used for the selection of highly favorable candidates for the extended eyespot proteome listed in **Table 1**. Thereby, we cannot exclude that we have missed certain components or that some false positives were included. For example, light signaling includes reversible phosphorylation, but it is hard to judge if a predicted kinase or phosphatase (without any further information) may be due to a contamination. Thus, additional functional studies as they were done for Casein kinase 1 (Schmidt et al., 2006) and Phototropin (Trippens et al., 2012) that is also present in the cytosol and flagella of *C. reinhardtii*, or the eyespot-specific SOUL3 (Schulze et al., 2013) and the newly identified EYE3 (**Table 1**; Boyd et al., 2011) are crucial. The present listed candidates in **Table 1** provide, however, a good basis for starting such functional tests.

Eyespot components involved in signal transduction are mainly in connection with the light signaling pathway. In the phototactic response of *C. reinhardtii* extracellular Ca^{2+} and Ca^{2+} fluxes are intricately involved. Both ChRs are directly light gated ion channels, which conduct Ca^{2+} under physiological conditions. Their excitation initiates fast inward-directed complex currents in the eyespot region, which finally produce a Ca^{2+} dependent alteration of the flagella beating and thereby leads to the steering of the cell toward or away from the light source (for reviews, see Witman, 1993; Hegemann and Berthold, 2009; Kreimer, 2009). Both ChRs as well as SOUL3, a protein important for the size and position of the eyespot, are targets of kinases (Wagner et al., 2008). Furthermore, in isolated green algal eyespots an increase in the free Ca^{2+} concentration from 10^{-8} to 10^{-7} M is known to affect protein phosphorylation and two protein phosphatases with PP2Cc domains are among the dominant proteins in the eyespot proteome (Linden and Kreimer, 1995; Schmidt et al., 2006). Thereby, reversible phosphorylation as well as Ca^{2+} signaling in the eyespot region are primary events after excitation of the ChRs. In this context, the increase in kinases and phosphatases as well as in calcium sensing components in the extended eyespot proteome is of high interest for future studies. Especially the identification of the Calcium dependent protein kinase 1 (CDPK 1) is noteworthy, as no CDPKs have been detected in the core eyespot proteome (Schmidt et al., 2006). The *Chlamydomonas* genome encodes 14 CDPKs; three of them (1,

3, and 11) are found in the flagellar proteome (Pazour et al., 2005; Liang and Pan, 2013). Although CDPK1 has important functions in the flagella, it is also strongly present in the cell body (Liang et al., 2014; Motiwalla et al., 2014). A similar situation is found for Casein kinase 1. This kinase is specifically enriched in both, flagella and the eyespot, and has been shown to be involved in circadian phototaxis as well as in different flagella functions (Schmidt et al., 2006; Wirschell et al., 2011; Boesger et al., 2012). Similarly, the identification of additional members of the ABC kinase family in the extended eyespot proteome could be of interest for eyespot function and development. One of them, EYE3, is already known to be important for eyespot development. Mutants in EYE3 lack a visible eyespot (Lamb et al., 1999; Boyd et al., 2011). Four members of this group found in the eyespot proteomes (Cre13.g581850t1.2; Cre03.g158500.t1.1; Cre09.g407800.t1.3; Cre13.g570350.t1.3) have homologs in PG of *A. thaliana*. Two of them, which were newly identified in the extended eyespot proteome, are known as AKC1 and AKC4. In higher plants, six of in total eight members of the ABC1-like kinases found in chloroplasts are associated with PG. They play a role in regulation of phylloquinone biosynthesis, redox recycling under high light and probably have other not yet known regulatory functions (Ytterberg et al., 2006; Lundquist et al., 2012; Martinis et al., 2013; Spicher and Kessler, 2015). With two 14-3-3 proteins, which interact with phosphoproteins, members of another protein group often involved in diverse signaling networks including those related to light perception were identified. For example, in higher plants 14-3-3 proteins interact with the blue light receptor Phototropin 1 (Sullivan et al., 2009). In this context, it is interesting that Phototropin in *C. reinhardtii* has recently been shown to affect eyespot size, the content of ChR1 as well as the sign of phototaxis (Trippens et al., 2012).

The procedure for purifying intact eyespots resulted also in an increase in transporters and membrane-associated proteins. Especially the presence of three P-type PM ATPases and a PM type Calmodulin-binding Ca^{2+}-transporting ATPase is of special interest, as, e.g., activation of PM ATPases could affect the speed of recovery of the resting membrane potential following excitation of the ChRs. This might be important for, e.g., desensitization and dark recovery of the cell (Govorunova et al., 1997). Also lowering of the cytosolic free Ca^{2+} concentration in the eyespot region following activation of the ChRs is important for signaling and adaptation. The function of the Ca^{2+}-ATPase might be complemented by light-induced Ca^{2+} uptake into the chloroplast, which has been demonstrated for isolated chloroplasts and appears to be important for the regulation of the sign of phototaxis in *C. reinhardtii* (Kreimer et al., 1985; Takahashi and Watanabe, 1993). Additionally, the discovery of two fascilin-like proteins with four (Cre12.g492650.t1.2) and three (Cre12.g492600.t1.2) FAS1 domains might be functionally relevant. These are thought to represent ancient cell adhesion domains. As the MORN-repeat motif, which has a critical role in several proteins with functions in the organization of membranous and cytoskeletal structures, these domains may be important for the close contact of the different membrane types in the eyespot region. A MORN-repeat protein is present in

the proteomes of both eyespot fractions (Schmidt et al., 2006). It should, however, be noted that for all proteins discussed so far, a role in eyespot development, ultrastructure, positioning or eyespot related signaling needs to be proven experimentally in the future. While the extended eyespot proteome revealed numerous novel eyespot proteins, some were also "lost" compared to the already published one (Schmidt et al., 2006). Thereby, one should consider that the former bioinformatics analysis of the proteome data was based on a so-called probability score. In the current analysis, we are applying a FDR of $\leq 1\%$, which is more restrictive. On the other hand, several of the missing candidates (10 out of 27) are putative contaminants. It may also be that the different cell rupture and eyespot isolation methods yielding either eyespot fragments (Schmidt et al., 2006) or the intact structure (present study), have different contaminants associated.

In the past years, it turned out that cellular signal transduction is not only frequently mediated by phosphorylation at Tyr, Ser and Thr but also by methylation at Arg and Lys (Biggar and Li, 2015). Protein methylation is meanwhile considered as an integral part of cellular biology. Protein Lys methyltransferases (PKMTs, often containing a so-called SET domain) and protein Arg methyltransferases (PRMTs) have been well characterized, while Lys and Arg demethylases are less well studied so far or still under debate in case of Arg demethylases (Alban et al., 2014). In *A. thaliana*, six of the SET-domain containing PKMT's are known or predicted to be targeted to the chloroplast (Table 1 in Alban et al., 2014). A search for homologous PKMTs in the *C. reinhardtii* genome, which was based on the *Arabidopsis* candidates, revealed five putative protein Lys methyltransferases. They have either a Rubisco-lysine *N*-methyltransferase domain [Cre16.g661350.t1.2 (RMT1), Cre12.g524500.t.1.2 (RMT2), and Cre12.g503800.t1.1 (RMT5)], a SET domain (Cre16.g649700.t1.1) or both (Cre12.g541777.t1.1). In case of the ATXR5 protein in *Arabidopsis*, which is supposed to be a histone-lysine methyltransferase, only a limited number of proteins with a very weak homology was found in the *C. reinhardtii* genome. None of them has a methyltransferase domain or a SET domain. Another distantly related group of PKMT's predicted for *Arabidopsis* chloroplasts (Table 1 in Alban et al., 2014) belongs to the seven-beta strand methyltransferases. One is a ribosomal protein L11 methyltransferase-like protein (PrmA-like) and is also found in *Chlamydomonas* (Cre09.g396735.t2.1). The other is a *S*-adenosyl-L-methionine-dependent methyltransferase (CaMKMT-like) and has only very limited homology (*E*-value: $5.6E^{-9}$) to a putative N^2,N^2-dimethylguanosine tRNA methyltransferase (Cre07.g347800.t1.1) in *Chlamydomonas*. In the case of the PRMT's, five enzymes are known in *C. reinhardtii* (summarized in Werner-Peterson and Sloboda, 2013). PRMTs 1, 2, 3, and 6 are Type I enzymes, which produce asymmetric dimethyl Arg residues, whereas PRMT5 is a Type II enzyme and produce symmetric dimethyl Arg's. While PRMT1 is known to be localized in flagella (Werner-Peterson and Sloboda, 2013), nothing is known about the cellular localization of the other proteins. In *Arabidopsis* (Alban et al., 2014), only PRMT7 is predicted to be localized in the chloroplast. In *C. reinhardtii*,

the closest two homologs to this protein are an uncharacterized PRMT (Cre02.g14626.t1.1) and a Protein/Histone-arginine *N*-methyltransferase [Cre.g558100.t1.2 (PRMT2)]. It seems likely that the methylation events of eyespot proteins located within the chloroplast part of this structure are catalyzed by chloroplast localized methyltransferases. This may even hold true for the methylated 14-3-3 protein, since members of this protein group are also reported to be present in the chloroplast (Sehnke et al., 2000, 2002).

In this context, methylation of known eyespot proteins and proteins forming complexes with eyespot proteins is of interest. Remarkably all of these proteins are localized in chloroplast parts of the eyespot. EYE2 is localized in the chloroplast envelope and important for the formation of the EG layer (Boyd et al., 2011). The photosystem I assembly protein Ycf4, which was found to be methylated at one Lys residue, is known to be in a complex with the eyespot protein COP2 (Ozawa et al., 2009) as well as certain PSI subunits including PsaB, which was also identified as a methylated protein in our analysis. Also the ATP synthase subunits alpha and beta, which are part of the soluble CF1 subunit, are of interest. Both subunits were found as methylated proteins in the chloroplast of *Arabidopsis* (Alban et al., 2014) and they are also present as methylated proteins in the *Chlamydomonas* eyespot. Former studies (Schmidt et al., 2007) showed that the alpha and beta subunits present in the eyespot fraction of *Chlamydomonas* are resistant against thermolysin treatment, which is not the case for the thylakoid-localized alpha and beta subunits of the ATP synthase and other membrane-associated proteins in the eyespot fraction. Therefore, it was assumed that a significant proportion of these ATP-synthase subunits have a specialized localization and function within the eyespot, possibly between the EG. Blue native PAGE of thermolysin-treated eyespots followed by SDS-PAGE even revealed that the alpha and beta subunits are present in conjunction with the gamma-subunit in a thermolysin resistant complex (Schmidt et al., 2007). Thus, methylation of these subunits is of special interest with regard to the conservation of methylation sites compared to *Arabidopsis* chloroplasts but also with regard to potential special functional features of methylation within the eyespot. In *Arabidopsis*, the alpha subunit reveals a methylation site on Arg141. In *Chlamydomonas* eyespots, we detected two methylation sites in this highly conserved protein at Arg161 and Lys470. Although an Arg is present at position 161 in *Arabidopsis*, it is not methylated there. On the other hand, at position 141 in *C. reinhardtii* also a non-methylated Arg is present. The methylated Lys at position 470 is not conserved in *Arabidopsis*. For the beta subunit, we identified six methylated residues in *C. reinhardtii* (Lys96, Lys104, Lys191, Arg418, Lys447, and Lys460) compared to two sites in the *A. thaliana* chloroplast (Alban et al., 2014). For three positions (Lys96, Lys104, Lys460) the corresponding Lys residues are not conserved in *A. thaliana*. Lys191 and Arg418 are conserved, but not methylated in *Arabidopsis*. One of the methylation sites (Lys447), however, fits exactly to one of the two methylation sites that were identified in the ATP synthase subunit beta in the chloroplast of *A. thaliana*

(Lys447, Arg52; Alban et al., 2014). It remains to be studied in the future whether the higher methylation status and rather distinct methylation pattern (with one exception) of these two subunits in the eyespot compared to the thylakoids is possibly related to their specialized location in the eyespot. The increased hydrophobicity without altering the charge of the methylated amino acid residues (Rice and Allis, 2001) might be beneficial for their localization between the highly hydrophobic EG.

Among the methylated proteins found in the eyespot fractions is also the SOUL heme binding protein SOUL3 that is localized at the EG and important for a correct positioning of the eyespot and its size (Schulze et al., 2013). It was shown before that SOUL3 is phosphorylated at two sites (Wagner et al., 2008). A crosstalk between methylation–phosphorylation events has been recently found (reviewed in Biggar and Li, 2015). If the methylation and phosphorylation sites are neighbored, this is called "methylation–phosphorylation switch". Moreover, a methylation–methylation crosstalk has been described. In case of SOUL3, a "methylation–phosphorylation switch" seems rather unlikely as the relevant sites are not directly neighbored. A methylation-methylation crosstalk, however, may exist. SOUL3 methylation sites are at Arg95 and Lys102 while the phosphorylation sites are at Thr42 and Ser44. Notably, both posttranslational modifications are situated at the N-terminal part of SOUL3 while the SOUL/HBP domain is situated at the C-terminus. Methylation of SOUL3 may be involved in regulation of protein–protein interactions. For example, dimethylation of p53 promotes its association with the co-activator protein p53-binding protein 1. Lys methylation can, however, also block protein–protein interactions as demonstrated for the MAPK kinase kinase 2 and its interaction with the serine/threonine protein phosphatase 2A complex (reviewed in Hamamoto et al., 2015). SOUL3 (approximately 45 kDa) has been found to be present in complexes during the day (approximately 100 kDa) and the night phase (approximately 270 kDa) over a circadian cycle (Schulze et al., 2013). It has to be investigated whether methylation affects complex formation of SOUL3 and whether its methylation status changes over a circadian cycle.

The knowledge about the protein composition of the eyespot proteomes as well as about posttranslational modifications such as methylation and phosphorylation provides now an efficient basis for further functional studies. For example, potential effects of protein methylation on protein–protein interactions, protein stability, or subcellular localization can now be put under focus. Signaling components such as EYE2, a protein of the thioredoxin superfamily, or the 14-3-3 protein might recruit interaction partners or induce/inhibit signaling pathways upon methylation. As mentioned before for the ATPase, it is also well visible that eyespot proteins may rely on methylation to increase their hydrophobicity profile especially when situated in between the EG. These emerging functional possibilities will need further attention in future approaches in order to understand this highly complex primordial visual system of a unicellular organism in depth with regard to its structural properties and signaling pathways.

AUTHOR CONTRIBUTIONS

FUNDING

ACKNOWLEDGMENTS

SUPPLEMENTARY MATERIAL

The Supplementary Material for this article can be found online at: http://journal.frontiersin.org/article/10.3389/fpls.2015.01085

REFERENCES

Alban, C., Tardif, M., Mininno, M., Brugiere, S., Gilgen, A., Ma, S., et al. (2014). Uncovering the protein lysine and arginine methylation network in *Arabidopsis* chloroplasts. *PLoS ONE* 9:e95512. doi: 10.1371/journal.pone.0095512

Altschul, S. F., Madden, T. L., Schäffer, A. A., Zhang, J., Zhang, Z., Miller, W., et al. (1997). Gapped BLAST and PSI-BLAST: a new generation of protein database search programs. *Nucleic Acids Res.* 25, 3389–3402. doi: 10.1093/nar/25.17.3389

Austin, J. R. II, Frost, E., Vidi, P.-A., Kessler, F., and Staehlin, L. A. (2006). Plastoglobules are lipoprotein subcompartments of the chloroplast that are permanently coupled to thylakoid membranes and contain biosynthetic enzymes. *Plant Cell* 18, 1693–1703. doi: 10.1105/tpc.105.039859

Biggar, K. K., and Li, S. S.-C. (2015). Non-histone protein methylation as a regulator of cellular signaling and function. *Nat. Rev. Mol. Cell Biol.* 16, 5–17. doi: 10.1038/nrm3915

Blifernez, O., Wobbe, L., Niehaus, K., and Kruse, O. (2011). Protein arginine methylation modulates light-harvesting antenna translation in *Chlamydomonas reinhardtii*. *Plant J.* 65, 119–130. doi: 10.1111/j.1365-313X.2010.04406.x

Boesger, J., Wagner, V., Weisheit, W., and Mittag, M. (2012). Application of phosphoproteomics to find targets of casein kinase 1 in the flagellum of *Chlamydomonas*. *Int. J. Plant Genomics* 2012, 581460. doi: 10.1155/2012/581460

Boyd, J. S., Mittelmeier, T. M., Lamb, M. R., and Dieckmann, C. L. (2011). Thioredoxin-family protein EYE2 and Ser/Thr kinase EYE3 play interdependent roles in eyespot assembly. *Mol. Biol. Cell* 22, 1421–1429. doi: 10.1091/mbc.E10-11-0918

Davidi, L., Levin, Y., Ben-Dor, S., and Pick, U. (2015). Proteome analysis of cytoplasmatic and plastidic β-Carotene lipid droplets in *Dunaliella* bardawil. *Plant Physiol.* 167, 60–79. doi: 10.1104/pp.114.248450

Decottignies, P., Le Maréchal, P., Jacquot, J. P., Schmitter, J. M., and Gadal, P. (1995). Primary structure and post-translational modification of ferredoxin-NADP reductase from *Chlamydomonas reinhardtii*. *Arch. Biochem. Biophys.* 316, 249–259. doi: 10.1006/abbi.1995.1035

Deininger, W., Kröger, P., Hegemann, U., Lottspeich, F., and Hegemann, P. (1995). Chlamyrhodopsin represents a new type of sensory photoreceptor. *EMBO J.* 14, 5849–5858.

Deng, X., Gu, L., Liu, C., Lu, T., Lu, F., Lu, Z., et al. (2010). Arginine methylation mediated by the *Arabidopsis* homolog of PRMT5 is essential for proper pre-mRNA splicing. *Proc. Natl. Acad. Sci. U.S.A.* 107, 19114–19119. doi: 10.1073/pnas.1009669107

Denison, F. C., Paul, A.-L., Zupanska, A. K., and Ferl, R. J. (2011). 14-3-3 proteins in plant physiology. *Semin. Cell Dev. Biol.* 22, 720–727. doi: 10.1016/j.semcdb.2011.08.006

Dieckmann, C. L. (2003). Eyespot placement and assembly in the green alga *Chlamydomonas*. *Bioessays* 25, 410–416. doi: 10.1002/bies.10259

Dodge, J. D. (1984). The functional and phylogenetic significance of dinoflagellate eyespots. *Biosystems* 16, 259–267. doi: 10.1016/0303-2647(83)90009-6

Erce, M. A., Pang, C. N., Hart-Smith, G., and Wilkins, M. R. (2012). The methylproteome and the intracellular methylation network. *Proteomics* 12, 564–586. doi: 10.1002/pmic.201100397

Foster, K. W., and Smyth, R. D. (1980). Light antennas in phototactic alga. *Microbiol. Rev.* 44, 572–630.

Fuhrmann, M., Stahlberg, A., Govorunova, E., Rank, S., and Hegemann, P. (2001). The abundant retinal protein of the *Chlamydomonas* eye is not the photoreceptor for phototaxis and photophobic responses. *J. Cell Sci.* 114, 3857–3863.

Gasteiger, E., Hoogland, C., Gattiker, A., Duvaud, S., Wilkins, M. R., Appel, R. D., et al. (2005). "Protein identification and analysis tools on the ExPASy server," in *The Proteomics Protocols Handbook*, ed. J. M. Walker (Totowa, StateNJ: Humana Press), 571–607.

Gavelis, G. S., Hayakawa, S., R. A. III, Gojobori, T., Suttle, C. A., Keeling, P. J., et al. (2015). Eye-like ocelloids are built from different endosymbiotically acquired components. *Nature* 523, 204. doi: 10.1038/nature14593

Govorunova, E. G., Sineshchekov, O. A., and Hegemann, P. (1997). Desensitization and dark recovery of the photoreceptor current in *Chlamydomonas reinhardtii*. *Plant Physiol.* 115, 633–642.

Hamamoto, R., Saloura, V., and Nakamuta, Y. (2015). Critical roles of non-histone protein lysine methylation in human tumorigenesis. *Nat. Rev.* 15, 110–124. doi: 10.1038/nrc3884

Harz, H., Nonnengässer, C., and Hegemann, P. (1992). The photoreceptor current of the green alga *Chlamydomonas*. *Philos. Trans. R. Soc. Lond. B Biol. Sci.* 338, 39–52. doi: 10.1098/rstb.1992.0127

Hayakawa, S., Takaku, Y., Hwang, J. S., Horiguchi, T., Suga, H., Gehring, W., et al. (2015). Function and evolutionary origin of unicellular camera-type eye structure. *PLoS ONE* 10:e0118415. doi: 10.1371/journal.pone.0118415

Hegemann, P., and Berthold, P. (2009). "Sensory photoreceptors and light control of flagellar activity," in *The Chlamydomonas Sourcebook*, Vol. 3, ed. G. B. Witman (San Diego, CA: Academic Press), 395–429.

Hegemann, P., and Nagel, G. (2013). From channelrhodopsins to optogenetics. *EMBO Mol. Med.* 5, 173–176. doi: 10.1002/emmm.201202387

Hofmann, K., and Stoffel, W. (1993). TMbase – A database of membrane spanning proteins segments. *Biol. Chem. Hoppe Seyler* 374, 166.

Kawai, H., and Kreimer, G. (2000). "Sensory mechanisms: light perception and taxis in algae," in *The Flagellates: Unity, Diversity and Evolution*, eds B. Leadbeater and J. Green (London: Taylor & Francis), 124–146.

Kreimer, G. (1994). Cell biology of phototaxis in flagellated algae. *Int. Rev. Cytol.* 148, 229–310. doi: 10.1016/S0074-7696(08)62409-2

Kreimer, G. (2009). The green algal eyespot apparatus: a primordial visual system and more? *Curr. Genet.* 55, 19–43. doi: 10.1007/s00294-008-0224-8

Kreimer, G., Brohsonn, U., and Melkonian, M. (1991). Isolation and partial characterization of the photoreceptive organelle for phototaxis of a flagellate green alga. *Eur. J. Cell Biol.* 55, 318–327.

Kreimer, G., and Melkonian, M. (1990). Reflection confocal laser scanning microscopy of eyespots in flagellate green alga. *Eur. J. Cell Biol.* 53, 101–111.

Kreimer, G., Melkonian, M., and Latzko, E. (1985). An electrogenic uniport mediates light-dependent Ca2+ influx into intact spinach chloroplasts. *FEBS Lett.* 180, 253–258. doi: 10.1016/0014-5793(85)81081-4

Kreimer, G., Overländer, C., Sineshchekov, O. A., Stolzis, H., Nultsch, W., and Melkonian, M. (1992). Functional analysis of the eyespot in *Chlamydomonas reinhardtii* mutant ey 627, mt-. *Planta* 188, 513–521. doi: 10.1007/BF00197043

Krogh, A., Larsson, B., von Heijne, G., and Sonnhammer, E. L. L. (2001). Predicting transmembrane protein topology with a hidden Markov model: application to complete genomes. *J. Mol. Biol.* 305, 567–580. doi: 10.1006/jmbi.2000.4315

Lamb, M. R., Dutcher, S. K., Worley, C. K., and Dieckmann, C. L. (1999). Eyespot-assembly mutants in *Chlamydomonas reinhardtii*. *Genetics* 153, 721–729.

Lehtimäki, N., Koskela, M. M., and Mulo, P. (2015). Post-translational modifications of chloroplast proteins: an emerging field. *Plant Physiol.* 168, 768–775. doi: 10.1104/pp.15.00117

Liang, Y., and Pan, J. (2013). Regulation of flagellar biogenesis by a calcium dependent protein kinase in *Chlamydomonas reinhardtii*. *PLoS ONE* 8:e69902. doi: 10.1371/journal.pone.0069902

Liang, Y., Pang, Y., Wu, Q., Hu, Z., Han, X., Xu, Y., et al. (2014). FLA8/KIF3B phosphorylation regulates kinesin-II interaction with IFT-B to control IFT entry and turnaround. *Dev. Cell* 30, 585–597. doi: 10.1016/j.devcel.2014.07.019

Lichtenthaler, H. K. (1987). Chlorophylls and carotenoids: pigments of photosynthetic biomembranes. *Methods Enzymol.* 148, 350–382. doi: 10.1016/0076-6879(87)48036-1

Linden, L., and Kreimer, G. (1995). Calcium modulates rapid protein phosphorylation/de-phosphorylation in isolated eyespot apparatuses of the green alga *Spermatozopsis similis*. *Planta* 197, 343–351. doi: 10.1007/BF00202656

Link, A. J., Eng, J., Schieltz, D. M., Carmack, E., Mize, G. J., Morris, D. R., et al. (1999). Direct analysis of protein complexes using mass spectrometry. *Nat. Biotechnol.* 17, 676–682. doi: 10.1038/10890

Lundquist, P. K., Poliakov, A., Bhuiyan, N. H., Zybailov, B., Sun, Q., and van Wijk, K. J. (2012). The functional network of the *Arabidopsis plastoglobule* proteome based on quantitative proteomics and genome-wide coexpression analysis. *Plant Physiol.* 158, 1172–1192. doi: 10.1104/pp.111.193144

Martinis, J., Glauser, G., Valimareanu, S., and Kessler, F. (2013). A chloroplast ABC1-like kinase regulates vitamin E metabolism in *Arabidopsis*. *Plant Physiol.* 162, 652–662. doi: 10.1104/pp.113.218644

Melkonian, M., and Robenek, H. (1984). The eyespot apparatus of green algae: a critical review. *Prog. Phycol. Res.* 3, 193–268.

Merchant, S. S., Prochnik, S. E., Vallon, O., Harris, E. H., Karpowicz, S. J., Witman, G. B., et al. (2007). The evolution of key animal and plant functions is revealed by analysis of the *Chlamydomonas* genome. *Science* 318, 245–251. doi: 10.1126/science.1143609

Motiwalla, M. J., Sequeira, M. P., and D'Souza, J. S. (2014). Two calcium-dependent protein kinases from *Chlamydomonas reinhardtii* are transcriptionally regulated by nutrient starvation. *Plant Signal. Behav.* 9, e27969. doi: 10.4161/psb.27969

Nacir, H., and Bréhélin, C. (2013). When proteomics reveals unsuspected roles: the plastoglobule example. *Front. Plant Sci.* 4:114. doi: 10.3389/fpls.2013.00114

Nagel, G., Ollig, D., Fuhrmann, M., Kateriya, S., Musti, A. M., Bamberg, E., et al. (2002). Channelrhodopsin-1: a light-gated proton channel in green algae. *Science* 296, 2395–2398. doi: 10.1126/science.1072068

Neuhoff, V., Phillip, K., Zimmer, H. G., and Mesecke, S. (1979). A simple versatile sensitive and volume-independent method for quantitative protein determination which is independent of other external influences. *Hoppe Seylers Z. Physiol. Chem.* 360, 1657–1670. doi: 10.1515/bchm2.1979.360.2.1657

Ozawa, S., Nield, J., Terao, A., Stauber, E. J., Hippler, M., Koike, H., et al. (2009). Biochemical and structural studies of the large Ycf4-photosystem I assembly complex of the green alga *Chlamydomonas reinhardtii*. *Plant Cell* 8, 2424–2442. doi: 10.1105/tpc.108.063313

Pazour, G. J., Agrin, N., Leszyk, J., and Witman, G. B. (2005). Proteomic analysis of a eukaryotic cilium. *J. Cell Biol.* 170, 103–113. doi: 10.1083/jcb.200504008

Reinders, J., and Sickmann, A. (2007). Modificomics: posttranslational modifications beyond protein phosphorylation and glycosylation. *Biomol. Eng.* 24, 169–177. doi: 10.1016/j.bioeng.2007.03.002

Renninger, S., Backendorf, E., and Kreimer, G. (2001). Subfractionation of eyespot apparatuses from the green alga *Spermatozopsis similis*: isolation and characterization of eyespot globules. *Planta* 213, 51–63. doi: 10.1007/s004250000473

Reynolds, E. (1963). The use of lead citrate at high pH as an electron-opaque stain in electron microscopy. *J. Cell Biol.* 17, 208–212. doi: 10.1083/jcb.17.1.208

Rice, J. C., and Allis, C. D. (2001). Histone methylation versus histone acetylation: new insights into epigenetic regulation. *Curr. Opin. Cell Biol.* 13, 263–273. doi: 10.1016/S0955-0674(00)00208-8

Roberts, D. G. W., Lamb, M. R., and Dieckmann, C. L. (2001). Characterization of the eye2 gene required for eyespot assembly in *Chlamydomonas reinhardtii*. *Genetics* 158, 1037–1049.

Rütgers, M., and Schroda, M. (2013). A role of VIPP1 as a dynamic structure within thylakoid centers as sites of photosystem biogenesis? *Plant Signal. Behav.* 8, e27037. doi: 10.4161/psb.27037

Schmidt, M., Geßner, G., Luff, M., Heiland, I., Wagner, V., Kaminski, M., et al. (2006). Proteomic analysis of the eyespot of *Chlamydomonas reinhardtii* provides novel insights into its components and tactic movements. *Plant Cell* 18, 1908–1930. doi: 10.1105/tpc.106.041749

Schmidt, M., Luff, M., Mollwo, A., Kaminski, M., Mittag, M., and Kreimer, G. (2007). Evidence for a specialized localization of the chloroplast ATP-synthase subunits α, ß and γ in the eyespot apparatus of *Chlamydomonas reinhardtii* (Chlorophyceae). *J. Phycol.* 43, 284–294. doi: 10.1111/j.1529-8817.2007.00331.x

Schulze, T., Schreiber, S., Iliev, D., Boesger, J., Trippens, J., Kreimer, G., et al. (2013). The SOUL heme-binding protein 3 of *Chlamydomonas reinhardtii* influences size and position of the eyespot. *Mol. Plant* 6, 931–944. doi: 10.1093/mp/sss137

Sehnke, P. C., Henry, R., Cline, K., and Ferl, R. J. (2000). Interaction of plant 14-3-3 protein with the signal peptide of a thylakoid-targeted chloroplast precursor protein and the presence of 14-3-3 isoforms in the chloroplast stroma. *Plant Physiol.* 122, 235–241. doi: 10.1104/pp.122.1.235

Sehnke, P. C., Rosenquist, M., Alsterfjord, M., DeLille, J., Sommarin, M., Larsson, C., et al. (2002). Evolution and isoform specificity of plant 14-3-3 proteins. *Plant Mol. Biol.* 50, 1011–1018. doi: 10.1023/A:1021289127519

Sineshchekov, O. A., Jung, K.-H., and Spudich, J. L. (2002). Two rhodopsins mediate phototaxis to low- and high-intensity light in *Chlamydomonas reinhardtii*. *Proc. Natl. Acad. Sci. U.S.A.* 99, 8689–8694. doi: 10.1073/pnas.122243399

Spalding, M. H. (2008). Microalgal carbon-dioxide-concentrating mechanisms: *Chlamydomonas* inorganic carbon transporters. *J. Exp. Bot.* 59, 1463–1473. doi: 10.1093/jxb/erm128

Spicher, L., and Kessler, F. (2015). Unexpected roles of plastoglobules (plastid lipid droplets) in vitamin K1 and E metabolism. *Curr. Opin. Plant Biol.* 25, 123–129. doi: 10.1016/j.pbi.2015.05.005

Sullivan, S., Thomson, C. E., Kaiserli, E., and Christie, J. M. (2009). Interaction specificity of *Arabidopsis* 14-3-3 proteins with phototropin receptor kinases. *FEBS Lett.* 583, 2187–2193. doi: 10.1016/j.febslet.2009.06.011

Suzuki, T., Yamasaki, K., Fujita, S., Oda, K., Iseki, M., Yoshida, K., et al. (2003). Archaeal-type rhodopsins in *Chlamydomonas*: model structure and intracellular localization. *Biochem. Biophys. Res. Commun.* 301, 711–717. doi: 10.1016/S0006-291X(02)03079-6

Takahashi, T., and Watanabe, M. (1993). Photosynthesis modulates the sign of phototaxis of wild-type *Chlamydomonas reinhardtii*. Effects of red background illumination and 3-(3',4'-dichlorophenyl)-1,1-dimethylurea. *FEBS Lett.* 336, 516–520. oi: 10.1016/0014-5793(93)80867-T

Trippens, J., Greiner, A., Schellwat, J., Neukam, M., Rottmann, T., Lu, Y., et al. (2012). Phototropin influence on eyespot development and regulation of phototactic behavior in *Chlamydomonas reinhardtii*. *Plant Cell* 24, 4687–4702. doi: 10.1105/tpc.112.103523

Veith, T., Brauns, J., Weisheit, W., Mittag, M., and Büchel, C. (2009). Identification of a specific fucoxanthin-chlorophyll protein in the light harvesting complex of photosystem I in the diatom *Cyclotella* meneghiniana. *Biochim. Biophys. Acta* 7, 905–912. doi: 10.1016/j.bbabio.2009.04.006

Vizcaino, J. A., Cote, R. G., Csordas, A., Dianes, J. A., Fabregat, A., Foster, J. M., et al. (2013). The proteomics identifications (PRIDE) database and associated tools: status in 2013. *Nucleic Acids Res.* 41, D1063–D1069. doi: 10.1093/nar/gks1262

von Heinjne, G. (1992). Membrane protein structure prediction: hydrophobicity analysis and the 'positive inside' rule. *J. Mol. Biol.* 225, 487–494. doi: 10.1016/0022-2836(92)90934-C

Vopalensky, P., Pergner, J., Liegertova, M., Benito-Gutierrez, E., Arendt, D., and Kozmik, Z. (2012). Molecular analysis of the amphioxus frontal eye unravels the evolutionary origin of the retina and pigment cells of the vertebrate eye. *Proc. Natl. Acad. Sci. U.S.A.* 109, 15383–15388. doi: 10.1073/pnas.1207580109

Wagner, V., Ullmann, K., Mollwo, A., Kaminski, M., Mittag, M., and Kreimer, G. (2008). The phosphoproteome of a *Chlamydomonas reinhardtii* eyespot fraction includes key proteins of the light signaling pathway. *Plant Physiol.* 146, 772–788. doi: 10.1104/pp.107.109645

Wang, Z. Y., Shimonaga, M., Kobayashi, M., and Nozawa, T. (2002). N-terminal methylation of the core light-harvesting complex in purple photosynthetic bacteria. *FEBS Lett.* 519, 164–168. doi: 10.1016/S0014-5793(02)02744-8

Werner-Peterson, R., and Sloboda, R. D. (2013). Methylation of structural components of the axoneme occurs during flagellar disassembly. *Biochemistry* 52, 8501–8509. doi: 10.1021/bi4011623

Wirschell, M., Yamamoto, R., Alford, L., Gokhale, A., Gaillard, A., and Sale, W. S. (2011). Regulation of ciliary motility: conserved protein kinases and phosphatases are targeted and anchored in the ciliary axoneme. *Arch. Biochem. Biophys.* 510, 93–100. doi: 10.1016/j.abb.2011.04.003

Witman, G. B. (1993). *Chlamydomonas* phototaxis. *Trends Cell Biol.* 3, 403–408. doi: 10.1016/0962-8924(93)90091-E

Ytterberg, A. J., Peltier, J., and van Wijk, K. J. (2006). Protein profiling of plastoglobules in chloroplasts and chromoplasts. A surprising site for differential accumulation of metabolic enzymes. *Plant Physiol.* 140, 984–997. doi: 10.1104/pp.105.076083

Zhang, K., Yau, P. M., Chandrasekhar, B., New, R., Kondrat, R., Imai, B. S., et al. (2004). Differentiation between peptides containing acetylated or tri-methylated lysines by mass spectrometry: an application for determinin lysine 9 acetylation and methylation of histone H3. *Proteomics* 4, 1–10. doi: 10.1007/s12014-008-9020-1

CrossMark

Analysis of Sensitive CO_2 Pathways and Genes Related to Carbon Uptake and Accumulation in *Chlamydomonas reinhardtii* through Genomic Scale Modeling and Experimental Validation

Flavia V. Winck[1]*[†], David O. Páez Melo[1], Diego M. Riaño-Pachón[2][†], Marina C. M. Martins[3], Camila Caldana[3,4] and Andrés F. González Barrios[1]

[1] Grupo de Diseño de Productos y Procesos, Department of Chemical Engineering, Universidad de los Andes, Bogotá, Colombia, [2] Group of Computational and Evolutionary Biology, Department of Biological Sciences, Universidad de los Andes, Bogotá, Colombia, [3] Brazilian Bioethanol Science and Technology Laboratory, Brazilian Center for Research in Energy and Materials, Campinas, Brazil, [4] Max Planck Partner Group, Brazilian Bioethanol Science and Technology Laboratory, Brazilian Center for Research in Energy and Materials, Campinas, Brazil

The development of microalgae sustainable applications needs better understanding of microalgae biology. Moreover, how cells coordinate their metabolism toward biomass accumulation is not fully understood. In this present study, flux balance analysis (FBA) was performed to identify sensitive metabolic pathways of *Chlamydomonas reinhardtii* under varied CO_2 inputs. The metabolic network model of *Chlamydomonas* was updated based on the genome annotation data and sensitivity analysis revealed CO_2 sensitive reactions. Biological experiments were performed with cells cultivated at 0.04% (air), 2.5, 5, 8, and 10% CO_2 concentration under controlled conditions and cell growth profiles and biomass content were measured. Pigments, lipids, proteins, and starch were further quantified for the reference low (0.04%) and high (10%) CO_2 conditions. The expression level of candidate genes of sensitive reactions was measured and validated by quantitative real time PCR. The sensitive analysis revealed mitochondrial compartment as the major affected by changes on the CO_2 concentrations and glycolysis/gluconeogenesis, glyoxylate, and dicarboxylate metabolism among the affected metabolic pathways. Genes coding for glycerate kinase (GLYK), glycine cleavage system, H-protein (GCSH), NAD-dependent malate dehydrogenase (MDH3), low-CO_2 inducible protein A (LCIA), carbonic anhydrase 5 (CAH5), E1 component, alpha subunit (PDC3), dual function alcohol dehydrogenase/acetaldehyde dehydrogenase (ADH1), and phosphoglucomutase (GPM2), were defined, among other genes, as sensitive nodes in the metabolic network simulations. These genes were experimentally responsive to the changes in the carbon fluxes in the system. We performed metabolomics analysis using mass spectrometry validating the modulation of carbon dioxide responsive pathways and metabolites. The changes on CO_2 levels mostly affected the metabolism of amino acids found in the photorespiration pathway. Our updated metabolic network was compared to

previous model and it showed more consistent results once considering the experimental data. Possible roles of the sensitive pathways in the biomass metabolism are discussed.

INTRODUCTION

The increase of air emissions originated from the burning of fossil fuels and the continuous rising of the demands and prices of energy have been an issue of world impact and socio-economic importance (O'Neill and Oppenheimer, 2002; Hoegh-Guldberg and Bruno, 2010). Microalgae-based technologies focused in the bioremediation of air emissions coupled to biomass production represents a potential alternative way for reducing levels of air contaminants, creating new sources of renewable biomass that can be used for bioenergy production, or even for the accumulation of other bioproducts (Li et al., 2010; Packer et al., 2011; Scranton et al., 2015). Microalgae can, through photosynthesis, capture CO_2 and accumulate biomass, reducing the net emission of CO_2 during the biofuel production, contributing to protect the environment through sustainable applications, including the development of third generation biofuels (Singh and Olsen, 2011; Singh et al., 2011; Behera et al., 2014). Therefore, microalgae have attracted more attention as suitable organisms with potential to be a sustainable source of biocompounds important for a number of areas such as nutrition, aquaculture, pharmaceuticals, and biofuels. Thanks to the advances in microalgae biology, bioengineering, and molecular biology, a better understanding of metabolic routes, gene expression regulation, and cellular mechanisms is being achieved, which may contribute to further improve microalgae capabilities toward sustainable applications (Rosenberg et al., 2008).

Since the efficiency to derive biofuels from microalgae seems to be comparable to those derived from crops plants (such as soy and canola), there is a great interest to develop research in biofuel production through maximizing biomass accumulation and improving derivatization processes (Savage, 2011). Biomass can be transformed into fuels by conversion of carbohydrates to ethanol, transesterification of lipids into biodiesel, gasification of biomass to syngas, cracking of hydrocarbons, and isoprenoids to gasoline (Matsumoto et al., 2003) and the direct synthesis of hydrogen gas (Carvalho et al., 2006).

Among the many species of microalgae, *Chlamydomonas reinhardtii* has been extensively considered as a model organism to the study of different cellular mechanisms under distinct environmental conditions (Harris, 2001). This knowledge may be applied to improve specific features and could be in some cases extrapolated to close evolutionary relative species. For example, it has been found that, although *Chlamydomonas* is not considered a good lipid-storing species, under N-starvation this capability is favored (Scranton et al., 2015). Additionally, several reports have indicated that by changing the cultivation conditions, such as carbon source, light intensity, nitrogen, sulfur, and microelements availability, the biomass production

could have significant improvement in microalgae cultivation (Rosenberg et al., 2008).

However, it is important to generate strategies that improve our capacity to predict the cellular behavior or to precisely identify the biological pathways that have an important role on determining biomass accumulation. Uncovering these pathways may allow us to perform permanent optimization of the capabilities of microalgae to accumulate biomass. An *in silico* method useful to analyze cell behavior under different growth conditions or disturbances and simulate metabolic changes occurring in microalgae cells consists of Flux Balance Analysis (FBA). This approach takes in consideration a linear programming strategy to solve and describe the fluxes in a systems at steady state (Orth et al., 2010).

FBA has emerged as a mathematical tool to study metabolic networks and has been successfully tested in prokaryotes including genus *Escherichia* (Edwards et al., 2002), *Lactobacillus* (Dishisha et al., 2014), *Nitrosomonas* (Perez-Garcia et al., 2014), to mention a few examples. In many of these studies, FBA was applied to detect main metabolic pathways, growth rates at specific genetic and environmental conditions, and revealed possible candidate genes for improvement of specific strains (Edwards et al., 2002). In *Chlamydomonas*, the FBA approach was previously employed to predict metabolic fluxes based on primary metabolism (Boyle and Morgan, 2009). Furthermore, FBA was used to estimate the cell growth rate at different photon flux inputs in an improved metabolic network (Chang et al., 2011).

From the perspective of the CO_2 uptake by microalgae and biomass production, the strategies of cell survival at low CO_2 have been well described with the characterization of the Carbon Concentrating Mechanism (CCM) (Badger et al., 1980). Through the understanding of the CCM, it is possible to explain, at least partially, the mechanisms by which microalgae are able to keep their photosynthesis performance and mitigate the stress caused by low CO_2 supply. Basically, cell machinery elevates the CO_2 concentration at the site of RubisCO (ribulose-bisphosphate carboxylase/oxygenase) enzyme by increasing the cellular inorganic carbon (Ci) pools favoring the carboxylase activity of RubisCO; thus, carbon fixation through photosynthesis. Moreover, some Ci transporters located in the plasma membranes and chloroplast have been suggested as main proteins on the carbon uptake process (Wang et al., 2011).

Since CCM is not fully activated at high CO_2 concentration and considering the fact that increasing the Ci concentration inside the cell alone does not guarantee full and effective carbon fixation due to reaction saturation problems, a deeper investigation of this process through *in silico* analysis is still needed. Moreover, the knowledge about the metabolic limitations

of microalgae to accumulate and fixate CO_2 even under high CO_2 concentrations is still incomplete. It has been previously suggested that some microalgae species are not able to fixate all carbon that is supplied to its growth and a possible saturation on the carbon fixation may occur (Melo et al., 2014). The identification of the pathways and biochemical routes that contribute to this saturation on the carbon fixation will continue to improve our understanding of the molecular control of the biomass accumulation.

Therefore, in the present study we investigated the effects of high CO_2 concentration in a metabolic perspective. We disclosed novel routes and genes related to CO_2 uptake and fixation through genomic scale metabolic network modeling. Our modeling strategy took in consideration the metabolic reconstruction reported by Chang et al. (2011) which was further updated and extended through homology-based sequence analysis on the annotated genome of the microalgae *C. reinhardtii*. Biomass production in this species was selected as the optimization function and evaluated under different CO_2 concentrations, ranging from 0.04 to 10%, using experimental data of biomass content as model constrains. The results from both models were compared, sensitive genes were selected, and their relative expression experimentally validated by quantitative real-time PCR. In addition, metabolome analysis was performed for the relative quantification of primary metabolites. Together, the detection and validation of sensitive genes and pathways under high CO_2 conditions through FBA, gene expression analysis and metabolomics, indicated that CCM, photorespiration and mitochondrial related processes have important roles in the control of biomass accumulation in *C. reinhardtii*. Our work revealed potential candidate pathways and genes for future maximization of microalgae biomass production.

MATERIALS AND METHODS

Metabolic Network Reconstruction

The *i*RC1080 model from Chang et al. (2011) was supplemented by genomic information and gap filling using metabolic databases. All the annotated protein sequences for *C. reinhardtii* (14,414 sequences) were retrieved from NCBI database (Sayers et al., 2009) and served as input for previous scripts developed in our research group that identify enzymes based on homology analysis by using BLASTp from NCBI. This analysis identified a total of 1632 enzymes (Supplemental Table 1). The recognized proteins were then used to extract all the metabolic reactions associated according to the KEGG database (Kanehisa and Goto, 2000) (Supplemental Table 2). An improved manual curation was performed due to the appearance of new reactions, substrates, and products that required new connections. Manual inspection was also needed to avoid generic metabolites and repeated reactions. The directionality of the new reactions was defined by the criteria of the free Gibb's energy at $27°C$ and pH 7 and calculated by the group contribution method as described in Mavrovouniotis (1990). Compartmentalization was needed to guarantee the placement and viability of the reaction according

to Chang et al. (2011), literature and databases based on signal peptide (Petersen et al., 2011). Exchange reactions were included in order to connect the new metabolites in the cellular compartments ensuring origin and consumption of reagents. Special attention was required for lipids and carbohydrates because generic or general names were found in KEGG database hindering the integration of new reactions.

Sensitivity Analysis

The two metabolic networks, the *i*RC1080 model given by Chang et al. (2011) and our complemented model, were reconstructed into the stoichiometric matrix and the fluxes of the transport reactions adjusted to represent autotrophic growth conditions. Light condition was fixed at cool-white fluorescent (57.54 mE/gDW.h, equivalent to $400 \, \mu E \cdot m^{-2} \cdot s^{-1}$) and the CO_2 fluxes modified to evaluate the effects of different conditions of CO_2 supply at the steady state of the cell metabolism and other parameters were established as previously described (Melo et al., 2014). In both cases, the Biomass function was not modified and was implemented as proposed by Chang et al. (2011). The lower and upper bounds of the new reactions were fixed according to standard values. The optimization problem was resolved using Xpress IVE® by setting constraints as follows:

$$\max_z c^T v(1)$$
$$subject \ to \ \mathbf{S}v = \mathbf{0}$$
$$LB \leq \boldsymbol{v} \leq UB$$
$$c^T \in R^n \left| c^T = [0\,0\,0\ldots1\ldots0\,0\,0] \right| pos(1) = Biomass \ reaction$$
$$\boldsymbol{v} \in R^n$$
$$\boldsymbol{S} \in R^{m \times n}$$
$$LB \in R^n$$

Where $\boldsymbol{S}$ is the stoichiometric matrix, $\boldsymbol{v}$ is the flux vector, *LB*: lower bound, *UB*: Upper bound, *c* is a vector of zeros that sets the objective function, *m* is the number of metabolites, *n* is the number of reactions, $pos(1)$ is the objective function (biomass).

The definition of candidate metabolic pathways and genes that could play an important role in CO_2 level response was performed through the identification of reactions affected under different CO_2 fluxes through FBA simulations. FBA was resolved at five different CO_2 conditions (0, 2.5, 8, 5, and 10% CO_2) and the resulting magnitudes defined the CO_2-sensitive reactions by the flux variation coefficient ρ [set to be significant when $\rho \geq 0.01$ (Melo et al., 2014)]. Experimental data of total biomass content were considered as model constrains for calculating the CO_2 fluxes, as previously described (Melo et al., 2014). The results from both models were compared to analyze the effects of the metabolic networks on the sensitivity of FBA.

Results from metabolomics analysis were used to further verify our sensitive reactions and support the FBA analysis. Thus, metabolites relatively quantified by metabolomics were compared to check compatibility between overexpression and knock-down according to our FBA results. For this, all the FBA-sensitive reactions for one specific metabolite were grouped with their calculated fluxes at low and high CO_2 concentrations. A

net flux was then calculated by adding production reactions, subtracting consumer reactions, and a rate between the net flux at low CO_2 over the net flux at high CO_2 was finally considered.

Cell Strain and Culture Conditions

The *C. reinhardtii* strain CC503 cw92mt+ (Chlamydomonas Resource Center University of Minnesota, USA) was cultivated in HSM medium at 27°C in autotrophic growth conditions, under different CO_2 concentrations [0.04 (air), 2.5, 5, 8, and 10% CO_2] in a R'ALF Plus solo 6.7 L bioreactor (Bioengineering, Inc., USA) in constant and continuous illumination with cool-white LED (average $400\,\mu E \cdot m^{-2} \cdot s^{-1}$). The cultures remained in a batch mode with starting culture volume of 4 L, in open system with automatic controlled CO_2 gas flow in air, no pH control and continuous stir at 60 rpm. Cell inoculation was carried out with a 10 mL pre-inoculum taken from a sample at steady state. Cells were harvested by centrifugation at the late exponential phase of cell growth (O.D._{750 nm} ≈ 0.9) for biomass characterization.

Cell growth monitoring was performed daily with measurements of O.D. at 750 nm and cell counting using Neubauer chamber. Growth rates were calculated as previously described (Sorokin and Krauss, 1958).

Total Biomass Measurement

Cell pellets from 50-mL cell culture aliquots at the late exponential phase were washed three times with 2 mL of demineralized water to remove inorganic salts and the final cell suspension was transferred to previously weigh empty Petri dishes. Plates containing the biomass were kept overnight at 90°C, and the dry weight was measured. Three (0.04 and 10% CO_2 conditions) or two biological replicates (2.5, 5, and 8% CO_2 conditions), each one with three technical replicates, were considered for statistical analysis.

Protein, Lipid, Pigment, and Starch Measurements

Cells at low (0.04%) and high CO_2 (10%) were harvested in 50-mL aliquots (three biological replicates and three technical replicates per sample) and centrifuged at 3000 × g in a swing rotor bench centrifuge for 5 min at 4°C. Cell pellets were kept at −80°C until further processing. Frozen cell pellets were macerated until conversion into a light green powder. Protein extraction was performed using a buffer containing 100 mM Tris pH 7.5, 4 mM EDTA, 5 mM 2-mercaptoethanol, 10% glycerol, and 0.05% Triton X-100. Protein content was determined by Bradford assay (Bradford, 1976). Pigments were extracted using ethanol and quantified using Kaczmar equations (Henriques et al., 2007). Lipids and carbohydrates were extracted using chloroform:methanol:water (1:2:0.8) mixture, and the resulting chloroform layer, which contains the lipids, was evaporated in a vacuum oven at 30°C for 24 h. The total lipid content was calculated by dry weight. Starch content was determined in the insoluble fraction after the chloroform:methanol:water extraction and solubilized in 0.1 M NaOH for 30 min at 95°C. After neutralization, starch was digested to glucose by the addition of amyloglucosidase and α-amylase at 37°C overnight. Determination of the glucose released by the enzymatic digestion of starch was assayed enzymatically by coupling to reduction of NADP+ to NADPH in a microplate reader (Stitt et al., 1989).

Gene Expression Analysis by Quantitative RT-PCR

Based on our results on the sensitivity analysis using FBA approach on the model described by Chang et al. (2011) and literature review, 40 sensitive genes related to CO_2 changes [low CO_2 (0.04%; air) and high CO_2 (10% CO_2)] were selected to further gene expression analysis through the relative quantification by qRT-PCR. These candidate genes were previously annotated to the following routes and mechanisms: CCM, Calvin cycle, Glycolysis/Gluconeogenesis metabolism, and Glyoxylate/dicarboxylated.

Cells for RNA extraction were harvested in 2-mL aliquots by centrifugation for 2 min, 3000 × g, at 4°C, and the cell pellets were immediately frozen and kept at −80°C until further use. Total RNA extraction was performed using the RNeasy Plant Mini Kit (Qiagen, Hilden, Germany) as previously described (Winck et al., 2013). Total RNA samples were treated with TURBO DNAse (Ambion, Darmstadt, Germany) as indicated by the manufacturer. Absence of genomic DNA contamination was accessed by qRT-PCR using primers annealing to an intergenic region of chromosome 16 (IGR1, IGR2). Primers were designed using QuantPrime tool (www.quantprime.de) following the criteria as follows: Tm = 60 ± 1°C, length 18–25 bases, preferentially on exon-exon junctions. When possible, primers were designed to have a GC content of 45–55%, generating a single PCR product sizing between 60 and 150 bp. Primers were synthesized by Macrogen (Macrogen, Korea).

Three micrograms of total RNA were used for cDNA synthesis employing the SuperScript III First Strand System (Invitrogen, Darmstadt, Germany) according to the manufacturer's instructions, using oligo-(dT_{20}) as primer for the synthesis of the first complementary DNA strand. Two genes [Actin (ACT) and Ubiquitin protein ligase (UBQ)] were selected as reference genes. All the cDNA samples were amplified in 96-well plates in an Applied BioSystems ABI7500 FAST system. The qPCR reaction was carried out in $10\,\mu L$ containing $1\,\mu M$ primers and SYBR Green qPCR Master Mix (Roche). The primer sequences used in this study are presented in Supplemental Table 3. Real-time PCR reaction parameter settings were as follow: 2 min at 50°C, 10 min at 95°C, followed by 40 cycles of 15 s at 95°C and 1 min at 60°C. Amplicons which dissociation curve resulted in double melting temperatures or doubled products in a 4% gel electrophoresis were discarded from further analysis. The relative expression ratio for each gene was calculated as previously described (Pfaffl, 2001). The PCR efficiency for each reaction was calculated based on the profile of the emitted fluorescence in the exponential phase (Rutledge and Stewart, 2008; Rutledge, 2011). Three biological replicates, each one with one technical replicate for the two conditions analyzed (0.04 and 10% CO_2) were performed.

Metabolomics Analysis

Aliquots of 50-mg pellet from cell culture were taken in the stationary phase (OD_{750} ≈ 0.9) at low (0.04%) and high CO_2

concentration (10%). Metabolites were extracted with methanol-chloroform-water HPLC grade (2.5:1:1.4) mixture and three biological replicates for low CO_2 (0.04%) and two biological replicates for high CO_2 (10%) were considered. Samples were immediately frozen in liquid nitrogen and lyophilized for storage. Extraction and derivatization of metabolites were performed as outlined previously (Lisec et al., 2006). GC-TOF-MS data were obtained using a PAL-Combi XT autosampler (PAL System http://www.palsystem.com/), coupled to an Agilent 7890 A gas chromatograph—Leco Pegasus HT time-of-flight mass spectrometer (LECO, St. Joseph, MI, USA; http://www.leco.com/). Identical chromatogram acquisition parameters were used as those previously described (Weckwerth et al., 2004). Chromatograms were exported from Leco ChromaTOF software (version 4.51.6.0) to R software. Peak detection, retention time alignment, and library matching were obtained using the TargetSearch package from bioconductor (Cuadros-Inostroza et al., 2009). Data obtained from GC-TOF-MS analysis were normalized by cell number, followed by sample total ion content (TIC) as described previously (Giavalisco et al., 2011).

RESULTS
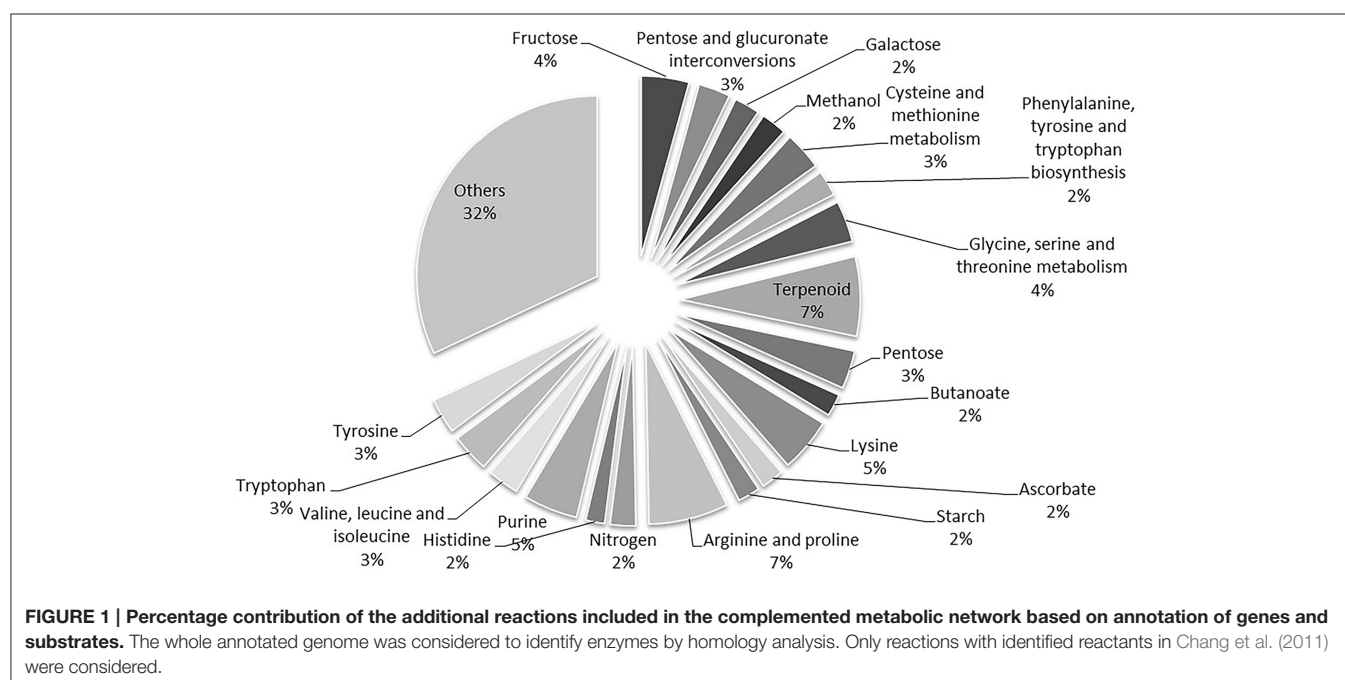
Metabolic Reconstruction Revealed Novel Reactions

Inspections through different metabolic databases [GoFORSYS—ChlamyCyc (http://chlamycyc.mpimp-golm.mpg.de/) or PMN (http://pmn.plantcyc.org/CHLAMY/) that report proteins and curated metabolic data, showed that only a small group of enzymes of *Chlamydomonas* has been discovered and functionally characterized. Considering this, our homology analysis was performed comparing all annotated proteins in

KEGG database to identify the EC numbers and the associated reactions. In order to simplify the reconstruction, only the reactions with reported reactants in Chang et al. (2011) were considered.

A total of 1632 enzymes were found by BLASTp analysis using our script and a total of 2599 reactions (without compartmentalization) were associated. After removing the reactions that already exist in the work of Chang et al. (2011), 1803 new reactions were identified. By following the proposed criteria, considering only the reactions with identified reactants described by Chang et al. (2011), we detected 1380 new compartmentalized reactions based on the homology analysis with KEGG database (Supplemental Table 2). Some products had to be connected by gap filling with manual inspection in KEGG database taking the shortest pathway for FBA purposes. The reactions were compartmentalized ensuring availability of substrate within the 10 compartments and a total of 87 reactions were defined as reversible based on Gibbs energy evaluation and previously reported studies. **Figure 1** depicts the percentage contribution of the main reaction categories, including substrates, and products for the updated of the metabolic network.

We found that some reactions and metabolites have generic names in KEGG database, especially those associated to lipid and starch metabolism. This inconsistent information provides new reactions and metabolites that cannot be interconnected affecting viable results from the FBA analysis. Gaps within the different pathways were observed when looking at the rows of the stoichiometric matrix and manual interconnection had to be assumed to consume products based on metabolic maps. Furthermore, unlikely reactions were found associated to homology parameters, reactions belonging to penicillin, and cephalosporin biosynthesis were rejected because no information

FIGURE 1 | Percentage contribution of the additional reactions included in the complemented metabolic network based on annotation of genes and substrates. The whole annotated genome was considered to identify enzymes by homology analysis. Only reactions with identified reactants in Chang et al. (2011) were considered.

was confronted with *Chlamydomonas*. These results indicated that manual curation is still necessary and mandatory to guarantee feasible models.

Curation Level of the Network Affects FBA Sensitivity Analysis

In a previous work, we have identified a total of 87 sensitive reactions solving the biomass function (Melo et al., 2014). A comparison of these sensitive reactions was performed against the previous model proposed by Chang et al. (2011), and 155 sensitive reactions were identified in our current complemented network (Supplemental Table 4). The percentage distribution of the annotation of the metabolic pathways corresponding to the sensitive reactions is shown (**Figure 2**). Data tendency is highly conserved between both models: reactions associated to mitochondrial transport, chloroplast transport, glycolysis/gluconeogenesis, and TCA cycle are both subjected to regulation under different CO_2 input fluxes. However, in our complemented reconstruction, more, and novel sensitive reactions appeared related to the amino acid metabolism of alanine, threonine, tryptophan, and propionate metabolism (resulting in production of valine and alanine) (Supplemental Table 5). Other reactions belonging to starch, sucrose, and methane metabolism were also glimpsed. Over 25 genes remained sensitive in both reconstructions and new ones were identified (**Table 1**). Our results showed that larger networks may lead to different results on the sensitive analysis

and may contribute to disclosing new candidate sensitive reactions.

Our sensitive analysis revealed that mitochondria is the most sensitive cellular compartment and showed the highest number of reactions affected by varying CO_2 concentrations, mainly related to amino acid transporters, carriers (phosphate, dicarboxylate), and transport of compounds such as ethanol, ammonia, and O_2. The mitochondria is important to the maintenance of intracellular redox gradients, impacting the rates of photorespiration, and efficiency of photosynthesis (Araújo et al., 2014). Therefore, our results of the sensitive analysis pointed to a possible role of mitochondria in modulating the biomass production in microalgae. In order to validate our results from the FBA analysis, the biomass objective function was compared with the experimental data on biomass production. As we have previously shown (Melo et al., 2014), the magnitudes of the growth rates in our simulations were similar to experimental values. However, *in silico* data showed a linear increment of biomass production that does not represent the saturation trends observed in our experimental conditions. High CO_2 concentration enhances biomass production through non-linear trend.

Cell growth was measured daily (**Figure 3A**) and a significant increase in the total dry weight biomass was evident at high CO_2 concentrations (above 0.04% CO_2), reaching the highest content when evaluated at 10% (**Figure 3B**). Therefore, there was a biomass increment of at least 300% in the cell culture in high CO_2 concentrations compared to cells cultured under low CO_2 concentration (air); this information corroborate previous results (Chang et al., 2011). The amount of proteins (**Figure 4A**), pigments (**Figure 4B**), lipids (**Figure 4C**), and dry weight (DW) (**Figure 4D**), quantified per cell and compared between the low CO_2 (0.04%) and high (10%) CO_2 conditions, showed a positive increase at high CO_2 concentration. However, no significant changes were found for starch (about 17 μmol/g or mg/dDW $\pm$ 2.5 at low CO_2 and 16 μmol/dDW $\pm$ 4.0 at high CO_2, $p > 0.05$). Moreover, we observed that cell culture at 5% CO_2 produced similar amounts of total biomass than cells cultured at 10% CO_2, suggesting the existence of a saturation trend in the biomass production once cells are cultivated in CO_2 concentration higher than 5%.

Furthermore, the cell growth curves observed on high CO_2 conditions (2.5, 5, 8, and 10% CO_2) showed similar profiles but cellular density was higher and statistically different from those cell cultures under low CO_2 (0.04%). Thus, the exposure to high CO_2 lead to an increased number of cells per culture volume and enhanced cellular capability to accumulate biomass, likely affecting mitosis-related cell cycle and energy metabolism.

Gene Expression Analysis Revealed Candidate Sensitive Genes

The experimental validation of our results on the identification of CO_2 sensitive metabolic reactions included gene expression analysis of selected genes and a metabolomics approach focused in the identification and relative quantification of the main metabolites of primary metabolism.
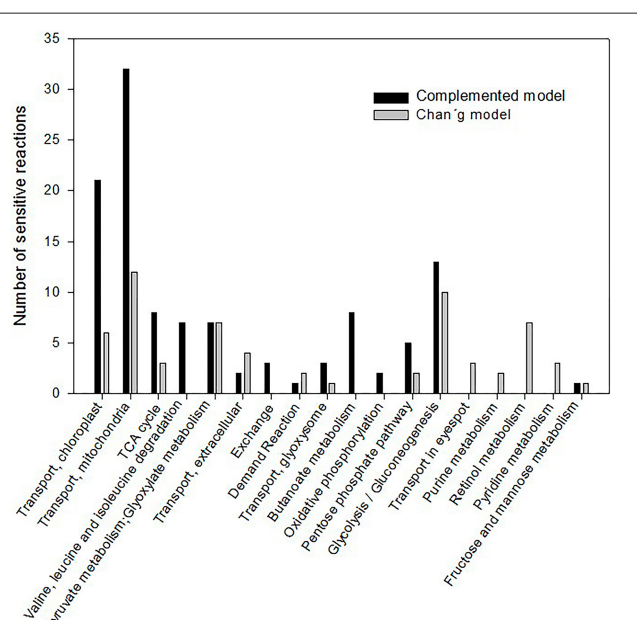
FIGURE 2 | Distribution of the metabolic pathways affected on sensitive analysis from the both metabolic models evaluated. FBA analysis was performed for the different CO_2 inputs in the system at autotrophic conditions. The same biomass function was established in both models and sensitive reactions were identified based on the flux variation coefficient. Metabolic pathways affected on sensitive analysis were annotated and the number of sensitive reactions is indicated.

TABLE 1 | Sensitive genes from FBA analysis of the complemented network.

Biological processes	Sensitive genes*
Transport, mitochondria	**MITC14**/MITC18/PTB8/PTB7/PTB1/PTB12/PTB4/PTB2/CRv4_Au5.213.g4507.t1
Phenylalanine tyrosine and tryptophan	**AST4/HIS5**
TCA cycle/CO$_2$ fixation	**ACH1**/IDH3/SDH1/SDH2/OGD1
Valine, leucine, and isoleucine degradation	CRv4_Au5.s4.g11844.t1/Crv4_Au5.s12.g3863.t1/CRv4_Au5.s6.g13618.t1/CRv4_Au5.s12.g3863.t1/g1910.t1
Pyruvate metabolism; Glyoxylate metabolism	**HYDA1/MFDX/HYDA2**/PFL1/ACK2/AACK1/ACK1/PAT1/PAT2/CRv4_Au5.s6.g13230.t1/CRv4_Au5.s2.g9723.t1
Alanine and aspartate metabolism; glycerine, serine, and threonine	**AST3/AST1**
Carbon fixation	AAT1/**AAT2**/MME3/MME6/MDH5/MME2
Glycolisis, Gluconeogenesis, Valine, Leucine, and isoleucine degradation	**DLDH1**/PDC2/PDH2/ALSS1/ALSL1/PYK1/PYK5/PHG1/GAP3/GAP1/PGM2/PGM5/PGM1B/PGK1/TPIC/FBA1/FBA2/PGI1/GPM2
Transport, extracellular	**NAR1.6/NAR1.3/NAR1.4**
Pentose phosphate pathway	TAL1/TRK1/RPE1/RPI1
Glycine, serine, and threonine metabolism	Crv4_Au5.s10.g124.t2/THD1/SHMT3
Transport, chloroplast	AOC6/**AOC5/AOT7/DAT1**/OMT1/AOT5/**FBB13**/NAR1.5/NAR1.2/NAR1.1/AAA3/AAA1/CRv4_Au5.s14.g5515.t1/CRv4_Au5.s15.g5921.t1/CRv4_Au5.g14736.t1/MOT20/**MIP1/MIP2**
Butanoate metabolism	CRv4_Au5.s7.g14479.t1/CRv4_Au5.s16.g6952.t1
Oxidative phosphorylation	**NDA3/NUO11/NUO10/NUO13/NUO21/NUO3/NUO5**/NUO6/NUO8/NUO9/IPY1/IPY3
Propanoate metabolism	PFL1
Nitrogen metabolism	CGL77/IBA57/GCST

*Bold type names represent common sensitive genes present in both metabolic reconstructions of Chang et al. (2011) and our present complemented reconstructed network.
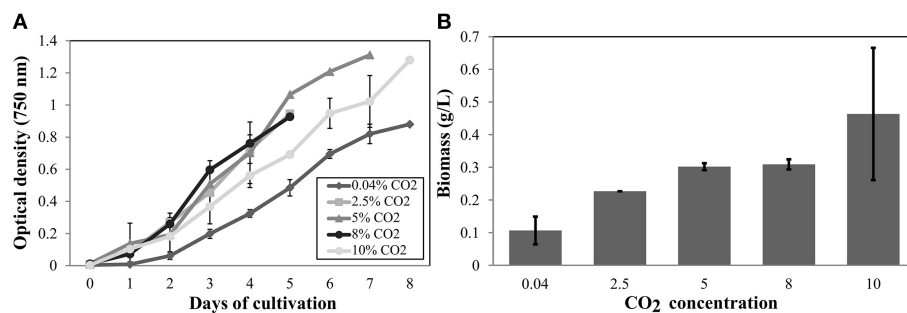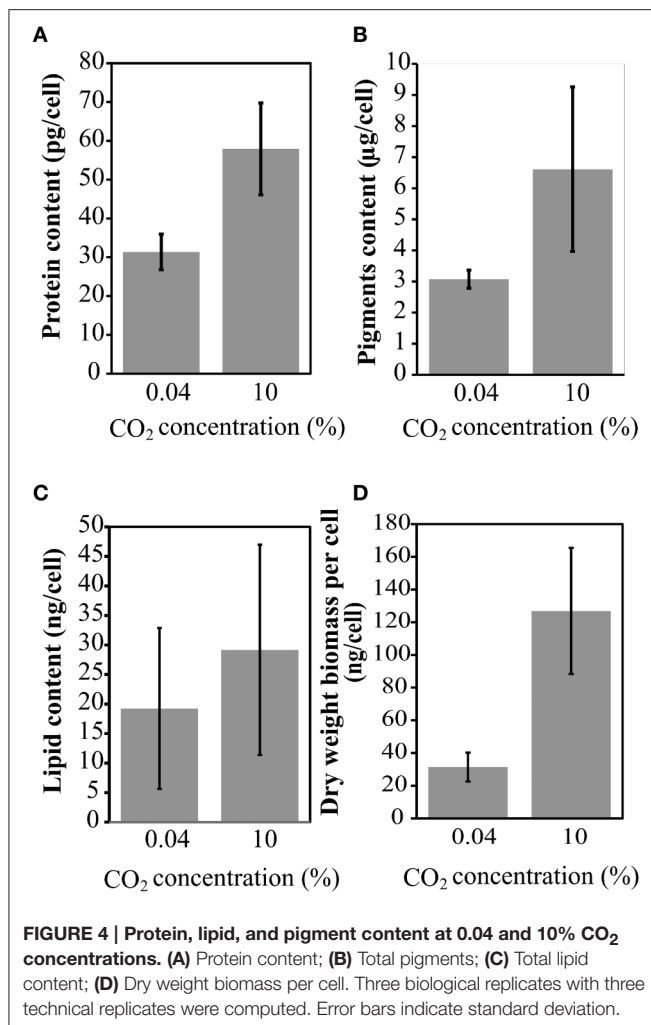
FIGURE 3 | Cell growth and biomass profiles at different CO$_2$ inputs in autotrophic conditions. (A) Cells were grown in a controlled bioreactor and autotrophic conditions (in HSM medium). Absorbance at 750 nm was daily measured. **(B)** Dry weight biomass (gDW/L). The data show the average of two biological replicates and three technical replicas for each sample. Error bars indicate standard deviation.

In **Figure 5A**, the relative expression levels of genes encoding carbonic anhydrases (CAHs) are shown. Carbonic anhydrases can catalyze the reversible interconversion of carbon dioxide to carbonic acid in order to increase the carbon uptake and availability in the site of photosynthesis at the chloroplast. The analysis of these genes was included because there were previous evidences that CO$_2$ related mechanisms may be determinant to biomass accumulation and CAHs play an important role on cellular carbon uptake (Fang et al., 2012; Winck et al., 2013). Our results showed that gene transcripts for CAH1, CAH4, CAH5, and LCI1 were found to be more abundant in low CO$_2$ concentration (0.04%). Similar results were shown by previous studies on the Carbon Concentrating Mechanism (Brueggeman et al., 2012). Moreover, our updated FBA sensitivity analysis revealed that metabolic pathways of glycolysis/gluconeogenesis, glyoxylate, and dicarboxylate metabolism are affected by the changes in CO$_2$ concentration. Genes coding for glycerate kinase (GLYK), glycine cleavage system, H-protein (GCSH), NAD-dependent malate dehydrogenase (MDH3), low-CO$_2$ inducible protein A (LCIA), low-CO$_2$-inducible protein 23 (LCI23), mitochondrial pyruvate dehydrogenase complex, E1 component, alpha subunit (PDC3), fructose-1,6-bisphosphate aldolase (FBA2), glyceraldehyde-3-phosphate dehydrogenase (GAP1), dual function alcohol dehydrogenase/acetaldehyde dehydrogenase (ADH1), and phosphoglucomutase (GPM2), were defined as sensitive nodes in the metabolic network simulations and found to be responsive to the changes in the carbon fluxes in the system.

FIGURE 4 | Protein, lipid, and pigment content at 0.04 and 10% CO₂ concentrations. (A) Protein content; **(B)** Total pigments; **(C)** Total lipid content; **(D)** Dry weight biomass per cell. Three biological replicates with three technical replicates were computed. Error bars indicate standard deviation.

As discussed previously, the sensitivity analysis may generate different outputs depending on the completeness of the metabolic network used as input for simulation. Genes coding for GLN1, CIS1, ATP2, PRK1, and FBP1, which were found to be sensitive in Chang et al. (2011), showed low variation in the gene expression levels in our network model (**Figure 5B**). These genes are involved in different metabolic processes such as carbon fixation, glutamate metabolism, and fructose metabolism, as previously shown (Melo et al., 2014). Moreover, genes coding for glycerate kinase (GLYK), phosphoglucomutase (GPM2), fructose-1,6-bisphosphate aldolase (FBA2), and glyceraldehyde-3-phosphate dehydrogenase (GAP1), sensitive in both metabolic network models compared, showed variations at the gene expression levels. This may suggest that our proposed network model could give complementary and valuable insights considering the results of transcriptional changes.

Metabolites are Affected by Changes on CO₂ Concentration Levels

The identification of sensitive reactions through FBA guided us to perform a quantitative analysis of the metabolites of cells

cultured in low (0.04%) and high (10%) CO₂ concentrations. The metabolomics analysis performed using GC-TOF-MS permitted the quantification of 67 metabolites in the two compared CO₂ concentrations (Supplemental Table 6).

We further explored the CO₂ sensitive reactions of 13 out of the 67 metabolites identified. Our model was able to predict the behavior of these 13 metabolites at high and low CO₂ concentrations regarding the amount and presence within the cells, being consistent with experimental results at the two growth conditions, except for the measurements of glycine, isocitrate, and sucrose, which were not good represented by the FBA.

Other 50 metabolites quantified did not show significant differences between the two growth conditions (0.04 and 10% CO₂) and 50% of these did not show any alteration through FBA. From this perspective, it is shown that the model assumptions in general terms seem to be consistent with real behavior of maximizing biomass. However, others mechanisms may be activated resulting in saturation trends for CO₂ processing and constraints.

We observed that the amino acids glycine, proline, b-alanine, phenylalanine, asparagine, and lysine are the ones that suffered the most prominent alterations in abundance in response to high CO₂ concentration (**Figure 6**) (Supplemental Table 7). Relative levels of sucrose have been significantly reduced and the amount of xylose increased in the cells cultivated at 10% CO₂ concentration. This is an important indication of the cellular metabolic shift at low and high CO₂ concentrations. We also observed that glycerate was more abundant in cells at 10% CO₂. Moreover, xylose, a potential inhibitor of photosynthesis, was more than five-fold more abundant in cells at 10% CO₂ (**Figure 7**). These results suggest that photorespiration or an alternative pathway with similar substrates and products may be modulated in cells at high CO₂ concentration, possibly leading to the saturation trend in the biomass accumulation observed in cells under this condition.

FBA analysis indicated that at low and high CO₂ concentrations the metabolic routes related to photorespiration may remain at least partially activated (it was not completely off) in order to satisfy the model constraints. The magnitude of the fluxes are >0 and are contributing to maximize the biomass function. Special attention to those magnitudes were taken into account for glycine transport from chloroplast to mitochondria, serine transport from mitochondria to chloroplast, hydroxypyruvate production, glycerate, and 3-phosphoglycerate production in the chloroplast. All these processes may be related to photorespiration and showed positive fluxes in both Chang et al. and our complemented metabolic network models. Although genomic-scale restriction was not considered in the FBA, it is shown that these routes contribute to maximize biomass production.

DISCUSSION

In the present work, we compared the effects of varying CO₂ concentrations in the biomass composition of *C. reinhardtii* cells. Moreover, we identified candidate genes sensitive to the variations on the CO₂ concentrations through the use
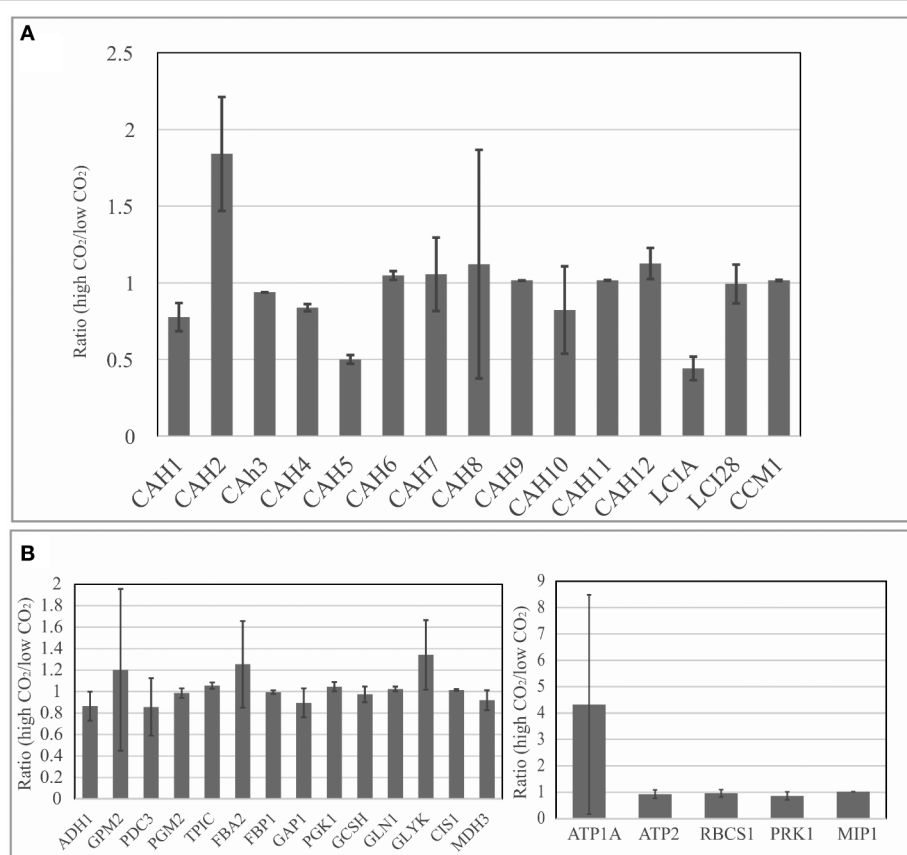
FIGURE 5 | Gene expression analysis through real-time qPCR. (A) Relative expression levels of genes related to carbon concentrating mechanism were compared at low (0.04%) and high CO_2 concentrations (10%); (B) Expression levels of genes related to glycolysis/gluconeogenesis and Calvin cycle were compared between low (0.04%) and high CO_2 concentrations (10%). Data normalization was performed using the expression level of gene coding for Actin (housekeeping gene) as reference for relative gene expression calculations. Three biological replicates were analyzed with two technical replicates. Error bars indicate standard deviation.
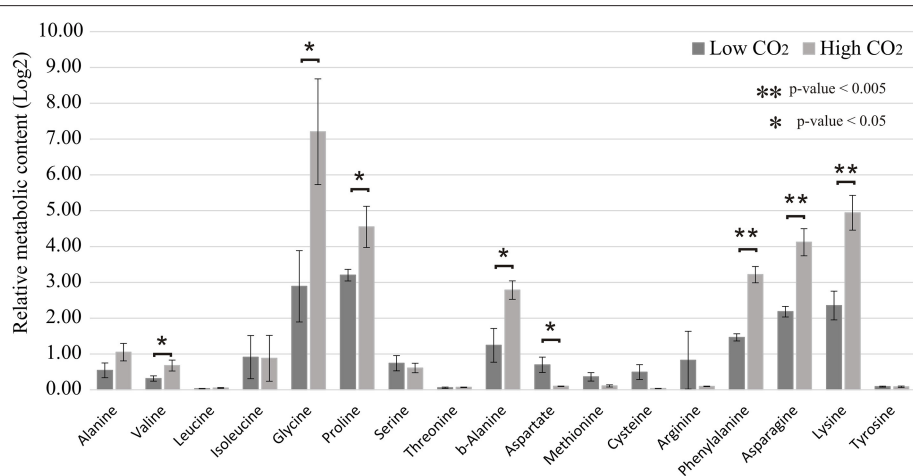
FIGURE 6 | Relative quantification of amino acids in low and high CO_2 concentrations. Metabolomics analysis was performed for the cells cultivated under low (0.04%) and high (10%) CO_2 concentrations. Amino acid content was measured by mass spectrometry analysis. Data is presented in Log_2 scale. Three biological replicates for low CO_2 (0.04%) and two biological replicates for high CO_2 (10%) were considered and three technical replicates were considered for each sample. Error bars indicate standard error.
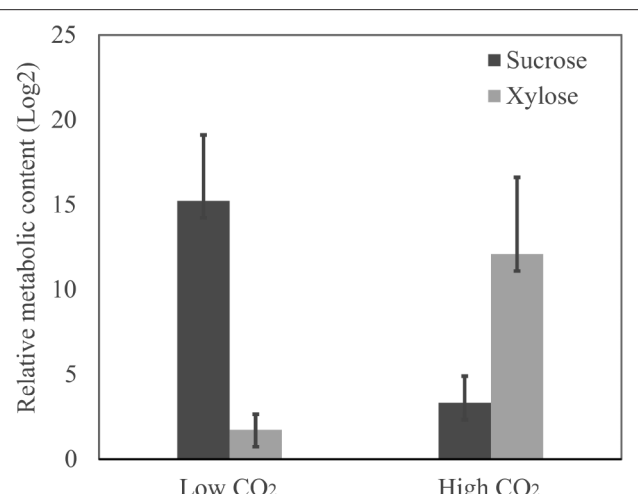
FIGURE 7 | Sucrose and xylose relative content in cells at low and high CO_2 concentrations. The relative content of sucrose and xylose was determined by metabolomics analysis through mass spectrometry. Data is presented in Log_2 scale. Three biological replicates for low CO_2 (0.04%) and two biological replicates for high CO_2 (10%) were considered and three technical replicates were considered for each sample. Error bars indicate standard error.

TABLE 2 | Candidate CO_2 sensitive genes which were identified as differentially expressed in a transcriptome dataset previously published comparing cells at high vs. low CO_2 concentrations using RNA-seq*.

Metabolic pathway or biological process Description	Candidate CO_2 sensitive genes	
	Complemented network (present work)	Chang et al., 2011
Mitochondrial transport	MIT28	
	PTB12	
	PTB4	
	PTB2	
Phenylalanine, tyrosine, and tryptophan biosynthesis	AST4	
Carbon fixation	MDH5	RBCS1
Pentose phosphate pathway	TAL1	*RPE1*
	RPE1	
	RPI1	
Transport, chloroplast	DAT1	
	NAR1.2	
Oxidative phosphorylation	NDA3	
	IPY1	
	IPY3	
Glycolysis, gluconeogenesis, valine, leucine, and isoleucine degradation	*PGK1*	*PGK1*
Extracellular transport		PTA3
		PTA4
Glycine, serine, and threonine metabolism		GCSP
		THS1
Glyoxylate metabolism		GLYK
Prphyrin and chlorophyll metabolism		GSA

Transcriptome dataset previously published (Fang et al., 2012).

of FBA in an extended metabolic network model presented here. Further experimental validation through gene expression analysis and metabolomics was performed. Our experimental results suggested that cells at high CO_2 have increased capability toward biomass production. However, it also indicated that cells cultivated at CO_2 concentrations higher than 5% achieved a saturation trend on total biomass accumulation. Although our FBA model was unable to describe this saturation trend, the magnitudes of the growth rate values were consistent between the different CO_2 concentrations compared. This may be explained by the fact that the model was resolved using linear optimization and a change in input values, such as any external metabolite, represents a proportional increase in the objective function.

Our results on the FBA sensitivity analysis of the two metabolic reconstructions showed a significant increase of flux in metabolic routes occurring in the chloroplast and mitochondria transport systems, including TCA cycle, glycolysis/gluconeogenesis, and amino acids biosynthesis in cells under high CO_2 concentrations. For the new sensitive routes and genes identified by our FBA, it was noted that many reactions were associated with energy metabolism. These sensitive routes have a number of genes which expression may be affected. Therefore, these genes may be interesting candidates on further biotechnological applications focused in the enhancement of biomass production. Reactions associated to the transport of amino acids, pyruvate, and carboxylate species into the mitochondria and chloroplast were shown to be the most sensitive ones. Moreover, mitochondria resulted as the most sensitive compartment as most reactions detected in our sensitive analysis may occur inside this organelle. Mitochondria presents a fundamental role in growth and biomass production, through its role on energy metabolism.

Sensitivity analysis also revealed a high dependence on the metabolic network quality and completeness on the identification of key routes. These routes can vary in differing models making it difficult to achieve consistent results; however, consensus in some main nodes were found and validated by qRT-PCR. Thus, our results revealed novel biochemical routes and candidate genes that may be relate to biomass production, through the modulation of the rate of biosynthetic processes.

The changes observed in the metabolite profiles of cells at low (0.04%) and high CO_2 (10%) concentrations suggest that high CO_2 concentration in microalgae cell culture may trigger mechanisms that are able to control the carbon fixation by the alternative synthesis of compounds that may have an inhibitory effect on the photosynthesis, or may enhance energy losses through photorespiration. These processes may have a role in

the control of the cell biomass content and microalgae cell population, even under non-limiting availability of CO_2. Further experiments are now necessary to provide more evidences of these effects.

Experimental validation also confirmed variations in the gene expression profiles of selected genes when cells are cultivated at different CO_2 concentrations. It was observed that many CCM-related genes are overexpressed at low CO_2, indicating, as expected, that cells change their metabolism to produce enzymes involved in enhanced carbon uptake and carbonic acid conversion, instead of redirecting energy to build biomass precursors. A previous transcriptomics analysis compared *Chlamydomonas* cells at high (5%), low (0.05%), and very low (0.02%) CO_2 concentrations (Fang et al., 2012) and revealed that the wild type strain cc125 vs. a cia5 mutant strain cc2702 showed at least 345 genes differentially expressed from low vs. high CO_2 and 696 genes from very low vs. high CO_2 in wild type cells. Several of those genes were found in our list of sensitive genes as it is summarized in **Table 2**.

Our results on the gene expression of carbonic anhydrases and genes related to CCM were consistent with previous findings. It was confirmed that the expression of CCM1 (or CIA5) itself does not depend on the CO_2 level (Fang et al., 2012). Previous studies have shown that proteins CAH1, CAH3, CAH4, CAH5, and CAH6 are responsive to variations on the CO_2 concentration. Moreover, protein LCIA, reported as induced at low CO_2, encodes a format/nitrite transporter that increase HCO3- transport in the stroma (CIA) was found highly expressed at low CO_2 concentration (Fang et al., 2012).

Besides the identification and validation of the expression of the main CA's under low and high CO_2 conditions, we further compared which metabolites were modulated in the two CO_2 concentrations (0.04 and 10%). Our metabolomics analysis indicated that the concentration of metabolites possibly related to photorespiration or other alternative route is modulated in response to high CO_2 concentration.

Our results on the experimental biomass characterization showed that the pigment content per cell is the most sensitive component and its amount is almost duplicated at high CO_2 concentration, indicating possible enhanced needs for light absorption and carbon fixation. However, starch content showed no significant changes which imply that the continuous light conditions may lead cells to control their carbohydrate stocks, probably due to the absence of a dark period and reduced need for starch accumulation or through the activation of alternative processes of carbon usage.

Altogether, these findings suggest that biomass accumulation does not enhances indefinitely with the enhanced availability of CO_2. The control of biomass accumulation may be closely connected to the regulation of biochemical pathways occurring in the mitochondria and the use of energy sources toward the accumulation of proteins and pigments.

AUTHOR CONTRIBUTIONS

FW, AG: conceived and designed the work; FW, DP, MM: performed experiments; FW and DP: drafted the manuscript; CC: performed metabolomics analysis; FW, DR, DP, AG: performed data analysis. All authors have read and approved the final version of the manuscript.

FUNDING

ACKNOWLEDGMENTS

SUPPLEMENTARY MATERIAL

The Supplementary Material for this article can be found online at: http://journal.frontiersin.org/article/10.3389/fpls.2016.00043

REFERENCES

Araújo, W. L., Nunes-Nesi, A., and Fernie, A. R. (2014). On the role of plant mitochondrial metabolism and its impact on photosynthesis in both optimal and sub-optimal growth conditions. *Photosyn. Res.* 119, 141–156. doi: 10.1007/s11120-013-9807-4

Badger, M. R., Kaplan, A., and Berry, J. A. (1980). Internal inorganic carbon pool of *Chlamydomonas reinhardtii*: evidence for a carbon dioxide-concentrating mechanism. *Plant Physiol.* 66, 407–413. doi: 10.1104/pp.66.3.407

Behera, S., Singh, R., Arora, R., Sharma, N. K., Shukla, M., and Kumar, S. (2014). Scope of algae as third generation biofuels. *Front. Bioeng. Biotechnol.* 2:90. doi: 10.3389/fbioe.2014.00090

Boyle, N. R., and Morgan, J. A. (2009). Flux balance analysis of primary metabolism in *Chlamydomonas reinhardtii. BMC Syst. Biol.* 3:4. doi: 10.1186/1752-0509-3-4

Bradford, M. M. (1976). A rapid and sensitive method for the quantitation of microgram quantities of protein utilizing the principle of protein-dye binding. *Anal. Biochem.* 72, 248–254. doi: 10.1016/0003-2697(76)90527-3

Brueggeman, A. J., Gangadharaiah, D. S., Cserhati, M. F., Casero, D., Weeks, D. P., and Ladunga, I. (2012). Activation of the carbon concentrating mechanism by CO_2 deprivation coincides with massive transcriptional restructuring in *Chlamydomonas reinhardtii. Plant Cell* 24, 1860–1875. doi: 10.1105/tpc.111.093435

Carvalho, A. P., Meireles, L. A., and Malcata, F. X. (2006). Microalgal reactors: a review of enclosed system designs and performances. *Biotechnol. Prog.* 22, 1490–1506. doi: 10.1002/bp060065r

Chang, R. L., Ghamsari, L., Manichaikul, A., Hom, E. F., Balaji, S., Fu, W., et al. (2011). Metabolic network reconstruction of Chlamydomonas offers insight into light-driven algal metabolism. *Mol. Syst. Biol.* 7, 518. doi: 10.1038/msb.2011.52

Cuadros-Inostroza, A., Caldana, C., Redestig, H., Kusano, M., Lisec, J., Peña-Cortés, H., et al. (2009). TargetSearch–a Bioconductor package for the efficient preprocessing of GC-MS metabolite profiling data. *BMC Bioinformatics* 10:428. doi: 10.1186/1471-2105-10-428

Dishisha, T., Pereyra, L. P., Pyo, S. H., Britton, R. A., and Hatti-Kaul, R. (2014). Flux analysis of the *Lactobacillus reuteri* propanediol-utilization pathway for

production of 3-hydroxypropionaldehyde, 3-hydroxypropionic acid and 1,3-propanediol from glycerol. *Microb. Cell Fact.* 13:76. doi: 10.1186/1475-2859-13-76

Edwards, J. S., Covert, M., and Palsson, B. (2002). Metabolic modelling of microbes: the flux-balance approach. *Environ. Microbiol.* 4, 133–140. doi: 10.1046/j.1462-2920.2002.00282.x

Fang, W., Si, Y., Douglass, S., Casero, D., Merchant, S. S., Pellegrini, M., et al. (2012). Transcriptome-wide changes in *Chlamydomonas reinhardtii* gene expression regulated by carbon dioxide and the CO_2-concentrating mechanism regulator CIA5/CCM1. *Plant Cell* 24, 1876–1893. doi: 10.1105/tpc.112.097949

Giavalisco, P., Li, Y., Matthes, A., Eckhardt, A., Hubberten, H. M., Hesse, H., et al. (2011). Elemental formula annotation of polar and lipophilic metabolites using (13) C, (15) N and (34) S isotope labelling, in combination with high-resolution mass spectrometry. *Plant J.* 68, 364–376. doi: 10.1111/j.1365-313X.2011.04682.x

Harris, E. H. (2001). Chlamydomonas as a model organism. *Annu. Rev. Plant Physiol. Plant Mol. Biol.* 52, 363–406. doi: 10.1146/annurev.arplant.52.1.363

Henriques, M., Silva, A., and Rocha, J. (2007). "Extraction and quantification of pigments from a marine microalga: a simple and reproducible method," in *Communicating Current Research and Educational Topics and Trends in Applied Microbiology*, Vol. 2, ed A. Méndez-Vilas (Badajoz: Formatex), 586–593.

Hoegh-Guldberg, O., and Bruno, J. F. (2010). The impact of climate change on the world's marine ecosystems. *Science* 328, 1523–1528. doi: 10.1126/science.1189930

Kanehisa, M., and Goto, S. (2000). KEGG: kyoto encyclopedia of genes and genomes. *Nucleic Acids Res.* 28, 27–30. doi: 10.1093/nar/28.1.27

Li, Y., Han, D., Hu, G., Dauvillee, D., Sommerfeld, M., Ball, S., et al. (2010). Chlamydomonas starchless mutant defective in ADP-glucose pyrophosphorylase hyper-accumulates triacylglycerol. *Metab. Eng.* 12, 387–391. doi: 10.1016/j.ymben.2010.02.002

Lisec, J., Schauer, N., Kopka, J., Willmitzer, L., and Fernie, A. R. (2006). Gas chromatography mass spectrometry-based metabolite profiling in plants. *Nat. Protoc.* 1, 387–396. doi: 10.1038/nprot.2006.59

Matsumoto, M., Yokouchi, H., Suzuki, N., Ohata, H., and Matsunaga, T. (2003). Saccharification of marine microalgae using marine bacteria for ethanol production. *Appl. Biochem. Biotechnol.* 105–108, 247–254. doi: 10.1385/ABAB:105:1-3:247

Mavrovouniotis, M. L. (1990). Group contributions for estimating standard gibbs energies of formation of biochemical compounds in aqueous solution. *Biotechnol. Bioeng.* 36, 1070–1082. doi: 10.1002/bit.260361013

Melo, D., Moncada, R.-P., Winck, F., and Barrios, A. (2014). "*In silico* analysis for biomass synthesis under different CO_2 levels for *Chlamydomonas reinhardtii* utilizing a flux balance analysis approach," in *Advances in Computational Biology*, eds L. F. Castillo, M. Cristancho, G. Isaza, A. Pinzón, and J. M. C. Rodríguez (Springer International Publishing), 279–285.

O'Neill, B. C., and Oppenheimer, M. (2002). Climate change: dangerous climate impacts and the Kyoto protocol. *Science* 296, 1971–1972. doi: 10.1126/science.1071238

Orth, J. D., Thiele, I., and Palsson, B. Ø. (2010). What is flux balance analysis? *Nat. Biotechnol.* 28, 245–248. doi: 10.1038/nbt.1614

Packer, A., Li, Y., Andersen, T., Hu, Q., Kuang, Y., and Sommerfeld, M. (2011). Growth and neutral lipid synthesis in green microalgae: a mathematical model. *Bioresour. Technol.* 102, 111–117. doi: 10.1016/j.biortech.2010.06.029

Perez-Garcia, O., Villas-Boas, S. G., Swift, S., Chandran, K., and Singhal, N. (2014). Clarifying the regulation of NO/N2O production in *Nitrosomonas europaea* during anoxic-oxic transition via flux balance analysis of a metabolic network model. *Water Res.* 60, 267–277. doi: 10.1016/j.watres.2014.04.049

Petersen, T. N., Brunak, S., von Heijne, G., and Nielsen, H. (2011). SignalP 4.0: discriminating signal peptides from transmembrane regions. *Nat. Methods* 8, 785–786. doi: 10.1038/nmeth.1701

Pfaffl, M. W. (2001). A new mathematical model for relative quantification in real-time RT-PCR. *Nucleic Acids Res.* 29:e45. doi: 10.1093/nar/29.9.e45

Rosenberg, J. N., Oyler, G. A., Wilkinson, L., and Betenbaugh, M. J. (2008). A green light for engineered algae: redirecting metabolism to fuel a biotechnology revolution. *Curr. Opin. Biotechnol.* 19, 430–436. doi: 10.1016/j.copbio.2008.07.008

Rutledge, R. G. (2011). A Java program for LRE-based real-time qPCR that enables large-scale absolute quantification. *PLoS ONE* 6:e17636. doi: 10.1371/journal.pone.0017636

Rutledge, R. G., and Stewart, D. (2008). A kinetic-based sigmoidal model for the polymerase chain reaction and its application to high-capacity absolute quantitative real-time PCR. *BMC Biotechnol.* 8:47. doi: 10.1186/1472-6750-8-47

Savage, N. (2011). Algae: the scum solution. *Nature* 474, S15–S16. doi: 10.1038/474S015a

Sayers, E. W., Barrett, T., Benson, D. A., Bryant, S. H., Canese, K., Chetvernin, V., et al. (2009). Database resources of the national center for biotechnology information. *Nucleic Acids Res.* 37, D5–D15. doi: 10.1093/nar/gkp382

Scranton, M. A., Ostrand, J. T., Fields, F. J., and Mayfield, S. P. (2015). Chlamydomonas as a model for biofuels and bio-products production. *Plant J.* 82, 523–531. doi: 10.1111/tpj.12780

Singh, A., and Olsen, S. I. (2011). A critical review of biochemical conversion, sustainability and life cycle assessment of algal biofuels. *Appl. Energy* 88, 3548–3555. doi: 10.1016/j.apenergy.2010.12.012

Singh, A., Olsen, S. I., and Nigam, P. S. (2011). A viable technology to generate third-generation biofuel. *J. Chem. Technol. Biotechnol.* 86, 1349–1353. doi: 10.1002/jctb.2666

Sorokin, C., and Krauss, R. W. (1958). The effects of light intensity on the growth rates of green algae. *Plant Physiol.* 33, 109–113. doi: 10.1104/pp.33.2.109

Stitt, M., Lilley, R. M., Gerhardt, R., and Heldt, H. W. (1989). Metabolite levels in specific cells and subcellular compartments of plant leaves. *Methods Enzymol.* 174, 518–552.

Wang, Y., Duanmu, D., and Spalding, M. H. (2011). Carbon dioxide concentrating mechanism in *Chlamydomonas reinhardtii*: inorganic carbon transport and CO_2 recapture. *Photosyn. Res.* 109, 115–122. doi: 10.1007/s11120-011-9643-3

Weckwerth, W., Wenzel, K., and Fiehn, O. (2004). Process for the integrated extraction, identification and quantification of metabolites, proteins and RNA to reveal their co-regulation in biochemical networks. *Proteomics* 4, 78–83. doi: 10.1002/pmic.200200500

Winck, F. V., Arvidsson, S., Riaño-Pachón, D. M., Hempel, S., Koseska, A., Nikoloski, Z., et al. (2013). Genome-wide identification of regulatory elements and reconstruction of gene regulatory networks of the green alga *Chlamydomonas reinhardtii* under carbon deprivation. *PLoS ONE* 8:e79909. doi: 10.1371/journal.pone.0079909

Deletion of Proton Gradient Regulation 5 (PGR5) and PGR5-Like 1 (PGRL1) proteins promote sustainable light-driven hydrogen production in *Chlamydomonas reinhardtii* due to increased PSII activity under sulfur deprivation

Janina Steinbeck[1], Denitsa Nikolova[1], Robert Weingarten[1], Xenie Johnson[2,3,4], Pierre Richaud[2,3,4], Gilles Peltier[2,3,4], Marita Hermann[1], Leonardo Magneschi[1†] and Michael Hippler[1]*

[1] Institute of Plant Biology and Biotechnology, University of Münster, Münster, Germany, [2] Laboratoire de Bioénergétique et Biotechnologie des Bactéries et Microalgues, Institut de Biologie Environnementale et de Biotechnologie, Direction des Sciences du Vivant, Commissariat à l'Energie Atomique et aux Energies Alternatives, Saint-Paul-lez-Durance, France, [3] CNRS, UMR 7265, Biologie Végétale et Microbiologie Environnementale, Saint-Paul-lez-Durance, France, [4] Laboratoire de Bioénergétique et Biotechnologie des Bactéries et Microalgues, Aix Marseille Université, Saint-Paul-lez-Durance, France

Continuous hydrogen photo-production under sulfur deprivation was studied in the *Chlamydomonas reinhardtii pgr5 pgrl1* double mutant and respective single mutants. Under medium light conditions, the *pgr5* exhibited the highest performance and produced about eight times more hydrogen than the wild type, making *pgr5* one of the most efficient hydrogen producer reported so far. The *pgr5 pgrl1* double mutant showed an increased hydrogen burst at the beginning of sulfur deprivation under high light conditions, but in this case the overall amount of hydrogen produced by *pgr5 pgrl1* as well as *pgr5* was diminished due to photo-inhibition and increased degradation of PSI. In contrast, the *pgrl1* was effective in hydrogen production in both high and low light. Blocking photosynthetic electron transfer by DCMU stopped hydrogen production almost completely in the mutant strains, indicating that the main pathway of electrons toward enhanced hydrogen production is via linear electron transport. Indeed, PSII remained more active and stable in the *pgr* mutant strains as compared to the wild type. Since transition to anaerobiosis was faster and could be maintained due to an increased oxygen consumption capacity, this likely preserves PSII from photo-oxidative damage in the *pgr* mutants. Hence, we conclude that increased hydrogen production under sulfur deprivation in the *pgr5* and *pgrl1* mutants is caused by an increased stability of PSII permitting sustainable light-driven hydrogen production in *Chlamydomonas reinhardtii*.

Keywords: PGR5, PGRL1, hydrogen production, PSII stability, sulfur deprivation

INTRODUCTION

Solar fuels are an important motive for the development of future renewable energy systems with zero CO_2 emission. This development is necessary to meet one of the most urgent challenges of our society today, to counter the problems of global warming, fossil fuel depletion, concurrent increasing energy demand, and consequently the maintenance of economic and political stability (Organisation for Economic Co-operation and Development (OECD)/International Energy Agency (IEA), 2011). Among other fuels, hydrogen is considered to be one of the most effective and clean fuels (Hankamer et al., 2007). Solar-driven H_2 production by photosynthetic microorganisms, particularly cyanobacteria and microalgae, is a promising complement to clean and sustainable technologies of hydrogen production beside chemical techniques.

Photobiological hydrogen production was first discovered by Gaffron and Rubin, 1942. In this process, electrons and protons from water splitting are directed via photosynthesis toward specific H_2-evolving enzymes, the hydrogenases. The algal Fe-Fe hydrogenase is very efficient compared to other hydrogenases (turnover rate in thousands per second, 100-fold higher than other hydrogenases; Volgusheva et al., 2013; Lubitz et al., 2014). However, direct light-to-hydrogen conversion efficiency is very low, because hydrogenase activity is extremely sensitive to oxygen (Ghirardi et al., 1997; Rupprecht et al., 2006; Stripp et al., 2009), thus oxygenic photosynthesis cannot easily be directly coupled to hydrogen production in green algae. Therefore, hydrogen production is a transient phenomenon in nature and stops after a few minutes of illumination (Bishop and Gaffron, 1963).

Melis et al. (2000) proposed an experimental protocol for prolong H_2 evolution based on sulfur deprivation that circumvents this limitation. This method allows the separation of photosynthetic oxygen evolution and hydrogen production by a two stage process: In the first phase of cell cultivation, oxygenic photosynthesis drives production of biomass and carbohydrate stores in the presence of acetate as an additional carbon source. Shifting cells to sulfur depleted medium in sealed flasks induces the switch to the second anaerobic stage, inducing hydrogenase expression and sustainable H_2 production for several days. During acclimation to this nutrient stress, cells stop dividing and undergo morphological changes (Zhang et al., 2002). Both light and dark reactions of photosynthesis are down-regulated, with the amounts of Rubisco being substantially reduced within the first 24 h of sulfur starvation (Zhang et al., 2002). Photosystem II activity drops gradually, attributed to an impaired PSII repair cycle due to the restricted *de novo* synthesis of the D1 reaction center protein (which contains methionines and cysteines) by S-limiting conditions, driving down O_2 evolution (Wykoff et al., 1998). When O_2 consumption overtakes O_2 evolution, anaerobic conditions are established. However, active PSII in the first hours of S-depletion was shown to be essential for H_2 generation, as no hydrogen evolution could be observed when the PSII inhibitor DCMU was added directly after transfer to S-free medium (Fouchard et al., 2005; Hemschemeier et al., 2008). Indeed, PSII activity was reported to contribute a substantial amount of electrons from water oxidation at PSII to hydrogen production

(Antal et al., 2003; Kosourov et al., 2003). Beside this direct PSII-dependent pathway, electrons toward the hydrogenase can also derive from an indirect pathway that relies on non-photochemical reduction of PQs from metabolites such as starch (Fouchard et al., 2005; Jans et al., 2008; Chochois et al., 2009). Starch is massively accumulated during the first hours of –S conditions and is subsequently degraded (Zhang et al., 2002). The direct sunlight to hydrogen pathway has nevertheless the potential for higher energy conversion efficiency.

The improvement in hydrogen production by the method of sulfur deprivation implicated the highest efficiency for photobiological systems reported by then (Rupprecht et al., 2006). Yet, this H_2 production efficiency has still to be advanced to reach economic profitability. Optimization of the electron supply to the hydrogenase appears to be a critical issue. Since the majority of electrons toward the hydrogenase have been shown to derive from PSII activity, but O_2 evolution by PSII has to be prevented not to inhibit hydrogenase activity, possible solution scenarios involve either a more O_2 tolerant hydrogenase or a more efficient oxygen scavenging system. Engineering resulting in a decrease in the O_2 sensitivity of the Fe–Fe hydrogenase has not been reported yet. Among some other *Chlamydomonas reinhardtii* mutant strains, the *state transition 6* (*stm6*) mutant lacking the mitochondrial respiratory chain assembly factor *moc1*, and the *proton gradient regulation like 1* (*pgrl1*) mutant displayed the highest improved hydrogen production rates (Kruse et al., 2005; Tolleter et al., 2011). The PGRL1 protein was first discovered in *Arabidopsis* (DalCorso et al., 2008) as an essential component of the PGR5 (proton gradient regulation 5) dependent cyclic electron flow (CEF) pathway (Munekage et al., 2002). Moreover, PGRL1 has been suggested to operate as the elusive ferredoxin-plastoquinone reductase (Hertle et al., 2013). In *Chlamydomonas*, PGRL1 is also required for effective CEF (Petroutsos et al., 2009; Tolleter et al., 2011) and suggested to be a functional component of a CEF-supercomplex formed under CEF promoting conditions (Iwai et al., 2010; Terashima et al., 2012). A *pgr5* mutant has recently been characterized in *Chlamydomonas* (Johnson et al., 2014), which revealed that PGR5 deficiency leads to a diminished proton gradient across the thylakoid membrane accompanied with less effective CEF capacity. The proton gradient across the thylakoid membrane was shown to restrict electron flow toward the hydrogenase in *pgrl1*, and also proton uncouplers like carbonyl cyanide-*p*-trifluoromethoxyphenylhydrazone (FCCP) and nigericin increased hydrogen evolution (Antal et al., 2009; Tolleter et al., 2011). Interestingly, both *stm6* and *pgrl1* share the characteristic of an increased respiration rate (Kruse et al., 2005; Petroutsos et al., 2009; Dang et al., 2014). Enhanced H_2 production in *stm6* was recently linked to prolonged PSII activity under sulfur starvation (Volgusheva et al., 2013). In this study, we investigated hydrogen production under similar conditions in the PGR5-deficient mutant and a *pgr5 pgrl1* double mutant in comparison to the *pgrl1* mutant. These mutants also exhibit enhanced hydrogen production and higher PSII stability under –S conditions. Since blocking PSII activity by DCMU abolished hydrogen production almost completely, we conclude

that electrons for enhanced hydrogen production mainly derive from PSII. Anaerobiosis and therefore hydrogenase activity can still be maintained due to a higher oxygen consumption capacity in the mutants.

MATERIALS AND METHODS

Strains and Growth Conditions

The *Chlamydomonas reinhardtii pgrl1* (Tolleter et al., 2011) mutant was back-crossed four times with the wild type (wt) strain CC124 (137c, nit2$^-$, mt$^-$) and then mated to *pgr5* (137c background; Johnson et al., 2014) in order to obtain *pgr5 pgrl1* double mutants in the 137c background. Zygotes were germinated on paromomycin plates (10 mg mL^{-1}) and progeny was screened for both insertion of the *AphVIII* resistance marker within the *PGRL1* coding sequence (primers AphVIII_Fw1, 5′-TCGGGCCGGAGTGTTCC-3′ and PGRL1_Rev, 5′-TTACGC AGCGGCCTTAGCC-3′) and deletion of the PGR5 locus (primers PGR5 FW2, 5′-CTACTCGCAGCCAAAACACA-3′ and PGR5 REV2, 5′-GGAAACCAGTGTGCAAGTCA-3′). Mating type of the isolated clones was assessed with primers MID_Fw (5′-ATGGCCTGTTTCTTAGC-3′), MID_Rev (5′-CTA CATGTGTTTCTTGACG-3′), FUS1_Fw (5′-ATGCCTATCTT TCTCATTCT-3′) and FUS1_Rev (5′-GCAAAATACACGTCT GGAAG-3′).

Wild-type, *pgrl1*, *pgr5,* and the *pgr5 pgrl1* double mutants were maintained on TAP medium (Harris, 1989), pH 7.0, solidified with 1.2% (w/v) agar at 25°C and 50 µE m^{-2} s^{-1} photosynthetically active, constant irradiance, and in case of the mutants supplemented with paromomycin (5 µg mL^{-1}). Strains were cultured in standard TAP medium at 25°C under continuous light of 50 µmol photons m^{-2} s^{-1} on a rotary shaker (120 rpm).

Long-term Hydrogen Production

Long-term hydrogen production was measured under conditions of sulfur deficiency (Melis et al., 2000). Cultures grown in TAP medium to a chlorophyll concentration of 20–25 mg L^{-1} were washed twice and resuspended (2500 × *g*, 5 min) in sulfur-deprived medium. Sealed in 250-ml glass flasks (Schott, conventional measuring system) or 1000-ml flasks (BlueSens gas measuring system) at a final chlorophyll concentration of 14–15 mg L^{-1}, cells were incubated at room temperature, constant stirring and under continuous one-side illumination at medium light (60 µE m^{-2} s^{-1}) or high light (200 µE m^{-2} s^{-1}). If indicated, DCMU (10 µM final concentration) or Lincomycin (2 mM final conc.) were added 48 h after sealing. For the conventional measuring system, the gas phase was removed daily, with H$_2$ and O$_2$ concentrations analyzed from a 0.2 ml gas sample each day by gas chromatography (GC-2010, Shimadzu). Liquid samples (1 ml) were taken for immunoblot and pulse-amplitude modulated (PAM) chlorophyll fluorometry analysis. For the BlueSens gas measuring system, the gas phase was constantly removed and analyzed every 20 s with online gas sensors (BCP, BlueSens gas sensor GmbH).

Chlorophyll Fluorescence Measurements

Fluorescence was measured at room temperature using a Maxi-Imaging PAM chlorophyll fluorometer (Heinz Walz GmbH). Samples were dark adapted for 20 min to maximally oxidize Q$_A$ before each measurement. The effective photochemical quantum yield of PSII was measured as PSII yield [Y(II) = (F$_m$′ − F)/F$_m$′].

Immunoblot Analysis

Whole cell samples (50 µg total protein, measured by Pierce$^{®}$ BCA^{TM} Protein Assay Kit) were analyzed by discontinuous 13% SDS-PAGE according to Laemmli (1970) and transferred to nitrocellulose membrane (Hybond ECL membrane, GE Healthcare), which was incubated with antibodies against PSAD (1:1000, Naumann et al., 2005), ATPB CF1 (1:10 000, Agrisera) and PSBA D1 (1:2500, Agrisera) as described (Hippler et al., 2001; Naumann et al., 2005). Secondary antibody was anti-rabbit (Invitrogen) and signal detection was by enhanced chemical luminescence (ECL).

Mass Inlet Membrane Spectroscopy (MIMS) Analysis of O$_2$ Exchange

Mass Inlet Membrane Spectroscopy (MIMS) analysis was performed as described in Johnson et al. (2014) and a detailed description of the protocols for analyzing MIMS data are provided in Cournac et al. (2002). For O$_2$ exchange experiments, cultures were grown in TAP at 10 µmol photons m^{-2} s^{-1} illumination. They were then centrifuged and resuspended in Minimal media and incubated for 24 h in 120 µmol photons m^{-2} s^{-1} of light with 2% CO$_2$ in an INFORS. Cells were then centrifuged and resuspended in fresh minimal medium without the addition of HCO$_3$$^-$ to a concentration of 10 mg mL^{-1} chlorophyll and left in the dark for 30 min before performing the experiments; 1.5 mL of the concentrated culture was added to the MIMS cuvette. Cells were incubated in the dark in the cuvette until the oxygen isotopes were in equilibrium and then exposed to a single light intensity at a time for around 10 min.

RESULTS

The depletion and/or absence of the PGRL1 induced increased hydrogen production under sulfur-deficiency in *Chlamydomonas reinhardtii* (Tolleter et al., 2011). Here, we investigate hydrogen production under similar conditions in a PGR5-deficient mutant and a *pgr5 pgrl1* double mutant.

Generation of the *pgr5 pgrl1* Double Mutant

Both *pgr5* (Johnson et al., 2014) and *pgrl1* (Tolleter et al., 2011) were obtained by insertional mutagenesis with the *AphVIII* cassette, conferring resistance to the antibiotic paromomycin. In *pgr5*, integration of this cassette resulted in a complete deletion of the PGR5 locus, a phenomenon already observed in other insertional mutants (Peers et al., 2009; Johnson et al., 2014). In *pgrl1,* on the other hand, insertion of the *AphVIII* cassette occurred at the level of the first exon, resulting in

lack of accumulation of the PGRL1 protein (Tolleter et al., 2011; Kukuczka et al., 2014). We took advantage of these genetic differences to screen for *pgr5 pgrl1* double mutants. Primers spanning the first 500 bp of the *PGR5* locus were used to differentiate wt-like (band) from *pgr5* (no band) progeny (Supplementary Figure S1). To select for absence of the PGRL1 protein in this *pgr5* background, we assessed integration of the resistance cassette inside the first exon of the *PGRL1* gene by *AphVIII*- and *PGRL1*-specific primers. Successful amplification of a ~800 bp fragment represents the signature of the *pgrl1* mutant background (Supplementary Figure S1). From this screening, three independent *pgr5 pgrl1* double mutants were isolated, two in the mating type minus (mt–) and one in the mating type plus (mt+). The mt– *pgr5 pgrl1* double mutant #15 was further characterized at the physiological level, since it revealed the highest H₂ production rates in a pre-screening test.

Enhanced Long-term Hydrogen Production in the *pgr* Mutants under Different Light Conditions

Continuous hydrogen production under sulfur deprivation was measured with two independent measuring systems over a period of up to 14 days (**Figures 1A** and **2**). The first approach used sealed flasks with a gas collection apparatus similar to that previously reported (Tolleter et al., 2011; **Figure 1**) from which gas was removed on a daily basis and analyzed using gas chromatography. Second, a continuous gas measuring system (BCP, BlueSens gas sensors GmbH) attached to the culture flasks was tested (**Figure 2**). Data collected with the BlueSens gas sensor system agreed well with data collected using the conventional apparatus, with a slight decrease in hydrogen production volumes (**Figures 1A** and **2B**). Continuous gas measurements have the ability to dissect more accurately the different phases of sulfur deprivation: (i) the O₂ evolution phase, (ii) the O₂ consumption phase, (iii) the anaerobic phase, and (iv) the H₂ production phase. All four phases could be observed with the continuous BlueSens gas measuring system in the wild type, with a short transition from anaerobiosis to hydrogen production (**Figure 2C**), while the transition from oxygen consumption to complete anaerobiosis toward the onset of hydrogen production was less discrete using the conventional apparatus (**Figure 1D**). Both experimental setups, however, independently showed that oxygen consumption capacity was increased in the *pgr* mutants (**Figures 1D** and **2C**). Therefore, they reached anaerobiosis faster and started producing hydrogen earlier than the wild type, and stayed anaerobic during the remaining time of sulfur deprivation (**Figures 1A,D** and **2B,C**). This was especially pronounced in the *pgr5* mutant under medium light conditions.

The *pgr* mutants showed enhanced hydrogen production with four times higher maximal production rates than the wild type (7 ml L⁻¹ culture per hour, **Figures 1A** and **2**). The *pgr5* mutant produced 7–10 times more hydrogen than the wild type in continuous medium light (**Figures 1A** and **2B**). With an overall volume of more than 800 ml hydrogen per liter (at 15 µg ml⁻¹ chlorophyll, **Figure 1A**), *pgr5* exceeded the hydrogen production of the *pgrl1* mutant by about 1.5 times (**Figure 1A**). Total
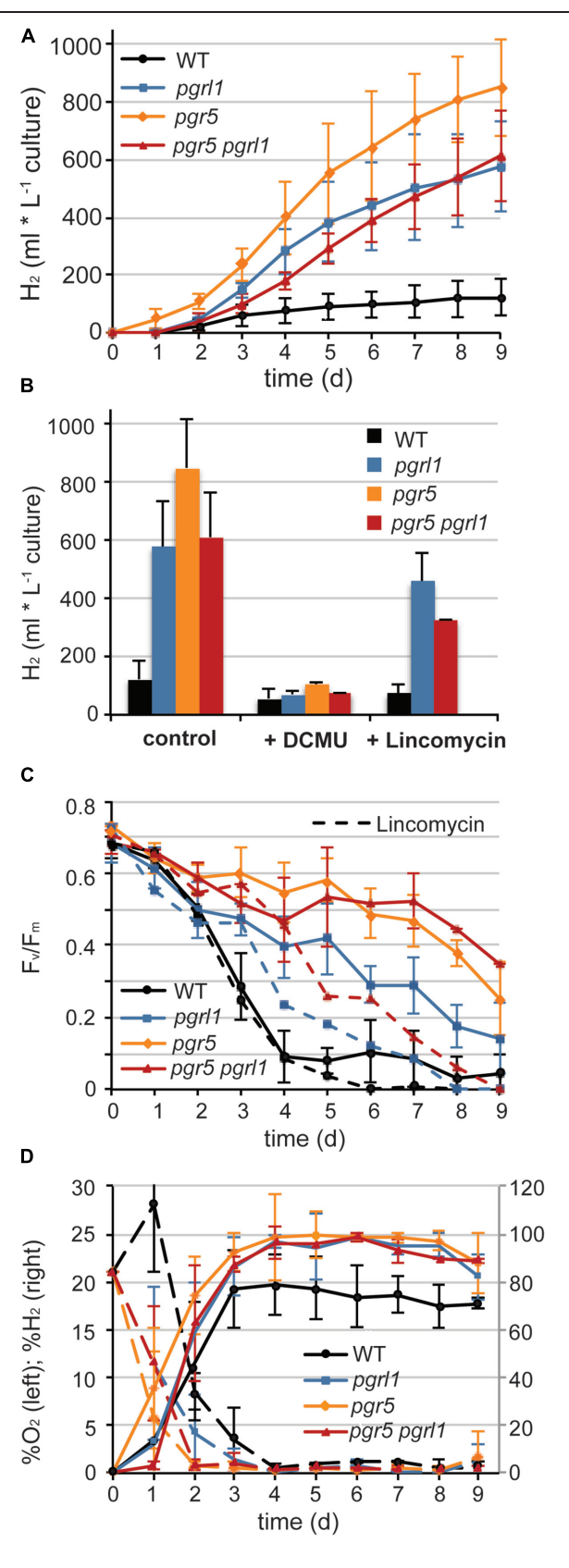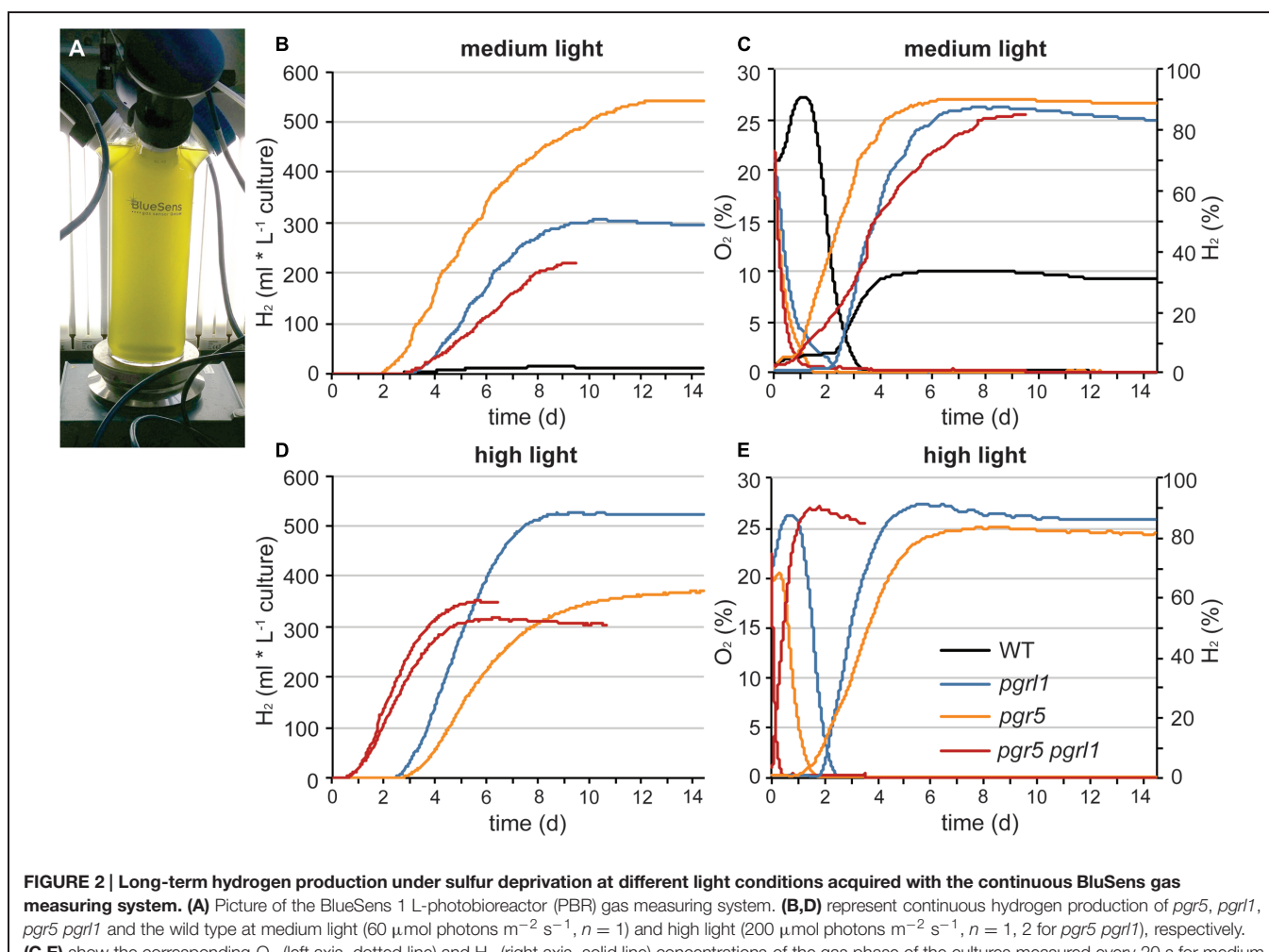
FIGURE 1 | Continued
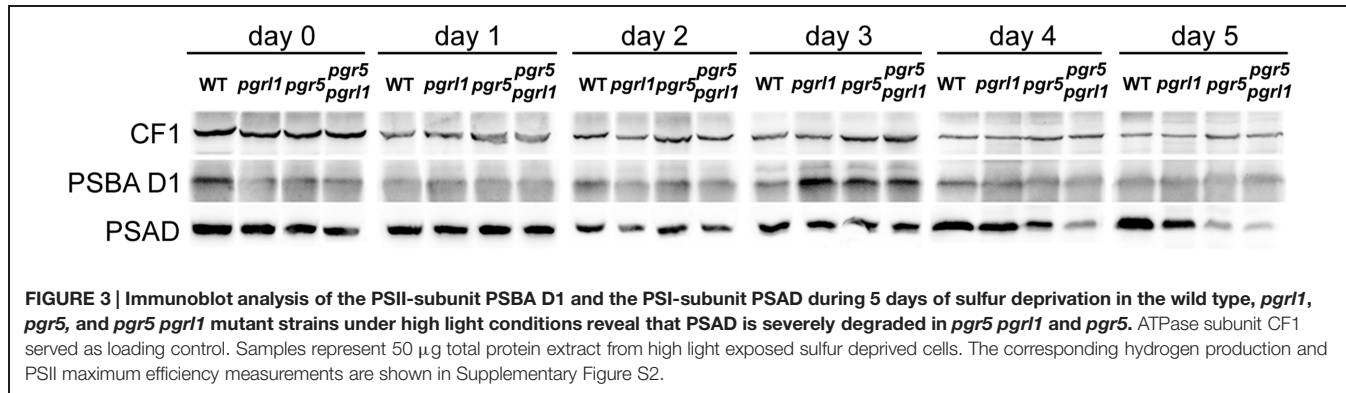
Continues hydrogen production is enhanced in *pgr5*, *pgrl1*, *pgr5 pgrl1* compared to the wild type. **(A)** Long-term hydrogen production of *pgr5*, *pgrl1*, *pgr5 pgrl1* and wild type under sulfur deprivation illuminated at 60 μmol photons m^{-2} s^{-1} ($n = 4$). **(B)** Total hydrogen volumes produced by *pgr* mutants and the wild type after 9 days of sulfur deprivation in the presence of DCMU (10 μM final conc.) or lincomycin (2 mM final conc.) compared to the control ($n = 2$). **(C)** Fv/Fm values measured after dark acclimation for 20 min of 200 μL aliquots from the S-deprived cultures ($n = 4$). **(D)** O$_2$ (left axis) and H$_2$ (right axis) concentrations of the gas phase of the cultures measured daily by gas chromatography. Concentrations remained constant after cells reached complete anaerobiosis on day 4 ($n = 3$). Data show mean ± SD.

hydrogen volumes by *pgrl1* of 600 ml L^{-1} culture correspond to ~1.6 μmol H$_2$ μg^{-1} chlorophyll and were therefore in good agreement with previous published results (Tolleter et al., 2011). The *pgr5 pgrl1* double mutant was as effective in hydrogen production as the *pgrl1* mutant under medium light.

Under elevated light conditions, oxygen evolution in *pgr5* and *pgrl1* was increased compared to medium light (**Figures 2C,E**), leading to a longer oxygen evolution phase. In contrast,

the double mutant reached the anaerobic phase even faster (**Figure 2E**) and showed an increased hydrogen burst at the beginning of sulfur deprivation (**Figure 2D**). However, it stopped producing hydrogen much earlier compared to medium light conditions. Also *pgr5* produced less hydrogen when exposed to high light, while *pgrl1* remained effective in H$_2$ production in both light settings (**Figure 2**, Supplementary Figure S2). Fractionation of whole cells by SDS-PAGE and immunoblotting using anti-PSAD and anti-PSBA antibodies revealed differences in the stability of the two photosystems (**Figure 3**). After 5 days of high light exposure under sulfur deprivation, the PSI complex in pgr5 was severely degraded as indicated by the strong decrease in the PSAD immunoblot signal (~70%). In the absence of both PGR5 and PGRL1, this effect was even greater, since by day 4, PSI levels were already low and the double mutant stopped hydrogen production completely by day 5. At the same time, levels of PSII, which is known to be prone to degradation under sulfur deprivation (Melis et al., 2000), remained comparably stable up to day 5. Thus the observed decrease in hydrogen production in *pgr5* and the double mutant can be attributed to increased photosensitivity of PSI in the absence of PGR5.

FIGURE 2 | Long-term hydrogen production under sulfur deprivation at different light conditions acquired with the continuous BluSens gas measuring system. (A) Picture of the BluSens 1 L-photobioreactor (PBR) gas measuring system. **(B,D)** represent continuous hydrogen production of *pgr5*, *pgrl1*, *pgr5 pgrl1* and the wild type at medium light (60 μmol photons m^{-2} s^{-1}, $n = 1$) and high light (200 μmol photons m^{-2} s^{-1}, $n = 1$, 2 for *pgr5 pgrl1*), respectively. **(C,E)** show the corresponding O$_2$ (left axis, dotted line) and H$_2$ (right axis, solid line) concentrations of the gas phase of the cultures measured every 20 s for medium and high light, respectively. Since gas concentrations remained constant after day 8, data are only shown till day 9 here ($n = 1$).

FIGURE 3 | Immunoblot analysis of the PSII-subunit PSBA D1 and the PSI-subunit PSAD during 5 days of sulfur deprivation in the wild type, *pgrl1*, *pgr5*, and *pgr5 pgrl1* mutant strains under high light conditions reveal that PSAD is severely degraded in *pgr5 pgrl1* and *pgr5*. ATPase subunit CF1 served as loading control. Samples represent 50 μg total protein extract from high light exposed sulfur deprived cells. The corresponding hydrogen production and PSII maximum efficiency measurements are shown in Supplementary Figure S2.

Moreover, the augmented decrease in PSI in the absence of PGR5 and PGRL1 indicate an additive effect between these two gene products, which are known to interact physically (DalCorso et al., 2008).

The *pgr* Mutants show Prolonged PSII Activity and Increased Oxygen Consumption Capacity under Sulfur Deprivation Leading to Increased Hydrogen Production

Sustainable hydrogen production under continuous light requires low oxygen concentrations due to the extremely oxygen sensitive Fe–Fe hydrogenases. Sulfur deprivation was reported to achieve anaerobiosis by down-regulating the activity of PSII (Melis et al., 2000). However, the maximum efficiency of PSII photochemistry, measured as the Fv/Fm values after 20 min of dark adaption (Baker, 2008), remained significantly higher in the *pgr* mutants under such sulfur limiting conditions compared to the control (wild type –S, **Figure 1C**). Despite this, *pgr* cells became anaerobic after 2 days of S deprivation, two times faster than the wild type (**Figures 1D** and **2D**). This suggests that in the *pgr* mutants, the driving force behind the more rapid attainment of anaerobiosis is not primarily the loss of PSII activity but instead is mediated by higher rates of respiration and light-dependent oxygen uptake, as demonstrated for *pgrl1* by Petroutsos et al. (2009), Tolleter et al. (2011), and Dang et al. (2014). This leads to a greater capacity to consume oxygen, even though some loss of PSII activity does occur. To test whether oxygen uptake is also increased in the *pgr5* mutant, we applied a MIMS technique that uses isotopic oxygen to differentiate between the rates of oxygen uptake in the light and photosynthetic oxygen evolution. Oxygen evolution (E) at different light intensities is similar between the wild type and *pgr5* showing that photosynthetic rates are not affected in *pgr5* under the conditions used (**Figure 4**, dotted lines). In contrast, oxygen uptake (U) rates in the light are higher at all light intensities in the *pgr5* strain compared to the wild type (**Figure 4**, solid lines). This is clearly demonstrated by the oxygen uptake in the light plotted as a percentage of total oxygen exchange (U/E + U = U/T): while wild type U/T is around 40%, the *pgr5* mutant is around 60%, with the highest tendency at the

lowest light intensity. This supports the idea that respiratory and/or light induced oxygen photo-reduction pathways are considerably more active in the *pgr5* mutant than in the wild type.

The decline in Fv/Fm is similar between *pgr* mutants and wild type up to 1.5 days of sulfur deprivation. By the time the wild type reached complete anaerobiosis after 3.5 days of sulfur starvation, PSII activity already dropped to 10% (**Figures 1C,D** and **2D**). In contrast, PSII activity in the *pgr* mutants remained at ∼60–85% of the starting cultures by the time they reached anaerobiosis and remained higher compared to the wild type throughout the entire period of sulfur deprivation (**Figure 1C**). Thus, higher oxygen consumption capacities in the *pgr* mutants lead to faster induction and maintenance of anaerobiosis, thereby preserving PSII activity under –S conditions.

To test whether the electrons for increased hydrogen evolution could be derived from residual PSII activity in the *pgr* mutants,
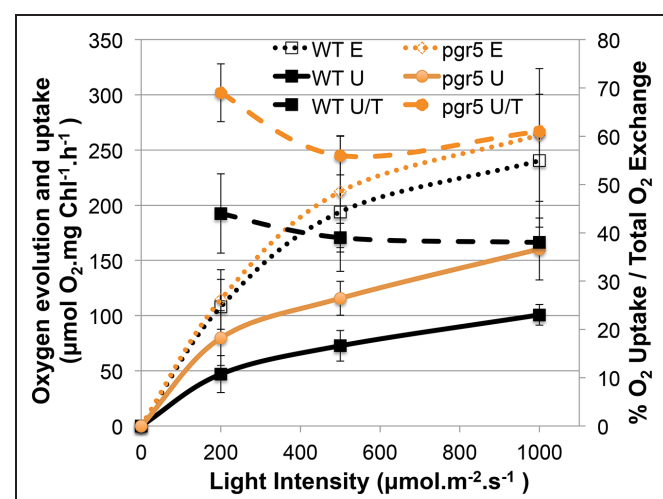
FIGURE 4 | Gas exchange analysis of competing O$_2$ flows in the light comparing the wt and *pgr5* strains. The left *y*-axis shows the rate of O$_2$ Evolution (E) or O$_2$ Uptake in the Light (U), normalized to the chlorophyll content of the cells. The right *y*-axis shows a ratio (U/T) between O$_2$ Uptake in the light (U) and Total O$_2$ exchange (U + E = T):. The *x*-axis shows the actinic light intensities used to excite photosynthesis in the cuvette. Data show mean ± SD (*n* = 3).

the inhibitor 3-(3,4-dichlorophenyl)-1,1-dimethylurea (DCMU) was added to the cultures after 2 days of sulfur starvation to block linear electron transfer at the level of the Q$_B$ side of PSII. This time point was chosen to be able to distinguish between the contribution of the PSII-direct and indirect pathway of electrons toward the hydrogenase (Fouchard et al., 2005; Hemschemeier et al., 2008). The link between photosynthetic water oxidation and hydrogen production, and the mechanism behind it, is important for understanding photobiological hydrogen production and its further development (Volgusheva et al., 2013). Indeed, addition of DCMU blocked hydrogen production immediately (**Figure 1B**). Hydrogen volumes displayed in **Figure 1B** were mainly produced prior to addition of DCMU, with a residual amount of only 1% produced after adding DCMU. This indicates that electrons from linear photosynthetic electron transfer driven by the residual PSII activity contribute to hydrogenase-mediated H$_2$-production, with elevated oxygen consumption being responsible for driving down O$_2$ levels to achieve rapid anaerobiosis.

While the chlorophyll content remained stable in all strains, the chlorophyll *a/b* ratio of the wild type increased by 20% from 2.3 to 2.8 within 5 days of sulfur starvation. In contrast, the chlorophyll *a/b* ratio remained constant at 2.35 in all *pgr* mutants, an indication that PSII could be less degraded. In agreement, the PSBA amounts as revealed by the immunoblots analyses of sulfur-deprived cells showed a higher stability than the wt at certain time points in the *pgr* mutants (**Figure 3**). To further investigate whether PSII is more stable in the thylakoid membranes of the *pgr* mutants, the effect of the prokaryotic translation inhibitor lincomycin on PSII activity and hydrogen production was investigated (**Figures 1B,C**). Inhibiting chloroplast translation at day 2 of sulfur starvation reduced the PSII activity of the mutants as well as the wild type in a similar manner with 50% decreased Fv/Fm levels by day 5 compared to the sulfur deprived control samples (**Figure 1C**). The decrease in hydrogen production by 33% $\pm$ 10% was also similar between strains (**Figure 1B**). However, Fv/Fm levels and hydrogen production rates still remained higher in the *pgr* mutants compared to the wild type. This supports the conclusion that a substantial amount of electrons for hydrogen production in the *pgr* mutants derived from PSII. Moreover, as lincomycin had a similar effect on wild type as well as the *pgr* mutants, it can be assumed that the larger residual PSII activity under

sulfur-deficiency is sustained due to the absence of PGR5 or PGRL1. However, it cannot be distinguished whether this is due to an altered repair cycle or a higher stability of PSII in the membrane.

DISCUSSION

In the present study, we investigated *pgr5* and *pgr5 pgrl1* double mutants in comparison to a PGRL1 deficient mutant and wild type in their capacity of light-driven hydrogen production. As already reported earlier for PGRL1 deficiency in *C. reinhardtii* (Tolleter et al., 2011), the absence of the *pgr5* gene product also increased the capacity of hydrogen production as compared to wild type significantly. Importantly, the *pgr5* mutant is, with hydrogen volumes of up to 10 times higher than the wild type, one of the highest hydrogen producers reported to date. The maximum amounts of 850 ml L^{-1} culture (at 15 μg ml^{-1} chlorophyll referring to 2.4 μmol H$_2$ μg^{-1} chlorophyll) exceed reported volumes of *pgrl1* and other high hydrogen producers like *stm6*, *stm6glc4*, *LO1*, or the PSII D1 mutant *L159I-N230Y* (see **Table 1**, Kruse et al., 2005; Doebbe et al., 2007; Torzillo et al., 2009; Oey et al., 2013). Our data indicate that (i) the ability to maintain linear photosynthetic electron flow rates under S deplete conditions in conjunction with (ii) an increased oxygen consumption capacity explains the increased hydrogen production in the *pgr* mutants.

Elevated Hydrogen Production in the pgr Mutants: Interplay between Capacities of Photosynthetic Electron Transfer and Oxygen Consumption

It is known that the hydrogenase is extremely sensitive to oxygen (Ghirardi et al., 1997; Stripp et al., 2009). On the other hand, linear electron transfer will produce oxygen. Compared to maximal wild type rates, the hydrogen amounts produced per hour were four times higher in the *pgr* mutants with maximal rates of 7 ml L^{-1} culture per hour over a period of 2–3 days (**Figure 1A**). The wild type stopped producing hydrogen slightly earlier than the mutants (**Figures 1A** and **2B**). After 2 days of sulfur deprivation (time point of DCMU addition, **Figure 1B**), the wild type produced already 46% vs. only 12% of hydrogen produced by the *pgr* mutants compared to the total hydrogen

TABLE 1 | Comparison of hydrogen amounts produced by different *Chlamydomonas* mutants.

Mutant	H$_2$ volume (ml/L culture)	Chlorophyll (μg/ml)	H$_2$ volume (μmol H2/μg chl)	PBR size (ml, ø in cm)	Reference
pgr5	850	15	2.4	250, 6.5	
pgrl1	580	15	1.6	250, 6.5	Also Tolleter et al., 2011
pgr5 pgrl1	610	15	1.7	250, 6.5	
stm6	540	26	0.9	500, 8.0	Kruse et al., 2005
stm6 glc4	150% of *stm6*	26	1.3	500, 8.0	Doebbe et al., 2007
LO1	400	15	1.1	500, 8.0	Oey et al., 2013
L159I-N230Y	504	12	1.75	1000, 5.0	Torzillo et al., 2009

Absolute H$_2$ volumes are taken from specified publications. For a better comparison, H$_2$ amounts are equalized to chlorophyll content (column 4). Photobioreactor (PBR) sizes are given as one possible factor introducing some variance between studies due to differences in experimental set-ups.

amounts produced over 9 days. This time point correlates with the drop in PSII activity in the wild type (**Figure 1C**). Thus, PSII activity of the *pgr* mutants remained higher until the late phase of sulfur deprivation (**Figures 1C** and **3**) suggesting that linear electron flow from PSII is responsible for the prolonged and significantly higher hydrogen production rates in the *pgr* mutants.

Why the hydrogenase is not inhibited by elevated PSII activity in the *pgr* mutants? This is because anaerobiosis can be maintained in the *pgr* mutants due to an increased oxygen consumption rate, as oxygen is removed much faster from the measuring system compared to wild type (**Figures 1D** and **2C,E**). This is further supported by the fact that light-induced oxygen uptake is increased in the *pgr5* mutant (**Figure 4**). Increased respiration rates were already reported for the *pgrl1 ko* and *kd* lines (Petroutsos et al., 2009; Tolleter et al., 2011). Recently, Dang et al. (2014) reported increased mitochondrial cooperation and increased O_2 photo-reduction in the *pgrl1* mutant and also in *Arabidopsis pgr5*, this cooperation was enhanced (Yoshida et al., 2007). Metabolic shuttles such as the malate-oxaloacetate shuttle can export reducing power from the stroma to the mitochondria (Scheibe, 2004; Shen et al., 2006). This cooperation is particularly enhanced under stress conditions, where ATP demand is increased (Lemaire et al., 1988). Mitochondrial inhibitors induced a drop in the PSII yield in *pgrl1* (Dang et al., 2014). Also light-dependent O_2 uptake and the abundance of flavodiiron proteins were higher in the mutant, indicating an increased capacity of Mehler-like reactions and possibly photorespiration. High antioxidant capacity was reported for *Arabidopsis pgr5* (Suorsa et al., 2012). A recent study showed an up-regulation of those proteins in the early acclimation phase of sulfur deprivation, suggesting an involvement of flavodiiron proteins in acclimation to anoxia during hydrogen production (Jokel et al., 2015). In addition to the very similar phenotype of the *pgrl1* and *pgr5* mutants in regard to CEF impairment, NPQ reduction and PSI photo-inhibition (Tolleter et al., 2011; Johnson et al., 2014; Kukuczka et al., 2014), O_2 consuming mechanisms are also up-regulated under S-deplete mixotrophic conditions in *pgr5* (**Figures 1D**, **2D,E** and **4**) and participate in a faster anaerobic induction at the onset of sulfur deprivation (**Figures 1D** and **2D,E**). This is in line with the conclusion, that increased oxygen consumption rates allow higher PSII activity under anaerobic –S conditions leading to increased hydrogen production in the *pgr* mutants. Interestingly, in a recent study using the *stm6* and PSII-D1 *L159I-N230Y* mutant (see also **Table 1**), the authors reported very similar phenotypes under sulfur deprivation as is shown here for the *pgr* mutants: the mutants reached anaerobiosis faster and increased hydrogen production was mainly achieved by an increased electron supply from PSII toward the hydrogenase due to an increased respiration rate (Torzillo et al., 2009; Scoma et al., 2012; Volgusheva et al., 2013).

The contribution of the indirect pathway of electrons from starch via NAD2 toward the hydrogenase to H_2 production has been reported to be variable, depending on experimental conditions and particularly on the phase of the sulfur deprivation process (Kosourov et al., 2003; Fouchard et al.,

2005; Hemschemeier et al., 2008; Jans et al., 2008). It might also contribute to increased hydrogen production in the *pgr* mutants. Starch breakdown was reported to be faster in the *pgrl1* mutant (Tolleter et al., 2011) and from a study with a starch deficient mutant and the inhibitor DCMU and proton uncoupler FCCP, it was concluded that the proton gradient generated by cyclic electron flow around PSI inhibits the indirect pathway of electrons from starch to the hydrogenase (Chochois et al., 2009). Tolleter et al. (2011) reported hydrogen production rates in *pgrl1* are enhanced compared to the wild type, and to a similar extent independent of the presence of DCMU. However, H_2 production was 10 times lower than in the absence of DCMU (Tolleter et al., 2011). In our hands, the hydrogen production in the presence of DCMU was even lower (**Figure 1B**), possibly because DCMU was added with a 1-day delay (48 h vs. 24 h of sulfur deprivation). Therefore, since blocking the PSII-dependent direct pathway by DCMU had such a dramatic effect on hydrogen production, the contribution of the indirect pathway to hydrogen production in the *pgr* mutants should be relatively small compared to the PSII-dependent pathway.

Deletion of PGRL1 and PGR5 Sustains PSII Activity under –S Conditions

The mechanisms contributing to the inhibition of photosynthetic O_2 evolution in S depleted conditions and their relative importance are still a matter of debate (Ghysels and Franck, 2010). Sulfur deprivation has a general effect on the transcription of the chloroplast (Irihimovitch and Stern, 2006; Irihimovitch and Yehudai-Resheff, 2008). It is well described that acclimation to sulfur deficiency is highly controlled and induces a down-regulation of photosynthesis, particularly of PSII (Davies et al., 1996). The absence of down-regulation of photosynthetic activity, as observed in the *sac1* mutant (Davies et al., 1996), is deleterious. It has been suggested that sulfur limitation will result in a general decrease in protein synthesis, which in turn would impact the capacity of D1 turn-over and repair cycle (Wykoff et al., 1998; Zhang et al., 2002). Hence, under low sulfur and in the absence of efficient PSII-repair, high activity of photosynthetic electron transfer would likely result in damage due to the production of reactive oxygen species, which could not be sustained by D1-repair. In the *pgr* mutants, however, PSII photochemistry efficiency remained high (**Figure 1C**) and amounts of the D1 protein in the mutants showed some stability compared to the wild type during sulfur starvation (**Figure 3**), at which PSII activity in the wild type had already dropped to 10% (**Figure 1C**). The inhibitory effect of chloroplastida translation by lincomycin on PSII activity and H_2 production further indicates that a substantial amount of PSII remains functional under sulfur deprivation (**Figures 1B,C**). Thus, the absence of PGRL1 and PGR5 sustained PSII activity under sulfur deprivation. How could this be explained?

The increased oxygen consumption capacity in the mutants, and the faster transition to anaerobiosis is, in its own right, sufficient to explain PSII preservation, via at least two

mechanisms. First, rapid attainment of anaerobiosis leads to early induction and high activity of the hydrogenase, the final electron acceptor of linear electron flow in –S conditions. This is important because CO$_2$ fixation is lost during S deprivation, which normally limits LEF by slowing down the reoxidation of its main final electron acceptor NADP$^+$: Rubisco is affected even earlier than D1 and declines by about 80% in the first 24 h of S deprivation, becoming undetectable after 60 h of starvation (Zhang et al., 2002). Loss of CO$_2$-fixation has been reported to slow down the D1 repair cycle and was therefore predicted to stimulate the loss of PSII activity during S deprivation (Takahashi and Murata, 2005, 2006). In summary, early anaerobiosis releases acceptor side limitation of LEF faster due to an earlier activation of the hydrogenase (**Figures 1D** and **2D**). Second, faster induction of anaerobiosis at the onset of sulfur starvation and induction of hydrogenase activity preserves existing PSII from photo-oxidative damage, as it reduces the amount of oxygen available to cause potential damage at PSII. All strains show an initial decline in Fv/Fm, which slows after the system becomes anaerobic, but as this occurs much later in the wt, the corresponding damage to PSII is much worse.

Under High Light Exposure, *pgr5 pgrl1* shows an Increased Hydrogen Burst at the Beginning of Sulfur Depletion and PSI becomes Photo-inhibited in the *pgr5* and *pgr5 pgrl1* Mutants

In this study, we report the generation of a *pgr5 pgrl1* double mutant. This double mutant displays a similar phenotype compared to its respective single mutants, confirming that PGR5 and PGRL1 both act on the same pathway as earlier proposed (DalCorso et al., 2008; Johnson et al., 2014). However, *pgrl1* and *pgr5* differ in the severity of one particular phenotype: While PSII remained stable in sulfur limiting conditions, PSI was degraded much faster in the *pgr5* and *pgr5 pgrl1* mutants when they were exposed to additional stress of high light (**Figure 3**), reducing the amount of hydrogen produced (**Figure 2**; Supplementary Figure S2). In contrast, *pgrl1* remained effective in hydrogen production also in high light and PSI was not degraded at the same rate (**Figures 2** and **3**). Although PGR5 was previously not detectable by western blot analysis in the *pgrl1* mutant (Johnson et al., 2014), the different phenotype of the *pgr5 pgrl1* and *pgr5* mutant compared to the *pgrl1* single mutant suggests that the PGR5 protein is present in the *pgrl1* mutant, though below the limit of detection of immunoblot analysis, which could detect about 50% of PGR5 wild type protein amounts (Johnson et al., 2014). High light sensitivity has already been reported for *pgr5* under photoautotrophic conditions (Johnson et al., 2014). In *pgrl1*, PSI becomes photo-inhibited under high light exposure (Kukuczka et al., 2014), although not degraded as severely as in *pgr5*. In the absence of both PGR5 and PGRL1, PSI becomes even more affected, indicating an additive role of these two proteins in terms of PSI protection and suggesting that both proteins operate in the same pathway.

PSI photo-inhibition in high light was also described in a *Chlamydomonas stt7-1* mutant locked in state 1 (Bergner et al., 2015). However, this phenotype was less severe than in the *pgr5* and *pgrl1* mutants (Johnson et al., 2014; Bergner et al., 2015). Furthermore, the *stt7-1* mutant displayed high CEF rates and enhanced formation of a CEF-supercomplex (Bergner et al., 2015). A non-successful acclimation to high light was recently also linked to altered dephosphorylation patterns of LHCII proteins in *Arabidopsis pgr5* (Mekala et al., 2015). These findings indicate a regulatory link between the PGR5/PGRL1 pathway, phosphorylation and dephosphorylation dynamics and the susceptibility of PSI to photo-inhibition.

In high light, the thylakoid lumen becomes acidified, which down-regulates linear electron flow and induces dissipation of excess energy at PSII in the form of heat. This so called non-photochemical quenching (NPQ) requires the induction of the LHCSR3 protein in algae (Peers et al., 2009) and acidification of the thylakoid lumen (Petroutsos et al., 2011). Both *pgr5* and *pgrl1* have reduced levels of NPQ due to a reduced proton gradient across the membrane, while LHCSR3 levels are unaltered in the mutants (Tolleter et al., 2011; Johnson et al., 2014). Without a sufficient proton gradient, linear electron flow is not down-regulated and the acceptor side of PSI becomes over-reduced. An indication that an increased electron drive toward the hydrogenase occurs under elevated light conditions is the enhanced hydrogen burst at the beginning of the hydrogen production phase in the *pgr5 pgrl1* mutant (**Figure 2C**). Hydrogen production at PSI was proposed to act as a safety valve to protect the photosynthetic electron transport chain from over-reduction under natural conditions by safely disposing of excess electrons from PSI (Melis and Happe, 2001; Happe et al., 2002; Hemschemeier et al., 2009). Now, the deletion of PGR5 and/or PGRL1 is deleterious for PSI under high light conditions. Thus, while PSII stability under sulfur deficiency is more affected in wild type, PSI integrity is most affected in the absence of PGR5 and/or PGRL1; a topic that certainly requires additional work for a more in-depth understanding.

CONCLUSION

Enhanced hydrogen production rates in the *pgrl1, pgr5,* and the *pgr5 pgrl1* double mutant under S deplete conditions lead to the highest continuous photobiological produced hydrogen amounts of eukaryotic cells reported so far. These rates are achieved by a prolonged residual PSII activity providing an increased electron supply toward the hydrogenase. PSII activity can be maintained in the mutants without inhibiting the oxygen sensitive hydrogenase, because the oxygen consumption capacity is increased. Our results suggest that respiration and light-dependent O$_2$-uptake rates are higher in the *pgr* mutants, and that this is responsible for the faster transition to anaerobiosis, especially when the greater residual PSII activity of the mutants is taken into account.

ACKNOWLEDGMENTS

SUPPLEMENTARY MATERIAL

The Supplementary Material for this article can be found online at: http://journal.frontiersin.org/article/10.3389/fpls.2015.00892

REFERENCES

Antal, T. K., Krendeleva, T. E., Laurinavichene, T. V., Makarova, V. V., Ghirardi, M. L., Rubin, A. B., et al. (2003). The dependence of algal H2 production on photosystem II and O2 consumption activities in sulfur-deprived *Chlamydomonas reinhardtii* cells. *Biochim. Biophys. Acta - Bioenerg* 1607, 153–160. doi: 10.1016/j.bbabio.2003.09.008

Antal, T. K., Volgusheva, A. A., Kukarskih, G. P., Krendeleva, T. E., and Rubin, A. B. (2009). Relationships between H2 photoproduction and different electron transport pathways in sulfur-deprived *Chlamydomonas reinhardtii*. *Int. J. Hydrogen Energy* 34, 9087–9094. doi: 10.1016/j.ijhydene.2009.09.011

Baker, N. R. (2008). Chlorophyll fluorescence: a probe of photosynthesis in vivo. *Annu. Rev. Plant Biol.* 59, 89–113. doi: 10.1146/annurev.arplant.59.032607.092759

Bergner, S. V., Scholz, M., Trompelt, K., Barth, J., Gäbelein, P., Steinbeck, J., et al. (2015). State transition7-dependent phosphorylation is modulated by changing environmental conditions and its absence triggers remodeling of photosynthetic protein complexes. *Plant Physiol.* 168, 615–634. doi: 10.1104/pp.15.00072

Bishop, N. I., and Gaffron, H. (1963). "Of the interrelation of the mechanisms for oxygen and hydrogen evolution in adapted algae," in *Photosynthetic Mechanisms in Green Plants*, eds B. Kok and A. T. Jagendorf (Washington, DC: National Academy of Sciences and National Research Council), 441–451.

Chochois, V., Dauvillée, D., Beyly, A., Tolleter, D., Cuiné, S., Timpano, H., et al. (2009). Hydrogen production in *Chlamydomonas*: photosystem II-dependent and -independent pathways differ in their requirement for starch metabolism. *Plant Physiol.* 151, 631–640. doi: 10.1104/pp.109.144576

Cournac, L., Mus, F., Bernard, L., Guedeney, G., Vignais, P., and Peltier, G. (2002). Limiting steps of hydrogen production in *Chlamydomonas reinhardtii* and *Synechocystis* PCC 6803 as analysed by light-induced gas exchange transients. *Int. J. Hydrogen Energy* 27, 1229–1237. doi: 10.1016/S0360-3199(02)00105-2

DalCorso, G., Pesaresi, P., Masiero, S., Aseeva, E., Schünemann, D., Finazzi, G., et al. (2008). A complex containing PGRL1 and PGR5 is involved in the switch between linear and cyclic electron flow in *Arabidopsis*. *Cell* 132, 273–285. doi: 10.1016/j.cell.2007.12.028

Dang, K.-V., Plet, J., Tolleter, D., Jokel, M., Cuiné, S., Carrier, P., et al. (2014). Combined increases in mitochondrial cooperation and oxygen photoreduction compensate for deficiency in cyclic electron flow in *Chlamydomonas reinhardtii*. *Plant Cell* 26, 3036–3050. doi: 10.1105/tpc.114.126375

Davies, J. P., Yildiz, F. H., and Grossman, A. (1996). Sacl, a putative regulator that is critical for survival of Chlamydomonas reinhardtii during sulfur deprivation. *EMBO J.* 15, 2150–2159.

Doebbe, A., Rupprecht, J., Beckmann, J., Mussgnug, J. H., Hallmann, A., Hankamer, B., et al. (2007). Functional integration of the HUP1 hexose symporter gene into the genome of *C. reinhardtii*: impacts on biological H(2) production. *J. Biotechnol.* 131, 27–33. doi: 10.1016/j.jbiotec.2007.05.017

Fouchard, S., Hemschemeier, A., Caruana, A., Happe, T., Peltier, G., and Cournac, L. (2005). Autotrophic and mixotrophic hydrogen photoproduction in sulfur-deprived *Chlamydomonas* cells. *Appl. Environ. Microbiol.* 71, 6199–6205. doi: 10.1128/AEM.71.10.6199

Gaffron, H., and Rubin, J. (1942). Fermentative and photochemical production of hydrogen in algae. *J. Gen. Physiol.* 26, 219–240. doi: 10.1085/jgp.26.2.219

Ghirardi, M. K., Togasaki, R. K., and Seibert, M. (1997). Oxygen sensitivity of algal h2-production. *Appl. Biochem. Biotechnol.* 63, 141–151. doi: 10.1007/978-1-4612-2312-2_14

Ghysels, B., and Franck, F. (2010). Hydrogen photo-evolution upon S deprivation stepwise: an illustration of microalgal photosynthetic and metabolic flexibility and a step stone for future biotechnological methods of renewable H(2) production. *Photosynth. Res.* 106, 145–154. doi: 10.1007/s11120-010-9582-4

Hankamer, B., Lehr, F., Rupprecht, J., Mussgnug, J. H., Posten, C., and Kruse, O. (2007). Photosynthetic biomass and H2 production by green algae: from bioengineering to bioreactor scale-up. *Physiol. Plant.* 131, 10–21. doi: 10.1111/j.1399-3054.2007.00924.x

Happe, T., Hemschemeier, A., Winkler, M., and Kaminski, A. (2002). Hydrogenases in green algae: do they save the algae's life and solve our energy problems? *Trends Plant Sci.* 7, 246–250. doi: 10.1016/S1360-1385(02)02274-4

Harris, E. H. (1989). *The Chlamydomonas Sourcebook: A Comprehensive Guide to Biology and Laboratory Use*. San Diego, CA: Academic Press.

Hemschemeier, A., Fouchard, S., Cournac, L., Peltier, G., and Happe, T. (2008). Hydrogen production by *Chlamydomonas reinhardtii*: an elaborate interplay of electron sources and sinks. *Planta* 227, 397–407. doi: 10.1007/s00425-007-0626-8

Hemschemeier, A., Melis, A., and Happe, T. (2009). Analytical approaches to photobiological hydrogen production in unicellular green algae. *Photosynth. Res.* 102, 523–540. doi: 10.1007/s11120-009-9415-5

Hertle, A. P., Blunder, T., Wunder, T., Pesaresi, P., Pribil, M., and Armbruster, U. (2013). PGRL1 is the elusive ferredoxin-plastoquinone reductase in photosynthetic cyclic electron flow. *Mol. Cell* 49, 511–523. doi: 10.1016/j.molcel.2012.11.030

Hippler, M., Klein, J., Fink, A., Allinger, T., and Hoerth, P. (2001). Towards functional proteomics of membrane protein complexes: analysis of thylakoid membranes from *Chlamydomonas reinhardtii*. *Plant J.* 28, 595–606. doi: 10.1046/j.1365-313X.2001.01175.x

Irihimovitch, V., and Stern, D. B. (2006). The sulfur acclimation SAC3 kinase is required for chloroplast transcriptional repression under sulfur limitation in *Chlamydomonas reinhardtii*. *Proc. Natl. Acad. Sci. U.S.A.* 103, 6–11. doi: 10.1073/pnas.0511042103

Irihimovitch, V., and Yehudai-Resheff, S. (2008). Phosphate and sulfur limitation responses in the chloroplast of *Chlamydomonas reinhardtii*. *FEMS Microbiol. Lett.* 283, 1–8. doi: 10.1111/j.1574-6968.2008.01154.x

Iwai, M., Takizawa, K., Tokutsu, R., Okamuro, A., Takahashi, Y., and Minagawa, J. (2010). Isolation of the elusive supercomplex that drives cyclic electron flow in photosynthesis. *Nature* 464, 1210–1213. doi: 10.1038/nature08885

Jans, F., Mignolet, E., Houyoux, P.-A., Cardol, P., Ghysels, B., Cuiné, S., et al. (2008). A type II NAD(P)H dehydrogenase mediates light-independent plastoquinone reduction in the chloroplast of *Chlamydomonas*. *Proc. Natl. Acad. Sci. U.S.A.* 105, 20546–20551. doi: 10.1073/pnas.0806896105

Johnson, X., Steinbeck, J., Dent, R. M., Takahashi, H., Richaud, P., Ozawa, S.-I., et al. (2014). Proton gradient regulation 5-mediated cyclic electron flow under ATP- or redox-limited conditions: a study of ΔATpase pgr5 and ΔrbcL pgr5 mutants in the green alga *Chlamydomonas reinhardtii*. *Plant Physiol.* 165, 438–452. doi: 10.1104/pp.113.233593

Jokel, M., Kosourov, S., Battchikova, N., Tsygankov, A. A., Aro, E. M., and Allahverdiyeva, Y. (2015). *Chlamydomonas* flavodiiron proteins facilitate acclimation to anoxia during sulfur deprivation. *Plant Cell Physiol.* 56, 1598–1607. doi: 10.1093/pcp/pcv085

Kosourov, S., Seibert, M., and Ghirardi, M. L. (2003). Effects of extracellular ph on the metabolic pathways in sulfur-deprived, H2-Producing *Chlamydomonas reinhardtii* cultures. *Plant Cell Physiol.* 44, 146–155. doi: 10.1093/pcp/pcg020

Kruse, O., Rupprecht, J., Bader, K.-P., Thomas-Hall, S., Schenk, P. M., Finazzi, G., et al. (2005). Improved photobiological H2 production in engineered green algal cells. *J. Biol. Chem.* 280, 34170–34177. doi: 10.1074/jbc.M503840200

Kukuczka, B., Magneschi, L., Petroutsos, D., Steinbeck, J., Bald, T., Powikrowska, M., et al. (2014). Proton gradient regulation5-like1-mediated cyclic electron flow is crucial for acclimation to anoxia and complementary to nonphotochemical quenching in stress adaptation. *Plant Physiol.* 165, 1604–1617. doi: 10.1104/pp.114.240648

Laemmli, U. K. (1970). Cleavage of structural proteins during the assembly of the head of bacteriophage T4. *Nature* 227, 680–685. doi: 10.1038/227680a0

Lemaire, C., Wollman, F., Bennoun, P., and Plant, J. E. (1988). Restoration of phototrophic growth in a mutant of *Chlamydomonas reinhardtii* in which the chloroplast atpB gene of the ATP synthase has a deletion: an example of mitochondria-dependent photosynthesis. *Proc. Natl. Acad. Sci. U.S.A.* 85, 1344–1348. doi: 10.1073/pnas.85.5.1344

Lubitz, W., Ogata, H., Ru, O., and Reijerse, E. (2014). Hydrogenases. *Chem. Rev.* 114, 4081–4148. doi: 10.1021/cr4005814

Mekala, N. R., Suorsa, M., Rantala, M., Aro, E.-M., and Tikkanen, M. (2015). Plants actively avoid state transitions upon changes in light intensity: role of light-harvesting complex ii protein dephosphorylation in high light. *Plant Physiol.* 168, 721–734. doi: 10.1104/pp.15.00488

Melis, A., and Happe, T. (2001). Update on hydrogen production. Green algae as a source of energy. *Plant Physiol.* 127, 740–748. doi: 10.1104/pp.010498.740

Melis, A., Zhang, L., Forestier, M., Ghirardi, M. L., and Seibert, M. (2000). Sustained photobiological hydrogen gas production upon reversible inactivation of oxygen evolution in the green alga *Chlamydomonas reinhardtii*. *Plant Physiol.* 122, 127–136. doi: 10.1104/pp.122.1.127

Munekage, Y., Hojo, M., Meurer, J., Endo, T., Tasaka, M., and Shikanai, T. (2002). PGR5 is involved in cyclic electron flow around photosystem I and is essential for photoprotection in *Arabidopsis*. *Cell* 110, 361–371. doi: 10.1016/S0092-8674(02)00867-X

Naumann, B., Stauber, E. J., Busch, A., Sommer, F., and Hippler, M. (2005). N-terminal processing of Lhca3 Is a key step in remodeling of the photosystem I-light-harvesting complex under iron deficiency in *Chlamydomonas reinhardtii*. *J. Biol. Chem.* 280, 20431–20441. doi: 10.1074/jbc.M414486200

Oey, M., Ross, I. L., Stephens, E., Steinbeck, J., Wolf, J., Radzun, K. A., et al. (2013). RNAi knock-down of LHCBM1, 2 and 3 increases photosynthetic H2 production efficiency of the green alga *Chlamydomonas reinhardtii*. *PLoS ONE* 8:e61375. doi: 10.1371/journal.pone.0061375

Organisation for Economic Co-operation and Development (OECD)/ International Energy Agency (IEA) (2011). *OECD Green Growth Studies: Energy*. Available at: http://www.oecd.org/greengrowth/greening-energy/49157219.pdf

Peers, G., Truong, T. B., Ostendorf, E., Busch, A., Elrad, D., Grossman, A. R., et al. (2009). An ancient light-harvesting protein is critical for the regulation of algal photosynthesis. *Nature* 462, 518–521. doi: 10.1038/nature08587

Petroutsos, D., Busch, A., Janssen, I., Trompelt, K., Bergner, S. V., Weinl, S., et al. (2011). The chloroplast calcium sensor CAS is required for photoacclimation in *Chlamydomonas reinhardtii*. *Plant Cell* 23, 2950–2963. doi: 10.1105/tpc.111.087973

Petroutsos, D., Terauchi, A. M., Busch, A., Hirschmann, I., Merchant, S. S., Finazzi, G., et al. (2009). PGRL1 participates in iron-induced remodeling of the photosynthetic apparatus and in energy metabolism in *Chlamydomonas reinhardtii*. *J. Biol. Chem.* 284, 32770–32781. doi: 10.1074/jbc.M109.050468

Rupprecht, J., Hankamer, B., Mussgnug, J. H., Ananyev, G., Dismukes, C., and Kruse, O. (2006). Perspectives and advances in biological H2 production in microorganisms. *Appl. Microbiol. Biotechnol.* 72, 442–449. doi: 10.1007/s00253-006-0528-x

Scheibe, R. (2004). Malate valves to balance cellular energy supply. *Physiol. Plant* 120, 21–26. doi: 10.1111/j.0031-9317.2004.0222.x

Scoma, A., Krawietz, D., Faraloni, C., Giannelli, L., Happe, T., and Torzillo, G. (2012). Sustained H2 production in a *Chlamydomonas reinhardtii* D1 protein mutant. *J. Biotechnol.* 157, 613–619. doi: 10.1016/j.jbiotec.2011.06.019

Shen, W., Wei, Y., Dauk, M., Tan, Y., and Taylor, D. C. (2006). Modulating the NADH/NAD+ ratio provides evidence of a mitochondrial glycerol-3-phosphate shuttle in *Arabidopsis*. *Plant Cell* 18, 422–441. doi: 10.1105/tpc.105.039750.similation

Stripp, S. T., Goldet, G., Brandmayr, C., Sanganas, O., Vincent, K. A., Haumann, M., et al. (2009). How oxygen attacks [FeFe] hydrogenases from photosynthetic organisms. *Proc. Natl. Acad. Sci. U.S.A.* 106, 17331–17336. doi: 10.1073/pnas.0905343106

Suorsa, M., Järvi, S., Grieco, M., Nurmi, M., Pietrzykowska, M., Rantala, M., et al. (2012). PROTON GRADIENT REGULATION5 is essential for proper acclimation of *Arabidopsis* photosystem I to naturally and artificially fluctuating light conditions. *Plant Cell* 24, 2934–2948. doi: 10.1105/tpc.112.097162

Takahashi, S., and Murata, N. (2005). Interruption of the Calvin cycle inhibits the repair of Photosystem II from photodamage. *Biochim. Biophys. Acta* 1708, 352–361. doi: 10.1016/j.bbabio.2005.04.003

Takahashi, S., and Murata, N. (2006). Glycerate-3-phosphate, produced by CO2 fixation in the Calvin cycle, is critical for the synthesis of the D1 protein of photosystem II. *Biochim. Biophys. Acta* 1757, 198–205. doi: 10.1016/j.bbabio.2006.02.002

Terashima, M., Petroutsos, D., Hüdig, M., Tolstygina, I., Trompelt, K., Gäbelein, P., et al. (2012). Calcium-dependent regulation of cyclic photosynthetic electron transfer by a CAS. ANR1, and PGRL1 complex. *Proc. Natl. Acad. Sci. U.S.A.* 109, 17717–17722. doi: 10.1073/pnas.1207118109

Tolleter, D., Ghysels, B., Alric, J., Petroutsos, D., Tolstygina, I., Krawietz, D., et al. (2011). Control of hydrogen photoproduction by the proton gradient generated by cyclic electron flow in *Chlamydomonas reinhardtii*. *Plant Cell* 23, 2619–2630. doi: 10.1105/tpc.111.086876

Torzillo, G., Scoma, A., Faraloni, C., Ena, A., and Johanningmeier, U. (2009). Increased hydrogen photoproduction by means of a sulfur-deprived *Chlamydomonas reinhardtii* D1 protein mutant. *Int. J. Hydrogen Energy* 34, 4529–4536. doi: 10.1016/j.ijhydene.2008.07.093

Volgusheva, A., Styring, S., and Mamedov, F. (2013). Increased photosystem II stability promotes H2 production in sulfur-deprived *Chlamydomonas reinhardtii*. *Proc. Natl. Acad. Sci. U.S.A.* 110, 7223–7228. doi: 10.1073/pnas.1220645110

Wykoff, D. D., Davies, J. P., Melis, A., and Grossman, A. R. (1998). The regulation of photosynthetic electron transport during nutrient deprivation in *Chlamydomonas reinhardtii* 1. *Plant Physiol.* 117, 129–139. doi: 10.1104/pp.117.1.129

Yoshida, K., Terashima, I., and Noguchi, K. (2007). Up-regulation of mitochondrial alternative oxidase concomitant with chloroplast over-reduction by excess light. *Plant Cell Physiol.* 48, 606–614. doi: 10.1093/pcp/pcm033

Zhang, L., Happe, T., and Melis, A. (2002). Biochemical and morphological characterization of sulfur-deprived and H2 -producing *Chlamydomonas reinhardtii* (green alga). *Planta* 214, 552–561. doi: 10.1007/s004250100660

Site-Directed Mutagenesis from Arg195 to His of a Microalgal Putatively Chloroplastidial Glycerol-3-Phosphate Acyltransferase Causes an Increase in Phospholipid Levels in Yeast

Long-Ling Ouyang[1], Hui Li[2], Xiao-Jun Yan[3], Ji-Lin Xu[3] and Zhi-Gang Zhou[1]*

[1] College of Aqua-Life Science and Technology, Shanghai Ocean University, Shanghai, China, [2] Department of Biology and Food Engineering, Bengbu University, Bengbu, China, [3] Key Laboratory of Applied Marine Biotechnology, Ningbo University, Ningbo, China

To analyze the contribution of glycerol-3-phosphate acyltransferase (GPAT) to the first acylation of glycerol-3-phosphate (G-3-P), the present study focused on a functional analysis of the GPAT gene from *Lobosphaera incisa* (designated as *LiGPAT*). A full-length cDNA of *LiGPAT* consisting of a 1,305-bp ORF, a 1,652-bp 5′-UTR, and a 354-bp 3′-UTR, was cloned. The ORF encoded a 434-amino acid peptide, of which 63 residues at the N-terminus defined a chloroplast transit peptide. Multiple sequence alignment and phylogeny analysis of GPAT homologs provided the convincible bioinformatics evidence that LiGPAT was localized to chloroplasts. Considering the conservation of His among the G-3-P binding sites from chloroplastidial GPATs and the substitution of His by Arg at position 195 in the LiGPAT mature protein (designated mLiGPAT), we established the heterologous expression of either *mLiGPAT* or its mutant (Arg195His) (*sdmLiGPAT*) in the GPAT-deficient yeast mutant *gat1*Δ. Lipid profile analyses of these transgenic yeasts not only validated the acylation function of *LiGPAT* but also indicated that the site-directed mutagenesis from Arg^{195} to His led to an increase in the phospholipid level in yeast. Semi-quantitative analysis of mLiGPAT and sdmLiGPAT, together with the structural superimposition of their G-3-P binding sites, indicated that the increased enzymatic activity was caused by the enlarged accessible surface of the phosphate group binding pocket when Arg^{195} was mutated to His. Thus, the potential of genetic manipulation of GPAT to increase the glycerolipid level in *L. incisa* and other microalgae would be of great interest.

Keywords: *Lobosphaera incisa* H4301, glycerol-3-phosphate acyltransferase (GPAT), plastid, site-directed mutagenesis, UPLC-Q-TOF-MS, glycerolipid

INTRODUCTION

In plants, *de novo* biosynthesis of fatty acids occurs exclusively in chloroplasts. The fatty acids generated are either directly metabolized into glycolipids and PG within the chloroplast or exported across the envelope to the ER to form phospholipids and neutral lipids. To synthesize these glycerolipids in both chloroplast and ER, glycerol-3-phosphate acyltransferase (GPAT, E.C. 2.3.1.15) is first required to acylate fatty acids in the glycerol backbone of G-3-P. This enzyme localized in ER was demonstrated to be crucial for cutin, suberin, or storage oil biosynthesis in *Arabidopsis thaliana* (Zheng et al., 2003; Gidda et al., 2009), *Ricinus communis* (Cagliari et al., 2010) and *Brassica napus* (Chen et al., 2010). In addition, it was found that a deficiency in the chloroplastidial GPAT activity could cause a reduction (10–25%) in the PG content of *Arabidopsis* (Kunst et al., 1988; Xu et al., 2006). Thus, GPAT has been found to play a pivotal role in initiating all glycerolipid biosynthesis in higher plants. In comparison, functional analyses of GPAT from microalgae are rare.

To understand the features of the first step of glycerolipid biosynthesis catalyzed by GPAT in microalgae, we attempted to identify one cloned GPAT gene from an oleaginous green microalga, *Lobosphaera incisa* Reisigl (designated as LiGPAT). This microalga possesses a high content of photosynthetic membrane lipids as suggested by a large incised chloroplast with many parallel thylakoid membranes (Merzlyak et al., 2007; Ouyang et al., 2012, 2013b), and it has the ability to accumulate TAG to form oil bodies in cells, especially under nitrogen starvation (Khozin-Goldberg et al., 2002; Zhang et al., 2002; Tong et al., 2011; Ouyang et al., 2013b). Thus, the study of the function of the GPAT gene from *L. incisa* might indicate the role of GPAT in microalgae. Given that GPAT in plants can localize to the chloroplast or the ER, the subcellular localization of the encoded protein LiGPAT was analyzed by bioinformatics technique. Heterologous complementation in a GPAT deficient mutant of yeast, *gat1*Δ (Zheng and Zou, 2001), was used to validate the function of *LiGPAT*, and the yeast lipids were analyzed by lipidomic approaches using UPLC-ESI-Q-TOF-MS and multivariate data analysis. Surprisingly, we found that the conserved His in the G-3-P binding sites from chloroplastidial GPATs was substituted by Arg at position 195 in this chloroplastidial LiGPAT mature protein, and site-directed mutagenesis at this site of LiGPAT improved the phospholipid level in yeast. These findings help us to understand the characteristics of a putatively chloroplastidial GPAT in *L. incisa* and thus provide a strategy for genetic engineering to improve the microalgae-based production of biofuels.

Abbreviations: AA, arachidonic acid; CDD, Conserved Domain Database; CIJF$_{JK}$, jack-knifed confidence interval; cTP, chloroplast transit peptide; CV-ANOVA, cross-validated analysis of variance; DAB, diaminobenzidine; ER, endoplasmic reticulum; G-3-P, Glycerol-3-phosphate; GPAT, Glycerol-3-phosphate acyltransferase; LPAAT, lysophosphatidic acid acyltransferase; m/z, mass-to-charge ratio; NC, nitrocellulose; OPLS-DA, orthogonal projection to latent structures with discriminant analysis; PC, phosphatidylcholine; PCA, principal components analysis; PE, phosphatidylethanolamine; PG, phosphatidylglycerol; PI, phosphatidylinositol; PLS-DA, projection to latent structures with discriminant analysis; PS, phosphatidylserine; RT, retention time; SDS-PAGE, SDS polyacrylamide gel electrophoresis; TAG, triacylglycerol; TAP, Tris acetate phosphate; UPLC-ESI-Q-TOF-MS, ultra performance liquid chromatography-electron spraying ionization-qadrupole-time-of-flight-mass spectrometry; VIP, variable importance in the projection.

MATERIALS AND METHODS

Strains, Medium and Growth Conditions

Lobosphaera incisa, deposited in the Culture Collection of Algae of Charles University in Prague under ID H4301 was cultivated in BG-11 medium (Stanier et al., 1971) in 500-mL glass flasks as described previously (Ouyang et al., 2013b). During culture, the flasks were shaken several times a day by hand at regular intervals.

Cloning of cDNA and DNA Encoding *LiGPAT*

A pair of degenerate primers (G1 and G2) (Supplementary Table S1) for the LiGPAT gene cDNA cloning were designed based on the amino acid sequences of GPAT from *Ostreococcus tauri* (GenBank Accession Number 116061306) and *Chlamydomonas reinhardtii* (GenBank Accession Number 159473711). Total RNA isolated by TRIzol reagent (Invitrogen) from *L. incisa* was used to synthesize cDNA with a Reverse Transcribed Kit II (TaKaRa). The full-length cDNA of *LiGPAT* was amplified by a SMART™ RACE cDNA Amplification Kit (Clontech). Two gene-specific primers (NGSP5-1 and GSP5-2) for the first 5′-RACE reaction, one gene-specific primer (GSP5-4) for the second 5′-RACE reaction, and two gene-specific primers (NGSP3-1 and GSP3-2) for the 3′-RACE reaction were designed (Supplementary Table S1). Genomic DNA extracted by the CTAB method from *L. incisa* (Dellaporta et al., 1983) was used to amplify both the coding region and the untranslated region of *LiGPAT* with four pairs of primers (Supplementary Table S1). All PCR products of the expected size were cloned into the pMD19-T cloning vector (TaKaRa). The resulting constructs were transformed into *Escherichia coli* DH5α and verified by sequencing. The BLAST Server[1] was used to annotate the cloned sequences.

Southern Blot Analysis of *LiGPAT*

Genomic DNA of *L. incisa* was double digested with *Xho*I/*Not*I or *Hind*III/*Not*I restriction endonucleases at 37°C for 4−6 h. The digested DNA samples were fractionated on a 1.0% agarose gel and then transferred to a NC filter membrane (Millipore). A pair of primers was designed based on the conserved domain of GPAT (Supplementary Table S1). A 311-bp biotin-labeled DNA sequence was prepared to use as a probe with a North2South® Biotin Random Prime Labeling Kit (Thermo Scientific). Subsequently, the hybridization was detected by the standard Southern blot procedure (Sambrook and Russell, 2001) with a North2South Chemiluminescent Hybridization and Detection Kit (Thermo Scientific). Signals were visualized by exposure to XBT-1 film (Kodak) at room temperature for 60−120 s.

---

[1]http://blast.ncbi.nlm.nih.gov/

Bioinformatics Analysis

The intron and exon regions from *LiGPAT* were analyzed using Spidey[2]. Signal peptide sites of the amino acid sequence of LiGPAT were predicted by the SignalP 4.1 Server[3], and the transit peptide sites were predicted by the TargetP 1.1 Server[4] and the ChloroP 1.1 Server[5]. Conserved domains were searched in NCBI's CDD (Marchler-Bauer et al., 2011). The PredictProtein program[6] was applied to predict protein structural and functional features (Rost et al., 2004). Protein structures were performed with I-TASSER[7] (Roy et al., 2010). The superimposed images of the LiGPAT tertiary structure were obtained from SuperPose 1.0[8] (Maiti et al., 2004) and displayed with UCSF Chimera 1.10 (Pettersen et al., 2004).

Multiple Sequence Alignment of GPAT Homologs

The available chloroplastidial GPAT amino acid sequences of *Arabidopsis thaliana* (GenBank Accession Number Q43307), *Auxenochlorella protothecoides* (GenBank Accession Number KFM22407), *Chlamydomonas reinhardtii* (GenBank Accession Number XP_001694977), *Coccomyxa subellipsoidea* C-169 (GenBank Accession Number XP_005643353), *Cucurbita moschata* (GenBank Accession Number BAB17755), *Cyanidioschyzon merolae* Strain 10D (GenBank Accession Number XP_006587606), *Glycine max* (GenBank Accession Number XP_006587606), *Micromonas pusilla* CCMP 1545 (GenBank Accession Number XP_003060587), *Micromonas* sp. RCC299 (GenBank Accession Number XP_002505030), *Ostreococcus lucimarinus* (GenBank Accession Number ABO94442), *Ostreococcus tauri* (GenBank Accession Number CAL52024), *Phaeodactylum tricornutum* (GenBank Accession Number XP_002184838), *Ricinus communis* (GenBank Accession Number XP_002518993), *Thalassiosira pseudonana* (GenBank Accession Number XP_002292905), and *Volvox carteri* f. *nagariensis* (GenBank Accession Number XP_002950506) were retrieved from GenBank. The amino acid sequences of the ER-bound GPAT isoform 4 (GenBank accession number Q9LMM0), isoform 5 (GenBank Accession Number NP_187750), isoform 6 (GenBank Accession Number NP_181346), and isoform 8 (GenBank Accession Number NP_191950) from *Arabidopsis thaliana*, and ER-bound GPAT from *Medicago truncatula* (GenBank Accession Number AES79440) and *Ricinus communis* (GenBank Accession Number XP_002511873) were also obtained from GenBank. Multiple sequence alignment of the chloroplastidial GPATs and the ER-bound GPATs were performed with the ClustalX program (Thompson et al., 1997). The web-based BLAST2 program (Altschul et al., 1990) at NCBI was employed to generate pairwise

similarity scores of the aligned sequences. The Multiple EM for Motif Elicitation (MEME) program (Bailey et al., 2006) was used to identify conserved sequence motifs.

Phylogeny Inference

The amino acid sequences of GPAT as well as LPAAT from higher plants and microalgae were retrieved from GenBank. Three GPATs from *Nitrosococcus halophilus*, *Bradyrhizobium japonicum*, and *Ralstonia pickettii* DTP0602 were chosen as an arbitrary outgroup. All accession numbers are presented in the phylogeny tree. All of the conserved domain sequences annotated by searching CDD were also aligned with the ClustalX program (Thompson et al., 1997). Phylogenetic analysis was conducted using maximum likelihood (ML) methods with MEGA 6.0 (Tamura et al., 2013) by using the most appropriate model (LG + G + Γ) determined by ProtTest v3.3 (Darriba et al., 2011). Branch points were tested for significance by bootstrapping with 1,000 replications (Felsenstein, 1985; Tamura et al., 2013).

Construction of *mLiGPAT* and *sdmLiGPAT* Expression Plasmids

To construct a bacterial plasmid, the 1,131-bp of the LiGPAT mature protein coding gene (designated as *mLiGPAT*) with *Bam*HI/*Xho*I digestion sites was amplified with a pair of primers (EcBamF and XhoR) (Supplementary Table S1). The PCR products were sticky-ended and subcloned into the *Bam*HI/*Xho*I sites of pET 28a to obtain the plasmid pET-mLiG.

For heterologous expression in yeast, *mLiGPAT* and the site-directed mutation (Arg195His) of *mLiGPAT* (designated as *sdmLiGPAT*) expression plasmids were constructed. An approximately 1.2 kb cDNA fragment containing the *Bam*HI/*Xho*I digestion sites of *mLiGPAT* was amplified with the primers ScBamF and XhoR (Supplementary Table S1). Site-directed mutagenesis by splicing overlap extension PCR (SOE-PCR) (Ge and Rudolph, 1997) was performed to generate *sdmLiGPAT* with *Bam*HI/*Xho*I digestion sites using four primers ScBamF, MuScR, XhoR, and MuScF (Supplementary Table S1). The PCR products of *mLiGPAT* and *sdmLiGPAT* were sticky-ended and subcloned into the *Bam*HI/*Xho*I sites of pYES2 (Invitrogen) to obtain the plasmids pY-mLiG and pY-sdmLiG, respectively. Prior to transforming the resulting plasmids into host cells, the correct orientation and in-frame fusion of all of the inserts was verified by sequencing.

Heterologous Expression of *LiGPAT*

To obtain soluble, recombinant mLiGPAT protein, the plasmid pET-mLiG and the vector pET 28a as a control were introduced into *E. coli* BL21 (DE3) pLysS (designated pmLiG/BL and pET/BL), respectively. Single colonies of pmLiG/BL or pET/BL were inoculated in LB medium. After incubation at 37°C for 12 h, the cells were collected and resuspended in LB medium with 1 mM IPTG to obtain an OD600 of 0.6. After incubation at 18°C overnight (Schein and Noteborn, 1988), soluble recombinant protein with a His-tag was expressed and detected by SDS-PAGE.

To express *mLiGPAT* and *sdmLiGPAT* in yeast for functional identification, we chose the GPAT deficient yeast mutant,

---

[2]http://www.ncbi.nlm.nih.gov/spidey/

[3]http://www.cbs.dtu.dk/services/SignalP/

[4]http://www.cbs.dtu.dk/services/TargetP/

[5]http://www.cbs.dtu.dk/services/ChloroP/

[6]http://www.predictprotein.org

[7]http://zhanglab.ccmb.med.umich.edu/I-TASSER/

[8]http://wishart.biology.ualberta.ca/SuperPose/

gat1Δ (BY4742, *Matα*, *his3Δ1*, *leu2Δ0*, *lys2Δ0*, *ura3Δ0*, *YKR067w::kanMX4*) as described by Zheng and Zou (2001). This strain was purchased from EUROSCARF[9]. Single colonies carrying pYES2 (plasmid-only as a control) or pY-mLiG or pY-sdmLiG (designated gPY, gmLiGPAT, and gsdmLiGPAT, respectively) were inoculated into SC-uracil medium with 2% glucose. The parental strain of *gat1Δ*, BY4742 (*Matα*, *his3Δ1*, *leu2Δ0*, *lys2Δ0*, *ura3Δ0*), was used as a positive control, while *gat1Δ* was used as a negative control. After incubation at 30°C for 30 h, cells of *gat1Δ*, gPY, BY4742, gmLiGPAT, and gsdmLiGPAT were collected by centrifugation and resuspended in SC-uracil medium with 2% galactose. After incubation at 30°C for 12 h to reach to the logarithmic phase, the yeast cells were transferred to 16°C and incubated for another 48 h. Cells were harvested by centrifugation at 4°C. For preparation of the yeast homogenates, the cell pellets were washed with 10 volumes of distilled H_2O and then immediately frozen in liquid nitrogen and stored at −80°C until use. For total lipid extraction, the cell pellets were lyophilized and stored at −20°C until use. Each sample was collected in duplicate. Colony PCR of each sample was accomplished using the primers pYF and pYR (Supplementary Table S1) to ensure the insertion of the target gene.

Polyclonal Antibody Preparation and Purification

Soluble recombinant mLiGPAT protein was purified by Ni-affinity column chromatography (Bio-Rad) and verified by HPLC-MS. New Zealand rabbits were immunized for LiGPAT polyclonal antibody preparation. The purified mLiGPAT protein was electrophoretically transferred from SDS polyacrylamide gels to NC membranes (Millipore) for polyclonal antibody preparation (Smith and Fisher, 1984). Next, the NC blots were incubated for l h in 3% BSA in PBS before an additional incubation in the prepared LiGPAT polyclonal antibody for 16 h at 4°C. Afterward, the blots were washed several times with PBS and eluted with 0.2 M glycine-HCl (pH 2.3) for 20 min. The eluate was immediately neutralized by the addition of 1 M Tris-HCl and PBS and stored at −20°C until use.

Western Blot Analysis

Fresh cells of *L. incisa* were ground in liquid nitrogen, resuspended in 50−100 μL breaking buffer (25 mM Tris-HCl, pH 6.5, 50 mM NaCl, 2 mM β-mercaptoethanol) and vortexed. Frozen cell pellets of yeast were resuspended in 500 μL breaking buffer (50 mM PBS, pH 7.4, 1 mM EDTA, 5% glycerol, 1 mM PMSF) and lysed by shear force using acid-washed glass beads according to the user manual (Invitrogen). Frozen cell pellets of *E. coli* were resuspended in 0.1 M PBS buffer and then sonicated on ice with a probe sonicator until the suspension was partially clear.

The lysed cells were centrifuged at 20,000 × *g* at 4°C, and the supernatant was collected and stored at −80°C until use. The protein concentration was determined by the Bradford protein assay (Bradford, 1976).

Crude proteins from *L. incisa*, *E. coli* or yeast were electrophoretically transferred to NC membranes (Millipore) as described above, and the Western blots were performed according to the standard protocol (Sambrook and Russell, 2001). The purified LiGPAT polyclonal antibody and the secondary antibody, peroxidase-conjugated goat anti-rabbit IgG (Shanghai Youke Biotechnology Co., Ltd.), were appropriately diluted. Immunoreactive bands were visualized by the addition of DAB according to the manufacturer's manual (Tiangen). The levels of mLiGPAT and sdmLiGPAT expressed in yeast were semi-quantified by measuring the band intensity on their corresponding blots with ImageJ software[10].

Total Lipid Extraction and Fractionation

Total lipid from yeast was extracted according to Bligh and Dyer (1959) with minor modifications. Acid washed glass beads with a diameter of 0.4−0.6 mm (Omega Bio-Tek) were used to break the cell walls. The extent of lysis was observed with a microscope, keeping the degree of breakage of each sample the same as far as possible.
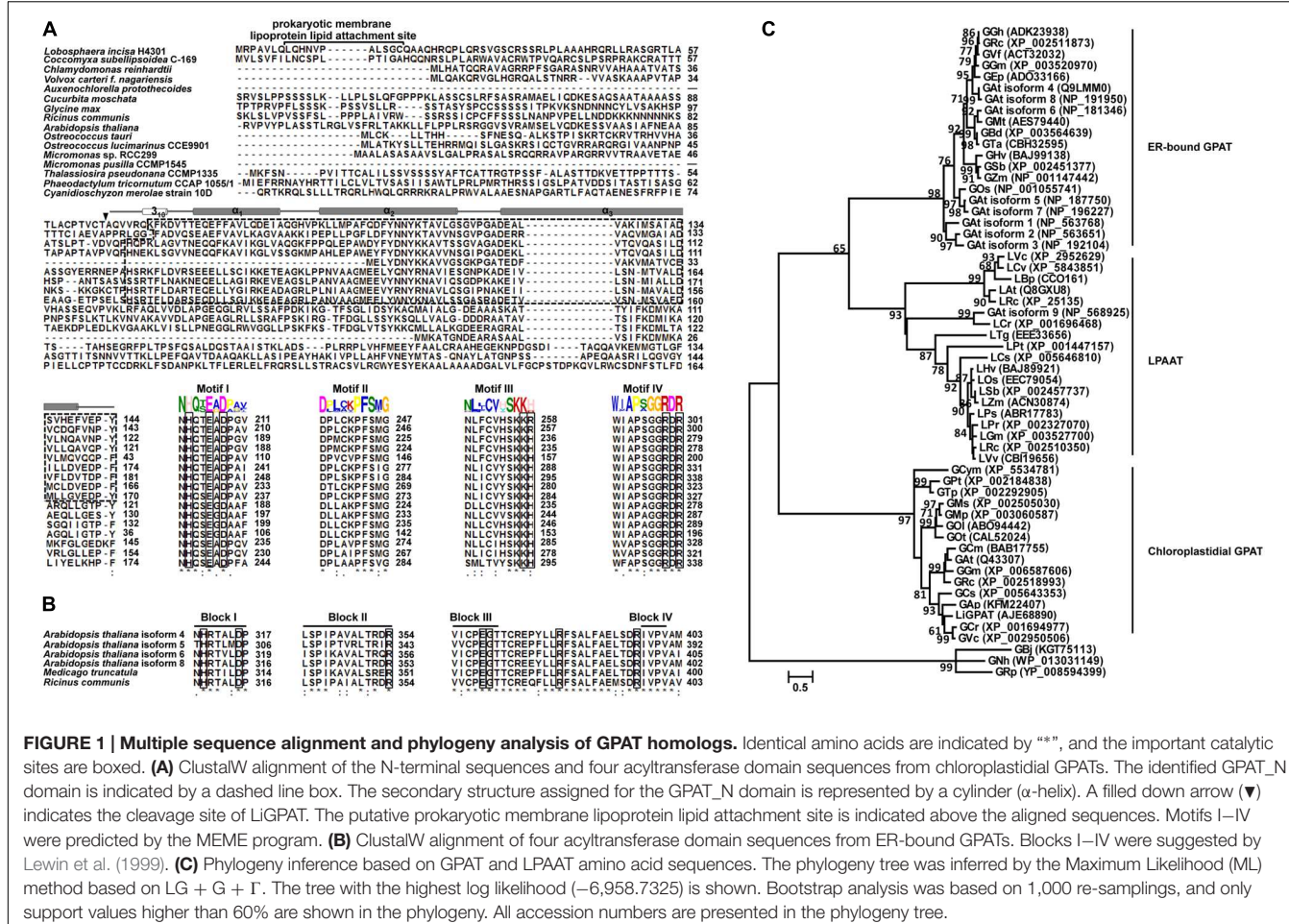
Phospholipids from the extracted total lipids of approximately 50 mg lyophilized yeast were separated using solid-phase extraction (Christie and Han, 2010). A 500 mg cartridge of silica gel (CNW) was first conditioned by elution with 5 mL of chloroform, and the total lipids from yeast were then applied to it. Elution with 10 mL of methanol yielded the phospholipids. This fraction was concentrated under a stream of nitrogen gas and then weighed.

UPLC-ESI-Q-TOF-MS Analysis

Reversed-phase analysis of lipids was performed on a Waters ACQUITY UPLC system using an ACQUITY UPLC BEH C8 analytical column (i.d. 2.1 × 100 mm, particle size 1.7 μm). The temperature of the sample chamber was set at 4°C, the column temperature was set at 40°C, and the injection volume was 4 μL for each analysis. A 1:4 split of the column effluent was used to achieve a flow rate of approximately 0.35 mL/min into the ESI source. To produce ions that could be readily fragmented, 0.001% lithium acetate and 0.1% formic acid were added to the mobile phase as the electrolyte. For efficient separation of the total lipids, water/tetrahydrofuran (3:1, v/v) was used as the mobile phase A and acetonitrile/methanol/tetrahydrofuran (2:1:1, v/v/v) as the mobile phase B. The initial composition of the mobile phase B was changed from 40 to 70% in 10 min and held for 7 min, then increased to 100% in 6 min and held for 1 min, and finally returned to the initial 40% in 1 min and equilibrated for 10 min. MS analysis was performed in a negative ion mode on a Waters Q-TOF Premier mass spectrometer. The mass range was from 100 to 1,200 with a scan duration of 0.3 s and an interscan delay of 0.02 s. High-purity nitrogen was used as the nebulizer and drying gas at a constant flow rate of 50 L/h, and the source temperature was set at 120°C. The capillary voltage was set at 2.6 kV, and the sampling cone voltage was set at the ramp of 35–80 V. MS/MS analysis was performed at a collision energy range of 25−35 V with argon as the collision gas. The

FIGURE 1 | Multiple sequence alignment and phylogeny analysis of GPAT homologs. Identical amino acids are indicated by "*", and the important catalytic sites are boxed. **(A)** ClustalW alignment of the N-terminal sequences and four acyltransferase domain sequences from chloroplastidial GPATs. The identified GPAT_N domain is indicated by a dashed line box. The secondary structure assigned for the GPAT_N domain is represented by a cylinder (α-helix). A filled down arrow (▼) indicates the cleavage site of LiGPAT. The putative prokaryotic membrane lipoprotein lipid attachment site is indicated above the aligned sequences. Motifs I–IV were predicted by the MEME program. **(B)** ClustalW alignment of four acyltransferase domain sequences from ER-bound GPATs. Blocks I–IV were suggested by Lewin et al. (1999). **(C)** Phylogeny inference based on GPAT and LPAAT amino acid sequences. The phylogeny tree was inferred by the Maximum Likelihood (ML) method based on LG + G + Γ. The tree with the highest log likelihood (−6,958.7325) is shown. Bootstrap analysis was based on 1,000 re-samplings, and only support values higher than 60% are shown in the phylogeny. All accession numbers are presented in the phylogeny tree.

TOF analyzer was used in a V mode and tuned for maximum resolution (>10,000 resolving power at m/z 1,000). Prior to the experiment, the instrument was calibrated with sodium formate, and the lock mass spray for precise mass determination was set with leucine enkephalin at a concentration 400 ng/μL, generating an [M-H]$^-$ ion at 554.2615 Da in ESI$^-$ mode. The lock spray frequency was set at 10 s.

Lipidomics Data Processing

The original data from the ESI$^-$ mode were acquired by the UPLC-Q-TOF-MS system and analyzed by a MassLynx 4.1 data processing system (Waters). The MarkerLynx matrices with peak numbers [based on the RT and mass-to-charge ratio (m/z)], sample names, and normalized peak intensities were exported to SIMCA-P+ 12.0 (Umetrics) and analyzed by PCA, PLS-DA, and OPLS-DA. The quality of the models PLS-DA and OPLS-DA was evaluated by two parameters, $R^2Y(cum)$ and $Q^2(cum)$. $R^2Y(cum)$ is the cumulative fraction of the sum of squares of all Y-variables that the model can explain using the latent variables, indicating the explanative ability of the model. $Q^2(cum)$ depicts the cumulative fraction of the total variation that can be predicted using the model via sevenfold cross-validation, indicating the predictability of the model. In general, $R^2Y(cum)$ and $Q^2(cum)$ values close to 1.0 indicate an excellent fit to the model, and the difference between these two values should be less than 0.3 (Wiklund, 2008). If the value of the $Q^2(cum)$ is higher than 0.9, the model is considered an excellent one (Wiklund, 2008). CV-ANOVA was systematically performed based on the PLS-DA model to rule out the non-randomness of the separation between groups. Generally, in permutation tests with 999 iterations, the intercept value of $Q^2 > 0.05$ indicates over-fit in the original model (Kang et al., 2008; Lu et al., 2012).
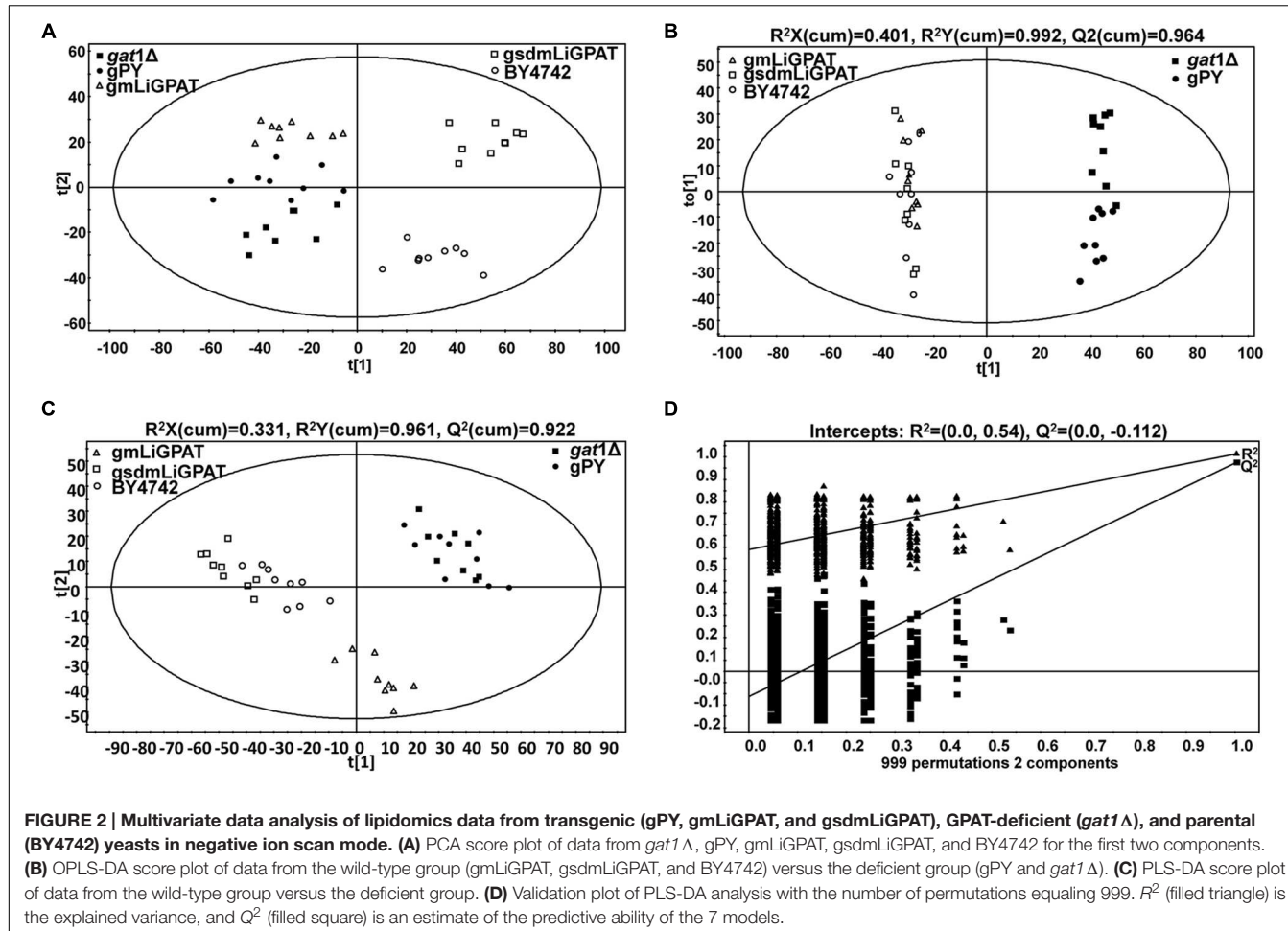
Identification of Lipid Metabolites

Variables meeting two criteria, specifically, high VIP and CIJF$_{JK}$ excluding zero, were selected as potential lipid biomarkers, which contributed to the separation between groups (Eriksson et al., 2006; Cai et al., 2015). The lipid metabolites were identified by the RT, m/z, and the characteristic fragment ions deduced by MS/MS (Yan et al., 2010). In addition, some public databases including HMDB[11], LIPID MAPS[12], and

[11]http://www.hmdb.ca

[12]http://www.lipidmaps.org

FIGURE 2 | Multivariate data analysis of lipidomics data from transgenic (gPY, gmLiGPAT, and gsdmLiGPAT), GPAT-deficient (gat1Δ), and parental (BY4742) yeasts in negative ion scan mode. (A) PCA score plot of data from gat1Δ, gPY, gmLiGPAT, gsdmLiGPAT, and BY4742 for the first two components. **(B)** OPLS-DA score plot of data from the wild-type group (gmLiGPAT, gsdmLiGPAT, and BY4742) versus the deficient group (gPY and gat1Δ). **(C)** PLS-DA score plot of data from the wild-type group versus the deficient group. **(D)** Validation plot of PLS-DA analysis with the number of permutations equaling 999. R^2 (filled triangle) is the explained variance, and Q^2 (filled square) is an estimate of the predictive ability of the 7 models.

METLIN[13] were also used to help elucidate the putative ion structures.

RESULTS

Cloning and Characterization of the LiGPAT Gene

Based on the amino acid sequences of GPAT proteins available from *Ostreococcus tauri* and *Chlamydononas reinhardtii*, a pair of degenerate primers (Supplementary Table S1) was designed, with which a 321-bp cDNA fragment was amplified from *L. incisa*. BLAST analysis revealed that this sequence was a GPAT homolog, and so it was designated *LiGPAT*. Subsequently, a 3,278-bp full-length cDNA of this gene, consisting of a 1,305-bp ORF, a 1,619-bp 5′-UTR, and a 354-bp 3′-UTR was obtained by the RACE technique. The nucleotide sequence of *LiGPAT* was identical to the unique annotated GPAT gene from the transcriptome of *L. incisa* (Ouyang et al., 2013a). A comparison of the cDNA sequence with its corresponding DNA sequence (Supplementary Figure S1A) revealed that the gene contained seven introns. The

introns, 279, 371, 404, 145, 307, 211, and 745 bp beginning from the 5′-end, contained splice sites that all conformed to the GT-AG rule. Both the cDNA and the DNA sequences of *LiGPAT* were deposited in GenBank under the accession numbers KM670441 and KM670442, respectively. Southern blot analysis of the genomic DNA digested by either *Not*I/*Xho*I or *Not*I/*Hind*III using a 311-bp specific probe suggested that *LiGPAT* was a single copy gene in *L. incisa* (Supplementary Figure S1B). The same result for nucleus-encoded chloroplastidial GPAT genes was observed in a number of angiosperm families (Ishizaki et al., 1988; Kunst et al., 1988; Weber et al., 1991; Nishida et al., 1993; Bhella and Mackenzie, 1994).

The ORF of *LiGPAT* encoded a 434-amino acid peptide, in which the domains GPAT_N (GenBank Accession Number cl20739) and LPLAT_GPAT (GenBank Accession Number cd07985) were annotated by searching CDD. A structural motif similar to a prokaryotic membrane lipoprotein lipid attachment site (Leu^8 − Cys^{18}) was identified by the PredictProtein program (**Figure 1A**). This motif was also identified in a chloroplastidial form of the acetyl-CoA carboxylase of pea (Shorrosh et al., 1996) and a chloroplastidial NEF1 of *Arabidopsis thaliana* (Ariizumi et al., 2004). Neither the transmembrane domain nor the signal peptide in LiGPAT was predicted, whereas the

---

[13]http://metlin.scripps.edu

N-terminal sequence of 63 residues was identified as a cTP (**Figure 1A**) as predicted by both the TargetP 1.1 Server and the ChloroP 1.1 Server. Characteristics of this cTP, including a high content (14.28%) of hydroxylated residues (Ser and Thr), a high content (19.05%) of hydrophobic residues (Ala and Val), the absence of the acidic residues (Asp and Glu), and very few Pro and Gly among the first 10 residues, were consistent with previously described cTP sequences (von Heijne et al., 1989). These results suggested that the LiGPAT might be a chloroplastidial GPAT.

Alignment and Phylogeny Analysis of GPAT Homologs

To ascertain the features of chloroplastidial GPAT amino acid sequences, a pairwise sequence alignment and a complete multiple sequence alignment were carried out separately. The results of the pairwise alignment showed a higher similarity among chloroplastidial GPAT proteins from higher plant species (67−74%) than from microalgal species (33−79%). LiGPAT was more conserved with GPATs from other Trebouxiophyceae species (*Coccomyxa subellipsoidea* and *Auxenochlorella prototothecoides*) and Chlorophyceae species (*Chlamydomonas reinhardtii* and *Volvox carteri*) (56−60%) than with Mamiellophyceae species (*Ostreococcus lucimarinus*, *Ostreococcus tauri*, *Micromonas pusilla*, and *Micromonas* sp.) (42−43%), Stramenopiles species (*Thalassiosira pseudonana* and *Phaeodactylum tricornutum*) (36−43%), and Rhodophyta species (*Cyanidioschyzon merolae*) (33%).

The complete multiple sequence alignment identified 39 fully conserved residues that corresponded to only 8.8% of the average 430 residues. The GPAT_N domain identified in LiGPAT was also found in GPATs from *Coccomyxa subellipsoidea*, *Chlamydomonas reinhardtii*, *Volvox carteri*, *Auxenochlorella prototothecoides*, *Cucurbita moschata*, *Glycine max*, *Ricinus communis*, and *Arabidopsis thaliana* (**Figure 1A**). The length of the domain GPAT_N was similar (74−78 amino acid residues) except for that from *Auxenochlorella prototothecoides*, due to the incomplete sequence, but its sequence was different from others (**Figure 1A**). In contrast, four motifs predicted by using the MEME program were relatively conserved (**Figure 1A**). The $H(X)_4D$ motif in Motif I was a conserved consensus sequence among many glycerolipid acyltransferases. The residues Lys, His, Arg, and Arg in Motif III and IV in chloroplastidial GPATs (**Figure 1A**) were considered to form a positive pocket to bind the phosphate group of G-3-P (Lewin et al., 1999; Turnbull et al., 2001). It is worth noting that these four G-3-P binding sites were well conserved except for the His residue, which was replaced by Arg in *L. incisa* and *Coccomyxa subellipsoidea* (**Figure 1A**).
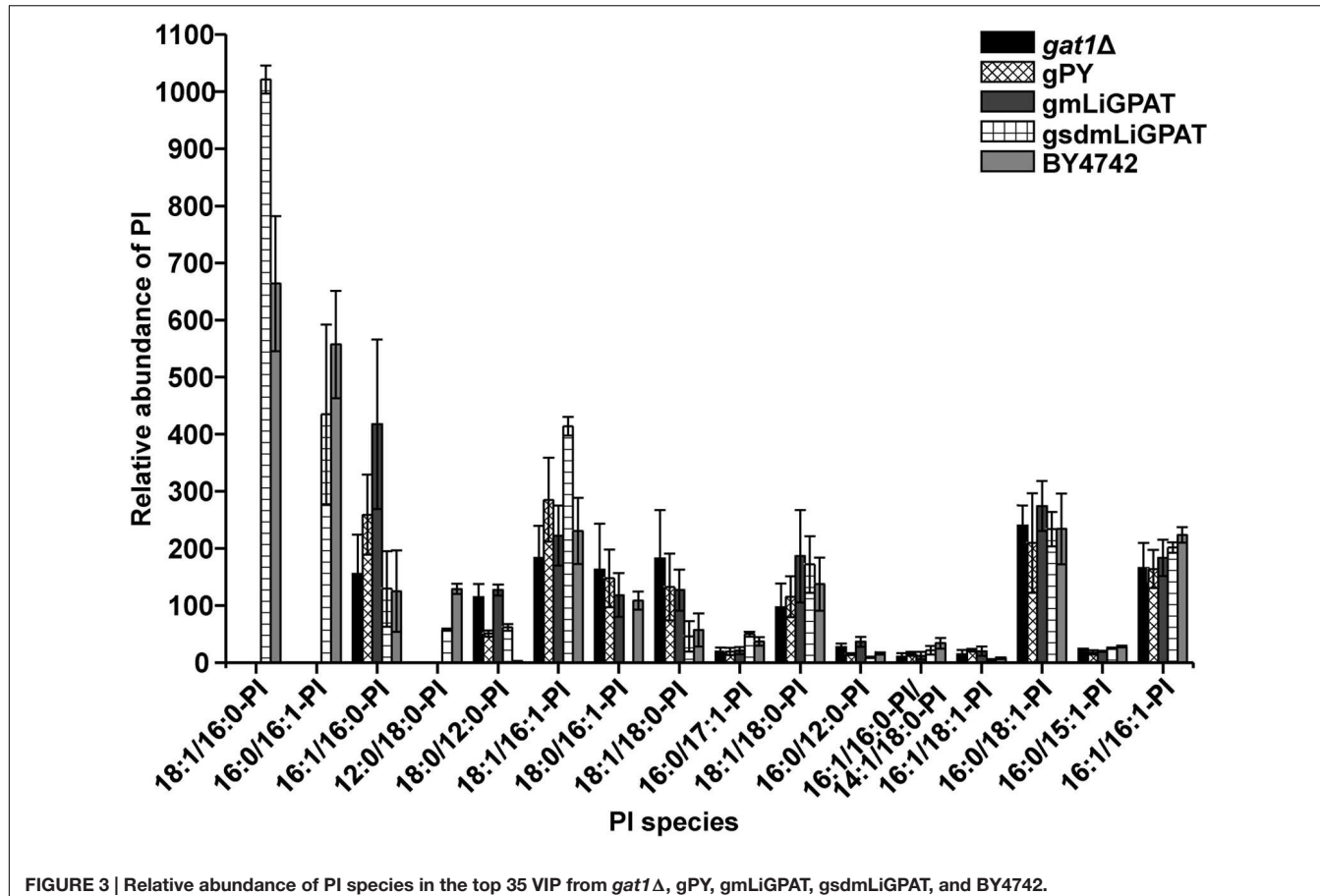
The ER-bound GPATs were aligned, and four acyltransferase domains were identified (**Figure 1B**). Interestingly, these acyltransferase domains were significantly different from those of chloroplastidial GPATs, except the His and Asp residues from the $H(X)_4D$ motif in Block I (**Figure 1B**). The Gly residue in Block III and the Pro residue in Block IV, both of which were suggested to be catalytically important sites (Lewin et al., 1999), were completely conserved (**Figure 1B**). In addition, the residues Arg in Block II and Glu and Ser in Block III were invariant among the cytoplasmic GPATs for G-3-P binding (**Figure 1B**).

Although the previously defined conserved domains of GPAT were similar to those of LPAAT (Heath and Rock, 1998; Lewin et al., 1999; Slabas et al., 2002), the phylogenetic tree showed an apparently different phylogenetic support between lineages of GPAT and LPAAT except that the GPAT isoform 9 from *Arabidopsis thaliana* was in the LPAAT clade (**Figure 1C**). The ER-bound GPATs and the mitochondrial GPATs formed a cluster apart from the chloroplastidial one comprising both higher plants and microalgae (**Figure 1C**), and this result was in agreement with a previous report (Cagliari et al., 2010). This separation could be explained by the differences in the G-3-P binding and catalytically important sites between the cytoplasmic and the chloroplastidial GPATs as mentioned above. The phylogeny

TABLE 1 | Identification of the top 35 metabolites contributing to differences between the wild-type group (gmLiGPAT, gsdmLiGPAT, and BY4742) and the deficient group (*gat1*Δ and gPY).

No	RT	m/z	VIP	Identification
1	11.11	835.5368	38.3386	18:1/16:0-PI
2	10.09	807.5041	27.1032	16:0/16:1-PI
3	6.82	339.2300	20.1118	Unknown
4	6.82	163.1099	16.6411	Unknown
5	10.30	807.5040	14.8547	16:1/16:0-PI
6	10.98	719.4896	11.6084	16:0/16:1-PG
7	9.97	781.4892	11.0091	12:0/18:0-PI
8	10.16	781.4890	8.2496	18:0/12:0-PI
9	10.72	833.5218	8.22112	18:1/16:1-PI
10	3.96	299.2570	8.06764	16:1/16:1-PE
11	11.66	835.5358	8.06364	18:0/16:1-PI
12	13.44	863.5690	6.98515	18:1/18:0-PI
13	11.04	821.5210	6.50701	16:0/17:1-PI
14	11.23	686.4771	5.83435	16:1/16:1-PE
15	10.98	745.5063	5.28594	18:1/16:1-PG
16	9.97	717.4710	5.25232	16:1/16:1-PG
17	10.16	717.4707	5.1447	16:1/16:1-PG
18	13.96	760.5160	5.11763	18:1/16:0-PS
19	13.63	760.5144	5.00298	16:0/18:1-PS
20	12.45	688.4934	4.12377	16:0/16:1-PE
21	2.80	271.2242	4.03169	Unknown
22	13.27	863.5690	4.02396	18:1/18:0-PI
23	9.33	753.4565	3.96868	16:0/12:0-PI
24	11.02	807.5054	3.78887	16:1/16:0-PI or 14:1/18:0-PI
25	4.60	353.2115	3.77584	Unknown
26	10.84	774.5312	3.75723	18:1/17:0-PS
27	19.04	1114.7429	3.68253	Unknown
28	11.36	833.5210	3.52542	16:1/18:1-PI
29	12.85	714.5086	3.37159	16:1/18:1-PE
30	12.06	835.5378	3.33699	16:0/18:1-PI
31	21.81	710.6666	3.1069	Unknown
32	10.00	793.4881	3.02204	16:0/15:1-PI
33	9.63	805.4902	2.82583	16:1/16:1-PI
34	10.14	722.4961	2.74706	12:0/16:0-PC
35	3.35	478.2912	2.59477	18:1-lysoPE

FIGURE 3 | Relative abundance of PI species in the top 35 VIP from *gat1*Δ, gPY, gmLiGPAT, gsdmLiGPAT, and BY4742.

also suggested a sister group relationship between the subclade, consisting of diatoms and red algae, and the one comprising higher plants and green microalgae (**Figure 1C**), which was consistent with the sequence similarity among these species.

These multiple-sequence alignments and phylogeny indicated that LiGPAT possessed the sequence features that conformed to those of chloroplastidial GPATs, providing further evidence that LiGPAT was localized in *L. incisa* chloroplasts.

Functional Identification of *LiGPAT* in a *gat1*Δ Mutant of Yeast

Multiple sequence alignment (**Figure 1A**) showed that the Arg[195] in mLiGPAT was different from His, which was considered one of the G-3-P binding sites in most chloroplastidial GPATs. When this residue His was mutated to Ser, the biological activity of squash chloroplastidial GPAT decreased (Slabas et al., 2002). Accordingly, it was inferred that the catalytic ability of this LiGPAT might be different from (probably lower than) the one with His at position 195. Thus, to identify the function of *LiGPAT*, heterologous expression of *mLiGPAT* as well as its mutant (Arg195His) *sdmLiGPAT* generated by site-directed mutagenesis was performed in the GPAT-deficient yeast strain *gat1*Δ.

To identify the function of GPAT in yeast, the activity of this enzyme was determined *in vitro*, for example, by routinely

using ^{14}C-labeled G-3-P as described by Zheng and Zou (2001). Because of the inconvenience in other ordinary laboratories without any protection from irradiation, a metabolomics approach by using UPLC-ESI-Q-TOF-MS and multivariate data analysis (Fiehn et al., 2000; Wiklund et al., 2005; Van Assche et al., 2015) was employed in this study.

A PCA model with two-components was constructed, which showed that gsdmLiGPAT (site-directed mutated) clustered with the parental yeast strain BY4742 (this group was designated as the wild-type) but was clearly separated from the *gat1*Δ (GPAT-deficient) and plasmid-only control yeast gPY (this group was designated as deficient) (**Figure 2A**). In this PCA model, which could not be well validated, gmLiGPAT (mLiGPAT-transformed) did not significantly separate from the deficient group. In comparison, both the OPLS-DA [$R^2Y(cum) = 0.992$ and $Q^2(cum) = 0.964$] and the PLS-DA [$R^2Y(cum) = 0.961$ and $Q^2(cum) = 0.922$] models with high $R^2Y(cum)$ and $Q^2(cum)$ values could provide reliable support for the separation of gmLiGPAT and the wild-type group from the deficient group (**Figures 2B,C**). Validation of the PLS-DA model with the number of permutations equaling 999 generated intercepts of $R^2 = 0.54$ and $Q^2 = −0.112$ (**Figure 2D**), giving an additional proof of the statistically valid and well fit model because the intercept of Q^2-point regression line was below zero. These statistical analyses indicated that lipid compositions of

gmLiGPAT and gsdmLiGPAT indeed significantly differed from those of gat1Δ and gPY but were similar to those of the parental strain BY4742. It was concluded that the deficiency of GPAT in the mutant gat1Δ was corrected by the introduction of *LiGPAT*, thus confirming the acylation function of the GPAT protein from *L. incisa*.

To understand which lipid mainly contributed to the separation of the wild-type group from the deficient group, 35 potential lipid biomarkers (VIP ranged from 38.34 to 2.59 with an average of 7.80) (**Table 1**) were selected according to both VIP values and the corresponding 95% confidence interval based on a jack-knife procedure (Eriksson et al., 2006). A total of 29 of these selected biomarkers were subsequently identified to be (PI, lyso-PI, PG, PS, PC, and PE (**Table 1**). Among these metabolites, PI accounted for 55.17% (16–29) and possessed relatively high VIP (ranging from 2.83 to 38.34 with an average of 9.613) (**Table 1**), indicating that this phospholipid was the main contributor to the separation. The relative abundance of most PI species from the wild-type group was higher than from the deficient group (**Figure 3**). This result was roughly consistent with the previous report (Redón et al., 2011) that the main increase of PI was observed when the yeast strain was cultured under low temperature. Therefore, the total relative abundance of PI species in the wild-type was compared with that in the deficient group. All of the PI species, 21 in total, were subsequently identified (**Table 2**), and the relative abundance was

TABLE 2 | List of identified PI species in the ESI⁻ model.

No	RT	m/z	Identification
1	6.72	723.4066	16:1/10:0-PI
2	7.68	725.4233	16:0/10:0-PI
3	9.32	753.4564	16:0/12:0-PI
4	9.00	753.4598	12:0/16:0-PI
5	9.57	779.4742	14:1/16:0-PI or
			14:0-16:1-PI or
			12:0/18:1-PI
6	10.15	781.4889	18:0/12:0-PI
7	9.97	781.4892	12:0/18:0-PI
8	10.00	793.4881	16:0/15:1-PI
9	9.61	805.4915	16:1/16:1-PI
10	10.30	807.504	16:1/16:0-PI
	10.21	807.5042	
	10.58	807.5052	
	11.01	807.5056	
11	10.09	807.5059	16:0/16:1-PI
12	10.14	819.5068	16:1/17:1-PI
13	11.03	821.5215	16:0/17:1-PI
14	11.35	833.5210	16:1/18:1-PI
15	10.70	833.5219	18:1/16:1-PI
16	11.66	835.5358	18:0/16:1-PI
17	11.11	835.5367	18:1/16:0-PI
18	12.06	835.5378	16:0/18:1-PI
19	12.47	861.5568	18:1/18:1-PI
20	13.43	863.5687	18:1/18:0-PI
	13.27	863.5690	
21	10.01	875.4960	16:0/21:2-PI

compared. The results showed that the total relative abundance of PI from gmLiGPAT was higher, although not significantly higher ($P > 0.05$), than from gat1Δ and gPY, whereas the total relative abundance of PI from gsdmLiGPAT was significantly higher ($P < 0.01$) than from gmLiGPAT, gat1Δ, and gPY, but there was no significant difference ($P > 0.05$) from BY4742 (**Figure 4C**). It was thus predicted that the site-directed mutagenesis of LiGPAT Arg195His might enhance the catalytic activity of this protein and result in an increase in the phospholipid level in yeast. The subsequent measurement of phospholipid content showed that the phospholipid level from gsdmLiGPAT was higher than from gmLiGPAT or BY4742 (**Figure 4D**), thus supporting the prediction.

DISCUSSION

Plastid-Localized GPAT from *L. incisa*

Glycerol-3-phosphate acyltransferases targeting the chloroplast, cytoplasm, and mitochondrion have been recognized in plants. The chloroplastidial GPAT localized in the stroma is a soluble protein, and it can utilize acyl-(acyl-carrier protein) as the acyl donor (Joyard and Douce, 1977). In contrast, the cytoplasmic form targeted to the ER is hydrophobic, and it is able to utilize acyl-CoA as the acyl donor (Frentzen et al., 1990). Genes of both chloroplastidial and ER-bound GPAT from several higher plants have been cloned, a total of 10 from *Arabidopsis* (Zheng et al., 2003; Xu et al., 2006; Gidda et al., 2009; Cagliari et al., 2010; Chen et al., 2010; Yang et al., 2012), 9 from *Ricinus communis* (Cagliari et al., 2010), and at least 2 from *Glycine max* (Eskandari et al., 2013), for instance. Examination of the algal genomes indicated that the microalgae *Chlamydomonas reinhardtii*, *Ostreococcus tauri*, *Cyanidioschyzon merolae* strain 10D, *Phaeodactylum tricornutum* CCAP 1055/1, and *Thalassiosira pseudonana* CCMP1335 were missing the recognizable extraplastidial GPAT homologs (Lykidis and Ivanova, 2008). It was suggested that the GPATs in these microalgae might have dual localization in both chloroplast and ER (Lykidis and Ivanova, 2008).

The present study provides the convincible bioinformatics evidence that one GPAT from the green microalga *L. incisa* is localized to chloroplasts (**Figures 1A,C**). In the latest NCBI database, there were deposited putative green microalgal GPATs, which were similar to the ER-bound GPAT9 from *Arabidopsis*. Therefore, it was inferred that the GPATs from *L. incisa* and the above-mentioned microalgae might be only localized to chloroplasts. Obviously, this idea would be more convincing and significant with analysis of accurate subcellular localization of the chloroplastidial GPATs and function of the cytoplasmic ones from these green microalgae.

Site-Directed Mutagenesis of LiGPAT Resulted in an Increase of the Phospholipid Level in Yeast

The phospholipid level of the yeast transformed with the site-directed mutated *LiGPAT* (Arg195His) was higher than that

of yeast transformed with the original *LiGPAT* (**Figure 4D**), indicating that the catalytic ability of LiGPAT was improved by site-directed mutagenesis. To explore whether this improvement resulted from an increased level of protein expression or an increased enzymatic activity, semi-quantitative analysis of LiGPAT introduced into yeast was performed using western blots with purified LiGPAT polyclonal antibody. The reliability of this antibody was supported by western blot analysis of the total proteins extracted from *L. incisa* and transformed *E. coli* pmLiG/BL (Supplementary Figure S2). Comparison of the band intensity on the blots indicated that the expression levels of mLiGPAT and sdmLiGPAT were not significantly difference ($P > 0.05$) (**Figures 4A,B**), suggesting that the site-directed mutagenesis from Arg^{195} to His had no effect on protein expression level but could enhance the enzymatic activity of LiGPAT. This prompted us to investigate the relationship between protein structure and enzymatic activity of LiGPAT because the mutated residue Arg is situated in the G-3-P binding pocket (**Figure 1A**).

The crystal structure of squash chloroplastidial GPAT protein (PDB entry 1K30) was the only structure solved with high-resolution that elucidated the structure-function relationship of GPAT (Heath and Rock, 1998; Turnbull et al., 2001; Tamada et al., 2004). Accordingly, 3D models

of mLiGPAT and sdmLiGPAT (**Figure 5**) were developed by using the I-TASSER server, which was an integrated platform for automated protein structure and function prediction based on the sequence-to-structure-to-function paradigm (Roy et al., 2010). The secondary structural elements of the mLiGPAT and sdmLiGPAT proteins were organized into two domains (**Figure 5A**), which were found well conserved in *Cucurbita moschata*, *Chlamydomonas reinhardtii*, *Arabidopsis thaliana*, and *Glycine max* (Turnbull et al., 2001; Misra and Panda, 2013). Domain I is the GPAT_N, and it forms a four-helix bundle (consisting of the 3_{10} helix linking residues 7–10 and helices α1–3) with a simple square, right-handed up–down-up–down topology (**Figures 1A** and **5A**). A loop region called the "interlinking loop" linked the small Domain I and the large Domain II. Domain II comprises the alternating α/β secondary structural elements (**Figure 5A**) and positively charged residues, which constitutes a positively charged pocket for binding the phosphate group of G-3-P. These residues were well conserved in most plants, except that the His residue at position 195 in mLiGPAT was substituted by Arg (**Figure 1A**). However, this replacement did not change the charge property and secondary structure of the pocket from mLiGPAT compared to that from its site-directed mutant sdmLiGPAT (**Figure 5A**). Structural
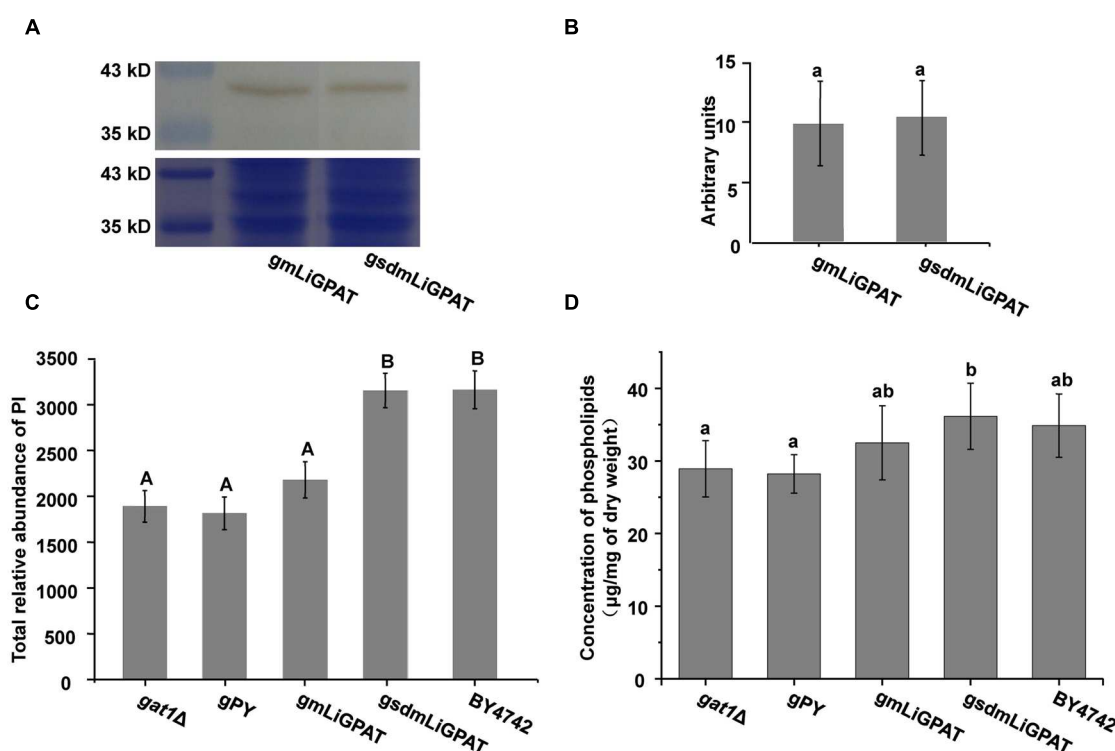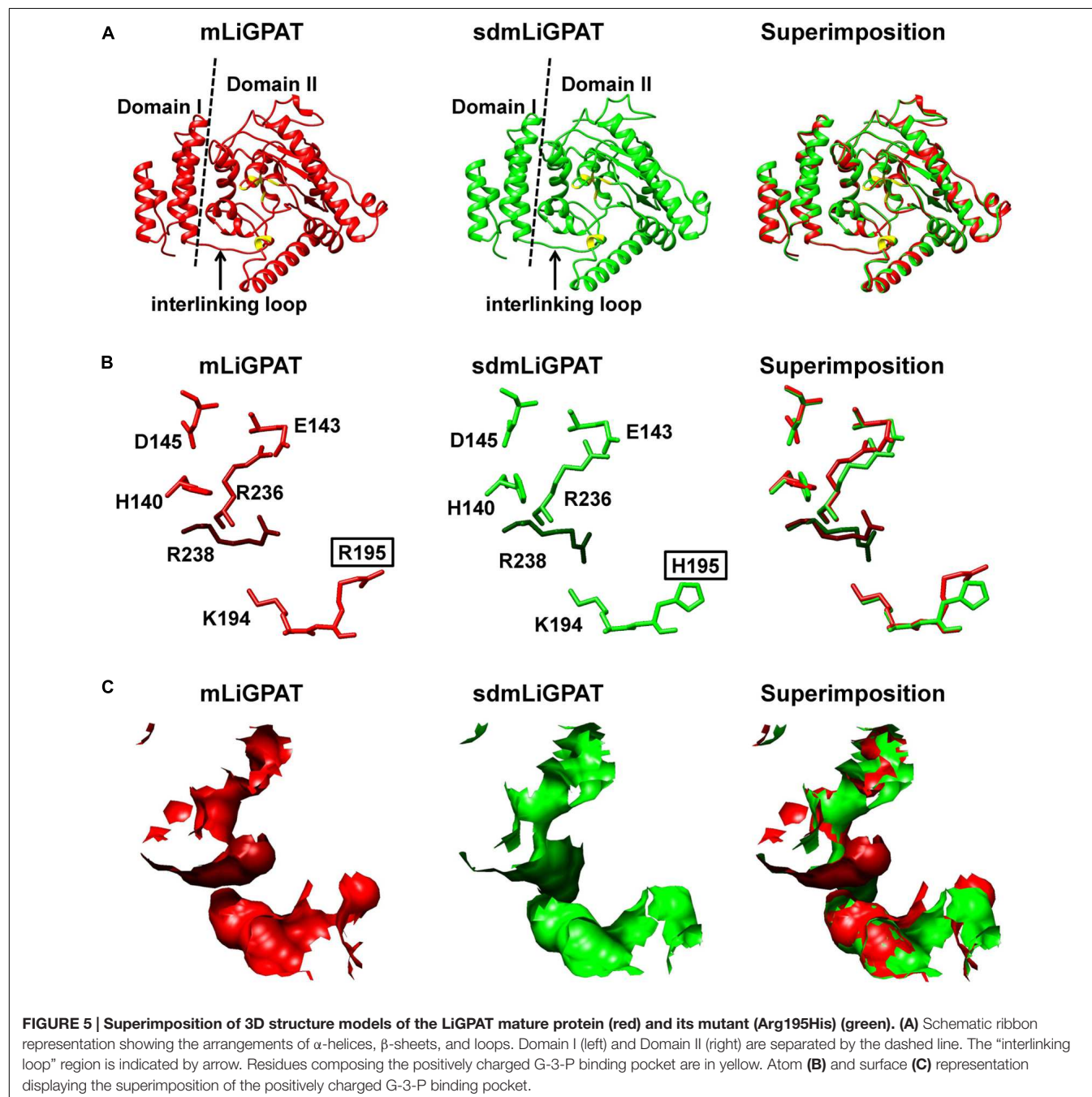
FIGURE 4 | The effect of site-directed mutagenesis of LiGPAT from Arg^{195} to His in yeast. (A) Western blot analysis of gmLiGPAT and gsdmLiGPAT with the LiGPAT antibody. **(B)** The density of the blots of gmLiGPAT and gsdmLiGPAT were measured with ImageJ software and expressed in arbitrary optical density units. Values are the mean ± SD, $n = 3$. The average levels of gmLiGPAT and gsdmLiGPAT showed no difference ($P > 0.05$). **(C)** Comparison of the total relative abundance of all PI species among *gat1*Δ, gPY, gmLiGPAT, gsdmLiGPAT, and BY4742. Values with the same letter showed no significant difference ($P > 0.05$); the others showed significant differences ($P < 0.01$). **(D)** Comparison of the concentration of phospholipids among *gat1*Δ, gPY, gmLiGPAT, gsdmLiGPAT, and BY4742. Values with the same letter showed no significant difference ($P > 0.05$); the others showed significant differences ($P < 0.05$).

superimposition of the binding sites for the phosphate group of G-3-P from mLiGPAT and sdmLiGPAT was illustrated by atom (**Figure 5B**) and surface (**Figure 5C**). The modeling indicated that the side-chain conformation of residues at positions 195 and 238 were different between these two proteins, suggesting a smaller accessible surface of the phosphate group binding pocket from mLiGPAT than from sdmLiGPAT. Therefore, changes of the side-chain conformation might be responsible for the difference in the enzymatic activity of mLiGPAT and sdmLiGPAT when they function in yeast.

In brief, acylation by GPAT is considered to be the rate-limiting step in the glycerolipid synthesis pathway and to regulate fatty acid flux through the pathway (Coleman and Lee, 2004; Wendel et al., 2009). In *Arabidopsis*, RNAi of the chloroplastidial *GPAT* in the *ats1-1* mutant background led to small leaves (Xu et al., 2006). Thus, it was inferred that the low growth rate of *L. incisa* (Ouyang et al., 2013b) might be partially associated with the relatively low enzymatic activity of LiGPAT. Recently, a modification of the GPAT-coding gene together with four other genes has been documented to improve the TAG content in

FIGURE 5 | Superimposition of 3D structure models of the LiGPAT mature protein (red) and its mutant (Arg195His) (green). (A) Schematic ribbon representation showing the arrangements of α-helices, β-sheets, and loops. Domain I (left) and Domain II (right) are separated by the dashed line. The "interlinking loop" region is indicated by arrow. Residues composing the positively charged G-3-P binding pocket are in yellow. Atom **(B)** and surface **(C)** representation displaying the superimposition of the positively charged G-3-P binding pocket.

Chlorella minutissima UTEX 2219 (Hsieh et al., 2012). Hence, genetic manipulation of the G-3-P binding sites of *GPAT* could be taken as a breakthrough to increase the growth rate and glycerolipid content of *L. incisa* and other microalgae.

AUTHOR CONTRIBUTIONS

Z-GZ and L-LO designed the study and wrote the paper. L-LO carried out the experiments and she and Z-GZ were involved in data analysis. HL assisted with heterologous expression of *LiGPAT* in yeast. X-JY and J-LX helped design the lipidomic experiments and interpret the data. Z-GZ gave the final approval of the version to be published. All authors have read and approved the final manuscript.

REFERENCES

Altschul, S. F., Gish, W., Miller, W., Myer, E. W., and Lipman, D. J. (1990). Basic local alignment search tool. *J. Mol. Biol.* 215, 403–410. doi: 10.1006/jmbi.1990.9999

Ariizumi, T., Hatakeyama, K., Hinata, K., Inatsugi, R., Nishida, I., Sato, S., et al. (2004). Disruption of the novel plant protein NEF1 affects lipid accumulation in the plastids of the tapetum and exine formation of pollen, resulting in male sterility in *Arabidopsis thaliana*. *Plant J.* 39, 170–181. doi: 10.1111/j.1365-313x.2004.02118.x

Bailey, T. L., Williams, N., Misleh, C., and Li, W. W. (2006). MEME: discovering and analyzing DNA and protein sequence motifs. *Nucleic Acids Res.* 34, W369–W373. doi: 10.1093/nar/gkl198

Bhella, R. S., and Mackenzie, S. L. (1994). Nucleotide sequence of a cDNA from *Carthamus tinctorius* encoding a glycerol-3-phosphate acyltransferase. *Plant Physiol.* 106, 1713–1714. doi: 10.1104/pp.106.4.1713

Bligh, E. G., and Dyer, W. J. (1959). A rapid method of total lipid extraction and purification. *Can. J. Biochem. Physiol.* 37, 911–917. doi: 10.1139/o59-099

Bradford, M. M. (1976). A rapid and sensitive method for the quantification of microgram quantities of protein using the principal of protein-dye binding. *Anal. Biochem.* 72, 248–254. doi: 10.1006/abio.1976.9999

Cagliari, A., Margis-Pinheiro, M., Loss, G., Mastroberti, A. A., de Araujo Mariath, J. E., and Margis, R. (2010). Identification and expression analysis of castor bean (*Ricinus communis*) genes encoding enzymes from the triacylglycerol biosynthesis pathway. *Plant Sci.* 179, 499–509. doi: 10.1016/j.plantsci.2010.07.015

Cai, D., Li, D., Zhao, S., Dou, X., Wang, F., Huang, G., et al. (2015). A correlation between diet and longevity characterization by means of element profiles in healthy people over 80 years from a chinese longevous region. *Biol. Trace Elem. Res.* 165, 18–29. doi: 10.1007/s12011-015-0233-7

Chen, X., Truksa, M., Snyder, C. L., El-Mezawy, A., Shah, S., and Weselake, R. J. (2010). Three homologous genes encoding sn-glycerol-3-phosphate acyltransferase 4 exhibit different expression patterns and functional divergence in *Brassica napus*. *Plant Physiol.* 155, 851–865. doi: 10.1104/pp.110.169482

Christie, W. W., and Han, X. (2010). *Lipid Analysis: Isolation, Separation, Identification and Lipidomic Analysis*. Bridgwater: The Oily Press.

Coleman, R. A., and Lee, D. P. (2004). Enzymes of triacylglycerol synthesis and their regulation. *Prog. Lipid Res.* 43, 134–176. doi: 10.1016/S0163-7827(03)00051-1

Darriba, D., Taboada, G. L., Doallo, R., and Posada, D. (2011). ProtTest 3: fast selection of best-fit models of protein evolution. *Bioinformatics* 27, 1164–1165. doi: 10.1093/bioinformatics/btr088

Dellaporta, S. L., Wood, J., and Hick, J. B. (1983). A plant DNA minipreparation: version II. *Plant Mol. Biol. Rep.* 1, 19–21. doi: 10.1007/bf02712670

ACKNOWLEDGMENTS

SUPPLEMENTARY MATERIAL

The Supplementary Material for this article can be found online at: http://journal.frontiersin.org/article/10.3389/fpls.2016.00286

Eriksson, L., Johansson, E., Kettaneh-Wold, N., Trygg, J., Wikström, C., and Wold, S. (2006). *Multi- and Megavariate Data Analysis. Basic principles and applications*, Part I. Umeå: Umetrics AB.

Eskandari, M., Cober, E. R., and Rajcan, I. (2013). Using the candidate gene approach for detecting genes underlying seed oil concentration and yield in soybean. *Theor. Appl. Genet.* 126, 1839–1850. doi: 10.1007/s00122-013-2096-7

Felsenstein, J. (1985). Confidence limits on phylogenies: an approach using the bootstrap. *Evolution* 39, 783–791. doi: 10.2307/2408678

Fiehn, O., Kopka, J., Dörmann, P., Altmann, T., Trethewey, R. N., and Willmitzer, L. (2000). Metabolite profiling for plant functional genomics. *Nat. Biotechnol.* 18, 1157–1161. doi: 10.1038/81137

Frentzen, M., Neuburger, M., Joyard, J., and Douse, R. (1990). Intraorganelle localization and substrate specificities of the mitochondrial acyl-CoA:sn-glycerol-3-phosphate O-acyl-transferase and acy-CoA:1-acyl-sn-glycerol-3-phosphate O-acyltransferase from potato tubers and pea leaves. *Eur. J. Biochem.* 187, 395–402. doi: 10.1111/j.1432-1033.1990.tb15317.x

Ge, L., and Rudolph, P. (1997). Simultaneous introduction of multiple mutations using overlap extension PCR. *Biotechniques* 22, 28–30.

Gidda, S. K., Shockey, J. M., Rothstein, S. J., Dyer, J. M., and Mullen, R. T. (2009). *Arabidopsis thaliana* GPAT8 and GPAT9 are localized to the ER and possess distinct ER retrieval signals: functional divergence of the dilysine ER retrieval motif in plant cells. *Plant Physiol. Biochem.* 47, 867–879. doi: 10.1016/j.plaphy.2009.05.008

Heath, R. J., and Rock, C. O. (1998). A conserved histidine is essential for glycerolipid acyltransferase catalysis. *J. Bacteriol.* 180, 1425–1430.

Hsieh, H. J., Su, C. H., and Chien, L. J. (2012). Accumulation of lipid production in *Chlorella minutissima* by triacylglycerol biosynthesis-related genes cloned from *Saccharomyces cerevisiae* and *Yarrowia lipolytica*. *J. Microbiol.* 50, 526–534. doi: 10.1007/s12275-012-2041-5

Ishizaki, O., Nishida, I., Agata, K., Eguchi, G., and Murata, N. (1988). Cloning and nucleotide sequence of cDNA for the plastid glycerol-3-phosphate acyltransferase from squash. *FEBS Lett.* 238, 424–430. doi: 10.1016/0014-5793(88)80525-8

Joyard, D., and Douce, R. (1977). Site of synthesis of phosphatidic acid and diacylglycerol in spinach chloroplasts. *Biochim. Biophys. Acta* 486, 273–285. doi: 10.1016/0005-2760(77)90023-6

Kang, J., Choi, M.-Y., Kang, S., Kwon, H. N., Wen, H., Lee, C. H., et al. (2008). Application of a 1H nuclear magnetic resonance (NMR) metabolomics approach combined with orthogonal projections to latent structure-discriminant analysis as an efficient tool for discriminating between Korean and Chinese herbal medicines. *J. Agric. Food Chem.* 56, 11589–11595. doi: 10.1021/jf802088a

Khozin-Goldberg, I., Bigogno, C., Shrestha, P., and Cohen, Z. (2002). Nitrogen starvation induces the accumulation of arachidonic acid in the freshwater green alga *Parietochloris incisa* (Trebouxiophyceae). *J. Phycol.* 38, 991–994. doi: 10.1046/j.1529-8817.2002.01160.x

Kunst, L., Browse, J., and Somerville, C. (1988). Altered regulation of lipid biosynthesis in a mutant of *Arabidopsis* deficient in chloroplast glycerol-3-phosphate acyltransferase activity. *Proc. Natl. Acad. Sci. U.S.A.* 85, 4143–4147. doi: 10.1073/pnas.85.12.4143

Lewin, T. M., Wang, P., and Coleman, R. A. (1999). Analysis of amino acid motifs diagnostic for the sn-glycerol-3-phosphate acyltransferase reaction. *Biochemistry* 38, 5764–5771. doi: 10.1021/bi982805d

Lu, N., Wei, D., Chen, F., and Yang, S.-T. (2012). Lipidomic profiling and discovery of lipid biomarkers in snow alga *Chlamydomonas nivalis* under salt stress. *Eur. J. Lipid Sci. Technol.* 114, 253–265. doi: 10.1002/ejlt.201100248

Lykidis, A., and Ivanova, N. (2008). "Genomic prospecting for microbial biodiesel production," in *Bioenergy*, eds J. D. Wall, C. S. Harwood, and A. Demain (Washington: ASM Press), 407–418.

Maiti, R., Van Domselaar, G. H., Zhang, H., and Wishart, D. S. (2004). SuperPose: a simple server for sophisticated structural superposition. *Nucleic Acids Res.* 32, W590–W594. doi: 10.1093/nar/gkh477

Marchler-Bauer, A., Lu, S., Anderson, J. B., Chitsaz, F., Derbyshire, M. K., DeWeese-Scott, C., et al. (2011). CDD: a conserved domain database for the functional annotation of proteins. *Nucleic Acids Res.* 39, D225–D229. doi: 10.1093/nar/gkq1189

Merzlyak, M. N., Chivkunova, O. B., Gorelova, O. A., Reshetnikova, I. V., Solovchenko, A. E., Khozin-Goldberg, I., et al. (2007). Effect of nitrogen starvation on optical properties, pigments, and arachidonic acid content of the unicellular green alga *Parietochloris incisa* (Trebouxiophyceae, Chlorophyta). *J. Phycol.* 43, 833–843. doi: 10.1111/j.1529-8817.2007.00375.x

Misra, N., and Panda, P. K. (2013). In search of actionable targets for agrigenomics and microalgal biofuel production: sequence-structural diversity studies on algal and higher plants with a focus on GPAT protein. *OMICS* 17, 173–186. doi: 10.1089/omi.2012.0094

Nishida, I., Tasaka, Y., Shiraisi, H., and Murata, N. (1993). The gene and the RNA for the precursor to the plastid-located glycerol-3-phosphate acyltransferase of *Arabidopsis thaliana*. *Plant Mol. Biol.* 21, 267–277. doi: 10.1007/bf00019943

Ouyang, L.-L., Chen, S.-H., Li, Y., and Zhou, Z.-G. (2013a). Transcriptome analysis reveals unique C4-like photosynthesis and oil body formation in an arachidonic acid-rich microalga *Myrmecia incisa* Reisigl H4301. *BMC Genomics* 14:396. doi: 10.1186/1471-2164-14-396

Ouyang, L.-L., Du, D. H., Yu, S. Y., Li, C. Y., Zhang, C. W., Gao, H. J., et al. (2012). Expressed sequence tags analysis revealing the taxonomic position and fatty acid biosynthesis in an oleaginous green microalga, *Myrmecia incisa* Reisigl (Trebouxiophyceae, Chlorophyta). *Chin. Sci. Bull.* 57, 3342–3352. doi: 10.1007/s11434-012-5159-2

Ouyang, L.-L., Li, H., Liu, F., Tong, M., Yu, S. Y., and Zhou, Z.-G. (2013b). "Accumulation of arachidonic acid in a green microalga, *Myrmecia incisa* H4301, enhanced by nitrogen starvation and its molecular regulation mechanism," in *Arachidonic acid: Dietary Sources and General Functions*, eds G. G. Dumancas, B. S. Murdianti, and E. A. Lucas (New York, NY: Nova Science Publishers), 1–20.

Pettersen, E. F., Goddard, T. D., Huang, C. C., Couch, G. S., Greenblatt, D. M., Meng, E. C., et al. (2004). UCSF Chimera–A visualization system for exploratory research and analysis. *J. Comput. Chem.* 25, 1605–1612. doi: 10.1002/jcc.20084

Redón, M., Guillamón, J. M., Mas, A., and Rozès, N. (2011). Effect of growth temperature on yeast lipid composition and alcoholic fermentation at low temperature. *Eur. Food Res. Technol.* 232, 517–527. doi: 10.1007/s00217-010-1415-3

Rost, B., Yachdav, G., and Liu, J. (2004). The predict protein server. *Nucleic Acids Res.* 32, W321–W326. doi: 10.1093/nar/gkh377

Roy, A., Kucukural, A., and Zhang, Y. (2010). I-TASSER: a unified platform for automated protein structure and function prediction. *Nat. Protoc.* 5, 725–738. doi: 10.1038/nprot.2010.5

Sambrook, J., and Russell, D. W. (2001). *Molecular Cloning: A Laboratory Manual*. New York, NY: Cold Spring Harbor Laboratory Press.

Schein, C. H., and Noteborn, M. H. M. (1988). Formation of soluble recombinant proteins in *Escherichia coli* is favored by lower growth temperature. *Nat. Biotechnol.* 6, 291–294. doi: 10.1038/nbt0388-291

Shorrosh, B. S., Savage, L. J., Soll, J., and Ohlrogge, J. B. (1996). The pea chloroplast membrane-associated protein, IEP96, is a subunit of acetyl-CoA carboxylase. *Plant J.* 10, 261–268. doi: 10.1046/j.1365-313x.1996.10020261.x

Slabas, A. R., Kroon, J. T. M., Scheirer, T. P., Gilroy, J. S., Hayman, M., Rice, D. W., et al. (2002). Squash glycerol-3-phosphate (1)-acyltransferase: alteration of substrate selectivity and identification of arginine and lysine residues important in catalytic activity. *J. Biol. Chem.* 277, 43918–43923. doi: 10.1074/jbc.m206429200

Smith, D. E., and Fisher, P. A. (1984). Identification, developmental regulation, and response to heat shock of two antigenically related forms of a major nuclear envelope protein in *Drosophila* embryos: application of an improved method for affinity purification of antibodies using polypeptides immobilized on nitrocellulose blots. *J. Cell Biol.* 99, 20–28. doi: 10.1083/jcb.99.1.20

Stanier, R. Y., Kunisawa, M. M., and Cohen-Bazir, G. (1971). Purification and properties of unicellular blue-green algae (order Chlorococcales). *Bacteriol. Rev.* 35, 171–201.

Tamada, T., Feese, M. D., Ferri, S. R., Kato, Y., Yajima, R., and Toguri, T. (2004). Substrate recognition and selectivity of plant glycerol-3-phosphate acyltransferases (GPATs) from *Cucurbita moscata* and *Spinacea oleracea*. *Acta Crystallogr. D Biol. Crystallogr.* 60, 13–21. doi: 10.1107/s0907444903020778

Tamura, K., Stecher, G., Peterson, D., Filipski, A., and Kumar, S. (2013). MEGA6: molecular evolutionary genetics analysis version 6.0. *Mol. Biol. Evol.* 30, 2725–2729. doi: 10.1093/molbev/mst197

Thompson, J. D., Gibson, T. J., Plewniak, F., Jeanmougin, F., and Higgins, D. G. (1997). The ClustalX windows interface: flexible strategies for multiple sequence alignment aided by quality analysis tools. *Nucleic Acids Res.* 25, 4876–4882. doi: 10.1093/nar/25.24.4876

Tong, M., Yu, S. Y., Ouyang, L.-L., and Zhou, Z.-G. (2011). Comparison of increased arachidonic acid content in *Myrmecia incisa* cultured during the course of nitrogen or phosphorus starvation. *J. Fish. China* 35, 763–773. doi: 10.3724/SP.J.1231.2011.17114

Turnbull, A. P., Rafferty, J. B., Sedelnikova, S. E., Slabas, A. R., Schierer, T. P., Kroon, J. T. M., et al. (2001). Analysis of the structure, substrate specificity, and mechanism of squash glycerol-3-phosphate (1)-acyltransferase. *Structure* 9, 347–353. doi: 10.1016/S0969-2126(01)00595-0

Van Assche, R., Temmerman, L., Dias, D. A., Boughton, B., Boonen, K., Braeckman, B. P., et al. (2015). Metabolic profiling of a transgenic *Caenorhabditis elegans* Alzheimer model. *Metabolomics* 11, 477–486. doi: 10.1007/s11306-014-0711-5

von Heijne, G., Steppuhn, J., and Herrmann, R. G. (1989). Domain structure of mitochondrial and chloroplast targeting peptides. *Eur. J. Biochem.* 180, 535–545. doi: 10.1111/j.1432-1033.1989.tb14679.x

Weber, S., Wolter, F. P., Buck, F., Frentzen, M., and Heinz, E. (1991). Purification and cDNA sequencing of an oleate-selective acyl-ACP:sn-glycerol-3-phosphate acyltransferase from pea chloroplasts. *Plant Mol. Biol.* 17, 1067–1076. doi: 10.1007/bf00037145

Wendel, A. A., Lewin, T. M., and Coleman, R. A. (2009). Glycerol-3-phosphate acyltransferases: rate limiting enzymes of triacylglycerol biosynthesis. *Biochim. Biophys. Acta* 1791, 501–506. doi: 10.1016/j.bbalip.2008.10.010

Wiklund, S. (2008). *Multivariate Data Analysis for Omics*. Umeå: Umetrics AB.

Wiklund, S., Karlsson, M., Antti, H., Johnels, D., Sjöström, M., Wingsle, G., et al. (2005). A new metabonomic strategy for analysing the growth process of the poplar tree. *Plant Biotechnol. J.* 3, 353–362. doi: 10.1111/j.1467-7652.2005.00129.x

Xu, C., Yu, B., Cornish, A. J., Froehlich, J. E., and Benning, C. (2006). Phosphatidylglycerol biosynthesis in chloroplasts of *Arabidopsis* mutants deficient in acyl-ACP glycerol-3-phosphate acyltransferase. *Plant J.* 47, 296–309. doi: 10.1111/j.1365-313X.2006.02790.x

Yan, X. J., Li, H. Y., Xu, J. L., and Zhou, C. X. (2010). Analysis of phospholipids in microalga *Nitzschia* closterium by UPLC-Q-TOF-MS. *Chin. J. Oceanol. Limnol.* 28, 106–112. doi: 10.1007/s00343-010-9263-3

Yang, W., Simpson, J. P., Li-Beisson, Y., Beisson, F., Pollard, M., and Ohlrogge, J. B. (2012). A land-plant-specific glycerol-3-phosphate acyltransferase family in *Arabidopsis*: substrate specificity, sn-2 preference, and evolution. *Plant Physiol.* 160, 638–652. doi: 10.1104/pp.112.201996

Zhang, C.-W., Cohen, Z., Khozin-Goldberg, I., and Richmond, A. (2002). Characterization of growth and arachidonic acid production of *Parietochloris*

incisa comb. nov (Trebouxiophyceae, Chlorophyta). *J. Appl. Phycol.* 14, 453–460. doi: 10.1023/A:1022375110556

Zheng, Z., Xia, Q., Dauk, M., Shen, W., Selvaraj, G., and Zou, J. (2003). *Arabidopsis* AtGPAT1, a member of the membrane-bound glycerol-3-phosphate acyltransferase gene family, is essential for tapetum differentiation and male fertility. *Plant Cell* 15, 1872–1887. doi: 10.1105/tpc.012427

Zheng, Z. F., and Zou, J. T. (2001). The initial step of the glycerolipid pathway: identification of glycerol 3-phosphate/dihydroxyacetone phosphate dual substrate acyltransferases in *Saccharomyces cerevisiae. J. Biol. Chem.* 276, 41710–41716. doi: 10.1074/jbc.m104749200

Identification of Characteristic Fatty Acids to Quantify Triacylglycerols in Microalgae

Pei-Li Shen[1,2†], Hai-Tao Wang[1,2†], Yan-Fei Pan[3], Ying-Ying Meng[4], Pei-Chun Wu[1] and Song Xue[1]*

[1] Marine Bioengineering Group, Department of Biotechnology, Dalian Institute of Chemical Physics, Chinese Academy of Sciences, Dalian, China, [2] University of Chinese Academy of Sciences, Beijing, China, [3] Department of Environmental Science and Engineering, College of Environment and Chemical Engineering, Dalian University, Dalian, China, [4] School of Life Science and Biotechnology, Dalian University of Technology, Dalian, China

The fatty acid profiles of lipids from microalgae are unique. Polyunsaturated fatty acids are generally enriched in polar lipids, whereas saturated and monounsaturated fatty acids constitute the majority of fatty acids in triacylglycerols (TAG). Each species has characteristic fatty acids, and their content is positively or negatively correlated with TAGs. The marine oleaginous diatom *Phaeodactylum tricornutum* was used as the paradigm to determine the quantitative relationship between TAG and characteristic fatty acid content. Fatty acid profiles and TAG content of *Phaeodactylum tricornutum* were determined in a time course. C16:0/C16:1 and eicosapentaenoic acid (EPA, C20:5n3) were identified as characteristic fatty acids in TAGs and polar lipids, respectively. The percentage of those characteristic fatty acids in total fatty acids had a significant linear relationship with TAG content, and thus, the correlation coefficient presenting r^2 were 0.96, 0.94, and 0.97, respectively. The fatty acid-based method for TAG quantification could also be applied to other microalgae such as *Nannochloropsis oceanica* in which the r^2 of C16:0 and EPA were 0.94 and 0.97, respectively, and in *Chlorella pyrenoidosa* r^2-values for C18:1 and C18:3 with TAG content were 0.91 and 0.99, repectively. This characteristic fatty acid-based method provided a distinct way to quantify TAGs in microalgae, by which TAGs could be measured precisely by immediate transesterification from wet biomass rather than using conventional methods. This procedure simplified the operation and required smaller samples than conventional methods.

Keywords: microalgae, triacylglycerols, neutral lipids, characteristic fattyacids, biofuels

INTRODUCTION

Microalgae are potential triacylglycerol (TAG) resource for biofuel production (Chisti, 2007; Williams and Laurens, 2010). Despite analyses indicating that biofuels may be able to substitute for petroleum-derived transport fuels in the future (Chisti, 2008; Sander and Murthy, 2010), biofuels from microalgae have not yet been commercialized due to high cost (Williams and Laurens, 2010). Increasing lipid production, especially TAGs, is critical to reduce the cost of microalgae-based biofuels. Therefore, a suitable method to quantify the lipid content in microalgae is necessary.

Oil content in microalgae is commonly assessed using a gravimetric method. Oil in microalgae is extracted with organic solvents, using the general rule of "like dissolves like" (Bligh and Dyer, 1959; Ryckebosch et al., 2012; Axelsson and Gentili, 2014). However, many cellular components, such as

pigments and unknown molecules, may be co-extracted with lipids due to their similar polarity, and these components may fluctuate during cultivation. Therefore, this method is unsuitable for assessing lipid production (Wang et al., 2009). Furthermore, this method requires a relatively large amount of sample, usually approximately 100 mg, and prevents conducting a time-course metabolic study of microalgae. Thin-layer chromatography (TLC) followed by capillary gas chromatography-flame ionization detection (GC-FID) is another method used to quantify lipids. This method separates lipids into individual classes by TLC after extraction from the cell using organic solvents. The lipids are then converted into fatty acid methyl esters (FAMEs) by GC-FID quantification. Due to the sensitivity of GC-FID, a few milligrams are sufficient for quantification. However, the method is time and labor intensive (Chen et al., 2009). High-performance liquid chromatography-mass spectrometry (HPLC-MS) has been used to detect lipids directly (MacDougall et al., 2011; Kind et al., 2012), but this approach is not routinely done due to the complex sample compositions. In addition, mutant screening is a powerful method to acquire an in-depth understanding of lipid metabolism (Doan and Obbard, 2012; Li et al., 2012; Manandhar-Shrestha and Hildebrand, 2013). Development of convenient and high-throughput methods to quantify lipids in microalgae has garnered increasing attention due to the labor-intensive nature of mutant screening (Terashima et al., 2015).

Lipids can be categorized into neutral and polar lipids, and neutral lipids are primarily referred to as TAGs. The fatty acid profiles in both microalgae and plants are unique to specific lipid classes. Neutral lipids mainly contain saturated (SFAs) and monounsaturated fatty acids (MUFAs), such as C16:0, C16:1, and C18:1, and more than 50% of C18:1 and C16:0 fatty acids that accumulate in the model algae *Chlamydomonas reinhardtii* are in the TAGs (Siaut et al., 2011). Contrarily, the neutral lipids in *Chlamydomonas reinhardtii*, polyunsaturated fatty acids (PUFAs), are enriched in polar lipids, such as C16:4, C18:3, and eicosapentaenoic acid (EPA, C20:5n3). C16:4 and C18:3 comprise the bulk of fatty acids in monogalactosyldiacylglycerols (MGDG), which account for more than 80% C16:4 and C18:3 of the total fatty acid content of *Chlamydomonas reinhardtii* (Zäuner et al., 2012). In the model plant *Arabidopsis thaliana*, C16:3 and C18:3 comprise the majority of MGDG and the main fatty acids in TAGs are C16:0, C18:0, and C18:1 (Fan et al., 2013). The total fatty acid profiles depend on the distinct fatty acid composition of the lipids. A strong correlation ($r^2 = 0.986$) has been reported between the 16:0/16:4 ratio in FAMEs derived directly from algal cells and the TAG/total acyl group ratio in *Chlamydomonas reinhardtii* (Liu et al., 2013). More recently, we have reported that the neutral lipid content in *Isochrysis zhangjiangensis* can be quantified based on the C18:1 or C18:4 content (Wang et al., 2014). Therefore, we propose that TAG content can be quantified using specific fatty acids.

Here, the marine microalgae *Phaeodactylum tricornutum*, which was an ideal candidate for producing biodiesel, was studied as an example to support this hypothesis. First, the principles of characteristic fatty acid identification were discussed based on an analysis of the fatty acid profile of

individual lipid in *Phaeodactylum tricornutum*. Subsequently, the relationship between the characteristic fatty acids and the TAG content was analyzed. This procedure was also applied to different microalgal species, such as *Nannochloropsis oceanica* and *Chlorella pyrenoidosa*, to expand its application.

MATERIALS AND METHODS

Strains and Culture Conditions

The marine microalgae *Phaeodactylum tricornutum* was provided by Dr. Weidong Liu of the Liaoning Institute of Marine Fisheries. The marine microalgae *Nannochloropsis oceanica* IMET1 was provided by Dr. Jian Xu of the Qingdao Institute of Bioenergy and Bioprocess Technology, Chinese Academy of Sciences. *Chlorella pyrenoidosa* was obtained from the Freshwater Algae Culture Collection of the Institute of Hydrobiology, Chinese Academy of Sciences.

To identify the characteristic fatty acids, enriched f/2 medium, which contained three-fold the concentration of all ingredients, was inoculated with *Phaeodactylum tricornutum* as described by Feng et al. (2011). The medium was supplemented with sodium nitrate (N+), and the algae were stressed by omitting sodium nitrate (N−).

To correlate the characteristic fatty acids with neutral lipids, *Phaeodactylum tricornutum* and *Nannochloropsis oceanica* IMET1 were cultured under N− (Meng et al., 2015). *Chlorella pyrenoidosa* was cultured in BG11 medium without sodium nitrate to generate the N− condition.

Total fatty acid profiles and TAG content of three species were determined in a time course. The sampling time of the three species were 0, 6, and 18 h of *Phaeodactylum tricornutum*; 0, 2, 4, 7, 9, 12, and 14 h of *Nannochloropsis oceanica* IMET1; and 0, 1, 5, 6, and 8 days of *Chlorella pyrenoidosa*, respectively. Three replicates were taken for each time point. Each data point was a biological replicate ($n = 3$).

An average irradiance of 70 µmol photons m^{-2} s^{-1} was provided by continuous illumination with cool white fluorescent lamps. Temperature was maintained at 25 ± 2°C.

Lipids Extraction and Fatty Acids Analysis

Cells were collected by centrifugation, and lipids were extracted according to the method described by Wang and Benning (2011) with slight modifications. A 300-µL aliquot of extraction solvent composed of methanol, chloroform, and formic acid (20:10:1, v/v/v) was added to approximately 5 mg biomass (dry weight). After shaking vigorously for 5 min, 150 µL of 0.2 M phosphoric acid and 1 M potassium chloride were added and vortexed for 1 min. Phase separation was achieved after centrifugation at 12,000 × g at room temperature for 5 min; the lipids dissolved in the lower chloroform phase were spotted onto TLC silica plates. Glycolipids (GL) and phospholipids (PL) were separated using a solvent system of acetone:toluene:water int the ration 91:30:7.5 mL, respectively. TAGs were separated with hexane:diethyl ether:acetic acid in the ratio 85:15:1, v/v/v, respectively.

The lipids separated by TLC or a microalgal biomass was added to methanol (2% H$_2$SO$_4$) and incubated for 1 h at 70°C

to prepare the FAMEs. After methylation, deionized water and hexane were added to extract the FAMEs. C17:0-TAG was added as an internal standard for quantification. The FAMEs were identified qualitatively by mass spectroscopy and quantitatively by gas chromatography with a FID. The FAMEs of samples were detected on a 7890B gas chromatograph with a DB-23 capillary column (30 m × 0.32 mm × 0.25 μm; Agilent Technologies, Santa Clara, CA, USA) and a FID. The injector temperature was 260°C with a split ratio of 50:1. The initial column temperature was 130°C and was maintained for 1 min. The temperature was then increased to 170°C at a rate of 10°C min^{-1}, followed by an increase to 215°C at a rate of 2.8°C min^{-1}. The temperature was then maintained at 215°C for 1 min.

Statistical Data Analysis

Correlation coefficients between characteristic fatty acids and TAG content were calculated using Origin Pro software, version 8.0 (Origin Lab, Hampton, Massachusetts, USA). Statistical significance in each result was calculated using the Two-tailed by SPSS 18.0 for windows (IBM, Armonk, New York City, USA), where the significance $P < 0.01$.

RESULTS

Identification of Characteristic Fatty Acids in *Phaeodactylum tricornutum*

Characteristic fatty acids were present in different classes of lipids, and it was necessary to identify the characteristic fatty acids to accurately quantify TAGs. The fatty acid profiles of different lipid classes and TAG content were determined under both N+ and N− to identify the characteristic fatty acids. The total lipids (TLs) extracted from *Phaeodactylum tricornutum* cells were separated into GLs, PLs, and TAGs by TLC. All lipids except

for TAGs were polar lipids. The fatty acid profile of individual lipid and TLs that were extracted from cells cultured under N+ and N− were analyzed (**Table 1**). PUFAs were the main fatty acids in GLs and PLs both under N+ and N−. EPA was the most abundant fatty acid in GLs and PLs and accounted for approximately 25% of the total fatty acids from these lipids. Therefore, EPA was the characteristic fatty acid of the polar lipids. TAGs were enriched with SFAs and MUFAs rather than PUFAs, such as C16:0, which was identified as a characteristic fatty acid. C16:1 almost evenly distributed across the aforementioned lipid classes and constituted 32–36% of the fatty acids in all lipid classes under N+. TAGs were specifically enriched with C16:1 under the N−, which was the most abundant fatty acid, accounting for almost 50% of fatty acid content. Although C16:1 content in PLs decreased dramatically, it remained largely unchanged in GLs and accounted for about 30% of its total fatty acids. Therefore, C16:1 was not specific to TAGs and could not serve as a characteristic fatty acid of TAGs.

The fatty acid distributions were determined in different lipid classes to evaluate the contributions of each FAME to the total fatty acid profiles (**Table 2**). EPA was present in polar lipids under the N+, and more than 70% of the EPA was detected in polar lipids under the N−, despite the decreased amount of EPA compared with that detected under the N+. Only about 20% of the C16:0 was detected in TAGs under the N+, but this proportion increased to 80% under the N−. Because most of the EPA was found in polar lipids, the variation in polar lipids could be represented by the proportion of characteristic fatty acids of total fatty acids. Given the inverse relationship between polar lipids and TAGs, EPA was negatively correlated with TAG content. Similar to the characteristic fatty acids of polar lipids, the proportion of TAG-characteristic fatty acids also represented changes in TAG content.

TABLE 1 | Fatty acid profiles of different lipid components (means ± *SD*, *n* = 3) in *Phaeodactylum tricornutum* under nitrogen replete (N+) and nitrogen deplete (N−) were obtained by capillary FID-GC.

Lipids	TL		GL		PL		TAG	
Medium	N+	N−	N+	N−	N+	N−	N+	N−
C14:0	3.0 ± 0.3	4.2 ± 0.1	3.1 ± 0.7	5.4 ± 0.6	2.9 ± 0.5	3.2 ± 0.3	2.8 ± 0.2	4.1 ± 0.0
C16:0	11.3 ± 0.4	27.5 ± 0.6	9.0 ± 0.2	17.8 ± 0.3	11.9 ± 1.0	15.7 ± 0.3	23.3 ± 1.9	32.4 ± 0.1
C16:1n7	35.5 ± 1.3	41.9 ± 1.0	35.0 ± 1.3	32.5 ± 0.3	37.1 ± 1.1	16.9 ± 0.7	33.8 ± 2.6	48.9 ± 0.3
C16:2n4	5.8 ± 0.1	1.9 ± 0.1	7.2 ± 0.2	4.2 ± 0.0	0.8 ± 0.1	0.2 ± 0.1	12.3 ± 0.6	1.5 ± 0.1
C16:3n4	8.4 ± 0.2	2.7 ± 0.1	13.6 ± 0.3	10.6 ± 0.5	0.7 ± 0.2	0.4 ± 0.1	0.3 ± 0.4	0.6 ± 0.0
C18:0	2.5 ± 0.5	1.6 ± 0.4	0.8 ± 0.3	1.7 ± 0.8	1.3 ± 0.6	2.1 ± 0.5	15.4 ± 2.5	1.5 ± 0.2
C18:1n9	2.1 ± 0.2	4.5 ± 0.1	0.5 ± 0.1	1.0 ± 0.2	5.6 ± 0.7	17.0 ± 0.8	1.7 ± 0.4	3.5 ± 0.1
C18:1n7	0.9 ± 0.3	1.1 ± 0.0	0.5 ± 0.1	0.8 ± 0.1	2.0 ± 0.5	1.8 ± 0.1	0.5 ± 0.0	1.1 ± 0.0
C18:2n6	1.6 ± 0.0	0.7 ± 0.3	0.5 ± 0.0	0.3 ± 0.2	3.8 ± 0.1	2.9 ± 0.2	1.0 ± 0.1	0.4 ± 0.3
C18:3n6	0.3 ± 0.0	0.4 ± 0.0	0.3 ± 0.0	0.0 ± 0.1	0.5 ± 0.0	1.0 ± 0.1	0 ± 0	0.4 ± 0.0
C18:3n3	0.3 ± 0.0	0.0 ± 0	0.2 ± 0.0	0 ± 0	0.7 ± 0.1	0 ± 0	0.1 ± 0.2	0.1 ± 0
C18:4n3	0.4 ± 0.1	0.2 ± 0.0	0.4 ± 0.0	0.4 ± 0.0	0.4 ± 0.1	0.1 ± 0.1	0.2 ± 0.2	0.2 ± 0.0
C18:5n3	1.2 ± 0.2	0.7 ± 0.2	1.1 ± 0.2	1.9 ± 0.7	0.9 ± 0.2	1.1 ± 0.4	2.6 ± 0.2	0.3 ± 0.1
C20:5n3	24.3 ± 0.6	11.8 ± 0.8	26.9 ± 1.2	23.4 ± 0.4	25.5 ± 0.9	33.1 ± 0.3	5.2 ± 2.2	4.7 ± 0.1
C22:6	2.4 ± 0.4	0.8 ± 0.1	0.9 ± 0.2	0.1 ± 0.1	5.9 ± 0.8	4.7 ± 0.1	0.8 ± 0.6	0.4 ± 0.0

TL, total lipid; GL, glycolipid; PL, phospholipid; TAG, triacylglycerol.

TABLE 2 | Fatty acids distribution in different lipid classes (means ± SD, $n = 3$) in *Phaeodactylum tricornutum* under nitrogen replete (N+) and nitrogen deplete (N−).

Lipids	GL		PL		TAG	
Medium	N+	N−	N+	N−	N+	N−
C14:0	61.0 ± 9.9	26.9 ± 2.6	29.8 ± 8.5	8.4 ± 2.0	9.1 ± 1.4	64.8 ± 3.2
C16:0	48.1 ± 2.7	13.9 ± 1.4	31.5 ± 3.4	6.2 ± 1.0	20.3 ± 1.6	79.9 ± 2.4
C16:1n7	59.3 ± 2.4	16.6 ± 1.7	31.2 ± 1.8	4.4 ± 0.9	9.4 ± 0.6	79.0 ± 2.5
C16:2n4	74.7 ± 1.5	46.9 ± 1.7	4.3 ± 0.3	1.2 ± 0.9	21 ± 1.2	51.9 ± 2.6
C16:3n4	97.1 ± 0.6	84.1 ± 0.7	2.6 ± 0.8	1.7 ± 0.4	0.3 ± 0.4	14.2 ± 1.1
C18:0	21.2 ± 7.7	21.5 ± 6.3	14.7 ± 6.7	13.7 ± 1.7	64.1 ± 12.8	64.8 ± 7.9
C18:1n9	13.4 ± 1.0	4.9 ± 0.8	78.7 ± 0.8	41.2 ± 3.7	8.0 ± 0.9	53.9 ± 4.0
C18:1n7	31.6 ± 2.0	15.4 ± 2.7	62.7 ± 2.5	17.8 ± 2.8	5.7 ± 0.5	66.8 ± 5.4
C18:2n6	20 ± 1.9	7.5 ± 5.3	73.4 ± 1.1	57.4 ± 23.0	6.6 ± 0.7	35.2 ± 17.7
C18:3n6	53.2 ± 0.9	1.8 ± 2.6	46.8 ± 0.9	27.3 ± 3.7	0 ± 0	70.9 ± 3.6
C18:3n3	34.0 ± 2.25	0 ± 0	63.1 ± 3.2	0 ± 0	2.8 ± 4.0	100.0 ± 0
C18:4n3	63.8 ± 7.0	36.2 ± 0.2	32.5 ± 2.4	4.6 ± 6.5	3.6 ± 5.2	59.2 ± 6.3
C18:5n3	55.2 ± 1.2	54.5 ± 1.9	22.7 ± 2.4	18.0 ± 7.9	22.2 ± 3.4	27.5 ± 6.7
C20:5n3	66.5 ± 1.2	42.3 ± 0.3	31.3 ± 0.3	30.4 ± 2.6	2.2 ± 1.2	27.3 ± 2.9
C22:6	22.3 ± 2.4	2.7 ± 3.8	74.3 ± 0.2	64.0 ± 5.0	3.3 ± 2.4	33.3 ± 4.2

TL, total lipid; GL, glycolipid; PL, phospholipid; TAG, triacylglycerol.

Correlations between Tag Content and Characteristic Fatty Acids in *Phaeodactylum tricornutum*

Characteristic fatty acids had positive or negative correlations with TAGs in microalgae. The fatty acid profiles of TLs and TAG content were determined over time after nitrogen depletion in *Phaeodactylum tricornutum* to quantify the relationship between the characteristic fatty acids and TAG content. A correlation analysis revealed that fatty acid levels were highly and significantly correlated with TAG content (**Figure 1**). Specifically, the correlation coefficients of C16:0, C16:1, and EPA with the TAG content were 0.96, 0.94, and 0.97, respectively. The linear relationship between the characteristic fatty acids and the TAG content revealed that characteristic fatty acids could be used to quantify TAG content.

DISCUSSION
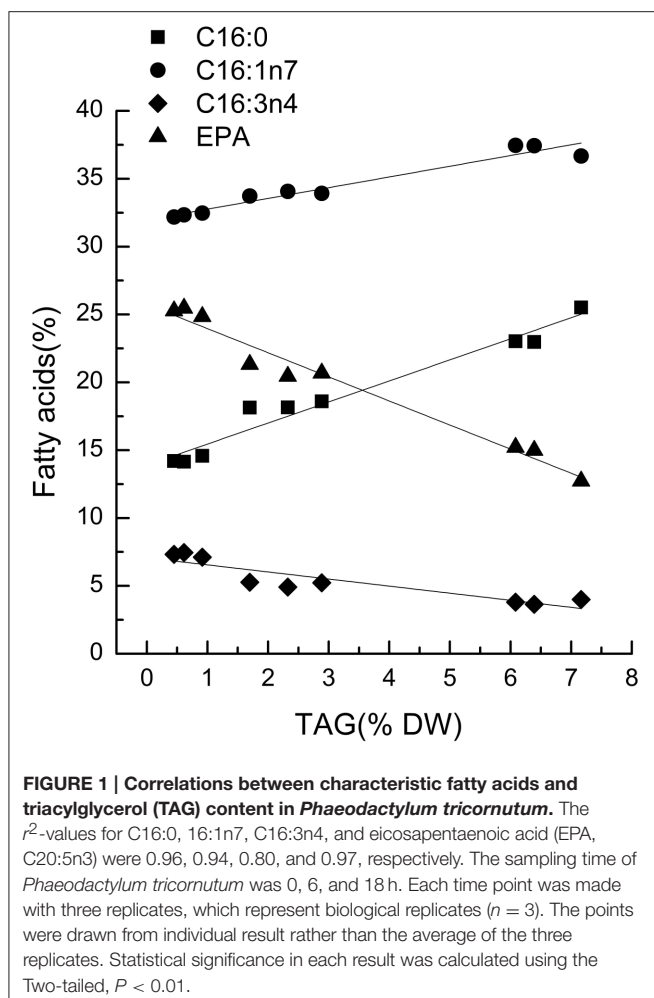
Principles to Identify Characteristic Fatty Acids

As some fatty acids were correlated with TAGs in microalgae, identifying the characteristic fatty acids was the first step to quantify TAG content. In order to quantify the characteristic fatty acid accurately, there was a threshold in the amount of characteristic fatty acids. Therefore, the proportion of fatty acids of TLs was a key rule for identifying characteristic fatty acids. Almost all C16:3 were found in GLs under the N− and N+ (**Table 2**). However, low total fatty acid content (**Table 1**) made it unsuitable to quantify TAGs. The correlation coefficient between the C16:3 content in total fatty acids and TAG content was only 0.798. We set 10% as the minimum content criterion for identifying characteristic fatty acids, therey considering a 10% variation in the percentage of each fatty acid determined by immediate transesterification of wet biomass (Liu et al., 2015), and C16:3 accounted for less than10% of total fatty acids in *Phaeodactylum tricornutum*. A significant change of cellular TAG

accumulation was another key point when to determine the characteristic fatty acids, and the minimum fold-change was set to 1.5. Although C16:1 was increased in the TAGs under the N−, the ~1.2-fold change in C16:1 of the total fatty acids was insufficient for quantification. Taken together, 10% total fatty acid content and a 1.5-fold change were the thresholds for defining the characteristic fatty acids.

Expanding the Characteristic Fatty Acid-based Method to Other Microalgae

Chlorella pyrenoidosa (Chlorophyta) and *Nannochloropsis oceanica* (Eustigmatophyceae) were chosen as examples to expand the characteristic fatty acid-based method to other taxa. The fatty acid profiles of total lipids and TAG content were determined in a time course after nitrogen depletion in *Nannochloropsis oceanica* (**Table 3**) and *Chlorella pyrenoidosa* (**Table 4**), as described for *Phaeodactylum tricornutum*. The principles discussed above were used to identify the characteristic fatty acids in the two species. C16:0 and EPA were determined to be characteristic fatty acids in *Nannochloropsis oceanica*. The linear relationship between the characteristic fatty acids and TAG content was shown in **Figure 2**. The correlation coefficients of C16:0 and EPA with TAG content were 0.94 and 0.97 in *Nannochloropsis oceanica*, respectively. Similar to *Nannochloropsis oceanica*, C18:1 and C18:3 were determined to be characteristic fatty acids in *Chlorella pyrenoidosa*. The correlation coefficients of C18:1 and C18:3 with TAG content were 0.91 and 0.99 in *Chlorella pyrenoidosa*, respectively (**Figure 3**). The high correlation coefficients between the characteristic fatty acids and TAG content demonstrated that the characteristic fatty acid-based method could accurately measure TAG content. In addition, two types of characteristic fatty acids, such as EPA and C18:1, were detected that were negatively or positively correlated with TAGs, respectively, because they were from GLs or TAGs, which were different sources.

FIGURE 1 | Correlations between characteristic fatty acids and triacylglycerol (TAG) content in *Phaeodactylum tricornutum*. The r^2-values for C16:0, 16:1n7, C16:3n4, and eicosapentaenoic acid (EPA, C20:5n3) were 0.96, 0.94, 0.80, and 0.97, respectively. The sampling time of *Phaeodactylum tricornutum* was 0, 6, and 18 h. Each time point was made with three replicates, which represent biological replicates ($n = 3$). The points were drawn from individual result rather than the average of the three replicates. Statistical significance in each result was calculated using the Two-tailed, $P < 0.01$.

TABLE 3 | Fatty acid profiles of total lipids (means ± SD, $n = 3$) in *Nannochloropsis oceanica* under nitrogen replete (N+) and nitrogen deplete (N−) were obtained by capillary FID-GC.

Lipids	TL	
Medium	N+	N−
C14:0	5.5 ± 0.1	5.3 ± 0.0
C16:0	21.6 ± 0.0	44.0 ± 0.3
C16:1n9	5.5 ± 0.4	2.1 ± 0.2
C16:1n7	24.0 ± 0.0	24.2 ± 0.4
C16:2n4	0.5 ± 0.0	0.3 ± 0.0
C18:0	0.4 ± 0.0	1.5 ± 0.1
C18:1n9	1.8 ± 0.0	2.9 ± 0.1
C18:1n7	0.2 ± 0.0	0.4 ± 0.0
C18:2n6	2.0 ± 0.2	1.7 ± 0.0
C18:3n6	0.3 ± 0.0	0.4 ± 0.0
C18:3n3	0.6 ± 0.1	0.0
C20:4n6	4.0 ± 0.1	3.0 ± 0.0
C20:5n3	30.5 ± 0.3	14.2 ± 0.2

TL, total lipid.

TABLE 4 | Fatty acid profiles of total lipids (means ± SD, $n = 3$) in *Chlorella pyrenoidosa* under nitrogen replete (N+) and nitrogen deplete (N−) were obtained by capillary FID-GC.

Lipids	TL	
Medium	N+	N−
C16:0	20.4 ± 0.0	25.6 ± 0.0
C16:1n7	1.1 ± 0	0.6 ± 0
C16:3	14.2 ± 0.0	7.6 ± 0.0
C18:0	3.2 ± 0	9.0 ± 0.0
C18:1n9	5.6 ± 0.0	21.5 ± 0.1
C18:1n7	0.1 ± 0	1.0 ± 0
C18:2n6	36.7 ± 0.0	25.5 ± 0.1
C18:3n3	18.6 ± 0.0	9.1 ± 0.0

TL, total lipid.

This idea was further supported by the statistical analysis of the microalgal fatty acid profiles under favorable and stressed conditions across eight phyla. The candidate characteristic fatty acids were shown in bold (Supplementary Material). Due to the diversity of microalgae, both fatty acid profiles and their response to the N− were species dependent. All species accumulated SFAs or MUFAs as TAG content increased in the same manner as in *Phaeodactylum tricornutum*, except in *Porphyridium cruentum* and *Spirulina platensis*, which accumulated C18:2n6. The level of PUFAs decreased in all microalgae following the accumulation of neutral lipids, such as C18:3n3 in *Chlamydomonas* sp. JSC4, C18:4n3 in *Rhodomonas* sp., and C18:5n3 in *Gymnodinium* sp.

The accumulation of SFAs or MUFAs coupled with the decrease in the level of PUFAs was also observed under high-light or salinity stress. *Chlorella zofingiensis* accumulated a large amount of C18:1 when exposed to high-light conditions, whereas the level of the PUFA C16:3 decreased by approximately 50% (Liu et al., 2012). The level of C18:1 increased from 17.8 to 39.4% in *Sphenolithus obtusus* XJ-15 under salinity stress (Xia et al., 2013). These results revealed that a linear relationship between specific fatty acids and TAG content may also be applicable to microalgae under stress conditions.

There were some microalgae of which PUFAs such as arachidonic acid (AA, C20:4n6), EPA, and docosahexaenoic

(DHA, C22:6n3) were accumulated in TAGs under stress condition. For example, the unicellular green alga *Parietochloris incise* (Trebuxiophyceae, Chlorophyta) accumulated TAGs with over 90% of total AA under nitrogen deprivation (Cohen et al., 2000; Khozin-Goldberg et al., 2002; Merzlyak et al., 2007). In the marine Haptophyte *Pavlova lutheri*, 55 and 67% of the overall cellular EPA and DHA content were attributed to the cellular TAG accumulation triggered by bicarbonate addition under nitrogen starvation (Guiheneuf and Stengel, 2013). In the red microalgae *Porphyridium cruentum* (Cohen et al., 1988) and Gracilaria (Gracilariales, Rhodophyta) (Araki et al., 1990), TAGs were predominantly constructed of AA and EPA. In this case, TAG content still could be quantified with the corresponding PUFAs, firstly to determine the quantitative correlation between them.

Advantage of the Characteristic Fatty Acid-based Method

The approach we have proposed differed from conventional approaches. All lipid quantification data presented previously relied on "like dissolves like" with many uncertain compounds, whereas quantification of TAGs in the proposed method relied
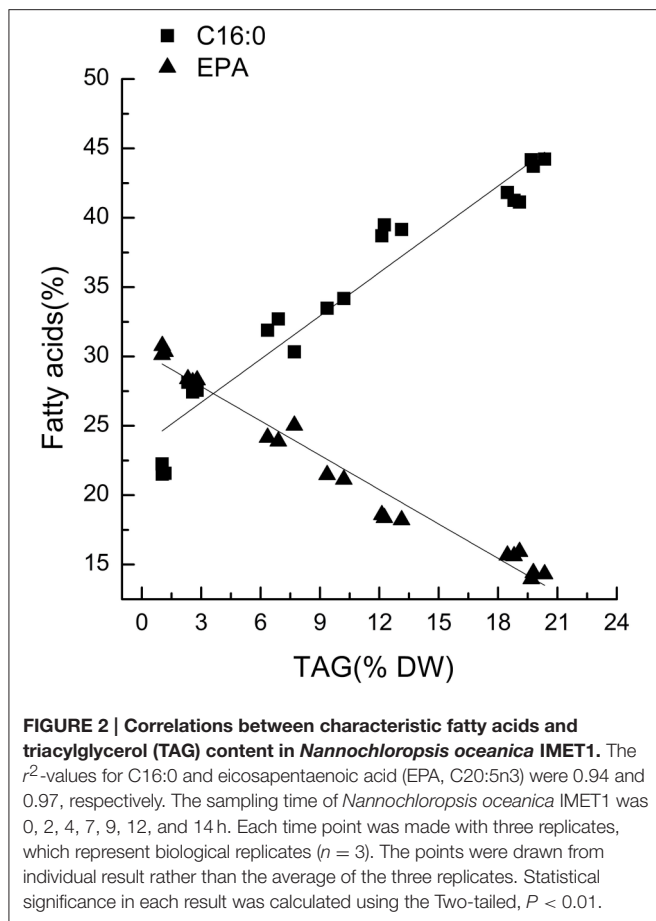
FIGURE 2 | Correlations between characteristic fatty acids and triacylglycerol (TAG) content in *Nannochloropsis oceanica* IMET1. The r^2-values for C16:0 and eicosapentaenoic acid (EPA, C20:5n3) were 0.94 and 0.97, respectively. The sampling time of *Nannochloropsis oceanica* IMET1 was 0, 2, 4, 7, 9, 12, and 14 h. Each time point was made with three replicates, which represent biological replicates ($n = 3$). The points were drawn from individual result rather than the average of the three replicates. Statistical significance in each result was calculated using the Two-tailed, $P < 0.01$.
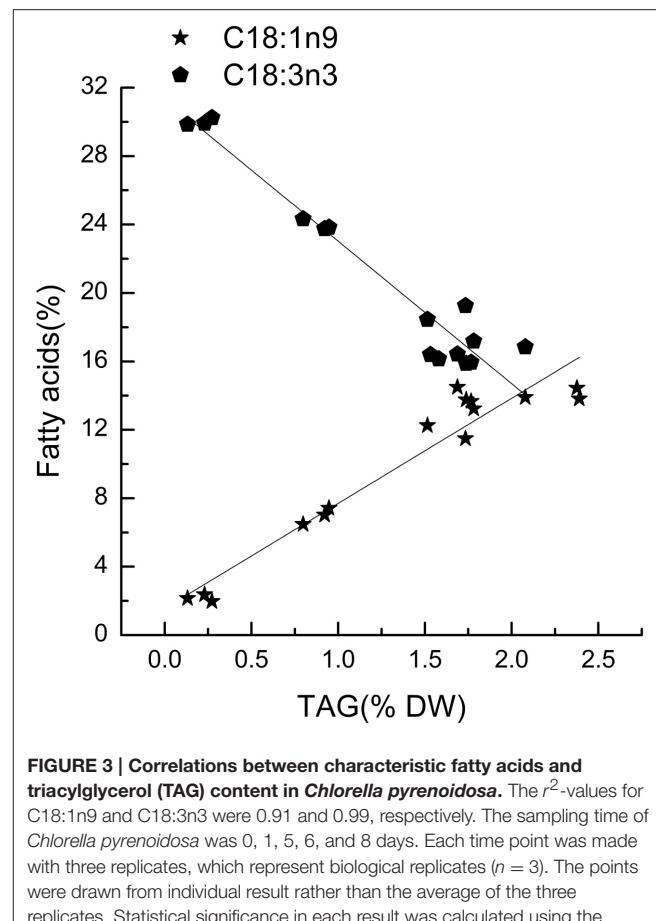
FIGURE 3 | Correlations between characteristic fatty acids and triacylglycerol (TAG) content in *Chlorella pyrenoidosa*. The r^2-values for C18:1n9 and C18:3n3 were 0.91 and 0.99, respectively. The sampling time of *Chlorella pyrenoidosa* was 0, 1, 5, 6, and 8 days. Each time point was made with three replicates, which represent biological replicates ($n = 3$). The points were drawn from individual result rather than the average of the three replicates. Statistical significance in each result was calculated using the Two-tailed, $P < 0.01$.

on the characteristic fatty acids, which was much easier to quantify than the entire TAG class because only one compound needs to be determined. Furthermore, the characteristic fatty acid content in total fatty acids could be determined by immediate transesterification from wet biomass. Therefore, drying the biomass and extracting the lipids could be omitted. Hence, this approach simplified sample preparation and lipid determination procedure. Furthermore, less than 5 mg of biomass is necessary due to the high sensitivity of the capillary GC-FID analysis, which is 20-times less than the amount required for conventional gravimetric determination methods. Therefore, this procedure could be used to monitor variations in lipids throughout a culture. Our procedure saved time and labor when quantifying TAGs.

In conclusion, our procedure used characteristic fatty acids to obtain lipid content and provided a unique way to quantify TAGs. The significant feature of this procedure was indirect quantification of lipids by direct detection of the individual characteristic fatty acid. Total fatty acid content of 10% and a 1.5-fold change during TAG accumulation were set as criteria to define the characteristic fatty acids. A significant linear relationship was observed between the characteristic fatty acids and TAG content. This characteristic fatty acid-based method provided a new method to quantify TAG content in different microalgal species.

AUTHOR CONTRIBUTIONS

PS and HW designed the experiments. PS, HW, and YP performed the experiments and interpreted the data. PS and HW wrote the draft manuscript. YM established analysis methods. PW provided the subculture of the strains. SX made the critical revision of the manuscript. All the authors discussed the results and commented on the manuscript.

FUNDING

SUPPLEMENTARY MATERIAL

The Supplementary Material for this article can be found online at: http://journal.frontiersin.org/article/10.3389/fpls.2016. 00162

REFERENCES

Araki, S., Sakurai, T., Oohusa, T., Kayama, M., and Nisizawa, K. (1990). Content of arachidonic and eicosapentaenoic acids in polarlipids from *Gracilaria* (Gracilariales, Rhodophyta). *Hydrobiologia* 204, 513–519. doi: 10.1007/BF00040279

Axelsson, M., and Gentili, F. (2014). A single-step method for rapid extraction of total lipids from Green Microalgae. *PLoS ONE* 9:e89643. doi: 10.1371/journal.pone.0089643

Bligh, E., and Dyer, W. (1959). A rapid method of total lipid extraction and purification. *Can. J. Biochem. Physiol.* 37, 911–917. doi: 10.1139/o59-099

Chen, W., Zhang, C., Song, L., Sommerfeld, M., and Hu, Q. (2009). A high throughput Nile red method for quantitative measurement of neutral lipids in microalgae. *J. Microbiol. Methods* 77, 41–47. doi: 10.1016/j.mimet.2009.01.001

Chisti, Y. (2007). Biodiesel from microalgae. *Biotechnol. Adv.* 25, 294–306. doi: 10.1016/j.biotechadv.2007.02.001

Chisti, Y. (2008). Biodiesel from microalgae beats bioethanol. *Trends Biotechnol.* 26, 126–131. doi: 10.1016/j.tibtech.2007.12.002

Cohen, Z., Khozin-Goldberg, I., Adlerstein, D., and Bigogno, C. (2000). The role of triacylglycerol as a reservoir of polyunsaturated fatty acids for the rapid production of chloroplastic lipids in certain microalgae. *Biochem. Soc. Trans.* 28, 740–743. doi: 10.1042/bst0280740

Cohen, Z., Vonshak, A., and Richmond, A. (1988). Effect of enviromental conditions on fatty acid composition of the red alga *porphyridiumcruentum* correlation to growth rate. *J. Phycol.* 24, 328–332.

Doan, T. T. Y., and Obbard, J. P. (2012). Enhanced intracellular lipid in Nannochloropsis sp. via random mutriglycerideenesis and flow cytometric cell sorting. *Algal Res.* 1, 17–21. doi: 10.1016/j.algal.2012.03.001

Fan, J., Yan, C., Zhang, X., and Xu, C. (2013). Dual role for phospholipid:diacylglycerol acyltransferase: enhancing fatty acid synthesis and diverting fatty acids from membrane lipids to triacylglycerol in *Arabidopsis* leaves. *Plant Cell* 25, 3506–3518. doi: 10.1105/tpc.113.117358

Feng, D., Chen, Z., Xue, S., and Zhang, W. (2011). Increased lipid production of the marine oleaginous microalgae *Isochrysis zhangjiangensis* (Chrysophyta) by nitrogen supplement. *Bioresour. Technol.* 102, 6710–6716. doi: 10.1016/j.biortech.2011.04.006

Guiheneuf, F., and Stengel, D. B. (2013). LC-PUFA-enriched oil production by microalgae: accumulation of lipid and triacylglycerols containing n-3 LC-PUFA is triggered by nitrogen limitation and inorganic carbon availability in the marine haptophyte *Pavlova lutheri*. *Mar. Drugs* 11, 4246–4266. doi: 10.3390/md11114246

Khozin-Goldberg, I., Bigogno, C., Shrestha, P., and Cohen, Z. (2002). Nitrogen starvation induces the accumulation of arachidonic acid in the freshwater green alga *Parietochloris incisa* (Trebuxiophyceae). *J. Phycol.* 38, 991–994. doi: 10.1046/j.1529-8817.2002.01160.x

Kind, T., Meissen, J. K., Yang, D., Nocito, F., Vaniya, A., Cheng, Y.-S., et al. (2012). Qualitative analysis of algal secretions with multiple mass spectrometric platforms. *J. Chromatogr. A* 1244, 139–147. doi: 10.1016/j.chroma.2012.04.074

Li, X., Moellering, E. R., Liu, B., Johnny, C., Fedewa, M., Sears, B. B., et al. (2012). A galactoglycerolipid lipase is required for triacylglycerol accumulation and survival following nitrogen deprivation in *Chlamydomonas reinhardtii*. *Plant Cell* 25, 3506–3518. doi: 10.1105/tpc.112.105106

Liu, B., Vieler, A., Li, C., Jones, A. D., and Benning, C. (2013). Triacylglycerol profiling of microalgae *Chlamydomonas reinhardtii* and *Nannochloropsis oceanica*. *Bioresour. Technol.* 146, 310–316. doi: 10.1016/j.biortech.2013.07.088

Liu, J., Liu, Y., Wang, H., and Xue, S. (2015). Direct transesterification of fresh microalgal cells. *Bioresour. Technol.* 176, 284–287. doi: 10.1016/j.biortech.2014.10.094

Liu, J., Sun, Z., Zhong, Y., Huang, J., Hu, Q., and Chen, F. (2012). Stearoyl-acyl carrier protein desaturase gene from the oleaginous microalga *Chlorella zofingiensis*: cloning, characterization and transcriptional analysis. *Planta* 236, 1665–1676. doi: 10.1007/s00425-012-1718-7

MacDougall, K., McNichol, J., McGinn, P., O'leary, S. B., and Melanson, J. (2011). Triacylglycerol profiling of microalgae strains for biofuel feedstock by liquid chromatography–high-resolution mass spectrometry. *Anal. Bioanal. Chem.* 401, 2609–2616. doi: 10.1007/s00216-011-5376-6

Manandhar-Shrestha, K., and Hildebrand, M. (2013). Development of flow cytometric procedures for the efficient isolation of improved lipid accumulation mutants in a *Chlorella* sp. microalga. *J. Appl. Phycol.* 25, 1643–1651. doi: 10.1007/s10811-013-0021-8

Meng, Y., Jiang, J., Wang, H., Cao, X., Xue, S., Yang, Q., et al. (2015). The characteristics of triglycerides and EPA accumulation in *Nannochloropsis oceanica IMET1* under different nitrogen supply regimes. *Bioresour. Technol.* 179, 483–489. doi: 10.1016/j.biortech.2014.12.012

Merzlyak, M. N., Chivkunova, O. B., Gorelova, O. A., Reshetnikova, I. V., Solovchenko, A. E., Khozin-Goldberg, I., et al. (2007). Effect of nitrogen starvation on optical properties, pigments, and arachidonic acid content of the unicellular green alga *Parietochloris incisa* (Trebouxiophyceae, Chlorophyta). *J. Phycol.* 43, 833–843. doi: 10.1111/j.1529-8817.2007.00375.x

Ryckebosch, E., Muylaert, K., and Foubert, I. (2012). Optimization of an analytical procedure for extraction of lipids from microalgae. *J. Am. Oil Chem. Soc.* 89, 189–198. doi: 10.1007/s11746-011-1903-z

Sander, K., and Murthy, G. S. (2010). Life cycle analysis of algae biodiesel. *Int. J. Life Cycle Assess.* 15, 704–714. doi: 10.1007/s11367-010-0194-1

Siaut, M., Cuine, S., Cagnon, C., Fessler, B., Nguyen, M., and Carrier, P. (2011). Oil accumulation in the model green alga *Chlamydomonas reinhardtii*: characterization, variability between common laboratory strains and relationship with starch reserves. *BMC Biotechnol.* 11:7. doi: 10.1186/1472-6750-11-7

Terashima, M., Freeman, E. S., Jinkerson, R. E., and Jonikas, M. C. (2015). A fluorescence-activated cell sorting-based strategy for rapid isolation of high-lipid *Chlamydomonas* mutants. *Plant J.* 81, 147–159. doi: 10.1111/tpj.12682

Wang, H.-T., Yao, C.-H., Liu, Y.-N., Meng, Y.-Y., Wang, W.-L., Cao, X.-P., et al. (2014). Identification of fatty acid biomarkers for quantification of neutral lipids in marine microalgae *Isochrysis zhangjiangensis*. *J. Appl. Phycol.* 27, 1–7. doi: 10.1007/s10811-014-0300-z

Wang, Z. H., and Benning, C. (2011). *Arabidopsis thaliana*polar glycerolipid profiling by thin layer chromatography (TLC) coupled with gas-liquid chromatography (GLC). *J. Vis. Exp.* 49, 1–6. doi: 10.1167/11.6.1

Wang, Z., Ullrich, N., Joo, S., Waffenschmidt, S., and Goodenough, U. (2009). Algal lipid bodies: stress induction, purification, and biochemical characterization in wild-type and starchless *Chlamydomonas reinhardtii*. *Eukaryot. Cell* 8, 1856–1868. doi: 10.1128/EC.00272-09

Williams, P. J. L. B., and Laurens, L. M. L. (2010). Microalgae as biodiesel & biomass feedstocks: review & analysis of the biochemistry, energetics & economics. *Energy Environ. Sci.* 3, 554–590. doi: 10.1039/b924978h

Xia, L., Ge, H., Zhou, X., Zhang, D., and Hu, C. (2013). Photoautotrophic outdoor two-striglyceridee cultivation for oleaginous microalgae Scenedesmus obtusus XJ-15. *Bioresour. Technol.* 144, 261–267. doi: 10.1016/j.biortech.2013.06.112

Zäuner, S., Jochum, W., Bigorowski, T., and Benning, C. (2012). A cytochrome b5-containing plastid-located fatty acid desaturase from *Chlamydomonas reinhardtii*. *Eukaryotic Cell* 11, 856–863. doi: 10.1128/EC.00079-12

Development of a Two-Stage Microalgae Dewatering Process – A Life Cycle Assessment Approach

Rizwan R. Soomro[1], Theoneste Ndikubwimana[2], Xianhai Zeng[3,4]*, Yinghua Lu[2,4], Lu Lin[3] and Michael K. Danquah[1]*

[1] Department of Chemical Engineering, Faculty of Engineering and Science, Curtin University of Technology, Sarawak, Malaysia, [2] Department of Chemical and Biochemical Engineering, College of Chemistry and Chemical Engineering, Xiamen University, Xiamen, China, [3] College of Energy, Xiamen University, Xiamen, China, [4] The Key Laboratory for Synthetic Biotechnology of Xiamen City, Xiamen University, Xiamen, China

Even though microalgal biomass is leading the third generation biofuel research, significant effort is required to establish an economically viable commercial-scale microalgal biofuel production system. Whilst a significant amount of work has been reported on large-scale cultivation of microalgae using photo-bioreactors and pond systems, research focus on establishing high performance downstream dewatering operations for large-scale processing under optimal economy is limited. The enormous amount of energy and associated cost required for dewatering large-volume microalgal cultures has been the primary hindrance to the development of the needed biomass quantity for industrial-scale microalgal biofuels production. The extremely dilute nature of large-volume microalgal suspension and the small size of microalgae cells in suspension create a significant processing cost during dewatering and this has raised major concerns towards the economic success of commercial-scale microalgal biofuel production as an alternative to conventional petroleum fuels. This article reports an effective framework to assess the performance of different dewatering technologies as the basis to establish an effective two-stage dewatering system. Bioflocculation coupled with tangential flow filtration (TFF) emerged a promising technique with total energy input of 0.041 kWh, 0.05 kg CO_2 emissions and a cost of $ 0.0043 for producing 1 kg of microalgae biomass. A streamlined process for operational analysis of two-stage microalgae dewatering technique, encompassing energy input, carbon dioxide emission, and process cost, is presented.

Keywords: microalgae, dewatering, biomass, biofuels, bioprocess

INTRODUCTION

The depletion of fossil resource reserves, climate change as well as the increasing price of crude oil are amongst the challenging problems of the world today, hence the search for alternative fuels is imperative (Shirvani et al., 2011). Biofuels, such as biodiesel and bioethanol, are considered as alternatives to fossil based fuels. They have much more advantages over fossil fuels as they have relatively low toxicity, high biodegradability, low net CO_2, are renewable and sustainable, and contains less or no sulfur (Zheng et al., 2012). Biofuels are currently produced from biological materials including sugar, corn, vegetable oils, plants, animal fats, woody biomass, and bio-wastes. However, due to competition with human food chain and the significant pretreatment operational

costs associated with woody biomass and bio-wastes, the search for new biomass sources has been a major research endeavor globally. Microalgal biomass is considered as an attractive feedstock for biofuel production due to its several significant advantages such as rapid growth rate, high lipid and carbohydrate contents, limited competition with food crops for arable land, and the great potential for carbon capture and biosequestration (Vandamme et al., 2011). However, high energy inputs and operational cost during the production of biomass are major limitations associated with microalgal biofuels development (Pienkos and Darzins, 2009; Wijffels and Barbosa, 2010). It has been reported that one of the most energy and cost intensive steps in algal biomass production process is the harvesting and dewatering or drying of microalgae suspension (Uduman et al., 2010; Rawat et al., 2013), this is due to the low concentration in the culture medium and the microalgae small cell sizes (a few micrometer) (Vandamme et al., 2011). Microalgal culture dewatering techniques commonly used are classified as chemical, mechanical, electrical, and biological. These methods can be applied as a single technique or combined (Danquah et al., 2009b). Chemical dewatering methods are mostly flocculation induced by inorganic or organic polyelectrolyte (polymer) flocculants. Mechanical techniques include centrifugation, filtration, natural sedimentation, flotation, and foam separation. Electrical dewatering techniques are based on electro-coagulation process. Biological dewatering techniques include auto-flocculation occurring at high pH, flocculation caused by secreted biopolymers, and microbial flocculation (Christenson and Sims, 2011). Though not fully developed for commercial application, biological dewatering techniques have recently gained research attention as low-cost sustainable techniques because of the absence of synthetic chemicals and minimal energy consumption (Christenson and Sims, 2011). It is imperative to find an efficient, cost effective and environmentally friendly harvesting and dewatering technique for commercializing biofuels from microalgal biomass. For biofuels production, the main objective of dewatering is to concentrate the dilute microalgae suspension of about 0.02–0.06% to 5–25%, and this is achievable in a two-step dewatering process where the primary stage is aimed at 2–7% and the secondary stage produces 15–25% of microalgae slurry (Uduman et al., 2010). However, with the introduction of innovative dewatering systems, the concentration of the slurry my exceed 25% in the secondary dewatering stage. The combination of two dewatering techniques has also been found to significantly improve the process by reducing the energy demands and/or total emissions (Khoo et al., 2011; Beach et al., 2012; Bilad et al., 2012; O'Connell et al., 2013; Weschler et al., 2014). The environmental impact analysis of the dewatering technique is a critical aspect in the assessment of microalgae as a potential biofuel feedstock. This is necessary to ensure reduced carbon footprint in the life cycle assessment (LCA) of the microalgal biofuel production process (Sander and Murthy, 2010; Uduman et al., 2010). The LCA illustrates the significance of dewatering to the scale up of microalgae-to-biofuels process engineering, hence there is a need for techno-economic and performance improvements

to make microalgae biofuels less energy intensive and more commercially viable (Uduman et al., 2010). This study will assess the performances of a wide range of technologies currently applied for microalgae dewatering through a comparative study of key process parameters as a basis for the development of two-stage microalgae dewatering systems. The complete performance and economic assessments of the two-stage dewatering systems are presented with an attempt to determine the most viable two-step dewatering technique.

CONVENTIONAL UNIT TECHNOLOGIES FOR MICROALGAE DEWATERING

Electrocoagulation

Electrocoagulation is described as environmentally friendly, highly selective, and potentially cost effective microalgae dewatering technique. **Table 1** presents some results on the performance and energy input of different electrocoagulation technologies reported as a means of microalgae dewatering. The main drawbacks associated with this technique are the cost of electricity, fouling of cathodes and periodic change of the anode materials (Uduman et al., 2011; Vandamme et al., 2011; Granados et al., 2012). The electrocoagulation process is influenced by many different factors such as the electrode material type, current density, temperature, pH, and any other coexisting ions (Gao et al., 2010). The electrocoagulation process is achieved by the combination of metal cations with negatively charged microalgal cells in the suspension carried towards the anode by electrophoretic motion (Mollah et al., 2004; Bukhari, 2008; Uduman et al., 2010). The amount of electricity which passes through the electrolytic solution determines the amount of metal dissolved into the solution (Mollah et al., 2004; Azarian et al., 2007; Bukhari, 2008).

Flocculation

Flocculation occurs once the solid particles in suspension collide and adhere to each other (Uduman et al., 2010). This dewatering process works well in separating algae cells from culture suspensions (Chen and Yeh, 2005; Knuckey et al., 2006; Henderson et al., 2008; Vandamme et al., 2010; Wyatt et al., 2012). The performance and energy input of some reported flocculation systems for microalgae dewatering are presented in **Table 2**. In the suspension, algae cells are stabilized by negative surface charge at wide pH values (Wyatt et al., 2012). Flocculation targets the development and sedimentation of flocs.

Theories on flocculation of microalgae have been described though some contradict (Schlesinger et al., 2012). Some of these theories state that flocculation occurs because the alkaline nature of the flocculants neutralizes surface charge of cells which could enable coalescence to larger flocs. Such theories are based on the assumption that electrostatic flocculation increases with increase in flocculant dosage in linear stoichiometric relations. This makes flocculation technology an expensive process as the performance hinges significantly on the amount of flocculant present. Contrary to the electrostatic flocculation theory, Schlesinger et al.

TABLE 1 | Performance and energy input of microalgae dewatering by electrocoagulation systems.

Electrocoagulation system	Process performance	Energy (kWh/m^3)	Reference
Electrocoagulation–Flocculation	Microalgal recovery efficiency: 80–95%	0.15–1	Vandamme et al., 2011
Electrolytic flocculation	Not precised	0.331	Coward et al., 2013
Electrocoagulation and electroflotation	Microalgal recovery efficiency: 99%	0.3	Weschler et al., 2014

TABLE 2 | Performance and energy input of microalgae dewatering by flocculation systems.

Mode of flocculation	Process performance	Energy (kWh/m^3)	Reference
Alum flocculation	Harvesting efficiency: 99.01%	0.1	Weschler et al., 2014
Polymer flocculation in conjunction with $Al_2(SO4)_3$	Suspended solids (%) in concentrate: 15	14.81	Danquah et al., 2009a
$FeCl_3$ – induced flocculation	Flocculation efficiencies: >90%	Not determined	Wyatt et al., 2012
Flocculation by Tanfloc and pH variation	Flocculation efficiencies: >96%	Not determined	Selesu et al., 2016

(2012) proposed that the amount of alkaline flocculants is a function of the logarithm of microalgae cell density with dense culture requiring an order of magnitude less base than dilute suspensions at low flocculation pH values. The principle of how flocculants work is based on the premise that the microalgae particulates have identical surface charges which repel them from each other. However, Chen et al. (2013), achieved effective flocculation for harvesting the microalgal cells of *Scenedesmus* sp. by simply increasing the pH of the culture without introducing any flocculants. Different types and flocculant dosage influence both the extent and the rate of flocculation. Both parameters are critical in the flocculation process, therefore extensive study should be undertaken to determine optimal flocculants dosage and sedimentation time (Schlesinger et al., 2012). Initial microalgal biomass concentration is one of the factors that influence flocculation efficiency. It has been found that a linear relation exists between the dosage needed and initial microalgal biomass concentration. The amount of suspended microalgal cells increases with increasing biomass concentration, thus higher flocculants dosages are required to interact with the surface charges of the microalgal cells (Kim et al., 2011).

Filtration

Filtration process consists of a permeable medium which restrains the movement of solid particles and allows liquid to pass through (Uduman et al., 2010). There are different types of filtration processes that are applicable for microalgae dewatering. These include magnetic filtration, vacuum filtration, pressure filtration, tangential flow filtration (TFF), and cross-flow filtration (Show et al., 2013). The performances and energy input of different filtration systems for microalgae dewatering have been studied extensively as depicted in **Table 3**. Filtration as a microalgae dewatering technology have many advantages. These include: high efficiency, low energy input (Danquah et al., 2009b), low cost, water recycle and reuse (Greenwell et al., 2010; Mata et al., 2010). However, it is generally difficult to filter biological feed because of the compressible nature of the biomass cake. The tendency of fouling with biological cells is high as biological feedstock may consist of mixtures of organic materials of different sizes, shapes and compressibility (Ríos et al., 2012). Microalgae cause

significant fouling to filtration membranes through the release of extracellular organic matter which significantly increases the cake resistance and this is independent on the membrane material, however, it is negligible at low feed concentrations. It however increases exponentially with microalgae deposition rate. Also the effect of trans-membrane pressure on cake resistance indicates that microalgal cake deposit is compressible and fouling of membrane by microalgae is proportional to the amount of organic polymers released (Babel and Takizawa, 2010).

Magnetic Separation

The principle of magnetic separation is based on the fact that materials with differing magnetic moments experience different forces in the presence of magnetic field gradients, thus an externally applied field can be used to drive a selection process (Svoboda and Fujita, 2003; Yavuz et al., 2009). Due to its attractive advantages such as low cost, energy efficient and simple operation, high permeation fluxes, small land area utilization, no clogging and fouling problems, magnetic separation process has been used in microalgae removal from freshwater using functionalized magnetic particles (Gao et al., 2009; Liu et al., 2009; Bucak et al., 2011; Toh et al., 2012). The technology presents the main drawback of low adsorptive capacity, also the high cost of nano magnetic particles should be considered while deciding on the magnetic separation system (Franzreb et al., 2006; Liu et al., 2009). The performance of different magnetic separation systems as reported by different researchers is presented in **Table 4**. The energy consumption during magnetic separation was not determined, thus not presented in the **Table 4**. In a mixture with a magnetic component, the magnetic material could be easily separated with electro-magnets or permanent magnets. Adsorption occurs due to electrostatic attraction between the magnetic particles and microalgae cells, and this is affected by the stirring speed, pH of the suspension, magnetic particle dosage, hydrodynamic resistance, magnetic field strength and the flow rate (Xu et al., 2011). Medium concentration, pH and particle concentration are critical to achieving high separation efficiencies (Cerff et al., 2012). During their studies on harvesting microalgae cells by magnetic separation, Cerff et al. (2012) reported that the presence of cations and anions in the medium could increase

TABLE 3 | The performance and energy input assessment of microalgae dewatering by filtration.

Filter type	Process performance	Energy (kWh/m^3)	Reference
Natural filtration	Suspended solids (%) in concentrate: 1–6	0.4	Uduman et al., 2010
Pressure filtration	Suspended solids (%) in concentrate: 5–27	0.88	Uduman et al., 2010
Tangential flow filtration (TFF)	Suspended solids (%) in concentrate: 2.5–8.9	0.2-2.6	Danquah et al., 2009a,b; Weschler et al., 2014
Vibrating screen filter	Harvesting efficiency: 89%	0.4	Weschler et al., 2014
Chamber filter	Harvesting efficiency: 89%	0.88	Coward et al., 2013
Belt filter press	Harvesting efficiency: 89%	0.5	Weschler et al., 2014
Vacuum filters	Suspended solids (%) in concentrate: 18	5.9	Coward et al., 2013
Submerged microfiltration	Recovery efficiency: 98%	0.25	Bilad et al., 2012

TABLE 4 | The performance and energy input assessment of microalgae dewatering by magnetic separation.

Magnetic separation system	Algal cell removal efficiency (%)	Reference
High gradient and low gradient magnetic separation	>90	Toh et al., 2012
High gradient magnetic separation	>95	Cerff et al., 2012
In situ magnetic separation	>98	Xu et al., 2011
Magnetic polymer separation	99	Liu et al., 2009
Coagulation-magnetic separation	>99	Liu et al., 2013a

the separation efficiency by five folds, however extensive studies should be undertaken on different media to substantiate the finding. Other research reports have established that lower pH and increase in magnetic particle dosage favor high recovery efficiency depending on the type of microalgae (Xu et al., 2011).

Flotation

Flotation as a separation technique was firstly applied in mineral industry, and recently have been found effective for removing algae from suspension (Phoochinda and White, 2003; Csordas and Wang, 2004; Phoochinda et al., 2004; Wiley et al., 2009). Flotation have many advantages such as less energy consumption than centrifugation (Wiley et al., 2009; Coward et al., 2013), and can achieve high efficiency at short operation time (Coward et al., 2013).

Flotation process is induced by bubbles generated from air or gas transformation within a solid-liquid suspension, the bubbles adhere to the particles to be separated carrying them at the top of the separator where they are collected (Pragya et al., 2013). Apart from microalgae harvesting, flotation is potentially applied in other fields for the recovery of valuable end-products such as oils (Al-Shamrani et al., 2002; Li et al., 2007; Hanotu et al., 2013), proteins (Aksay and Mazza, 2007; Jiang et al., 2011; Liu et al., 2013b), water and wastewaters remediation (Christenson and Sims, 2011). **Table 5** presents the performance and energy requirement of some reported flotation systems. Even though flotation is believed favorable for microalgae harvesting, there is a number of limitations associated with this technology including the use of surfactants or collectors at different dosage to improve the performance,

which requires additional separation units and thus subsequently increasing the process cost. More studies in this area are still needed such as the use of natural surfactants or collectors, and non-consumable electrodes materials (for electroflotation systems) in order to render flotation processes more applicable in commercial microalgae harvesting.

Centrifugation

Microalgae centrifugation involves a phase separation of microalgal cells from the suspension by the application of centrifugal force, and it is dependent on the particle size and density of the medium components (Uduman et al., 2010; Rawat et al., 2013). Centrifugation is an advantageous microalgae dewatering technique as it is rapid, easy and effective (Molina Grima et al., 2003). However, the exposure of microalgae cells to high gravitational and shear forces can lead to cell disruption and structural damage (Knuckey et al., 2006), and considering the processing of large volumes of microalgal cultures combined with increased energy consumption, centrifugation process is time consuming and economically unattractive (Rawat et al., 2013). Different centrifugation systems have been reported for microalgae dewatering (**Table 6**).

Bioflocculation

Bioflocculation refers to naturally induced flocculation due to secreted biopolymers of either the microalgal or bacterial cells. Microalgae dewatering costs could be greatly reduced with bioflocculation because no chemical costs are incurred with little to no energy consumption (Christenson and Sims, 2011). **Table 7** presents the performances of some reported microalgae bioflocculation methodologies. The addition of bioflocculants or bacterial microorganisms that naturally produce flocculants, to a culture of microalgae has been shown to enhance bioflocculation processes and the harvesting efficiency of multiple microalgal species (Christenson and Sims, 2011). Some fungi, for instance, have positively charged hyphae that can interact with the negatively charged microalgal cell surface and cause flocculation (Su et al., 2011; Van Den Hende et al., 2011; Zhang and Hu, 2012; Zhou et al., 2012). The dewatering of microalgae with bioflocculation using bacteria or fungi as a flocculating agent in co-cultivation with microalgae presents the main drawback of microbiological contamination, and possible interference with food or feedstock applications of the microalgal biomass. Naturally occurring microbial flocculants have been used to

TABLE 5 | The performance and energy input assessment of microalgae dewatering by flotation.

Mode of separation	Process performance	Energy (kWh/m^3)	Reference
Foam flotation	Total suspended solids (%) in concentrate: 1.4–2.4	0.015	Coward et al., 2013
Foam fractionation	Harvesting efficiency: >90%	Not determined	Csordas and Wang, 2004
Dissolved air flotation	Harvesting efficiency: 99.9%	1.5	Weschler et al., 2014
Dissolved air flotation	Total suspended solids (%) in concentrate: 5	7.6	Wiley et al., 2009
Jameson cell flotation	Harvesting efficiency: 97.4%	Not determined	Garg et al., 2014

TABLE 6 | The performance and energy input assessment of microalgae dewatering by centrifugation.

Centrifuge	Process performance	Energy (kWh/m^3)	Reference
Self-cleaning plate separator	Algal recovery efficiency: 95%	1	Weschler et al., 2014
Self-cleaning centrifuge	Total suspended solids (%) in concentrate: 12	1	Molina Grima et al., 2003
Nozzle discharge centrifuge	Total suspended solids (%) in concentrate: 2–15	0.9	Coward et al., 2013
Decanter bowl centrifuge	Total suspended solids (%) in concentrate: 22	8	Coward et al., 2013
Hydrocyclone	Total suspended solids (%) in concentrate: 0.4	0.3	Coward et al., 2013

harvest microalgae for aquaculture and biodiesel production because of their high harvesting efficiency and biodegradability (Oh et al., 2001; Manheim and Nelson, 2013).

MATERIALS AND METHODS

Life Cycle Assessment

By definition, LCA means a systematic environmental management tool used to assess the environmental factors associated with the product system through its life cycle stages, and projecting the environmental performance based on selected functional value of the products (Gnansounou et al., 2009; Khoo et al., 2010, 2011). The assessment takes into consideration the relevant inputs and outputs of a system and evaluates the potential environmental impacts associated with it (Yee et al., 2009; Clarens et al., 2010; Sanz Requena et al., 2011). The primary focus of the LCA investigation may be on the energy demands (Jorquera et al., 2010) and/or CO_2 emissions of the process chain (Stephenson et al., 2010), especially when LCA is applied for comparing the bioenergy products. This study was performed based on the principles of ISO 14040 (International Standardization Organization [ISO], 2006). The LCA model was

TABLE 7 | The performance of microalgae dewatering by bioflocculation systems.

Mode of bioflocculation	Harvesting efficiency (%)	Reference
γ-PGA broth bioflocculant	99	Ndikubwimana et al., 2014
Commercial γ-PGA bioflocculant	90–95	Zheng et al., 2012
Bioflocculant from *Paenibacillus* sp. AM49	83	Oh et al., 2001
Co-cultivation of microalgae with filamentous fungi	99	Xie et al., 2013
Fungal pelletization-assisted bioflocculation technology	100	Zhou et al., 2012

utilized for energy input and CO_2 emissions assessment during microalgae dewatering stages considered in this study.
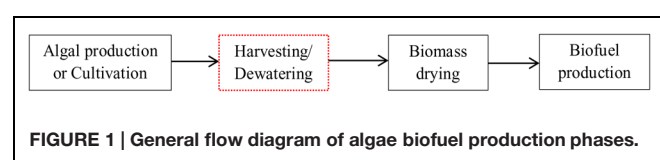
Goal and Scope

The general goal of this study is to compare life cycle energy and life cycle CO_2 of different dewatering technologies for potential application at industrial level of algal biofuel production. Different dewatering technologies and scenarios are evaluated and compared for the development of a most economical, with least energy consumption and low emissions two-stage microalgae dewatering system. The process energy for microalgae dewatering includes energy used directly by the dewatering technology (e.g., for mixing), raw materials (e.g., flocculants or electrode materials), but exclude other form of energy associated with other process units as would be included in the traditional cradle-to-grave life cycle assessment (LCA). The process energy input and CO_2 emissions during microalgae dewatering stage was the only elements considered in analysis. The scope of analysis was limited in this regard to focus mainly on the unit processes used for microalgae dewatering and avoid the uncertainty associated with upstream and downstream process options. The information provided by this study will serve for full LCA study.

The functional unit selected for all dewatering scenarios evaluated is 1000 kg of biomass harvested. **Figure 1** presents a general overview flow diagram of algae biofuel production phases and highlights (with red dashed line) the system boundary of the phase considered in this work. The comprehensive energy input and CO_2 emissions of different dewatering techniques will assist in finding the most efficient, economic, and environmental friendly two-stage microalgae dewatering configuration. The

FIGURE 1 | General flow diagram of algae biofuel production phases.

algal cultivation is not considered in this study; also the drying stage is omitted as some alternative downstream production methods such as wet lipid extraction may be applied.

Energy Balance

As harvesting/dewatering is the main bottleneck for the commercialization of microalgae based biofuel due to its high cost resulting from high energy input, it is the stage considered in this work. The volume (V) of the microalgae to be processed, the energy input (EI) of a single unit dewatering process, total energy input (TEI) of the whole dewtering system, were calculated using Eqs (1), (2), and (3), respectively.

$$V_x = \frac{FU}{C_x \times RE} \qquad (1)$$

$$EI_x = V_x \times E_x \qquad (2)$$

$$TEI_x = \sum EI_x \qquad (3)$$

where, TEI: Total energy input (kWh/1000 kg dry microalgae), EI_x: Energy input for unit process x (kWh/1000 kg dry microalgae), x: Unit process, where $1 =$ first stage dewatering, $2 =$ second stage dewatering, V_x: Volume of slurry (for $x = 1, 2$) in unit process x (m^3), E_x: Volumetric energy consumption for unit process x (kWh/m^3), FU: Functional unit (1000 kg of biomass recovered), RE: Recovery efficiency and C_x: Concentration of slurry entering unit process x. It is assumed that there is no biomass lost during the downstream process.

The CO₂ Balance

The greenhouse gas (GHG) emissions contributing most apparently to global warming are CO_2, CH_4, and N_2O (Houghton et al., 2001), whereby methane contributes almost 7%, N_2O about 0.8%, and CO_2 emissions make up the rest (Dones et al., 2003). Most of LCA studies describe the CO_2 balance considering the total emissions from fossil fuels and resources consumption vs. the CO_2 intake by microalgae in cultivation stage. However in this study, the CO_2 balance is described as the total CO_2 emitted during dewatering stage based on the amount of the energy required for each process.

System Boundaries

To facilitate the development of the analytical framework of the process evaluation, the system boundaries is simulated according to the following conditions and assumptions to typify a large-scale microalgae dewatering system:
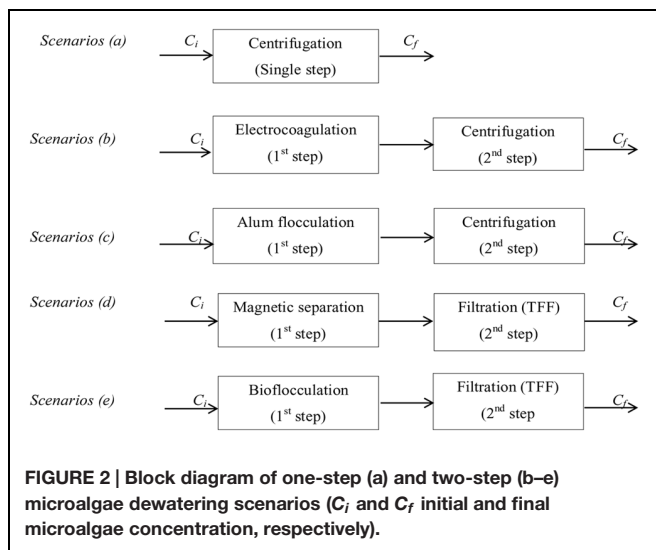
✓ The case study considered in this work is dewatering stage of a microalgae based biofuel system as presented in **Figure 1**.
✓ As this is a comparative operational life cycle analysis, some of the components of the full life cycle analysis framework, such as energy production and distribution, for the different technologies will cancel out. Thus the main LCA driving component is the energy consumption/requirement of the different dewatering technologies.

✓ The functional unit which is the measure of the performance and functional output of the system is chosen as 1000 kg of microalgae biomass in the final slurry.
✓ The initial microalgae biomass concentration is 0.3 g/L, which reflect the biomass concentration in open pond cultivation systems.
✓ The electricity consumed during the process is generated from black coal with associated environmental impacts (Norgate and Rankin, 2001).
✓ The amount of CO_2 emitted was calculated based on the amount of energy required for each process.
✓ The operational cost calculated includes the aluminum cost and nano particles costs.
✓ The leakage or malfunction of the system is not taken into consideration.
✓ The emissions of wastewater and other air pollutants are not covered in this study.
✓ The treatment of wastes (such as solids or wastewater) is not considered in this study.

Process Development and Evaluation of Two-Step Microalgae Dewatering Techniques

Most existing microalgal biomass production systems use energy intensive centrifuges for harvesting and dewatering microalgae (Heasman et al., 2000), making harvesting and dewatering a major fraction of the total energy demand (Molina Grima et al., 2003; Uduman et al., 2010). The application of two-stage dewatering techniques has been found to significantly improve the process (Can et al., 2006). LCA is important to assess the environmental aspects and potential impacts associated with the technology. Classical LCA implements a 'cradle to grave' principle which investigates the environmental aspects throughout the life of the product; raw material acquisition, product manufacturing, product use and disposal. The two-step microalgae dewatering techniques proposed for evaluation are presented in **Figure 2** as follows: (b) electro-coagulation with aluminum anodes coupled with centrifugation, (c) alum flocculation coupled with centrifugation, (d) magnetic separation coupled with TFF, and (e) bioflocculation coupled with filtration. Centrifugation (a) is used as the single-step dewatering base scenario for the analysis since it is the most conventional method used in the industry. All dewatering systems are assumed to be operated in batch mode. Considering different existing microalgae dewatering techniques, it is possible to have several various combinations in two-step system. In this study, only four combinations were proposed and further studies can evaluate other combinations.

For the electrocoagulation, aluminum anodes were chosen over steel 430 anodes as coagulation rate is faster with aluminim anodes, maximum recovery of microalgae is obtained at shorter run times, and smaller quantities dissolved aluminim is required under the same electro-coagulation conditions (Uduman et al., 2011). Moreover, Vandamme et al. (2011), realized that ECF was more efficient with aluminum anode than with iron anode. For the purpose of this study, aluminum metal dissolution and

FIGURE 2 | Block diagram of one-step (a) and two-step (b–e) microalgae dewatering scenarios (C_i and C_f initial and final microalgae concentration, respectively).

requirement are determined based on the batch analysis, alum flocculation dosage is determined from batch experiments, and the electrocoagulation energy requirement is based on optimal reported conditions (Uduman et al., 2011). Reported LCA and experimental data are used in this study to determine the energy requirements, carbon dioxide emissions, and cost for the proposed dewatering techniques.

Parameters and data sources essential to carry out this analysis are summarized in **Table 8**. The data presented in **Table 8** are the representative averages of different reported values of the same unit operation. Other sources of data are: Fe_3O_4 nano particles price: $ 114.2/kg (Alibaba/Beijing Dekedaoin Tech. Co. Ltd, 2014), CO_2 emission rate: 1.115 kg/kWh (Dones et al., 2003), Energy to produce Aluminum: 58.61 kWh/kg (Norgate and Rankin, 2001), Energy to produce alum: 3.06×10^{-4} kWh/kg (Arpke and Hutzler, 2006), the cost of aluminum anodes, flocculants and magnetic nano particles were also included in cost calculations. Aluminum cost was taken to be $ 1.733/kg[1], alum cost $ 0.2/kg[2], the electricity cost was $ 0.105/kWh (The State Grid Corporation of China/Fujian Province (2012), The industry power price), and the industrial price of Fe_3O_4 nano

[1]http://www.alibaba.com/product-detail/2012-August-Price-for-Ammonium-Alum 622064205.html

[2]http://www.metalprices.com/metal/aluminum/lme-aluminum-cash-official, 2014

particle, size of 20 nm (99% of purity) was 700 RMB/kg (Alibaba/Beijing Dekedaoin Tech. Co. Ltd, 2014). The exchange rate was: 100USD = 613.2RMB[3]. Aluminum and alum production energy requirements were included in calculations of energy inputs for electrocoagulation and alum flocculation, respectively.

The mixing energy required for magnetic separation was calculated by determining the mixing power consumption of the stirrer blades for the total mixing time (Sinnott, 2005). The shaft power required to drive an agitator can be estimated using the power number:

$$N_p = \frac{P}{D^5 N^3 \rho} \tag{4}$$

Where D is the agitator diameter (m), N is the agitator speed (s^{-1}), ρ is the fluid density (kg/m^3), and P is the shaft power (w). Equation (4) can be rearranged to solve for the shaft power. The power number can be obtained by using the power correlation for a single three bladed propeller and the Reynolds number (Re).

$$Re = \frac{D^2 N \rho}{\mu} \tag{5}$$

Where μ is the fluid viscosity (Ns/m^2).

RESULTS AND DISCUSSION OF TWO-STAGE DEWATERING SYSTEMS

After LCA calculations and process cost evaluation, the total energy demands, CO_2 emissions and the costs for the different scenarios of microalgae dewatering are presented in **Table 9** and **Figure 3**.

The two-step dewatering system of electrocoagulation coupled with centrifugation emerged the most energy intensive (**Table 9**), with highest CO_2 emissions but with relatively low cost (**Figure 3**). Different studies conducted on electrocoagulation show that it is a promising microalgae dewatering technique due to its lower energy demand. Vandamme et al. (2011) found that under optimal conditions, power consumption of Electrocoagulation–Flocculation using aluminum anode, was around 2 kWh/kg of microalgal biomass harvested for *C. vulgaris* and 0.3 kWh/kg for *P. tricornutum,* thus authors concluded that ECF is more energy efficient compared to centrifugation. In

[3]http://www.boc.cn/sourcedb/whpj/

TABLE 8 | Data sources for energy input, carbon dioxide emission, and cost analysis.

| Unit	Microalgae recovery (%)	Energy (kWh/m^3)	Reference
Self-cleaning plate centrifuge	95	1	Weschler et al., 2014
Electrocoagulation	88	0.6	Vandamme et al., 2011
Flocculation	99	0.1	Weschler et al., 2014
Magnetic separation	98	Not determined*	Xu et al., 2011
TFF	89	0.2	Weschler et al., 2014
Bioflocculation	99	Negligible	Xie et al., 2013
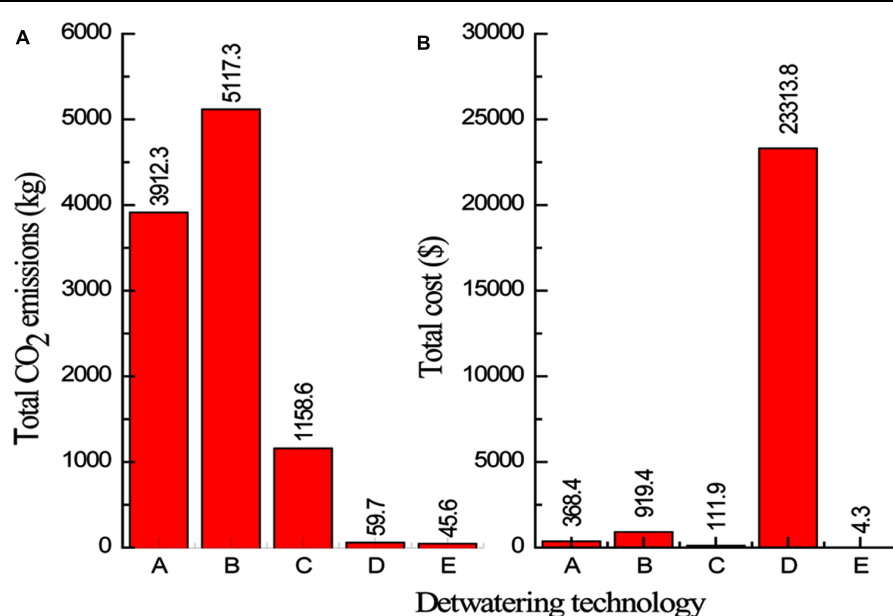
*The energy input required for magnetic separation will be calculated in this study based on mixing energy.

TABLE 9 | Energy requirements for the dewatering technologies evaluated.

Unity process		Energy input (kWh)
Centrifuge	Centrifugation	3508.8
Electrocoagulation/Centrifuge	Al production	1722.2
	Electrocoagulation	2272.7
	Centrifugation	594.5
	Total	**4589.4**
Alum flocculation/Centrifuge	Alum production	0.6
	Alum flocculation	336.7
	Centrifugation	701.8
	Total	**1039.1**
Magnetic separation/TFF	Magnetic separation	0.03
	TFF	53.5
	Total	**53.5**
Bioflocculation/TFF	Bioflocculation	Negligible
	TFF	40.9
	Total	**40.9**

their study on the removal of COD from wastewater with alum flocculation and electrocoagulation, Can et al. (2006), reported that energy input of 1.2 kWh/kg COD and an operating cost of \$ 0.31/kg COD were necessary for electrocoagulation, while energy requirement of 0.02 kWh/kg COD and an operating cost of \$ 0.08/kg COD are for alum flocculation. However, these studies only accounted for the energy and costs associated with the operation and did not consider the energy, CO_2 emissions and costs associated with raw material production which is an important parameter to consider for a complete life cycle assessment (LCA).

The two-step dewatering systems of magnetic separation and bioflocculation pared with TFF are almost in the same range of energy input (**Table 9**), and CO_2 emission (**Figure 3**), per 1000 kg of microalgae biomass recovered, however, the system of magnetic separation coupled with TFF is the most costing compared to all other microalgae dewatering systems evaluated (**Figure 3**). This is due to the high cost of magnetic nano particles. The recycle and reusability frequency of nano particles should be evaluated in order to cut-down the cost of magnetic separation process. Xu et al. (2011), reported that magnetic separation was energy-saving and environmental friendly microalgae dewatering technique but authors did not consider the process cost effectiveness because the cost of magnetic nano particles was not included in the study. Therefore, for the system of magnetic separation coupled with TFF to be cost effective, the use of cheaper and reusable magnetic nano particles is imperative. From the analysis, the two-step microalgae dewatering by bioflocculation pared with TFF process is the most attractive in terms of energy consumption, CO_2 emissions, and cost, showing significant low values for each parameter compared to centrifugation as a single step and other two-step dewatering systems considered in this study. However, initial capital investment for TFF is greater than flocculation as reported by Danquah et al. (2009a), but the payback period is 1.5 years earlier than 6 years for flocculation thus greater profits can be obtained with TFF, therefore this renders the two-step microalgae dewatering technique of bioflocculation coupled with TFF a viable, effective and cost efficient microalgae dewatering technique that can be applied at industrial level. Previous alum flocculation studies have deemed it unsuitable for microalgae dewatering due to high dosage requirement

FIGURE 3 | Total CO_2 emissions (A) and total cost (B) for the dewatering technologies evaluated. (A: Centrifugation, B: Electrocoagulation coupled with centrifugation, C: Alum flocculation coupled with centrifugation, D: Magnetic separation coupled with Tangential flow filtration (TFF), and E: Bioflocculation coupled with filtration).

(Buelna et al., 1990). However, from their studies on alum flocculation of marine microalgae, Uduman et al. (2011), reported that the alum dosage was in moderate quantities for commercial considerations thus making alum flocculation a possible industrial microalgae dewatering technique. Moreover, the coupling of alum flocculation with centrifugation in a two-step microalgae dewatering process for microalgae biomass production is profitable with the lowest energy input and CO_2 emissions compared to centrifugation as a single step and electrocoagulation coupled with centrifugation dewatering processes.

The results from this study demonstrate that a two-step microalgae dewatering technique, though it requires a high initial capital investment, is more efficient, economic viable and environmental friendly compared to a single step. Also Can et al. (2006), and Sander and Murthy (2010), reported that two-step dewatering technique is more energy efficient compared to a single step. Bilad et al. (2012), reported that the energy consumption to dewater *C. vulgaris* and *P. tricornutum* was 0.84 and 0.91 kWh/m^3, respectively, when the submerged microfiltration was combined with centrifugation in a two-step dewatering system. However, the results from the present study clearly show that bioflocculation coupled with TFF would be the best choice for microalgae dewatering with the lowest energy consumption. Different LCA studies have also confirmed that the two-step microalgae dewatering is the most efficient with low energy consumption and low emissions. Weschler et al. (2014) compared the process energy of different cultivation and harvesting technologies combined in various production scenarios for the production of microalgae biomass as a biofuel feedstock. Authors realized that the scenarios which used open ponds for cultivation, followed by settling and membrane filtration were the most energy efficient. Khoo et al. (2011), during their study on life cycle energy and CO_2 analysis of microalgae to biodiesel, they employed air sparging assisted coagulation flocculation (ASACF) process followed by centrifugation for harvesting and dewatering. They found that on the basis of a functional unity of 1 MJ of biofuel, the total energy demands were 4.44 MJ with 13% from biomass production, 85% from lipid extraction, and 2% from biodiesel production. O'Connell et al. (2013) reported the LCA of dewatering routes for algae derived biodiesel processes. Authors performed an analysis of the life cycle emissions associated with harvesting, dewatering, extraction, reaction, and product purification stages for algae biodiesel. From this base-case, they found that the total emissions were 10,500 kg per 1 t of biodiesel with 96% of those attributed to the spray dryer used for dewatering. However, by evaluating different alternative cases for various sequences of mechanical and thermal dewatering techniques, authors realized that the best case consisted of a disk-stack centrifuge followed by the chamber filter press and a heat integrated dryer, which resulted in 875 kg emissions per 1 t of biodiesel, equivalent to a 91% reduction from the base-case.

CONCLUSION

This study provides viable information about the energy input, environmental impact, and cost related to a two-step microalgae dewatering technique compared to a single step. The information provided by this study will contribute much essentially for a full LCA of a microalgae based biofuel process. The comparison of the two-step dewatering processes proposed in this study, and centrifugation as a single dewatering technique demonstrated that two-step dewatering technique can be less energy intensive, with low CO_2 emissions, cost efficiency, and high microalgae recovery. Life cycle energy analysis and related carbon dioxide emission revealed that bioflocculation coupled with TFF is the most promising industrial microalgae dewatering technique having the lowest energy consumption and carbon dioxide emissions. Magnetic separation required low energy for its operation as a dewatering process, but the overall process was highly costing, due to the cost associated with the Fe_3O_4 nano particles. Even though, a two-step microalgae dewatering technique is promising, more work is required to investigate process conditions required for optimal recovery at low energy requirement, carbon emission and overall cost of the dewatering process for a complete LCA study. Moreover, to minimize the production cost of biofuels from microalgae, extensive studies including strains engineering as the dewatering might be strain dependent, further combination of other different single dewatering technologies, optimization of different working parameters, choice of process materials and chemicals, and rigorous life cycle assessments are required to develop an efficient process for large-scale microalgae dewatering.

AUTHOR CONTRIBUTIONS

MKD, XZ, conceived, designed and supervised the study with the help of YL and LL. RRS and TN collected the sources data and wrote the draft of the manuscript. All authors revised the manuscript and contributed to the discussion and approved the final manuscript.

ACKNOWLEDGMENTS

REFERENCES

Aksay, S., and Mazza, G. (2007). Optimization of protein recovery by foam separation using response surface methodology. *J. Food Eng.* 79, 598–606. doi: 10.1016/j.jfoodeng.2006.02.024

Al-Shamrani, A., James, A., and Xiao, H. (2002). Destabilisation of oil-water emulsions and separation by dissolved air flotation. *Water Res.* 36, 1503–1512. doi: 10.1016/S0043-1354(01)00347-5

Alibaba/Beijing Dekedaoin Tech. Co. Ltd (2014).

Arpke, A., and Hutzler, N. (2006). Domestic water use in the united states: a lifecycle approach. *J. Ind. Ecol.* 10, 169–184. doi: 10.1162/108819806775545312

Azarian, G., Mesdaghinia, A., Vaezi, F., Nabizadeh, R., and Nematollahi, D. (2007). Algae removal by electro-coagulation process, application for treatment of the effluent from an industrial wastewater treatment plant. *Iran. J. Public Health* 36, 57–64.

Babel, S., and Takizawa, S. (2010). Microfiltration membrane fouling and cake behavior during algal filtration. *Desalination* 261, 46–51. doi: 10.1016/j.desal.2010.05.038

Beach, E. S., Eckelman, M. J., Cui, Z., Brentner, L., and Zimmerman, J. B. (2012). Preferential technological and life cycle environmental performance of chitosan flocculation for harvesting of the green algae *Neochloris oleoabundans*. *Bioresour. Technol.* 121, 445–449. doi: 10.1016/j.biortech.2012.06.012

Bilad, M. R., Vandamme, D., Foubert, I., Muylaert, K., and Vankelecom, I. F. (2012). Harvesting microalgal biomass using submerged microfiltration membranes. *Bioresour. Technol.* 111, 343–352. doi: 10.1016/j.biortech.2012.02.009

Bucak, S., Sharpe, S., Kuhn, S., and Hatton, T. A. (2011). Cell clarification and size separation using continuous countercurrent magnetophoresis. *Biotechnol. Prog.* 27, 744–750. doi: 10.1002/btpr.594

Buelna, G., Bhattarai, K., De la Noue, J., and Taiganides, E. (1990). Evaluation of various flocculants for the recovery of algal biomass grown on pig-waste. *Biol. Wastes* 31, 211–222. doi: 10.1016/0269-7483(90)90160-T

Bukhari, A. A. (2008). Investigation of the electro-coagulation treatment process for the removal of total suspended solids and turbidity from municipal wastewater. *Bioresour. Technol.* 99, 914–921. doi: 10.1016/j.biortech.2007.03.015

Can, O., Kobya, M., Demirbas, E., and Bayramoglu, M. (2006). Treatment of the textile wastewater by combined electrocoagulation. *Chemosphere* 62, 181–187. doi: 10.1016/j.chemosphere.2005.05.022

Cerff, M., Morweiser, M., Dillschneider, R., Michel, A., Menzel, K., and Posten, C. (2012). Harvesting fresh water and marine algae by magnetic separation: screening of separation parameters and high gradient magnetic filtration. *Bioresour. Technol.* 118, 289–295. doi: 10.1016/j.biortech.2012.05.020

Chen, J. J., and Yeh, H. H. (2005). The mechanisms of potassium permanganate on algae removal. *Water Res.* 39, 4420–4428. doi: 10.1016/j.watres.2005.08.032

Chen, L., Wang, C., Wang, W., and Wei, J. (2013). Optimal conditions of different flocculation methods for harvestin Scenedesmus sp. cultivated in an open-pond system. *Bioresour. Technol.* 133, 9–15. doi: 10.1016/j.biortech.2013.01.071

Christenson, L., and Sims, R. (2011). Production and harvesting of microalgae for wastewater treatment, biofuels, and bioproducts. *Biotechnol. Adv.* 29, 686–702. doi: 10.1016/j.biotechadv.2011.05.015

Clarens, A. F., Resurreccion, E. P., White, M. A., and Colosi, L. M. (2010). Environmental life cycle comparison of algae to other bioenergy feedstocks. *Environ. Sci. Technol.* 44, 1813–1819. doi: 10.1021/es902838n

Coward, T., Lee, J. G., and Caldwell, G. S. (2013). Development of a foam flotation system for harvesting microalgae biomass. *Algal Res.* 2, 135–144. doi: 10.1016/j.algal.2012.12.001

Csordas, A., and Wang, J. K. (2004). An integrated photobioreactor and foam fractionation unit for the growth and harvest of *Chaetoceros* spp. in open systems. *Aquacult. Eng.* 30, 15–30. doi: 10.1016/j.aquaeng.2003.07.001

Danquah, M. K., Ang, L., Uduman, N., Moheimani, N., and Forde, G. M. (2009a). Dewatering of microalgal culture for biodiesel production: exploring polymer flocculation and tangential flow filtration. *J. Chem. Technol. Biotechnol.* 84, 1078–1083. doi: 10.1002/jctb.2137

Danquah, M. K., Gladman, B., Moheimani, N., and Forde, G. M. (2009b). Microalgal growth characteristics and subsequent influence on dewatering efficiency. *Chem. Eng. J.* 151, 73–78. doi: 10.1016/j.cej.2009.01.047

Dones, R., Heck, T., and Hirschberg, S. (2003). Greenhouse gas emissions from energy systems: comparison and overview. *Energy* 100:2300.

Franzreb, M., Siemann-Herzberg, M., Hobley, T. J., and Thomas, O. R. (2006). Protein purification using magnetic adsorbent particles. *Appl. Microbiol. Biotecnol.* 70, 505–516. doi: 10.1007/s00253-006-0344-3

Gao, S., Yang, J., Tian, J., Ma, F., Tu, G., and Du, M. (2010). Electro-coagulation-flotation process for algae removal. *J. Harzard Mater.* 177, 336–343. doi: 10.1016/j.jhazmat.2009.12.037

Gao, Z., Peng, X., Zhang, H., Luan, Z., and Fan, B. (2009). Montmorillonite-Cu (II)/Fe (III) oxides magnetic material for removal of cyanobacterial *Microcystis aeruginosa* and its regeneration. *Desalination* 247, 337–345. doi: 10.1016/j.desal.2008.10.006

Garg, S., Wang, L., and Schenk, P. M. (2014). Effective harvesting of low surface-hydrophobicity microalgae by froth flotation. *Bioresour. Technol.* 159, 437–441. doi: 10.1016/j.biortech.2014.03.030

Gnansounou, E., Dauriat, A., Villegas, J., and Panichelli, L. (2009). Life cycle assessment of biofuels: energy and greenhouse gas balances. *Bioresour. Technol.* 100, 4919–4930. doi: 10.1016/j.biortech.2009.05.067

Granados, M., Acien, F., Gomez, C., Fernández-Sevilla, J., and Molina Grima, E. (2012). Evaluation of flocculants for the recovery of freshwater microalgae. *Bioresour. Technol.* 118, 102–110. doi: 10.1016/j.biortech.2012.05.018

Greenwell, H., Laurens, L., Shields, R., Lovitt, R., and Flynn, K. (2010). Placing microalgae on the biofuels priority list: a review of the technological challenges. *J. R. Soc. Interface* 7, 703–726. doi: 10.1098/rsif.2009.0322

Hanotu, J., Bandulasena, H., Chiu, T. Y., and Zimmerman, W. B. (2013). Oil emulsion separation with fluidic oscillator generated microbubbles. *Int. J. Multiphase Flow* 56, 119–125. doi: 10.1016/j.ijmultiphaseflow.2013.05.012

Heasman, M., Diemar, J., O'connor, W., Sushames, T., and Foulkes, L. (2000). Development of extended shelf-life microalgae concentrate diets harvested by centrifugation for bivalve molluscs-a summary. *Aquacult. Res.* 31, 637–659. doi: 10.1046/j.1365-2109.2000.00492.x

Henderson, R., Parsons, S. A., and Jefferson, B. (2008). The impact of algal properties and pre-oxidation on solid-liquid separation of algae. *Water Res.* 42, 1827–1845. doi: 10.1016/j.watres.2007.11.039

Houghton, J. T., Ding, Y., Griggs, D. J., Noguer, M., van der Linden, P. J., Dai, X., et al. (2001). *Climate Change 2001: The Scientific Basis*. Cambridge: Cambridge university press.

International Standardization Organization [ISO] (2006). *Environmental Management-Life Cycle Assessment-Principles and Framework, ISO14040*. London: British Standards Institution.

Jiang, C., Wu, Z., Li, R., and Liu, Q. (2011). Technology of protein separation from whey wastewater by two-stage foam separation. *Biochem. Eng. J.* 55, 43–48. doi: 10.1016/j.bej.2011.03.005

Jorquera, O., Kiperstok, A., Sales, E. A., Embiruçu, M., and Ghirardi, M. L. (2010). Comparative energy life-cycle analyses of microalgal biomass production in open ponds and photobioreactors. *Bioresour. Technol.* 101, 1406–1413. doi: 10.1016/j.biortech.2009.09.038

Khoo, H. H., Lim, T. Z., and Tan, R. B. (2010). Food waste conversion options in Singapore: environmental impacts based on an LCA perspective. *Sci. Total Environ.* 408, 1367–1373. doi: 10.1016/j.scitotenv.2009.10.072

Khoo, H., Sharratt, P., Das, P., Balasubramanian, R., Naraharisetti, P., and Shaik, S. (2011). Life cycle energy and CO_2 analysis of microalgae-to-biodiesel: preliminary results and comparisons. *Bioresour. Technol.* 102, 5800–5807. doi: 10.1016/j.biortech.2011.02.055

Kim, D. G., La, H. J., Ahn, C. Y., Park, Y. H., and Oh, H. M. (2011). Harvest of Scenedesmus sp. with bioflocculant and reuse of culture medium for subsequent high-density cultures. *Bioresour. Technol.* 102, 3163–3168. doi: 10.1016/j.biortech.2010.10.108

Knuckey, R. M., Brown, M. R., Robert, R., and Frampton, D. M. (2006). Production of microalgal concentrates by flocculation and their assessment as aquaculture feeds. *Aquacult. Eng.* 35, 300–313. doi: 10.1016/j.aquaeng.2006.04.001

Li, X. B., Liu, J. T., Wang, Y. T., Wang, C. Y., and Zhou, X. H. (2007). Separation of oil from wastewater by column flotation. *J. China University Min. Technol.* 17, 546–577. doi: 10.1016/S1006-1266(07)60143-6

Liu, D., Li, F., and Zhang, B. (2009). Removal of algal blooms in freshwater using magnetic polymer. *Water Sci. Technol.* 59, 1085–1091. doi: 10.2166/wst.2009.046

Liu, D., Wang, P., Wei, G., Dong, W., and Hui, F. (2013a). Removal of algal blooms from freshwater by the coagulation-magnetic separation method. *Environ. Sci. Pollut. Res. Int.* 20, 60–65. doi: 10.1007/s11356-012-1052-4

Liu, Z., Wu, Z., Li, R., and Fan, X. (2013b). Two-stage foam separation technology for recovering potato protein from potato processing wastewater using the column with the spiral internal component. *J. Food Eng.* 114, 192–198. doi: 10.1016/j.jfoodeng.2012.08.011

Manheim, D., and Nelson, Y. (2013). Settling and bioflocculation of two species of algae used in wastewater treatment and algae biomass production. *Environ. Progr. Sustain. Energy* 32, 946–954. doi: 10.1002/ep.11861

Mata, T. M., Martins, A. A., and Caetano, N. S. (2010). Microalgae for biodiesel production and other applications: a review. *Renewable Sustain. Energy Rev.* 14, 217–232. doi: 10.1016/j.rser.2009.07.020

Molina Grima, E., Belarbi, E. H., Acién Fernández, F., Robles Medina, A., and Chisti, Y. (2003). Recovery of microalgal biomass and metabolites: process options and economics. *Biotechnol. Adv.* 20, 491–515. doi: 10.1016/S0734-9750(02)00050-2

Mollah, M. Y., Morkovsky, P., Gomes, J. A., Kesmez, M., Parga, J., and Cocke, D. L. (2004). Fundamentals, present and future perspectives of electrocoagulation. *J. Harzard Mater.* 114, 199–210. doi: 10.1016/j.jhazmat.2004.08.009

Ndikubwimana, T., Zeng, X., Liu, Y., Chang, J.-S., and Lu, Y. (2014). Harvesting of microalgae *Desmodesmus* sp. F51 by bioflocculation with bacterial bioflocculant. *Algal Res.* 6, 186–193. doi: 10.1016/j.algal.2014.09.004

Norgate, T., and Rankin, W. (2001). "Greenhouse gas emissions from aluminium production-a life cycle approach," in *Proceedings of Symposium on Greenhouse Gas Emissions in the Metallurgical Industries: Policies, Abatement and Treatment, COM2001* (Toronto, ON: METSOC of CIM), 275–290.

O'Connell, D., Savelski, M., and Slater, C. S. (2013). Life cycle assessment of dewatering routes for algae derived biodiesel processes. *Clean Technol. Environ. Policy* 15, 567–577. doi: 10.1007/s10098-012-0537-7

Oh, H. M., Lee, S. J., Park, M. H., Kim, H. S., Kim, H. C., Yoon, J. H., et al. (2001). Harvesting of *Chlorella vulgaris* using a bioflocculant from *Paenibacillus* sp. AM49. *Biotechnol. Lett.* 23, 1229–1234. doi: 10.1023/A:1010577319771

Phoochinda, W., and White, D. (2003). Removal of algae using froth flotation. *Environ. Technol.* 24, 87–96. doi: 10.1080/09593330309385539

Phoochinda, W., White, D., and Briscoe, B. (2004). An algal removal using a combination of flocculation and flotation processes. *Environ. Technol.* 25, 1385–1395. doi: 10.1080/09593332508618466

Pienkos, P. T., and Darzins, A. (2009). The promise and challenges of microalgal-derived biofuels. *Biofuels Bioprod. Biorefining* 3, 431–440. doi: 10.1002/bbb.159

Pragya, N., Pandey, K. K., and Sahoo, P. (2013). A review on harvesting, oil extraction and biofuels production technologies from microalgae. *Renewable Sustain. Energy Rev.* 24, 159–171. doi: 10.1016/j.rser.2013.03.034

Rawat, I., Kumar, R. R., Mutanda, T., and Bux, F. (2013). Biodiesel from microalgae: a critical evaluation from laboratory to large scale production. *Appl. Energy* 103, 444–467. doi: 10.1016/j.apenergy.2012.10.004

Ríos, S. D., Salvadó, J., Farriol, X., and Torras, C. (2012). Antifouling microfiltration strategies to harvest microalgae for biofuel. *Bioresour. Technol.* 119, 406–418. doi: 10.1016/j.biortech.2012.05.044

Sander, K., and Murthy, G. S. (2010). Life cycle analysis of algae biodiesel. *Int. J. Life Cycle Assess.* 15, 704–714. doi: 10.1007/s11367-010-0194-1

Sanz Requena, J., Guimaraes, A., Quiros Alpera, S., Relea Gangas, E., Hernandez-Navarro, S., Navas Gracia, L., et al. (2011). Life Cycle Assessment (LCA) of the biofuel production process from sunflower oil, rapeseed oil and soybean oil. *Fuel Process. Technol.* 92, 190–199. doi: 10.1016/j.fuproc.2010.03.004

Schlesinger, A., Eisenstadt, D., Bar-Gil, A., Carmely, H., Einbinder, S., and Gressel, J. (2012). Inexpensive non-toxic flocculation of microalgae contradicts theories; overcoming a major hurdle to bulk algal production. *Biotechnol. Adv.* 30, 1023–1030. doi: 10.1016/j.biotechadv.2012.01.011

Selesu, N. F., de Oliveira, T. V., Corrêa, D. O., Miyawaki, B., Mariano, A. B., Vargas, J. V., et al. (2016). Maximum microalgae biomass harvesting via flocculation in large scale photobioreactor cultivation. *Can. J. Chem. Eng.* 94, 304–309. doi: 10.1002/cjce.22391

Shirvani, T., Yan, X., Inderwildi, O. R., Edwards, P. P., and King, D. A. (2011). Life cycle energy and greenhouse gas analysis for algae-derived biodiesel. *Energy Environ. Sci.* 4, 3773–3778. doi: 10.1039/c1ee01791h

Show, K. Y., Lee, D. J., and Chang, J. S. (2013). Algal biomass dehydration. *Bioresour. Technol.* 135, 720–729. doi: 10.1016/j.biortech.2012.08.021

Sinnott, R. K. (2005). *Chemical Engineering Design.* Oxford: Elsvier Butterworth-Heinemann.

Stephenson, A. L., Kazamia, E., Dennis, J. S., Howe, C. J., Scott, S. A., and Smith, A. G. (2010). Life-cycle assessment of potential algal biodiesel production in the United Kingdom: a comparison of raceways and air-lift tubular bioreactors. *Energy Fuels* 24, 4062–4077. doi: 10.1021/ef1003123

Su, Y., Mennerich, A., and Urban, B. (2011). Municipal wastewater treatment and biomass accumulation with a wastewater-born and settleable algal-bacterial culture. *Water Res.* 45, 3351–3358. doi: 10.1016/j.watres.2011.03.046

Svoboda, J., and Fujita, T. (2003). Recent developments in magnetic methods of material separation. *Miner. Eng.* 16, 785–792. doi: 10.1016/S0892-6875(03)00212-7

The State Grid Corporation of China/Fujian Province (2012).

Toh, P. Y., Yeap, S. P., Kong, L. P., Ng, B. W., Chan, D. J. C., Ahmad, A. L., et al. (2012). Magnetophoretic removal of microalgae from fishpond water: feasibility of high gradient and low gradient magnetic separation. *Chem. Eng. J.* 211, 22–30. doi: 10.1016/j.cej.2012.09.051

Uduman, N., Lee, H., Danquah, M. K., and Hoadley, A. F. (2011). *Electrocoagulation of Marine Microalgae. Chemeca 2011.* Sydney, NSW: Engineering a Better World, 18–21.

Uduman, N., Qi, Y., Danquah, M. K., Forde, G. M., and Hoadley, A. (2010). Dewatering of microalgal cultures: a major bottleneck to algae-based fuels. *J. Renewable Sustain. Energy* 2, 012701–012715. doi: 10.1063/1.3294480

Vandamme, D., Foubert, I., Meesschaert, B., and Muylaert, K. (2010). Flocculation of microalgae using cationic starch. *J. Appl. Phycol.* 22, 525–530. doi: 10.1007/s10811-009-9488-8

Vandamme, D., Pontes, S. C. V., Goiris, K., Foubert, I., Pinoy, L. J. J., and Muylaert, K. (2011). Evaluation of electro-coagulation-flocculation for harvesting marine and freshwater microalgae. *Biotechnol. Biong.* 108, 2320–2329. doi: 10.1002/bit.23199

Van Den Hende, S., Vervaeren, H., Saveyn, H., Maes, G., and Boon, N. (2011). Microalgal bacterial floc properties are improved by a balanced inorganic/organic carbon ratio. *Biotechnol. Bioeng.* 108, 549–558. doi: 10.1002/bit.22985

Weschler, M. K., Barr, W. J., Harper, W. F., and Landis, A. E. (2014). Process energy comparison for the production and harvesting of algal biomass as a biofuel feedstock. *Bioresour. Technol.* 153, 108–115. doi: 10.1016/j.biortech.2013.11.008

Wijffels, R. H., and Barbosa, M. J. (2010). An outlook on microalgal biofuels. *Science* 329, 796–799. doi: 10.1126/science.1189003

Wiley, P. E., Brenneman, K. J., and Jacobson, A. E. (2009). Improved algal harvesting using suspended air flotation. *Water Environ. Res.* 81, 702–708. doi: 10.2175/106143009X407474

Wyatt, N. B., Gloe, L. M., Brady, P. V., Hewson, J. C., Grillet, A. M., Hankins, M. G., et al. (2012). Critical conditions for ferric chloride-induced flocculation of freshwater algae. *Biotechnol. Biong.* 109, 493–501. doi: 10.1002/bit.23319

Xie, S., Sun, S., Dai, S. Y., and Yuan, J. S. (2013). Efficient coagulation of microalgae in cultures with filamentous fungi. *Algal Res.* 2, 28–33. doi: 10.1016/j.algal.2012.11.004

Xu, L., Guo, C., Wang, F., Zheng, S., and Liu, C.-Z. (2011). A simple and rapid harvesting method for microalgae by in situ magnetic separation. *Bioresour. Technol.* 102, 10047–10051. doi: 10.1016/j.biortech.2011.08.021

Yavuz, C. T., Prakash, A., Mayo, J., and Colvin, V. L. (2009). Magnetic separations: from steel plants to biotechnology. *Chem. Eng. Sci.* 64, 2510–2521. doi: 10.1016/j.ces.2008.11.018

Yee, K. F., Tan, K. T., Abdullah, A. Z., and Lee, K. T. (2009). Life cycle assessment of palm biodiesel: revealing facts and benefits for sustainability. *Appl. Energ.* 86, S189–S196. doi: 10.1016/j.apenergy.2009.04.014

Zhang, J., and Hu, B. (2012). A novel method to harvest microalgae via co-culture of filamentous fungi to form cell pellets. *Bioresour. Technol.* 114, 529–535. doi: 10.1016/j.biortech.2012.03.054

Zheng, H., Gao, Z., Yin, J., Tang, X., Ji, X., and Huang, H. (2012). Harvesting of microalgae by flocculation with poly (γ-glutamic acid). *Bioresour. Technol.* 112, 212–220. doi: 10.1016/j.biortech.2012.02.086

Zhou, W., Cheng, Y., Li, Y., Wan, Y., Liu, Y., Lin, X., et al. (2012). Novel fungal pelletization-assisted technology for algae harvesting and wastewater treatment. *Appl. Biochem. Biotechnol.* 167, 214–228. doi: 10.1007/s12010-012-9667-y

Lipid Extracted Microalgal Biomass Residue as a Fertilizer Substitute for *Zea mays* L.

Rahulkumar Maurya[1, 2], Kaumeel Chokshi[1, 2], Tonmoy Ghosh[1, 2], Khanjan Trivedi[2, 3], Imran Pancha[1, 2], Denish Kubavat[2, 3], Sandhya Mishra[1, 2]* and Arup Ghosh[2, 3]*

[1] Salt and Marine Chemicals Division, CSIR-Central Salt and Marine Chemicals Research Institute, Bhavnagar, India,
[2] Academy of Scientific and Innovative Research, CSIR-Central Salt and Marine Chemicals Research Institute, Bhavnagar, India, [3] Wasteland Research Division, CSIR-Central Salt and Marine Chemicals Research Institute, Bhavnagar, India

High volumes of lipid extracted microalgal biomass residues (LMBRs) are expected to be produced upon commencement of biodiesel production on a large scale, thus necessitating its value addition for sustainable development. LMBRs of *Chlorella variabilis* and *Lyngbya majuscula* were employed to substitute the nitrogen content of recommended rate of fertilizer (RRF) for *Zea mays* L. The pot experiment comprised of 10 treatments, i.e., T1 (No fertilizer); T2 (RRF-120 N: 60 P_2O_5: 40 K_2O kg ha^{-1}); T3 to T6—100, 75, 50, and 25% N through LMBR of the *Chlorella* sp., respectively; T7 to T10—100, 75, 50, and 25% N through LMBR of *Lyngbya* sp., respectively. It was found that all LMBR substitution treatments were at par to RRF with respect to grain yield production. T10 gave the highest grain yield (65.16 g plant^{-1}), which was closely followed by that (63.48 g plant^{-1}) under T5. T10 also recorded the highest phosphorus and potassium contents in grains. T4 was markedly superior over control in terms of dry matter accumulation (DMA) as well as carbohydrate content, which was ascribed to higher pigment content and photosynthetic activity in leaves. Even though considerably lower DMA was obtained in *Lyngbya* treatments, which might have been due to the presence of some toxic factors, no reduction in grain yield was apparent. The length of the tassel was significantly higher in either of the LMBRs at any substitution rates over RRF, except T6 and T7. The ascorbate peroxidase activity decreased with decreasing dose of *Chlorella* LMBR, while all the *Lyngbya* LMBR treatments recorded lower activity, which were at par with each other. Among the *Chlorella* treatments, only T5 recorded significantly higher values of glutathione reductase activity over RRF, while the rest were at par. There were significant increases in carbohydrate and crude fat, respectively, only in T4 and T3 over RRF, while no change was observed in crude protein due to LMBR treatments. Apparently, there was no detrimental effect on soil properties, suggesting that both the LMBRs can be employed to reduce the usage of chemical fertilizers, thus promoting maize crop production in a sustainable manner.

Keywords: *Chlorella*, *Lyngbya*, fertilizer, de-oiled microalgae, maize, soil properties, photosynthesis

INTRODUCTION

The effect of climate change due to the incessant burning of fossil fuels is now being felt across the globe (Ghosh, 2012) which has necessitated the search for alternate sources of cleaner energy (Ghosh et al., 2007; Ghosh, 2014). In the last few years, there has been intensive research on microalgae as it is an attractive feedstock for biofuel production (Chisti, 2007). Microalgae have been reported to have much higher primary productivity as compared to other terrestrial plants having biofuel potential (Mata et al., 2010). Processes for conversion of microalgal oil to biodiesel have already been developed (Mishra et al., 2012) and it is expected that once the microalgal cultivation technology is sufficiently optimized, adequate feedstock would be available from large scale cultivation for biofuel production. During algal biodiesel production, lipid is extracted from microalgal biomass through suitable solvent and converted to biodiesel through trans-esterification process. After lipid extraction, a huge amount of de-oiled microalgal biomass remains left.

Algae biomass is a complex material comprising of carbohydrates, lipids, proteins, and several potentially interesting molecules. The biofuel sector is specifically interested in carbohydrates (mainly C6) and lipids (mainly C16–C22), the amount of which could vary as a function of the algae species, strains, and the cultivation methods adopted (Chiaramonti et al., 2015). The current worldwide algae biomass production has been projected to be at more than 20,000 dry tons per year (Verdelho, 2013; Zittelli et al., 2013a,b; Chiaramonti et al., 2015). However, the algae market is expected to grow as the constraints of algal production are overcome and the cost of production is reduced. As per Studt (2010) and Rodolfi et al. (2009), the potential oil yield from microalgae on equal acreage basis is 5–20 times higher than that of oil from palm species. Assuming a conservative figure of 25% extractable oil from microalgal biomass (Chisti, 2007), for every metric ton of biodiesel manufactured, three times the amount of lipid extracted microalgal biomass residue (LMBR) will be produced. To make the biodiesel sustainable, it is also necessary to valorize such biomass for various applications, thus also offsetting the cost of biodiesel. Such value addition of LMBRs may be by its use as feed and fertilizer; fermentation to bio-methane and bio-ethanol; as a nutrient source for organisms; thermo-chemical conversion into various fuels and chemicals and as biosorbents for removal of dye and heavy metals from wastewater (Mata et al., 2010; Scott et al., 2010; Rashid et al., 2013; Maurya et al., 2014). Depending on the species, LMBRs are rich in protein and therefore rich in nitrogen content besides the presence of other essential plant macro- and micro-nutrients. Because of low carbon-nitrogen ratio, it cannot be utilized directly for bio-methane production, although such biomass can be utilized as animal feed, fertilizer, or nutrient source for organisms (Mata et al., 2010; Bryant et al., 2012; Gao et al., 2012). There are reports that shed light on the use of microalgae

as a potential source of nutrients and bioactive compounds that can be utilized for sustainable plant production either directly as an inoculum (Metting and Rayburn, 1983; Grzesik and Romanowska-Duda, 2014), as unprocessed dried algae (Mulbry et al., 2005), and sonicated biomass (Grzesik and Romanowska-Duda, 2015). However, no such studies have been reported yet that validate the use of LMBRs as a source of plant nutrients.

Urea, which is the most commonly used chemical nitrogenous fertilizers, is produced through very well-known Haber-Bosch process which rely on fossil fuels (Vance, 2001; Pfromm et al., 2011). Excessive use of chemical fertilizers is responsible for global warming, for example, assuming a recommended rate of 150:60:40 kg $N:P_2O_5:K_2O$ hectare^{-1} applied through urea, di-ammonium phosphate (DAP) and muriate of potash (MOP) for the cultivation of maize, $\sim$599 kg CO_2 equivalents are produced on account of fertilizer production and their transport (Singh et al., 2015). Using carbon rich residues as a chemical fertilizer substitute may also have other benefits such as improved soil health, stability of soil aggregates, soil water retention, carbon sequestration, and prevention of nutrient losses (Metting and Rayburn, 1983; Anand et al., 2015). Enhancing the productivity of crops in a sustainable manner without adversely affecting soil health should be the focus of the approaches to meet the increasing food demand (Singh et al., 2015).

In the present study, lipid-extracted biomass residues of two microalgal species, namely, *Chlorella variabilis* (ATCC PTA 12198) and *Lyngbya majuscula* have been evaluated for its nitrogen substitution potential for maize (*Zea mays* L.—a heavy feeder of nutrients) crop in a pot experiment. Different N substitution levels were used to evaluate their effects on crop growth, yield, quality, and soil properties.

MATERIALS AND METHODOLOGY

LMBR Preparation and Characterization

Initially, 1 kg biomass of each algae was taken for the lipid extraction. The lipid was extracted in soxhlet extractor using 3 L n-hexane per kg dry biomass. The extraction time of five cycles was 4 h in total. At the end of extraction, lipid, hexane, and de-oiled biomass were recovered. The de-oiled biomass was sundried for a day and powdered by grinding in mixture grinder (Boss Cyclone B219, Boss Home Appliances, Mumbai, India). The chemical composition of *Chlorella* and *Lyngbya* LMBR has been presented in **Table 1**. TVS and ash were obtained by subjecting the ovendried biomass in a muffle furnace at 575 ± 25°C (van Wychen and Laurens, 2013). Carbon, hydrogen, nitrogen and sulfur were analyzed using a CHNS analyzer (Perkin-Elmer Model 2 400, USA). Na and K was analyzed after wet ashing the LMBR samples with ternary acid mixture (Jackson, 1973), followed by their estimation using flame photometer (Toth et al., 1948); other micro and macro elements were analyzed by the X-Ray Fluorescence analyzer (Bruker AXS, S4 Pioneer, Billerica, Massachusetts, USA). Crude protein was calculated from nitrogen content using a multiplication factor of 6.25 (Jones, 1941).

Abbreviations: LMBR, lipid extracted microalgal biomass residues; RRF, recommended rate of fertilizer; CRD, completely randomized design; DMA, dry matter accumulation; APX, ascorbate peroxidase; GR, glutathione reductase; SSP, single super phosphate; MOP, muriate of potash; DAS, days after sowing; TVS, total volatile solid; DAP, di-ammonium phosphate; ROS, reactive oxygen species.

Parameters	LMBR	
	Chlorella	*Lyngbya*
TVS (%)	67.66 ± 0.071	55.82 ± 2.58
Ash (%)	32.34 ± 0.071	40.73 ± 1.57
Crude protein (%)	36.31 ± 0.98	24.75 ± 0.28
C (%)	28.36 ± 2.51	23.40 ± 1.56
H (%)	4.75 ± 0.32	4.42 ± 0.28
N (%)	5.810 ± 0.157	3.960 ± 0.045
S (%)	0.27 ± 0.04	0.43 ± 0.03
P (%)	0.273 ± 0.072	0.097 ± 0.004
K (%)	0.634 ± 0.031	0.579 ± 0.044
Na (%)	1.466 ± 0.016	0.183 ± 0.005
Ca (%)	0.017 ± 0.002	0.007 ± 0.001
Mg (%)	0.07 ± 0.01	0.037 ± 0.004
Fe (%)	1.84 ± 0.19	6.61 ± 1.21
Mn (%)	0.05 ± 0.008	0.27 ± 0.08
Cu (PPM)	6 ± 1.35	6 ± 1.00
Zn (PPM)	31 ± 3.88	24 ± 4.36
Cl (PPM)	69 ± 8.56	64 ± 9.27

Pot Experiment

The experiment was carried out during *Rabi* season in 2013–14 (i.e., cold months during November to February) at pot culture facility of CSIR-CSMCRI, Bhavnagar, Gujarat, India (21°44′57.6″N latitude, 72°08′39.3″E longitude). The experimental soil was sandy clay loam in texture, slightly alkaline (pH: 8.08 ± 0.03) and non-saline (0.41 dS m^{-1}). The soil was low in organic carbon ($0.21 \pm 0.05\%$), medium in available N (0.2 ± 0.06 g kg^{-1}), and high with respect to available P (0.027 ± 0.004 g kg^{-1}) and available K (0.30 ± 0.01 g kg^{-1}). The experiment was carried out in pots with 35 kg soil in each of them. The experiment was laid out in completely randomized design (CRD) comprising of 10 treatments including control (recommended rate of fertilizers through chemical means) and absolute control receiving no nutrients at all. Random number table was used for randomization. Each of the 10 treatments had five replicates, each represented by an individual pot having one plant. The recommended rate of fertilizer (RRF) application was 120:60:40 kg N:P$_2$O$_5$:K$_2$O hectare^{-1} supplied through urea, single super phosphate (SSP), and MOP, respectively. The test variety employed was F1 hybrid sweet corn, variety: Sugar-75 (Syngenta India Ltd.). This variety has very good plant vigor, plant height and is recommended for winter sowing. The maturity of the plant is about 90 days. The variety has long uniform cylindrical cobs, golden yellow kernels, excellent tip filling, high yield, and very sweet taste (16% total soluble sugar).

The treatments T$_1$ and T$_2$ represented absolute control and RRF, respectively. The treatments T$_3$–T$_6$ represented substitution of 100, 75, 50, and 25% N, respectively, through *Chlorella* derived LMBR. Similarly, treatments T$_7$–T$_{10}$ represented substitution of 100, 75, 50, and 25% N, respectively, through *Lyngbya* derived LMBR. The remaining proportion of nitrogen (i.e., 0, 25, 50, and 75% of RRF) in the respective treatments was supplemented through urea fertilizer (containing 46% N) to accomplish RRF in all the treatments except T1. The phosphorus and potassium inadvertently supplied through biomass were calculated and remaining dose was supplied through SSP and MOP to accomplish the RRF in all the treatments except T1. The biomass and chemical fertilizers were applied to the soil on the day of sowing according to the respective treatments. The crop was harvested at maturity (110th day after sowing).

Recording of Growth Parameters

Observations on growth parameters [plant height at 20, 40, 60, and 80 days after sowing (DAS), dry matter accumulation (DMA) in leaves, stem, and roots at harvest], grain yield and yield attributes (100-grain weight, number of kernel (grain) rows per cob and number of kernels per row) were recorded. Chlorophyll index of leaves at 20, 40, 60, 80, and 100 DAS was measured using Chlorophyll meter (Opti-Sciences, CCM-200). Photosynthetic rate was measured at 30 and 60 DAS by infrared gas analyzer (LI-6400XT, portable photosynthesis system, LI-COR, USA).

Enzyme Assays

Enzyme assays were carried at 60 DAS, which corresponded to 10 days pre-tasseling. Any kind of environmental stresses like nutrient or moisture deficiency at this late vegetative growth stage greatly affects the crop performance and therefore this time was chosen to assess any stress response due to the different nutrient management treatments (McWilliams et al., 1999). For carrying out enzyme assays, leaf tissues (0.1 g fresh weight) were collected at 60 DAS and homogenized using a mortar and pestle with liquid nitrogen. The tissue was then extracted with 50 mM Tris extraction buffer (pH 7.5) containing 0.2% (w/v) Triton X-100, 0.1 mM EDTA, 1 mM polymethylsulphonylfluoride, and 2 mM dithiothreitol for glutathione reductase (GR) activity. For ascorbate peroxidase (APX) assay, instead of Tris, 50 mM potassium phosphate buffer (pH 7.0) amended with 2 mM ascorbate was used for extraction. Both the homogenates were vortexed and centrifuged at $20,000 \times$ g for 30 min at $4°C$. The supernatants were collected and stored at $-80°C$ until further analysis. Protein content was estimated according to Bradford method (1976) using bovine albumin as a standard and measured using UV–Vis spectrophotometer. The APX (EC 1.11.1.1) and GR (EC 1.6.4.2) activity were measured according to Nakano and Asada (1981) and Edwards et al. (1990), respectively. The concentration of oxidized ascorbate was calculated using an extinction coefficient of 2.8 mM^{-1}cm^{-1}, while GR activity was calculated using an extinction coefficient of 6.22 M^{-1}cm^{-1} for NADPH. One unit of APX is defined as 1 mmol ascorbate oxidized per min per ml and expressed in units per mg protein. One unit of GR is defined as 1 μmol NADPH oxidized per min per ml at $25°C$ and expressed in units per mg protein.

Analytical Methods

The total nitrogen content in the grain was estimated by standard semi-micro-Kjeldahl method (Thimmaiah, 1999) and expressed in terms of crude protein using a conversion factor of 6.25 (Jones, 1941), while Na and K content was determined using flame

photometry (Flame photometer 128, Systronics, India) according to the method prescribed by Jackson (1973). Phosphorus (P) content in grains was determined by the Vanado-Molybdate yellow method (Jackson, 1973) following wet digestion with HNO_3–$HClO_4$ (10:4) di-acid mixture. Carbohydrate in grains was estimated by the method of Dubois et al. (1956). Fat content in grains was determined using petroleum ether (at 70°C) in a Soxhlet apparatus (AACC, 1987)

The available N in soil was analyzed by alkaline permanganate method (Subbiah and Asija, 1956). The available K in soil was extracted by neutral normal ammonium acetate method (Hanway and Heidel, 1952) and available P by sodium bicarbonate as per Olsen et al. (1954) and estimated by flame photometer (Flame photometer 128, Systronics, India) and spectrophotometer (Varian Cary-50 Bio, Varian Inc., USA), respectively. Organic carbon was analyzed according to the method of Walkley and Black (1934).

Statistical Analysis

The treatments were subjected to statistical analysis by analysis of variance (ANOVA) using InfoStat statistical software V 2012 (Di Rienzo et al., 2011). *Post-hoc* comparison of means was carried out using Fisher's Least Significant Difference (LSD) at the probability level of 5% and presented in the tables.

RESULTS

Effects on Growth Parameters of Maize

The plant heights recorded in different treatments at 20, 40, 60, and 80 DAS are presented in **Table 2**. The lowest plant height was recorded at all the growth stages under the absolute control treatment where no fertilizer was applied (T1). Compared to RRF, the treatment receiving N nutrition equally through LMBR from *Chlorella* and chemical source (T5) gave an initial fillip to the plant height as early as 20 DAS that was maintained significantly till 80 DAS ($P < 0.001$). However, all the treatments employing LMBR from *Lyngbya* were at par with RRF with respect to plant height at all the days of observations, except T8 at 60 DAS; however, there was no

change in the number of nodes due to any of the treatments. Interestingly, the length of the tassels formed by applying either of the LMBRs at any of the substitution rates was markedly higher than that formed under RRF ($P < 0.05$), except that in the treatments employing the lowest level of LMBR from *Chlorella* and the highest level of that from *Lyngbya,* where were at par.

Leaf chlorophyll index and net photosynthetic rates recorded at different growth stages are tabulated in **Table 3**. The chlorophyll index of LMBR treated plants was significantly higher than that of RRF only at 60 DAS ($P < 0.001$) and that also in the T4 and T5 treatments in which 75 and 50% chemical N substitution was done through LMBR from *Chlorella* and in T10 which replaced 25% of N. All these three treatments were at par. The treatment T10 maintained this advantage even at 100 DAS. T5 and T10, which recorded the highest chlorophyll index at 60 DAS using *Chlorella* and *Lyngbya* LMBR, respectively, also recorded the significantly highest net photosynthetic rate ($P < 0.001$) compared to RRF for the respective LMBR at the corresponding time of observation. Both these treatments recorded higher rate of photosynthesis at the early growth stage (30 DAS) as well, however, they were at par with T4 and T6.

The DMA in stem, leaves, and roots and their total at harvest are presented in **Table 4**. Supplying 75% of N through LMBR from *Chlorella* (T4) resulted in the maximum DMA in stem and roots which were significantly higher over RRF ($P < 0.001$). The leaf dry biomass in this treatment was nevertheless at par with RRF. However, this treatment recorded the significantly highest ($P < 0.001$) total dry matter in the vegetative parts than that in any of the other treatments. There was a marked decline in the DMA in stem and root in all the treatments receiving *Lyngbya* LMBR, although interestingly, none of them except T10 showed decline in leaf dry weight compared to RRF. This, however, resulted in overall significant decline in the total vegetative DMA, compared to RRF. Further, all the *Lyngbya* substitution treatments were found at par with respect to total DMA.

TABLE 2 | Effect of different LMBR treatments on plant height and tassel height of maize.

Treatments	Plant height (cm)				Tassel height(cm)
	20 DAS	40 DAS	60 DAS	80 DAS	
T1	21.60 ± 1.14[d]	68.40 ± 3.85[f]	102.60 ± 4.28[d]	164.60 ± 2.07[e]	34.20 ± 2.17[d]
T2	23.00 ± 1.00[c]	76.00 ± 2.85[bcde]	151.80 ± 7.09[c]	199.80 ± 4.92[bc]	37.20 ± 1.92[cd]
T3	24.80 ± 0.84[ab]	83.40 ± 6.35[a]	167.60 ± 4.98[b]	203.40 ± 7.16[bc]	40.60 ± 1.95[ab]
T4	23.20 ± 1.64[c]	78.40 ± 3.51[abc]	164.40 ± 3.36[b]	221.80 ± 12.01[a]	40.80 ± 3.70[ab]
T5	26.00 ± 1.00[a]	80.20 ± 3.17[ab]	177.60 ± 5.94[a]	225.40 ± 8.82[a]	42.60 ± 2.97[a]
T6	23.20 ± 1.30[c]	72.60 ± 5.86[def]	153.80 ± 7.79[c]	185.40 ± 7.54[d]	38.60 ± 2.97[bc]
T7	23.40 ± 1.14[c]	76.20 ± 2.59[bcde]	150.20 ± 6.76[c]	207.60 ± 10.55[b]	39.80 ± 1.79[abc]
T8	24.20 ± 0.84[bc]	77.80 ± 4.40[bcd]	163.60 ± 4.04[b]	206.80 ± 5.76[b]	41.60 ± 1.14[ab]
T9	23.80 ± 0.45[bc]	74.30 ± 3.07[cde]	151.40 ± 5.41[c]	194.40 ± 2.30[cd]	41.00 ± 2.00[ab]
T10	23.80 ± 1.10[bc]	72.00 ± 5.00[ef]	151.80 ± 3.70[c]	195.80 ± 5.63[c]	41.00 ± 3.00[ab]

Values followed by different alphabets in columns are significantly different at p < 0.05 by LSD.

TABLE 3 | Effect of different LMBR treatments on leaf chlorophyll index and photosynthesis rate of maize.

Treatments	Leaf chlorophyll index					Photosynthesis (μmole CO_2/m^{2}leaf/day)	
	20 DAS	40 DAS	60 DAS	80 DAS	100 DAS	30 DAS	60 DAS
T1	22.70 ± 3.27^e	31.48 ± 4.30^c	25.38 ± 2.47^d	24.86 ± 2.93^d	19.44 ± 4.10^f	25.45 ± 1.38^e	16.63 ± 1.13^g
T2	32.90 ± 3.65^{abc}	37.08 ± 3.52^{ab}	36.88 ± 3.60^c	47.18 ± 3.56^a	34.36 ± 3.68^{bc}	34.45 ± 2.01^{cd}	26.29 ± 1.72^f
T3	31.80 ± 4.45^{bcd}	32.72 ± 2.22^{bc}	37.12 ± 3.17^c	37.72 ± 4.83^{bc}	27.40 ± 3.30^d	33.32 ± 0.34^d	29.63 ± 1.38^{de}
T4	34.58 ± 3.33^{ab}	37.22 ± 2.74^{ab}	44.22 ± 5.73^a	36.12 ± 2.48^{bc}	36.26 ± 2.57^{ab}	41.51 ± 4.92^a	28.10 ± 1.28^e
T5	36.68 ± 2.59^a	35.34 ± 2.53^{bc}	47.24 ± 5.00^a	38.66 ± 4.95^{bc}	32.00 ± 1.60^c	40.95 ± 2.16^{ab}	30.41 ± 0.62^{cd}
T6	31.52 ± 4.69^{bcd}	36.42 ± 4.22^{abc}	43.48 ± 1.50^{ab}	41.68 ± 4.25^{ab}	35.80 ± 3.68^{abc}	41.21 ± 1.83^a	28.61 ± 2.72^e
T7	28.04 ± 3.30^d	31.44 ± 5.23^c	36.40 ± 3.63^c	37.20 ± 4.35^{bc}	24.12 ± 2.74^{de}	34.55 ± 3.06^{cd}	35.65 ± 1.54^b
T8	29.14 ± 5.17^{cd}	36.54 ± 4.86^{abc}	38.80 ± 4.82^{bc}	38.58 ± 6.45^{bc}	20.54 ± 2.17^{ef}	33.73 ± 1.46^d	31.51 ± 0.85^c
T9	28.20 ± 3.18^{cd}	31.62 ± 6.63^c	38.42 ± 4.73^{bc}	33.26 ± 5.31^c	27.76 ± 2.85^d	37.35 ± 3.07^c	27.87 ± 0.19^{ef}
T10	28.66 ± 2.78^{cd}	41.80 ± 4.22^a	45.58 ± 4.30^a	40.26 ± 2.75^b	38.52 ± 3.58^a	37.65 ± 2.82^{bc}	37.83 ± 0.91^a

Values followed by different alphabets in columns are significantly different at p < 0.05 by LSD.

TABLE 4 | Effect of different LMBR treatments on dry matter accumulation in above-ground vegetative parts and roots of maize plant.

Treatments	Dry matter accumulation (g)			
	Stem	Leaves	Root	Total
T1	82.00 ± 4.95^{cd}	79.92 ± 4.55^{bcde}	76.64 ± 8.78^{bc}	238.56 ± 9.70^{cd}
T2	86.45 ± 9.02^c	82.27 ± 3.02^{abc}	85.84 ± 7.81^b	254.56 ± 12.71^{bc}
T3	87.14 ± 6.73^{bc}	84.18 ± 11.32^{ab}	76.92 ± 5.14^{bc}	248.24 ± 18.10^{bc}
T4	109.14 ± 13.57^a	75.57 ± 3.10^{cde}	114.74 ± 13.12^a	299.45 ± 15.10^a
T5	97.61 ± 11.34^b	88.71 ± 6.16^a	72.16 ± 6.00^c	258.48 ± 18.44^b
T6	77.49 ± 5.83^{cd}	74.33 ± 5.31^{de}	75.78 ± 11.15^{bc}	227.59 ± 17.78^d
T7	81.08 ± 6.76^{cd}	81.81 ± 7.83^{abcd}	$44.003.66^d$	206.89 ± 8.16^e
T8	73.13 ± 7.16^d	75.25 ± 4.87^{cde}	52.88 ± 7.63^d	201.27 ± 14.52^e
T9	73.73 ± 10.90^d	75.83 ± 3.60^{cde}	53.24 ± 4.20^d	202.80 ± 12.88^e
T10	79.25 ± 6.40^{cd}	73.28 ± 5.29^e	47.62 ± 8.78^d	200.15 ± 17.25^e

Values followed by different alphabets in columns are significantly different at p < 0.05 by LSD.

Stress Enzymes

Preliminary studies on LMBR treated plants also revealed positive results with respect to the stress enzymes studied which was carried out with a view to assess whether the application of the LMBRs on maize plants elicit any stress response. Two key enzymes, namely, ascorbate peroxidase (APX) and glutathione reductase (GR) activities were assayed (**Figure 1**). It was found that the treatment receiving no external nutrition recorded the highest APX activity, which was significantly higher than that in RRF ($P = 0.011$). Higher APX is suggestive of greater oxidative stress. All the other LMBR treatments had significantly lower activity of this enzyme ($P \leq 0.027$) than RRF except in T3, which received N nutrition solely through LMBR of *Chlorella*. Interestingly, the APX activity decreased with decreasing dose of *Chlorella* LMBR. However, all the treatments employing LMBR of *Lyngbya* recorded significantly lower activity ($P < 0.001$) over RRF, which were at par with each other and thus was suggestive of decreased oxidative stress. GR activity was lowest in T1, which was, however, at par to RRF. Among the *Chlorella* treatments, only T5 recorded significantly higher values of GR

activity over RRF ($P = 0.015$), while the rest were at par. All the *Lyngbya* treatments except that utilizing LMBR solely as N source recorded significantly higher GR activity over RRF, the highest being in T9, which was superior to all the other nine treatments ($P < 0.001$).

Effect on Yield Attributes and Grain Yield

The length, width, fresh weight as well as the dry weight of the maize cobs with or without the outer husk remained statistically similar in all the LMBR treatments comparable to that in the RRF. Similarly, the same trend was found in number of kernel rows per cob and number of kernels (grains) per row, which determine the total number of grains formed (**Table 5**). Notably, T8 treatment that substituted 75% of chemical N by *Lyngbya* LMBR had significantly heavier grains compared to RRF ($P = 0.008$), which however was at par with all other LMBR treatments except in T7 where 100% of N was supplied by LMBR from *Lyngbya*. The highest grain weight (65.16 g plant^{-1}) was measured in T10 where 25% of the total N was supplied by *Lyngbya* derived LMBR and rest by urea, which was closely followed by that (63.48 g

plant^{-1}) measured in T5 treatment where N was supplied to the plants in equal proportion through *Chlorella* LMBR and urea. However, both these treatments were found at par with other levels of substitutions with LMBRs from either of the algae and were also equivalent to RRF. The yield and its attributes were found the lowest in the absolute control treatment where no external nutrition was supplied.

Effect on Nutritional Quality of Maize

The carbohydrate, crude protein, and crude fat in maize grains were determined and are presented in **Table 6**. The carbohydrate content was the maximum where 75% of N was supplied through LMBR of *Chlorella*. This treatment was at par to all the other combinations of *Chlorella* LMBR, but was significantly superior to RRF ($P = 0.018$) as well as all other *Lyngbya* treatments ($P \leq 0.021$). However, all the *Lyngbya* treated plants were at par with RRF treated ones. There was no change in crude protein content in grains due to either of the two LMBR treatments as compared to that in RRF. All the algal biomass treated plants were equivalent with respect to crude fat content, except T3 where 100% N was supplied through *Chlorella* derived LMBR. With respect to nutritional quality, it was found that there was no change in nitrogen content of the grains due to any of the LMBR treatments when compared to RRF. Compared to RRF, T3, and T10 had the significantly ($P < 0.05$) highest phosphorus content in the *Chlorella* and *Lyngbya* derived LMBR treatments, respectively. However, all the LMBR treatments were at par with each other with respect to P content in grains. Compared to RRF, there was significantly ($P < 0.001$) higher potassium uptake in grains in all the LMBR treatments except where N was entirely supplied through *Chlorella* derived LMBR. There was a marked increase in sodium as well as potassium content of grains in T10 treatment when compared to that in RRF.

Effects on Physico-chemical Properties of Soil at Harvest

The changes in physico-chemical properties brought out due to the various treatments are presented in **Table 7**. It was found that there was no significant difference in pH, EC, organic carbon, and available N content in the LMBR treated soil when compared to RRF treated ones. Other than the treatments supplying 100% (T3) and 75% (T4) N through *Chlorella* derived LMBR, all other treatments were at par to RRF with respect to available P content. The two aforesaid treatments were significantly ($P \leq 0.006$) better than all other treatments, but at par with each other. T4 and T5 in case of *Chlorella* based LMBR and T8 and T10 in case of *Lyngbya* based LMBR treatments recorded significantly lower available K in soil at harvest, while all other treatments were at par with RRF.

DISCUSSION

Among the LMBR from the two algal species, *Chlorella* derived one apparently was found to be more responsive in improving the plant height as no response was found through LMBR from *Lyngbya* when compared to RRF (**Table 2**). Nitrogen nutrition
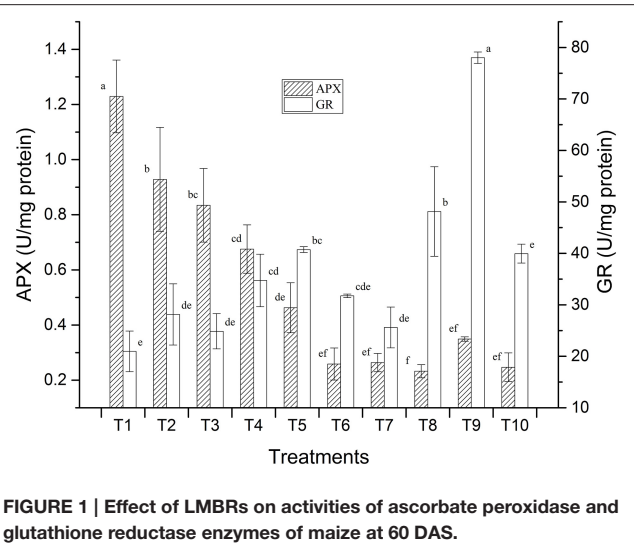
FIGURE 1 | Effect of LMBRs on activities of ascorbate peroxidase and glutathione reductase enzymes of maize at 60 DAS.

TABLE 5 | Effect of different LMBR treatments on yield attributes and grain yield of maize.

Treatments	Grains dry weight per plant (g)	100 grains dry weight (g)	Length of kernel set on cob (cm)	No of kernels line on cob	No of kernels per line
T1	40.99 ± 6.11[b]	8.06 ± 1.81[c]	13.73 ± 2.90[b]	14.40 ± 2.61[b]	30.47 ± 0.90[b]
T2	61.21 ± 10.84[a]	8.60 ± 0.86[bc]	18.96 ± 2.33[a]	16.00 ± 0.00[ab]	32.13 ± 14.10[ab]
T3	60.36 ± 5.26[a]	9.63 ± 0.87[ab]	17.82 ± 1.69[ab]	16.80 ± 1.10[a]	40.40 ± 4.25[ab]
T4	59.20 ± 3.58[a]	10.05 ± 1.68[ab]	17.56 ± 2.94[ab]	14.80 ± 2.28[ab]	38.80 ± 8.13[ab]
T5	63.48 ± 4.45[a]	10.02 ± 0.74[ab]	18.25 ± 1.49[a]	16.00 ± 1.41[ab]	39.87 ± 3.20[ab]
T6	55.70 ± 11.33[a]	9.94 ± 1.38[ab]	15.67 ± 3.46[ab]	15.60 ± 0.89[ab]	34.40 ± 7.95[ab]
T7	56.29 ± 13.34[a]	9.11 ± 0.86[bc]	16.61 ± 2.85[ab]	16.40 ± 1.67[ab]	36.20 ± 6.30[ab]
T8	64.93 ± 3.68[a]	10.68 ± 0.72[a]	18.25 ± 7.38[a]	15.60 ± 0.89[ab]	32.87 ± 13.01[ab]
T9	60.46 ± 6.92[a]	10.05 ± 1.32[ab]	17.62 ± 1.81[ab]	15.60 ± 1.67[ab]	39.53 ± 5.74[ab]
T10	65.16 ± 9.45[a]	9.67 ± 0.91[ab]	18.91 ± 1.96[a]	15.60 ± 1.67[ab]	41.00 ± 3.54[a]

Values followed by different alphabets in columns are significantly different at p < 0.05 by LSD.

TABLE 6 | Effect of different LMBR treatments on nutritional quality of maize.

Treatments	Carbohydrate (%)	Crude protein (%)	Crude fat (%)	Nitrogen (%)	Phosphorus (%)	Potassium (%)	Sodium (%)
T1	57.19 ± 2.06[cd]	8.73 ± 1.46[b]	10.57 ± 0.82[c]	1.40 ± 0.23[b]	0.28 ± 0.06[ab]	0.51 ± 0.08[bc]	0.039 ± 0.014[c]
T2	57.97 ± 3.23[bcd]	9.02 ± 0.91[ab]	10.63 ± 1.30[bc]	1.44 ± 0.15[ab]	0.18 ± 0.05[b]	0.33 ± 0.02[d]	0.043 ± 0.010[c]
T3	60.68 ± 3.67[abc]	11.27 ± 3.76[a]	11.82 ± 0.98[a]	1.80 ± 0.60[a]	0.39 ± 0.41[a]	0.27 ± 0.10[d]	0.046 ± 0.012[c]
T4	63.21 ± 3.59[a]	9.85 ± 0.87[ab]	11.26 ± 0.78[abc]	1.58 ± 0.14[ab]	0.28 ± 0.03[ab]	0.44 ± 0.09[c]	0.048 ± 0.025[bc]
T5	61.49 ± 4.78[ab]	9.68 ± 1.20[ab]	11.26 ± 0.78[abc]	1.55 ± 0.19[ab]	0.28 ± 0.05[ab]	0.56 ± 0.04[ab]	0.044 ± 0.004[c]
T6	60.47 ± 1.54[abc]	9.62 ± 1.02[ab]	11.30 ± 0.97[abc]	1.54 ± 0.16[ab]	0.35 ± 0.12[ab]	0.58 ± 0.06[ab]	0.047 ± 0.004[bc]
T7	58.08 ± 3.45[bcd]	9.59 ± 2.36[ab]	11.05 ± 0.85[abc]	1.53 ± 0.38[ab]	0.36 ± 0.14[ab]	0.58 ± 0.11[ab]	0.044 ± 0.005[c]
T8	57.02 ± 4.06[cd]	9.31 ± 0.75[ab]	11.75 ± 0.59[ab]	1.49 ± 0.12[ab]	0.30 ± 0.06[ab]	0.52 ± 0.02[abc]	0.042 ± 0.006[c]
T9	57.24 ± 1.84[bcd]	9.71 ± 1.82[ab]	11.53 ± 0.90[abc]	1.55 ± 0.29[ab]	0.28 ± 0.05[ab]	0.52 ± 0.02[abc]	0.078 ± 0.013[a]
T10	53.92 ± 3.90[d]	10.28 ± 2.47[ab]	11.07 ± 0.75[abc]	1.64 ± 0.40[ab]	0.41 ± 0.22[a]	0.62 ± 0.16[a]	0.062 ± 0.004[b]

Values followed by different alphabets in columns are significantly different at p < 0.05 by LSD.

TABLE 7 | Effect of different LMBR treatments on physico-chemical properties of soil at harvest.

Treatments	Moisture (%)	pH	EC (dS/m)	Available N (g/kg)	Available P (g/kg)	Available K (g/kg)	Organic carbon (%)
T1	15.89 ± 1.65[a]	7.69 ± 0.24[a]	1.14 ± 0.12[b]	0.13 ± 0.03[b]	0.03 ± 0.01[bc]	0.39 ± 0.06[a]	0.20 ± 0.03[a]
T2	13.24 ± 2.30[b]	7.47 ± 0.17[a]	1.29 ± 0.24[ab]	0.12 ± 0.02[b]	0.05 ± 0.02[b]	0.40 ± 0.06[a]	0.15 ± 0.04[b]
T3	13.68 ± 1.82[ab]	7.58 ± 0.15[a]	1.56 ± 0.27[a]	0.13 ± 0.05[b]	0.08 ± 0.03[a]	0.39 ± 0.11[a]	0.20 ± 0.03[ab]
T4	13.78 ± 0.95[ab]	7.59 ± 0.22[a]	1.32 ± 0.24[ab]	0.13 ± 0.04[b]	0.08 ± 0.02[a]	0.29 ± 0.01[b]	0.18 ± 0.03[ab]
T5	15.00 ± 2.43[ab]	7.66 ± 0.42[a]	1.19 ± 0.20[b]	0.15 ± 0.04[b]	0.03 ± 0.02[bc]	0.29 ± 0.05[b]	0.19 ± 0.03[ab]
T6	13.83 ± 3.75[ab]	7.63 ± 0.21[a]	1.25 ± 0.10[b]	0.15 ± 0.03[b]	0.03 ± 0.01[bc]	0.34 ± 0.08[ab]	0.19 ± 0.02[ab]
T7	13.64 ± 1.43[ab]	7.63 ± 0.26[a]	1.24 ± 0.21[b]	0.16 ± 0.10[b]	0.02 ± 0.01[b]	0.31 ± 0.09[ab]	0.16 ± 0.06[ab]
T8	15.37 ± 0.81[ab]	7.79 ± 0.21[a]	1.32 ± 0.38[ab]	0.41 ± 0.24[a]	0.03 ± 0.01[b]	0.36 ± 0.08[b]	0.18 ± 0.02[ab]
T9	13.44 ± 1.39[ab]	7.76 ± 0.23[a]	1.29 ± 0.22[ab]	0.14 ± 0.05[b]	0.02 ± 0.00[b]	0.34 ± 0.08[ab]	0.17 ± 0.05[ab]
T10	14.50 ± 1.22[ab]	7.76 ± 0.39[a]	1.30 ± 0.27[ab]	0.26 ± 0.18[b]	0.04 ± 0.02[bc]	0.29 ± 0.04[b]	0.19 ± 0.03[ab]

Values followed by different alphabets in columns are significantly different at p < 0.05 by LSD.

derived equally from both organic and chemical sources seemed to be the best balanced dose that sustained higher plant height relative to RRF starting from as early as 20 DAS till 80 DAS. It was observed that substitution of 100–50% of total N (T3–T5) through *Chlorella* LMBR treatments maintained the plant height at par with RRF or was even higher until 60 DAS. However, lowest rate of substitution in T6 (25%) brought about a diminution suggesting the role of the algal biomass toward sustained supply of nutrients or other active factors to the plants.

With respect to total DMA in the above ground vegetative parts and roots, contrasting results were found between LMBR from *Chlorella* and *Lyngbya* (**Table 4**). Whereas, 100 to 50% N substitutions through *Chlorella* biomass resulted in higher or equivalent DMA, similar levels of substitution by *Lyngbya* resulted in significant decrease when compared to that in RRF, suggesting the presence of one or more factor in the latter that are responsible for diminution of growth. Substitution of 25% N through either of the LMBR invariably brought a significant decrease in the aforesaid total DMA, connoting the requirement of *Chlorella* in higher amounts and confirming the retardant activity of LMBR from *Lyngbya* even at lower doses of substitution. The differential response between the two algal LMBRs might be on the account of their composition, which thus needs to be fully unraveled. This may indicate the presence of

some toxic ingredients in *Lyngbya* species that negatively affect the plant growth. There are reports of toxicity of the microalgal extracts affecting the growth of plants (Romanowska-Duda and Tarczyñska, 2002) thus validating the argument (Grzesik and Romanowska-Duda, 2015) that untested algal residues should not be employed for treatment on plants.

Interestingly, there was no decrease in DMA in leaf due to the *Lyngbya* treatments except that in T10 where least level of substitution (25%) was done, which was also equivalent to all the other *Lyngbya* treatments. T4 fared the best among all the treatments for total DMA which could be primarily attributed to increase in stem and root biomass, while T5 formed the highest leaf biomass, which was although similar to that in RRF. The highest plant height and leaf biomass found in the LMBR treatment using biomass of *Chlorella* in equal proportion as chemical N (T5) at 60 DAS can be well-corroborated by the leaf chlorophyll index and net photosynthetic rate recorded during this time (**Table 3**), which were found to be the highest among all the *Chlorella* treatments and significantly superior to RRF. Notably, in spite of lower DMA in the vegetative biomass in all the *Lyngbya* treatments, compared to RRF, there was no significant decrease in net photosynthetic rate at the leaf level, as evident from its values recorded at 30 and 60 DAS (**Table 3**). Rather, it was significantly higher than all other treatments at

60 DAS. This treatment also showed the best chlorophyll index among all the *Lyngbya* LMBR treatments at all the times and was significantly higher than RRF before (60 DAS) as well as after tasseling stage (100 DAS) of the plant. Grzesik and Romanowska-Duda (2015) also similarly reported intensification of several metabolic processes such as net photosynthesis and other gas exchange parameters, stability of cytomembranes which eventually led to enhanced shoot and root dry weight of willow plants by application of sonicated biomass of two species of Cyanobacteria (*Microcystis* sp. and *Anabaena* sp.) and one green algae (*Chlorella* sp.).

Thus, the observations recorded on plant height, leaf chlorophyll index, net photosynthetic rate and above ground vegetative DMA in the treatments using LMBR from *Chlorella* suggest that any level of substitution resulted in either maintaining the growth parameters or improving it in some of the treatments. This possibly explained for the equivalent grain yield obtained from all the *Chlorella* derived LMBR treatments, compared to RRF. Besides, microalgae, which itself is photosynthetic, have all the plant essential elements in its biomass (**Table 1**) which are left in the residue after oil extraction and upon decomposition are available to the plants fertilized with it. Even though there was a detrimental effect on the total DMA by using LMBR from *Lyngbya* (**Table 4**), the maintenance of similar or higher photosynthetic rate leading to attainment of similar leaf biomass might have resulted in better partitioning of photosynthates to the grains, thus explaining for the similar grain yields despite the mentioned limitations. Evidently, even though the grain yield of maize was found similar to RRF in all the LMBR treatments, irrespective of the species of algae it was derived from, there were differences in the quality of grains due to the different treatments (**Table 6**). Whereas, there was no change in the protein content, T4 was nutritionally superior in terms of carbohydrate content, while T3 was superior with respect to fat and phosphorus content when compared over RRF. T10 was superior in terms of P, K as well as Na content when compared to RRF.

Strikingly, it was found that all the LMBR treatments except T3 had marked enhancement in the potassium content. Potassium has a prominent role in imparting stress tolerance in plants (Zörb et al., 2014). Another notable observation was that all the LMBR treatments exhibited a significantly longer tassel compared to that in RRF except that in T6 and T7, which were also numerically superior (**Table 1**). A longer tassel has been reported to be desirable under stress environment to ensure sufficient and extended pollen availability (Sofi, 2007). Even though the plants in the present experiment were not subjected to any specific stress, nevertheless, plants do experience biotic and abiotic stress, even at different times of the day during its growth and reproductive phase when grown under uncontrolled conditions (Layek et al., 2015). Such stress may be due to temperature extremities during day or night, incipient wilting during mid-day, variation in soil moisture, pest attack, etc., all of which could induce instantaneous production of reactive oxygen species (ROS). The results obtained from our studies on ROS scavengers like APX suggests that LMBRs may also be important for imparting tolerance under environmental stress

and may be explored in the future on this aspect. The presence of bioelicitors in the LMBRs may also be explored which can perhaps trigger plant defense pathways in response to biotic and abiotic stresses. Such elicitors have been reported in other green algae like *Ulva lactuca* (Grzesik and Romanowska-Duda, 2015).

Evidently, no detrimental effect was found in the pH and EC of the soil due to the various LMBR treatments (**Table 7**). Although, there was no change in organic carbon content of soil, continuous application of the carbon rich LMBR may have a significant beneficial effect in the long run. The treatments employing 100% (T3) and 75% (T4) N through *Chlorella*-derived LMBR had a striking effect in improving available phosphorus in soil which may be ascribed to the improved microbial and associated biochemical activity of such carbonaceous materials (Anand et al., 2015). Interestingly, T3 also had the highest P content in the grains, all of which connote toward greater mineralization of soil phosphorus and also the higher mobilization of phosphorus to the grains of soil, which needs to be investigated in future. Grzesik and Romanowska-Duda (2014) recently reported that application of microalgal residues to corn plants significantly enhanced the activity of phosphatase enzyme, which is responsible for distribution of P in plants. The use of LMBR may also confer another advantage by preventing the loss of soil nutrients by way of leaching or volatilization, thus being a sustainable release nutrient source. Mulbry et al. (2005) reported that only 3% of algal N was present as plant available N in soil at the time of application of dried algal biomass (day 0). Similar to our studies, they also found that dried algal biomass was equivalent to fertilizer in supplying N and P to cucumber and corn. It was further conjectured that NH_3 volatilization would not occur by use of dried algal biomass as manure in contrast to the use of chemical fertilizers.

Chemical solvent extraction is the most common method to effectively extract lipids from algae cells, but use of solvents like n-hexane and electric power, makes the cost of oil production high. In our case, LMBR was produced on a smaller scale for the purpose of conducting pot experiments. Other methods like wet extraction (Reddy et al., 2014), supercritical fluid technologies using CO_2 (Halim et al., 2011), milking extraction methods (Kleinegris et al., 2010) are emerging as newer technologies for lipid extraction that would considerably economize on the cost and energy requirement. Even though efforts to extract the microalgal lipids and recover the solvent used has been recently demonstrated by using solar driven solvent extractor (Ghosh et al., 2013), nevertheless, it is extremely important that the algal residue obtained after extraction of the main product (oil) should be used in a biorefinery approach, which was the primary objective of the study. We found that the LMBRs deserved proper exploitation as fertilizer substitute as they are rich in plant nutrients. Considering the state of the art of algal production and post-harvest technology, the current production of biofuel from microalgae is technically feasible, but its economic feasibility is still a major challenge (Chiaramonti et al., 2015). The results of the present experiment applying the biorefinery concept to valorize the LMBR as a plant nutrient source is one of the ways to achieve economic sustainability of algal biofuel.

In view of promising results and due to the limited information available in the literature on this aspect of worldwide interest, further studies are required to evaluate the effect of the use of LMBRs on crop plants over the long term and understand the mechanism of action as well. The effects of LMBRs on soil microbial and biochemical properties, which have bearing on the nutrient cycle, also need to be studied in the future. Other active ingredients or anti-nutrients present in LMBRs also need to be characterized.

CONCLUSION

In the present study, nitrogen-rich LMBRs of two microalgal species, namely, *Chlorella* and *Lyngbya* were utilized to substitute for the chemical nitrogen fertilizer requirement of maize plants in different proportions viz., 100, 75, 50, and 25%. The grain yield obtained using either of the LMBRs were equivalent to that under treatment employing RRF solely through chemical fertilizers. Even though LMBR of *Lyngbya* resulted in diminution of the stem and root biomass, there was no reduction observed in the formation of leaf biomass and photosynthetic rate as a result of which the translocation of assimilates from the source to sink was maintained and similar grain yields to that in RRF were obtained using it. Substitution of 75% of the total chemical N through *Chlorella* LMBR (T4) resulted in the highest DMA in above-ground vegetative biomass and roots and this treatment also recorded the highest grain carbohydrate content, all of which were significantly superior to that in RRF. Among the *Lyngbya* treatments, substitution at 25% level (T10) was found to be the best in terms of grain yield production as well as phosphorus

and potassium content in grains, while carbohydrate, protein as well as fat content were found at par with RRF. Decreased APX enzyme activity, indicative of lower plant stress was also apparent in most of the LMBR treatments. There was also no detrimental effect of the various LMBR treatments on soil properties. Based on the results, it is concluded that both of the LMBRs can substitute, wholly or partially, the chemical nitrogen fertilizer without affecting the yield and quality of the maize crop, thereby reducing the usage of chemical fertilizers in agriculture and simultaneously making gainful use of the LMBRs generated during biodiesel preparation. The results obtained from the present study thus helps to valorize the LMBR in the commodity markets, thereby advancing toward the economic sustainability of algae production for biofuels.

REFERENCES

AACC (1987). *Approved Methods of the AACC*. St Paul, MN: American Association of Cereal Chemists Inc.

Anand, K. G. V., Kubavat, D., Trivedi, K., Agarwal, P. K., Wheeler, C., and Ghosh, A. (2015). Long-term application of *Jatropha* press cake promotes seed yield by enhanced soil organic carbon accumulation, microbial biomass and enzymatic activities in soils of semi-arid tropical wastelands. *Eur. J. Soil Biol.* 69, 57–65. doi: 10.1016/j.ejsobi.2015.05.005

Bradford, M. M. (1976). A rapid and sensitive method for the quantitation of microgram quantities of protein utilizing the principle of protein-dye binding. *Anal. Biochem.* 72, 248–254. doi: 10.1016/0003-2697(76)90527-3

Bryant, H. L., Gogichaishvili, I., Anderson, D., Richardson, J. W., Sawyer, J., Wickersham, T., et al. (2012). The value of post-extracted algae residue. *Algal Res.* 1, 185–193. doi: 10.1016/j.algal.2012.06.001

Chiaramonti, D., Tredici, M. R., Prussi, M., and Biondi, N. (2015). *Algae Biofuels. Handbook of Clean Energy Systems*. New Jersey: John Wiley & Sons, Ltd.

Chisti, Y. (2007). Biodiesel from microalgae. *Biotechnol. Adv.* 25, 294–306. doi: 10.1016/j.biotechadv.2007.02.001

Di Rienzo, J. A., Casanoves, F., Balzarini, M. G., Gonzalez, L., Tablada, M., and Robledo, Y. C. (2011). *InfoStat Versión 2011. Grupo InfoStat, FCA*. Universidad Nacional de Córdoba, Argentina. Available online at: http://www.infostat.com.ar

Dubois, M., Gilles, K. A., Hamilton, J. K., Rebers, P. A., and Smith, F. (1956). Colorimetric method for determination of sugars and related substances. *Anal. Chem.* 28, 350–356. doi: 10.1021/ac60111a017

Edwards, E. A., Rawsthorne, S., and Mullineaux, P. M. (1990). Subcellular distribution of multiple forms of glutathione reductase in leaves of pea (*Pisum sativum* L.). *Planta* 180, 278–284. doi: 10.1007/BF00194008

Gao, M. T., Shimamura, T., Ishida, N., and Takahashi, H. (2012). Investigation of utilization of the algal biomass residue after oil extraction to lower the total production cost of biodiesel. *J. Biosci. Bioeng.* 114, 330–333. doi: 10.1016/j.jbiosc.2012.04.002

Ghosh, A. (2012). Indra's net and the midas touch: living sustainably in a connected world. *Int. J. Environ. Stud.* 69, 859–863. doi: 10.1080/00207233.2012.705079

Ghosh, A. (2014). Plane truth: aviation's real impact on people and the environment. *Int. J. Environ. Stud.* 71, 888–898. doi: 10.1080/00207233.2014.964063

Ghosh, A., Chaudhary, D. R., Reddy, M. P., Rao, S. N., Chikara, J., Pandya, J. B., et al. (2007). Prospects for *Jatropha* methyl ester (biodiesel) in India. *Int. J. Environ. Stud.* 64, 659–674. doi: 10.1080/00207230701766499

Ghosh, P. K., Mishra, S., Maiti, S., Paliwal, C., Mishra, S. K., Ghosh, T., et al. (2013). *Solar Driven Solvent Extractor and Process for Extraction of Microalgal Lipids Using the Same*. U.S. Patent No 14/389,824. Alexandria, VA: USPTO.

Grzesik, M., and Romanowska-Duda, Z. (2014). Improvements in germination, growth, and metabolic activity of corn seedlings by grain conditioning and root application with cyanobacteria and microalgae. *Pol. J. Environ. Stud.* 23, 1147–1153. Available online at: http://www.pjoes.com/pdf/23.4/Pol.J.Environ.Stud.Vol.23.No.4.1147-1153.pdf

Grzesik, M., and Romanowska-Duda, Z. (2015). Ability of cyanobacteria and green algae to improve metabolic activity and development of willow plants. *Pol. J. Environ. Stud.* 24, 1003–1012. doi: 10.15244/pjoes/34667

Halim, R., Gladman, B., Danquah, M. K., and Webley, P. A. (2011). Oil extraction from microalgae for biodiesel production. *Bioresour. Technol.* 102, 178–185. doi: 10.1016/j.biortech.2010.06.136

Hanway, J. J., and Heidel, H. (1952). Soil analysis methods as used in Iowa state college soil testing laboratory. *Iowa Agric.* 57, 1–31.

Jackson, M. L. (1973). *Soil Chemical Analysis*. New Delhi: Prentice Hall of India Pvt. Ltd.

Jones, D. B. (1941). *Factors for Converting Percentages of Nitrogen in Foods and Feeds into Percentages of Proteins*. Washington, DC: US Department of Agriculture.

Kleinegris, D. M., Janssen, M., Brandenburg, W. A., and Wijffels, R. H. (2010). The selectivity of milking of *Dunaliella salina*. *Marine Biotechnol.* 12, 14–23. doi: 10.1007/s10126-009-9195-0

Layek, J., Das, A., Ramkrushna, G. I., Trivedi, K., Yesuraj, D., Chandramohan, M., et al. (2015). Seaweed sap: a sustainable way to improve productivity of maize in North-East India. *Int. J. Environ. Stud.* 72, 305–315. doi: 10.1080/00207233.2015.1010855

Mata, T. M., Martins, A. A., and Caetano, N. S. (2010). Microalgae for biodiesel production and other applications: a review. *Renew. Sustain. Energy Rev.* 14, 217–232. doi: 10.1016/j.rser.2009.07.020

Maurya, R., Ghosh, T., Paliwal, C., Shrivastav, A., Chokshi, K., Pancha, I., et al. (2014). Biosorption of methylene blue by de-oiled algal biomass: equilibrium, kinetics and artificial neural network modelling. *PLoS ONE* 9:e109545. doi: 10.1371/journal.pone.0109545

McWilliams, D. A., Berglund, D. R., and Endres, G. J. (1999). *Corn Growth and Management Quick Guide*. North Dakota State University and University of Minnesota. A-1173.

Metting, B., and Rayburn, W. R. (1983). The influence of a microalgal conditioner on selected Washington soils: an empirical study. *Soil Sci. Soc. Am. J.* 47, 682–685. doi: 10.2136/sssaj1983.03615995004700040015x

Mishra, S. C. P., Ghosh, P. K., Gandhi, M. R., Bhattacharya, S., Maiti, S., Upadhyay, S. C., et al. (2012). *Engine Worthy Fatty Acid Methyl Ester (biodiesel) from Naturally Occuring Marine Microalgal Mats and Marine Microalgae Cultured in Open Salt Pans Together with Value Addition of Co-products*. U.S. Patent No US20140099684 A1. Alexandria, VA: USPTO.

Mulbry, W., Westhead, E. K., Pizarro, C., and Sikora, L. (2005). Recycling of manure nutrients: use of algal biomass from dairy manure treatment as a slow release fertilizer. *Bioresour. Technol.* 96, 451–458. doi: 10.1016/j.biortech.2004.05.026

Nakano, Y., and Asada, K. (1981). Hydrogen peroxide is scavenged by ascorbate-specific peroxidase in spinach chloroplasts. *Plant Cell Physiol.* 22, 867–880.

Olsen, S. R., Cole, C. V., Watanabe, F. S., and Dean, L. A. (1954). Estimation of available phosphorus in soils by extraction with sodium bicarbonate. *USDA Circular*, 939.

Pfromm, P. H., Amanor-Boadu, V., and Nelson, R. (2011). Sustainability of algae derived biodiesel: a mass balance approach. *Bioresour. Technol.* 102, 1185–1193. doi: 10.1016/j.biortech.2010.09.050

Rashid, N., Rehman, M. S. U., and Han, J. I. (2013). Recycling and reuse of spent microalgal biomass for sustainable biofuels. *Biochem. Eng. J.* 75, 101–107. doi: 10.1016/j.bej.2013.04.001

Reddy, H. K., Muppaneni, T., Patil, P. D., Ponnusamy, S., Cooke, P., Schaub, T., et al. (2014). Direct conversion of wet algae to crude biodiesel under supercritical ethanol conditions. *Fuel* 115, 720–726. doi: 10.1016/j.fuel.2013.07.090

Rodolfi, L., Chini Zittelli, G., Bassi, N., Padovani, G., Biondi, N., Bonini, G., et al. (2009). Microalgae for oil: strain selection, induction of lipid synthesis and outdoor mass cultivation in a low-cost photobioreactor. *Biotechnol. Bioeng.* 102, 100–112. doi: 10.1002/bit.22033

Romanowska-Duda, Z., and Tarczyńska, M. (2002). The influence of microcystin-LR and hepatotoxic cyanobacterial extract on the water plant

Spirodela oligorrhiza. Environ. Toxicol. 17, 434–440. doi: 10.1002/tox. 10076

Scott, S. A., Davey, M. P., Dennis, J. S., Horst, I., Howe, C. J., Lea-Smith, D. J., et al. (2010). Biodiesel from algae: challenges and prospects. *Curr. Opin. Biotechnol.* 21, 277–286. doi: 10.1016/j.copbio.2010.03.005

Singh, S., Singh, M. K., Pal, S. K., Trivedi, K., Yesuraj, D., Singh, C. S., et al. (2015). Sustainable enhancement in yield and quality of rain-fed maize through *Gracilaria edulis* and *Kappaphycus alvarezii* seaweed sap. *J. Appl. Phycol.* doi: 10.1007/s10811-015-0680-8. [Epub ahead of print].

Sofi, P. A. (2007). Genetic analysis of tassel and ear characters in maize (*Zea mays* L.) using triple test cross. *Asian J. Plant Sci.* 6, 881–883. doi: 10.3923/ajps.2007.881.883

Studt, T. (2010). Algae promise biofuel solutions. *INFORM* 21, 319–324.

Subbiah, B. V., and Asija, G. L. (1956). A rapid procedure for the estimation of available nitrogen in soil. *Curr. Sci.* 25, 259–260.

Thimmaiah, S. K. (1999). *Standard Methods of Biochemical Analysis*. New Delhi: Kalyani Publishers.

Toth, S. J., Prince, A. I., Wallace, A., and Mikkelsen, D. S. (1948). Rapid quantitative determination of eight mineral elements in plant tissues by a systematic procedure involving use of a flame photometer. *Soil Sci.* 66, 459–466. doi: 10.1097/00010694-194812000-00006

Vance, C. P. (2001). Symbiotic nitrogen fixation and phosphorus acquisition. Plant nutrition in a world of declining renewable resources. *Plant Physiol.* 127, 390–397. doi: 10.1104/pp.010331

van Wychen, S., and Laurens, L. M. L. (2013). *Determination of Total Solids and Ash in Algal Biomass. Laboratory Analytical Procedure*. Colorado: Technical Report. NREL/TP-5100–60956

Verdelho, V. (2013). "European projects and ventures for large-scale algae biomass production" in *1st LIMBAC* (Lisbon).

Walkley, A. J., and Black, C. A. (1934). An examination of the method for determining soil organic matter and a proposed modification of the chromic acid titration method. *Soil Sci.* 37, 29–38. doi: 10.1097/00010694-193401000-00003

Zittelli, G. C., Biondi, N., Rodolfi, L., and Tredici, M. R. (2013b). "Photobioreactors for mass production of microalgae," in *Handbook of Microalgal Culture. Applied Phycology and Biotechnology, 2nd Edn.*, eds A. Richmond and Q. Hu (Chichester: Wiley Blackwell), 225–266.

Zittelli, G. C., Rodolfi, L., Bassi, N., Biondi, N., and Tredici, M. R. (2013a). "Photobioreactors for microalgal biofuel production," in *Algae for Biofuels and Energy*, eds M. A. Borowitzka and N. R. Moheimani (Dordrecht: Springer), 115–132.

Zörb, C., Senbayram, M., and Peiter, E. (2014). Potassium in agriculture-status and perspectives. *J. Plant physiol.* 171, 656–669. doi: 10.1016/j.jplph.2013.08.008

Astaxanthin-Producing Green Microalga *Haematococcus pluvialis*: From Single Cell to High Value Commercial Products

Md. Mahfuzur R. Shah[1], Yuanmei Liang[1], Jay J. Cheng[1,2] and Maurycy Daroch[1]*

[1] School of Environment and Energy, Peking University, Shenzhen Graduate School, Shenzhen, China, [2] Department of Biological and Agricultural Engineering, North Carolina State University, Raleigh, NC, USA

Many species of microalgae have been used as source of nutrient rich food, feed, and health promoting compounds. Among the commercially important microalgae, *Haematococcus pluvialis* is the richest source of natural astaxanthin which is considered as "super anti-oxidant." Natural astaxanthin produced by *H. pluvialis* has significantly greater antioxidant capacity than the synthetic one. Astaxanthin has important applications in the nutraceuticals, cosmetics, food, and aquaculture industries. It is now evident that, astaxanthin can significantly reduce free radicals and oxidative stress and help human body maintain a healthy state. With extraordinary potency and increase in demand, astaxanthin is one of the high-value microalgal products of the future.This comprehensive review summarizes the most important aspects of the biology, biochemical composition, biosynthesis, and astaxanthin accumulation in the cells of *H. pluvialis* and its wide range of applications for humans and animals. In this paper, important and recent developments ranging from cultivation, harvest and postharvest bio-processing technologies to metabolic control and genetic engineering are reviewed in detail, focusing on biomass and astaxanthin production from this biotechnologically important microalga. Simultaneously, critical bottlenecks and major challenges in commercial scale production; current and prospective global market of *H. pluvialis* derived astaxanthin are also presented in a critical manner. A new biorefinery concept for *H. pluvialis* has been also suggested to guide toward economically sustainable approach for microalgae cultivation and processing. This report could serve as a useful guide to present current status of knowledge in the field and highlight key areas for future development of *H. pluvialis* astaxanthin technology and its large scale commercial implementation.

Keywords: *Haematoccocus pluvialis*, astaxanthin, nutraceuticals, algae cultivation and processing, biorefinery

INTRODUCTION

"Green microalgae" comprise more than 7000 species growing in a variety of habitats. *Haematococcus pluvialis* (Chlorophyceae, Volvocales) is unicellular fresh water microalga distributed in many habitats worldwide. It is considered as the best natural source of astaxanthin and the main producing organism of this commercial product

(Lorenz, 1999; Ranga Rao et al., 2010). Astaxanthin (3,3'-dihydroxy-ß-carotene-4,4'-dione) is a bright red secondary carotenoid from the same family as lycopene, lutein, and β-carotene, synthesized *de novo* by some microalgae, plants, yeast, bacteria, and present in many of our favored seafood including salmon, trout, red sea bream, shrimp, lobster, and fish eggs (Higuera-Ciapara et al., 2006; Ranga Rao et al., 2014). Astaxanthin contains two chiral centers and can exist in three different stereoizomers, (3*S*, 3'*S*); (3*R*, 3'*S*), and (3*R*, 3'*R*). The ratio of 1:2:1 of these isomers is obtained during chemical synthesis of this compound. *H. pluvialis* biosynthesizes predominantly the 3*S*, 3'*S* stereoisomer, the most valuable one (Yang et al., 2013; Al-Bulishi et al., 2015). Astaxanthin synthesis in *H. pluvialis* is directly correlated in space and time with deposition of cellular reserves in lipid droplets under conditions of cellular stress (Solovchenko, 2015). From biochemical perspective astaxanthin is synthesized through carotenoid pathway from glyceraldehyde-3-phosphate and pyruvate. Both of these compounds are products of photosynthesis and/or glycolysis depending on cultivation conditions. These two key metabolic intermediates then enter non-mevalonate (MEP) pathway to generate IPP—key intermediate for the synthesis of all carotenoids including astaxanthin. Astaxanthin has a wide range of applications in the food, feed, cosmetic, aquaculture, nutraceutical, and pharmaceutical industries because of its free radical scavenging capacity. In terms of antioxidant activity astaxanthin is 65 times more powerful than vitamin C, 54 times stronger than β-carotene, 10 times more potent than β-carotene, canthaxantin, zeaxanthin, and lutein; and 100 times more effective than α-tocopherol (Miki, 1991; Borowitzka, 2013; Koller et al., 2014; Pérez-López et al., 2014; Cyanotech, 2015). Currently, over 95% of the astaxanthin available in the market is produced synthetically; while *H. pluvialis* derived natural astaxanthin corresponds to <1% of the commercialized quantity (Koller et al., 2014). Synthetic astaxanthin, synthesized from asta-C_{15} -triarylphosphonium salt and the C_{10} -dialdehyde in a Wittig reaction (Krause et al., 1997), has 20 times lower antioxidant capacity than its natural counterpart and to date has not been approved for human consumption (Lorenz and Cysewski, 2000; Koller et al., 2014). Moreover, there are concerns about the safety of using synthetic astaxanthin for direct human consumption due to both different stereochemistry and potential carryover of synthesis intermediates. These concerns make natural astaxanthin from *H. pluvialis* a preferred choice for high-end markets (Li et al., 2011). In addition, *H. pluvialis* has been already approved as a color additive in salmon feeds and as a dietary-supplement ingredient for human consumption in the USA, Japan, and several European countries (Yuan et al., 2011). Nevertheless, there is no EFSA (European Food Safety Authority) approval for the therapeutic application so far. Supercritical CO_2 extracts from *H. pluvialis* have been granted "novel food" Status by the UK Food Standards Agency (FSA), whilst US FDA (Food and Drug Administration) granted astaxanthin from *H. pluvialis* "GRAS" status (Generally Recognized As Safe) (Grewe and Griehl, 2012; Capelli and Cysewski, 2013).

The increasing demand for natural astaxanthin and its high price raises interest in efficient systems to produce astaxanthin from *H. pluvialis*. Various cultivation and astaxanthin production methods in photoautotrophic, heterotrophic, and mixotrophic growth conditions, both indoors; in open raceway ponds or closed photobioreactors using batch or fed-batch approach have been reported (Kang et al., 2005, 2010; Kaewpintong et al., 2007; Ranjbar et al., 2008; García-Malea et al., 2009; Issarapayup et al., 2009; Zhang et al., 2009; Li et al., 2011; Han et al., 2013; Wang et al., 2013a,b). The most recent advances in *H. pluvialis* cultivation for astaxanthin production include a two-stage mixotrophic culture system (Park et al., 2014) and an "attached cultivation" system using the immobilized biofilm (Zhang et al., 2014). Along with the cultivation process, the induction of carotenoid synthesis in *H. pluvialis* has a direct correlation with the astaxanthin content of cells and total astaxanthin productivity. The accumulation of astaxanthin is affected by both environmental factors such as light (Saha et al., 2013; Park et al., 2014); temperature (Yoo et al., 2012); pH (Hata et al., 2001); salt concentration (Kobayashi et al., 1993); and nutritional stresses (Boussiba et al., 1999; Chekanov et al., 2014), as well as various plant hormones and their derivatives (Yu et al., 2015). Attempts were made to genetically enhance the capacity of *H. pluvialis* to produce astaxanthin using both classical mutagenesis (Hu et al., 2008), and more recently genetic engineering (Sharon-Gojman et al., 2015). Once biomass is successfully grown and achieved high cell density, efficient harvesting, cell disruption, dehydration, and recovery/extraction of astaxanthin from *H. pluvialis* biomass are important factors. Harvesting have been so far achieved through a combination of passive settling and subsequent centrifugation (Han et al., 2013; Pérez-López et al., 2014), or flotation and centrifugation (Panis, 2015). Mechanical processes such as expeller pressing and bead milling are commonly used cell disruption methods to enhance recovery of astaxanthin from *H. pluvialis* (Razon and Tan, 2011). For the dehydration of *H. pluvialis* biomass, spray drying (Li et al., 2011; Panis, 2015), freeze drying, lyophilization, and cryodesiccation (Milledge, 2013) methods have been utilized. There are several methods of astaxanthin extraction utilizing solvents, acids, edible oils, enzymes, pressurized liquids (Jaime et al., 2010; Zou et al., 2013; Dong et al., 2014), supercritical carbon dioxide (SC-CO_2) (Wang et al., 2012; Reyes et al., 2014), and liquefied dimethyl ether (DME) (Boonnoun et al., 2014). Although many studies have explored various methods of extraction and downstream processing of astaxanthin from *H. pluvialis* biomass, more comprehensive investigation is required to take an advantage of the biological potential of this microalga and its highly valuable product. Since astaxanthin has a great potential in the global market (280 mt, $447 million in 2014 for both synthetic and natural astaxanthin) and high market value ($2500–7000/kg); (Koller et al., 2014; Pérez-López et al., 2014; Industry Experts, 2015), in depth investigation of *H. pluvialis* biology, physiology, efficient culture techniques, downstream bioprocessing, and product formation are highly desired for further development of this sector. Even though currently several commercial companies (Cyanotech Corporation, Mera Pharmaceuticals Inc, AIgatechnologies, Fuji Chemical Industry Co. Ltd etc.) are involved in large scale production of *H. pluvialis*

and astaxanthin, the production capacity is far beyond the global demand of natural astaxanthin.

This review summarizes both classical knowledge and most recent advances in the cell biology, physiological, and biochemical characteristics, responses to environmental stresses, and their effect on astaxanthin accumulation, genetic engineering, growth conditions, and different cultivation techniques, harvesting, and post harvest downstream bioprocessing of *H. pluvialis*. The biorefinery concept, global market potential, challenges, and future direction for development of *H. pluvialis* and astaxanthin production in commercial scale also are discussed.

BIOLOGY OF *H. PLUVIALIS*

Taxonomy and Occurrence

The freshwater unicellular biflagellate green microalgae *H. pluvialis* Flotow belongs to the class Chlorophyceae, order Volvocales and family Haematococcaseae (Bold and Wynne, 1985; Eom et al., 2006). It is also known as *Haematococcus lacustris* or *Sphaerella lacustris*. *Haematococcus* was first described by J. Von Flotow in 1844 and later in 1899 Tracy Elliot Hazen extensively presented its biology and life cycle (Hazen, 1899; Leonardi et al., 2011). *H. pluvialis* is common in small transient freshwater bodies and widely distributed in many habitats worldwide. It occurs primarily in temporary water bodies like ephemeral rain pools, artificial pools, natural and man-made ponds, and birdbaths (Czygan, 1970; Burchardt et al., 2006). This microalga can be usually found in temperate regions around the world and has been isolated from Europe, Africa, North America, and Himachal Pradeslv India (Pringsheim, 1966; Suseela and Toppo, 2006). It has been also found across diverse environmental and climate conditions: in brackish water on the rocks on the seashore (Chekanov et al., 2014); freshwater basin in the rock filled with melted snow on Blomstrandhalvøya Island (Norway) (Klochkova et al., 2013); dried fountain near Rozhen, Blagoevgrad in Bulgaria Gacheva et al., 2015, freshwater fishpond in Bihor, Romania (Dragos et al., 2010); rooftop surface of a building of KIOST in Seoul Korea (Kim et al., 2015). It is well suited for survival under conditions of expeditious and extreme in light, temperature, and salt concentration that would be deleterious to many other microalgae, due to its ability to encyst (become enclosed by thick membrane) in a rapid manner (Proctor, 1957).

Cellular Morphology and Life Cycle

Cellular structure of *H. pluvialis* is similar to most of other members of volvocalean unicellular green algae. The life cycle of *H. pluvialis* consists of four types of distinguishable cellular morphologies: macrozooids (zoospores), microzooids, palmella, and hematocysts (aplanospores) (Hazen, 1899; Elliot, 1934). Macrozooids (zoospores), microzooids, and palmella stages are usually called "green vegetative phase" (**Figures 1A,B**). Hematocysts (aplanospores) are referred as "red nonmotile astaxanthin accumulated encysted phase" of the *H. pluvialis* life cycle (**Figures 1C,D**). Macrozooids (zoospores) are spherical, ellipsoidal, or pear-shaped cells with two flagella of equal length

emerging from anterior end, and a cup-shaped chloroplast with numerous, scattered pyrenoids (**Figure 1A**). The macrozooid cells are between 8 and 20 μm long with a distinct gelatinous extracellular matrix of variable thickness. Numerous contractile vacuoles are irregularly distributed near the protoplast surface of the cell (Hagen et al., 2002). These flagellated fast-growing vegetative cells predominate under favorable culture conditions in the early vegetative growth stage (**Figure 1A**) Macrozooids may divide into 2–32 daughter cells by mitosis (Wayama et al., 2013) (**Figures 2A,B**). Under unfavorable environmental or culture conditions, macrozooids start losing flagella, and expand their cell size. They form an amorphous multilayered structure in the inner regions of the extracellular matrix or the primary cell wall as they develop into non-motile "palmella" and become resting vegetative cells (Hagen et al., 2002) (**Figure 1B**). With the continued environmental stress (i.e., nutrient deprivation, high light irradiance, high salinity) and cessation of cell division, "palmella" transform into the asexual "aplanospores" (**Figures 1C,D**). At this stage, cells contain two distinct structures, a thick and rigid trilaminar sheath, and secondary cell wall of acetolysis-resistant material. Such cells become resistant to prevailing extreme environmental conditions (Santos and Mesquita, 1984; Boussiba and Vonshak, 1991). Mature aplanospores; accumulate large amounts of secondary carotenoids, particularly astaxanthin, in lipid droplets deposited in the cytoplasm, which results in a characteristic bright red color of these cells (Hagen et al., 2002). Some *H. pluvialis* strains are reported to be capable of accumulating astaxanthin without forming aplanospores (Brinda et al., 2004). Once environmental or culture conditions return to optimal, red aplanospores germinate to form flagellated zoospores to initiate a new vegetative growth cycle (**Figure 1A**). In some cases, gametogenesis may occur in aplanospores (**Figures 3A–D**). Such process requires an exposure to extreme adverse conditions (freezing, desiccation, or nutrient starvation) followed by return to favorable culture conditions. During gametogenesis, aplanospore cells can produce up to 64 gametes which are known as microzooids. The microzooids are smaller in size (<10 μm) compared to the zoospores (20–50 μm), and exhibit high-speed motility after their release from gametocysts. Sexual reproduction is rarely observed in *H. pluvialis*, and has been largely replaced by vegetative reproduction (Triki et al., 1997).

Ultrastructural Changes of *H. pluvialis* during the Life Cycle

In *H. pluvialis* cells, large amount of ultrastructural changes occurs during their life cycle which is frequently associated with responses to stress conditions in the environment. In the green vegetative palmella cells, a thick cell wall surrounds the cell, and two layers of extracellular matrix present near the cell wall (**Figure 4A**). Nucleus is located in the center of the cell, and highly developed chloroplasts are located at the periphery (**Figure 4A**). Few astaxanthin granules are present which located around the nucleus (**Figure 4A**). Conspicuous pyrenoids with electron-dense matrix can be found in the stroma (**Figures 4A,B**) (Wayama et al., 2013). During the starting of encystment process,
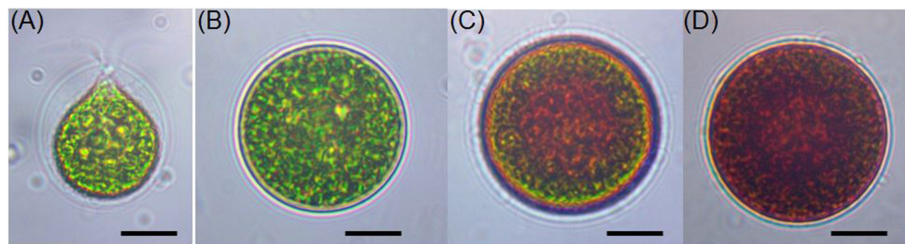
FIGURE 1 | Light microscopic images of *H. pluvialis* cells in life cycle. (A) Green vegetative motile cell; **(B)** Green vegetative palmella cell; **(C)** Astaxanthin accumulating palmella cell in transition to aplanospore; **(D)** Astaxanthin accumulated aplanospore cell. Scale bar: 10 μm.
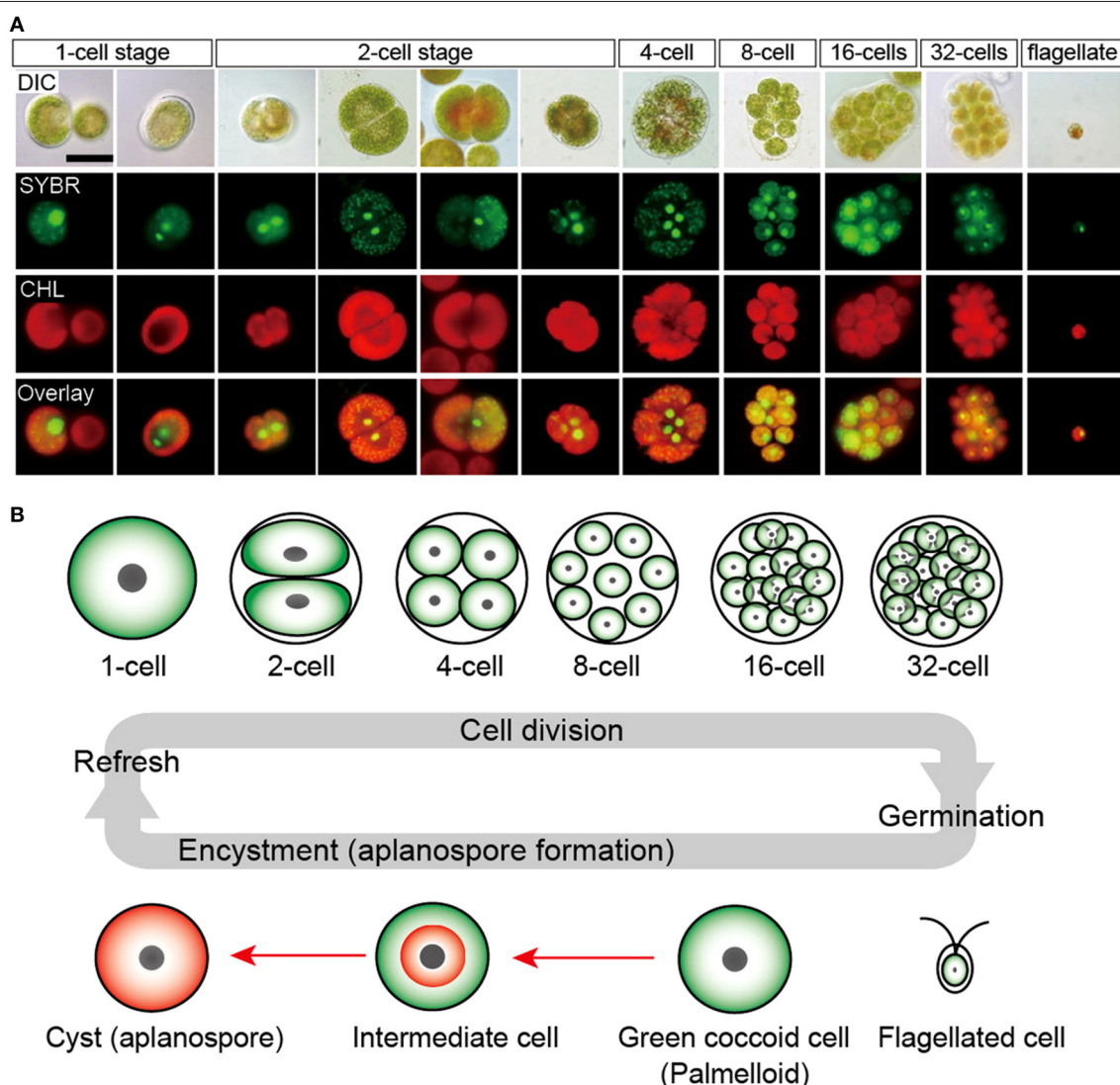
FIGURE 2 | Life cycle of *H. pluvialis*. (A) Fluorescence microscopy images, showing the 1- to 32-cell stages, and the flagellated stage. DIC, differential interference contrast image; SYBR, SYBR Green I-stained cells (green); CHL, chlorophyll autofluorescence (red); and Overlay, overlaid images of SYBR and CHL. **(B)** Illustration of life cycle of *H. pluvialis*. Refresh, when old cultures are transplanted into fresh medium, coccoid cells undergo cell division to form flagellated cells within the mother cell wall. Germination, Flagellated cells settle and become coccoid cells. Continuous and/or strong light accelerate the accumulation of astaxanthin during encystment (red arrows). Figure reproduced from Wayama et al. (2013) distributed under the terms of the Creative Commons Attribution License.

Haematococcus turned into greenish-orange cells (with some astaxanthin accumulation) which can be referred as intermediate stage cells. In this stage, conspicuous pyrenoids with electron-dense matrix located in the stroma, remain surrounded by thick starch capsules and many starch grains are located around the pyrenoids (**Figure 5**). Round oil droplets with various sizes, containing astaxanthin located around the nucleus (**Figure 5**). At this stage, thylakoids become partial degraded (Wayama et al.,

2013). With the gradual accumulation of astaxanthin chloroplast reduce in volume but photosynthetic activity remains. In the aplanosopre or cyst stage, astaxanthin accumulates and cells form cysts. Oil droplets and astaxanthin accumulation patterns may differ among cyst cells. For example, electron-dense astaxanthin granules in oil droplets (**Figures 6A,B**) occurred in some cells. In other cells, relatively large oil droplets occurred throughout the cell (**Figures 6C,D**). Chloroplasts are degenerated and localized in the interspace between oil droplets (Wayama et al., 2013).

BIOCHEMICAL COMPOSITION OF *H. PLUVIALIS*

Because of the unique life cycle of *H. pluvialis*, cellular composition of this microalga varies tremendously between its "green" and "red" stages of cultivation (**Table 1**).

Protein

In green stage, during favorable growth conditions most *H. pluvialis* strains are rich in protein (29–45) (**Table 1**), lower protein content (23.6%) have been however observed in a Bulgarian strain *Haematococcus* cf. *pluvialis* Rozhen-12 during green stage cultivation (Gacheva et al., 2015). It was estimated that proteins contribute to 21 (Kim et al., 2015) and 23% (Lorenz, 1999) of cellular content during red stage cultivation of *H. pluvialis*. Amino acid composition of proteins in the red stage indicated that proteins were mainly composed of aspartic acid, glutamic acid, alanine, and leucine with total amino acid content of 10.02/100 mg, 46.0% of which belonged to essential amino acids (Lorenz, 1999; Kim et al., 2015).

Carbohydrates

In green stage, carbohydrate content approximates to 15–17%, about a half of the red stage (**Table 1**). In the red stage, under conditions of stress (e.g., nutrient starvation, light stress, high acidity, temperature variations etc.), *H. pluvialis* accumulates

FIGURE 3 | Gametogenesis in *H. pluvialis*. **(A)** C, cyst; G, gametocyst; S, a sporocyst; **(B)** vegetative zoospore, F, flagella (indicated by arrow); **(C)**: gametocyst before releasing gametes; **(D)**: release of gametes from gametocyst. Reproduced with permission from Triki et al., 1997, Phycologia, Allen Press Publishing Services. Copyright (1997) Allen Press Publishing Services.
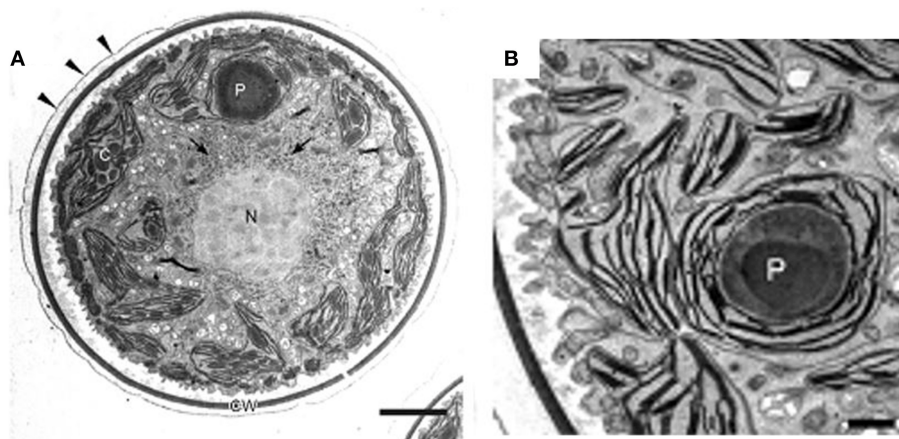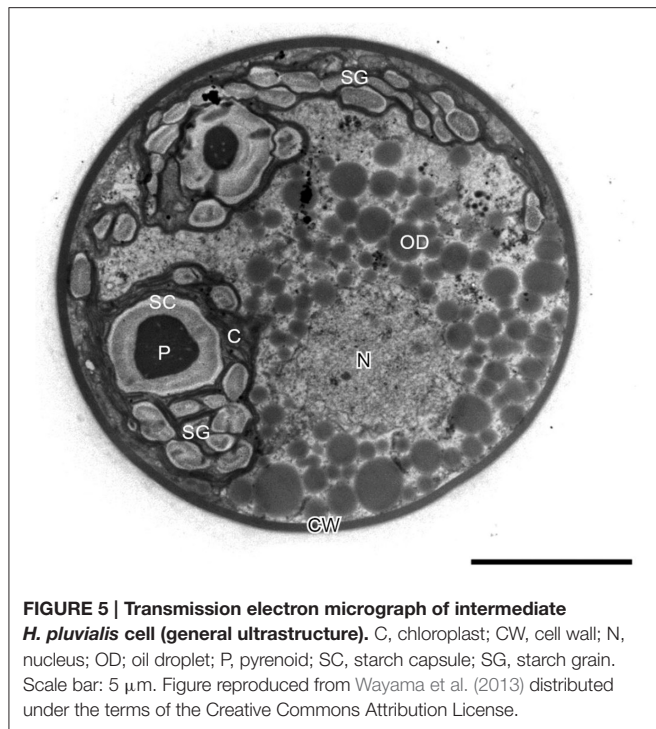
FIGURE 4 | Transmission electron micrographs of green vegetative cells of *H. pluvialis*. **(A)** General ultrastructure. The cell wall is surrounded by extracellular matrix (arrowheads). Arrows indicate astaxanthin granules. **(B)** Chloroplast and pyrenoid. C, chloroplast; CW, cell wall; N, nucleus; P, pyrenoid. Scale bars in **(A,B)**: 5 and 1 μm, respectively. Figure reproduced from Wayama et al. (2013) distributed under the terms of the Creative Commons Attribution License.

FIGURE 5 | Transmission electron micrograph of intermediate *H. pluvialis* cell (general ultrastructure). C, chloroplast; CW, cell wall; N, nucleus; OD; oil droplet; P, pyrenoid; SC, starch capsule; SG, starch grain. Scale bar: 5 μm. Figure reproduced from Wayama et al. (2013) distributed under the terms of the Creative Commons Attribution License.

higher content of carbohydrates (starch), for example 38 (Lorenz, 1999), 60 (Recht et al., 2012), and 74% (Boussiba and Vonshak, 1991). Under prolonged stress conditions starch is consumed in the cell.

Lipid

In green stage, total lipid content varies from 20 to 25%, with approximately 10% lipids composed predominantly of short (C16, C18) polyunsaturated fatty acids deposited in the chloroplasts. Neutral lipids are predominant lipid class in both green and red cells (**Table 1**). In red stage, prolonged stress conditions direct larger flux toward the synthesis of neutral lipids—triacylglycerols (TAG). Red stage cells can accumulate up to 40% of their cell weight as cytoplasmic lipid droplets (LD), and considerable amount of secondary metabolites including up to 4% of the ketocarotenoid astaxanthin (Boussiba et al., 1992, 1999; Saha et al., 2013). The phospholipid content does not change compared to the green stage, while the glycolipid fraction nearly doubles in red cells when compared with green vegetative cells (Damiani et al., 2010). The total fatty acid profile of *H. pluvialis* is relatively complex. Palmitic (16:0), linoleic (18:2), and linolenic (18:3) acids are predominant components of the profile with highly polyunsaturated species also present in considerable amounts (**Table 2**). Based on the comparative studies on fatty acids profile of two different *H. pluvialis*, it was revealed that both strains varied in composition, especially of palmitic (16:0), oleic (18:1), linoleic (18:2), and linolenic (18:3) acids. This variation might be associated with several factors such as culture environment, stress conditions, culture parameters, variation of strain origin, nutrient etc. Higher lipid content of *H. pluvialis* grown under nutrient starvation and

the suitable profile of its fatty acids indicate a possibility of biodiesel production from this microalga (Damiani et al., 2010; Saha et al., 2013). The massive astaxanthin accumulation in *H. pluvialis* is a cellular response to stress conditions and is accompanied by the enhanced biosynthesis of triacylglycerols (TAG) (Zhekisheva et al., 2002, 2005; Cerón et al., 2007), and the reduction in photosynthetic activity of PSII, loss of cytochrome *f*, and subsequent reduction in electron transport, and increased respiration rate (Boussiba, 2000). During transition from green vegetative cells to red aplanospores after exposure to stress conditions astaxanthin start to accumulate as fatty acid mono- or diesters in cytoplasmic lipid droplets (LD) (Aflalo et al., 2007). As cells undergo transition to red stage, both chlorophyll and protein contents drop.

Carotenoid

The carotenoid fraction of green vegetative cells consists of mostly lutein (75–80%), β-carotene (10–20%) and others, including chlorophyll a and b, primary carotenoids, violaxanthin, neoxanthin, lactucaxanthin, and zeaxanthin (Renstrøm et al., 1981; Harker et al., 1996a). In the red stage, the total carotenoid content is markedly enhanced, and the characteristic primary carotenoid pattern of vegetative stage is replaced by secondary carotenoids, mainly astaxanthin (80–99% of total carotenoids) (Harker et al., 1996a; Dragos et al., 2010). The ratio of carotenoids to chlorophylls is about 0.2 in the green stage and increases in the red stage by an order of magnitude and reaches about 2–9. The majority of astaxanthin is not deposited in its free form but it exists within the cell as fatty acid esters of astaxanthin, usually mono- or diesters of palmitic (16:0), oleic (18:1), or linoleic (18:2) acids. This type of modification is required for the deposition of this highly polar molecule within non-polar matrix of lipid droplets. Approximately 70% monoesters, 25% diesters, and only 5% of the free ketocarotenoid is present in the mature "red" cells of *H. pluvialis* (Zhekisheva et al., 2002; Solovchenko, 2015). Under certain conditions of stress *H. pluvialis* has been shown to accumulate up to 3–5% DW of astaxanthin (Han et al., 2013; Chekanov et al., 2014).

H. PLUVIALIS-DERIVED ASTAXANTHIN

H. pluvialis as a Major Source of Astaxanthin

H. pluvialis can accumulate up to 5% DW of astaxanthin and is considered as the best natural source of this high-value carotenoid pigment (Wayama et al., 2013). Dietary supplements containing *Haematococcus* astaxanthin has proved to be safe to humans and widely used for over 15 years as a nutraceutical supplement with no adverse side-effects of its supplementation (Capelli and Cysewski, 2013; Yang et al., 2013). Natural astaxanthin from *H. pluvialis* or krill oil is available in the market as a dietary supplement in dosages from 3.8 to 7.6 mg per day due to potential health benefits (Yang et al., 2013). As societies nowadays are looking toward "green" solutions, natural astaxanthin form *H. pluvialis* seems to be more favorable than its synthetic counterpart due to structure, function, application, and
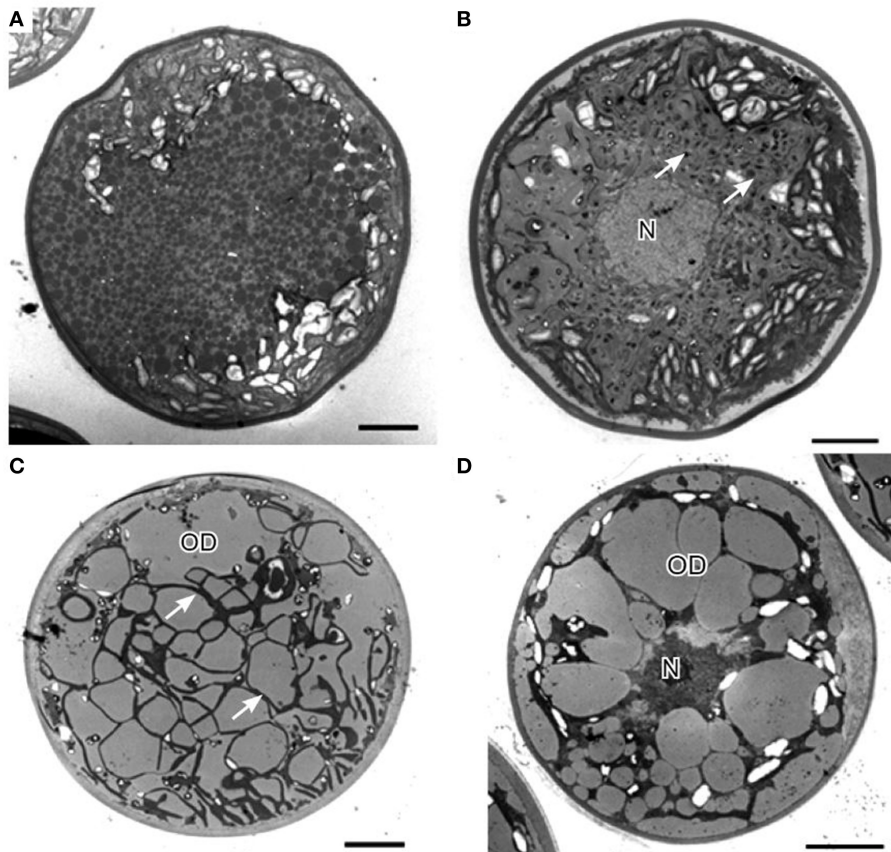
FIGURE 6 | Transmission electron micrographs of *H. pluvialis* cyst cells. (A) General ultrastructure of cyst cells, showing small granules that contain astaxanthin. **(B)** General ultrastructure of a cyst cell, showing astaxanthin accumulation in oil droplets. **(C)** General ultrastructure of a cyst cell, showing large oil droplets. Chloroplasts localize in the interspace between oil droplets (arrows). **(D)** Some oil droplets are fused. C, chloroplast; N, nucleus; OD, oil droplet. Scale bars in **(A–D)**: 5 μm. Figure reproduced from Wayama et al. (2013) distributed under the terms of the Creative Commons Attribution License.

security (Choubert and Heinrich, 1993; Capelli and Cysewski, 2013; Pérez-López et al., 2014).

Biosynthesis of Astaxanthin in *H. pluvialis*

Biosynthesis of astaxanthin in *H. pluvialis* is a complex process that is highly up-regulated in conditions of stress and which coincides with the accumulation of triacylglycerols (TAGs). Both compounds are deposited in the cytosolic lipid bodies during the "red" stage of *H. pluvialis* cultivation. Astaxanthin belongs to carotenoids, a C_{40} tetraterpenes, synthesized from isoprene units. Isopentenyl pyrophosphate (IPP) is a key intermediate of carotenoid synthesis. In principle, IPP can originate from two dissimilar pathways: mevalonate pathway (MVA) located in cytosol and non-mevalonate (MEP) located in the chloroplast (Lichtenthaler et al., 1997; Lichtenthaler, 1999; Eisenreich et al., 2001). Alternative name for MEP is DOXP, due to the formation of 1-deoxy-D-xylulose-5-phosphate in the first stage of the pathway. Comparative transcriptomic analysis of astaxanthin biosynthesis in *H pluvialis* have shown that the key intermediate-IPP is most likely synthesized using the DOXP pathway. *H. pluvialis* lacks three key enzymes of

the mevalonate pathway (MVA) catalyzing the formation of isopentenyl pyrophosphate (IPP) from acetoacetyl-CoA (Gwak et al., 2014). There has been numerous evidence of the full set of enzymes required for the conversion of photosynthesis-derived products i.e., pyruvate and glyceraldehyde-3-phosphate into isopentenyl pyrophosphate through DOXP pathway inside *H. pluvialis* chloroplasts (Gwak et al., 2014). It makes it the most likely source of IPP in *H. pluvialis* cells. The process of astaxanthin biosynthesis is presented on **Figure 7**. IPP derived from DOXP pathway is an initial building block of astaxanthin synthesis. In the subsequent step the IPP undergoes isomerization to dimethylallyl diphosphate (DMAPP). It has been long assumed that this conversion was catalyzed exclusively by isopentenyl pyrophosphate isomerase (*IPI*) (Sun et al., 1998; Lichtenthaler, 1999). However, recent transcriptomic studies suggest that neither of the two *ipi* genes of *H pluvialis* (*ipi1* and *ipi2IPI2*) are up-regulated during cellular accumulation of astaxanthin (Gwak et al., 2014). Suggestions have been made that another enzyme of similar activity, 4-hydroxy-3-methylbut-2-enyl diphosphate reductase (HDR) was more likely to be responsible for catalyzing interconversion between IPP and

TABLE 1 | Typical composition of *H. pluvialis* biomass in green and red cultivation stages.

Composition content (% of DW)	Green stage	Red stage
Proteins	29–45	17–25
Lipids (% of total)	20–25	32–37
Neutral lipids	59	51.9–53.5
Phospholipids	23.7	20.6–21.1
Glycolipids	11.5	25.7–26.5
Carbohydrates	15–17	36–40
Carotenoids (% of total)	0.5	2–5
Neoxanthin	8.3	n.d
Violaxanthin	12.5	n.d
β -carotene	16.7	1.0
Lutein	56.3	0.5
Zeaxanthin	6.3	n.d
Astaxanthin (including esters)	n.d	81.2
Adonixanthin	n.d	0.4
Adonirubin	n.d	0.6
Canthaxanthin	n.d	5.1
Echinenone	n.d	0.2
Chlorophylls	1.5–2	0

Adapted from Grewe and Griehl (2012). *n.d., no data.*

TABLE 2 | Comparison of fatty acid composition (%) of two different *H. pluvialis* strains.

Fatty acids	*Haematococcus* sp. KORDI03 (Kim et al., 2015)	*H. pluvialis* (Lorenz, 1999)
C12:0 lauric	N/A	0.1
C14:0 myristic	0.1	0.5
C15:0 pentadecanoic acid	0.1	N/A
C16:0 palmitic	13.7	29.0
C16:1 palmitoleic	0.5	0.6
C16:2	0.4	N/A
C16:3	3.5	N/A
C16:4	3.3	N/A
C17:0 margaric	N/A	0.2
C17:1 margaroleic	N/A	1.3
C18:0 stearic	0.7	2.1
C18:1 oleic	4.9	25.9
C18:2 linoleic	24.9	20.8
C18:3 linolenic	39.7	12.8
C18:4 octadecatetraenoic	5.8	1.4
C20:0 arachidic	N/A	0.6
C20:1 gadoleic	0.5	0.3
C20:2 eicosadenoic	N/A	1.2
C20:3 eicosatrienoic gamma	N/A	0.5
C20:4 arachidonic	0.9	1.4
C20:5 eicosapentaenoic	0.6	0.6
C22:0 behenic	N/A	0.4
C24:0 lignoceric	0.3	0.2
C24:1 nervonic acid	0.1	0.1
∑ SFAs	15.0	33.2
∑ MUFAs	6.0	28.1
∑ PUFAs	79.1	38.7
Total	100.0	100.0

DMAPP (Hoeffler et al., 2002; Rohdich et al., 2002; Gwak et al., 2014). Further studies are required to assess the contribution of these three enzymes to this key biosynthetic step of astaxanthin formation. Elongation of the isoprenoid chain is initiated with a molecule of DMAPP and a subsequent linear additions of three molecules of IPP catalyzed by an enzyme geranylgeranyl pyrophosphate synthase (GGPS) (Britton, 1993; Cunningham and Gantt, 1998). The final step of this process is the formation of a C_{20} compound, geranylgeranyl pyrophosphate (GGPP), a shared precursor with other isoprenoids. The first committed step of carotenoid synthesis is catalyzed by phytoene synthase (PSY) and results in a head-to-tail condensation of two GGPP molecules to form a C_{40} compound—phytoene that serves as a precursor for astaxanthin and other carotenoids (Cunningham and Gantt, 1998). The expression of the phytoene synthase gene (*psy*) was up-regulated in *Haematococcus* cells stressed with high light and undergoing transformation from "green" to "red" stage (Steinbrenner and Linden, 2001; Vidhyavathi et al., 2008; Gwak et al., 2014). The subsequent formation of highly unsaturated compound—lycopene proceeds through four desaturation steps catalyzed by two phytoene desaturases (PDS) and a ζ-carotene desaturase (ZDS) with two plastid terminal oxidase (PTOX 1, PTOX 2) acting as co-factors for electron transfer between C_{40} carotenoid intermediates, plastoquinone and final electron acceptor—oxygen (Li et al., 2010; Nawrocki et al., 2015). Of the two, PTOX 1 was found to be co-regulated with astaxanthin synthesis in *H. pluvialis* (Wang et al., 2009; Nawrocki et al., 2015). Desaturation reactions increase the number of conjugated carbon-carbon double bonds that form the chromophore in carotenoids and convert a colorless molecule of ζ-carotene to a pink colored lycopene (Cunningham and Gantt, 1998). Both termini of lycopene undergo cyclization catalyzed by lycopene

cyclases (LCY-e and LCY-b). Cyclization is a branching point of the carotenoid biosynthesis in most organisms, yielding α-carotene (precursor of lutein) and β-carotene (precursor of other carotenoids including astaxanthin). In *H. pluvialis* vast majority of the carbon flux is directed into the latter (Gwak et al., 2014), and high level of LCY-b transcripts have been observed under stress conditions (Lorenz and Cysewski, 2000; Gwak et al., 2014). Final two oxygenation steps catalyzed by β-carotene ketolase (BKT) and β-carotene hydroxylase (CrtR-b) are rate limiting steps of astaxanthin synthesis (Linden, 1999; Steinbrenner and Linden, 2001; Vidhyavathi et al., 2008). Although in principle the reactions catalyzed by these two enzymes can proceed in any order, higher substrate specificity of BKT toward β-carotene than zeaxanthin favors initial addition of keto group before enantio-selective hydroxylation of canthaxanthin to astaxanthin is catalyzed by CrtR-b (Lotan and Hirschberg, 1995). Enantioselectivity of astaxanthin synthesis is of primary importance for the nutraceuticals market and the major advantage of *H. pluvialis* astaxanthin over its synthetic counterpart. Since astaxanthin has two identical chiral centers at the positions of 3 and 3′ it can exist in four different

configurations which yield three different isomers: (3R, 3′S); (3R, 3′R); (3S, 3′S) depending on the spatial orientation of the hydroxyl (OH) groups in chiral carbon. During chemical synthesis these isomers are present in the ratio of 2:1:1, respectively, yielding only 25% of the naturally occurring (3S, 3′S) isoform. *H. pluvialis* synthesizes the (3S, 3′S) stereoisomer of astaxanthin and is therefore a much sought-off product in the nutraceutical market.

Effect of Small Molecules on Astaxanthin Synthesis

Astaxanthin is a secondary metabolite, a carotenoid synthesized by *H. pluvialis* in a response to stress conditions such as high light, salinity, or carbon to nitrogen ratio (Gao et al., 2012a). Regulation of these pathways can be affected by numerous small molecules like plant hormones or their analogs. An array of such molecules has been explored to modulate astaxanthin accumulation by *H. pluvialis*. Plant hormones that are usually associated with stress response mechanisms e.g., abscisic acid (ABA), jasmonic acid (JA), methyl jasmonate (MJ) or growth regulators like gibberellic acid (GA3), salicylic acid (SA) or brassinosteroid—2, 4-epibrassinolide (EBR) were found particularly promising in increasing astaxanthin accumulation in *H. pluvialis* (Kobayashi et al., 1997b; Gao et al., 2012a,b, 2013a,b; Yu et al., 2015). It was found that these compounds affect numerous genes involved in astaxanthin biosynthesis and result in their even six to 10 fold up-regulation. All of these compounds were tested in various concentrations and the highest improvement of astaxanthin accumulation was achieved with salicylic acid. At relatively low concentrations of the hormone 50 mg L^{-1} and low light 25 μmol photons m^{-2} s^{-1} the content of astaxanthin raised seven fold from 0.391 mg L^{-1} to 2.74 mg L^{-1}. Higher levels of these hormones had however deleterious effect on both growth and astaxanthin accumulation (Gao et al., 2012a). Correlation between mRNA transcript levels of five key enzymes of astaxanthin synthesis pathway (*ipi*, *psy*, *pds*, *crtO*, and *crtR-b* encoding respectively isopentenyl-diphosphate δ-isomerase (IPI), phytoene synthase (PSY), phytoene desaturase (PDS), β-carotene oxygenase (CrtO), and β-carotene hydroxylase (CrtR-b) with alga growth and astaxanthin production suggested a complex, multiple regulatory mechanisms at transcriptional, translational, and post-translational levels controlling entire process of carotenoid synthesis in *H. pluvialis* (Li et al., 2010). Small molecules can have multiple effects on the regulation of each of these genes and more detailed investigation of the molecular responses to their application is required for both understanding gene regulation in *H. pluvialis* and enhancing its capacity as commercial astaxanthin producer.

Genetic Improvement of *H. pluvialis* for Astaxanthin Production

Green eukaryotic microalgae are among the organisms that are notoriously difficult to genetically engineer. In principle, genetic engineering of microalgae has been reported for over 30 strains of various species, including *Haematococcus* (Rosenberg et al.,

2008; Radakovits et al., 2010; Forján et al., 2015). In majority of these reports however, only a transient transgene expression has been achieved and a desired, stable, hereditary, and efficient genetic modification existed only for model species such as *Chlamydomonas reinhardtii* and *Volvox carteri*. Due to these constrains genetic improvement of *H. pluvialis* strains have been long limited to classical mutagenesis. Combination of mutagenic treatment and various screening methods resulted in the development of numerous interesting mutants of *H. pluvialis* including those of higher astaxanthin accumulation capacity (Tjahjono et al., 1994a; Chumpolkulwong et al., 1997; Tripathi et al., 2001; Chen et al., 2003; Hu et al., 2008; Hong et al., 2012; Gomez et al., 2013). Various mutagenic treatments have been tested, and can be broadly divided into UV and chemical mutagenesis. Chemical mutagenesis has been generally found to be more suitable for *H. pluvialis* due to alga's intrinsic capacity to limit the damage from light. Typical chemicals used for mutagenesis include ethyl methanesulphonate (EMS) and N-methyl-N-nitro-N-nitrosoguanidine (MNNG). In all studies their concentrations were adjusted to target 85–95% cell mortality. Successful mutants are usually screened using a combination of factors that promote identification of mutants capable of high astaxanthin accumulation. Typically, herbicides that affect carotenoid synthesis pathway such as norflurazon, fluridone, nicotine, compactin, or diphenylamine are used (Tjahjono et al., 1994a; Chumpolkulwong et al., 1997; Tripathi et al., 2001; Chen et al., 2003; Gomez et al., 2013). Screening relies on identifying colonies that are capable of surviving and/or growing well in the presence of inhibitory concentrations of these compounds and high illumination. Surviving strains should in principle exhibit better capacity to synthesize carotenoids and divert larger, or more efficient carbon flux toward these compounds. A number of successful mutants have been isolated this way and typical improvement of astaxanthin accumulation ranges from several percent (Gomez et al., 2013) to two or three fold improvement (Hu et al., 2008). In former case the mutated strain was tested in commercial scale cultivation system (120,000 L) and retained the improved capacity for astaxanthin production. An alternative approach to strain improvement relying on selection of photosensitive mutants was recently attempted (Hong et al., 2012). Photosensitive mutant with an ability to grow under hetero or mixotrophic conditions should be in principle advantageous over wild type strains due to faster growth rates and more efficient stress trigger. Screening for successful mutants was performed in a three stage process. Since photosensitivity is connected with impaired photosynthesis, these impaired mutants were selected in the first screening. Secondary screening tested for the ability of heterotrophic growth of these photosensitive isolates. Tertiary screening involved mixotrophic conditions with moderate illumination to obtain mixotrophic photosensitive strain that accumulated 4.7% (w/w) of astaxanthin under much shorter induction time (Hong et al., 2012). The mutated strain was stable for at least 1.5 year and is an interesting example of using classical mutagenesis for improvement of *H. pluvialis*. Mutagenic strain improvement can be expanded by breeding or creating hybrid strains from previous genetic improvement efforts. Technique of protoplast
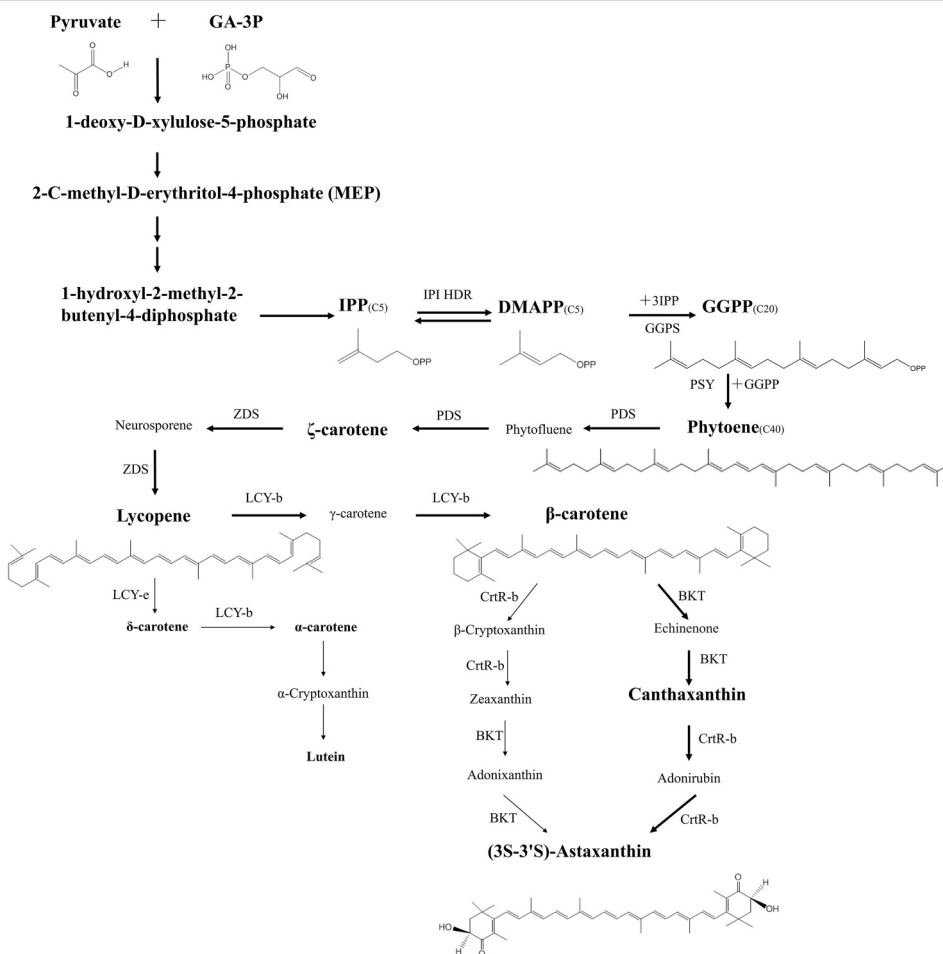
FIGURE 7 | Pathway of (3S-3′S)-astaxanthin biosynthesis in *H. pluvialis*. Major carbon flux during the red stage of *H. pluvialis* cultivation is indicated with thick arrows, minor products are indicated with thin arrows. Major intermediates of biosynthesis are indicated in large fonts, minor intermediates in small fonts. Enzyme abbreviations are as follows: IPI, Isopentenyl pyrophosphate isomerase; HDR, 4-hydroxy-3-methylbut-2-enyl diphosphate reductase; GGPS, geranylgeranyl pyrophosphate synthase; PSY, phytoenesysthase; PDS, phytoenedesaturase; ZDS, ζ-carotene desaturase; LCY-b, lycopene β-cyclase; LCY-e, lycopene ε-cyclase; BKT, β-carotene ketolase; CrtR-b, β-carotene 3,3′-hydroxylase; Intermediates: Phytofluene, Neurosporene, γ-carotene, β-Cryptoxanthin, Adonixanthin, Echinenone, Adonirubin.

fusion has been successfully applied to *H. pluvialis* (Tjahjono et al., 1994a). Two mutagenized strains, norflurazon-resistant and nicotine-resistant have been fused to create a hybrid containing genetic material of two initial strains and showed 30% higher astaxanthin accumulation than the initial wild type strain, when neither of the fused strains showed such characteristics (Tjahjono et al., 1994a). Till very recently *H. pluvialis* was one of the organisms in which genetic engineering of its nuclear genome was considered difficult due to lack of suitable shuttle vectors and satisfactory transformation efficiencies (Sharon-Gojman et al., 2015). A number of unsuccessful approaches have been tried that included various transformation methods (particle bombardment, electroporation, *Agrobacterium*), vectors, promoters, and strains (Sharon-Gojman et al., 2015). To address these limitations and open a new array of possibilities in *H. pluvialis* and astaxanthin biology and technology new developments were required. In recent years these developments

emerged and stable transformations of *H. pluvialis* chloroplast (Gutiérrez et al., 2012) and nuclear genomes (Sharon-Gojman et al., 2015) were achieved. Most recent nuclear transformation vectors are capable to transform one or two transgenes into the nuclear genome either 5′ or 3′ of the endogenous dominant selection marker, in the absence of any additional antibiotic resistance genes. The selection marker used in this system is a phytoene desaturase (*pds*) variant that confers resistance to a herbicide norflurazon due to a single point mutation (L504A). Successful transformation of *H. pluvialis* was obtained with particle bombardment and numerous constructs based on *pds* selection marker were delivered and incorporated to the genome showing stability of integration for over 16 months of subculturing (Sharon-Gojman et al., 2015). Genetic engineering of chloroplast genome of *H. pluvialis* have been also achieved relatively recently (Gutiérrez et al., 2012). So far these studies are limited to expressing exogenous antibiotic resistance gene (*aadA*

cassette) between Internal Transcribed Spacer region and 16S gene of *H. pluvialis* chloroplast genome, but this technique may in the near future have significant impact on protein production in *H. pluvialis* (Gutiérrez et al., 2012) as higher protein yields are generally obtained during chloroplast expression of transgenes in other microalgal strains (Li et al., 2015). These new developments in genetic engineering of *H. pluvialis* can open a new chapter for the development of this organism as both industrial astaxanthin producer and an interesting model for carotenoid synthesis and accumulation studies.

APPLICATIONS OF *H. PLUVIALIS* ASTAXANTHIN

Astaxanthin in Human Health and as Nutraceutical

Astaxanthin possesses various human health benefits and nutraceutical applications and plenty of published information available with evidences, mainly from *in vitro* and animal models (Guerin et al., 2003; Chew et al., 2004; Higuera-Ciapara et al., 2006; Palozza et al., 2009; Yuan et al., 2011). The effect of *Haematococcus* derived astaxanthin on various physiological systems in animal and human subject is presented in **Table 3**. Astaxanthin is considered as "super anti-oxidant" which possesses one of the strongest known antioxidant effects. Its unique structure allows it to span biological membranes and act as an antioxidant by reducing and stabilizing free radicals (Hussein et al., 2006; Liu and Osawa, 2007; Ranga Rao et al., 2010). It is very good at protecting membrane phospholipids and other lipids against peroxidation (Naguib, 2000). There are several studies which showed high antioxidant activity of astaxanthin from *H. pluvialis* in rats supplemented with diet (Kamath et al., 2008; Ranga Rao et al., 2010, 2013; Augusti et al., 2012). Astaxanthin can terminate the induction of inflammation in biological systems. It can help to fight symptoms of ulcer disease from *Helicobacter pylori* (Liu and Lee, 2003); protect against gastric lesions (ulcers), improve gastrointestinal health (Nishikawa et al., 2005; Kamath et al., 2008); and treat gastrointestinal discomfort (Andersen et al., 2007; Kupcinskas et al., 2008). Astaxanthin offers protection against free radical damage to preserve immune-system defenses. The immunomodulating capacity of astaxanthin has been found to be superior to that of β-carotene and canthaxanthin (Chew and Park, 2004). Astaxanthin has shown significant effect on immune function in a number of *in vitro* and *in vivo* assays using both animal models (Chew et al., 2004) and humans (Park et al., 2010). Astaxanthin is a potential therapeutic agent against atherosclerotic cardiovascular disease (Fassett and Combes, 2011). Astaxanthin supplementation can be beneficial for people with enhanced risk for heart attacks. It is carried by VLDL, LDL, and HDL (high-density lipoprotein) in human blood and protects LDL-cholesterol against oxidation (Iwamoto et al., 2000); has a role in the reduction of blood plasma level (Karppi et al., 2007); and increases basal arterial blood flow (Miyawaki et al., 2008). Oxidative stress is a causative or at least ancillary factor in the pathogenesis of

major neurodegenerative diseases (Alzheimer's, Huntington's, Parkinson's, and amyotrophic lateral sclerosis-ALS). Diets high in antioxidants offer the potential to lower the associated risks (Ferrante et al., 1997). Natural astaxanthin can cross the blood-brain barrier in mammals and can extend its antioxidant benefits beyond that barrier. Therefore, astaxanthin can help to alleviate the effects of Alzheimer's disease and other neurological diseases. Astaxanthin can improve respiratory and sympathetic nervous system activities (Nagata et al., 2006), inhibit the growth of fibrosarcoma, breast, and prostate cancer cells and embryonic fibroblasts (Palozza et al., 2009); cell death, cell proliferation and mammary tumors (Nakao et al., 2010). Astaxanthin supplementation can help to protect against UV-induced photooxidation; as an oral sun-protectant; can prevent skin thickening and reduce collagen reduction against UV induced skin damage (Ranga Rao et al., 2013) and can improve skin condition across its layers i.e., corneocyte, epidermis, basal, and dermis by combining oral supplementation and topical treatment (Seki et al., 2001; Yamashita, 2002; Tominaga et al., 2012). Results have shown that semen quality, pregnancy rate and sperm velocity in human subject can be improved (Elgarem et al., 2002; Comhaire et al., 2005) whereas idiopathic infertility can be decreased by astaxanthin (Andrisani et al., 2015).

Astaxanthin in Aquaculture and Poultry Industry

During last 20 years, synthetic astaxanthin has been widely used for pigmentation of fish. *Haematococcus* astaxanthin has great potential in aquaculture industry, due to increasing consumer demands for natural products and ability of *Haematococcus* astaxanthin to provide necessary supplementation for adequate growth and reproduction of commercially valuable fishes (Salmonid, Red sea bream), rainbow trouts, and shrimps. Microalgae- derived astaxanthin has been demonstrated as safe and effective compound for flesh pigmentation of these fish (Torrissen and Naevdal, 1984; Tolasa et al., 2005). Utilization of *H. pluvialis* meal for pigmenting has resulted in significant astaxanthin deposition in flesh and skin, flesh coloration enhancement, enhanced antioxidant system, fish egg quality, better growth and survival of fry of Salmonid, sea bream, and rainbow trout (Arai et al., 1987; Sommer et al., 1991; Choubert and Heinrich, 1993; Sheikhzadeh et al., 2012a,b), ornamental fishes (Ako and Tamaru, 1999), and shrimp (Arai et al., 1987; Parisenti et al., 2011). A recent study indicated that diets supplemented with *H. pluvialis* can improve large yellow croaker fish growth more than diets supplemented with synthetic astaxanthin (Li et al., 2014). *H. pluvialis*-derived natural astaxanthin has shown to be efficient in pigmentation of egg yolks, egg production (Elwinger et al., 1997) in hen and breast muscle tissue improvement and higher feed efficiency in broiler chicken (Inborr and Lignell, 1997; Inbbor, 1998). It has also been proved to improve health and fertility of chicken and to decrease their mortality (Lignell and Inborr, 1999, 2000).

TABLE 3 | Effect of *H. pluvialis*-derived astaxanthin on various physiological systems in human and animal subjects.

Physiological System	Subject	Effect followed	Main outcome	References
Anti-oxidation	Rabbits	Thioredoxin reductase; Paraoxonase activity	Enhanced; No effect	Augusti et al., 2012
	Rats	Hepatoprotective and antioxidant activity	Improved	Ranga Rao et al., 2015
	Rats	Antioxidant enzymes, catalase, superoxide dismutase, peroxidase, and lipid peroxidation in plasma and liver	Increased	Ranga Rao et al., 2010, 2013
	Men (bilateral cataract)	Antioxidative effects through changes in superoxide scavenging activity, and hydroperoxides production in aqueous humor	Enhanced; Suppressed	Hashimoto et al., 2013
Eye function	18 healthy men	Deep vision	Improved	Sawaki et al., 2002
	10 healthy men	Eye function	Improved	Iwasaki and Tawara, 2006
	40 asthenopia patients	Eye accommodation power	Improved	Kenji et al., 2005
	49 healthy men	Uncorrected far visual acuity	Improved	Nakamura et al., 2004
	87 men (visual display terminal workers)	Eye accommodation amplitude (the adjustment in the lens of the eye that allows it to focus);	Improved;	Nagaki et al., 2002
		Eye soreness, dryness, tiredness, and blurred vision	Reduced	Nagaki et al., 2006
Skin	Healthy female or male	Skin wrinkle, corneocyte layer, epidermis, and dermis	Improved	Tominaga et al., 2012
	46 healthy women	Skin elasticity and moisture	Improved	Seki et al., 2001; Yamashita, 2002
Immune response	14 healthy women	Oxidative stress and inflammation markers; Immune response	Reduced; Improved	Park et al., 2010
Inflammation	Rats	Gastrointestinal health	Improved	Nishikawa et al., 2005
Gastric ulcer	*H. pylori*-infected mice	Bacterial load Gastric inflamation	Reduced	Liu and Lee, 2003
	Rats	Gastric ulcer markers	Reduced	Kamath et al., 2008
	44 patients with functional dyspepsia	Inflammatory markers; gastrointestinal discomfort	No effect; No effect	Andersen et al., 2007; Kupcinskas et al., 2008
Cardiovascular system	20 adult men	Blood flow time	Improved	Miyawaki et al., 2008
	Men	Blood plasma levels	Reduced	Karppi et al., 2007
Muscle endurance	16 non-trained men	Lactic acid accumulation after run	Reduced	Sawaki et al., 2002
	19 non-trained men	Respiratory and sympathetic nervous system activities	Improved	Nagata et al., 2006
	20 non-trained men	Strength/explosiveness test; strength/endurance test	No effect; Improved	Lignell, 2001
	20 resistance-trained men	Markers of skeletal muscle injury	No effect	Bloomer et al., 2005
Cancer	Rats	Growth of colon cancer cells	Inhibited	Palozza et al., 2009
Central nervous system	Healthy mice	Memory	Improved	Zhang et al., 2007
	10 healthy men (50–69 years)	Response time and accuracy of several tasks	Improved	Satoh et al., 2009
	Middle aged/elderly men and women	Cog Health battery scores (Nuropsychological memory test)	Improved	Katagiri et al., 2012
Male fertility	20 sub-fertile men	Semen quality, pregnancy rate	Improved	Elgarem et al., 2002
	30 sub-fertile men	Sperm velocity; oxidation markers; pregnancy rate	Improved; Reduced; Improved	Comhaire et al., 2005
	24 healthy men	Idiopathic infertility	Decreased	Andrisani et al., 2015
Metabolic Syndrome (MS)	Obese rats	Body weight; adipose tissue weight; MS markers	Reduced; Reduced; Improved	Ikeuchi et al., 2007

CULTIVATION AND PROCESSING OF *H. PLUVIALIS* FOR ASTAXANTHIN PRODUCTION

Culture Conditions and Requirements for Cell Growth and Astaxanthin Formation

Optimization of the various culture parameters, such as growth medium composition, light, pH, temperature etc. is necessary to achieve high biomass and astaxanthin production. Most of these parameters have different optima for biomass accumulation and astaxanthin production. For carotenogenesis induction, the stronger exposure to stress conditions, the higher astaxanthin accumulation. The origins of this stress can be diverse and successful astaxanthin accumulation has been induced with both, high levels of one stressor, or from a combination of multiple stress factors. In some cases, if cells are exposed to strong stress, cells growth completely ceases and cells begin to die in a relatively short time (Su et al., 2014). Various types of growth media are used for cultivation of *H. pluvialis*. The most commonly used media are BG- 11 (Rippka et al., 1979), BBM (Bischoff and Bold, 1963), OHM (Fábregas et al., 2000); KM1-basal medium with organic carbon sources in the form of sodium acetate (Kobayashi et al., 1993), and their modifications. An ideal composition of the medium to achieve high growth rate and biomass accumulation is different from ideal composition for high accumulation of astaxanthin. Sodium nitrate was found to be the most optimal inorganic nitrogen source (Sarada et al., 2002a), alternatively an organic source such as urea can be used. When culture is subjected to nutrient deficiency, it leads to accumulation of astaxanthin within the cells (Saha et al., 2013). Nitrogen limitation leads to approximately twice the rate of astaxanthin production than the limitation of phosphorus. It can be due to higher cellular damage resulting from a lack of nitrogen, which manifests in significant degradation of chlorophyll, compared to the phosphorus starvation (Boussiba et al., 1999). Micronutrients such as selenium and chromium result in an increased biomass and astaxanthin production (Tripathi et al., 1999; Fábregas et al., 2000; Domínguez-Bocanegra et al., 2004). Formation of astaxanthin can also be induced by adding NaCl (0.25–0.5% w/v) to the media. Also, when NaCl is added together with 2.2 mM sodium acetate, astaxanthin accumulation can be increased (Sarada et al., 2002b). Addition of 0.45 mM Fe^{2+} in the form of ferrous sulfate may significantly increase the biosynthesis of carotenoids in cysts due to formation of hydroxyl radicals. (Kobayashi et al., 1997b). This effect may be enhanced by combining Fe^{2+} treatment with an addition of sodium acetate and high temperature exposure (Kobayashi et al., 1993; Tjahjono et al., 1994b). According to most studies, the suitable temperature for the growth and astaxanthin accumulation of *H. pluvialis* is between 20 and 28°C (Fan et al., 1994; Hata et al., 2001; Lababpour et al., 2005; Kang et al., 2010; Yoo et al., 2012; Wan et al., 2014a). However, temperature above 30°C induces a transition from green vegetative stage to red stage and formation of red cysts can be observed within 2 days. This transition is combined with a significant slowdown in growth, while astaxanthin accumulation is 2–3 times higher than at 20°C.

The increased temperature is likely to affect the synthesis of astaxanthin through stimulation of oxygen radicals formation and their higher reactivity (Tjahjono et al., 1994b). It is preferred that the temperature change takes place gradually, allowing better acclimation to the new conditions (Hata et al., 2001). pH can also significantly affect the cell growth and synthesis of chlorophyll and carotenoids in *H. pluvialis*. In terms of biomass and astaxanthin production optimal pH is within the range of 7.00–7.85 (Hata et al., 2001; Sarada et al., 2002a). The typical irradiation for *H. pluvialis* cultivation ranges between 40 and 50 µmol photons $m^{-2}s^{-1}$ (Hata et al., 2001; Chekanov et al., 2014; Park et al., 2014). Optimal irradiation to achieve a high growth rates tend to be higher, namely 70 (Zhang et al., 2014), 80 (Saha et al., 2013), 90 (Fan et al., 1994), or even up to 177 µmol photons $m^{-2}s^{-1}$ (Domínguez-Bocanegra et al., 2004). These different optimal values may be caused by other cultivation parameters such as media composition, temperature, or the strain of *H. pluvialis*. During vegetative stage cultivation of *H. pluvialis*, the regular cycles of alternating light and dark 12:12 or 16: 8 h are often used (Saha et al., 2013; Park et al., 2014), but the higher density cultures are achieved with continuous illumination (Domínguez-Bocanegra et al., 2004). The best practice to date appears to be white or blue LED lighting (Saha et al., 2013) or the mixture of both at the ratio of 3:1 at 7000 lx (∼95 µmol photons $m^{-2}s^{-1}$). These conditions promote morphologic changes from green vegetative cells to red cyst cells (Sun et al., 2015). Carotenogenesis is induced in cells upon exposure to higher light intensity than the corresponding light saturation point (LSP). However, specific optimum value of LSP differ between studies. The lowest intensities that have been reported utilized irradiation of around 100–150 µmol photons $m^{-2}s^{-1}$ (Zhang et al., 2014) followed by 240 (Saha et al., 2013), 345 (Domínguez-Bocanegra et al., 2004), and 480 µmol photons $m^{-2}s^{-1}$ (Chekanov et al., 2014). Lower optimal irradiation was found to be influenced by other stress conditions, such as deficiency of nutrients (Saha et al., 2013; Zhang et al., 2014) or elevated temperature (Tjahjono et al., 1994b). It proves that for effective induction of carotenogenesis excessive irradiation may not be necessary if other stressors are present. With the reduced requirements of light for cultivation in photobioreactors, the costs of cultivation can be minimized which is essential for astaxanthin production in an industrial scale. Regarding the type of illumination, the highest carotenoid content was obtained by using a continuous PAR lighting (Saha et al., 2013). An interesting alternative to an immediate change in the radiation intensity to induce the transition from the vegetative phase to carotenoid production is gradually increasing the level of lighting. Gradual increase of light intensity can result in gradual transformation of cells to cysts and can also contribute to better accumulation of astaxanthin, because the cells are capable to cope with increasing higher levels of stress (Park et al., 2014).

Culture Systems

Astaxanthin-producing *H. pluvialis* is capable of growing in photoautotrophic, heterotrophic, or mixotrophic growth

conditions in indoors, open raceway ponds or closed photobioreactors in batch, fed batch, or continuous modes.

Photoautotrophic Culture

Photoautotrophic culture of *H. pluvialis* is mainly carried out in open raceway ponds or closed photobioreactors. Typical photobioreactors used for its cultivation include tubular, bubble column and airlift photobioreactors. As the culture conditions for maximum growth and maximum astaxanthin content are mutually exclusive, a two-step cultivation strategy is commonly adopted for the commercial production. The first step, green vegetative growth phase ("green stage") is to promote algal growth under favorable culture conditions (e.g., low light and nitrogen-replete) (Boussiba, 2000; Aflalo et al., 2007; Del Rio et al., 2007). When high cell density is reached, the culture enters into the second step, reddish inductive production phase ("red stage"), where algal cells are subjected to stress conditions such as high light intensity and nitrogen depletion, excess acetate addition, pH or salt stress, phosphate deficiency, or the addition of specific cell division inhibitors. These stress factors (either one or combination of more) induce the astaxanthin production in *H. pluvialis* (Fábregas et al., 2001; Torzillo et al., 2003; Orosa et al., 2005; He et al., 2007; Hu et al., 2008; Li et al., 2010; Choi et al., 2011). Therefore, carotenoid induction method has a direct correlation with both the astaxanthin content and total astaxanthin productivity. The optimal environmental and nutritional conditions for each stage are quite different (Del Rio et al., 2007). The reported biomass productivities in green stage and red stage ranged from 0.01 to 0.5 g L^{-1} d^{-1} and 0.01 to 4.8 g L^{-1} d^{-1}, respectively. Astaxanthin productivity and astaxanthin content ranged from 0.44 to 21 mg L^{-1} d^{-1} and 0.8 to 4.8% of DW, respectively (**Table 4**). Astaxanthin can be also produced efficiently by *H. pluvialis* using a simpler "one-step strategy." This strategy involves the administration of nitrate starvation and specific average irradiance in the culture medium, resulting in simultaneous algal cell growth and astaxanthin accumulation (Del Río et al., 2005; Del Rio et al., 2007; Del Río et al., 2008; García-Malea et al., 2009). At the laboratory scale and under continuous illumination, mean astaxanthin productivity of 20.8 mg L^{-1} d^{-1} has been reported for the one-step method (Del Río et al., 2008). The technical feasibility of this approach at a pilot scale was demonstrated in an outdoor tubular photobioreactor, which resulted in biomass and astaxanthin productivities of 0.7 g L^{-1} d^{-1} and 8 mg L^{-1} d^{-1}, respectively (García-Malea et al., 2009). One-stage cultivation seems attractive, since it is less complicated than the two-stage process and the production of astaxanthin takes place in a continuous mode. It has however two serious drawbacks. First, the actual astaxanthin production is significantly lower compared to the two-stage approach. Second, this cultivation is unsuitable for outdoor setting, since it requires incessant illumination during night as well what makes the process too expensive (Aflalo et al., 2007). An "attached cultivation" approach was successfully applied in the induction of *H. pluvialis* for astaxanthin production. In this method green cells are cultured in the conventional water column and then deposited on the membrane to increase light stress surface area in the second

phase of cultivation. Under the optimized conditions, biomass, and astaxanthin productivities in the attached cultivation system were 2.8 (3.7 g m^{-2} d^{-1}) and 2.4-fold (65.8 mg m^{-2} d^{-1}) higher than those of the suspended bioreactor, respectively (Wan et al., 2014b). Other studies that used similar approach have reported higher astaxanthin productivities of 124 mg m^{-2} d^{-1} (Yin et al., 2015) and 164.5 mg m^{-2} d^{-1} (Zhang et al., 2014). Attached cultivation approach is superior to suspended induction in several aspects such as, lower water consumption and smaller risk of contamination. This indicates that attached induction approach can provide a promising way to boost economic benefits and considerably reduce production cost of astaxanthin from *H. pluvialis* (Zhang et al., 2014; Wan et al., 2014b). Recently, Park et al. (2014) established a two-stage "perfusion culture" system for *H. pluvialis* combining it with stepwise increase of light irradiance. Approach is based on repeated replacement of the growth medium. Cells are grown in a photobioreactor and are periodically retained in the cell settling chamber whilst growth medium is being replaced in the photobioreactor. Cells are later recycled to the bioreactor and can efficiently utilize fresh growth medium which is free of inhibitory metabolic by-products. Perfusion culture can provide high biomass productivities of 0.18 g L^{-1} d^{-1}. Under stepwise increased light irradiance (150–450 µE/m²/s), cellular density of 12.3 g L^{-1} of have been obtained which is 3.09 and 1.67 times higher than batch and fed-batch processes, respectively whilst the productivity of astaxanthin reached 602 mg L^{-1} (Park et al., 2014).

Heterotrophic and Mixotrophic Culture

High light irradiance is often employed for enhancing astaxanthin formation in *H. pluvialis* cultures. However, light absorption and scattering caused by mutual shading of cells in large-scale cultures severely affects the productivity and quality of algal biomass and products. The high cost of illumination is another problem hindering the commercialization of *Haematococcus* products. To overcome this drawback, heterotrophic culture approach may be considered. Under heterotrophic growth conditions light is not needed as organic substrates serve as carbon and energy sources for growth and synthesis of secondary metabolites. Also, since lipid accumulation and astaxanthin biosynthesis are connected in space and time the effect of carbon source on lipid accumulation can have significant effect on overall productivity. It has been shown in *Haematococcus* and other microalgae lipid content and lipid profiles of microalgae are dependent on the cultivation conditions with various stress factors such as starvation or salt stress are efficient triggers of lipid accumulation, and can result in the alteration of fatty acid profiles due to cellular adjustment to particular stressor (Damiani et al., 2010; Lei et al., 2012; Saha et al., 2013; Chen et al., 2015). Various types of organic carbon sources have been used for heterotrophic cultivation and induction using acetate has been found effective for *Haematococcus* encystment and initiation of astaxanthin production (Kobayashi et al., 1991; Kakizono et al., 1992; Orosa et al., 2000; Hata et al., 2001; Kang et al., 2005). However, unlike many microalgae in which oversupply of easily accessible carbon in combination with nitrogen limitation yields diversion of

TABLE 4 | Summary of various methods of *H. pluvialis* biomass cultivation and corresponding astaxanthin productivities.

PBRs type	Outdoor/Indoor	Mode	Culture medium*	Biomass productivity in Green stage (g L⁻¹ d⁻¹)	Biomass productivity in Red stage (g L⁻¹ d⁻¹)	Astaxanthin content (%, DW)	Astaxanthin productivity (mg L⁻¹ d⁻¹)	References
Airlift column (30 L)	Indoor	Batch	Modified Bold's Basal medium	0.03	0.01	2.7	0.44[b]	Harker et al., 1996b
Tubular /open pond (25,000 L)	Outdoor	–	Modified Bold's Basal Medium	0.036–0.052	N/A	2.8–3.0	N/A	Olaizola, 2000
Tubular (50 L)	Indoor	Semi continuous	BG-11 medium	N/A	0.05	3.6	7.2[c,d]	Torzillo et al., 2003
Bubbling column (1.8)	Indoor	Batch	Basal inorganic culture medium	N/A	0.6	0.8	5.6[a]	Del Río et al., 2005
Airlift Tubular (55 L)		–	Inorganic medium free of acetate	N/A	0.41	1.1	4.4[a]	López et al., 2006
Bubbling column (0.5 L)	Indoor	Batch	BG-11 medium	0.5	0.21	4	11.5[b]	Aflalo et al., 2007
Tubular (200 L)	Outdoor	Batch	BG-11 medium	0.37	0.21	3.8	10.1[b,c]	Aflalo et al., 2007
Bubbling column (1.8 L)	Indoor	Batch	Basal inorganic culture medium	N/A	1.9	1.1	21[a]	Del Río et al., 2008
Bubbling column (1 L)	Indoor	Batch	Standard inorganic medium	0.36	0.14	3.6	12[b]	Ranjbar et al., 2008
Tubular (1.8 L), outdoor	Outdoor	Continuous	Standard inorganic medium	N/A	0.7	1	8[a]	García-Malea et al., 2009
Open pond	Indoor	Batch	BG-11 medium	N/A	0.15	2.79	4.3[a]	Zhang et al., 2009
Flat type (1 L)	Indoor	Fed batch	NIES-C medium	0.33	0.44	4.8	14[b]	Kang et al., 2010
Airlift column	Indoor	Batch	*Haematococcus* medium (OHM)	N/A	0.14	N/A	3.3[a]	Choi et al., 2011
Bubbling column (6 L)	Indoor	Batch	NIES-C medium	N/A	0.047	N/A	1.4[a]	Yoo et al., 2012
Bubbling column (0.6 L)	Outdoor	Batch	BG-11 medium	N/A	0.58	2.7	17.1[b,d]	Wang et al., 2013a
Bubbling column (0.6 L)	Outdoor	Batch	BG-11 medium	N/A	0.30	3.8	16.0[b,d]	Wang et al., 2013b

[a]Obtained from one-step culture process. [b]Obtained from two-step culture process. Productivity value was calculated based on total time required by the "green stage" and "red stage" of cultivation. [c]Induction of astaxanthin was performed outdoors; [d]Obtained from a two-step process in which astaxanthin productivity was calculated based on time spent on the "red stage" only.
*Detail medium composition can be found in relevant references.

the carbon flux toward lipid accumulation (Miao and Wu, 2006; Jia et al., 2014), *H. pluvialis* grows at a relatively low rate (0.22 d^{-1}) and accumulates negligible amount of astaxanthin, too low to be considered for commercial scale production if single step cultivation is considered (Kobayashi et al., 1992, 1997a; Moya et al., 1997). Additionally, heterotrophic cultivation of *Haematococcus* increases the risk of bacterial or fungal contamination (Hata et al., 2001; Olguín et al., 2012). *H. pluvialis* can be also produced indoors mixotrophically employing an organic acid (e.g., acetate) or carbohydrates as an additional carbon and energy source (Kobayashi et al., 1993). Studies have shown that both growth and astaxanthin production can be enhanced under mixotrophic culture conditions. A final cell density of 0.9–2.65 g L^{-1} and a maximum astaxanthin content of 1–2% DW were obtained from mixotrophic cultures of *H. pluvialis* (Chen et al., 1997; Zhang et al., 1999; Wang et al., 2003). A sequential, heterophotric-photoautotrophic culture mode was also explored. Heterotrophic culture was used in the green stage to produce algal biomass, while astaxanthin production was induced in photoautotrophic culture conditions. The induction of astaxanthin accumulation was performed under nitrogen deprivation conditions and whilst using bicarbonate or CO_2 as carbon sources. As a result, a very high cellular astaxanthin content of 7% (DW) was achieved, 3.4-fold higher than heterotrophic induction whilst astaxanthin productivity of 6.25 mg L^{-1} d^{-1} was obtained (Kang et al., 2005). Results indicate that photoautotrophic induction of astaxanthin production in *H. pluvialis* is more effective than heterotrophic one. Based upon the information obtained thus far, heterotrophic and mixotrophic culture modes are less cost-effective than the photoautotrophic one for *Haematococcus* mass culture.

Microbial Contamination and Possible Control Measures

Since interest in commercial microalgae cultivation is increasing, microbial contaminants that hamper production by resulting in reduced biomass yield and quality received great attention recently. Mass culture of *H. pluvialis* is reported to be contaminated by fungal parasites and zooplanktonic predators (e.g., amoebas, ciliates, and rotifers), as well as other microalgae and cyanobacteria (Han et al., 2013). A parasitic chytrid/blastoclad fungus *Paraphysoderma sedebokerenses* is found to be responsible for reduced astaxanthin productivity and frequent culture collapses in commercial *Haematococcus* cultivation facilities (Hoffman et al., 2008; Strittmatter et al., 2015). Detection of contaminants is prerequisite for preventing and controlling of microbial contamination in mass microalgal culture. Methods of detection usually include microscopy and staining, flow cytometry, molecular based detection and monitoring. In order to cope with microalgae culture contamination, the techniques that are generally used include abiotic stresses such as NO_3^- limitation, pH stress, temperature stress, light stress, toxic substances, and shear forces. There are some other techniques for parasite removal including salvage harvest, chemical agents (abscisic acid, copper sulfate), physical methods, biological methods (selective breeding and biological

agents) (Carney and Lane, 2014). Recently, several patent applications relating to control of fungus *P. sedebokerenses* have been developed in the USA and China to protect production losses in commercial *Haematococcus* culture facilities across the world (McBride et al., 2013; Zhang et al., 2013; Carney and Sorensen, 2015).

Harvesting

Harvesting remains one of the most challenging issues and a limiting factor for commercial algal biomass production. Harvesting of *H. pluvialis* refers to the selection of appropriate techniques to recover the "red" biomass, after the accumulation of astaxanthin in the cells and also that can facilitate cost-efficient astaxanthin extraction in the extraction phase. For the large scale harvesting of *H. pluvialis* centrifugation is the most common method and combined with other processes. Usually haematocysts are separated from the water through passive settling and subsequently concentrated with centrifugation (Lorenz and Cysewski, 2000; Olaizola, 2000; Li et al., 2011; Han et al., 2013; Pérez-López et al., 2014). Through the combination of these processes total suspended solid of 13.5% in the algal cake is achieved (Li et al., 2011). Flotation and disk-stack centrifugation have been also reported as another alternative for *H. pluvialis* harvest. Both showed more than 95% biomass recovery efficiency (Panis, 2015).

Cell Disruption

Different techniques have been developed in order to disrupt the algal cell and recover the intracellular metabolites. The most appropriate cell disruption methods to enhance recovery of astaxanthin from *H. pluvialis* at a commercial scale involve mechanical processes and more specifically expeller pressing and bead milling (Lorenz and Cysewski, 2000; Olaizola, 2003; Mercer and Armenta, 2011; Razon and Tan, 2011). During pressing (pulverization) microalgae cells are squeezed under high pressure in order to rupture the thick sporopollenin wall. Main advantage of expeller pressing is simple operation and minimization of contamination from external sources. Algal oil recovery efficiency of 75% can be achieved in a single step. Bead milling utilizes vessels filled with tiny glass, ceramic or steel beads that are agitated at high speeds. The dried biomass is fed in these vessels, where continuous exposure of biomass to the grinding media (beads) leads to cell-wall rupture, and subsequent release of intracellular compounds. This method is most effective when biomass concentration in the algal cake after harvesting is between 100 and 200 g/l (Greenwell et al., 2010). Both methods are reliable and widely applied for the *H. pluvialis* cells disruption at a commercial scale.

Dehydration

In commercial scale astaxanthin production, dehydration (drying) ensures the quality of the pigment and leads to the formulation of the final product (Mata et al., 2010; Li et al., 2011). After algal cell walls have been disrupted, biomass must be processed rapidly within few hours to avoid spoilage. Thus, dehydration is a process applied prior to recovery of the desired metabolite, in order to extend the shelf-life of the algal biomass

(Mata et al., 2010). The most known dehydration techniques that have been employed on microalgae are solar drying, spray drying, and freeze drying (Molina Grima et al., 2003; Brennan and Owende, 2010; Milledge, 2013). Spray drying has been considered as the most appropriate method to dry high-value microalgal products including *H. pluvialis* astaxanthin (Leach et al., 1998; Brennan and Owende, 2010; Li et al., 2011; Han et al., 2013; Milledge, 2013; Panis, 2015). The recovery efficiency of dry biomass (in powder) using this method exceeds 95% and in some occasions may approach 100% (Leach et al., 1998). After spray drying, the moisture content in "red" biomass is lowered to about 5% (Pérez-López et al., 2014). The main drawbacks of spray drying include high operational costs and the risk of microalgae pigments deterioration (Molina Grima et al., 2003). Freeze drying (lyophilization or cryodesiccation), involves the freezing of algal cake, the technique causes less damage than spray drying, but it is even more expensive, especially on a commercial scale (Milledge, 2013).

Recovery of Astaxanthin

Once the cell wall is disrupted and the biomass is fully dried, the recovery of the desired product is possible. Astaxanthin is a lipophilic compound and can be dissolved in solvents and oils. There is an abundance of astaxanthin extraction methods from *H. pluvialis* utilizing solvents, acids, edible oils, supercritical carbon dioxide (SC-CO_2) as well as microwave-assisted and enzyme-assisted approaches. Among the recovery methods used solvent extraction and supercritical carbon dioxide (SC-CO_2) extraction are considered as the most efficient, compatible, and widely used methods for astaxanthin extraction from *H. pluvialis*. The summary of various extraction methods of astaxanthin from *H. pluvialis* with recent updates is presented in **Table 5** Supercritical carbon dioxide (SC-CO_2) extraction has been widely used for industrial applications due to its many processing advantages. Due to low critical temperature of carbon dioxide, the SC-CO_2 system can be operated at moderate temperatures, preventing the degradation of valuable substances (Machmudah et al., 2006). Several studies have reported experiments on supercritical CO_2 extraction for the recovery of astaxanthin from *H. pluvialis.* Considering astaxanthin quality as the most important criterion, supercritical CO_2 extraction is the most favorable option. Supercritical CO_2 provides shorter extraction time and limits the use of toxic organic solvents. By contrast to most solvents, CO_2 is relatively cheap, chemically inert, non-toxic, and stable (Guedes et al., 2011). Supercritical fluid extraction has also been tested with *Haematococcus*, aiming at improving the extraction efficiency. For instance, supercritical carbon dioxide (SC-CO_2) coupled with ethanol or vegetable oil as a co-solvent can further increase the extraction efficiency of astaxanthin (80–90%) (Nobre et al., 2006; Krichnavaruk et al., 2008). There is an array of alternative approaches that can assist astaxanthin extraction from *H. pluvialis* such as solvents, acids, edible oils, enzymes, or pressurized liquids (Sarada et al., 2006; Kang and Sim, 2008; In, 2009; Jaime et al., 2010; Zou et al., 2013; Dong et al., 2014) Pressurized liquid extraction has several advantages over traditional solvent extraction. PLE requires shorter time, can be automated, uses less solvent, and

retains the sample in an oxygen-free and light-free environment in contrast to traditional organic solvent extraction (Jaime et al., 2010). Recently, a simple method for the direct extraction of lipids from high moisture *H. pluvialis* microalgae was successfully achieved using liquefied dimethyl ether (Boonnoun et al., 2014).

BIOREFINERY APPROACH FOR *H. PLUVIALIS*

Microalgae have been often proposed as third generation feedstock for biofuel production that does not compete for freshwater or land resources (Daroch et al., 2013a). However, despite significant advances in recent years it becomes apparent that cultivation of microalgae for the sole purpose of biofuel production is unlikely to be possible unless a major low-energy breakthrough technologies in algae cultivation, dewatering, and harvesting are developed (Li et al., 2015). In the meantime, microalgae are extremely important producers of many high-value nutraceutical compounds such as polyunsaturated fatty acids or astaxanthin that can justify high cost of microalgae cultivation and processing technologies. Integration of simultaneous production of numerous compounds within one system maximizing the benefits and limiting the costs is called biorefining (Li et al., 2015). Taking into consideration these findings *H. pluvialis* emerges as a very useful organism for the development of a dedicated microalgal biorefinery. It fits numerous requirements of for the development of first microalgal biorefineries especially the "high value product first" principle (Li et al., 2015). First, *H. pluvialis* is the best-known producer of astaxanthin-high value product worth in excess of several thousand US $ per kilogram. This product itself can easily justify expensive cultivation systems required for this organism. Second, *H. pluvialis* grown under nutrient starvation conditions induces both carotenogenesis (astaxanthin formation) and deposition of storage materials (triglycerides). It has been shown that these two responses are closely related and coincide in both space and time and triglycerides are essential for deposition of astaxanthin inside lipid bodies to confer its protective function (Solovchenko, 2015). In traditional approaches of microalgae to biofuels starvation-induced lipid accumulation is considered as significant challenge for commercialization of these systems as the overall lipid productivity of culture can drop significantly due to impaired growth rates under starvation conditions (Daroch et al., 2013b). In case of high value product like astaxanthin this drop becomes much less of the burden as the high value of the main product will compensate for this delay in final product formation. Due to the coexistence of astaxanthin and triglycerides in space and time it is possible to simultaneously obtain high value product (astaxanthin) and a biofuel feedstock (triglycerides) from a single algal feedstock. Since fatty acid content in the astaxanthin-containing 'red' cells can be as high as 30–60% of algae dry weight (Solovchenko, 2015) making *H. pluvialis* a very good candidate for biorefining strain. The fatty acid profiles of the alga have been evaluated by several studies and are summarized in **Table 2**, indicating that fatty acid profiles of the algae are suitable for biodiesel production

TABLE 5 | Summary of astaxanthin extraction methods from *H. pluvialis*.

| Astaxanthin Extraction/Purification method	Astaxanthin yield/Extraction efficiency	References
SC-CO$_2$ at 20 MPa, 55°C and13% (w/w) ethanol for 120 min of extraction time.	83% recovery	Reyes et al., 2014
CO$_2$ expanded ethanol (50% %w/w ethanol), 7 MPa, 45°C, 120 min of extraction time.	124.2% recovery	Reyes et al., 2014
SC- CO$_2$ at at 20 MPa, 60°C, 2 ml of ethanol for 1 h of extraction time	2.45 mg/g DW	Fujii, 2012
SC- CO$_2$, co-solvent 0.154–1% (v/v) ethanol, 7–34 MPa, 30–80°C, 0–100 min	74% recovery	Pan et al., 2012
SC- CO$_2$, co-solvent 1.25–8.75% (v/v) ethanol, 30–50 MPa, 35–75°C, 210 min	87.4% recovery	Wang et al., 2012
SC- CO$_2$, co-solvent 0–12% (v/v) vegetable oils, 30–50 MPa 50–80°C 300 min	51% recovery	Krichnavaruk et al., 2008
SC- CO$_2$, co-solvent 30–50 MPa 40–80°C 60–240 min	84% recovery	Thana et al., 2008
SC- CO$_2$, co-solvent,1.67–7.5% (v/v) ethanol 20–55 MPa 40–80°C, 240 min	80% recovery	Machmudah et al., 2006
SC- CO$_2$, co-solvent 0, 10% (v/v) ethanol 20–30 MPa, 40–60°C	90% recovery	Nobre et al., 2006
SC- CO$_2$, co-solvent 0, 9.4% (w/w) ethanol, 30 MPa at 60°C	97% recovery	Valderrama et al., 2003
Cell germination (12 h), Ionic liquid (1-ethyl-3- methylimidazolium ethylsulfate) (24 h),	32.5 pg/cell	Praveenkumar et al., 2015
Direct extraction using liquefid dimethyl ether (DME) at 0.59 MPa and 25°C, without drying, cell disruption, or heating,	1 (mg/g cell)	Boonnoun et al., 2014
HCl:acetone (5:5), 70°C, 20 min	19.8 mg/g cell	Dong et al., 2014
Ultrasound in solvent (EtOH and EA),16 min, 41°C, 40 kHz, 200 W, EtOH: ethyl acetate (20:1)	28 (mg/g)	Zou et al., 2013
Grinding three repetitions, pressurized hexane (10.3 Mpa)	35 (mg/g cell)	Jaime et al., 2010
Treating with enzymes (Viscozyme, Alcalase) at 50°C, 2 h	2649 ± 359 μg/g cell	In, 2009
Dodecane mixing 48 h, saponification with methanolic NaOH (0.02 M), sedimentation in darkness at 4°C, 12 h.	85% efficiency	Kang and Sim, 2008
Acid digestion, 2 N HCl, 70°C. Acetone extraction for 1 h	87% efficiency	Sarada et al., 2006
NaOH 30 min, Acetone (16 h)	7 (mg/g cell)	Mendes-Pinto et al., 2001
40% (v/v) acetone for 2 min at 80°C, followed by lyophilization or treatment with specific lytic enzymes	70% recovery	Kobayashi et al., 1997c

SC, supercritical; EA, ethyl acetate.

(Damiani et al., 2010). Third, *H. pluvialis* have been found to be a mixotrophic alga what is highly advantageous for development of microalgae biorefineries. *H. pluvialis* is capable of utilizing carbon dioxide, carbonates, and carbohydrates as carbon sources, this opens a possibilities of lowering cultivation costs and/or speeding up the cultivation of the strain through using various waste streams like flue gasses or waste streams containing carbon and nutrient compounds (Wu et al., 2013). Auto-, hetero-, and mixo-trophic cultivation modes require energy and nutrients, both of which can be to an extent recycled from anaerobic digestion process. Carbon sources vary depending on cultivation mode. Photoautotrophic cultivation requires CO$_2$ that can be recycled from energy production at anaerobic digestion stage. Heterotrophic cultivation requires reduced carbon source—such as carbohydrates or acetate which need to be supplied from alternative source. These compounds can also originate from waste streams. For example, food industry is rich in carbohydrate-rich waste streams that can be used in heterotrophic cultivation of *H. pluvialis* (Wang, 2014). Mixotrophic cultivation can take advantage of both sources of carbon. After simultaneous extraction of both high value product-astaxanthin and biofuel product-triglycerides algal cake composed of residual biomass can be utilized as a supplementary feedstock for biogas production using anaerobic digestion that would further assist in extraction of residual energy from this integrated bioprocess. These three features of *H. pluvialis* make it a suitable strain for the development of algal biorefineries

producing high value product (astaxanthin) and biofuel molecule (biodiesel and/or biogas). The proposed biorefinery scheme is presented on **Figure 8** and employs a classical two stage cultivation of *H. pluvialis* in green and red stage.

CURRENT GLOBAL MARKET AND MARKET PLAYERS OF *H. PLUVIALIS* ASTAXANTHIN

Synthetic astaxanthin dominates current commercial market, of the total value exceeding $200 million, corresponding to 130 metric tons of product per year (Li et al., 2011). According to recent reports, microalgae-derived astaxanthin corresponds to less than 1% of the commercialized quantity due to much lower price of synthetic astaxanthin and technological problems associated with large-scale algae cultivation (Koller et al., 2014; Pérez-López et al., 2014). In recent years, there has been a growing trend toward using natural ingredients in food, nutraceutical, and cosmetic markets, resulting from increasing concerns for consumer safety and regulatory issues over the introduction of synthetic chemicals into the human food chain. The demand for natural astaxanthin derived from *H. pluvialis* in the global market has been "sky-rocketing" in recent years owing to increasing consumer awareness of its health benefits. Global market for both synthetic and natural source astaxanthin in aquaculture feed, nutraceuticals, cosmetics, and food and
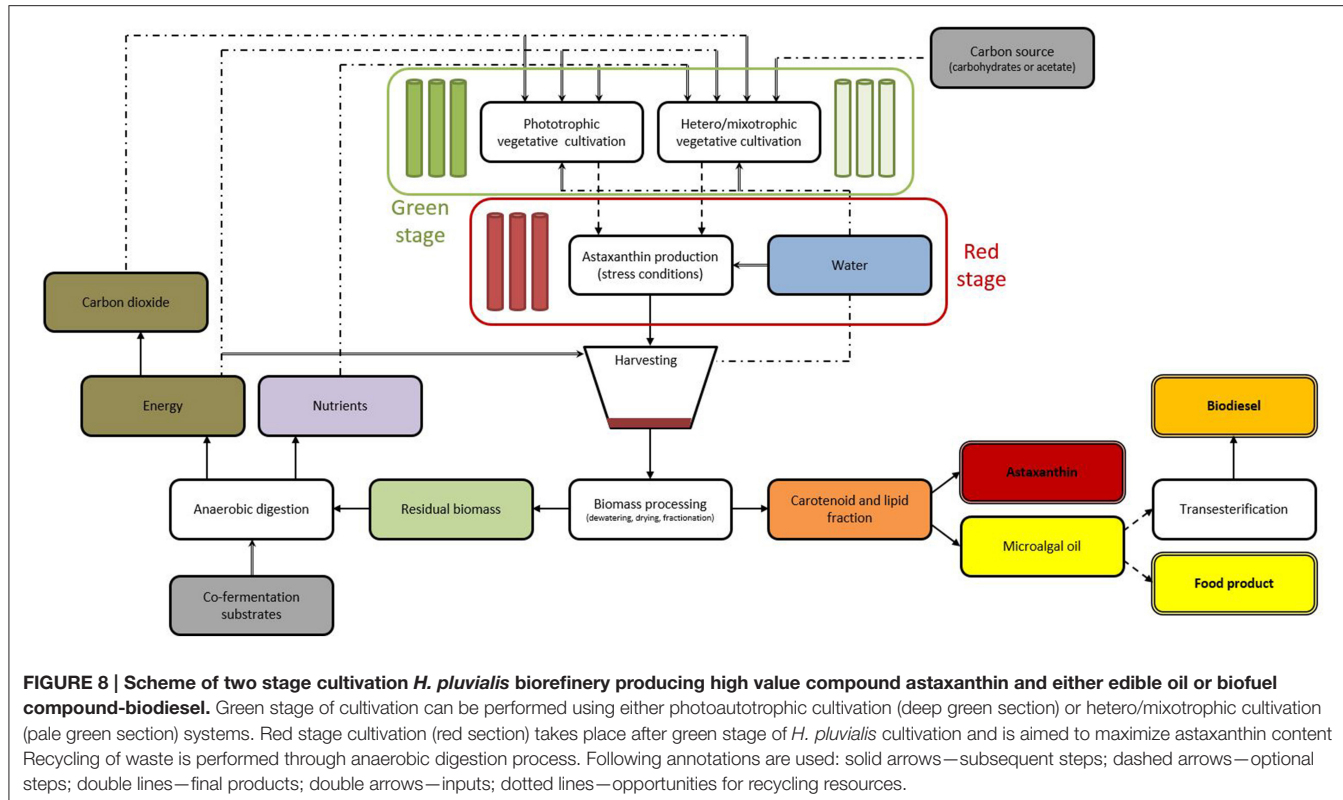
FIGURE 8 | Scheme of two stage cultivation *H. pluvialis* biorefinery producing high value compound astaxanthin and either edible oil or biofuel compound-biodiesel. Green stage of cultivation can be performed using either photoautotrophic cultivation (deep green section) or hetero/mixotrophic cultivation (pale green section) systems. Red stage cultivation (red section) takes place after green stage of *H. pluvialis* cultivation and is aimed to maximize astaxanthin content Recycling of waste is performed through anaerobic digestion process. Following annotations are used: solid arrows—subsequent steps; dashed arrows—optional steps; double lines—final products; double arrows—inputs; dotted lines—opportunities for recycling resources.

beverages is estimated at 280 metric tons valued at $447 million in 2014. It is further projected to reach 670 metric tons valued at $1.1 billion by 2020 (Industry Experts, 2015; Panis, 2015). Synthetic astaxanthin, astaxanthin rich *Phaffia* yeast, and *Paracoccus* bacteria are predominantly used in the aquaculture sector, while the astaxanthin derived from *H. pluvialis* is the main source for human applications such as dietary supplements, cosmetics, and food and beverages. Nowadays, the estimated market value of astaxanthin depending on products' purity varies from $2500–7000/kg to about $15,000/kg pigment from *H. pluvialis* in some cases (Borowitzka, 2013; Koller et al., 2014; Pérez-López et al., 2014; Industry Experts, 2015), while the production cost is estimated at about $1000 per kg of astaxanthin from *H. pluvialis* (Li et al., 2011). Natural astaxanthin is three to four times more valuable than the synthetic alternative in nutraceutical and pharmaceutical markets (Han et al., 2013). Since there is growing market demand for natural astaxanthin for specific commercial applications (e.g., the nutraceuticals market) to replace the synthetic astaxanthin, mass cultivation of *H. pluvialis* in industrial scale has great potential and attractive business opportunity. However, current market demand for natural astaxanthin is not met. It is expected that in the foreseeable future after the optimization of the production technology, the production costs of the natural astaxanthin from *H. pluvialis* should be more competitive to these of the synthetic alternative (Pérez-López et al., 2014). Since the mid 1990's, several leading companies are successfully producing *H. pluvialis* at commercial scale and marketing natural astaxanthin from *H. pluvialis* worldwide. The list of the leading companies with their

products is presented in **Table 6**. The size of the nutraceutical astaxanthin market is growing day by day and this market is very attractive to *Haematococcus* astaxanthin producers since the price of these products is significantly higher than those of feed applications. *Haematococcus* producers need to invest their attention for increasing astaxanthin production capacity to meet the global demand. It is worthy to mention that several manufacturers already have doubled the cultivation capacities in recent years. Apart from an increase in existing players' capacities, new producers, such as BGG in China, have entered the market with significant production capacities.

MAJOR CHALLENGES FOR THE IMPROVEMENT OF *H. PLUVIALIS* BIOMASS AND ASTAXANTHIN PRODUCTION

There are many challenges and problems for the development of large scale production of biomass and astaxanthin from *H. pluvialis.* Due to these obstacles the productivity can be hampered and in some cases a failure of the production system can make the production process economically unsustainable. Following issues are considered as most important challenges for the development of *H. pluvialis* astaxanthin production process:

- Lack of effective solution to prevent or treat microbial contaminations of mass cultures in a commercial scale.

TABLE 6 | Leading commercial companies and their *H. pluvialis*-derived astaxanthin and related products in the world market.

Company Name	Country	Brand Name	Product particulars
Cyanotech Corporation (www.cyanotech.com)	USA	BioAstin®	Astaxanthin extract packaged in soft gel, beadlets; dietary supplement
		Naturose™	Algae meal; pigmentation source for ornamental fish and animals
Mera Pharmaceutigals Inc. (www.merapharma.com)	USA	AstaFactor®	Astaxanthin packaged as soft gel; dietary supplement
Stazen Inc. (www.stazen.com)	USA	Stazen®	Dietary supplement containing algae crushed and dried algae meal
Valensa International (www.valensa.com)	USA	Zanthin®	Astaxanthin extract, soft gel, beadlets
Algatechnologies Ltd. (www.algatech.com)	Israel	AstaPure™	Dry algal biomass, astaxanthin beadlets, and oleoresin
Fuji Chemical Industry Co. Ltd. (AstaReal Co Tld) (www.fujichemical.co.jp; www.astareal.com)	Japan, Sweden, USA	AstaREAL®	Astaxanthin oleoresin products, water dispersible, and soluble powders
BioReal (Sweden) AB (subsidiary of Fuji Chemical) (www.bioreal.se)	Sweden	AstaXine® AstaCaroxe®	Dietary supplement containing algae crushed, and dried algae meal
		AstaEquus®	Astaxanthin extract feed supplement for horses
		Novaasta®	Astaxanthin extract feed supplement for animals
Britannia Health Products Ltd. (www.britanniahealth.co.uk)	UK	Britaxan®	Astaxanthin complex with other carotenoids packaged as capsule- dietary supplement
Supreme Biotechnologies NZ Ltd. (www.supremebiotech.com)	New Zealand	AstaSupreme®	Algal biomass, Oleoresins, beadlets, and soft gels of Astaxanthin
Atacama Bio Natural (www.atacamabionatural.com)	Chile	Supreme Asta Oil™ Supreme Asta powder™	Oleoresin for food, nutraceutic, and cosmetic products, and powder for animal feed supplement
Jingzhou Natural Astaxanthin Inc. (www.asta.cn)	China	NaturAsta™	Dry algal biomass and astaxanthin soft gel
Kunming Biogenic Co. Ltd. (www.bgenic.com)	China	AstaBio®	Algal biomass, oleoresins, beadlets, and soft gels of Astaxanthin
Beijing Ginko Group (BGG) Biological Technology Co. Ltd. (www.gingkogroup.com.cn)	China	AstaZine®	Astaxanthin oil, powder, and beadlets
Wefirst Biotechnology Co. Ltd. (www.astawefirst.com)	China	AstaFirst™	Dried algal powder, Astaxanthin oleoresin, and soft gel
Algaetech International SDN BHD (www.algaetech.com.my)	Malaysia	Astaxanthin Premia-*Ex*	Algae biomass, oleoresin, and soft gel
Parry Nutraceuticals Ltd. (EID Parry) (www.eidparry.com/)	India	Zanthin®	Astaxanthin oleoresins, beadlets, and soft gel

- Slow cell growth rate, sensitivity of the cells to hydrodynamic stress, and changes in cell morphology under various environmental conditions.
- Inadequate and cost ineffective cultivation, drying, and astaxanthin extraction technologies at the commercial scale.
- Unavailability of genetically improved/engineered strains of *H. pluvialis* and genetic transformation tools for engineering astaxanthin biosynthesis pathways in this organism for improved astaxanthin production.
- Lack of sufficient number of skilled workers in production farms and insufficient collaboration between universities and commercial enterprises.
- Lack of adequate scientific research on the economic performance and viability of commercial scale astaxanthin production process.

CONCLUSION AND PERSPECTIVES

This review provides an insight about the latest scientific and technological advancements in various aspects of astaxanthin-producing microalga *H. pluvialis* such as cell biology, reproduction, biosynthesis pathway, stress mechanism, biomass production, and downstream processing. It also contemplates a broader image including potential benefits, global market opportunities and integration of astaxanthin production into biorefining. In recent years there is an increased interest for natural astaxanthin from green microalga *H. pluvialis*. Wide ranges of scientific improvements have been achieved during the last decade in terms of productivity and bioprocessing in order to obtain a refined astaxanthin product. Yet its commercial production, especially for low-end markets is

too expensive for mass adoption of natural astaxanthin over its synthetic counterpart. *H. pluvialis* has been shown to be cultured in photoautotrophic, heterotrophic or mixotrophic growth conditions in various culture systems. Research have been conducted on the optimization of the various culture parameters, such as growth medium composition, light, pH, temperature etc. to achieve high biomass and astaxanthin production. Most of these parameters have been optimized and found different for biomass accumulation and astaxanthin production. Little can be done to address this limitatiaion as it is funadamentally connected with the life cycle of this microalgae. We believe there exist three key areas where further improvements are required and interesting novel approaches have been recently developed: cultivation efficiency and cost; good cultivation practice and predator control; and astaxanthin isolation and purification.

First, due to complex life-cycle of *H. pluvialis* it is important to maximase cell densities of alga at "green stage" of cultivation to maximize astaxanthin yield from the "red stage." We think that a number of recent developments can make significant impact in maximizing cell densities. Especially attached cultivation approach and a two-stage "perfusion culture" system can be considered most promising due to the capability of producing several fold higher biomass and astaxanthin productivity and some other benefits such as lower water consumption and smaller risk of contamination. These improvements may boost economic benefits and reduce production cost of astaxanthin from *H. pluvialis* (Park et al., 2014; Wan et al., 2014b; Zhang et al., 2014). Alternatively, utilization of supplementary carbon source and adoption a two-stage sequential heterotrophic-photoautotrophic approach could improve biomass and astaxanthin production. Especially utilization of waste carbon and nutrient sources in biorefinery setup could help to decrease cultivation costs. Unfortunately, these researches are still in laboratory stage and need to be tested in large-scale commercial production for further validation.

Second, control of contaminants, parasites, and predators remains to be primary concern for *Haematococcus* growers and major issue in culture stability and astaxanthin productivity. Since there is very little that can be done once contamination takes place it is important to limit the possibility of such disruption and identify it as soon as possible, and avoid spreading to other parts of culture. Traditional detection methods such as microscopy and staining can be used to visualize algal parasites, however this technique may be too labor intensive to perform on a routine basis for most commercial operations. For routine detection, more automated systems such as flow cytometry would be ideal. Alternatively, molecular-based techniques that are considered as the most informative and sensitive for the detection and identification of parasites. Following techniques are worth further exploring DNA sequencing (Sanger, shotgun, or next generation) and then monitoring for these specifically using qPCR or phylochip technology. Decreasing costs of next generation DNA sequencing can make DNA sequencing for culture diagnostic purposes more accessible in the near future.

Third, combination of low cell densities and robust trilayer cell walls of astaxanthin-containing aplanospores make isolation of astaxanthin difficlut and expensive. Currentlly harvesting by centrifugation, cell wall disruption by expeller pressing and bead milling are the most common described methods for commercial scale astaxanthin production from *H. pluvialis*. After cell walls disruption, biomass is usually processed by spray drying or freeze drying. A number of astaxanthin extraction methods such as (solvents, acids, edible oils, supercritical carbon dioxide, microwave-assisted, and enzyme-assisted approaches have been reported for *H. pluvialis* and supercritical carbon dioxide (SC- CO_2) extraction has been widely used for industrial applications. Two recently developed methods allow efficient extraction of astaxanthin-containing lipids from wet biomass at yields comparable to conventional drying-solvent extraction method. Efficient extraction of astaxanthin from wet *H. pluvialis* biomass was achieved with liquefied dimethyl ether (Boonnoun et al., 2014) and also cell germination process in conjunction with ionic liquids treatment (Praveenkumar et al., 2015).

Despite significant advances in research and development of *H. pluvialis* astaxanthin production is still in laboratory stage and often faces difficulties to become implemented in large-scale commercial production. There is a number of other areas of improvement that will contribute to the expansion of *Haematococcus* production capacity, lowering the production cost, and increasing market penetration at low end applications. These include: next-generation culture systems along with advanced management practices; better understanding of astaxanthin biosynthesis, metabolic pathways and their regulation, genetic engineering, and omics-scale understanding of astaxanthin accumulation; development of genetic manipulation toolbox; exploration of integration of *H. pluvialis* cultivation with other processes. Yet, we firmly believe that three key areas of focus should be: cultivation efficiency and cost; good cultivation practice and predator control; and astaxanthin isolation and purification. Further developments in these fields can have a profound effect on the commercial deployment of *H. pluvialis* astaxanthin products and can act as a catalyst for the development of an entire microalgae industry in the near future.

AUTHOR CONTRIBUTIONS

FUNDING

REFERENCES

Aflalo, C., Meshulam, Y., Zarka, A., and Boussiba, S. (2007). On the relative efficiency of two- vs. one-stage production of astaxanthin by the green alga *Haematococcus pluvialis. Biotechnol. Bioeng.* 98, 300–305. doi: 10.1002/bit.21391

Ako, H., and Tamaru, C. S. (1999). Are feeds for food fish practical for aquarium fish? *Int. Aqua Feeds* 2, 30–36.

Al-Bulishi, M. S. M., Changhu, X., and Tang, Q. J. (2015). Health aspects of astaxanthin: a review. *Canad. J. Clin. Nutr.* 3, 71–78. doi: 10.14206/canad.j.clin.nutr.2015.02.08

Andersen, L. P., Holck, S., Kupcinskas, L., Kiudelis, G., Jonaitis, L., Janciauskas, D., et al. (2007). Gastric inflmmatory markers and interleukins in patients with functional dyspepsia treated with astaxanthin. *FEMS Immunol. Med. Microbiol.* 50, 244–248. doi: 10.1111/j.1574-695X.2007.00257.x

Andrisani, A., Donà, G., Tibaldi, E., Brunati, A. M., Sabbadin, C., Armanini, D., et al. (2015). Astaxanthin improves human sperm capacitation by inducing lyn displacement and activation. *Mar. Drugs* 13, 5533–5551. doi: 10.3390/md13095533

Arai, S., Mori, T., Miki, W., Yamaguchi, K., Konosu, S., Satake, M., et al. (1987). Pigmentation of juvenile coho salmon with carotenoid oil extracted from Antarctic krill. *Aquaculture* 66, 255–264. doi: 10.1016/0044-8486(87)90111-6

Augusti, P. R., Quatrin, A., Somacal, S., Conterato, G. M., Sobieskim, R., Ruviaro, A. R., et al. (2012). Astaxanthin prevents changes in the activities of thioredoxin reductase and paraoxonase in hypercholesterolemic rabbits. *J. Clin. Biochem. Nutr.* 51, 42–49. doi: 10.3164/jcbn.11-74

Bischoff, H. W., and Bold, H. C. (1963). "Phycological studies IV," in *Some Soil Algae from Enchanted Rock and Related Algal Species*. (Austin, TX: University of Texas Publications), 95.

Bloomer, R. J., Fry, A., Schilling, B., Chiu, L., Hori, N., and Weiss, L. (2005). Astaxanthin supplementation does not attenuate muscle injury following eccentric exercise in resistance-trained men. *Int. J. Sport Nutr. Exerc. Metab.* 15, 401–412.

Bold, H. C., and Wynne, M. J., (1985). *Introduction to the Algae*. Texas: Prentice-Hall Inc.

Boonnoun, P., Kurita, Y., Kamo, Y., Machmudah, S., Okita, Y., Ohashi, E., et al. (2014). Wet extraction of lipids and astaxanthin from *Haematococcus pluvialis* by liquefied dimethyl ether. *J. Nutr. Food Sci.* 4:305. doi: 10.4172/2155-9600.1000305

Borowitzka, M. A. (2013). High-value products from microalgae—their development and commercialisation. *J. Appl. Phycol.* 25, 743–756. doi: 10.1007/s10811-013-9983-9

Boussiba, S. (2000). Carotenogenesis in the green alga *Haematococcus pluvialis*: cellular physiology and stress response. *Physiol. Plantarum* 108, 111–117. doi: 10.1034/j.1399-3054.2000.108002111.x

Boussiba, S., and Vonshak, A. (1991). Astaxanthin accumulation in the green alga *Haematococcus pluvialis. Plant Cell Physiol.* 32, 1077–1082.

Boussiba, S., Bing, W., Yuan, J. -P., Zarka, A., and Chen, F. (1999). Changes in pigments profie in the green alga *Haeamtococcus pluvialis* exposed to environmental stresses. *Biotechnol. Lett.* 21, 601–604. doi: 10.1023/A:1005507514694

Boussiba, S., Fan, L., and Vonshak, A. (1992). "Enhancement and determination of astaxanthin accumulation in green alga *Haematococcus pluvialis*," in *Carotenoids Part A: Chemistry, Separation, Quantitation, and Antioxidation*, Enzymology (Academic Press), 386–391.

Brennan, L., and Owende, P. (2010). Biofuels from microalgae-A review of technologies for production, processing, and extractions of biofuels and co-products. *Renew. Sust. Energ. Rev.* 14, 557–577. doi: 10.1016/j.rser.2009.10.009

Brinda, B. R., Sarada, R., Kamath, B. S., and Ravishankar, G. A. (2004). Accumulation of astaxanthin in flgellated cells of *Haematococcus pluvialis* - cultural and regulatory aspects. *Curr. Sci.* 87, 1290–1294.

Britton, G. (1993). "Biosynthesis of carotenoids," in *Carotenoids in Photosynthesis SE - 4*, eds A. Young and G. Britton (London: Springer), 96–126. doi: 10.1007/978-94-011-2124-8_4

Burchardt, L., Balcerkiewicz, S., Kokocinski, M., Samardakiewicz, S., and Adamski, Z. (2006). Occurrence of *Haematococcus pluvialis* Flotow emend. Wille in a small artificial pool on the university campus of the collegium biologicum in poznan (Poland). *Biodiv. Res. Conserv.* 1, 163–166.

Capelli, G. C., and Cysewski, G. (2013). *The Worlds' Best Kept Health Secret Natural Astaxanthin*. Kailua-Kona, HI: Cyanotech Corporation.

Carney, L. T., and Lane, T. W. (2014). Parasites in algae mass culture. *Front. Microbiol.* 5:278. doi: 10.3389/fmicb.2014.00278

Carney, L. T., and Sorensen, K. (2015). *Methods for Treating a Culture of Haematococcus pluvialis for Contamination using Hydrogen Peroxide*. US Patent 9113607 B1.

Cerón, M. C., García-Malea, M. C., Rivas, J., Acien, F. G., Fernandez, J. M., Del Río, E., et al. (2007). Antioxidant activity of *Haematococcus pluvialis* cells grown in continuous culture as a function of their carotenoid and fatty acid content. *Appl. Microbiol. Biotechnol.* 74, 1112–1119. doi: 10.1007/s00253-006-0743-5

Chekanov, K., Lobakova, E., Selyakh, I., Semenova, L., Sidorov, R., and Solovchenko, A. (2014). Accumulation of astaxanthin by a new *Haematococcus pluvialis* strain BM1 from the White Sea coastal rocks (Russia). *Mar. Drugs.* 12, 4504–4520. doi: 10.3390/md12084504

Chen, F., Chen, H., and Gong, X. (1997). Mixotrophic and heterotrophic growth of *Haematococcus lacustris* and rheological behaviour of the cell suspensions. *Bioresour. Technol.* 62, 19–24. doi: 10.1016/S0960-8524(97)00115-6

Chen, G., Wang, B., Han, D., Sommerfeld, M., Lu, Y., Chen, F., et al. (2015). Molecular mechanisms of the coordination between astaxanthin and fatty acid biosynthesis in *Haematococcus pluvialis* (Chlorophyceae). *Plant J.* 81, 95–107. doi: 10.1111/tpj.12713

Chen, Y., Li, D., Lu, W., Xing, J., Hui, B., and Han, Y. (2003). Screening and characterization of astaxanthin-hyperproducing mutants of *Haematococcus pluvialis. Biotechnol. Lett.* 25, 527–529. doi: 10.1023/A:1022877703008

Chew, B. P., Park, J. S., Hayek, M. G., Massimino, S., and Reinhart, G. A. (2004). Dietary astaxanthin stimulates cell-mediated and humoral immune response in cats. *FASEB J.* 18, 533.

Chew, B. P., and Park, J. S.(2004). Carotenoid action on the immune reponse. *J. Nutr.* 134, 257–261.

Choi, Y. E., Yun, Y. S., Park, J. M., and Yang, J. W. (2011). Determination of the time transferring cells for astaxanthin production considering two-stage process of *Haematococcus pluvialis* cultivation. *Bioresour. Technol.* 102, 11249–11253. doi: 10.1016/j.biortech.2011.09.092

Choubert, G., and Heinrich, O. (1993). Carotenoid pigments of the green alga *Haematococcus pluvialis*: assay on rainbow trout, *Oncorhynchus mykiss*, pigmentation in comparison with synthetic astaxanthin and canthaxanthin. *Aquaculture* 112, 217–226. doi: 10.1016/0044-8486(93)90447-7

Chumpolkulwong, N., Kakizono, T., Handa, T., and Nishio, N. (1997). Isolation and characterization of compactin resistant mutants of an astaxanthin synthesizing green alga *Haematococcus pluvialis. Biotechnol. Lett.* 19, 299–302. doi: 10.1023/A:1018330329357

Comhaire, F. H., El Garem, Y., Mahmoud, A., Eertmans, F., and Schoonjans, F. (2005). Combined conventional/ antioxidant "Astaxanthin" treatment for male infertility: a double blind randomized trial. *Asian J. Androl.* 7, 257–262. doi: 10.1111/j.1745-7262.2005.00047.x

Cunningham, F. X., and Gantt, E. (1998). Genes and enzymes of carotenoid biosynthesis in plants. *Annu. Rev. Plant Physiol. Plant Mol. Biol.* 49, 557–583. doi: 10.1146/annurev.arplant.49.1.557

Cyanotech (2015). *BioAstin - Natural Astaxanthin*. Available online at: http://www.cyanotech.com/bioastin.html (Retrieved 21 October, 2015).

Czygan, F. C. (1970). Blood-rain and blood-snow: nitrogendefiient cells of *Haematococcus pluvialis* and *Chlamydomonas nivalis. Arch. Mikrobiol.* 74, 69–76. doi: 10.1007/BF00408689

Damiani, M. C., Popovich, C. A., Constenla, D., and Leonardi, P. I. (2010). Lipid analysis in *Haematococcus pluvialis* to assess its potential use as a biodiesel feedstock. *Bioresour. Technol.* 101, 3801–3807. doi: 10.1016/j.biortech.2009.12.136

Daroch, M., Geng, S., and Wang, G. (2013a). Recent advances in liquid biofuel production from algal feedstocks. *Appl. Energy* 102, 1371–1381. doi: 10.1016/j.apenergy.2012.07.031

Daroch, M., Shao, C., Liu, Y., Geng, S., and Cheng, J. J. (2013b). Induction of lipids and resultant FAME profiles of microalgae from coastal waters of pearl river delta. *Bioresour. Technol.* 146, 192–199. doi: 10.1016/j.biortech.2013.07.048

Del Río, E., Acién, F. G., García-Malea, M. C., Rivas, J., Del Rio, E., Acién, F. G., et al. (2005). Efficient one-step production of astaxanthin by the microalga *Haematococcus pluvialis* in continuous culture. *Biotechnol. Bioeng.* 91, 808–815. doi: 10.1002/bit.20547

Del Rio, E., Acien, F. G., Garcia-Malea, M. C., Rivas, J., Molina-Grima, E., and Guerrero, M. G. (2007). Efficiency assessment of the one-step production of astaxanthin by the microalga *Haematococcus pluvialis*. *Biotechnol. Bioeng.* 100, 397–402. doi: 10.1002/bit.21770

Del Río, E., Acién, F. G., García-Malea, M. C., Rivas, J., Molina-Grima, E., and Guerrero, M. G. (2008). Efficiency assessment of the one-step production of astaxanthin by the microalga *Haematococcus pluvialis*. *Biotechnol. Bioeng.* 100, 397–402. doi: 10.1002/bit.21770

Domínguez-Bocanegra, A. R., Guerrero Legarreta, I., Martinez Jeronimo, F., and Tomasini Campocosio, A. (2004). Influence of environmental and nutritional factors in the production of astaxanthin from *Haematococcus pluvialis*. *Bioresour. Technol.* 92, 209–214. doi: 10.1016/j.biortech.2003.04.001

Dong, S., Huang, Y., Zhang, R., Wang, S., and Liu, Y. (2014). Four different methods comparison for extraction of astaxanthin from green alga *Haematococcus pluvialis*. *Sci. World J.* 7, 694–705. doi: 10.1155/2014/694305

Dragos, N., Bercea, V., Bica, A., Druga, B., Nicoara, A., and Coman, C. (2010). Astaxanthin production from a new strain of *Haematococcus pluvialis* grown in batch culture. *Ann. Roman. Soc. Cell Biol.* 15, 353–361.

Eisenreich, W., Rohdich, F., and Bacher, A. (2001). Deoxyxylulose phosphate pathway to terpenoids. *Trends Plant Sci.* 6, 78–84. doi: 10.1016/S1360-1385(00)01812-4

Elgarem, Y., Lignell, A., and Comhaire, F. H. (2002). "Supplementation with Astaxanthin (Astacarox) improves semen quality in infertile men," in *Proceedings of the 13th International Carotenoid Symposium* (Honolulu, HI), 180–197.

Elliot, A. M. (1934). Morphology and life history of *Haematococcus pluvialis*. *Arch. Protistenk.* 82, 250–272.

Elwinger, K., Lignell, A., and Wilhelmson, M. (1997). "Astaxanthin rich algal meal (*Haematococcus pluvialis*) as carotenoid source in feed for laying hens," in *Proceedings of the VII European Symposium on the Quality of Eggs and Egg Products* (Poznan), 52–59.

Eom, H., Lee, C. G., and Jin, E. (2006). Gene expression profile analysis in astaxanthin-induced *Haematococcus pluvialis* using a cDNA microarray. *Planta* 223, 1231–1242. doi: 10.1007/s00425-005-0171-2

Fábregas, J., Domínguez, A., Regueiro, M., Maseda, A., and Otero, A. (2000). Optimization of culture medium for the continuous cultivation of the microalga *Haematococcus pluvialis*. *Appl. Microbiol. Biotechnol.* 53, 530–535. doi: 10.1007/s002530051652

Fábregas, J., Otero, A., Maseda, A., and Domínguez, A. (2001). Two-stage cultures for the production of astaxanthin from *Haematococcus pluvialis*. *J. Biotechnol.* 89, 65–71. doi: 10.1016/S0168-1656(01)00289-9

Fan, L., Vonshak, A., and Boussiba, S. (1994). Effect of temperature and irradiance on growth of *Haematococcus pluvialis* (Chlorophyceae). *J. Phycol.* 30, 829–833. doi: 10.1111/j.0022-3646.1994.00829.x

Fassett, R. G., and Combes, J. S. (2011). Astaxanthin: a potential therapeutic agent in cardiovascular disease. *Mar. Drugs* 9, 447–465. doi: 10.3390/md9030447

Ferrante, R. J., Browne, S. E., Shinobu, L. A., Bowling, A. C., Baik, M. J., MacGarvey, U., et al. (1997). Evidence of increased oxidative damage in both sporadic and familial amyotrophic lateral sclerosis. *J. Neurochem.* 69, 2064–2074. doi: 10.1046/j.1471-4159.1997.69052064.x

Forján, E., Navarro, F., Cuaresma, M., Vaquero, I., Ruíz-Domínguez, M. C., Gojkovic, Ž., et al. (2015). Microalgae: fast-growth sustainable green factories. *Crit. Rev. Environ. Sci. Technol.* 45, 1705–1755. doi: 10.1080/10643389.2014.966426

Fujii, K. (2012). Process integration of supercritical carbon dioxide extraction and acid treatment for astaxanthin extraction from a vegetative microalga. *Food Bioprod. Process.* 90, 762–766. doi: 10.1016/j.fbp.2012.01.006

Gacheva, G., Dimitrova, P., and Pilarski, P. (2015). New strain *Haematococcus cf. pluvialis* Rozhen-12 - growth, biochemical characteristics and future perspectives. *Genet. Plant Physiol.* 5, 29–38.

Gao, Z., Meng, C., Gao, H., Li, Y., Zhang, X., Xu, D., et al. (2013b). Carotenoid genes transcriptional regulation for astaxanthin accumulation in fresh water unicellular alga *Haematococcus pluvialis* by gibberellin A3 (GA3). *Ind. J. Biochem. Biophys.* 50, 548–553.

Gao, Z., Meng, C., Gao, H., Zhang, X., Xu, D., Su, Y., et al. (2013a). Analysis of mRNA expression profiles of carotenogenesis and astaxanthin production

of *Haematococcus pluvialis* under exogenous. *Biol. Res.* 46, 201–206. doi: 10.4067/S0716-97602013000200012

Gao, Z., Meng, C., Zhang, X., Xu, D., Miao, X., Wang, Y., et al. (2012a). Induction of salicylic acid (SA) on transcriptional expression of eight carotenoid genes and astaxanthin accumulation in *Haematococcus pluvialis*. *Enzyme Microb. Technol.* 51, 225–230. doi: 10.1016/j.enzmictec.2012.07.001

Gao, Z., Meng, C., Zhang, X., Xu, D., Zhao, Y., Wang, Y., et al. (2012b). Differential expression of carotenogenic genes, associated changes on astaxanthin production and photosynthesis features induced by JA in *H. pluvialis*. *PLoS ONE* 7:e42243. doi: 10.1371/journal.pone.0042243

García-Malea, M. C., Acién, F. G., Del Río, E., Fernández, J. M., Cerón, M. C., Guerrero, M. G., et al. (2009). Production of astaxanthin by *Haematococcus pluvialis*: taking the one-step system outdoors. *Biotechnol. Bioeng.* 102, 651–657. doi: 10.1002/bit.22076

Gomez, P. I., Inostroza, I., Pizarro, M., and Perez, J. (2013). From genetic improvement to commercial-scale mass culture of a Chilean strain of the green microalga *Haematococcus pluvialis* with enhanced productivity of the red ketocarotenoid astaxanthin. *AoB Plants* 5:plt026. doi: 10.1093/aobpla/plt026

Greenwell, H. C., Laurens, L. M. L., Shields, R. J., Lovitt, R. W., and Flynn, K. J. (2010). Placing microalgae on the biofuels priority list: a review of the technological challenges. *J. Royal Soc. Int.* 7, 703–726. doi: 10.1098/rsif.2009.0322

Grewe, C. B., and Griehl, C. (2012). "The carotenoid astaxanthin from *Haematococcus pluvialis*," in *Microalgal Biotechnology: Integration and Economy* eds C. Posten and C. Walter (Berlin; Boston, MA: De Gruyter), 129–144. doi: 10.1515/9783110298321.129

Guedes, A. C., Amaro, H. M., and Malcata, F. X. (2011). Microalgae as sources of carotenoids. *Mar. Drugs* 9, 625–644. doi: 10.3390/md9040625

Guerin, M., Huntley, M. E., and Olaizola, M. (2003). *Haematococcus* astaxanthin: applications for human health and nutrition. *Trends Biotechnol.* 21, 210–216. doi: 10.1016/S0167-7799(03)00078-7

Gutiérrez, C. L., Gimpel, J., Escobar, C., Marshall, S. H., and Henríquez, V. (2012). Chloroplast genetic tool for the green microalgae *Haematococcus pluvialis* (Chlorophyceae, Volvocales)1. *J. Phycol.* 48, 976–983. doi: 10.1111/j.1529-8817.2012.01178.x

Gwak, Y., Hwang, Y. S., Wang, B., Kim, M., Jeong, J., Lee, C. G., et al. (2014). Comparative analyses of lipidomes and transcriptomes reveal a concerted action of multiple defensive systems against photooxidative stress in *Haematococcus pluvialis*. *J. Exp. Bot.* 65, 4317–4334. doi: 10.1093/jxb/eru206

Hagen, C., Siegmund, S., and Braune, W. (2002). Ultrastructural and chemical changes in the cell wall of *Haematococcus pluvialis* (Volvocales, Chlorophyta) during aplanospore formation. *Eur. J. Phycol.* 37, 217–226. doi: 10.1017/S0967026202003669

Han, D., Li, Y., and Hu, Q. (2013). "Biology and commercial aspects of *Haematococcus pluvialis*," in *Handbook of Microalgal Culture: Applied Phycology and Biotechnology, 2nd Edn.*, eds A. Richmond and Q. Hu (Hoboken, NJ: Blackwell), 388–405. doi: 10.1002/9781118567166.ch20

Harker, M., Tsavalos, A. J., and Young, A. J. (1996a). Factors responsible for astaxanthin formation in the chlorophyte *Haematococcus pluvialis*. *Bioresour. Technol.* 55, 207–214. doi: 10.1016/0960-8524(95)00002-X

Harker, M., Tsavalos, A. J., and Young, A. J. (1996b). Autotrophic growth and carotenoid production of *Haematococcus pluvialis* in a 30 liter air-lift photobioreactor. *J. Ferment. Bioeng.* 82, 113–118. doi: 10.1016/0922-338X(96)85031-8

Hashimoto, H., Arai, K., Hayashi, S., Okamoto, H., Takahashi, J., Chikuda, M., et al. (2013). Effects of astaxanthin on antioxidation in human aqueous humor. *J. Clin. Biochem. Nutr.* 53, 1–7. doi: 10.3164/jcbn.13-6

Hata, N., Ogbonna, J. C., Hasegawa, Y., Taroda, H., and Tanaka, H. (2001). Production of astaxanthin by *Haematococcus pluvialis* in a sequential heterotrophic-photoautotrophic culture. *J. Appl. Phycol.* 13, 395–402. doi: 10.1023/A:1011921329568

Hazen, T. E. (1899). The life history of *Sphaerella lacustris*. *Mem. Torrey Bot. Club* 6, 211–244.

He, P., Duncan, J., and Barber, J. (2007). Astaxanthin accumulation in the green alga *Haematococcus pluvialis*: effects of cultivation parameters. *J. Integr. Plant. Biol.* 49, 447–451. doi: 10.1111/j.1744-7909.2007.00468.x

Higuera-Ciapara, I., Felix-Valenzuela, L., and Goycoolea, F. M. (2006). Astaxanthin: a review of its chemistry and applications. *Crit. Rev. Food Sci. Nutr.* 46, 185–196. doi: 10.1080/10408690590957188

Hoeffler, J. F., Hemmerlin, A., Grosdemange-Billiard, C., Bach, T. J., and Rohmer, M. (2002). Isoprenoid biosynthesis in higher plants and in *Escherichia coli*: on the branching in the methylerythritol phosphate pathway and the independent biosynthesis of isopentenyl diphosphate and dimethylallyl diphosphate. *Biochem. J.* 366, 573–583. doi: 10.1042/bj20020337

Hoffman, Y., Aflalo, C., Zarka, A., Gutman, J., James, T. Y., and Boussiba, S. (2008). Isolation and characterization of a novel chytrid species (phylum Blastocladiomycota), parasitic on the green alga *Haematococcus. Mycol. Res.* 112, 70–81. doi: 10.1016/j.mycres.2007.09.002

Hong, M.-E., Choi, S. P., Park, Y.-I., Kim, Y.-K., Chang, W. S., Kim, B. W., et al. (2012). Astaxanthin production by a highly photosensitive *Haematococcus* mutant. *Process. Biochem.* 47, 1972–1979. doi: 10.1016/j.procbio.2012.07.007

Hu, Z., Li, Y., Sommerfeld, M., Chen, F., and Hu, Q. (2008). Enhanced protection against oxidative stress in an astaxanthin-overproduction *Haematococcus* mutant (Chlorophyceae). *Eur. J. Phycol.* 43, 365–376. doi: 10.1080/09670260802227736

Hussein, G., Sankawa, U., Goto, H., Matsumoto, K., and Watanabe, H. (2006). Astaxanthin, a carotenoid with potential in human health and nutrition. *J. Nat. Prod.* 69, 443–449. doi: 10.1021/np050354+

Ikeuchi, M., Koyama, T., Takahashi, J., and Yazawa, K. (2007). Effects of astaxanthin in obese mice fed a high-fat diet. *Biosci. Biotechnol. Biochem.* 71, 893–899. doi: 10.1271/bbb.60521

In, M. (2009). Effect of enzyme treatments on the extraction efficacy and antioxidant activity of haematococcus extract from *Haematococcus pluvialis. J. Korea Acad. Indus. Cooperat. Soc.* 10, 194–199. doi: 10.5762/KAIS.2009.10.1.194

Inbbor, J. (1998). *Haematococcus*, the poultry pigmentor. *Feed Mix.* 6, 31–34.

Inborr, J., and Lignell, Å. (1997). "Effect of feeding astaxanthin-rich algae meal (*Haematococcus pluvialis*) on performance and carotenoid concentration of different tissues of broiler chickens," in *Proceedings of the XIII WPSA Conference on Poultry Meat Quality in Poznan* (Poland: Session M1), 39–43.

Industry Experts (2015). *Global Astaxanthin Market – Sources, Technologies and Applications.* Available online at: http://industry-experts.com/verticals/healthcare-and-pharma/global-astaxanthin-market-sources-technologies-and-applications

Issarapayup, K., Powtongsook, S., and Pavasant, P. (2009). Flat panel airlift photobioreactors for cultivation of vegetative cells of microalga *Haematococcus pluvialis. J. Biotechnol.* 142, 227–232. doi: 10.1016/j.jbiotec.2009.04.014

Iwamoto, T., Hosoda, K., Hirano, R., Kurata, H., Matsumoto, A., Miki, W., et al. (2000). Inhibition of low-density lipoprotein oxidation by astaxanthin. *J. Atheroscler. Thromb.* 7, 216–222. doi: 10.5551/jat1994.7.216

Iwasaki, T., and Tawara, A. (2006). Effects of astaxanthin on eyestrain induced by accommodative dysfunction. *J. Eye (Atarashii Ganka).* 6, 829–834.

Jaime, L., RodrIguez-Meizoso, I., Cifuentes, A., Santoyo, S., Suarez, S., and Ibánez, E. (2010). Pressurized liquids as an alternative process to antioxidant carotenoids extraction from *Haematococcus pluvialis* microalgae. *LWT Food Sci. Tech.* 43, 105–112. doi: 10.1016/j.lwt.2009.06.023

Jia, Z., Liu, Y., Daroch, M., Geng, S., and Cheng, J. J. (2014). Screening, growth medium optimisation and heterotrophic cultivation of microalgae for biodiesel production. *Appl. Biochem. Biotechnol.* 173, 1667–1679. doi: 10.1007/s12010-014-0954-7

Kaewpintong, K., Shotipruk, A., Powtongsook, S., and Pavasant, P. (2007). Photoautotrophic high-density cultivation of vegetative cells of *Haematococcus pluvialis* in airlift bioreactor. *Bioresour. Technol.* 98, 288–295. doi: 10.1016/j.biortech.2006.01.011

Kakizono, T., Kobayashi, M., and Nagai, S. (1992). Effect of carbon/nitrogen ratio on encystment accompanied with astaxanthin formation in a green alga *Haematococcus pluvialis. J. Ferment. Bioeng.* 74, 403–405.

Kamath, B. S., Srikanta, B. M., Dharmesh, S. M., Sarada, R., and Ravishankar, G. A. (2008). Ulcer preventive and antioxidative properties of astaxanthin from *Haematococcus pluvialis. Eur. J. Pharmacol.* 590, 387–395. doi: 10.1016/j.ejphar.2008.06.042

Kang, C. D., and Sim, S. J. (2008). Direct extraction of astaxanthin from *Haematococcus* culture using vegetable oils. *Biotechnol. Lett.* 30, 441–444. doi: 10.1007/s10529-007-9578-0

Kang, C. D., Han, S. J., Choi, S. P., and Sim, S. J. (2010). Fed-batch culture of astaxanthin-rich *Haematococcus pluvialis* by exponential nutrient feeding and stepwise light supplementation. *Bioproc. Biosys. Eng.* 33, 133–139. doi: 10.1007/s00449-009-0362-5

Kang, C. D., Lee, J. S., Park, T. H., and Sim, S. J. (2005). Comparison of heterotrophic and photoautotrophic induction on astaxanthin production by *Haematococcus pluvialis. Appl. Microbiol. Biotechnol.* 68, 237–241. doi: 10.1007/s00253-005-1889-2

Karppi, J., Rissanen, T. H., Nyyssönen, K., Kaikkonen, J., Olsson, A. G., Voutilainen, S., et al. (2007). Effects of astaxanthin supplementation on lipid peroxidation. *Int. J. Vitam. Nutr. Res.* 77, 3–11. doi: 10.1024/0300-9831.77.1.3

Katagiri, M., Satoh, A., Tsuji, S., and Shirasawa, T. (2012). Effects of astaxanthin-rich *Haematococcus pluvialis* extract on cognitive function: a randomised, double-blind, placebo-controlled study. *J. Clinic. Biochem. Nutr.* 51, 102–107. doi: 10.3164/jcbn.D-11-00017

Kenji, S., Kazuhiro, O., Takuya, N., Yasuhiro, S., Shinki, C., Kazuhiko, Y., et al. (2005). Effect of astaxanthin on accommodation and asthenopia-efficacy - identification study in healthy volunteers. *J. Clin. Ther. Med.* 21, 637–650.

Kim, J. H., Affan, M. A., Jang, J., Kang, M. H., Ko, A. R., Jeon, S. M., et al. (2015). Morphological, molecular, and biochemical characterization of astaxanthin-producin g green microalga *Haematococcus* sp. KORDI03 Haematococcaceae, Chlorophyta) isolated from Korea. *J. Microbiol. Biotechnol.* 25, 238–246. doi: 10.4014/jmb.1410.10032

Klochkova, T. A., Kwak, M. S., Han, J. W., Motomura, T., Nagasato, C., and Kim, G. H. (2013). Cold-tolerant strain of *Haematococcus pluvialis* (Haematococcaceae, Chlorophyta) from Blomstrandhalvoya (Svalbard). *Algae* 28, 185–192. doi: 10.4490/algae.2013.28.2.185

Kobayashi, M., Hirai, N., Kurimura, Y., Ohigashi, H., and Tsuji, Y. (1997b). Abscisic acid-dependent algal morphogenesis in the unicellular green alga *Haematococcus pluvialis. Plant Growth Regul.* 22, 79–85. doi: 10.1023/A:1005862809711

Kobayashi, M., Kakizono, T., and Nagai, S. (1993). Enhanced carotenoid biosynthesis by oxidative stress in acetateinduced cyst cells of a green unicellular alga, *Haematococcus pluvialis. Appl. Environ. Microbiol.* 59, 867–873.

Kobayashi, M., Kakizono, T., and Nagai,. S. (1991). Astaxanthin production by a green alga, *Haematococcus pluvialis* accompanied with morphological changes in acetate media. *J. Ferment. Bioeng.* 71, 335–339. doi: 10.1016/0922-338X(91)90346-I

Kobayashi, M., Kakizono, T., Yamaguchi, K., Nishio, N., and Nagai, S. (1992). Growth and astaxanthin formation of *Haematococcus pluvialis* in heterotrophic and mixotrophic conditions. *J. Ferment. Bioeng.* 74, 17–20. doi: 10.1016/0922-338X(92)90261-R

Kobayashi, M., Kurimura, Y., and Tsuji, Y. (1997a). Light independent, astaxanthin production by the green microalga *Haematococcus pluvialis* under salt stress. *Biotechnol. Lett.* 19, 507–509. doi: 10.1023/A:1018372900649

Kobayashi, M., Kurimura, Y., Sakamoto, Y., and Tsuji, Y. (1997c). Selective extraction of astaxanthin and chlorophyll from the green alga *Haematococcus pluvialis. Biotechnol. Technol.* 11, 657–660. doi: 10.1023/A:1018455209445

Koller, M., Muhr, A., and Braunegg, G. (2014). Microalgae as versatile cellular factories for valued products. *Algal Res.* 6, 52–63. doi: 10.1016/j.algal.2014.09.002

Krause, W., Henrich, K., Paust, J., and Ernst, H. (1997). *Preparation of Astaxanthin.* Available online at: https://www.google.com/patents/US5654488

Krichnavaruk, S., Shotipruk, A., Goto, M., and Pavasant, P. (2008). Supercritical carbon dioxide extraction of astaxanthin from *Haematococcus pluvialis* with vegetable oils as co-solvent. *Bioresour. Technol.* 99, 5556–5560. doi: 10.1016/j.biortech.2007.10.049

Kupcinskas, L., Lafolie, P., Lignell, A., Kiudelis, G., Jonaitis, L., Adamonis, K., et al. (2008). Efficacy of the natural antioxidant astaxanthin in the treatment of functional dyspepsia in patients with or without *Helicobacter pylori* infection: a prospective, randomized, double blind, and placebo-controlled study. *Phytomedicine* 15, 391–399. doi: 10.1016/j.phymed.2008.04.004

Lababpour, A., Shimahara, K., Hada, K., Kyoui, Y., Katsuda, T., and Katoh, S. (2005). Fedbatch culture under illumination with blue light emitting diodes (LEDs) for astaxanthin production by *Haematococcus pluvialis. J. Biosci. Bioeng.* 100, 339–342. doi: 10.1263/jbb.100.339

Leach, M., Hamilton, L. C., Olbrich, A., Wray, G. M., and Thiemermann, C. (1998). Effects of inhibitors of the activity of cyclooxygenase-2 on the hypotension and multiple organ dysfunction caused by endotoxin: a comparison with dexa-methasone. *Br. J. Pharmacol.* 124, 586-592. doi: 10.1038/sj.bjp.0701869

Lei, A., Chen, H., Shen, G., Hu, Z., Chen, L., and Wang, J. (2012). Expression of fatty acid synthesis genes and fatty acid accumulation in *Haematococcus pluvialis* under different stressors. *Biotechnol. Biofuels* 5:18. doi: 10.1186/1754-6834-5-18

Leonardi, P. I., Popovich, C. A., Damiani, M. C. (2011). "Feedstocks for second-generation biodiesel: microalgae's biology and oil composition," in *Economic Effects of Biofuel Production*, ed M. A. d. S. Bernardes (InTech), 317–347. doi: 10.5772/23125

Li, J., Liu, Y., Cheng, J. J., Mos, M., and Daroch, M. (2015). Biological potential of microalgae in China for biorefinery-based production of biofuels and high value compounds. *N. Biotechnol.* 32, 588–596. doi: 10.1016/j.nbt.2015.02.001

Li, J., Zhu, D. L., Niu, J., Shen, S. D., and Wang, G. (2011). An economic assessment of astaxanthin production by large scale cultivation of *Haematococcus pluvialis*. *Biotechnol. Adv.* 29, 568–574. doi: 10.1016/j.biotechadv.2011.04.001

Li, M., Wu, W., Zhou, P., Xie, F., Zhou, Q., and Kangsen Mai, K. (2014). Comparison effect of dietary astaxanthin and *Haematococcus pluvialis* on growth performance, antioxidant status and immune response of large yellow croaker *Pseudosciaena crocea*. *Aquaculture* 434, 227–232. doi: 10.1016/j.aquaculture.2014.08.022

Li, Y., Sommerfeld, M., Chen, F., and Hu, Q. (2010). Effect of photon flux densities on regulation of carotenogenesis and cell viability of *Haematococcus pluvialis* (Chlorophyceae). *J. Appl. Phycol.* 22, 253–263. doi: 10.1007/s10811-009-9453-6

Lichtenthaler, H. K. (1999). the 1-Deoxy-D-Xylulose-5-Phosphate pathway of isoprenoid biosynthesis in plants. *Annu. Rev. Plant Physiol. Plant Mol. Biol.* 50, 47–65. doi: 10.1146/annurev.arplant.50.1.47

Lichtenthaler, H. K., Rohmer, M., and Schwender, J. (1997). Two independent biochemical pathways for isopentenyl diphosphate and isoprenoid biosynthesis in higher plants. *Plant Physiol.* 101, 643–652. doi: 10.1111/j.1399-3054.1997.tb01049.x

Lignell, A. (2001). *Medicament for Improvement of Duration of Muscle Function or Treatment of Muscle Disorders or Diseased*. Varmdo: US patent # 6,245,818 Astacarotene AB.

Lignell, A., and Inborr, J. (1999). *Agent for Increasing the Production of/in Breeding and Production Mammals*. Varmdo: European patent. EP0912106.

Lignell, A. N. G. K., and Inborr, J. (2000). *Agent for Increasing the Production of/in Breeding and Production Mammals*. Varmdo: United States patent and trademark office granted patent. WO97/35491.

Linden, H. (1999). Carotenoid hydroxylase from *Haematococcus pluvialis*: cDNA sequence, regulation and functional complementation. *Biochim. Biophys. Acta Gene Struct. Expr.* 1446, 203–212. doi: 10.1016/S0167-4781(99)00088-3

Liu, B. H., and Lee, Y. K. (2003). Effect of total secondary carotenoids extracts from Chlorococcum sp. on Helicobacter pylori-infected BALB/c mice. *Int. Immunopharmacol.* 3, 979–986. doi: 10.1016/S1567-5769(03)00096-1

Liu, X., and Osawa, T. (2007). Cis astaxanthin and especially 9-cis astaxant hin exhibits a higher antioxidant activity *in vitro* compared to the all-trans isomer. *Biochem. Biophys. Res. Commun.* 357, 187–193. doi: 10.1016/j.bbrc.2007.03.120

López, M. C. G.-M., Sanchez, E. D. R., López, J. L. C., Fernández, F. G. A., Sevilla, J. M. F., Rivas, J., et al. (2006). Comparative analysis of the outdoor culture of *Haematococcus pluvialis* in tubular and bubble column photobioreactors. *J. Biotechnol.* 123, 329–342. doi: 10.1016/j.jbiotec.2005.11.010

Lorenz, R. T. (1999). *A Technical Review of Haematococcus Algae*. NatuRose™ Technical Bulletin #060 (Kailua-Kona, HI: Cyanotech Corporation).

Lorenz, R. T., and Cysewski, G. R. (2000). Commercial potential for *Haematococcus* microalgae as a natural source of astaxanthin. *Trends Biotechnol.* 18, 160–167. doi: 10.1016/S0167-7799(00)01433-5

Lotan, T., and Hirschberg, J. (1995). Cloning and expression in *Escherichia coli* of the gene encoding beta-C-4-oxygenase, that converts beta-carotene to the ketocarotenoid canthaxanthin in *Haematococcus pluvialis*. *FEBS Lett.* 364, 125–128. doi: 10.1016/0014-5793(95)00368-J

Machmudah, S., Shotipruk, A., Goto, M., Sasaki, M., and Hirose, T. (2006). Extraction of astaxanthin from *Haematococcus pluvialis* using supercritical CO2 and ethanol as entrainer. *Ind. Eng. Chem. Res. Dev.* 45, 3652–3657. doi: 10.1021/ie051357k

Mata, T. M., Martins, A. A., and Caetano, N. S. (2010). Microalgae for biodiesel production and other applications: a review. *Renew. Sust. Energ. Rev.* 14, 217–232. doi: 10.1016/j.rser.2009.07.020

McBride, R., Behnke, C., Botsch, K., Heaps, N., and Meenach, C. (2013). *Use of Fungicides in Liquid Systems*. Merryfield Row San Diego, CA: PCT Patent Application WO2013056166 A1.

Mendes-Pinto, M. M., Raposo, M. F. J., Bowen, J., Young, A. J., and Morais, R. (2001). Evaluation of different cell disruption processes on encysted cells of *Haematococcus pluvialis*: effects on astaxanthin recovery and implications for bioavailability. *J. Appl. Phycol.* 13, 19–24. doi: 10.1023/A:1008183429747

Mercer, P., and Armenta, R. E. (2011). Developments in oil extraction from microalgae. *Eur. J. Lipid Sci. Tech.* 113, 539–547. doi: 10.1002/ejlt.201000455

Miao, X., and Wu, Q. (2006). Biodiesel production from heterotrophic microalgal oil. *Bioresour. Technol.* 97, 841–846. doi: 10.1016/j.biortech.2005.04.008

Miki, W. (1991). Biological functions and activities of animal carotenoids. *Pure Appl. Chem.* 63, 141–146. doi: 10.1351/pac199163010141

Milledge, J. J. (2013). *Energy Balance and Techno-economic Assessment of Algal Biofuel Production Systems*. Doctoral Thesis, University of Southampton, Faculty of Engineering and the Environment.

Miyawaki, H., Takahashi, J., Tsukahara, H., and Takehara, I. (2008). Effects of astaxanthin on human blood rheology. *J. Clin. Biochem. Nutr.* 43, 69–74. doi: 10.3164/jcbn.2008048

Molina Grima, E., Belarbi, E. H., Acién Fernández, F. G., Robles Medina, A., and Chisti, Y. (2003). Recovery of microalgal biomass and metabolites: process options and economics. *Biotechnol Adv.* 20, 491–515. doi: 10.1016/S0734-9750(02)00050-2

Moya, M. J., Sánchez-Guardamino, M. L., Vilavella, A., and Barbera, E. (1997). Growth of *Haematococcus lacustris*: a contribution to kinetic modelling. *J. Chem. Technol. Biotechnol.* 68, 303–309.

Nagaki, Y., Hayasaka, S., Yamada, T., Hayasaka, Y., Sanada, M., and Uonomi, T. (2002). Effects of astaxanthin on accommodation, critical flicker fusion, and pattern visual evoked potential in visual display terminal workers. *J. Trad. Med.* 19, 170–173.

Nagaki, Y., Mihara, M., Tsukuhara, H., and Ohno, S. (2006). The supplementation effect of astaxanthin on accommodation and asthenopia. *J. Clin. Therap. Med.* 22, 41–54.

Nagata, A., Tajima, T., and Takahashi, J. (2006). Effect of astaxanthin 5 mg on anti fatigue and task performance of human. *Carotenoid Sci.* 10, 102–106.

Naguib, Y. M. A. (2000). Antioxidant activities of astaxanthin and related carotenoids. *J. Agric. Food Chem.* 48, 1150–1154. doi: 10.1021/jf991106k

Nakamura, A., Isobe, R., Otaka, Y., Abematsu, Y., Nakata, D., Honma, C., et al. (2004). Changes in visual function following peroral astaxanthin. *Jpn. J. Clin. Opthal.* 58, 1051–1054.

Nakao, R., Nelson, O. L., Park, J. S., Mathison, B. D., Thompson, P. A., and Chew, B. P. (2010). Effect of astaxanthin supplementation on inflammation and cardiac function in BALB/c mice. *Anticancer Res.* 30, 2721–2725.

Nawrocki, W. J., Tourasse, N. J., Taly, A., Rappaport, F., and Wollman, F. A. (2015). The plastid terminal oxidase: its elusive function points to multiple contributions to plastid physiology. *Annu. Rev. Plant Biol.* 66, 49–74. doi: 10.1146/annurev-arplant-043014-114744

Nishikawa, Y., Minenaka, Y., Ichimura, M., Tatsumi, K., Nadamoto, T., and Urabe, K. (2005). Effects of astaxanthin and vitamin C on the prevention of gastric ulcerations in stressed rats. *J. Nutr. Sci. Vit.* 51, 135–141. doi: 10.3177/jnsv.51.135

Nobre, B., Marcelo, F., Passos, R., Beirao, L., Palavra, A., Gouveia, L., et al. (2006). Supercritical carbon dioxide extraction of astaxanthin and other carotenoids from the microalga *Haematococcus pluvialis*. *Eur. Food Res. Technol.* 223, 787–790. doi: 10.1007/s00217-006-0270-8

Olaizola, M. (2000). Commercial production of astaxanthin from *Haematococcus pluvialis* using 25,000-liter outdoor photobioreactors. *J. Appl. Phycol.* 12, 499–506. doi: 10.1023/A:1008159127672

Olaizola, M. (2003). Commercial development of microalgal biotechnology: from the test tube to the marketplace. *Biomol. Eng.* 20, 459–466. doi: 10.1016/S1389-0344(03)00076-5

Olguín, E. J., Giuliano, G., Porro, D., Tuberosa, R., and Salamin, F. (2012). Biotechnology for a more sustainable world. *Biotechnol. Adv.* 30, 931–932. doi: 10.1016/j.biotechadv.2012.06.001

Orosa, M., Franqueira, D., Cid, A., and Abalde, J. (2005). Analysis and enhancement of astaxanthin accumulation in *Haematococcus pluvialis*. *Bioresour. Technol.* 96, 373–378. doi: 10.1016/j.biortech.2004.04.006

Orosa, M., Torres, E., Fidalgo, P., and Abalde, J. (2000). Production and analysis of secondary carotenoids in green algae. *J. Appl. Phycol.* 12, 553–556. doi: 10.1023/A:1008173807143

Palozza, P., Torelli, C., Boninsegna, A., Simone, R., Catalano, A., Mele, M. C., et al. (2009). Growth-inhibitory effects of the astaxanthin-rich alga *Haematococcus pluvialis* in human colon cancer cells. *Cancer Lett.* 283, 108–117. doi: 10.1016/j.canlet.2009.03.031

Pan, J. L., Wang, H. M., Chen, C. Y., and Chang, J. S. (2012). Extraction ofastaxanthin from *Haematococcus pluvialis* by supercritical carbon dioxide fluid with ethanol modifier. *Eng. Life Sci.* 12, 638–647.

Panis, G. (2015). *Commercial Astaxanthin Production Derived by Green Alga Haematococcus pluvialis: A Microalgae Process Model and a Techno-Economic Assessment All Through Production Line.* Master Thesis (45 EC), Utrecht University, Netherlands.

Parisenti, J., Beirao, L. H., Maraschin, M., Mourino, J. L., Nascimento, V.iera F.,Do Nascimento Vieira, F., Bedin, L. H., et al. (2011). Pigmentation and carotenoid content of shrimp fed with *Haematococcus pluvialis* and soy lecithin. *Aquacult. Nutr.* 17, 530–535. doi: 10.1111/j.1365-2095.2010.00794.x

Park, J. C., Choi, S. P., Hong, M. E., and Sim, S. J. (2014). Enhanced astaxanthin production from microalga, *Haematococcus pluvialis* by two-stage perfusion culture with stepwise light irradiation. *Bioprocess Biosyst. Eng.* 37, 2039–2047. doi: 10.1007/s00449-014-1180-y

Park, J. S., Chyun, J. H., Kim, Y. K., Line, L. L., and Chew, B. P. (2010). Astaxanthin decreased oxidative stress and inflammation and enhanced immune response in humans. *Nutr. Metab. (Lond).* 7:18. doi: 10.1186/1743-7075-7-18

Pérez-López, P., González-García, S., Jeffryes, C., Agathos, S. N., McHugh, E., Walsh, D., et al. (2014). Life-cycle assessment of the production of the red antioxidant carotenoid astaxanthin by microalgae: from lab to pilot scale. *J. Clea. Prod.* 64, 332–344. doi: 10.1016/j.jclepro.2013.07.011

Praveenkumar, R., Lee, K., Lee, J., and Oh, Y.-K. (2015). Breaking dormancy: an energy- efficient means of recovering astaxanthin from microalgae. *Green Chem.* 17, 1226–1234. doi: 10.1039/C4GC01413H

Pringsheim, E. G. (1966). Nutritional requirements of *Haematococcus pluvialis* and related species. *J. Phycol.* 2, 1–7. doi: 10.1111/j.1529-8817.1966.tb04584.x

Proctor, V. W. (1957). Some controlling factors in the distribution of *Haematococcus pluvialis*. *Ecology* 38, 457–462. doi: 10.2307/1929890

Radakovits, R., Jinkerson, R. E., Darzins, A., and Posewitz, M. C. (2010). Genetic engineering of algae for enhanced biofuel production. *Eukaryot. Cell* 9, 486–501. doi: 10.1128/EC.00364-09

Ranga Rao, A., Harshvardhan Reddy, A., and Aradhya, S. M. (2010). Antibacterial properties of *Spirulina platensis*, *Haematococcus pluvialis*, *Botryococcus braunii* micro algal extracts. *Curr. Trends Biotechnol. Pharm.* 4, 809–819.

Ranga Rao, A., Sarada, R., Shylaja, M. D., and Ravishankar, G. A. (2015). Evaluation of hepatoprotective and antioxidant activity of astaxanthin and astaxanthin esters from microalga-*Haematococcus pluvialis*. *J. Food Sci. Tech.* 52, 6703–6710. doi: 10.1007/s13197-015-1775-6

Ranga Rao, A., Siew Moi, P., Ravi, S., and Aswathanarayana, R. G. (2014). Astaxanthin: sources, extraction, stability, biological activities and its commercial applications—a review. *Mar. Drugs* 12, 128–152. doi: 10.3390/md12010128

Ranga Rao, A., Sindhuja, H. N., Dharmesh, S. M., Sankar, K. U., Sarada, R., and Ravishankar, G. A. (2013). Effective inhibition of skin cancer, tyrosinase, and antioxidative properties by astaxanthin and astaxanthin esters from the green alga *Haematococcus pluvialis*. *J. Agric. Food Chem.* 61, 3842–3851. doi: 10.1021/jf304609j

Ranjbar, R., Inoue, R., Shiraishi, H., Katsuda, T., and Katoh, S. (2008). High efficiency production of astaxanthin by autotrophic cultivation of *Haematococcus pluvialis* in a bubble column photobioreactor. *Biochem. Eng. J.* 39, 575–580. doi: 10.1016/j.bej.2007.11.010

Razon, L. F., and Tan, R. R. (2011). Net energy analysis of the production of biodiesel and biogas from the microalgae: *Haematococcus*

pluvialis and *Nannochloropsis*. *Appl. Energ.* 88, 3507–3514. doi: 10.1016/j.apenergy.2010.12.052

Recht, L., Zarka, A., and Boussiba, S. (2012). Patterns of carbohydrate and fatty acid changes under nitrogen starvation in the microalgae *Haematococcus pluvialis* and *Nannochloropsis* sp. *Appl. Microbiol. Biotechnol.* 94, 1495–1503. doi: 10.1007/s00253-012-3940-4

Renstrøm, B., Borch, G., Skulberg, O. M., and Liaaen-Jensen, S. (1981). Optical purity of (3S,3′S)-astaxanthin from Haematococcus pluvialis. *Phytochemistry* 20, 2561–2564. doi: 10.1016/0031-9422(81)83094-4

Reyes, F. A., Mendiola, J. A., Ibanez, E., and del Valle, J. M. (2014). Astaxanthin extraction from *Haematococcus pluvialis* using CO2-expanded ethanol. *J. Supercrit. Fluids* 92, 75–83. doi: 10.1016/j.supflu.2014.05.013

Rippka, R., Deruelles, J., Waterbury, M., Herdman, M., and Stanier, R. (1979). Generic assignments, strain histories and properties of pure culture of cyanobacteria. *J. Gen. Microbiol.* 111, 1–61. doi: 10.1099/00221287-111-1-1

Rohdich, F., Hecht, S., Gärtner, K., Adam, P., Krieger, C., Amslinger, S., et al. (2002). Studies on the nonmevalonate terpene biosynthetic pathway: metabolic role of IspH (LytB) protein. *Proc. Natl. Acad. Sci. U.S.A.* 99, 1158–1163. doi: 10.1073/pnas.032658999

Rosenberg, J. N., Oyler, G. A., Wilkinson, L., and Betenbaugh, M. J. (2008). A green light for engineered algae: redirecting metabolism to fuel a biotechnology revolution. *Curr. Opin. Biotechnol.* 19, 430–436. doi: 10.1016/j.copbio.2008.07.008

Saha, S. K., McHugh, E., Hayes, J., Moane, S., Walsh, D., and Murray, P. (2013). Effect of various stressregulatory factors on biomass and lipid production in microalga *Haematococcus pluvialis*. *Bioresour. Technol.* 128, 118–124. doi: 10.1016/j.biortech.2012.10.049

Santos, M. F., and Mesquita, J. F. (1984). Ultrastructural study of *Haematococcus lacustris* (Girod.) Rostafinski (Volvocales) I. Some aspects of carotenogenesis. *Cytologia* 49, 215–228. doi: 10.1508/cytologia.49.215

Sarada, R., Bhattacharya, S., and Ravishankar, G. A. (2002a). Optimization of culture conditions for growth of the green alga *Haematococcus pluvialis*. *World J. Microbiol. Biotechnol.* 18, 517–521. doi: 10.1023/A:101634 9828310

Sarada, R., Tripathi, U., and Ravishankar, G. A. (2002b). Influence of stress on astaxanthin production in *Haematococcus pluvialis* grown under different culture conditions. *Process Biochem.* 37, 623–627. doi: 10.1016/S0032-9592(01)00246-1

Sarada, R., Vidhyavathi, R., Usha, D., and Ravishankar, G. A. (2006). An efficient method for extraction of astaxanthin from green alga *Haematococcus pluvialis*. *J. Agric. Food Chem.* 54, 7585–7588. doi: 10.1021/jf060737t

Satoh, A., Tsuji, S., Okada, Y., Murakami, N., Urami, M., Nakagawa, K., et al. (2009). Preliminary clinical evaluation of toxicity and efficacy of a new astaxanthin-rich *Haematococcus pluvialis* extract. *J. Clin. Biochem. Nutr.* 44, 280–284. doi: 10.3164/jcbn.08-238

Sawaki, K., Yoshigi, H., Aoki, K., Koikawa, N., Azum ane, A., Kaneko, K., et al. (2002). Sports performance benefits from taking natural astaxanthin characterized by visual acuity and muscle fatigue improvements in humans. *J. Clinic. Therap. Med.* 18, 73–88.

Seki, T., Sueki, H., Kono, H., Suganuma, K., and Yamashita, E. (2001). Effects of astaxanthin from *Haematococcus pluvialis* on human skin-patch test; skin repeated application test; effect on wrinkle reduction. *Fragrance J.* 12, 98–103.

Sharon-Gojman, R., Maimon, E., Leu, S., Zarka, A., and Boussiba, S. (2015). Advanced methods for genetic engineering of *Haematococcus pluvialis* (Chlorophyceae, Volvocales). *Algal Res.* 10, 8–15. doi: 10.1016/j.algal.2015.03.022

Sheikhzadeh, N., Panchah, I. K., Asadpour, R., Tayefi-Nasrabadi, H., and Mahmoudi, H. (2012a). Effects of *Haematococcus pluvialis* in maternal diet on reproductive performance and egg quality in rainbow trout (*Oncorhynchus mykiss*). *Anim. Reprod. Sci.* 130, 119–123. doi: 10.1016/j.anireprosci.2011.12.010

Sheikhzadeh, N., Tayefi-Nasrabadi, H., Oushani, A. K., and Najafi Enferadi, M. H. (2012b). Effects of *Haematococcus pluvialis* supplementation on antioxidant system and metabolism in rain- bow trout (*Oncorhynchus mykiss*). *Fish Physiol. Biochem.* 38, 413–419. doi: 10.1007/s10695-011-9519-7

Solovchenko, A. E. (2015). Recent breakthroughs in the biology of astaxanthin accumulation by microalgal cell. *Photosynth. Res.* 125, 437–449. doi: 10.1007/s11120-015-0156-3

Sommer, T. R., Potts, W. T., and Morrissy, N. M. (1991). Utilization of microalgal astaxanthin by rainbow trout (*Oncorhynchus mykiss*). *Aquaculture* 94, 79–88.

Steinbrenner, J., and Linden, H. (2001). Regulation of two carotenoid biosynthesis genes coding for phytoene synthase and carotenoid hydroxylase during stress-induced astaxanthin formation in the green alga *Haematococcus pluvialis*. *Plant Physiol.* 125, 810–817. doi: 10.1104/pp.125.2.810

Strittmatter, M., Guerra, T., Silva, J., and Gachon, C. M. M. (2015). A new flagellated dispersion stage in *Paraphysoderma sedebokerense*, a pathogen of *Haematococcus pluvialis*. *J. Appl. Phycol.* 27, 1–6. doi: 10.1007/s10811-015-0700-8

Su, Y., Wang, J., Shi, M., Niu, X., Yu, X., Gao, L., et al. (2014). Metabolomic and network analysis of astaxanthin-producing *Haematococcus pluvialis* under various stress conditions. *Bioresour. Technol.* 170, 522–529. doi: 10.1016/j.biortech.2014.08.018

Sun, H., Kong, Q., Geng, Z., Duan, L., Yang, M., and Guan, B. (2015). Enhancement of cell biomass and cell activity of astaxanthin-rich *Haematococcus pluvialis*. *Bioresour. Technol.* 186, 67–73. doi: 10.1016/j.biortech.2015.02.101

Sun, Z., Cunningham, F. X. Jr., and Gantt, E. (1998). Differential expression of two isopentenyl pyrophosphate isomerases and enhanced carotenoid accumulation in a unicellular chlorophyte. *Proc. Natl. Acad. Sci. U.S.A.* 95, 11482–11488. doi: 10.1073/pnas.95.19.11482

Suseela, M. R., and Toppo, K. (2006). *Haematococcus pluvialis*—a green alga, richest natural source of astaxanthin. *Curr. Sci.* 90, 1602–1603.

Thana, P., Machmudah, S., Goto, M., Sasaki, M., Pavasant, P., and Shotipruk, A. (2008). Response surface methodology to supercritical carbon dioxide extraction of astaxanthin from *Haematococcus pluvialis*. *Bioresour. Technol.* 99, 3110–3115. doi: 10.1016/j.biortech.2007.05.062

Tjahjono, A. E., Hayama, Y., Kakizono, T., Terada, Y., Nishio, N., and Nagai, S. (1994b). Hyper accumulation of astaxanthin in a green alga *Haematococcus pluvialis* at elevated temperatures. *Biotechnol. Lett.* 16, 133–138. doi: 10.1007/BF01021659

Tjahjono, A. E., Kakizono, T., Hayama, Y., Nishio, N., and Nagai, S. (1994a). Isolation of resistant mutants against carotenoid biosynthesis inhibitors for a green alga *Haematococcus pluvialis*, and their hybrid formation by protoplast fusion for breeding of higher astaxanthin producers. *J. Ferment. Bioeng.* 77, 352–357. doi: 10.1016/0922-338X(94)90003-5

Tolasa, S., Cakli, S., and Ostermeyer, U. (2005). Determination of astaxanthin and canthaxanthin in salmonid. *Eur. Food. Res. Technol.* 221, 787–791. doi: 10.1007/s00217-005-0071-5

Tominaga, K., Hongo, N., Karato, M., and Yamashita, E. (2012). Cosmetic benefits of astaxanthin on humans subjects. *Acta Biochim Pol.* 59, 43–47.

Torrissen, O. J., and Naevdal, G. (1984). Pigmentation of salmonids — Genetical variation in carotenoid deposition in rainbow trout. *Aquaculture* 38, 59–66. doi: 10.1016/0044-8486(84)90137-6

Torzillo, G., Goksan, T., Faraloni, C., Kopecky, J., and Masojidek, J. (2003). Interplay between photochemical activities and pigment composition in an outdoor culture of *Haematococcus pluvialis* during the shift from the green to red stage. *J. Appl. Phycol.* 15, 127–136. doi: 10.1023/A:1023854904163

Triki, A., Maillard, P., and Gudin, C. (1997). Gametogenesis in *Haematococcus pluvialis* Flotow (Volvocales, Chlorophyta). *Phycologia* 36, 190–194. doi: 10.2216/i0031-8884-36-3-190.1

Tripathi, U., Sarada, R., Ramachandra Rao, S., and Ravishankar, G. A. (1999). Production of astaxanthin in *Haematococcus pluvialis* cultured in various media. *Bioresour. Technol.* 68, 197–199. doi: 10.1016/S0960-8524(98)00143-6

Tripathi, U., Venkateshwaran, G., Sarada, R., and Ravishankar, G. A. (2001). Studies on *Haematococcus pluvialis* for improved production of astaxanthin by mutagenesis. *World J. Microbiol. Biotechnol.* 17, 143–148. doi: 10.1023/A:1016609815405

Valderrama, J. O., Perrut, M., Majewski, W., and Serena, L. (2003). Extraction of Astaxantine and Phycocyanine from Microalgae with Supercritical Carbon Dioxide, *J. Chem. Eng. Data* 48, 827–830. doi: 10.1021/je020128r

Vidhyavathi, R., Venkatachalam, L., Sarada, R., and Ravishankar, G. A. (2008). Regulation of carotene biosynthetic genes expression and carotenoid accumulation in the green alga *Haematococcus pluvialis* under nutrient stress conditions. *J. Exp. Bot.* 59, 1409–1418. doi: 10.1093/jxb/ern048

Wan, M., Hou, D., Li, Y., Fan, J., Huang, J., Liang, S., et al. (2014b). The effective photoinduction of *Haematococcus pluvialis* for accumulating astaxanthin with attached cultivation. *Bioresour. Technol.* 163, 26–32. doi: 10.1016/j.biortech.2014.04.017

Wan, M., Zhang, J., Hou, D., Fan, J., Li, Y., Huang, J., et al. (2014a). The effect of temperature on cell growth and astaxanthin accumulation of *Haematococcus pluvialis* during a light–dark cyclic cultivation. *Bioresour. Technol.* 167, 276–283. doi: 10.1016/j.biortech.2014.06.030

Wang, B., Zarka, A., Trebst, A., and Boussiba, S. (2003). Astaxanthin accumulation in *Haematococcus pluvialis* (Chlorophyceae) as an active photoprotective process under high irradiance. *J. Phycol.* 39, 1116–1124. doi: 10.1111/j.0022-3646.2003.03-043.x

Wang, J. F., Han, D. X., Sommerfeld, M. R., Lu, C. M., and Hu, Q. (2013a). Effect of initial biomass density on growth and astaxanthin production of *Haematococcus pluvialis* in an outdoor photobioreactor. *J. Appl. Phycol.* 25, 253–260. doi: 10.1007/s10811-012-9859-4

Wang, J. F., Sommerfeld, M. R., Lu, C. M., and Hu, Q. (2013b). Combined effect of initial biomass density and nitrogen concentration on growth and astaxanthin production of *Haematococcus pluvialis* (Chlorophyta) in outdoor cultivation. *Algae* 28, 193–202. doi: 10.4490/algae.2013.28.2.193

Wang, J., Sommerfeld, M., and Hu, Q. (2009). Occurrence and environmental stress responses of two plastid terminal oxidases in *Haematococcus pluvialis* (Chlorophyceae). *Planta* 230, 191–203. doi: 10.1007/s00425-009-0932-4

Wang, L., Yang, B., Yan, B., and Yao, X. (2012). Supercritical fluid extraction of astaxanthin from *Haematococcus pluvialis* and its antioxidant potential in sunflower oil. *Innovative Food Sci. Emerg. Technol.* 13, 120–127. doi: 10.1016/j.ifset.2011.09.004

Wang, P. (2014). *Culture Medium and Culture Method for Culturing Haematococcus pluvialis by using Brewery Wastewater*. Available online at: https://www.google.com/patents/CN103966103A?cl=en

Wayama, M., Ota, S., Matsuura, H., Nango, N., Hirata, A., and Kawano, S. (2013). Three-dimensional ultrastructural study of oil and astaxanthin accumulation during encystment in the green alga *Haematococcus pluvialis*. *PLoS ONE* 8:e53618. doi: 10.1371/journal.pone.0053618

Wu, Y. H., Yang, J., Hu, H. Y., and Yu, Y. (2013). Lipid-rich microalgal biomass production and nutrient removal by *Haematococcus pluvialis* in domestic secondary effluent. *Ecol. Eng.* 60, 155–159. doi: 10.1016/j.ecoleng.2013.07.066

Yamashita, E. (2002). Cosmetic benefit of dietary supplements containing astaxanthin and tocotrienol on human skin. *Food Style* 21, 112–117.

Yang, Y., Kim, B., and Lee, J. Y. (2013). Astaxanthin structure, metabolism, and health benefits. *J. Hum. Nutr. Food Sci.* 1, 1003:1–1003:11.

Yin, S., Wang, J., Chen, L., and Liu, T. (2015). The water footprint of biofilm cultivation of *Haematococcus pluvialis* is greatly decreased by using sealed narrow chambers combined with slow aeration rate. *Biotechnol. Lett.* 37, 1819–1827. doi: 10.1007/s10529-015-1864-7

Yoo, J. J., Choi, S. P., Kim, B. W., and Sim, S. J. (2012). Optimal design of scalable photobioreactor for phototropic culturing of *Haematococcus pluvialis*. *Bioprocess Biosyst. Eng.* 35, 309–315. doi: 10.1007/s00449-011-0616-x

Yu, X., Chen, L., and Zhang, W. (2015). Chemicals to enhance microalgal growth and accumulation of high-value bioproducts. *Front. Microbiol.* 6:56. doi: 10.3389/fmicb.2015.00056

Yuan, J. P., Peng, J., Yin, K., and Wang, J. H. (2011). Potential health promoting effects of astaxanthin: a high-value carotenoid mostly from microalgae. *Mol. Nutr. Food Res.* 55, 150–165. doi: 10.1002/mnfr.201000414

Zhang, B., Geng, Y., Li, Z., Hu, H., and Li, Y. (2009). Production of astaxanthin from *Haematococcus* in open pond by two-stage growth one-step process. *Aquaculture* 295, 275–281. doi: 10.1016/j.aquaculture.2009.06.043

Zhang, J., Luo, Z., Li, J., and Liu, Z. (2013). Production method and device for preventing and treating contamination of *Paraphysoderma sedebokerensis* in *Haematococcus pluvialis*. PCT Patent Application WO2013127280 A1.

Zhang, W., Wang, J., Wang, J., and Liu, T. (2014). Bioresource Technology. *Attached cultivation of Haematococcus pluvialis for astaxanthin production*. *Bioresour. Technol.* 158, 329–335. doi: 10.1016/j.biortech.2014.02.044

Zhang, X. W., Gong, X. D., and Chen, F. (1999). Kinetic models for astaxanthin production by high cell density mixotrophic culture of the microalga *Haematococcus pluvialis*. *J. Ind. Microbiol. Biotechnol.* 23, 691–696. doi: 10.1038/sj.jim.2900685

Zhang, X., Pan, L., Wei, X., Gao, H., and Liu, J. (2007). Impact of astaxanthin-enriched algal powder of *Haematococcus pluvialis* on memory improvement in

BALB/c mice. *Environ. Geochem. Health* 29, 483–489. doi: 10.1007/s10653-007-9117-x

Zhekisheva, M., Boussiba, S., Khozin-Goldberg, I., Zarka, A., and Cohen, Z. (2002). Accumulation of oleic acid in *Haematococcus pluvialis* (Chlorophyceae) under nitrogen starvation or high light is correlated with that of astaxanthin esters. *J. Phycol.* 38, 325–331. doi: 10.1046/j.1529-8817.2002.01107.x

Zhekisheva, M., Zarka, A., Khozin-Goldberg, I., Cohen, Z., and Boussiba, S. (2005). Inhibition of astaxanthin synthesis under high irradiance does not abolish triacylglycerol accumulation in the green alga *Haematococcus pluvialis* (Chlorophyceae). *J. Phycol.* 41, 819–826. doi: 10.1111/j.0022-3646.2005.05015.x

Zou, T. B., Jia, Q., Li, H. W., Wang, C.-X., and Wu, H.-F. (2013). Response surface methodology for ultrasound-assisted extraction of astaxanthin from *Haematococcus pluvialis*. *Mar. Drugs* 11, 1644–1655. doi: 10.3390/md11051644

frontiers
in Bioengineering and Biotechnology

Industrial fermentation of *Auxenochlorella protothecoides* for production of biodiesel and its application in vehicle diesel engines

Yibo Xiao[†], Yue Lu[†], Junbiao Dai* and Qingyu Wu*

Ministry of Education Key Laboratory of Bioinformatics, Center for Synthetic and Systems Biology, School of Life Sciences, Tsinghua University, Beijing, China

Microalgae-derived biodiesel has been regarded as a promising alternative for fossil diesel. However, the commercial production of microalgal biodiesel was halted due to its high cost. Here, we presented a pilot study on the industrial production of algal biodiesel. We began with the heterotrophic cultivation of *Auxenochlorella protothecoides* in a 60-m³ fermentor that produced biomass at 3.81 g L⁻¹ day⁻¹ with a neutral lipid content at 51%. Next, we developed plate-frame filter, natural drying, and ball milling methods to harvest, dry, and extract oil from the cells at low cost. Additionally, algal biodiesel was produced for a vehicle engine test, which indicated that the microalgal biodiesel was comparable to fossil diesel but resulted in fewer emissions of particulate matter, carbon monoxide, and hydrocarbon. Altogether, our data suggested that the heterotrophic fermentation of *A. protothecoides* could have the potential for the future industrial production of biodiesel.

Keywords: microalgae biodiesel, *Chlorella*, heterotrophic cultivation, cost assessment, diesel engine test

INTRODUCTION

We will eventually have to face the time when all fossil fuels, i.e., petroleum, natural gas, and coal, run out. Even before that time, climate change might destroy the entire planet if we continue to rely heavily on fossil fuels as we have, and we are now already experiencing warming of over 1°C (http://news.yahoo.com/not-run-fossil-fuels-op-ed-231243174.html). Recent advances in drilling and hydraulic fracturing technology to explore shale gas (Weber and Clavin, 2012) are exciting and may relieve concerns about fossil fuels for some time. However, even this resource may eventually be exhausted, as it is still not infinite. Meanwhile, concerns are rising due to its potential damage to the environment, especially land and habitat fragmentation, and its impact on air and water quality (Entrekin et al., 2011; Olmstead et al., 2013; Vidic et al., 2013). Therefore, there continues to be interest in developing new technologies to utilize other renewable and sustainable energy sources, such as solar, wind, geothermal, and biomass (Hidy, 2012).

Due to their faster growth rate, higher lipid content and less impact on food security than agriculture-based feedstocks, algae have attracted increasing amounts of attention for biofuel production in recent years (Brennan and Owende, 2010; Weyer et al., 2010). However, projections have largely depended upon small-scale experimental data. Most open pond systems and photobioreactors have been used to culture microalgae for high-value products but not for biodiesel due to the limitations of the lipid content under such cultivation conditions and the high cost for biomass (Rawat et al., 2013). To simultaneously achieve fast cell growth and high lipid content, the heterotrophic cultivation of

Auxenochlorella protothecoides has been developed (Miao and Wu, 2006; Xiong et al., 2008; Ceron-Garcia et al., 2013). After optimization, the lipid productivity of *A. protothecoides* could reach 11.8 g L^{-1} day^{-1} (Xiong et al., 2010), much higher than that of photoautotrophic algae [0.2 g L^{-1} day^{-1} as reported by Rodolfi et al. (2009)]. It could, therefore, potentially be applicable for the commercial production of microalgal biodiesel. In addition, a previous study to evaluate microalgal biodiesel prepared from an 11-ton bioreactor suggested that it was comparable to conventional fossil fuels and complied with the US biodiesel standard (Li et al., 2007). Lately, many improvements at the lab scale for biodiesel preparation from algal lipids or directly from dry and wet cells using chemical or enzymatic approaches have been made to increase the efficiency of transesterification and to obtain high quality final products (Miao and Wu, 2004; Johnson and Wen, 2009; Levine et al., 2010). However, due to the difficulty in obtaining enough biomass for industrial production of microalgal biodiesel, only a few studies in recent years have been able to apply algal biodiesel to original or unmodified vehicle engines (Haik et al., 2011; Al-Lwayzy and Yusaf, 2013).

With the aim to produce microalgal biodiesel for commercial application, we report here the first large-scale trial of an algal biodiesel manufacturing and evaluation process, including the step-wise enlargement of biomass production, cell harvesting and drying, and biodiesel preparation by transesterification followed by quality assessment. After generating enough algal biodiesel for application tests, combustion experiments in a four-cylinder vehicle diesel engine were conducted, and several main features, including engine torque and emission, were monitored.

MATERIALS AND METHODS

Microalga Strain and Basal Culture Medium

The microalga *A. protothecoides* strain was originally obtained from the Culture Collection of Algae at University of Texas (Austin, TX, USA) and screened in the Laboratory of Microalgae Fermentation and Bioenergy at Tsinghua University, Beijing, China. The basic culture media were the same as reported previously (Xiong et al., 2008).

Production and Harvest of Microalga Biomass

The production of *A. protothecoides* biomass was carried out at North China Pharmaceutical Huasheng Co., Ltd., and the scaling-up fermentation was divided into three steps (**Figure 1**). First, the seed cultivation was performed in three 700 L stirred tank bioreactors containing 300 L basal medium with turbine impellers. Two liters of *A. protothecoides* cells at the exponential stage was inoculated into each fermentor, for which the temperature, pH, aeration rate, and agitation speed were initially set at 28 ± 0.5°C, 6.3 ± 0.1, 25 m^3 h^{-1} (1:1 vvm), and 360 rpm, respectively. The pressure of the inner fermentor was kept at 0.04 Mpa except for the 60-m^3 fermentor, which was kept at 0.2 Mpa. After 10 days of cultivation, the cells were partly inoculated into an 11-m^3 fermentor containing 5 m^3 of medium and kept at the same conditions
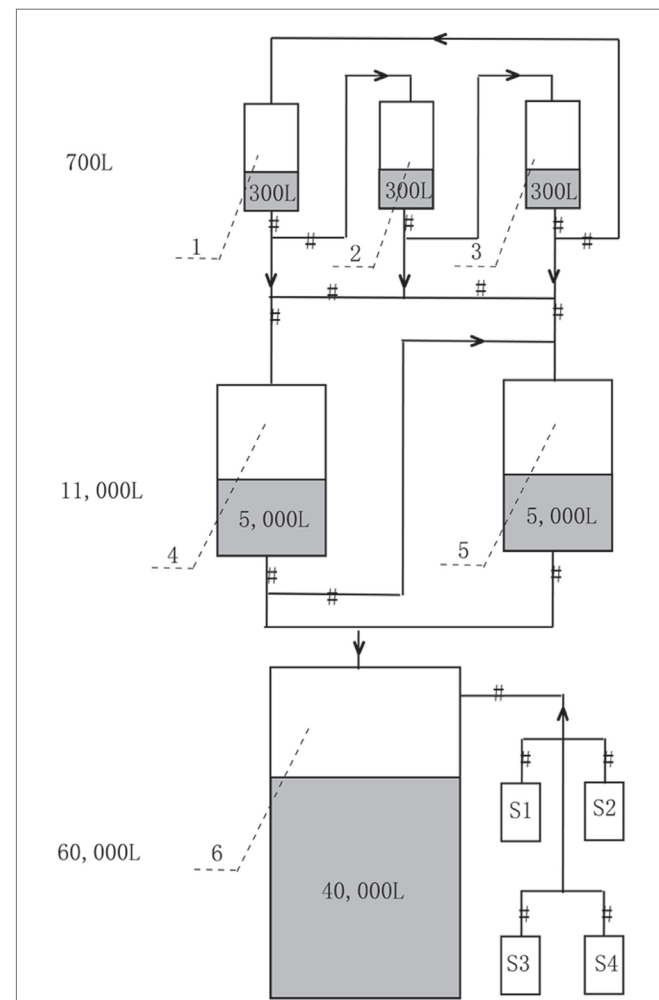

FIGURE 1 | Mass production strategy of heterotrophic *A. protothecoides* biomass in 700 L (Tanks 1–3, with 300 L medium each), 11 m^3 (Tanks 4 and 5, with 5 m^3 medium each), and 60 m^3 (Tank 6, with 40 m^3 medium) industrial fermentors. S1–S4 are supplemental tanks for feeding glucose, nitrogen, NaOH, and antifoam, respectively.

as those of the 700 L fermentors. Finally, cells at the exponential stage from the 11-m^3 fermentor were completely inoculated into a 60-m^3 fermentor with 40 m^3 of medium. We followed the optimized concentration of nitrogen and carbon source according to our previous published paper (Xiong et al., 2008). During fermentation, the cells were sampled every 6 h to determine their glucose concentration by the dinitrosalicylic acid (DNS) method (Miller, 1959) and the organic nitrogen concentration by the Nessler's reagent method (Thompson and Morrison, 1951). Concentrated glucose solution (40%), corn steep liquor (0.3%), and antifoam solution (10%) were fed depending upon the substrate consumption. Five molar KOH was injected continuously to keep the pH at ~6.0.

Cell Growth Estimation

To monitor the cell growth, 10 mL cell suspensions were collected. After centrifugation followed by twice washing with

distilled water, the cells were oven dried until constant weight to determine the cell density (dry cell weight g L^{-1}).

At the end of the fermentation, the cells were harvested by filtration at 0.05–0.12 MPa using plate-frame vertical pressure filters with 32 pieces of cloth for 12 h and were then spread on the open ground under sunlight for 2 days to dry. The water fraction of the algal biomass, represented by the moisture content (MC), was calculated as

$$MC = \left(W_w - W_d\right)/W_w \times 100\% \qquad (1)$$

where W_d is the weight of the completely dried cells using a frozen vacuum dryer and W_w is the weight of the biomass ($W_w - W_d$ was the water left in the biomass).

Oil Content Determination and Extraction

For the oil content (OC) determination, 10 g freeze-dried cells was hand-ground with silica in a mortar. The oil was extracted with *n*-hexane by the Soxhlet extraction method for 72 h. The *n*-hexane was subsequently evaporated, and the OC (weight of oil/weight of biomass × 100%) was calculated. For large-scale oil extraction, 30 kg dry cells, 30 kg steel grinding balls (3–5 mm in diameter) and 30 L isopropyl alcohol (IPA) were loaded into a 100-L steel ball mill machine (an industrial piece of equipment used in the food, oil and mining industries, XQM-100, Tianchuang Powder Equipment Co., Ltd., China) and ground at 200 rpm for 1 h. After recovering the milling balls using a stainless steel screen with a mesh size of 2 mm, the solution was filtered by a plate and frame filter. The oil-IPA miscella was vacuum distilled to recover the IPA. The crude oil was refined, and the oil extraction efficiency (OEE) was calculated as follows:

$$OEE = OW_x /\left(BW_x \times OC\right)\times 100\% \qquad (2)$$

where OW_x is the weight of the oil extracted with the ball milling process and BW_x is the weight of the dried biomass.

To investigate the effects of the ball mill machine on cell breakage and OEE, the microstructure of the broken cells (after oil extraction) was examined by scanning electron microscopy (Oberkochen, Germany). Both intact and broken cells were dehydrated sequentially with 50, 75, 90, and 100% ethanol (volume fraction) for 1 h each. After natural volatilization, the samples were spread on conductive tape, coated with gold powder and subjected to microscope examination.

Preparation of Microalgal Biodiesel

The transesterification of the microalga oil was catalyzed by liquid lipase (12,000 U g^{-1}, Sichuan Habio Bioengineering Co., Ltd., China) with the volume fraction of catalyzer:methanol (batch addition):oil at 1:10:100. The reaction was carried out in a 50-L bioreactor under constant stirring at 180 rpm and a temperature of 50°C for 8 h. The processes of methanol feeding and product separation were conducted according to a previous report (Li et al., 2007). After washing and distilling the remaining methanol, catalyst, and glycerol, the crude biodiesel at the top layer was rectified to obtain high quality biodiesel in a 100-L distillation

tower with a maximum temperature at 220°C and vacuum degree at 0.1 Pa.

Components and Quality Analysis of Algal Biodiesel

The biodiesel components were analyzed by gas chromatography–mass spectroscopy (GC–MS) (Thermo, USA). A dual-stage quadrupoles GC apparatus was equipped with a Varian VF-5 ms column (30 m × 0.25 mm ID DF = 0.25 μm), and the GC was manipulated with a flow rate at 10 mL min^{-1}. The physical and chemical properties of the biodiesel were determined according to ASTM D6751 standards at the Institute Analysis Center, SINOPEC CORP. The petroleum diesel (PD) on the market was used for comparison.

Vehicle Diesel Engine Test

Three types of fuel samples (100 L each) including 100% algal biodiesel (MBD100), 20% algal biodiesel blended with 80% PD (MBD20), and 100% PD were fueled and tested separately in a 3.0 L vehicle diesel engine (ZD-30, Nissan Motor Company, Japan) for their dynamic properties and emissions. The stationary bench tests were conducted in the National Key Laboratory of Automotive Engineering in Tsinghua University, Beijing, China. To apply load on the vehicle diesel engine, a dynamometer (GW300, Hunan Xiang Yi Dynamic Test Instrument Co., Ltd.) was used. The dynamometer was modified by adding a load cell and digital monitor to measure the engine speed (r min^{-1}) and torque (Nm) to calculate the power (kW). The engine thermal efficiency was calculated as follows:

$$\eta = 3.6 \times 10^6 /\left(b \times H\right) \qquad (3)$$

where η, b, and H are the engine efficiency, brake-specific fuel consumption (BSFC), and heat value of the fuels, respectively.

A gas analyzer (BEA 460 Bosch, Combustion Products Group, Ltd., UK) was used to monitor the engine exhaust gases for carbon monoxide (CO), hydrocarbon (HC), and nitrogen oxides (NOx). Particulate matter (PM) was measured by a 5–1000 nm particulate analyzer (DMS500, Combustion Products Group, Ltd., UK). Prior to the test, the device was subjected to maintenance and calibration by the manufacturer followed by daily standard calibration.

RESULTS

Production of Heterotrophic *A. protothecoides* Biomass

The cell growth, pH, and glucose and nitrogen content in the 60-m^3 fermentor were monitored throughout the fermentation process, and concentrated glucose solutions (40%), corn steep liquors (0.3%), and antifoam solutions (10%) were batch-fed accordingly (**Figure 2**). The pH was controlled at ~6.0 ± 0.2 to ensure optimal cell growth conditions. The amount of glucose and residual nitrogen in the container, which are critical to maintain the heterotrophic growth of *A. protothecoides*, were carefully controlled. According to our previous trials (data not shown),
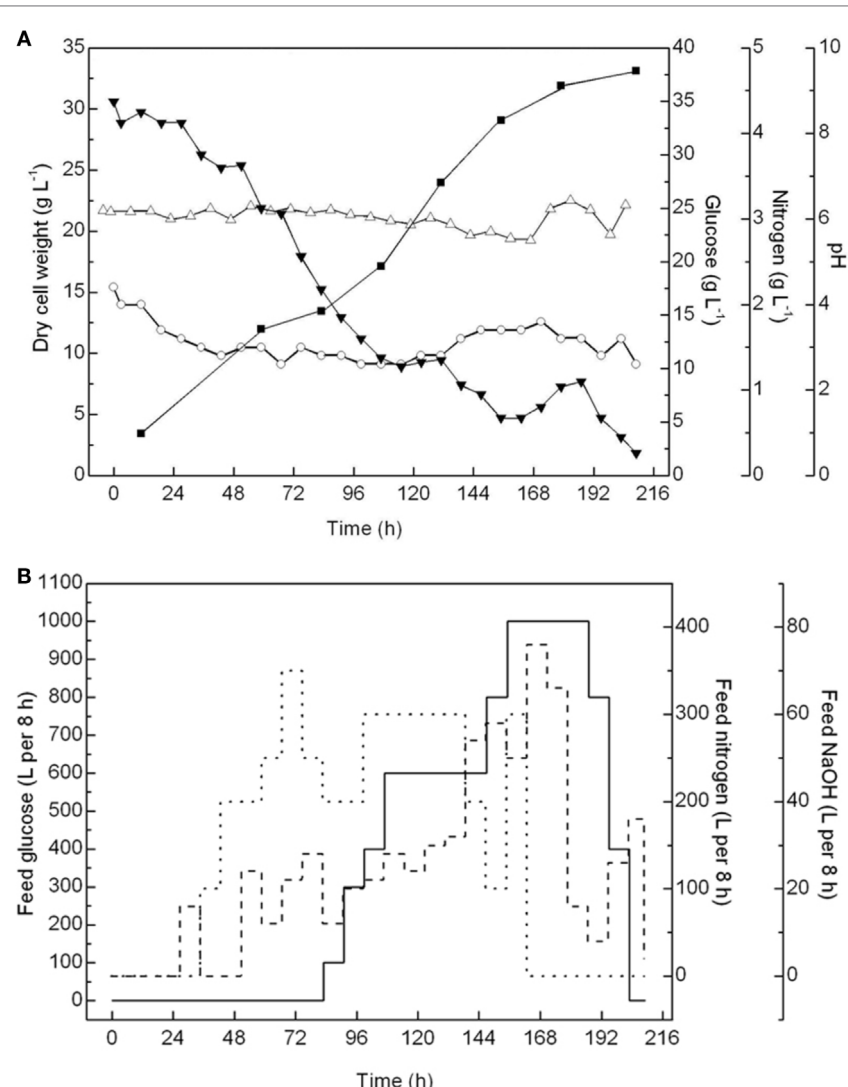
FIGURE 2 | Monitor and control of fed-batch cultivations of *A. prototheocoides* in a 60-m³ fermentor. (A) Time courses monitor records of cell growth (■), pH variation (Δ), residential concentration of glucose (▼), and nitrogen (O). **(B)** Time course profiles of feeding glucose (—), nitrogen (…), and NaOH (- - -).

when cells escaped from the lag phase, a low residual concentration of glucose below 10 g L^{-1} in the culture medium could avoid the inhibition of cell growth, especially when both the glucose consumption rate and glucose feeding rate were high. Therefore, after 84 h, when the glucose content dropped to near 10 g L^{-1}, the glucose feeding was initiated but was carefully regulated to ensure a residual concentration between 5 and 10 g L^{-1}. Meanwhile, the amount of residual nitrogen was maintained at ~1.5 ± 0.2 g L^{-1}, enough for the cells to proliferate.

After 216 h of fermentation in the 60-m³ fermentor, the final cell density reached 33.14 g L^{-1}, with an average biomass productivity at 3.81 g L^{-1} day^{-1}. Notably, before the cell density reached 30 g L^{-1} in the initial 144 h, the biomass productivity was above 6.87 g L^{-1} day^{-1}. However, the cell growth was greatly inhibited after that, resulting in the biomass productivity in the last 48 h being <2.5 g L^{-1} day^{-1}. This result suggested that under

this fermentation condition, the cells may enter a stationary phase once the density is over 30 g L^{-1}. Therefore, it becomes uneconomical to continue the fermentation process. In the future, we can either stop this fermentation or initiate the semi-continuous fermentation process at this time point. The biomass productivity in this 60-m³ fermentation was more than twice that (1.71 g L^{-1} day^{-1}) in an 11-m³ fermentor in a previous study and 10 times more than that in outdoor photobioreactors (on average 0.30 g L^{-1} day^{-1}) (Rodolfi et al., 2009).

Sugar-Lipid Conversion Ratio in a 60-m³ Fermentor

The total glucose consumed in the 60-m³ fermentation was 5120 kg, and the yield of dry biomass was 1540 kg, indicating that the conversion ratio of glucose to biomass was ~0.301 kg/kg.

Within these cells, the OC was determined to be 51%. Therefore, the total oil yield per fermentation was 739.5 kg, the oil productivity was 82.16 kg day^{-1}, and the conversion ratio of glucose to oil was 0.154 kg/kg. However, during the oil production through carbon metabolism, glucose is first converted to pyruvate via glycolysis and is then transformed to acetyl-CoA. The theoretical maximum conversion ratio of glucose to oil is 51.1% (mass fraction, i.e., 66.7% mole fraction) (Xiong et al., 2010). However, a previous study indicated that the conversion ratios in 5 L and

11 m^3 fermentors were 31.2 and 27%, respectively (Li et al., 2007), suggesting that the increased volume may reduce the conversion rate. Additional studies should be performed to increase the conversion rate, especially in larger fermentors.

Algal Harvest, Drying, and Oil Extraction

The processes to harvest and dry the microalgae biomass and to extract oil from the cells are the other important energy- and labor-consuming steps in microalgal biofuel production and
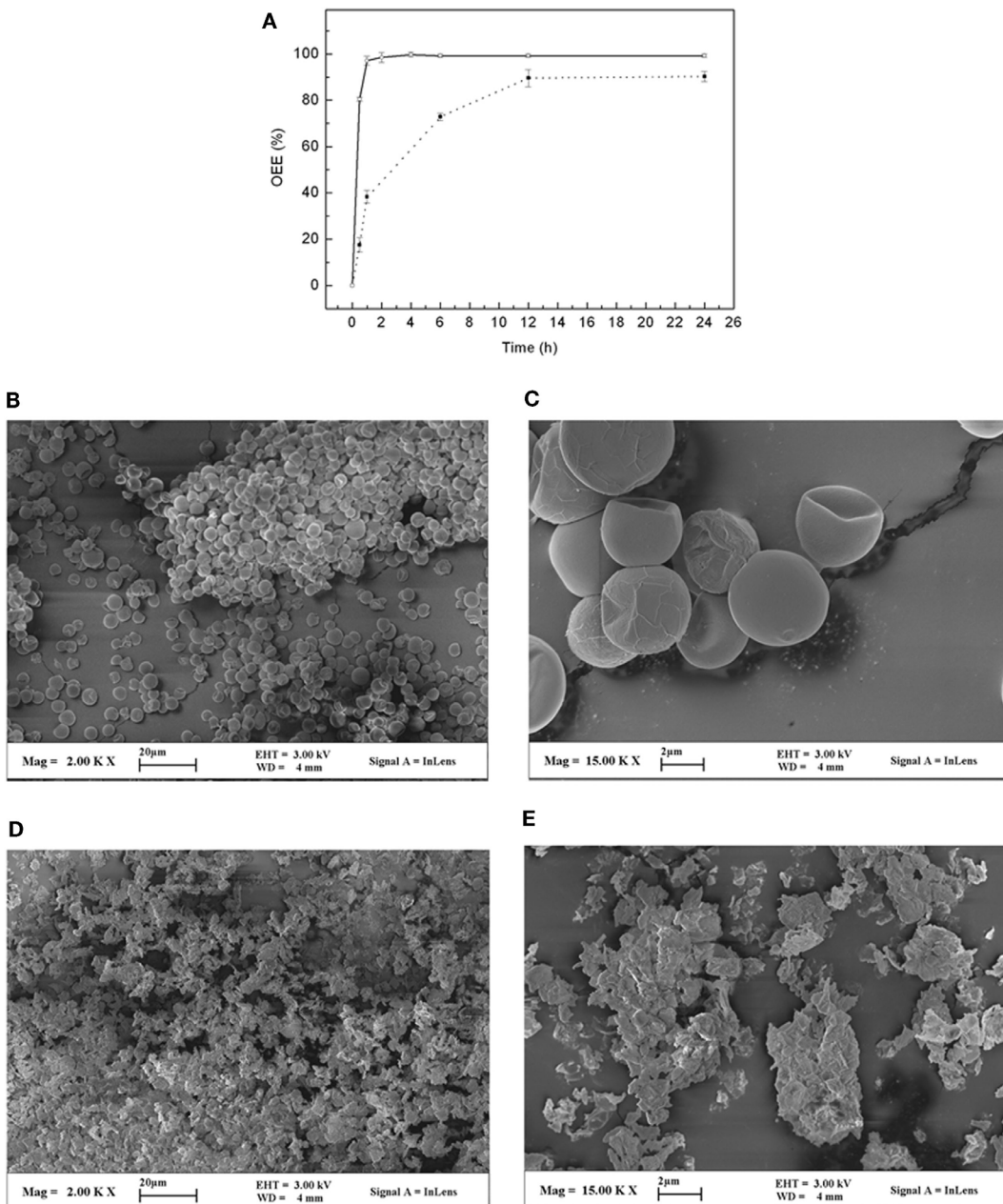

FIGURE 3 | Oil extraction from *A. prototecoides* cells by ball milling with IPA as solvent. **(A)** Effects of ball mill time on oil extraction efficiency (OEE) of algal biomass with MC at 5% (○) and 66% (■). **(B,C)** Photos of scanning electron microscopy of *A. prototecoides* cells before ball milling at small **(B)** and large **(C)** magnifications, see scale bar. **(D,E)** Photos of scanning electron microscopy of cell residues after ball milling with IPA at small **(D)** and large **(E)** magnifications, see scale bar.

could account for a significant fraction of the total cost (Islam et al., 2014). In the laboratory, centrifugation is commonly used to collect the algal biomass followed by freeze or spray drying (Xu et al., 2011; Wang et al., 2012), and the method of Soxhlet was generally used to extract oil (Yan et al., 2011; Mohan and Devi, 2014). However, these methods require either high-cost equipment or high energy consumption, and their processing capacity is only limited to a small amount of biomass. Therefore, it is not feasible to apply these methods in commercial production.

To handle the large volume of final fermented suspension from a 60-m³ fermentor and simultaneously avoid the high energy and high-cost centrifugation process, we developed a filtering method that enables us to obtain wet biomass by gravity supplemented with vertical pressure (0.05–0.12 MPa) through the plate-frame filter with 32 pieces cloth (a patent filter device, Chinese patent application No. 201310285550.8). This method could recover ~98% of algae, and the medium after filtering could theoretically be recycled and used for another round of fermentation. The MC showed that the wet biomass from the plate-frame filter contained 66% water, which could be further dried. In addition, there are several recent reports on direct oil extraction using wet biomass (Islam et al., 2014), and similar processes could potentially be applied here. Meanwhile, we tested two different methods to dry the cells. One method is using a commercial oven to bake the wet algae, and the other is to simply expose the wet biomass on the open ground under natural sunlight. We found that both methods worked well by reducing the MC to 0 or 5% after 48 h, respectively. However, when the cells were taken out of the oven, they formed a solid plaque that was very hard to break and prevented the subsequent oil extraction process. However, the cells dried under natural sunlight remained as a soft powder and could be easily processed. In addition, natural drying also avoided an extra electricity cost, and we, therefore, think it is a better method for cell drying. Furthermore, we also tested if the naturally dried cells could potentially affect the oil extraction process and found no difference between normal dried cell samples (**Figure 3A**). Overall, the energy consumption for the plate-frame filter was calculated as 0.014 MJ kg⁻¹. Compared with that using centrifuge and freeze or spray drying, which required at least 80.9 MJ kg⁻¹ (Xu et al., 2011), the method presented in this study was economical and feasible for industrial application.

Oil extraction from algal cells is another challenge for the commercial production of biofuel. The laboratory-scale Soxhlet method is not applicable, as it could only deal with a very small amount of dried cells (generally <100 g) and took a long time (generally 3 days). To overcome this problem, we tested whether oil could be directly extracted by organic solvent when cell disruption was performed simultaneously in a 100-L steel ball mill machine, which allowed us to process a biomass of ~360 kg/day. Considering the lipid composition of heterotrophic *A. protothecoides* and also safety issues, IPA was used due to its high boiling point and low toxicity. As shown in **Figure 3A**, the OEE was 65.89 ± 1.31% after immersing the dry algal cell (MC at 2%) in IPA for 1 h without physical disruption. However, when the cells were subjected to ball milling in IPA, the OEE increased up to 97.12 ± 1.84%. In addition, we also tested whether we can directly extract oil from the aforementioned wet algal cells (MC

TABLE 1 | Comparison of the properties of microalgae biodiesel, 0# petroleum diesel, and ASTM biodiesel's standard.

Properties	Unit	Microalgae biodiesel	0# petroleum diesel[a]	ASTM D6751 Standard
Flash point	°C	160	75	≥130.0
Viscosity	mm² s⁻¹	4.354	1.9–4.1	1.9–6.0
Density	kg m⁻³	876.9	838	820–900
Acid number	mg(KOH) g⁻¹	0.2	≤0.5	≤0.50
Cetane number	–	52.6	40–51	≥47
Copper strip corrosion	Class	1	1	≤1
Cold filter plugging point	°C	1	≤4	Report
Heat value	MJ kg⁻¹	38.25	40–45	Report
90% recovery temperature	°C	341.0	NA	≤360
Oxidation stability	h	1.2	NA	≥3
Water content	mg kg⁻¹	26	NA	≤50
Sediments	–	None	None	None
Sulfated ash	% Mass	0.005	NA	≤0.02
10% Carbon residue	% Mass	0.09	NA	≤0.3
H/C ratio	% Mass	1.81	1.81	Report
Total glycerol content	% Mass	0.02	NA	≤0.24
Oxygen content	% Mass	10.66	NA	Report
Sulfur content	% Mass	8.3×10^{-6}	0.95	≤0.02

[a]The data for diesel fuel are from published studies; NA indicates not available.

at 66%). We found that it required a longer processing time and had a lower OEE than when using the dried cells (**Figure 3A**). To further confirm the effect of the ball milling method, a scanning electron microscope (SEM) was used to evaluate the cell integrity. We found that before ball milling, all algal cells were intact but shriveled due to dehydration (**Figures 3B,C**). After ball milling, the cells were almost completely crushed into tiny fragments (<0.2 μm) (**Figures 3D,E**). Most of the oil and intracellular constituents were taken into the IPA.

Properties of the Algal Biodiesel

Given that enough crude oil could be obtained through above processes, we next carried out enzymatic transesterification to produce algal biodiesel and analyzed its composition. We found that the overall quality of the biodiesel was similar to what has been previously reported (Miao and Wu, 2006). A comprehensive evaluation of the derived algal biodiesel was conducted by comparing its chemical and physical properties with PD and the ASTM D6751 Standard. As shown in **Table 1**, the algal biodiesel was characterized by a flash point of 160°C, viscosity of 4.354 mm² s⁻¹, density of 876.9 kg m⁻³, acid number of 0.2, and heat value of 38.25 MJ kg⁻¹. These properties satisfied most ASTM D6751 standards, except that the oxidation stability exceeded the designated range and could be improved (Schober and Mittellbach, 2004). The cetane number at 52.6 indicated that the microalgal biodiesel would combust better
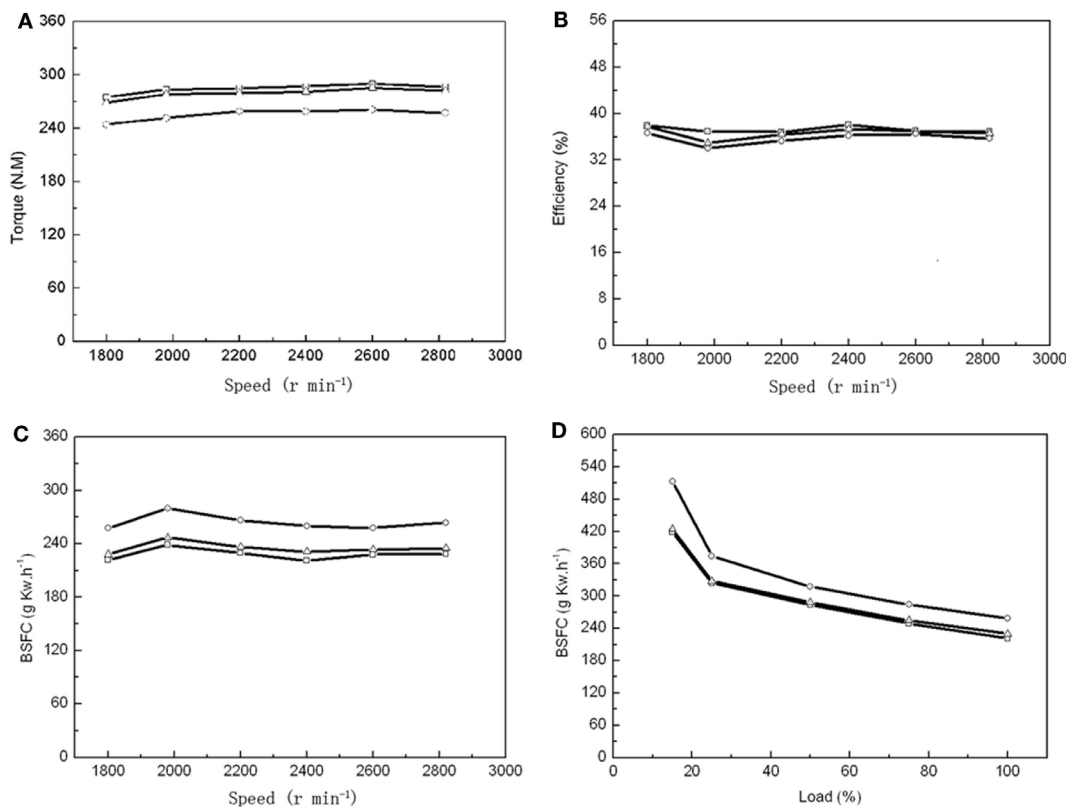
FIGURE 4 | Performance of vehicle diesel engine using petroleum diesel (PD, □), 20% microalgal biodiesel blend with 80% PD (MBD20, △), and pure microalga biodiesel (MBD100, ○), respectively. **(A)** The relationship between engine torque and engine speed. **(B)** The relationship between engine efficiency and engine speed. **(C)** The relationship between engine brake-specific fuel consumption (BSFC) and engine speed. **(D)** The relationship between engine BSFC and engine load.

than number 0 fossil diesel. Overall, our study suggested that the microalgal oil derived from cells in a 60-m³ industrial fermentor could be used as feedstock for the production of high quality biodiesel.

Application of Microalgal Biodiesel for Vehicle Engine Operation

Biodiesel has been tested in direct-injection engines or diesel tractors. For example, Dorado et al. (2003) tested biodiesel from olive waste cooking oil in a direct-injection engine. For microalgae-derived biodiesel, a recent report (Al-Lwayzy and Yusaf, 2013) suggested that it could satisfy the requirement in a diesel agriculture tractor engine, in which 20% microalgal biodiesel was used. However, there are still no reports if pure microalgal biodiesel (100%) could be used and how it will perform in a direct-injection engine.

As a single 60-m³ fermentor could produce 1540 kg dry biomass with an OC over 50%, it enabled us to prepare enough algal biodiesel for 24 h combustion to test multiple parameters. Number 0 diesel, 20% microalgal biodiesel (B20), and 100% microalgal biodiesel (B100) were tested in a vehicle diesel engine to compare the BSFC, engine torque, thermal efficiency, NOx and PM emissions between these different fuels. The maximum torques was found at an engine speed of 2600 r min⁻¹ for PD,

MBD20, and MBD100 (**Figure 4A**). The engineering efficiency did not change significantly among PD, MBD20, and MBD100 at different speed (**Figure 4B**). The average dynamics reached ~98 and 90% of the peak values with MBD20 and MBD100, respectively, indicating no significant differences between PD and MBD20 at a speed of 2600 r min⁻¹ at the peak torque. The BSFC (**Figures 4C,D**) was observed to increase with a higher proportion of algal biodiesel in the blend compared to PD at all engine speeds. No significant difference was found between PD and MBD20 in the entire load range, suggesting that MBD20 could be an optimal biodiesel blend.

Emissions of gas and PM are the other important parameters to evaluate in biodiesel. When the air supply was insufficient at a low engine speed and load, carbon monoxide (CO) was the main pollutant in the exhaust gas. We found that the CO emissions were 35 and 53% lower from the combustion of MBD20 and MBD100, respectively, than that from PD when the engine speed was below 1900 r min⁻¹ and the engine load was below 20% (**Figures 5A,B**). This indicates better combustion for MBD20 and MBD100, which potentially resulted from the extra oxygen in the biodiesel. With increasing engine speed up to 2000 r min⁻¹ or engine load up to 25%, the CO emission decreased greatly and did not subsequently show differences among PD, MBD20, and MBD100 (**Figures 5A,B**).
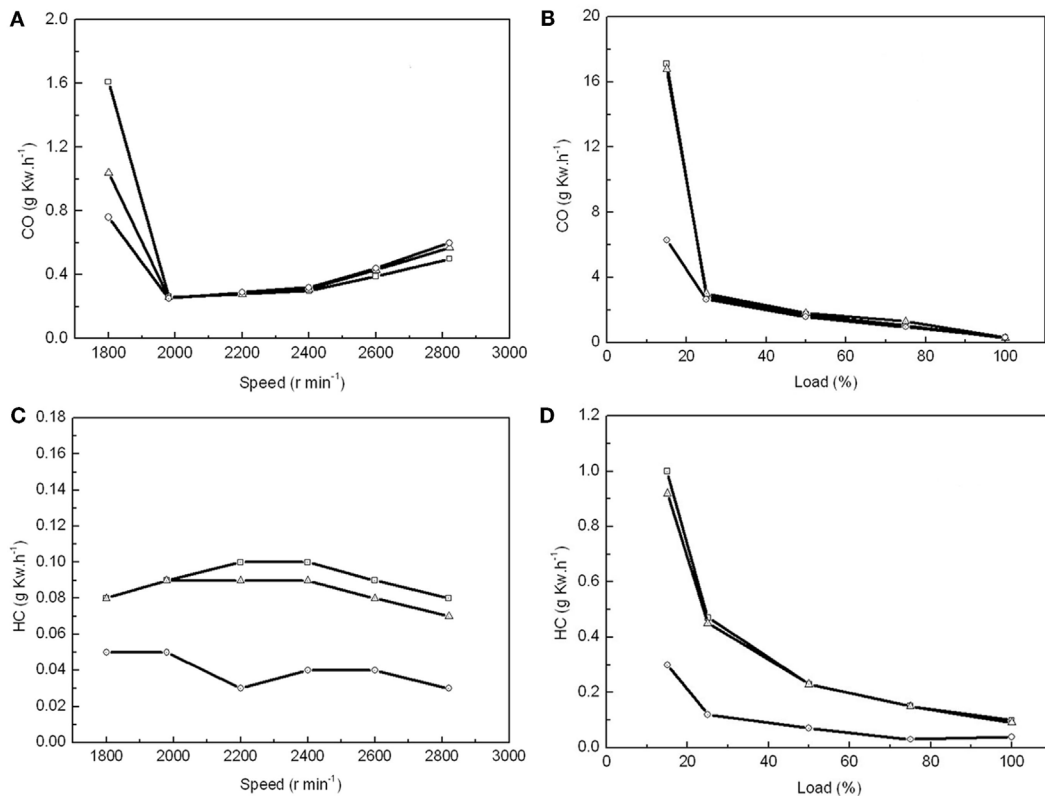
FIGURE 5 | The effects of combustion with PD, MBD20, and MBD100 on emissions of CO and HC. (A) CO emission from different engine speeds. (B) CO emission at different engine loads. (C) HC emission at different engine speeds. (D) HC emission at different engine loads. PD (□), MBD20 (△) and MBD100 (○).

Hydrocarbon, as one of the main greenhouse gases that negatively impacts the formation of ozone, is another pollution gas from fuel combustion. The lowest HC emission at 0.03 g k Wh^{-1} was recorded at 2200 r min^{-1} for MBD100, which was only one-third of that for PD (**Figure 5C**). HC emissions for MBD20 were close to PD, which decreased significantly with increasing engine load (**Figure 5D**). In general, MBD100 produced less HC did PD and MBD20 under most conditions.

In addition, NOx, including NO and NO$_2$ as pollution gases from fuel combustion, were detected in the engine test. No significant difference was observed among BMD 100, BMD 20 and PD for the test fuels (data not shown). In contrast, the PM emissions detected showed that the PM emissions from both MBD20 and MBD100 were obviously lower than those of PD under different engine speeds and loads (**Figure 6**). Compared with PD, the PM emission reduced from 37 to 42% in the MBD20 test and 57 to 75% in the MBD100 test, respectively. As a bio-oil derived fuel, the 10.66% oxygen content in the biodiesel molecules and the low sulfur content (mass fraction of 8.3×10^{-6}) may contribute to a complete fuel oxidation, causing a significant decrease in the PM concentration. When the engine load doubled or the speed increased, the PM emissions were clearly reduced (**Figure 6**) as the formation of soot from the exhaust emission was proportional with the change of combustion temperature.

DISCUSSION

At the moment, it is still not economically viable to industrially produce microalgal biofuel, despite the potential for microalgae to be a sustainable and green bioenergy resource, largely because of limitations on microalgal productivity (Pienkos and Darzins, 2009; Davis et al., 2011). Several technologies have been developed to reduce the cost, including strain improvement, cultivation optimization, and chemical treatment (Specht et al., 2010; Scranton et al., 2015). Here, we extended the heterotrophic cultivation of *A. protothecoides* for biomass production from a laboratory to an industrial scale (Miao and Wu, 2006; Xu et al., 2006; Li et al., 2007). A 60-m³ fermentor of *A. protothecoides* was established, which produced microalgal biomass at 3.81 g L^{-1} day^{-1} on average and an OC of ~51%, comparable to what we previously obtained on a smaller scale (Miao and Wu, 2006; Xu et al., 2006; Li et al., 2007).

Plate-frame filter, natural drying, and ball milling methods were developed as subsequent energy-saving processing technologies. The plate-frame filter and natural drying procedure could replace the commonly used, high-cost centrifugation, which requires not only a large investment in equipment but also significant energy consumption. In addition, our study suggested that the ball mill disruption method could also be a feasible and scalable process to meet the industrial requirement for oil extraction besides its
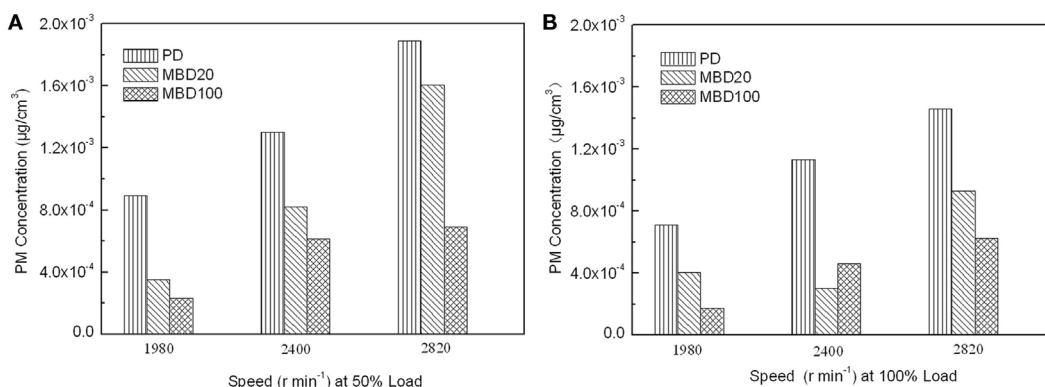
FIGURE 6 | The effects of combustion with PD, MBD20, and MBD100 on emissions of particulate matter. **(A)** PM emission at different engine speeds with 50% engine load. **(B)** PM emission at different engine speeds with 100% engine load.

application in the recovery of bioproducts from cyanobacteria (Balasundaram et al., 2012). Compared with high-pressure single solvent (hexane) extraction (Islam et al., 2014), ball mill disruption consumes less energy and has low requirements for equipment.

Subsequently, the vehicle diesel engine test indicated that the microalgal biodiesel is comparable to fossil diesel but produces fewer emissions of PM, carbon monoxide, and HC emissions. Two types of biodiesel (MBD 20 and MBD 100) performed well and resulted in an acceptable increment of the volumetric fuel consumption in an unmodified vehicle diesel engine with fewer emissions of carbon monoxide, HC, and PM, which could potentially reduce damage to the environment.

Finally, based on a previous study on the commercial production process of biodiesel, the cost of crude oil feedstock contributes to 88% of the overall production cost (Haas et al., 2006). Accordingly, the cost of our microalgal biodiesel could be estimated at 18.73 US\$/kg, which is equivalent to 15.70 US\$/L (density of algal biodiesel measured at 0.838 kg/L). Although the minimum production cost of algal biodiesel in this study was higher than the current petrol diesel price in China (1.2 US\$/L), it was much lower than the reported microalgae biodiesel produced from an outdoor photobioreactor (73.5 US\$/L) (Lam and Lee, 2014), suggesting that the fermentation process could become competitive in the future once the production costs are further reduced. Several approaches could be adapted to cut the costs in

the future, including (1) the substrate (glucose) feeding and process control in the fermentor can be further optimized to obtain a higher cell density and OC, reduce the fermentation period or improve the actual conversion ratio from sugar to oil; (2) the cost for the glucose substrate might be reduced by using other feedstocks, such as cassava (Lu et al., 2010), Jerusalem artichoke (Cheng et al., 2009), or waste molasses (Yan et al., 2011); (3) the off-gas from the fermentor could be recycled to agitate the medium in the photobioreactor and provide CO_2 for photoautotrophic cells, which can be coupled with heterotrophic fermentation to address carbon reuse and cost reduction (Lu et al., 2013); (4) replacing the current 60-m³ stirring fermentor with an airlift bioreactor could save on electricity consumption for driving the big agitator blade; (5) a continuous fermentation process could be used to shorten the fermentation period and cut down on the corresponding consumption of electricity and aseptic air; and (6) high-value byproducts or co-products, such as carotene and lutein, might be explored to supplement algal biodiesel production.

ACKNOWLEDGMENTS

REFERENCES

Al-Lwayzy, S. H., and Yusaf, T. (2013). *Chlorella protothecoides* microalgae as an alternative fuel for tractor diesel engines. *Energies* 6, 766–783. doi:10.3390/en6020766

Balasundaram, B., Skill, S. C., and Llewellyn, C. A. (2012). A low energy process for the recovery of bioproducts from cyanobacteria using a ball mill. *Biochem. Eng. J.* 69, 48–56. doi:10.1016/j.bej.2012.08.010

Brennan, L., and Owende, P. (2010). Biofuels from microalgae – a review of technologies for production, processing, and extractions of biofuels and co-products. *Renew. Sust. Energ. Rev.* 14, 557–577. doi:10.1016/j.rser.2009.10.009

Ceron-Garcia, M. C., Macias-Sanchez, M. D., Sanchez-Miron, A., Garcia-Camacho, F., and Molina-Grima, E. (2013). A process for biodiesel production

involving the heterotrophic fermentation of *Chlorella protothecoides* with glycerol as the carbon source. *Appl. Energy* 103, 341–349. doi:10.1016/j.apenergy.2012.09.054

Cheng, Y., Zhou, W. G., Gao, C. F., Lan, K., Gao, Y., and Wu, Q. Y. (2009). Biodiesel production from Jerusalem artichoke (*Helianthus tuberosus* L.) tuber by heterotrophic microalgae *Chlorella protothecoides*. *J. Chem. Technol. Biotechnol.* 84, 777–781. doi:10.1002/jctb.2111

Davis, R., Aden, A., and Pienkos, P. T. (2011). Techno-economic analysis of autotrophic microalgae for fuel production. *Appl. Energy* 88, 3524–3531. doi:10.1016/j.apenergy.2011.04.018

Dorado, M. P., Ballesteros, E., Arnal, J. M., Gomez, J., and Gimenez, F. J. L. (2003). Testing waste olive oil methyl ester as a fuel in a diesel engine. *Energy Fuel* 17, 1560–1565. doi:10.1021/ef0202485

Entrekin, S., Evans-White, M., Johnson, B., and Hagenbuch, E. (2011). Rapid expansion of natural gas development poses a threat to surface waters. *Front. Ecol. Environ.* 9:503–511. doi:10.1890/110053

Haas, M. J., McAloon, A. J., Yee, W. C., and Foglia, T. A. (2006). A process model to estimate biodiesel production costs. *Bioresour. Technol.* 97, 671–678. doi:10.1016/j.biortech.2005.03.039

Haik, Y., Selim, M. Y. E., and Abdulrehman, T. (2011). Combustion of algae oil methyl ester in an indirect injection diesel engine. *Energy* 36, 1827–1835. doi:10.1016/j.energy.2010.11.017

Hidy, G. M. (2012). Energy supplies and future engines for land, sea, and air. *J. Air Waste Manag. Assoc.* 62, 605–606. doi:10.1080/10962247.2012.737277

Islam, M. A., Brown, R. J., O'Hara, I., Kent, M., and Heimann, K. (2014). Effect of temperature and moisture on high pressure lipid/oil extraction from microalgae. *Energy Convers. Manag.* 88, 307–316. doi:10.1016/j.enconman.2014.08.038

Johnson, M. B., and Wen, Z. Y. (2009). Production of biodiesel fuel from the microalga *Schizochytrium limacinum* by direct transesterification of algal biomass. *Energy Fuel* 23, 5179–5183. doi:10.1021/ef900704h

Lam, M. K., and Lee, K. T. (2014). Cultivation of *Chlorella vulgaris* in a pilot-scale sequential-baffled column photobioreactor for biomass and biodiesel production. *Energy Convers. Manag.* 88, 399–410. doi:10.1016/j.enconman.2014.08.063

Levine, R. B., Pinnarat, T., and Savage, P. E. (2010). Biodiesel production from wet algal biomass through in situ lipid hydrolysis and supercritical transesterification. *Energy Fuel* 24, 5235–5243. doi:10.1021/ef1008314

Li, X. F., Xu, H., and Wu, Q. Y. (2007). Large-scale biodiesel production from microalga *Chlorella protothecoides* through heterotropic cultivation in bioreactors. *Biotechnol. Bioeng.* 98, 764–771. doi:10.1002/bit.21489

Lu, Y., Dai, J. B., and Wu, Q. Y. (2013). Photosynthesis-fermentation hybrid system to produce lipid feedstock for algal biofuel. *Environ. Technol.* 34, 1869–1876. doi:10.1080/09593330.2013.824011

Lu, Y., Zhai, Y., Liu, M. S., and Wu, Q. Y. (2010). Biodiesel production from algal oil using cassava (Manihot esculenta Crantz) as feedstock. *J. Appl. Phycol.* 22, 573–578. doi:10.1007/s10811-009-9496-8

Miao, X. L., and Wu, Q. Y. (2004). High yield bio-oil production from fast pyrolysis by metabolic controlling of *Chlorella protothecoides*. *J. Biotechnol.* 110, 85–93. doi:10.1016/j.jbiotec.2004.01.013

Miao, X. L., and Wu, Q. Y. (2006). Biodiesel production from heterotrophic microalgal oil. *Bioresour. Technol.* 97, 841–846. doi:10.1016/j.biortech.2005.04.008

Miller, G. L. (1959). Use of dinitrosalicylic acid reagent for determination of reducing sugar. *Anal. Chem.* 31, 426–428. doi:10.1021/ac60147a030

Mohan, S. V., and Devi, M. P. (2014). Salinity stress induced lipid synthesis to harness biodiesel during dual mode cultivation of mixotrophic microalgae. *Bioresour. Technol.* 165, 288–294. doi:10.1016/j.biortech.2014.02.103

Olmstead, S. M., Muehlenbachs, L. A., Shih, J. S., Chu, Z. Y., and Krupnick, A. J. (2013). Shale gas development impacts on surface water quality in Pennsylvania. *Proc. Natl. Acad. Sci. U.S.A.* 110, 4962–4967. doi:10.1073/pnas.1213871110

Pienkos, P. T., and Darzins, A. (2009). The promise and challenges of microalgal-derived biofuels. *Biofuels Bioprod. Biorefin.* 3, 431–440. doi:10.1002/bbb.159

Rawat, I., Kumar, R. R., Mutanda, T., and Bux, F. (2013). Biodiesel from microalgae: a critical evaluation from laboratory to large scale production. *Appl. Energy* 103, 444–467. doi:10.1016/j.apenergy.2012.10.004

Rodolfi, L., Zittelli, G. C., Bassi, N., Padovani, G., Biondi, N., Bonini, G., et al. (2009). Microalgae for oil: strain selection, induction of lipid synthesis and outdoor mass cultivation in a low-cost photobioreactor. *Biotechnol. Bioeng.* 102, 100–112. doi:10.1002/bit.22033

Schober, S., and Mittelbach, M. (2004). The impact of antioxidants on biodiesel oxidation stability. *Eur. J. Lipid Sci. Technol.* 106, 382–389. doi:10.1002/ejlt.200400954

Scranton, M. A., Ostrand, J. T., Fields, F. J., and Mayfield, S. P. (2015). Chlamydomonas as a model for biofuels and bio-products production. *Plant J.* 82, 523–531. doi:10.1111/tpj.12780

Specht, E., Miyake-Stoner, S., and Mayfield, S. (2010). Micro-algae come of age as a platform for recombinant protein production. *Biotechnol. Lett.* 32, 1373–1383. doi:10.1007/s10529-010-0326-5

Thompson, J. F., and Morrison, G. R. (1951). Determination of organic nitrogen – control of variables in the use of Nessler reagent. *Anal. Chem.* 23, 1153–1157. doi:10.1021/ac60056a029

Vidic, R. D., Brantley, S. L., Vandenbossche, J. M., Yoxtheimer, D., and Abad, J. D. (2013). Impact of shale gas development on regional water quality. *Science* 340, 1235009. doi:10.1126/science.1235009

Wang, H. Y., Xiong, H. R., Hui, Z. L., and Zeng, X. B. (2012). Mixotrophic cultivation of *Chlorella pyrenoidosa* with diluted primary piggery wastewater to produce lipids. *Bioresour. Technol.* 104, 215–220. doi:10.1016/j.biortech.2011.11.020

Weber, C. L., and Clavin, C. (2012). Life cycle carbon footprint of shale gas: review of evidence and implications. *Environ. Sci. Technol.* 46, 5688–5695. doi:10.1021/es300375n

Weyer, K. M., Bush, D. R., Darzins, A., and Willson, B. D. (2010). Theoretical maximum algal oil production. *Bioenerg. Res.* 3, 204–213. doi:10.1007/s12155-009-9046-x

Xiong, W., Gao, C. F., Yan, D., Wu, C., and Wu, Q. Y. (2010). Double CO2 fixation in photosynthesis-fermentation model enhances algal lipid synthesis for biodiesel production. *Bioresour. Technol.* 101, 2287–2293. doi:10.1016/j.biortech.2009.11.041

Xiong, W., Li, X. F., Xiang, J. Y., and Wu, Q. Y. (2008). High-density fermentation of microalga *Chlorella protothecoides* in bioreactor for microbio-diesel production. *Appl. Microbiol. Biotechnol.* 78, 29–36. doi:10.1007/s00253-007-1285-1

Xu, H., Miao, X. L., and Wu, Q. Y. (2006). High quality biodiesel production from a microalga *Chlorella protothecoides* by heterotrophic growth in fermenters. *J. Biotechnol.* 126, 499–507. doi:10.1016/j.jbiotec.2006.05.002

Xu, L. X., Brilman, D. W. F., Withag, J. A. M., Brem, G., and Kersten, S. (2011). Assessment of a dry and a wet route for the production of biofuels from microalgae: energy balance analysis. *Bioresour. Technol.* 102, 5113–5122. doi:10.1016/j.biortech.2011.01.066

Yan, D., Lu, Y., Chen, Y. F., and Wu, Q. Y. (2011). Waste molasses alone displaces glucose-based medium for microalgal fermentation towards cost-saving biodiesel production. *Bioresour. Technol.* 102, 6487–6493. doi:10.1016/j.biortech.2011.03.036

Conflict of Interest Statement: The authors declare that the research was conducted in the absence of any commercial or financial relationships that could be construed as a potential conflict of interest.

Advantages of publishing in Frontiers

OPEN ACCESS

Articles are free to read, for greatest visibility

COLLABORATIVE PEER-REVIEW

Designed to be rigorous – yet also collaborative, fair and constructive

FAST PUBLICATION

Average 85 days from submission to publication (across all journals)

COPYRIGHT TO AUTHORS

No limit to article distribution and re-use

TRANSPARENT

Editors and reviewers acknowledged by name on published articles

SUPPORT

By our Swiss-based editorial team

IMPACT METRICS

Advanced metrics track your article's impact

GLOBAL SPREAD

5'100'000+ monthly article views and downloads

LOOP RESEARCH NETWORK

Our network increases readership for your article

Frontiers
EPFL Innovation Park, Building I • 1015 Lausanne • Switzerland
Tel +41 21 510 17 00 • Fax +41 21 510 17 01 • info@frontiersin.org
www.frontiersin.org

Find us on